Escuela de Doctorado Universitat Jaume I

Programa de Doctorado en Química Sostenible

SISTEMAS PSEUDOPEPTÍDICOS MULTIFUNCIONALES APLICACIÓN EN QUÍMICA SUPRAMOLECULAR

PhD Thesis

ADRIANA VALLS TEN

Directors:

Dr. Santiago Vicente Luis Lafuente

Dr. Belén Altava Benito

December, 2020

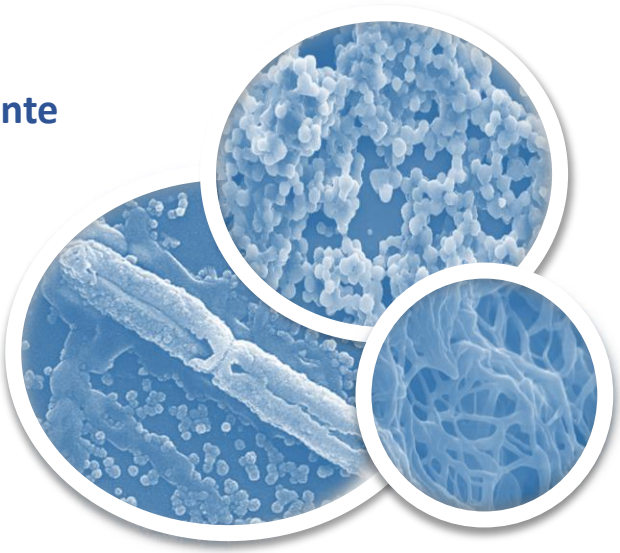

Programa de Doctorat en **Química Sostenible**

Escuela de Doctorado de la Universitat Jaume I

Título de la tesis

SISTEMAS PSEUDOPEPTÍDICOS MULTIFUNCIONALES. APLICACIÓN EN QUÍMICA SUPRAMOLECULAR.

Memoria presentada por **Adriana Valls Ten** para optar al **grado de doctora** por la Universitat Jaume I

Doctoranda:

ADRIANA|VALLS|TEN Firmado digitalmente por ADRIANA|VALLS|TEN Fecha: 2020.12.22 18:02:20 +01'00'

Adriana Valls Ten

Directores de la Tesis:

Dra. Belén Altava Benito

SANTIAGO VICENTE|LUIS|LAFUENTE Firmado digitalmente por SANTIAGO VICENTE|LUIS|LAFUENTE Fecha: 2020.12.22 17:58:50 +01'00'

Dr. Santiago Vicente Luis Lafuente

Castelló de la Plana, Diciembre de 2020

FINANCIACIÓN RECIBIDA

La realización de esta Tesis Doctoral ha sido posible gracias a la concesión de una ayuda en forma de contrato predoctoral de Formación de Profesorado Universitario (**FPU15/01191**) por parte del Ministerio de Educación, Cultura y Deporte del Gobierno de España.

La financiación de la actividad investigadora ha sido posible gracias a los proyectos concedidos por el Ministerio de Economía y Competitividad del Gobierno de España (RTI2018-098233-B-C22 o CTQ2015-68429-R), al Pla de Promoció de la Investigació de la Universitat Jaume I (UJI-B2019-40) y por la Generalitat Valenciana (PROMETEO/ 2016/071).

AGRADECIMIENTOS

En primer lugar, me gustaría agradecer al grupo de Química Sostenible y Supramolecular de la Universidad Jaume I y a sus miembros: Santiago Luis, Maribel Burguete, Belén Altava y Eduardo García, la gran oportunidad que me brindaron al abrirme las puertas hacia el mundo de la investigación universitaria. He sentido su apoyo, cariño, ayuda y guía durante todo este bonito proceso de aprendizaje, del cual les estoy muy agradecida.

A mis directores de tesis, convirtiéndose en mis pilares esenciales en este camino de formación. Gracias Santiago y Belén por todos los consejos, dedicación, cercanía y por transmitirme tanto amor por el conocimiento.

Agradecer también a las personas responsables de mis dos estancias en la Universidad de Helsinki y en la Universidad de Preston de los cuales he tenido el placer de aprender mucha química y sentirme muy integrada, a las personas con las que hemos realizado colaboraciones científicas que han sido de mucha ayuda para poder completar este camino, a los técnicos del Servicio Central de Instrumentación Científica de la UJI, a los compañeros del Departamento de Química Inorgánica y Orgánica por los buenos momentos compartidos y a aquellas personas que me han permitido crecer en mi formación como docente dándome buenos consejos y confiando en mí para impartir más docencia.

Y como no, a mi familia, al amor de mi vida, a mis compañeros y amigos de laboratorio tanto más recientes como más antiguos, a mis amigos de la Vall, a mis amigos de carrera y amigos que han aparecido durante este camino, gracias, gracias y mil gracias. Ya sabéis que siento por cada uno de vosotros y todo lo que os quiero. Gracias por las risas, abrazos, cariño, besos, consejos, apoyo y por hacerme de esta experiencia una vivencia inolvidable.

Muchísimas gracias a todos.

ABBREVIATION LIST

3D	Three-Dimensional
AAILs	Amino Acid based Ionic Liquids
ACN	Acetonitrile
ATR	Attenuated total reflection
Bn	Benzyl
CAC	Critical Aggregation Concentration
Cbz	Carboxybenzyl
CD	Circular Dichroism
CF	Carboxyfluorescein
CILs	Chiral Ionic Liquids
CMC	Critical Micellar Concentration
CSAs	Chiral Shift Agents
DDC	Dynamic Combinatorial Chemistry
DEA	Diethylenetriamine
DMEM	Dulbecco's modified Eagle's medium
DMF	Dimethylformamide
DILs	Dicationic Ionic Liquids
DMSO	Dimethyl sulfoxide
DNA	Deoxyribonucleic acid
DSC	Differential Scanning Calorimeter
DVB	Divinylbenzene
ESI-MS	Electrospray ionization mass spectrometry
FTIR	Fourier-Transform Infrared spectroscopy
GAPs	Gemini Amphiphilic Pseudopeptides
GC	Gas Chromatography
HEK-293	Human Embryonic Kidney cell line
ILs	Ionic Liquids
iPr	Isopropyl
IR	Infrared spectroscopy
LMWGs	Low-Molecular-Weight-Gelators
Me	Methyl
MeOH	Methanol
MBC	Minimal Bactericidal Concentration
MIC	Minimum Inhibitory Concentration
MILs	Monocationic Ionic Liquids
mim	1-alkyl-3-methylimidazole
MMFF	Merk Molecular Force Field

mp	Melting point
NMR	Nuclear Magnetic Resonance spectroscopy
NSAIDs	Non-Steroidal AntiInflamatory Drugs
O/W	Oil in Water
Ph	Phenyl
Phe	Phenylalanine
PILs	Polymers Ionic Liquids
PNPG	Poly(N-propergyl glycine)
POPC	1-palmitoyl-2-oleoyl-sn-glycero-3-phosphocoline
PVP	PolyVinylPyrrolidone
QDs	Quantum Dots
QUILL	Queen's University Ionic Liquid Laboratories
ROESY	Rotating frame Overhause Effect SpectroscopY
SEM	Scanning Electron Microscopy
TAEA	2,2',2"-triaminotriethylamine
TDD	Transdermal Drug Delivery
TEM	Transmission Electron Microscopy
TGA	Thermogravimetric Analysis
TILs	Tricationic Ionic Liquids
TSILs	Task-Specific ILs
TSs	Transition States
UV	Ultraviolet-Visible spectroscopy
Val	Valine
W/O	Water in Oil

SYMBOLS

η	Viscosity of a fluid
λ	Wavelength
T	Temperature
I	Intensity
γ	Deformation
τ	Shear stress
G^*	Complex shear module
G'	Elastic module
G''	Viscous module
w	Frequency
φ or **δ**	Offset
Jss	Solute steady-state flux

ΔC	Concentration increment
k_{ass}	Association constant
K	Skin/vehicle partition coefficient of the permeant
L	skin pathlength
D	Skin diffusion coefficient of the permeant
P	Skin permeability
J_x	Local permeant flux at position x
D_x	Local permeant diffusion coefficient
C_x	Concentration at position x
t_L	Lag time
T_1	Spin-lattice relaxation time
J_{max}	The maximum flux
S_V	Solubility of the permeant in the formulation
C_V	Experimental permeant's concentration
C	Concentration
M_t	Amount of drug released at time t
M_0	Total mass of drug loaded into the device
h	Thickness of the device
M_∞	Absolute cumulative amount of drug released at infinitive
k_D	Diffusional constant
k_R	Relaxation contribution constant
m	The purely Fickian diffusion exponent for a device

RESUMEN DE LA TESIS

La presente Tesis Doctoral se engloba dentro del área de la Química Supramolecular y más concretamente en el ámbito del autoensamblaje con la formación de distintos tipos de agregados supramoleculares y sus diferentes implicaciones en un gran número de aplicaciones. El principal objetivo es el diseño y desarrollo de nuevos compuestos pseudopeptídicos polifuncionales derivados de aminoácidos como la Valina y la Fenilalanina, compuestos muy interesantes por sus propiedades biológicas.

La memoria de la tesis se ha estructurado en 4 capítulos. El tercero de ellos consta de los resultados y discusión de la investigación realizada, que se ha redactado siguiendo el formato de artículos científicos a partir del trabajo de investigación desarrollado. Los resultados obtenidos han permitido la publicación de tres artículos en la revista Organic Chemistry Frontiers, de la Royal Society of Chemistry, en la revista Journal of Agricultural and Food Chemistry, de la ACS publications y en la revista Polymers, de MPDI, revistas de alto índice de impacto. Además, el trabajo expuesto ha permitido la elaboración de otro manuscrito ya enviado a una revista de alto impacto, así como otros tres manuscritos que serán enviados en breve, esperando ser publicados también en revistas de alto impacto.

El primer capítulo incluye una introducción general que se estructura en tres apartados, en el primero se realiza una breve introducción a la química supramolecular, el segundo apartado se adentra en los compuestos pseudopeptícos y el tercero desarrolla los líquidos iónicos, todos ellos con sus respectivas aplicaciones. Este capítulo tiene el objetivo de poner en antecedentes al lector y facilitar el posterior seguimiento de la tesis a través de los siguientes capítulos.

A continuación, en el segundo capítulo se exponen y detallan los objetivos generales de la tesis, así como los específicos para cada apartado, de forma que el lector pueda centrar su atención y comprender las motivaciones.

A partir de este punto, en el capítulo tercero se detallan los resultados obtenidos y la discusión de los mismos durante siete apartados. La primera sección estudia la fuerte preferencia por la formación de sistemas tripodales sobre los compuestos monotópicos y ditópicos relacionados para la reacción entre tris(halometil)bencenos e imidazoles derivados de aminoácidos y que contienen

un fragmento de amida, incluso cuando una mezcla equimolar de los compuestos de partida reacciona. Las reacciones se controlaron usando espectroscopía de RMN y espectrometría de masas ESI y se caracterizaron cinéticamente. También se realizaron estudios computacionales para racionalizar la preferencia observada del producto trisustituido. Esta investigación permitió la publicación de un artículo en la revista Organic Chemistry Frontiers.

La segunda sección recoge las investigaciones realizadas para obtener potenciales agentes quimioterapéuticos. Una serie de sales de imidazolio tripodales derivadas de *L*-valina y *L*-fenilalanina que contienen diferentes grupos hidrófobos se probaron contra cuatro líneas celulares cancerosas a pHe fisiológico y ácido (6.2). También se estudió el papel de la lipofilicidad, así como se llevó a cabo el estudio de transporte de aniones en vesículas POPC utilizando en presencia de estos compuestos para lograr una mejor comprensión de su acción terapéutica. Este trabajo resultó en la elaboración de un manuscrito listo para ser enviado a una revista especializada.

La tercera sección consta de los estudios realizados para desarrollar compuestos anfifílicos basados en sales de imidazolio derivados de la *L*-valina como potenciales tensioactivos. El patrón de sustitución del espaciador central aromático se utilizó para ajustar sus propiedades. Se estudió el autoensamblaje de estas moléculas en medio acuoso obteniendo concentraciones críticas de agregación (CACs) del orden de micromolar. Este estudio resultó en la preparación de un manuscrito listo para ser enviado a la revista Advanced Healthcare Materials.

La cuarta sección se centra en el diseño de nuevas sales de imidazol e imidazolio derivadas de *L*-valina y *L*-fenilalanina que contienen diferentes grupos hidrófobos y probar su actividad antibacteriana contra dos cepas bacterianas modelo, *E. coli* Gram-negativas y *B. subtilis* Gram-positivas. También se estudia el valor de citotoxicidad IC_{50} para la línea celular de control HEK-293 y la agregación de los compuestos para determinar si las especies monoméricas son responsables de la actividad antibacteriana observada. Esta investigación permitió la elaboración de un manuscrito enviado a la revista especializada Pharmaceuticals.

La quinta sección se desvía ligeramente de las anteriores que consiste en la síntesis de fases estacionarias líquidas iónicas poliméricas (PIL) soportadas sobre sílice derivadas de un monómero líquido iónico de *L*-valina vinílico y divinilbenceno (DVB) como agente de reticulación y estudiarlos como fases estacionarias de cromatografía de gases. Se comprobó la selectividad de separación y resolución de diferentes compuestos. Este trabajo permitió la publicación de un artículo en la revista especializada Polymers.

La sexta sección informa sobre una nueva familia de compuestos pseudopeptídicos de cadena abierta funcionalizados con un grupo carboxílico como hidrogelantes para la administración controlada de fármacos utilizando una celda de difusión de Franz y empleando una membrana biológica. También se estudió la capacidad de la formación del gel ante diferentes estímulos externos. Este estudio resultó en la preparación de un manuscrito listo para ser enviado a la revista Advanced Healthcare Materials.

Finalmente, la última sección se centró en la síntesis de organogelantes de bajo peso molecular que contienen fragmentos de alquil urea unidos al extremo amino de diferentes estructuras pseudopeptídicas miminalistas. Estos compuestos se estudiaron para gelar sustancias activas relevantes como aceite natural terpénico. Este estudio permitió la publicación de un artículo en el Journal of Agricultural and Food Chemistry.

Para concluir, en el capítulo cuarto y último, se exponen las conclusiones más importantes y destacables derivadas del trabajo descrito en cada uno de los artículos desarrollados en esta tesis.

Las abreviaciones utilizadas se recogen al principio de la tesis por orden alfabético. Del mismo modo, también se ha elaborado un listado con las estructuras y la numeración de los compuestos que aparecen en cada uno de los artículos.

Las referencias aparecen a pie de página y en el caso de citar varias veces la misma, ésta aparecerá indicada con el número correspondiente a la primera vez en la que ha sido citada. La numeración de las referencias, así como la de las figuras y tablas, se inicia en cada uno de los capítulos abordados.

SUMMARY OF THE THESIS

This Doctoral Thesis is framed in the area of Supramolecular Chemistry and more specifically in the field of self-assembly with the formation of different types of supramolecular aggregates and their different implications in a large number of applications. The main objective is the design and development of new polyfunctional pseudopeptide compounds derived from amino acids such as Valine and Phenylalanine, very interesting compounds due to their biological properties.

The thesis report has been structured in 4 chapters. The third of them consists of the results and discussion of the research carried out, which has been written following the format of scientific articles describing the research work developed. The results obtained have allowed the publication of three articles in the journal Organic Chemistry Frontiers, from the Royal Society of Chemistry, another in the Journal of Agricultural and Food Chemistry, from the ACS publications, and another in Polymers, from MPDI, which have a high impact index. In addition, the exposed work has allowed the elaboration of another manuscript already sent to a high impact journal, as well as three other drafts that will be sent shortly waiting to be published also in high impact specialised journals.

The first chapter includes a general introduction that is structured in three sections, the first one contains a brief introduction to supramolecular chemistry, the second one delves into pseudopeptic compounds and the third one develops ionic liquids, all of them with their respective applications. This chapter aims to provide the context to the reader and highlight the background, as to facilitate the reader the subsequent follow-up of the thesis through the following chapters.

Then, in the second chapter the general objectives of the thesis, as well as the specific ones for each section, have been exposed and detailed, so that the reader can focus their attention and achieve a better comprehension of the motivations for this work.

After this, the third chapter details the results obtained and their discussion throughout seven sections. The first section reports the strong preference for the formation of tripodal systems over the related monotopic and ditopic compounds for the reaction between tris(halomethyl)benzenes and imidazoles

derived from amino acids and containing an amide fragment, even when an equimolar mixture of the starting compounds is reacted. The reactions were monitored using 1H NMR spectroscopy and ESI mass spectrometry and kinetically characterized. Computational studies were also performed in order to rationalize the observed preference of the tri-substituted product. This investigation allowed the publication of an article in the journal Organic Chemistry Frontiers.

The second section collects the research carried out to obtain potential chemotherapeutic agents. A series of tripodal imidazolium salts derived from *L*-valine and *L*-phenylalanine containing different hydrophobic groups were tested against four cancer cell lines at physiologic and acidic pHe (6.2). The role of the lipophilicity of the compounds and their anion transport through POPC vesicles were also studied to achieve a better comprehension about their therapeutic action. This work resulted in the elaboration of a manuscript ready to be sent to a specialised journal.

The third section consists of the studies carried out to develop imidazolium amphiphiles derived from *L*-valine as potential surfactants. The substitution pattern of the aromatic central spacer was used to tune their properties. The self-assembly of these molecules in aqueous medium was studied, obtaining critical aggregation concentrations (CACs) of micromolar order. This study resulted in the preparation of a manuscript ready to be sent to the Advanced Healthcare Materials journal.

The fourth section focuses on the designing of new imidazole and imidazolium salts derived from *L*-valine and *L*-phenylalanine containing different hydrophobic groups and testing their antibacterial activity against two model bacterial strains, Gram-negative *E. coli* and Gram-positive *B. subtilis*. It is also studied IC_{50} cytotoxicity value for the control cell line HEK-293 and the aggregation of the compounds to determine whether the monomeric species were responsible for the observed antibacterial activity. This investigation allowed the preparation of a manuscript sent to the specialised Pharmaceuticals journal.

The fifth section deviates slightly from the previous ones which consists on the synthesis of silica-supported polymeric ionic liquid (PIL)-based stationary phases derived from a vinylic *L*-valine ionic liquid monomer and divinylbenzene

(DVB) as the crosslinking agent and study them as gas chromatographic stationary phases. It was checked the separation selectivity and resolution of different compounds. This work allowed the publication of an article in the specialised journal Polymers.

The sixth section reports a new family of open chain-pseudopeptidic compounds functionalized with a pendant carboxylic group as hydrogelators for controlled drug delivery using a Franz diffusion Cell and employing a biological membrane. The capacity of the gel formation in the face of different external stimuli was also studied. This study resulted in the preparation of a manuscript ready to be sent to the Advanced Healthcare Materials journal.

Finally, the last section focused on synthesizing low-molecular-weight organogelators containing alkylurea fragments attached to the amino end of different miminalistic pseudopeptidic structures. These compounds were studied to gelate relevant active substances as terpene natural oil. This study allowed the publication of an article in the Journal of Agricultural and Food Chemistry.

To conclude, in the fourth and last chapter, the most important and remarkable conclusions derived from the work described in each of the articles of the thesis have been gathered.

The abbreviations used are listed at the beginning of the thesis in alphabetical order. In the same way, a list has also been drawn up with the structures and the numbering of the compounds that appear in each of the articles.

References appear at the bottom of the page and in the case of citing it several times, it will appear indicated with the number corresponding to the first time it has been cited. The numbering of the references, as well as that of the figures and tables, begins in each of the chapters addressed.

TABLE OF CONTENTS

CHAPTER 3. General discussion of the results

CHAPTER 1. General Introduction

CHAPTER 1. General Introduction

1. Supramolecular Chemistry

Supramolecular Chemistry could be defined as "*the chemistry beyond the molecule*" or "*the chemistry of non-covalent bond*".[1] It involves the study of new molecular systems in which the components are linked by non-covalent interactions like electrostatic interactions, aromatic interactions, hydrogen bonding, van der Waals forces or hydrophobic effects.[2] These interactions allow the molecules to organize themselves in well-defined structures called *supramolecules*.[3]

In biology, these non-covalent interactions play critical roles and are responsible for many processes, such as, for example, the transcription of signals, the selective transport of ions and small molecules through membranes, enzymatic reactions, adhesive hydrogels, etc.[4] On the other hand, in abiotic chemistry, these interactions are very important because determine different physical properties of the molecules. Therefore, the interest in understanding this kind of interactions in the scientific world has made supramolecular chemistry one of the areas of greatest growth and interest in the chemistry field (Figure 1).[5]

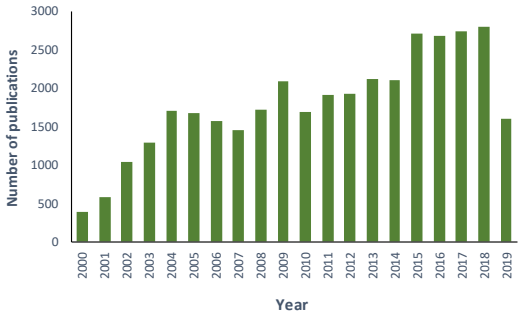

Figure 1 Evolution of number of publications from the last 20 years in the field of Supramolecular chemistry (Search "Supramolecular chemistry" as a keyword in Scopus database).

---

[1] (a) *Perspectives in Supramolecular Chemistry—From Molecular Recognition towards Molecular Information Processing and Self-Organization;* Lehn, J. M.; *Angew. Chem. Int. Ed.* **1990**, *29*, 1304-1319, (b) *Supramolecular Chemistry—Scope and Perspectives Molecules, Supermolecules, and Molecular Devices (Nobel Lecture);* Lehn, J. M.; *Angew. Chem. Int. Ed.* **1988**, *27*, 89-112.

[2] (a) *Towards Complex Matter: Supramolecular Chemistry and Self-organization;* Lehn, J. M.; *Eur. Rev.* **2009**, *17*, 263-280, (b) *Supramolecular chemistry: Functional structures on the mesoscale*; Nguyen, S. T.; Gin, D. L.; Hupp, J. T.; Zhang X.; *Proc. Natl. Acad. Sci.* **2001**, *98*, 11849-11850.

[3] Lehn, J.-M. *Supramolecular Chemistry;* John Wiley & Sons, Ltd, **1995**. https://doi.org/10.1002/3527607439.fmatter.

[4] *Plant-inspired adhesive and tough hydrogel based on Ag-Lignin nanoparticles-triggered dynamic redox catechol chemistry*; Gan, D.; Xing, W.; Jiang, L.; Fang, J.; Zhao, C.; Ren, F.; Fang, L.; Wang, K.; Lu, X.; *Nat. Commun.,* **2019**, *1*, 1-10.

[5] *Supramolecular chemistry: Where from? Where to?*; Lehn; J. M.; *Chem. Soc. Rev.* **2017**, *46*, 2378-2379.

This area of chemistry was born with Donald J. Cram, Jean-Marie Lehn and Charles J. Pedersen who received the Nobel Prize in 1987 for their development and use of molecules with structure-specific interactions of high selectivity called as molecular recognition or host-guest chemistry.[6] Hence, supramolecular chemistry involves a "host" and a "guest" molecule as can be seen in Figure 2, which illustrates the relationship between molecular and supramolecular chemistry in terms of structures.[7]

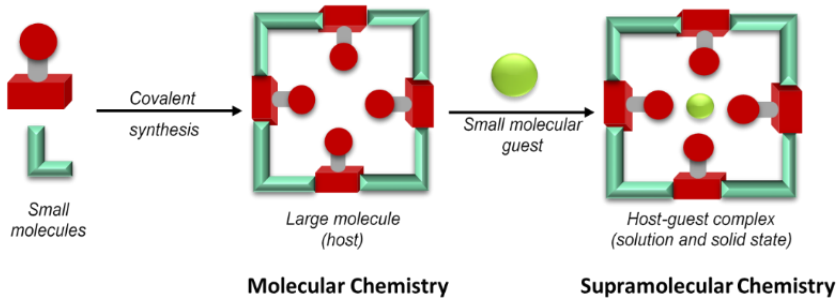

Figure 2 Comparison between molecular and supramolecular chemistry.[8]

In the beginning, the discovery of crown ethers by Pedersen (Figure 3) in the 1960s strongly activated the interest in studying weak and non-covalent molecular interactions, opening new avenues and providing one of the key elements for this area: molecular recognition.[9]

---

[6] (a) https://www.nobelprize.org/prizes/chemistry/1987/summary/, (b) *A new macrocyclic polyphenolic receptor for quaternary ammonium cations;* Dhaenens, M.; Lehn, J. M.; Fernandez, M. J.; Vigneron, J. P.; *New Journal of Chemistry* **1991**, *15*, 12, 873-877, (c) *Binding of acetylcholine and other quaternary ammonium cations by sulfonated calixarenes - crystal-structure of a [choline-tetrasulfonated calix[4]arene] complex;* Lehn, J. M.; Meric, R.; Vigneron, J. P.; Cesario, M.; Guilhem, J.; Pascard, C.; Asfari, Z.; Vicens, J.; *Supramol. Chem.* **1995**, *5*, 2, 97-103, DOI: 10.1080/10610279508029480, (d) *The utilization of persistent H-bonding motifs in the self-assembly of supramolecular architectures;* Krische, M. J.; Lehn, J. M.; *Mol. Self-assem.: Org. vs Inorg. App.* **2000**, *96*, 3-29, (e) *Metallo-Controlled Dynamic Molecular Tweezers: Design, Synthesis, and Self-Assembly by Metal-Ion Coordination;* Ulrich, S.; Petitjean, A.; Lehn, J. M.; *Eur. J. Inorg. Chem.* **2010**, *13*, 1913-1928.

[7] (a) *Tight and Selective Caging of Chloride Ions by a Pseudopeptidic Host*; Martí, I.; Bolte, M.; Burguete, M. I.; Vicent, C.; Alfonso, I.; Luis S. V.; *Chem. Eur. J.* **2014**, *20*, 7458 – 7464, (b) *Acyclic Pseudopeptidic Hosts as Molecular Receptors and Transporters for Anions;* Martí, I.; Burguete, M. I.; Gale, P. A.; Luis, S. V.; *Eur. J. Org. Chem.* **2015**, 5150–5158, (c) *Molecules with Large Cavities in Supramolecular Chemistry;* Seel, C.; Vögtle, F.; *Angew.* **1992**, *31*, 5, 528-549, (d) *Mechanisms of Molecular Recognition: Investigations of Organic Host–Guest Complexes;* Schneider, H-J.; *Angew.* **1991**, *30*, 11, 1417-1436, (e) *Self-Assembly in Synthetic Routes to Molecular Devices. Biological Principles and Chemical Perspectives: A Review;* Lindsey, J. S.; *New Journal of Chemistry* **1991**, *15*, 2-3, 153-180.

[8] *Lipoidal Soft Hybrid Biocarriers of Supramolecular Construction for Drug Delivery;* Kumar, D.; Sharma, D.; Singh, G.; Singh, M.; Rathore, M. S.; ISRN Pharm. **2012**, 1-14.

[9] *Cyclic polyethers and their complexes with metal salts;* Pedersen, C. J.; *J. Am. Chem. Soc.* **1967**, *89*, 26, 7017-7036.

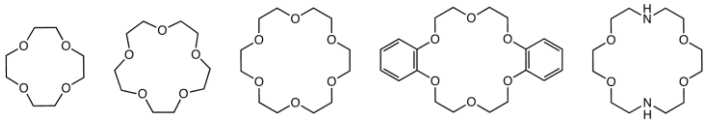

Figure 3 Five crown ethers developed by Pedersen.[8]

Afterwards, other researchers such as Donald J. Cram,[10] Jean-Marie Lehn and Fritz Vogtle became active in synthesizing shape- and size ion-selective receptors, and throughout the 1980s research in this area gathered a rapid pace with concepts such as mechanically interlocked molecular architectures emerging.[11] Nowadays, artificial receptors can selectively recognize different kind of molecules, mimicking as artificial biosensors.[12]

The three main themes that outline the development of supramolecular chemistry are described below.[13] Firstly, supramolecular chemistry focused on the design of molecular receptors.[14] These receptors were used for selective molecular recognition of different molecules. Molecular recognition is one of the main topics of supramolecular chemistry because this one is based on how to recognize molecules, how to influence molecules and how to express specific functions due to molecular interactions. It relies on the design and preorganization and implements information storage and processing.

Later, due to the greater understanding of non-covalent interactions, self-assembling processes were used for the synthesis of new molecular entities that were inaccessible using traditional methods involving breaking and formation of covalent bonds.[15] Self-assembly is the spontaneous and reversible

---

[10] *The design of molecular hosts, guests, and their complexes;* Cram, D. J.; *Angew. Chem.* **1988**, *100,* 1041–1052.

[11] Vögtle, F.; Alfter, F. *Supramolecular chemistry: an introduction*; Wiley, **1991**.

[12] (a) *Supramolecular Chemistry of Cyclodextrins in Enzyme Technology*; Villalonga, R.; Cao, R.; Fragoso, A.; *Chem. Rev.* **2007**, *107*, 7, 3088-3116, (b) *A nano-molar sensitive disposable biosensor for determination of dopamine;* Tu, Y. F.; Chen, H. Y.; *Biosens. Bioelectron.* **2002**, *17*, 19-24.

[13] *Toward Self-Organization and Complex Matter*; Lehn, J.-M.; *Science* **2002**, *295*, 5564, 2400-2403.

[14] (a) Wagner, B. D. *Host-Guest Chemistry: Supramolecular Inclusion in Solution*; De Gruyter, **2020**, (b) *Advances in Anion Supramolecular Chemistry: From Recognition to Chemical Applications;* Evans, N. H.; Beer, P. D.; *Angew.* **2014**, *53*, 44, 11716-11754, (c) *Polyazacyclophanes. 2,6,9,13-Tetraaza[14] paracyclophane as a cationic and anionic receptor;* Andrés, A.; Burguete, M. I.; García-España, E.; Luis, S. V.; Miravet, J. F.; Soriano, C.; *J. Chem. Soc. Perkin Trans. 2* **1993**, 749-755, (d) Bianchi, A.; Bowman-James, K.; Garcia-España, E. *The Supramolecular Chemistry of Anions;* Wiley-VCH, Weinheim, **1997**.

[15] (a) *Molecular Architecture: Coordination as the Motif in the Rational Design and Assembly of Discrete Supramolecular Species—Self-Assembly of Metallacyclic Polygons and Polyhedra;* Stang, P. J.; *Chem. Eur. J.* **1998**, *4*, 1, 19-27, (b) *Self-Assembling Capsules*; Conn, M. M.; Rebek, J.; *Chem. Rev.* **1997**, *97*, 5, 1647- 1668, (c) *Self-assembly of ten molecules into nanometre-sized organic host frameworks;* Fujita, M.; Oguro, D.; Miyazawa, M.; Oka, H.; Yamaguchi, K.; Ogura, K.; *Nature* **1995**, *378*, 6556, 469-471, (d) *Self-Assembling Supramolecular Complexes;* Lawrence, D. S.; Jiang, T.; Levett, M.; *Chem. Rev.* **1995**, *95*, 6, 2229-2260.

association of two or more components to produce an aggregate with a structure that is dependent only on the information contained within the chemical building blocks.[11]

The third feature defining supramolecular chemistry essence, resides in its dynamic nature introducing adaptation and evolution. It relies on self-organization through selection in addition to design and implements chemical diversity and "informed" dynamics. The advantage of non-covalent synthesis is that it is dynamic nature due to the lability of the interactions that connect its components.[16] In addition, the reversibility of these associations allows a continuous change in the constitution, either by internal reorganization or by the exchange, incorporation and extrusion of the components. Therefore, Supramolecular Chemistry can be easily associated with a dynamic combinatorial chemistry (DCC).[17] This type of chemistry considers that the different elements obtained from a dynamic system are able to respond to external stimuli by modifying its constitution.

In addition, supramolecular chemistry is an interdisciplinary field linking chemistry, physics and biology. Many significant advances have been achieved in the diverse fields of supramolecular chemistry over last years leading to a large number of applications in medicine, catalysis, chromatography, information storage and processing of nano-technological devices.[18] Due to the broadness of the field, it will continue to expand ensuring this area of the chemistry will remain one of the most active fields of research in the next future.

The present thesis is outlined within supramolecular chemistry and more specifically in the field of self-assembly and molecular recognition. The following chapters describe the synthesis and study of new pseudopeptidic and ionic liquid supramolecular systems as well as their possible applications.

---

[16] *Constitutional Dynamic Chemistry*; Barboiu, M., Ed.; Topics in Current Chemistry; Springer-Verlag: Berlin Heidelberg, **2012**. https://doi.org/10.1007/978-3-642-28344-4

[17] *From supramolecular chemistry towards constitutional dynamic chemistry and adaptive chemistry;* Lehn, J. M.; *Chem. Soc. Rev.* **2007**, *36*, 151-160.

[18] (a) *Effect of Bile Salts on Self-Assembly and Construction of Micro-/nanomaterials;* Jiao, J.; Xu, G.; Xin, X.*; Acta Phys.-Chim. Sin.* **2019**, *35*, 684-696, (b) *Symposium on Host-Guest Molecular Interactions: from Chemistry to Biology*; Chadwick, D.; Widdows, K.; Ciba Foundation. Host-Guest Molecular Interactions: From Chemistry to Biology.; Wiley: Chichester, England; New York, **1991**.

1.1 Supramolecular Interactions

In Supramolecular chemistry, non-covalent interactions are responsible of the formation of supramolecules by creating huge attractive and repulsive effects, in particular when larges surfaces and multiple interactions are involved.[19] Covalent bonds hold atoms together; nevertheless, weak chemical forces or noncovalent bonds are intramolecular or intermolecular attractions between atoms. None of these weak forces are strong enough to bind free atoms together.[20] Thus, these weak forces create interactions that are constantly forming and breaking at different stimulus (for instance, temperature or pH), unless by cumulative number they impart stability to the structures generated by their collective action.

Table 1 Main types of supramolecular interactions.[22]

Interaction	**Direction**	**Bond energy (kJ mol^{-1})**	**Examples**
Hydrogen Bonding	Directional	10-65	Carboxylic dimers
Ion-Ion	Non-directional	100-350	KI, Na_2SO_4
Ion-Dipole	Partially directional	50-200	Na^+ - Crown ether
Dipole-Dipole	Partially directional	5-50	CH_3OH – $CHCl_3$
Cation-π	Directional	5-80	Acetylcholine - Tryptophan[23]
Anion-π	Directional	2-40	Azadendtriz - $CuCl_2$[24]
π-π	Directional	0-50	Benzene - DNA
Van der Waals	Non-directional	<5	Hydrocarbons,[25] amino acids
Halogen bonds	Directional	~200	Iodine monochloride - trimethylamine[26]

[19] (a) Varshey, D. B.; Sander, J. R. G.; Friščić, T.; MacGillivray, L. R. *Supramolecular Interactions. In Supramolecular Chemistry*; American Cancer Society, **2012**, (b) Schmittel, M.; Kalsani, V. *Functional, Discrete, Nanoscale Supramolecular Assemblies*; Schlüter, A. D., Ed.; Topics in Current Chemistry; Springer: Berlin, Heidelberg, **2005**; pp 1–53. https://doi.org/10.1007/b98165

[20] Voet, D.; Voet, J. G. Biochemistry, 4th Edition | Wiley https://www.wiley.com/en-us/Biochemistry%2C+4th+Edition-p-9780470570951

[22] Steed, J. W.; Atwood, J. L. *Supramolecular Chemistry;* John Wiley & Sons: Chichester, **2000**. ISBN 0-471-98791-3.

[23] *The discovery of potential acetylcholinesterase inhibitors: A combination of pharmacophore modeling, virtual screening, and molecular docking studies;* Lu, S-H.; Wu, J. W.; Liu, H-L.; Zhao, J-H.; Liu, K-T.; Chuang, C-K.; Lin, H-Y.; Tsai, W-B.; Ho, Y.; *J. Biomed. Sci.* **2011**,*18*, 8.

[24] *An aromatic anion receptor: anion-pi interactions do exist;* De Hoog, P.; Gamez, P.; Mutikainen, I.; Turpeinen, U.; Reedijk, J.; *Angew.Chem. Int. Ed.* **2004**, *43*, 5815 –5817.

[25] Parsegian, V. A. *Van der Waals Forces: A Handbook for Biologists, Chemists, Engineers, and Physicists*; Cambridge University, **2006**. Press. ISBN 978-0-521-83906-8.

[26] (a) *An overview of halogen bonding*; Politzer, P.; Lane, P.; Concha, M. C.; Ma, Y.; Murray, J. S.*; J. Mol. Model* **2007**, *13,* 2, 305–311, doi:10.1007/s00894-006-0154-7, PMID 17013631, (b) *Halogen bonds and s-holes*; Clark, T.; *Faraday Discuss.* **2017**, *203*, 9–27.

These forces are very important not only in host-guest systems, but also in their surroundings.[27] Non-covalent interactions as mention above, include hydrogen bonding, electrostatic interactions, aromatic-interactions, van der Waals forces or hydrophobic effects, as detailed in Table 1.

1.1.1 Hydrogen bonding

Hydrogen bonding has been the most non-covalent interaction exploited historically, that involves highly directional forces due to the wealth of such non-covalent interactions in biological systems, its structural diversity and moderate to very high association constants. Hydrogen bonds form between an electronegative atom (such as oxygen or nitrogen) that serves as the hydrogen bond acceptor and a hydrogen atom covalently bonded to a second electronegative atom. Consequently, this kind of interaction can be considered as a special case of dipole-dipole interaction.[28]

In the design of artificial receptor molecules, the main driving force in the recognition events between some hosts and their guests is H-bonding interaction, as can be observed in the Figure 4 for the macrocyclic receptor and the chloride anion.[29]

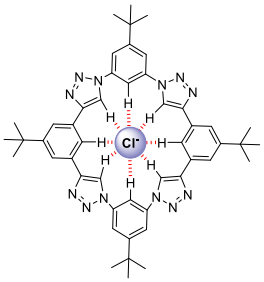

Figure 4 Hydrogen bond interactions between the hydrogens of the macrocyclic receptor and the chloride group.

1.1.2 Electrostatic interactions

Electrostatic interactions can be categorized in ion-ion (species possessing discrete charges), ion-dipole and dipole-dipole interactions (having a permanent or a temporary separation of positive and negative charge respectively). They are

[27] *Binding mechanisms in supramolecular complexes;* Schneider, H.-J.*; Angew. Chem. Int. Ed.* **2009**, *48, 22,* 3924-3977.
[28] Jeffrey, G. A. *An Introduction to Hydrogen Bonding;* Oxford University Press: Oxford, **1997**. ISBN 978-0195095494.
[29] *Pure C_H Hydrogen Bonding to Chloride Ions: A Preorganized and Rigid Macrocyclic Receptor;* Li, Y.; Flood, A. H.; *Angew. Chem. Int. Ed.* **2008**, *47,* 2649 –2652.

based on the Coulomb attraction between opposite charges, such as negative carboxylate groups and positive amonium groups (Figure 5).

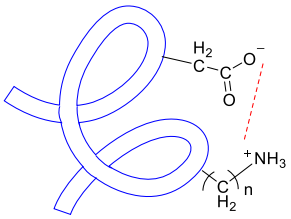

Figure 5 Ionic bonds in protein strand.

The strength of electrostatic interactions is highly dependent on the nature of the interacting species and the distance between them. Therefore, ion-ion is non-directional interaction while ion-dipole and dipole-dipole are partially directional interaction. The high strength of electrostatic interactions has made them an optimized tool for achieving strong binding.[30]

1.1.3 Aromatic-system interactions

π-system interactions are non-covalent attractive directional interactions between the electron-rich or electron-poor aromatic system and a metal (cationic or neutral), an anion, another molecule or even another aromatic system (Figure 6).[31] They are involved in many biological phenomena such as the vertical base-base interactions, which stabilize the double helical structure of DNA,[32] the intercalation of drugs into DNA,[33] or the complexation in many host-guest systems. [34]

---

[30] (a) *The effects of amino acids on the gel properties of potassium iota carrageenan*; Dong, Y.; Wen, C.; Li, T.; Wu, C.; Qi, H.; Liu, M.; Wang, Z.; Zhu, B.; Song, S.; *Food Hydrocolloids* **2019**, *95*, 378–384, (b) *Effects of the Molecular Design on the Supramolecular Organization of Luminescent Pt(II) Complexes;* Aliprandi, A.; Capaldo, L.; Bobica, C.; Silvestrini, S.; De Cola, L.; *Isr. J. Chem.* **2019**, *59,* 1–7, (c) *Macroscopic Supramolecular Assembly through Electrostatic Interactions Based on a Flexible Spacing Coating;* Zhang, Q.; Liu, C.; Ju, G.; Cheng, M.; Shi, F.; *Macromol. Rapid Comm.* **2018**, *39*, 20.

[31] (a) *Minimalistic amino amides as models to study N–H···π interactions and their implication in the side chain folding of pseudopeptidic molècules;* Faggi, E.; Luis, S. V.; Alfonso, I.; *RSC Adv.*, **2013**, *3*, 11556–11565, (b) *Molecular Rotors as Simple Models to Study Amide NH–Aromatic Interactions and Their Role in the Folding of Peptide-like Structures;* Alfonso, I.; Burguete, M. I.; Galindo, F.; Luis, S. V.; Vigara, L.; *J. Org. Chem.* **2007**, *72*, 7947-7956.

[32] Saenger, W. *Principles of Nucleic Acid Structure;* Springer-Verlag: New York, **1984**. ISBN 978-0123695079

[33] *Polyfunctional DNA intercalating agents;* Wakelin, L. P. G.; *Med. Res. Rev.* **1986**, *6*, 3, 275-340.

[34] *Molecular recognition with convergent functional groups. VII. Energetics of adenine binding with model receptors*; Williams, K.; Askew, B.; Ballester, P.; Buhr, C; Jeong, K. S.; Jones, S.; Rebek, J. Jr.; *J. Am. Chem. Soc.* **1989**, *111*, 3, 1090-1094.

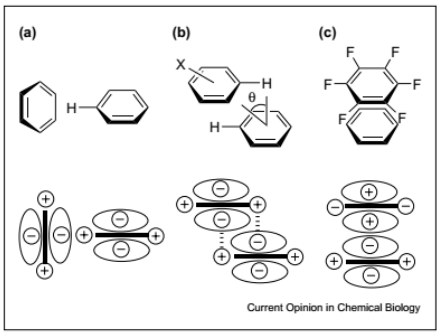

Figure 6 Geometries of aromatic interactions. (a) edge-face, (b) offset stacked and (c) face-to-face stacked.[35]

1.1.4 Van der Waals forces

Van der Waals forces are the result of induced electrical interactions between closely approaching atoms or molecules that occur between the positively charged nuclei and the electrons of nearby atoms. These forces operate only over a very limited interactions distance (~0.5 nm) and they are nondirectional and weaker than electrostatic interactions providing additional enthalpy stabilization to the coordination of a guest into a host molecule (Figure 7).[36]

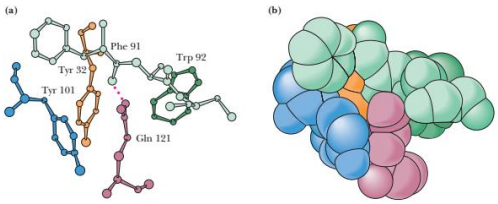

Figure 7 Van der Waals packing is enhanced in molecules that are structurally complementary. Gln121, a surface protuberance on lysozyme, is recognized by the antigen-binding site of an antibody against lysozyme. Gln121 (pink) fits nicely in a pocket formed by Tyr32 (orange), Phe91 (light green), Trp92 (dark green), and Tyr101 (blue) components of the antibody. (a) Ball-and-stick model. (b) Space-filling representation.[37]

---

[35] (a) *Aromatic interactions in model Systems*; Waters, M. L.; *Curr Opin Chem Biol.* **2002**, *6*, 6, 736-741, (b) Gräbner, D.; Hoffmann, H. *Rheology of Cosmetic Formulations.* 27. Cosmetic Science and Technology, Theoretical Principles and Applications, Elsevier, **2017**, 471-488.

[36] (a) *Highly stable oil-in-water emulsions with a gemini amphiphilic pseudopeptide;* Lotfallah, A. H.; Burguete, M. I.; Alfonso, I.; Luis, S. V.; *RSC Adv.* **2015**, *5*, 36890-36893, (b) *Multiple weak forces in ion-binding molecules;* Shanzer, A.; Libman, J.; Lifson, S.; *Pure and Appl. Chem.* **1992**, *64*, 10, 1421-1435. DOI: 10.1351/pac199264101421, (c) Schneider, H. J.; Schiestel, T.; Zimmermann, P. *Host-Guest Supramolecular Chemistry.* 34. The Incremental Approach to Noncovalent Interactions: Coulomb and van Der Waals Effects in Organic Ion Pairs. J. Am. Chem. Soc. **1992**, 114 (20), 7698–7703.

[37] *Three-dimensional structure of an antigenantibody complex at 2.8 Å resolution;* Amit, A. G.; Mariuzza, R. A.; Phillips, S. E.; Poljak, R. J.; *Science* **1986**, *15,* 233, 747–753, figure 5.

1.1.5 Hydrophobic effect

Hydrophobic interactions are important specific driving forces that describe the relations between water and nonpolar molecules. These interactions can be more varied and numerous if nonpolar molecules come together to form a distinct organic phase. The entropy of water increases in this phase separation because fewer water molecules are arranged in orderly arrays around individual apolar molecules.[38] These preferential interactions between water molecules "exclude" hydrophobic substances from aqueous solution and drive the tendency of apolar molecules to cluster together.

The hydrophobic effect is seen as the driving force for a variety of phenomena, such as protein folding, poor solubility of non-polar solvent in aqueous media and formation of aggregates.[39] American chemist Walter Kauzmann discovered that nonpolar substances like fat molecules tend to form micelles because this allows the fat molecules to have minimal contact with water.[40]

1.2 Supramolecular materials

1.2.1 Self-assembly and self-association processes

In Nature there are structures made up of small molecules that interact with each other through non-covalent links.[41] This mode of union is the responsible for assembling essential complex structures in living organisms and it is present, for example, in the formation of the DNA double helix from two complementary strands of oligonucleostrands. Hydrogen bonds between purine and pyrimidine bases and other intermolecular forces are the responsible which allow that the two chains are held together to maintain the double helical structure.[42] In proteins as well, the linear polypeptide chain sequences fold into significant secondary structures such as α-helices and β-sheets. They are held

[38] *Enthalpy–Entropy Interplay in π-Stacking Interaction of Benzene Dimer in Water;* Lee, H.; Dehez, F.; Chipot, C.; Lim, H-K.; Kim H.; *J. Chem. Theory Comput.* **2019**, *15*, 3, 1538−1545. DOI: 10.1021/acs.jctc.8b00880.
[39] *Control of the Ketone to gem-Diol Equilibrium by Host−Guest Interactions;* Thangavel, A.; Rawashdeh, A. M. M.; Sotiriou-Leventis, C.; Leventis, N.; *Org. Lett.,* **2008**, *10*, 6, 1131-1134.
[40] Kauzmann, W.; McElroy, W. D.; Glass, B. *In The Mechanism of Enzyme Action;* The John Hopkins Press: Baltimore, **1954**.
[41] (a) Li Dequan, A. *Molecular Self-Assembly: Advances and Applications;* 1st Edition, Jenny Stanford Publishing, **2012**, (b) Kimizuka, N. *Self-Assembly of Supramolecular Nanofibers. In Self-Assembled Nanomaterials I: Nanofibers*; Shimizu, T., Ed.; Advances in Polymer Science; Springer: Berlin, Heidelberg, **2008**; pp 1–26. https://doi.org/10.1007/12_2008_170.
[42] *Molecular structure of nucleic acids: a structure for deoxyribose nucleic acid;* Watson, J. D.; Crick, F. H. C.; *Am. J. Psychiatry* **2003**, *160*, 623-624.

together by hydrophobic effects in aqueous solution and amide hydrogen bonding interactions (NH---O=C). Moreover, these components can further self-assembly to generate well-defined nanostructures in biological systems.[43]

Therefore, self-assembly can be considered as a key concept in supramolecular chemistry and it is defined as the spontaneous and reversible non-covalent association of molecules or ions to form larger, more complex supramolecular entities according to the intrinsic information contained in the molecules themselves.[44] Self-assembly of the constituent blocks of a supramolecular system can occur spontaneously or induced by an external stimulus. In both cases this self-assembly can lead to the formation of organized nanostructure. Similarly, the disassembly of this non-covalent suprastructure may be induced by external stimulus, thus achieving total control of the supramolecular process.[45] Some of these simple external stimuli may be pH,[46] temperature,[47] light,[48] electrical potential,[49] ions,[50] etc.

Nature has many examples of self-assembly, so, over the past few decades, some researchers have based their studies on the observation of nature and on how it was able to use reversible and non-covalent interactions between components, having sizes from molecular to macroscopic, to generate systems of great interest.[51] Although covalent bonds provide the strongest connection between atoms of a molecule when the non-covalent bonds act cooperative can provide very powerful unions. So, it is not surprising the extensive development of Supramolecular Chemistry which was born as a discipline of studying new

---

[43] Voet, D.; Voet, J. G. *Biochemistry*; 2nd Edition, John Wiley & Sons, Inc.: New York, **1995**. https://doi.org/10.1016/0307-4412(95)90658-4.

[44] *Toward complex matter: Supramolecular chemistry and self-organization;* Lehn, J. M.; *Proc. Natl. Acad. Sci.* **2002**, *99*, 4763-4768.

[45] *Programmed disassembly of supramolecular nanoparticles stabilized by heteroternary CB[8] host-guest interactions;* Stoffelen, C.; Voskuhl, J.; Jonkheijm, P.; Huskens, J.; *J. Photochem. Photobiol. A: Chem.* **2016,** *331,* 146–152.

[46] *Self-Assembly Behavior and pH-Stimuli-Responsive Property of POSS-Based Amphiphilic Block Copolymers in Solution;* Xu, Y.; He, K.; Wang, H.; Li, M.; Shen, T.; Liu, X.; Yuan, C.; Dai, L.; *Micromachines* **2018**, *9*, 258, 1-15.

[47] *Unique Temperature-Dependent Supramolecular Self-Assembly: From Hierarchical 1D Nanostructures to Super Hydrogel;* Qiao, Y.; Lin, Y.; Yang, Z.; Chen, H.; Zhang, S.; Yan, Y.; Huang, J.; *Phys. Chem. B* **2010**, *114*, 36, 11725-11730.

[48] *Light-Switchable Supramolecular Self-Assembly of Soft Colloids;* Wang, P.; Yang, Q.; Ye, Z.; Zhao, C.; Yang, J.; *Macromol. Chem. Phys.* **2017**, *218*, 1700280.

[49] *Beyond molecules: Self-assembly of mesoscopic and macroscopic components;* Whitesides, G. M.; Boncheva, M.; *Proc Natl Acad Sci U S A.* **2002**, *99*, 8, 4769–4774.

[50] *An octahedral aluminium(iii) complex as a three-fold node for supramolecular heterometallic self assemblies: solution and solid state chemistry;* Simond, D.; Clifford, S. E.; Vieira, A. F.; Besnard, C.; Williams, A. F.; *RSC Adv.* **2014**, *4*, 16686–16693.

[51] (a) *Low Molecular Mass Gelators of Organic Liquids and the Properties of Their Gels;* Terech, P.; Weiss, R. G.; *Chem. Rev.* **1997**, *97*, 8, 3133-3160, (b) *Water Gelation by Small Organic Molecules,* Estroff, L. A.; Hamilton, A. D.; *Chem. Rev.* **2004**, *104*, 3, 1201-1217.

molecular systems in which its components are held through non-covalent interactions. Bioengineers are interested in copying these systems to create useful new materials or devices.

Thus, for example, Rebek et al., have developed and synthetized "molecular tennis balls" (and related systems) through the self-assembly of the molecules involving hydrogen bonding interactions.[52] A diphenyl glycoluril subunit is self-complementary and self-associates in solution by hydrogen bonds to form a dimer having an internal cavity, which is remarkably stable, and it can encapsulate small molecules within the self-assembled cavities (Figure 8).[53]

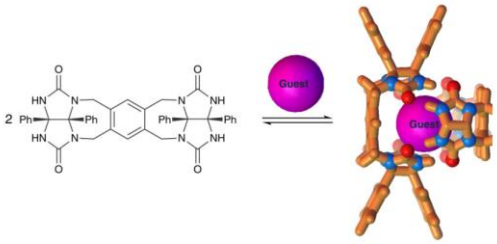

Figure 8 Presence of guest drives dimerization of diphenyl glycoluril subunit to form the tennis ball.[54]

There is a wide variety of elements that can be used as a constituent blocks of a final supramolecular system. In this regard, ionic liquids (ILs) have attracted great attention as a constituent block. [55] Moreover, ionic liquids can also act as new media for molecular self-assembly, capable of producing novel soft materials with unique features never observed for conventional soft materials containing organic and aqueous solvents.[56]

---

[52] *Molecules within molecules: Recognition through self-assembly;* Hof, F.; Rebek, J.; *Proc. Natl. Acad. Sci.* **2002**, *99*, 4775-4777.

[53] *The ins and outs of molecular encapsulation;* Palmer, L. C.; Rebek, J. J.; *Org. Biomol. Chem.* **2004**, *2*, 3051-3059.

[54] *Synthesis and Self-Assembly of the "Tennis Ball" Dimer W and Subsequent Encapsulation of Methane;* Hof, F.; Palmer, L. C.; Rebek J. Jr.; *J. Chem. Ed.* **2001**, *78*, 11, 1519-1521.

[55] (a) *Supramolecular Self-Assembly of Nanoconfined Ionic Liquids for Fast Anisotropic Ion Transport;* Cherian, T; Nunes, D. R.; Dane, T. G.; Jacquemin, J.; Vainio, U.; Myllymaki, T. T. T.; Timonen, J. V. I.; Houbenov, N.; Marechal, M.; Rannou, P.; Ikkala, O.; *Adv. Funct. Mater.* **2019**, 1905054, (b) *Self-assembly of ionic-liquid-type imidazolium gemini surfactant with polyoxometalates into supramolecular architectures for photocatalytic degradation of dye;* Sun, P.; Zhang, S.; Pang, J.; Tan, Y.; Sun, D.; Xia, C.; Cheng, X.; Xin, X.; *J. Mol. Liq.* **2018**, *272*, 180–187, (c) *Spontaneous Self-Assembly of Glycolipid Bilayer Membranes in Sugar-philic Ionic Liquids and Formation of Ionogels;* Kimizuka, N.; Nakashima, T.; *Langmuir* **2001,** *17,* 6759-6761.

[56] (a) *Block copolymer self-assembly in ionic liquids;* Tamate, R.; Hashimoto, K.; Ueki, T.; Watanabe, M.; *Phys.Chem.Chem.Phys.* **2018**, *20,* 25123-25139, (b) *Ionicity in ionic liquids: correlation with ionic structure and physicochemical properties*; Ueno, K.; Tokuda, H.; Watanabe, M.; *Phys. Chem. Chem. Phys.* **2010**, *12,* 1649–1658.

Although it is possible to find a huge range of elements that can be used as a constituent blocks of a final supramolecular system, those based on peptide compounds have a special appeal. The biocompatibility of these systems, their chemical diversity, their stability (especially for derivatives of unnatural amino acids) and the possibility of being synthesized at large scale are some of the advantages that are making the self-assembly of peptides structures considered a useful tool for the design of new materials.[57] Self-assembly of peptides, proteins, and pseudopeptides is of great biological relevance. They are involved in abnormal processes being associated with important diseases.[58] For instance, one of the most important natural macromolecules leading to self-association is the amyloid-b peptide Ab42, which is involved in the pathogenesis of the Alzheimer's disease.[59]

However, amyloid proteins can also form very useful materials, such as spider silk, or biofilms around living cells.[60] Researchers have now come up with methods to manipulate natural proteins so that they self-assemble into amyloid fibrils. But the ultimate mechanism for fibril formation in living systems remains unknown. In this biomedical context it has been described the role of some non-steroidal anti-inflammatory drugs (NSAIDs), like ibuprofen and flurbiprofen, on the progression of the disease.[61] It is believed that those low molecular weight molecules interact with the fibrillar peptidic aggregates or its precursors in such a way that aggregation is disrupted.[62] However, there is much debate around this topic and related issues.

In many vital processes it has been observed that there is a close and intimate relationship with molecular chirality, since most biological functions are inherently chiral. [63] The therm "chiral molecule" is refered to a molecule which

---

[57] *Peptide Self-Assembled Nanostructures for Drug Delivery Applications;* Fan, T.; Yu, X.; Shen, B.; Sun L.; *J. Nanomater.* **2017**, *2017*, 1-16.
[58] *A Century-Old Debate on Protein Aggregation and Neurodegeneration Enters the Clinic;* Lansbury, P. T.; Lashuel, H. A.; *Nature* **2006**, *443*, 774–779.
[59] *Nanoparticle formulations in the diagnosis and therapy of Alzheimer's disease*; Gupta, J.; Fatima, M. T.; Islamb, Z.; Khan, R. H.; Uversky, V. N.; Salahuddin, P.; *Int. J. Biol. Macromol.* **2019**, *130*, 515–526.
[60] *Amyloid self-assembling peptides: Potential applications in nanovaccine engineering and biosensing;* Al-Halifa, S.; Babych, M.; Zottig, X.; Archambault, D.; Bourgault, S.; *Pept. Sci.* **2019**, 111:e24095. https://doi.org/10.1002/pep2.24095
[61] *Nonsteroidal Anti-Inflammatory Drugs Can Lower Amyloidogenic Aß$_{42}$ by Inhibiting Rho*; Zhou, Y.; Zhou, Y.; Su, Y.; Li, B.; Liu, F.; Ryder, J. W.; Wu, X.; Gonzalez-DeWhitt, P. A.; Gelfanova, V.; Hale, J. E.; May, P. C.; Paul, S. M.; Ni, B.; *Science* **2003**, *302*, 1215-1217.
[62] *Non-steroidal anti-inflammatory drugs (NSAIDs) in Alzheimer's disease: old and new mechanisms of action;* Gasparini, L.; Ongini, E.; Wenk, G.; *J. Neurochem* **2004**, *91,* 521-536.
[63] *From parity to chirality: Chemical implications revisited;* Avalos, M.; Babiano, R.; Cintas, P.; Jiménez, J. L.; Palacios, J. C.; *Tetrahedron Asymmetry* **2000,** *11, 14,* 2845-2874.

is non-superposable on its mirror image. It contains an asymmetric carbon center that induce chirality in organic and inorganic molecules. This discovery of chirality, more than a century ago, led chemists to become aware of the need to design and develop methods that allow obtaining enantiomerically enriched or pure substances.

Thus, simpler models of the complex aggregates of natural molecules are needed in order to approach to a full understanding of the natural processes. In this regard, it is widely studied the self-assembling of the proper design of low molecular weight peptides and pseudopeptides under physiological conditions to form well-defined nanostructures like hydrogels or organogels with important applications as well as in tissue engineering.[64]

1.2.2 Gels

The processes of self-association and self-assembly of organic molecules, based on non-covalent intermolecular interactions, can lead to the formation of a large number of nano-, micro- and/or macro-structured materials of interest in different fields.[65] Among these non-covalently linked materials, molecular gels represent one of the fields that has aroused the greatest interest. [66]

The formation of molecular gels is based on the creation of a fibrillary structure, through a process of self-association and self-assembly of a functional molecule, being the molecules of the solvent trapped in the small cavities formed in the complex fibrillation network created (Figure 9).[67] Despite its solid appearance, inside the gel the liquid component is mobile and is only retained by capillary forces between the fibres of the gelator. The solid network can be produced by

---

[64] *Selective Differentiation of Neural Progenitor Cells by High-Epitope Density Nanofibers;* Silva, G. A.; Czeisler, C.; Niece, K. L.; Beniash, E.; Harrington, D. A.; Kessler, J. A.; Stupp, S. I.; *Science,* **2004**, *303*, 1352–1355.

[65] (a) *Design and applications of dipyrrin-based fluorescent dyes and related organic luminophores: From individual compounds to supramolecular selfassembled Systems;* Solomonova, A. V.; Marfina, Y. S.; Rumyantseva, E. V.; *Dyes and Pigments* **2019**, 162, 517–542, (b) *DNA-Decorated, Helically Twisted Nanoribbons: AScaffold for the Fabrication of One-Dimensional, Chiral, Plasmonic Nanostructures;* Golla, M.; Albert, S. K.; Atchimnaidu, S.; Perumal, D.; Krishnan, N.; Varghese, R.; *Angew.Chem. Int. Ed.* **2019**, *58*, 3865 –3869, (c) *Supramolecular Photothermal Nanomaterials as an Emerging Paradigm toward Precision Cancer Therapy;* Zhao, L.; Liu, Y.; Chang, R.; Xing, R.; Yan, X.; *Adv. Funct. Mater.* **2019**, *29*, 1806877, (d) *Supramolecular Chemistry in Microflow Fields: Toward a New Material World of Precise Kinetic Control;* Numata, M.; *Chem. - Asian J.* **2015**, *10*, 12, 2574-2588.

[66] *Molecular recognition of melamine and cyanuric acid by C2-symmetric phenylalanine based supramolecular hydrogels;* Mehwish, N.; Kousar, A.; Yinme Dang-i, A.; Huang, J.; Dou, X.; Feng, C.; *Eur. Polym. J.* **2019,** *118,* 170–175.

[67] *Supramolecular gels formed from multi-component low molecular weight species;* Buerkle, L. E.; Rowan, S. J.; *Chem. Soc. Rev.* **2012**, *41,* 6089–6102.

a covalent polymer or by the supramolecular interaction of a set of small molecules.

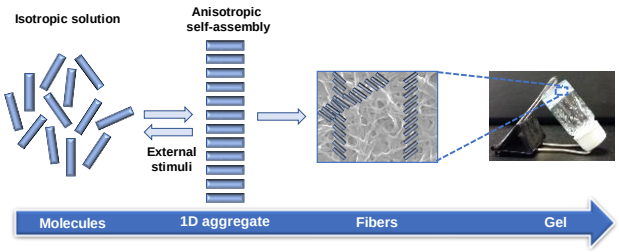

Figure 9 Gel formation by the supramolecular interaction of a set of small functional molecules through a process of self-association and self-assembly.

At the macroscale, the main property to define gels is that they do not flow. Therefore, the simplest test to determine the formation of a gel is to invert the vial containing the gel and observe if it is maintained without flowing towards the cap, this method was first referenced by Suzuki et al in 2003.[68] On the other hand, at the microscale, the solid-type component generally comprises fibrillary networks of high aspect ratio and generally follows certain steps:[69]

1. Two adjacent molecules form a dimer.
2. Two or more dimers interact to give oligomers
3. These oligomers evolve to supramolecular polymeric fibrils
4. The fibrils roll up into larger fibers
5. The fibers interact forming an interconnected network
6. The fibrillary framework immobilizes the solvent due to surface tension effects

In the case of chiral gels, these fibrillary networks can adopt a helical morphology.

Some gels also exhibit thixotropy, that is, they flow when shaken, but they re-form when the movement stops. The mechanical forces involved in the agitation are sufficient to temporarily break the bonds that hold the gel fibres.

However, at the macroscale, the inversion of the vial is not reliable enough. Hence, there is a technique which allow researchers to measure the features of the gels in a more faithful way. This technique is known as rheology which is

[68] *In situ organogelation at room temperature: direct synthesis of gelators in organic solvents;* Suzuki, M.; Nakajima, Y.; Yumoto, M.; Kimura, M.; Shirai, H.; Hanabusa, K.; *Org. Biomol. Chem.* **2004**, *2,* 8, 1155-1159.
[69] *Peptide hydrogels; Dasgupta,* A.; Mondal, J. H.; Das, D.; *RSC Ad.* **2013**, *3,* 9117–9149.

useful in a vast fields, as well as in mathematics, physics, biology, technology, engineering or chemistry. Rheology gives us information about the relation between force and deformation of the gels. It establishes relationships between the strains caused by mechanical stresses acting on a material and the changes of the strains over time. Moreover, rheology provides us information about the flow of matter involving the term of viscosity. Thus, the viscosity of a fluid, **η**, can be described as the resistance to flow or movement.

The flow is directly related to the deformation. This refers to adjacent points in the fluid that move relatively with each other. The deformation is commonly represented by the symbol **γ**. There are two basic types of flow known as shear flow and extensional flow. In Figure 10 it can be seen that the shear flow is the continuous movement of fluid particles one above the other; while in the extensional flow the particles move away or towards each other. All flows are resisted by viscosity. For a determined speed, when viscosity increases, the resulting force increases, while for a given force, when the viscosity increases, the speed decreases.

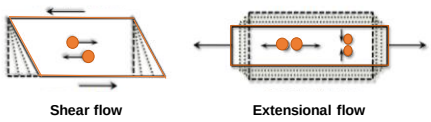

Figure 10 Particles movement in shear flow and extensional flow respectively.

In this regard, it can be defined two relevant terms. Shear rate is the rate at which a fluid is sheared or "worked" during flow and shear stress, **τ**, is the force per area, being the viscosity the relationship between the shear stress and the shear rate.

In terms of viscosity, it is crucial to highlight the viscoelasticity, which intrinsically considers the simultaneous existence of viscous and elastic properties in a material. All materials can behave as liquids or solids, depending on the time scale of the rheological experiment. The time scale of the deformation determines the ratio of viscosity (liquids) to elasticity (solids) in the properties of a given material. Thus, **G'** (storage or elastic modulus) measures the elastic component and **G''** (loss or viscous modulus) the plastic component, being **G*** the complex shear module. The units of these modules are pascal (Pa) in the International System and are defined by the Equation 1 and Equation 2:

$$G' = G^* \cdot \cos \delta$$

Equation 1

$$G'' = G^* \cdot \operatorname{sen} \delta$$

Equation 2

Oscillatory analysis is often the most used type of viscoelastic test. This test consists in subjecting a fluid to a sinusoidal stress (**τ**) or deformation (**γ**) of a given frequency (**ω**). During this periodic movement, the stress and the strain rate evolve sinusoidally with the same pulse as a function of time but present a certain offset (**φ** or **δ**) with respect to each other. Both lags are related by the Equation 3:

$$\delta = \left(\frac{\pi}{2}\right) - \varphi$$

Equation 3

The offset (**δ**) can be related to the elastic (**G'**) and viscous (**G''**) modulus by the Equation 4:

$$\tan\delta = \frac{G''}{G'}$$

Equation 4

If the value of δ is between 0° and 45° the fluid has a more elastic than viscous behavior and vice versa.

The sinusoidal deformation that is imposed on the fluid and that varies over time with frequency, can be represented by the Equation 5:

$$\gamma(t) = \gamma 0 \cdot e^{i\omega t}$$

Equation 5

The stress that accompanies this deformation generally presents an offset (**δ**) and is given by the Equation 6:

$$\tau_{(t)} = \tau_0 . e^{i(\omega t + \delta)}$$

Equation 6

All these rheological properties vary with respect to the composition of the gel considered and the temperature.[70]

[70] (a) *Rheological properties of peptide-based hydrogels for biomedical and other Applications;* Yan, C.; Pochan, D. J.; *Chem. Soc. Rev.* **2010**, *39,* 3528–3540, (b) *Molecular Gels: Materials with Self-*

A test commonly used in oscillatory rheology to characterize gelled structures is the dependence of G´ and G´´ with the shear frequency (**ω**) applied. Considering a regular gel, the spectrum obtained consists of two almost horizontal lines. G´ is normally one or two orders of magnitude greater than G´´, and both can show a slight increase at higher frequencies (Figure 11). Thus, a gel is a viscoelastic material for which G´ is larger than G´´ and therefore the storage and loss moduli are almost independent of frequency, and break at relatively low strain.[71]

Hence, the rheological properties of a viscoelastic material tend to be independent of applied stress, up to a critical level. The critical stress above which a material undergoes crucial structural alterations and starts to flow is known as yield stress. The material would behave as elastic (G'>G") below that point and its complex moduli are independent of the applied stress.

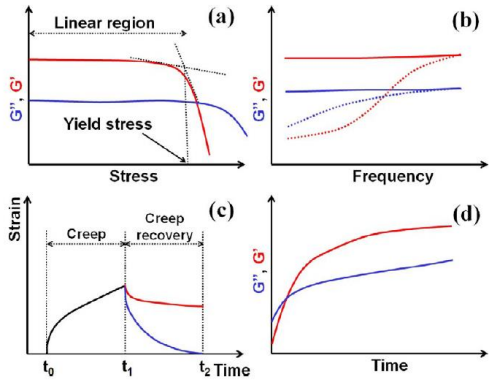

Figure 11 Illustrative rheological experiments on soft viscoelastic material performed at a constant temperature: (a) Determination of yield stress and linear region at a constant frequency; (b) Frequency sweep at constant stress in the linear region; solid lines corresponds to the materials with pronounced elastic behaviour and the dotted lines correspond to the materials with pronounced viscous behaviour; (c) Creep test: stress is suddenly raised to a given value at t0, which kept constant until t1; in the creep recovery, stress is removed completely at t_1 and t_2. Resulting strain is measured as a function of time, where the red lines signifies a viscoelestic materials and blue line corresponds to a typical elastic material; (d) Time evolution of moduli of a mechano-responsive viscoelastic material after the release of shear applied over the linear region.[70]

The essential properties of gelating compounds and formed gels are based on four fundamental parameters: the chemical structure of the gelator, the range

Assembled Fibrillar Networks; Weiss, R. G., Terech, P., Eds.; Springer Netherlands, **2006**. https://doi.org/10.1007/1-4020-3689-2

[71] *Low Molecular Weight Supramolecular Gels Under Shear: Rheology as the Tool for Elucidating Structure–Function Correlation;* Dawn, A.; Kumari, H.; *Chem. Eur. J.* **2018**, *24*, 762 –776.

of solvents for which the gelator is able to produce gelation, the thermal stability of the formed gels and the minimum concentration to produce the phenomenon (CGC).[72]

Thus, the gelation capacity depends on the structure of the chemical compounds that can be used as gelators. The chemical nature of these compounds is very wide, but taking into account their fundamental chemical features, gelating compounds are usually classified into two large groups: gelators of high molecular weight – natural or synthetic macromolecules- and low-molecular-weight organic gelators [LMWGs].[73] The high capacity of chemists for the design, synthesis and characterization of structure-activity relationships for molecules of small molecular weight makes LMWGs greater interested between the other gelators.[74]

On the other hand, depending on the solvents in which this phenomenon is produced, the resulting gels can be classified as aerogels,[75] organogeles[76] or

---

[72] (a) *Rheological and structural properties of ovomucin from chicken eggs with different interior quality;* Shan, Y.; Tang, D.; Wang, R.; Tu, A.; Yi, Y.; Wang, X.; Liu, B.; Zhou, Y.; Huang, Q.; Lü, X.; *Food Hydrocolloids* **2020,** *100,* 105393, (b) *Design of ß-lactoglobulin micro- and nanostructures by controlling gelation through physical variables;* Simões, L. S.; Araújo, J. F.; Vicente, A. A.; Ramos, O. L.; *Food Hydrocolloids* **2020**, *100,* 105357, (c) *Local viscosity and solvent relaxation experienced by rod-like fluorophores in AOT/4-chlorophenol/m-xylene organogels;* Dandapat, M.; Mandal, D.; *Spectrochim. Acta A Mol. Biomol. Spectrosc.* **2017**, *170,* 150–156, (d) *Gelation property and water holding capacity of heat treated collagen at different temperature and pH vàlues;* Correa de Moraes, M.; Cunha, R. L.; *Food Res. Int.* **2013**, *50,* 213–223, *(e) Organogels, hydrogels and bigels as transdermal delivery systems for diltiazem hydrochloride;* Ibrahim, M. M.; Hafez, S. A.; Mahdy, M. M.; *Asian J. Pharm. Sci.* **2013**, *8,* 48–57.

[73] *Hydrogelation Induced by Fmoc-Protected Peptidomimetics;* Zanna, N.; Merlettini, A.; Tatulli, G.; Milli, L.; Focarete, M. L.; Tomasini, C.; *Langmuir* **2015**, *31*, 12240−12250.

[74] (a) *Low Molecular Weight Gelators Based on Functionalized l-Dopa Promote Organogels Formation*; Giuri, D.; Zanna, N.; Tomasini, C.; *Gels* **2019**, *5,* 27, 1-11, (b) *Characterization and biocompatibility of organogels based on L-alanine for parenteral drug delivery implants;* Motulsky, A.; Lafleur, M.; Couffin Hoarau, A. C.; Hoarau, D.; Boury, F.; Benoit, J. P.; Leroux, J. C.; *Biomaterials* **2005**, *26,* 6242–6253, (c) *In situ-forming pharmaceutical organogels based on the self-assembly of L-alanine derivatives;* Couffin Hoarau, A. C.; Motulsky, A.; Delmas, P.; Leroux, J. C.; *Pharm. Res.* **2004**, *21,* 454–457.

[75] (a) *3D Nitrogen-Doped Graphene Aerogel-Supported Fe_3O_4 Nanoparticles as Efficient Electrocatalysts for the Oxygen Reduction Reaction;* Wu, Z-S; Yang, S.; Sun, Y.; Parvez, K.; Feng, X.; Müllen, K.; *J. Am. Chem. Soc.* **2012**, *134,* 9082−9085, (b) *Mechanical structure-property relationship of aerogels;* Ma, S. H.; Roberts, A. P.; Prévost, J-H.; Jullien, R.; Scherer, G. W.; *J. Non-Cryst. Solids* **2000**, *277,* 127-141.

[76] (a) *L-Cysteine-Derived Ambidextrous Gelators of Aromatic Solvents and Ethanol/Water Mixtures;* Pal, A.; Dey, J.; *Langmuir* **2013**, *29*, 2120−2127, (b) *Photoluminescence Enhancement of CdSe Quantum Dots: A Case of Organogel−Nanoparticle Symbiosis;* Wadhavane, P. D.; Galian, R. E.; Izquierdo, M. A.; Aguilera-Sigalat, J.; Galindo, F.; Schmidt, L.; Burguete, M. I.; Pérez-Prieto, J.; Luis, S. V.; *J. Am. Chem. Soc.* **2012**, *134*, 20554−20563, (c) *Highly Conductive Ionic-Liquid Gels Prepared with Orthogonal Double Networks of a Low-Molecular-Weight Gelator and CrossLinked Polymer;* Kataoka, T.; Ishioka, Y.; Mizuhata, M.; Minami, H.; Maruyama, T.; *ACS Appl. Mater. Interfaces* **2015**, *7,* 23346−23352, (d) *Two-Component Gel-Phase Materials—Highly Tunable Self-Assembling Systems;* Hirst, A. R.; Smith, D. K.; *Chem. Eur. J.* **2005**, *11,* 19, 5496-5508, (e) *Systematic Design of Amide- and Urea-Type Gelators with Tailored Properties;* Hanabusa, K.; Yamada, M.; Kimura, M.; Shirai, H.; *Angew. Chem. Int. Ed.* **1996**, *35,* 17, 1949-1951.

hydrogels.[77] Aerogels are defined as synthetic porous ultralight solid materials derived from gels, in which the liquid component of the gels have been replaced with a gas during a supercritical drying process. However, hydrogels contain water as solvent while organogels possess an organic solvent as their continuous phase. The aggregation mechanism of the gels in water is generally dominated by hydrophobic interactions, whereas in organic solvents hydrogen bonding usually dominates. Moreover, there is another kind of gels named metallogens. These are gels in which the fibrillar network is created with the participation of metal ions for the establishment of supramolecular interactions.[78] One of the most important parameters characterizing gels is their T_{gel}, the temperature above which the gel is converted into an isotropic solution.[79] This value can be obtained by the rheological instrument when G' and G" intersect during tan δ versus time experiment, while the frequency ω and the deformation γ parameters remain constants. In the ideal situation, cooling the solution below the indicated temperature regenerates the organogel. This thermal stability is directly related to the strength of the interaction of organic molecules in the fibrillar network.[80] The high interaction forces between the organic molecules which act as organogelators are necessary to obtain a high thermal stability of the gel. Greater thermal stability implies the maintenance of the gel structure in a greater range of temperatures. These intermolecular interactions can be achieved, for example, by combining multiple complementary hydrogen bonds, such as those associated with the amide and urea clusters that exhibit high interaction energy. In addition to these hydrogen

---

[77] (a) *A pH-Responsive Amphiphilic Hydrogel Based on Pseudopeptides and Poly(ethylene glycol) for Oral Delivery of Hydrophobic Drugs*; Wang, S.; Attah, R.; Li, J.; Chen, Y.; Chen, R.; *ACS Biomater. Sci. Eng.* **2018**, *4*, 4236−4243, (b) *Pseudopeptide-Based Hydrogels Trapping Methylene Blue and Eosin Y;* Milli, L.; Zanna, N.; Merlettini, A.; Di Giosia, M.; Calvaresi, M.; Focarete, M. L.; Tomasini, C.; *Chem. Eur. J.* **2016**, *22*, 12106–12112, (c) *Multicomponent hydrogels from enantiomeric amino acid derivatives: helical nanofibers, handedness and self-sorting;* Adhikari, B.; Nanda, J.; Banerjee, A.; *Soft Matter* **2011**, *7*, 8913–8922, (d) *Microscopic and macroscopic anisotropy in supramolecular hydrogels of histidine-based surfactants;* Pasc, A.; Gizzi, P.; Dupuy, N.; Parant, S.; Ghanbaja, J.; Gérardin, G.; *Tetrahedron Lett.* **2009,** *50*, 6183–6186, (e) *Selective and highly efficient dye scavenging by a pH-responsive molecular hydrogelator;* Rodríguez-Llansola, F.; Escuder, B.; Miravet, J. F.; Hermida-Merino, D.; Hamley, I. W.; Cardin, C. J.; Hayes, W.; *Chem. Commun.* **2010**, *46,* 42, 7960-7962.

[78] (a) *Luminescent metallomesogens based on platinum complex containing triphenylene unit;* Shi, J.; Wang, Y.; Xiao, M.; Zhong, P.; Liu, Y.; Tan, H.; Zhu, M.; Zhu, W.; *Tetrahedron* **2015**, *71*, 3, 463-469, (b) *Metallomesogens: a promise or a fact?;* Giménez, R.; Lydon, D. P.; Serrano, J. L.; *Curr. Opin. Solid State Mater. Sci.* **2002**, *6*, 6, 527-535.

[79] *The process of heat-induced gelation in Litopenaeus vannamei;* Yang, Y.; Liu, X.; Xue, Y.; Xue, C.; Zhao, Y.; *Food Hydrocolloids* **2020,** *98,* 105260.

[80] (a) *Rheometry of an Androstanol Steroid Derivative Paramagnetic Organogel. Methodology for a Comparison with a Fatty Acid Organogel;* Terech, P.; Friol, S. F.; *Tetrahedron* **2007,** *63,* 31, 7366-7374; (b) *Active Polymer Gel Actuators;* Maeda, S.; Hara, Y.; Yoshida, R.; Hashimoto, *S.; Int. J. Mol. Sci.* **2010**, *11,* 52-66.

bond interactions, Van der Waals forces between the different alkyl groups of the molecule, and other non-covalent interactions, also play an important role in gel stability.[81]

Thus, substitution of amine by urea linkages for the tails provides stronger H-bonds, producing gels with high thermal stability for a variety of solvents.[82] Therefore, this property makes it an ideal group to be included in the design of new gelling systems.[83] In 2002, Hamilton and collaborators designed and synthesized a family of compounds derived from the urea group. The bis-ureas obtained acted as excellent organogelators, forming 0.2% wt gels in a wide variety of solvents.[84] A year later, the same researchers presented a new family of amino acid derived compounds which present urea groups in their structure and behave like hydrogelants.[85] During the following years until now, new gelators have been developed that include urea groups in their structure.[86]

Nowadays, gels can be easily found in our daily life. Although organogels have been known for decades, their industrial applications are more recent. They are now used in a variety of fields such as dermocosmetics and personal care

[81] *Supramolecular gel chemistry: developments over the last decade;* Steed, J. W.; *Chem. Commun.* **2011**, *47,* 5, 1379-1383.
[82] *(a) Anion receptor chemistry;* Gale, P. A.; *Chem. Commun.* **2011**, *47,* 1, 82-86, (b) *Anion recognition by hydrogen bonding: urea-based receptors;* Amendola, V.; Fabbrizzi, L.; Mosca, L.; *Chem. Soc. Rev.* **2010**, *39,* 10, 3889-3915, (c) *Compressed alkanes in reversible encapsulation complexes;* Ajami, D.; Rebek, J.; *Supramol. Chem.* **2009**, *21,* 1, 103-106, (d) *Synthetic lectins*; Davis, A. P.; *Org. Biomol. Chem.* **2009**, *7,* 18, 3629-3638.
[83] (a) *Folding and self-assembly of aromatic and aliphatic urea oligomers: Towards connecting structure and function;* Fischer, L.; Guichard, G.; *Org. Biomol. Chem.* **2010**, *8,* 14, 3101-3117, (b) *The Design of Organic Gelators: Solution and Solid State Properties of a Family of Bis-Ureas;* Carr, A. J.; Melendez, R.; Geib, S. J.; Hamilton, A. D.; *Tetrahedron Lett.* **1998**, *39,* 41, 7447-7450.
[84] *Synthesis and Self-Assembling Properties of Polymerizable Organogelators;* Wang, G.; Hamilton, A. D.; *Chem. Eur. J.* **2002**, *8,* 1954-1961.
[85] (a) *Low molecular weight organogelators for water;* Wang, G.; Hamilton, A. D.; *Chem. Commun.,* **2003**, *3,* 310-311, (b) *Fiber formation in water by a mono-urea dicarboxylic acid;* Estroff, L. A.; Huang, J. S.; Hamilton, A. D.; *Chem. Commun.* **2003**, *24,* 2958-2959.
[86] (a) *Anion-tuned supramolecular gels: a natural evolution from urea supramolecular chemistry;* Steed, J. W.; *Chem. Soc. Rev.* **2010**, *39,* 10, 3686-3699, (b) *Epoxy modified with urea-based ORMOSIL and isocyanate-functionalized polybutadiene: Viscoelastic and adhesion properties;* Soaresa, B. G.; Bezerrab, B. M.; Barrosb, D. N.; Silvac, A. A.; *Composites Part B* **2019,** *168,* 334–341.

products,[87] cleaning materials and paints,[88] food processing and nutraceutics.[89] Moreover, organogels allow entrapping a vast variety of therapeutic compounds due to their incredibly entangled fibrous nano/microstructures, which makes them useful as drug delivery platforms.

Drug delivery through the skin has been a promising concept for a long time because skin has a large surface area with a wide exposure to the circulatory and lymphatic networks, is also easy to access and the route is noninvasive.[90] In this regard, organogels have recently regained interest following many reports on their in vitro and in vivo applications, at various development stages. So organogels has been studied especially as drug and vaccine delivery platforms via various routes such as transdermal, oral, ophthalmic and parenteral administrations.[91] Transdermal delivery is of great importance for drugs that may cause systemic side effects such as non-steroidal anti-inflammatory drugs.[92] However, despite the good results obtained, success of translation into actual clinical products is hampered by a lack of biocompatibility for the organogels; due to the toxicity of most of the used organic solvents. More recently, researchers are trying to use more biocompatible, biodegradable

---

[87] (a) *Development and characterization of sorbitan monostearate and sesame oil-based organogels for topical delivery of antimicrobials;* Singh, V. K.; Pramanik, K.; Ray, S. S.; Pal, K.; *AAPS PharmSciTech* **2015**, *16,* 293–305, (b) *Aqueous dispersions of organogel nanoparticles - potential systems for cosmetic and dermo-cosmetic applications;* Kirilov, P.; Rum, S.; Gilbert, E.; Roussel, L.; Salmon, D.; Abdayem, R.; Serre, C.; Villa, C.; Haftek, M.; Falson, F.; Pirot, F.; *Int. J. Cosmet. Sci.* **2014**, *36,* 336–346, (c) *Study and description of hydrogels and organogels as vehicles for cosmetic active ingredients;* Morales, M. E.; Gallardo, V.; Clares, B.; Garcia, M. B.; Ruiz, M. A.; *J. Cosmet. Sci.* **2009**, *60,* 627–636.

[88] (a) *Organogel formulations for the cleaning of easel paintings;* Baglioni, P.; Bonelli, N.; Chelazzi, D.; Chevalier, A.; Dei, L. G.; Domingues, J.; Fratini, E.; Giorgi, R.; Martin, M.; *Appl. Phys. A Mater. Sci. Process* **2015**, *12,* 857–868, (b) *Rheoreversible polymeric organogels: the art of science for art conservation;* Carretti, E.; Dei, L.; Macherelli, A.; Weiss, R. G.; *Langmuir* **2004,** *20,* 8414–8418.

[89] (a) Kanekanian, A. *Encapsulation Technologies and Delivery Systems for Food Ingredients and Nutraceuticals*, Garti, N.; McClements, D. J., Woodhead Publishing Ltd., Cambridge, UK, **2012**. ISBN 978-1-8456-9801-0, (b) *Olive oil/policosanol organogels for nutraceutical and drug delivery purposes;* Lupi, F. R.; Gabriele, D.; Baldino, N.; Mijovic, P.; Parisi, O. I.; Puoci, F.; *Food Funct.* **2013**, *4,* 1512–1520, (c) *Development of a food-grade organogel with high bioaccessibility and loading of curcuminoids;* Yu, H.; Shi, K.; Liu, D.; Huang, Q.; *Food Chem.* **2012**, *131,* 48–54.

[90] *Galenics of dermal productsvehicles, properties and drug release;* Daniels, R.; Knie, U.; *JDDG* **2007**, *5,* 367-381.

[91] (a) *Organogels, promising drug delivery systems: an update of state-of-the-art and recent applications;* Esposito, C. L.; Kirilov, P.; Roullina, V. G.; *J. Controlled Release* **2018**, *271*, 1–20, (b) *Formulation and clinical evaluation of silymarin pluronic-lecithin organogels for treatment of atopic dermatitis;* Mady, F. M.; Essa, H.; El-Ammawi, T.; Abdelkader, H.; Hussein, A. K.; *Drug Des. Dev. Ther.* **2016**, *10,* 1101–1110, (c) *Tyrosine-based rivastigmine-loaded organogels in the treatment of Alzheimer's disease;* Bastiat, G.; Plourde, F.; Motulsky, A.; Furtos, A.; Dumont, Y.; Quirion, R.; Fuhrmann, G.; Leroux, J. C.; *Biomaterials* **2010**, *31,* 6031–6038, (d) *Organogels in drug delivery;* Murdan, S.; *Expert Opin. Drug Deliv.* **2005**, *2,* 489–505.

[92] *Piroxicam release from dermatological bases: in vitro studies using cellulose membrane and hairless mouse skin;* Babar, A.; Solanki, U. D.; Cutie, A. J.; Plakogiannis, F.; *Drug Dev. Ind. Pharm.,* **1990**, *16,* 523-540.

organic solvents and organogelators proved more pharmaceutically-acceptable and environmental-friendly.[93]

By the other hand, pharmaceutical hydrogels have been extensively studied due to their nature and characteristics, for instance, water-soluble and also providing a good biocompatibility.[94] Thus, there are recent studies using hydrogels as drug platform via transdermal route, enhancing dermal drug delivery and therapeutic outcomes in inflammatory skin diseases (Figure 12).[95]

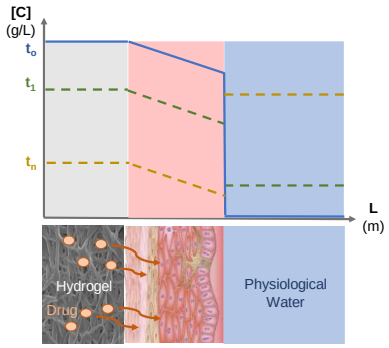

Figure 12 Drug delivery from a hydrogel through epidermis membrane.

The *in vitro* studies are mainly carried out using the Franz diffusion cell. This cell consists of a donor and a receptor compartment, where the formulated product containing the drug and the receptor fluid are placed, respectively (Figure 13). The membrane is placed between the receptor and donor compartments of the Franz cell, being porcine skin one the most common

[93] (a) *Studies on the in vitro and in vivo degradation behavior of amino acid derivative-based organogels;* Li, Z.; Cao, J.; Hu, B.; Li, H.; Liu, H.; Han, F.; Liu, Z.; Tong, C.; Li, S.; *Drug Dev. Ind. Pharm.* **2016**, *42*, 1732–1741, (b) *A vegetable oilbased organogel for use in pH-mediated drug delivery;* Khuphe, M.; Mukonoweshuro, B.; Kazlauciunas, A.; Thornton, P. D.; *Soft Matter* **2015**, *11,* 9160–9167, (c) *Encapsulation of vegetable organogels for controlled delivery applications;* Sagiri, S. S.; Sethy, J.; Pal, K.; Banerjee, I.; Pramanik, K.; Maiti, T. K.; *Des. Monomers Polym.* **2013**, *16*, 366–376, (d) *Nanoengineering of a biocompatible organogel by thermal processing;* Li, J. L.; Wang, R. Y.; Liu, X. Y.; Pan, H. H.; *J. Phys. Chem. B* **2009**, *113,* 5011–5015, (e) *Biocompatible lecithin organogels: structure and phase equilibria;* Angelico, R.; Ceglie, A.; Colafemmina, G.; Lopez, F.; Murgia, S.; Olsson, U.; Palazzo, G.; *Langmuir* **2005**, *21*, 140–148.

[94] (a) *A biocompatible and biodegradable protein hydrogel with green and red autofluorescence: preparation, characterization and in vivo biodegradation tracking and modelling;* Ma, X.; Sun, X.; Hargrove, D.; Chen, J.; Song, D.; Dong, Q.; Lu, X.; Fan, T.-H.; Fu, Y.; Lei, Y.; *Sci. Rep.* **2016,** *6,* 19370, (b) *Biocompatible hydrogels for microarray cell printing and encapsulation;* Datar, A.;Joshi, P.; Lee, M.-Y.; *BIOS* **2015**, *5,* 647–663, (c) *Building biocompatible hydrogels for tissue engineering of the brain and spinal cord; Aurand*, E. R.; Wagner, J.; Lanning, C.; Bjugstad, K. B.; *J. Funct. Biomater.* **2012**, *3,* 839–863, *(d) Light controlled protein release from a supramolecular hydrogel;* Peng, K.; Tomatsu, I.; Kros, A.; *Chem. Commun.* **2010**, *46,* 4094–4096.

[95] *Enhanced delivery of naproxen to the viable epidermis from an activated poly N-isopropylacrylamide (PNIPAM) Nanogel: Skin penetration, modulation of COX-2 expression and rat paw oedema;* Yurdasiper, A.; Ertan, G.; Heard, C. M.; *Nanomedicine: Nanotechnology, Biology, and Medicine* **2018**, *14,* 2051–2059.

membranes, used in one of the following chapter, although some researchers are also used synthetic membranes[96] or animals skin (Figure 13).[97]

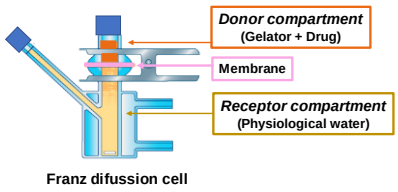

Figure 13 Representation of Franz diffusion cell.

To analyse skin permeation, Fick's diffusion laws (First Law and Second Law) have been used extensively since Scheuplein and Blank[98] reported that Fick's First Law was satisfied quite well in describing the transdermal diffusion of various permeants (a gas, an ion, or a nonelectrolyte, except in cases when the permeant damages the skin). Thus, the Fick's diffusion laws mathematically describe the process of diffusion of matter or energy in a medium in which there is initially no chemical or thermal equilibrium.[99] They received their name by Adolf Fick in 1855 who proposed them.

Fick's First Law expresses the proportionality between the solute steady-state flux, **Jss**, and the applied solute concentration difference, **ΔC**. The Equation 7 shows the steady state global form of Fick's First Law, where **K** is the skin/vehicle partition coefficient of the permeant, **L** is the skin pathlength, **D** is the skin diffusion coefficient of the permeant and **P** is the skin permeability, under the assumption that **D** and **P** are constant everywhere in the skin, assuming a homogeneous membrane.

$$Jss=(\frac{KD}{L})\Delta C=P\ \Delta C$$

Equation 7

However, a more general local expression of Fick's First Law is given in Equation 8, where **Jx** is the local permeant flux at position x in the membrane, **Dx** is the

[96] *Development and Evaluation of Ibuprofen Transdermal Gel Formulations;* Rasool; B. K. A.; Abu-Gharbieh, E. F.; Fahmy, S. A.; Saad, H. S.; Khan, S. A.; *Trop J Pharm Res* **2010**; *9,* 355-363.
[97] *Hyaluronic acid-containing ethosomes as a potential carrier for transdermal drug delivery;* Xie, J.; Ji, Y.; Xue, W.; Ma, D.; Hu, Y.; *Colloids and Surfaces B: Biointerfaces* **2018**, *172,* 323–329.
[98] *Permeability of the skin;* Scheuplein, R. J.; Blank, I. H.; *Phys Rev* **1971**, *51,* 702–747.
[99] *Prediction of Steady-State Skin Permeabilities of Polar and Nonpolar Permeants across Excised Pig Skin Based on Measurements of Transient Diffusion: Characterization of Hydration Effects on the Skin Porous Pathway;* Tang, H.; Blankschtein, D.; Langer, R.; *J. Pharm. Sci.* **2002**, *91,* 1891-1907.

local permeant diffusion coefficient and **Cx** is the concentration at position x in the membrane.

$$Jx = -Dx\left(\frac{dCx}{dx}\right)$$

Equation 8

Moreover, Jss could be calculated from the slope of the linear portion of the plots of the cumulative amount of the permeated drug versus time. The lag time ($\mathbf{t_L}$) is the time where the release and permeation of the drug through the membrane has not yet occurred. Lag time could be calculated from the x-axis intercept of the linear portion of the plots of the cumulative amount of the permeated drug versus time.[100]

The maximum flux ($\mathbf{J_{max}}$) is the applicable flux to saturated solutions that can be estimated from the experimental steady-state flux corrected for the known solubility in the formulation by the following Equation 9:

$$J_{max} = J_{ss}\left(\frac{S_v}{C_v}\right)$$

Equation 9

where $\mathbf{S_V}$ is the solubility of the permeant in the formulation and $\mathbf{C_V}$ is the experimental permeant's concentration used.[101]

On the other hand, Fick's Second Law assumes that the concentration, **C**, varies only in the direction perpendicular to the membrane surface, denoted by x. This law describes the time-dependent variation of permeant concentration in the membrane (Equation 10).

$$\frac{dC}{dt} = D\left(\frac{d^2C}{dx^2}\right)$$

Equation 10

Derived from Fick's second law of diffusion under initial and boundary conditions, the following Equation 11 and Equation 12 are obtained:[102]

---

[100] *Evaluation of the barrier potential of some synthetic membranes in testing the in vitro tenoxicam release from hydrogels, using the experimental model with franz diffusion cells;* Olariu, I.; Coneac, G.; Hirjau, M.; Popoiu, C.; Mut, A. M.; Vlaia, V.; Sevastre, A-S.; Lupuliasa, D.; Vlaia, L.; *Farmacia* **2019**, *67,* 73-80.

[101] *Synergistic Skin Penetration Enhancer and Nanoemulsion Formulations Promote the Human Epidermal Permeation of Caffeine and Naproxen;* Abd, E.; Namjoshi, S.; Mohammed, Y. H.; Roberts, M. S.; Grice, J. E.*; J. Pharm. Sci.* **2016**, *105,* 212-220.

[102] *Drug transport mechanisms and release kinetics from molecularly designed poly(acrylic acid-g-ethylene glycol) hydrogels;* Serra, L.; Doménech, J.; Peppas, N. A.; *Biomaterials* **2006**, *27,* 5440–5451.

$$\frac{M_t}{M_o} = 4\left(\frac{D_E t}{\pi h^2}\right)^{1/2}$$

Equation 11

$$\frac{M_t}{M_o} = 1 - \frac{8}{\pi^2} exp\left(-\frac{\pi^2 D_L t}{\delta\, h^2}\right)$$

Equation 12

$\mathbf{M_t}$ is the amount of drug released at time **t**, $\mathbf{M_0}$ is the total mass of drug loaded into the device, $\mathbf{D_E}$ and $\mathbf{D_L}$ are the early-time and late-time diffusion coefficients of the drug within the gelator network, respectively, and **h** is the thickness of the device. This is an approximation that holds for the release of the first 60% of cumulative release.[102]

Nevertheless, the drug delivery between a membrane not always can be followed by the Fick's diffusion laws. When the gelator network comes in contact with aqueous solutions causes the swelling of the gelator. As water penetrates inside the glassy network, the glass transition temperature of the gelator decreases and the gel becomes rubbery. The drug trapped inside the gel dissolves with the imbibed water and starts diffusing out of the network. It is relevant to highlight the three driving forces that contribute to this phenomenon which are a penetrant concentration gradient, a gelator stress gradient and osmotic forces. In the case of nonswelling controlled delivery systems, the relaxation rate of the gelator is very slow in comparison to the water transport inside the gel. Then, the transport mechanism in this type of systems follows Fickian diffusion. In the contrary, when the relaxation rate of the gelator is the dominating driving force, other type of transport has to be considered.

Therefore, in order to describe the Fickian and non-Fickian release behavior of swelling-controlled release systems, Ritger and Peppas introduced exponential relation $M_t/M_o = kt^n$" in 1987.[103] The diffusional exponent, n, is an important indicator of the mechanism of transport of a drug through the gel. The authors analysed the drug delivery from different sort of devices: sheets, cylinders and spheres obtaining the following Table 2:

[103] *A simple equation for description of solute release I. Fickian and non-fickian release from non-swellable devices in the form of slabs, spheres, cylinders or discs;* Ritger, P. L.; Peppas, N. A.; *J Control Release* **1987**, *5,* 23-36.

Table 2 Diffusional exponent and mechanism of diffusional release from various swellable controlled release systems[101]

Diffusional exponent n			**Drug release mechanism**
Thin film	*Cylindrical sample*	*Spherical sample*	
0,5	0,45	0,43	Fickian diffusion
0,5<n<1,0	0,45<n<0,89	0,43<n<0,85	Anomalous (non-Fickian) transport
1,0	0,89	0,85	Case II transport

In the wake of these results, different diffusion models have been developed to study the drug delivery transport mechanism from the gel and fit the experimental data,[104] which are illustrated in Table 3.[105]

Table 3 Diffusion models.

Model	**Expression**	**Application**
Higuchi[106]	$\frac{M_t}{M_\infty}=Kt^{1/2}$	Fickian diffusion
Ritger-Peppas or Korsmeyer–Peppas[101]	$\frac{M_t}{M_\infty}=Kt^n$	n=1, another transport (Case II), n=0.5, Fickian diffusion; 0.5 <n <1, non-Fickian diffusion
Peppas-Sahlin[107]	$\frac{M_t}{M_\infty}=K_D(t-t_L)^m+K_R(t-t_L)^{2m}$	m=1, another transport (Case II), m=0.5, Fickian diffusion; 0.5 <m <1, anomalous transport
Alfrey[108]	$\frac{M_t}{M_\infty}=K_Dt+K_Rt^{1/2}$	Non-Fickian diffusion (sigmoid)
Zero order[103]	$\frac{M_t}{M_\infty}=Kt$	Another transport (Case II)
First order	$\ln(1-\frac{M_t}{M_\infty})=-Kt$	Another transport (Case II)

$\mathbf{M_t}$ and $\mathbf{M_\infty}$are the absolute cumulative amount of drug released at time t and infinitive time respectively, the coefficient **m** is the purely Fickian diffusion exponent for a device of any geometrical shape which exhibits controlled release (**n**=**m** when the relaxational mechanism is negligible), $\mathbf{k_D}$ is the diffusional constant (referred to the molecular diffusion of the

[104] *Drug transport mechanisms and release kinetics from molecularly designed poly(acrylic acid-g ethylene glycol) hydrogels;* Serra, L.; Doménech, J.; Peppas, N. A.; *Biomaterials* **2006**, *27,* 5440–5451.
[105] *Drug release kinetics and transport mechanisms of non-degradable and degradable polymeric delivery systems;* Fu, W.; Kao, W. *J.; Expert Opin. Drug Deliv.* **2010**, *7,* 429-444.
[106] *Mechanism of Sustained- Action Medication. Theoretical Analysis of Rate of Release of Solid Drugs Dispersed in Solid Matrices;* Higuchi, T.; *J Pharm Sci.* **1963**, *52,* 1145-1149.
[107] *A simple equation for the description of solute release. III. Coupling of diffusion and relaxation;* Peppas, N. A.; Sahlin, J. J.; *Int. J. Pharm. Sci.* **1989**, *57,* 169-172.
[108] *Diffusion in glassy polymers;* Alfrey, T.; Gurnee, E. F.; Lloyd, W. G.; *J Polymer Sci C Polym Symp.* **1966**, *12,* 249-261.

drug as consequence of the chemical potential gradient, Fickian contribution) and $\mathbf{k_R}$ is the relaxation contribution constant (referred to another kind of transport set by the stress and state transition of swelling-controlled drug release), being k_D values always superior to k_R.[109] Therefore, Fickian diffusional release occurs by the usual molecular diffusion of the drug due to a chemical potential gradient. Case-II relaxational release is the drug transport mechanism associated with stresses and state-transition in hydrophilic glassy polymers which swell in water or biological fluids. In general, lower release rates are consistently observed for denser materials, which can be explained by the most obstructed pathways that the drug must overcome.[110]

Although hydrogels possess highly attractive physicochemical properties that make them suitable for biomedical applications, such as cell therapeutics, wound healing, cartilage/bone regeneration and the sustained release of drugs, hydrogels have also drawn great attention to be used in a wide variety of products, as well as, diapers, watering beads for plants, perfume delivery, contact lenses or cosmetics.[111]

1.2.3 Solid state

Supramolecular chemistry has been one of the main topics of chemical research, with the aim of understanding chemistry beyond the covalent bond. The long-range periodicity in crystals is a product of the directionally specific short-range intermolecular interactions that are responsible for molecular assembly, due to this fact, the analysis of crystalline solids is relevant to understand intermolecular interactions and recognition phenomena.[112] In this

[109] *Smart Hydrogel for the pH-Selective Drug Delivery of Antimicrobial Compounds;* Pinho, E.; Machado, S.; Soares, G.; *Macromol. Symp.* **2019**, *385,* 1800182.
[110] *Tailoring drug release profile of low-molecular-weight hydrogels by supramolecular co-assembly and thiol–ene orthogonal coupling;* Díaz, D. D.; Morin, E.; Schön, E. M.; Budin, G.; Wagner, A.; Remy, J-S.; *J. Mater. Chem.* **2011**, *21,* 641–644.
[111] (a) *History and Applications of Hydrogels; Chirani,* N.; Yahia, L. H.; Gritsch, L.; Motta, F. L.; Chirani, S.; Faré, S.; *J Biomedical Sci* **2015**, *4,* 2-13, (b) *Biomedical applications of hydrogels: A review of patents and commercial products;* Caló, E.; Khutoryanskiy, V. V.; *Eur. Polym. J.* **2015**, *65,* 252–267, (c) *Hydrogels for biomedical applications;* Hoffman, A. S.; *Adv. Drug Delivery Rev.* **2012**, *64,* 18–23.
[112] *Intermolecular Interactions in Functional Crystalline Materials: From Data to Knowledge;* Vologzhanina, A. V.; Crystals **2019**, 9, 9, 478. DOI: 10.3390/cryst9090478

regard, a common approach to the study of supramolecular interactions consist in analysing a crystal structure in different conditions.[113]

The solid-state crystal structures of compounds can be described geometrically in terms of a close-packing arrangement, which are held together by non-covalent interactions. All forms of non-covalent interactions, such as hydrogen bonds, halogen bonds, stacking interactions, van der Waals interactions, etc., can be characterized by their geometry (distances and angles) and energy (vibrational and optical absorption band wavenumbers, intensities, widths).[114] In the final structure of the crystal compounds, a maximum number of contacts will be achieved with other adjacent molecules leading to stabilizing the final structure. In supramolecular chemistry many crystal structures which have large ions are closely packed with the smaller ions filling the spaces in between them. They have shown very useful properties in molecular recognition and catalysis.

The solid-state structures can present different sort of aggregates depending on the intermolecular forces involved. The self-assembling abilities of these aggregates can be thoroughly studied in the solid state using different techniques like SEM, TEM, FTIR or X-ray. These techniques allow researchers to have an idea of the possible structural factors that dominate the aggregation process of the different compounds.[115] Thus, SEM and TEM microscopy allows the observation of the structures' morphology in inorganic and organic materials at nano- and micrometric scales.[116] They are techniques that also allow to check very fast if the materials are nanostructured, that is, if they form an organized structure at the nanoscopic level providing direct visual information of size, shape and aggregation extent of a sample i.e. the formation of fibres, micelles or vesicles (Figure 14).[117]

---

[113] *From Solid-State Structure and Dynamics to Crystal Engineering;* Braga, D.; Grepioni, F.; Maini, L.; d'Agostino, S.; *Eur. J. Inorg. Chem.* **2018**, 3597–3605.

[114] *Supramolecular assembly of conjugated polymers: From molecular engineering to solid-state properties;* Leclère, P.; Surin, M.; Brocorens, P.; Cavallini, M.; Biscarini, F.; Lazzaroni, R.; *Mater. Sci. Eng. R.* **2006**, *55,* 1-56.

[115] Urbanc, B.; Borreguero, J. M.; Cruz, L.; Stanley, H. E. *Ab Initio Discrete Molecular Dynamics Approach to Protein Folding and Aggregation. In Methods in Enzymology*; Amyloid, Prions, and Other Protein Aggregates, Part B; Academic Press, **2006**; Vol. 412, pp 314–338. https://doi.org/10.1016/S0076-6879(06)12019-4.

[116] *Peptides Co-Assembling into Hydrangea-Like Microstructures;* Guo, Z.; Shen, Z.; Wang, Y.; Tan, T.; Zhang, Y.; *J. Nanosci. Nanotechnol.* **2020**, *20, 5,* 3239-3245.

[117] *Transmission electron microscopy as an orthogonal method to characterize protein aggregates,* Sung, J. J.; Pardeshi, N. N.; Mulder, A. M.; Mulligan, S. K.; Quispe, J.; On, K.; Carragher, B.; Potter, C. S.; Carpenter, J. F.; Schneemann, A.; *J Pharm Sci.* **2015**, *104, 2,* 750–759.

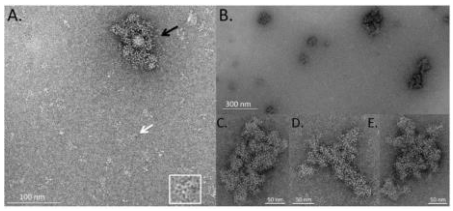

Figure 14 TEM images of negatively stained, stressed IVIg. (A) Representative image showing sub-micron IVIg aggregate (black arrow) surrounded by small oligomeric antibody complexes and monomeric IVIg molecules. A view of the monomeric IVIg molecule identified by the white arrow is shown at increased scale in the lower right corner. This antibody is oriented in a planar fashion on the grid, giving it a Y-shaped appearance. The three arms of the molecule are visible in the form of small rings. (B) Field of view at lower magnification showing distribution and size range of IVIg aggregates. (C to E) Individual IVIg aggregates at high magnification. The aggregates are compact and appear to be formed from smaller globules.[116]

Moreover, in the last few decades, the halogen bonding has been at the forefront to understand the crystal structures.[118] The $Br_2\cdots O(CH_2CH_2)_2O$ adduct was the first reported X-ray structure of a halogen-bonded system[119] (Figure 15a) and several related crystal structures of adducts involving dihalogens and halocarbons were then established in rapid sequence.[120] The crystal structures of $Br_2\cdots C_6H_6$ (Figure 15b) was particularly noteworthy as it proved that π-systems work as donor of electron density to electrophilic halogens in the solid state.[121]

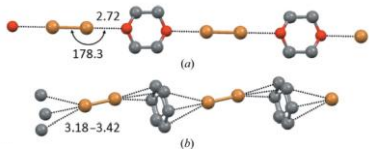

Figure 15 One-dimensional chains formed by Br_2 (working as a bidentate XB donor) with 1,4-dioxane (a) and benzene (b), both working as bidentate XB acceptors. H atoms are omitted. XBs are shown as black dotted lines. Distances are given in A° and angles in degrees. Colour code: grey, C; red, O; brown, Br.[122]

---

[118] *Halogen bonding, chalcogen bonding, pnictogen bonding, tetrel bonding: origins, current status and discussion;* Brammer, L.; *Faraday Discuss.* **2017**, *203,* 485-507.
[119] *The Structure of Bromine 1,4-Dioxanate;* Hassel, O.; Hvoslef, J.; Vihovde, E. H.; Sorensen, N. A.; *Acta Chem. Scand.* **1954**, *8,* 873.
[120] *Structural Aspects of Interatomic Charge-Transfer Bonding;* Hassel, O.; *Science* **1970**, *170,* 497–502.
[121] *Noncovalent binding of the halogens to aromatic donors. Discrete structures of labile Br_2 complexes with benzene and toluene;* Vasilyev, A. V.; Lindeman, A. V.; Kochi, J. K.; *Chem. Commun.* **2001**, 909-910.
[122] *Supramolecular interactions in the solid state;* Resnati, G.; Boldyreva, E.; Bombicz, P.; Kawano, M.; *IUCrJ* **2015**, *2,* 675–690.

Regarding the crystal as a supramolecular entity, the collective properties of molecules mediated by intermolecular interactions are crucial. The fine-tuning of the structural properties performs the control of the physicochemical properties of materials. This might be achieved by introduction of substituents on molecules or guest molecules of different sizes, shapes and chemical composition. The balance of spatial requirements and electrostatic effects ultimately determine the packing arrangement. The capability of fine-tuning requires first the recognition, then a better understanding of supramolecular interactions in the solid state, along with consideration of molecular, supramolecular and crystallographic symmetry.

In 1995, Fan and co-workers designed self-complementary molecules in which binding groups on one part of the structure fitted precisely with complementary groups on a different region of an adjacent molecule, performing the controlled formation of different three-dimensional shapes.[123] The orientation of the interacting groups determined the nature and size of the aggregate. They created three-dimensional structures with the urea hydrogen bonding motif using cis,cis-cyclohexane-1,3,5-tricarboxamide derivatives for the central core (Figure 16). The resulting conformation possessed three carbonyl oxygens on one surface of the molecule ideally positioned to hydrogen bond with the three amide-NH on the opposite surface of an adjacent molecule.

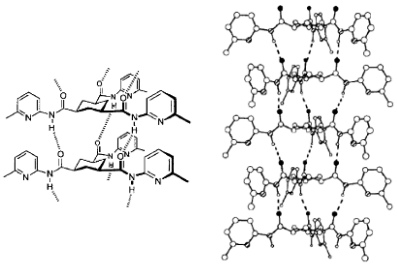

Figure 16 Crystal structure of the compound from a 1:1 mixture of MeOH-CH_2Cl_2 in ball and stick representation.[109]

X-Ray diffraction analysis showed a compact packing arrangement in which the triamide monomers formed an extended column structure stabilized by three

[123] *Hydrogen-bonding control of molecular aggregation: self-complementary subunits lead to rod-shaped structures in the solid state;* Fan, E.; Yang, J.; Geib, S. J.; Stoner, T. C.; Hopkins, M. D.; Hamilton, A. D.; *J. Chem. Soc. Chem. Commun.* **1995**, 1251-1252.

inter- molecular hydrogen bonds between each monomer. It resulted in large rod-shaped crystals.

1.2.4 Other materials in solution

An amphiphilic substance is defined from the physicochemical point of view as a polar-apolar duality, showing a double affinity. Thus, the typical molecule of an amphiphilic compound has two parts: a polar part and a nonpolar part. The polar part is hydrophilic, while the apolar part is hydrophobic (lipophilic), having or not an affinity for water, respectively (Figure 17).

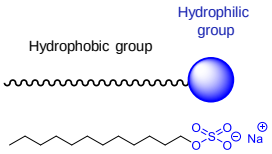

Figure 17 Example of the amphiphilic compound: sodium dodecyl sulfate.

On the other hand, the surfactant (or tensioactive) compounds show surface or interfacial activity, thanks to their double affinity. Thus, due to it, a part of the amphiphilic molecule does not have much affinity in a solvent, polar or nonpolar. In this regard, these compounds show a strong tendency to migrate to the interfaces. However, it should be noted that all amphiphilic compounds do not possess such activity and, therefore, cannot be called surfactants. An amphiphilic compound is considered a surfactant when it has relatively balanced properties, it is not too hydrophilic or hydrophobic.[124]

Surfactant compounds are chemical compounds that are used daily throughout the world.[125] This class of compounds is well known for its solubility and its usefulness in cleaning processes. Therefore, from a commercial point of view, surfactants are classified according to their applications. Nevertheless, it is observed that many surfactants are likely to be used in different applications, which can cause confusion. Hence, surfactants are classified by their chemical structure, more precisely, according to how they are dissociated in water.[126] Thus, surfactants can be classified, according to the nature of their hydrophilic

[124] *Supramolecular amphiphiles;* Zhang, X.; Wang, C.; *Chem. Soc. Rev.* **2011**, *40,* 1, 94-101.
[125] *Basics and Potential Applications of Surfactants-A Review;* Mishra, M.; Muthuprasanna, P.; Prabha, K. S.; Rani, P. S.; Babu, I. A. S.; Chandiran, I. S.; Arunachalam, G.; Shalini, S.; *Int.J. PharmTech Res.* **2009**, *1,* 4, 1354-1365.
[126] Salaguer, J. L. Cuaderno - S201A *Surfactantes en Solucion Acuosa. Laboratorio FIRP*, **1992**.

group, in amphoteric, anionic, cationic and non-ionic.[127] The type of surfactant defines its physicochemical features, its properties and applications.[128]

- *Amphoteric surfactants.* Its behavior depends on the pH. Thus, its molecules are capable of changing the charge, from positive to negative, increasing or decreasing the pH, and presenting a "zwitterionic" behaviour at intermediate pH values. The best-known amphoteric surfactants contain an amino group and an acidic group such as sulfonate, carboxylate, sulfate or phosphate type. The amino group is protonated at acidic pH and the acidic group is deprotonated at basic pH, resulting a zwitterion compound at intermediate pH.[129] These are used in the textile industry, rubber, as antibacterial agents, as catalysts and so on.

- *Anionic surfactants*: the most common and most used type. The hydrophobic part of the molecule is generally an alkyl radical of different length, while the hydrophilic part is usually formed by carboxyl, sulfate, sulphonate or phosphate groups. Its utilities are wide and very diverse. The main one is to obtain detergents[130], however, they are also used successfully in the field of biotechnology and other industrial processes.[131] Moreover, they are used in pharmaceutical formulations to increase the efficiency of the active product[132] and so on.

- *Cationic surfactants*. The most common types of cationic surfactants are quaternary ammonium compounds. These contain at least one hydrocarbon hydrophobic chain (large size alkyl group) attached to a positively charged nitrogen atom, while other alkyl groups such as methyl or benzyl groups are also present as substituents on the nitrogen.[133] Cationic surfactants are used

---

[127] Porter, M. R. *Handbook of surfactants;* Springer Netherlands, **1994**, 26-93.
[128] Salaguer, J. L. Cuaderno - S201A *Surfactantes. Tipos y usos. Laboratorio FIRP*, **2002**.
[129] *Progress in synthesis and application of zwitterionic Gemini surfactants;* Cheng, Y.; Yang, Y.; Niu, C.; Feng, Z.; Zhao, W.; Lu, S.; *Front. Mater. Sci.* **2019**, *13, 3,* 242-257.
[130] *Development of Surfactants and Builders in Detergent Formulations;* Yangxin, Y. U.; Jin, Z.; Bayly, A. E.; *Chin. J. Chem. Eng.* **2008**, *16,* 4, 517-527.
[131] *Biological activity and environmental impact of anionic surfactants;* Cserhati, T.; Forgacs, E.; Oros, G.; *Environ. Int.* **2002***, 28,* 5, 337-348.
[132] *In vitro study on the interaction of mechanism of tricyclic compounds with bovine serum albumin;* Kamat, B. P.; Seetharamappa, J.; *J. Pharm. Biomed. Anal.* **2004**, *35,* 3, 655-664.
[133] *The aggregation and micellization of ionic surfactants in aqueous solution detected using surface-confined redox and ion-pairing reactions;* Tauzin, A.; Dionne, E. R.; Badia, A.; *Electrochimica Acta* **2019**, *326,* 134991.

as detergents, hair conditioners, disinfectants, softeners, antibacterials and so on.[134]

- *Non-ionic surfactants.* The surface activity of non-ionic surfactants derives from the balance between the hydrophobic and hydrophilic groups contained in their structure, none of which charged. The solubility of these compounds is usually defined by the polarity of the polar head group. Its hydrophobic part is generally formed by a derivative of an alkylated phenol, a fatty acid or a linear chain of alcohols. Its hydrophilic part is formed by ethylene oxide chains of various lengths. These types of compounds are widely used as emulsifiers, wetting agents and so on.[135]

Surfactants can self-assemble creating interesting structures. In an aqueous medium, from a certain concentration, the hydrophobic interactions between surfactant molecules become sufficiently important regarding hydrophilic surfactant/water interactions. This results in the spontaneous formation of an aggregate. Therefore, critical aggregation concentration (CAC) can be defined as the minimum concentration of compound from which aggregates are spontaneously formed in a solution.[136] In most cases, surfactants are associated forming micelles. Thus, critical micellar concentration (CMC) is the concentration of compound above which the individual molecules of the compound are aggregated forming micelles. In compounds with aliphatic chains, the CMC value tends to decrease when the length of the compound's aliphatic chain increases. On the other hand, long spacers contribute to increase the hydrophobicity of the compound, thus reducing its solubility in water and improving its tendency towards self-assembly. The CMC values of dimeric surfactant, also called gemini surfactant (which usually contains two aliphatic long tails and a polar head) are much smaller than those of the

---

134 *Cationic Surfactants: Self-Assembly,Structure-Activity Correlation and Their Biological Applications;* Zakharova, L. Y.; Pashirova, T. N.; Doktorovova, S.; Fernandes, A. R.; Sanchez-Lopez, E.; Silva, A. M.; Souto, S. B.; Souto, E. B.; *Int. J. Mol. Sci.* **2019**, *20,* 5534-5565.

135 *Synergistic stabilization of Pickering emulsions by in situ modification of kaolinite with non ionic surfactant;* Nallamilli, T.; Basavaraj, M. G.; *Appl. Clay Sci.* **2017**, *148,* 68-76.

136 *(a) Self-Assembly and Critical Aggregation Concentration Measurements of ABA Triblock Copolymers with Varying B Block Types: Model Development, Prediction, and Validation;* Aydin, F.; Chu, X.; Uppaladadium, G.; Devore, D.; Goyal, R.; Murthy, N. S.; Zhang, Z.; Kohn, J.; Dutt, M.; *J. Phys. Chem. B* **2016**, *120,* 3666−3676, (b) *Stoichiometry and Physical Chemistry of Promiscuous Aggregate-Based Inhibitors;* Coan, K. E. D.; Shoichet, B. K.; *J. Am. Chem. Soc.* **2008**, *130,* 9606–9612, (c) *Determination of the aggregation properties of weakly self-associating systems by NMR techniques: the self-association of propranolol hydrochloride in aqueous electrolyte solution;* Ruso, J. M.; Taboada, P.; Attwood, D.; Mosquera, V.; Sarmiento, F.; *Phys. Chem. Chem. Phys.* **2000**, *2,* 1261-1265.

corresponding monomeric surfactant, because two alkyl chains are transferred from water to the micelle pseudophase at the same time.[137] Hence, gemini surfactants consist of two conventional surfactant molecules (the two terminal hydrocarbon tails can be short or long and the two polar head groups can be cationic, anionic or nonionic) chemically bonded together by a spacer which can be short or long, flexible or rigid. The gemini surfactants need not be symmetrically disposed about the center of the spacer and they can self-assemble at much lower concentrations being superior in surface activity as compared to conventional surfactants.

In aqueous medium the micelles can group several tens and even some hundreds of molecules. The size and geometry of these conglomerates essentially depend on the structure of the surfactant (Figure 18) and the solution conditions, such as surfactant concentration, temperature, pH, and ionic strength.[138] The critical packing factor ($\boldsymbol{C_{pp}}$) allows to estimate the shape and size of the aggregates, according to Equation 13:

$$C_{pp} = V_o/A_{mic}l_c$$

Equation 13[139]

where V_o is the effective volume occupied by hydrophobic chains in the aggregate core, A_{mic} is the effective hydrophilic head group surface area at the aggregate-solution interface and l_c is the maximum effective length (critical chain length). Depending on the Cpp value, it is possible to find different structures of aggregates: spherical (Cpp ≤ 1/3), cylindrical (1/3 ≤ Cpp ≤ 1/2), vesicles (1/2 ≤ Cpp ≤ 1), lamellar (Cpp = 1) and inverse micelles (Cpp > 1).

The vesicles generated correspond to ellipsoidal or spherical closed amphiphile bilayer structures with an internal cavity containing the dispersion solution.[140] In aqueous solution, they tend to be metastable structures and, depending on

[137] *Studies of mixed surfactant solutions of cationic dimeric (gemini) surfactant with nonionic surfactant C12E6 in aqueous mèdium;* Sharma, K. S.; Rodgers, C.; Palepu, R. M.; Rakshit, A. K.; *J. Colloid Interface Sci.* **2003**, *268,* 2, 482-488.

[138] *Amphiphiles Self-Assembly: Basic Concepts and Future Perspectives of Supramolecular Approaches;* Lombardo, D.; Kiselev, M. A.; Magazù, S.; Calandra, P.; *Adv. Condens. Matter Phys.* **2015**, *2015,* 1-22.

[139] Israelachvili, J. N. *Intermolecular and Surface Forces*; Elsevier, **2011**. https://doi.org/10.1016/C2009-0-21560-1

[140] Israelachvili, J. N. *Thermodynamic and geometric aspects of amphiphile aggregation into micelles, vesicles and bilayers, and the interactions between them.* Physics of Amphiphiles: Micelles, Vesicles and Microemulsions, Degiorgio, V., Corti, M., Eds., North-Holland, Amsterdam, The Netherlands, **1985**.

the conditions of preparation (i.e., extrusion, stirring, or sonication), some energy is required to dissolve the amphiphile in water and to induce self-aggregation. The vesicles obtained are generally from 10 nm to 10 μm and they may contain one (unilamellar) or more (multilamellar) concentric bilayer surfaces in an onion-like structure (hydrated multilayers).[141]

In the inverse micelles, the hydrophobic chains radiate away from centrally aggregated headgroups, the water solvent is found inside them.

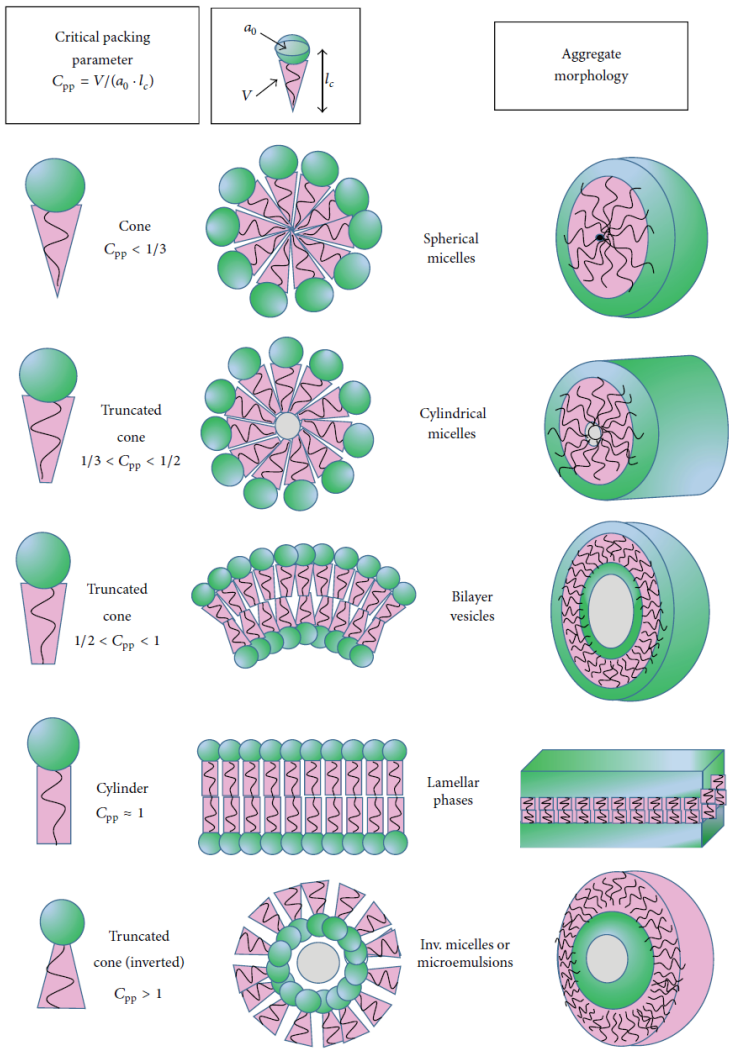

Figure 18 Amphiphile shape factors and summary of the aggregate structures that can be predicted from the critical packing parameter *C*pp.[137]

Due to the aggregation of the surfactants, they can be used in multiple applications. One that is recently increasing the interest of the researchers is

[141] *A sucrose solutions application to the study of model biological membranes;* Kiselev, M. A.; Lesieur, P.; Kisselev, A. M.; Lombardo, D.; Killany, M.; Lesieur, S.; Ollivon, M.; *Nucl. Instrum. Methods Phys. Res. Sect. A.* **2001**, *470, 1-2,* 409–416.

the control release of drugs and fragrances.[142,143] The surfactant is capable to form micelles through self-assembly process and the fragrance is found inside these (Figure 19). When the solvent starts to evaporate it, the fragrance is released slower than without the use of the surfactants that retains the fragrance longer in time.[144]

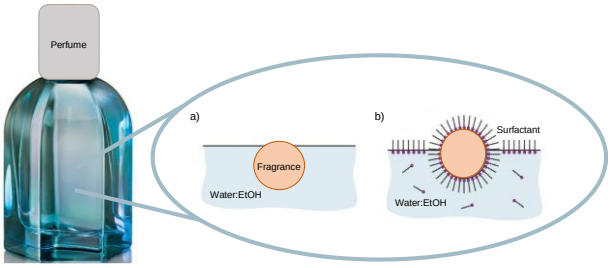

Figure 19 (a) General representation of the composition of a perfume (b) including also the surfactant.

Hence, when there is two immiscible phases' system, the surfactant generates an emulsion that looks like milk. This is thermodynamically unstable, and it is separated over time. The emulsion is considered oil in water (O/W) when the disperse phase is nonpolar and the continuous phase is polar, being water in oil (W/O) the opposite phases. On the other hand, if the interfacial tension is low, it could be achieved dispersed systems in which the size of the surfactant's aggregate is less than one micra, this is called microemulsion. It is a transparent solution.

These different emulsions are not stable and can be broken following different mechanisms (Figure 20):

- *Creaming*

Creaming is referred to the formation of a superior phase constituted by emulsion's drops. The density of this phase is considerably lower than the continuous phase.

---

[142] *Encapsulation of oils and fragrances by core-in-shell structures from silica particles, polymers and surfactants: The brick-and-mortar concept;* Radulova, G. M.; Slavova, T. G.; Kralchevsky, P. A.; Basheva, E. S.; Marinova, K. G.; Danov, K. D.; *Colloids Surf., A* **2018**, *559,* 351–364.
[143] dos Santos, S.; Medronho, B.; dos Santos, T.; Antunes, F. E. *Amphiphilic Molecules in Drug Delivery Systems;* Coelho J., Eds., Drug Delivery Systems: Advanced Technologies Potentially Applicable in Personalised Treatment. Advances in Predictive, Preventive and Personalised Medicine, Springer, Dordrecht, **2013**, *4*, 35-85.
[144] *The effect of surfactant chain length on the morphology of poly(methyl methacrylate) microcapsules for fragrance oil encapsulation;* Tasker, A. L.; Hitchcock, J. P.; He, L.; Baxter, E. A.; Biggs, S.; Cayre, O. J.; *J. Colloid Interface Sci.* **2016**, *484,* 10–16.

- *Sedimentation*

Sedimentation is the tendency for particles in suspension to settle out of the fluid in which they are entrained and come to rest against a barrier.

- *Flocculation*

Flocculation is known as the adherence of droplets to form aggregates or clusters and the build-up of these aggregates. When the attractive forces between the droplets exceeds that of the repulsive forces take place the flocculation mechanism, without a breakdown in the structural integrity of the interfacial film surrounding the droplets. These phenomena could be reversible.

- *Coalescence*

Coalescence occurs when aggregates or flocculates of the dispersed phase combine to form a single, larger drop. Coalescence is really a reflection of the nature of the interfacial film on the surface of the droplet. A strong, stable film on the surface of the droplet, owing to the addition of the correct concentration of the appropriate emulsifier, will minimize this type of destabilization.

- *Phase inversion*

Phase inversion occurs when the discontinuous phase will become the continuous phase. The viscosity of an emulsion will increase gradually as more and more of a given phase is added until a critical volume is reached. If more of that same phase is added, exceeding the critical volume, the emulsion will invert.

- *Ostwald ripening*

If the two phases forming the emulsion are not totally immiscible, and there are differences in droplet size within the emulsion, larger droplets will form at the expense of smaller droplets owing to a process known as 'Ostwald ripening.' This mechanism is always a factor since variations in initial droplet size always occur in macroemulsions, and both phases are never completely immiscible. The driving force for Ostwald ripening is the difference in chemical potential between droplets of difference sizes. Equilibrium will only exist when all droplets are the same size, which really means a single 'drop' or the presence of two continuous and separate phases.

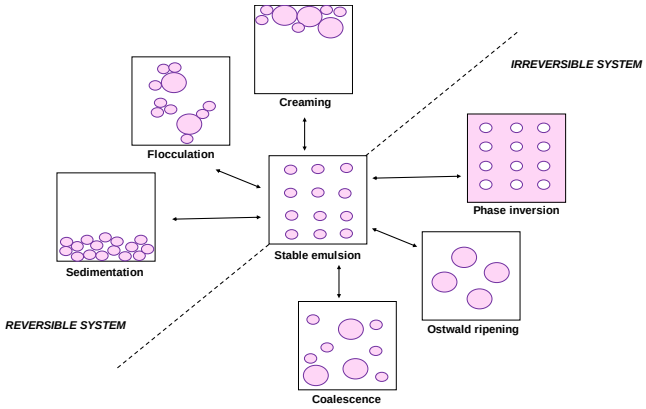

Figure 20 Rupture emulsions' mechanisms.

Although there are many phenomena that can alter the emulsions properties, they can be stabilized in order to avoid their rupture.[145] The emulsion stability is known as the ability of an emulsion to keep its properties unchanged over a certain period of time. In this regard, two relevant parameters to be considered are the thermodynamic and kinetic stability. Thermodynamics gives information about processes taking place during emulsification or at quiescent conditions (after homogenisation)[146] while kinetics refers to the rate at which these processes occur. During the emulsification, the overall free energy is positive, due to the increase of interfacial area, being thermodynamically unfavourable. For instance, the coalescence phenomenon occurs due to the thermodynamic instability.

In addition, spherical aggregates can be generally stabilized by different methods:[147]

- *Addition of emulsifiers:* compounds that facilitate the formation of emulsion by lowering the oil/water interfacial tension producing a protective film around the droplets. The most effective emulsifiers are nonionic surfactants that can be used to emulsify O/W or W/O. They can stabilize the emulsion against flocculation and coalescence.
- *Addition of stabilizers*: compounds that impart long-term stability to emulsions by restricting interfacial interactions not being generally surface active.

[145] *The Theory of Emulsification, III.;* Bancroft, W. D.; *J. Phys. Chem.* **1912**, *16,* 475-512.
[146] *Food Emulsions: Principles, Practices, and Techniques,* 3rd Edition, McClements, D. J. M., Eds.; CRC Press, **2015**.
[147] *Stability of emulsions under equilibrium and dynamic conditions;* Ivanov, I. B.; Kralchevsky, P. A.; *Colloids Surf., A* **1997**, *128,* 155-175.

- *Formation of Liquid Crystals*: compounds formed by mixing different emulsifiers in water. It is also called mesophase structure.
- *Pickering emulsions*: solid particles provide the stability of the emulsion.[148]

Methods to control the gravitational separation: The reduction of droplet size to neglect the gravitational force and the increment of the viscosity of continuous phase surroundings the droplets, producing the decrease of droplets rate. These are useful against sedimentation or creaming.

There are currently several techniques that allow us to determine CAC value in solution state like NMR, UV, CD, GC, FTIR or Fluorimetry techniques.[149] The last one consists in the measurement of fluorescence intensity, using the pyrene method. In this method the pyrene acts as a fluorescent probe, allowing the emission of fluorescence. In general, in this method when aggregate's formation occurs, the ratio between intensities (I1/I3) decreases from 1.8 to 1.2.[150] The behaviour of the compounds in solution is deepened using the fluorescence study, in particular it is important the study of the behaviour in a solvent such as water, a biological medium.

1.2.5 Molecular receptors

Molecular receptors are structures capable of selectively complexing ionic or molecular substrates, through intermolecular interactions, with the formation of a supramolecular structure. They can be classified as a function of the stoichiometry of the complex formed. Thus, it is possible to find two different types of molecular receptors:

- *Monotopic receptor*: it is composed by only one molecular region abled to act as a receptor and therefore complex a single substrate.[151]

---

[148] *The Theory of Emulsification I.;* Bancroft, W. D.; *J. Phys. Chem.* **1912**, *16,* 177-233.
[149] (a) *Fluorescence probes for critical micelle concentration determination;* Ananthapadmanabhan, K. P.; Goddard, E. D.; Turro, N. J.; Kuo, P. L.; *Langmuir* **1985**, *1,* 3, 352-355, (b) *Critical Micellization Concentration of Surfactants in Aqueous Solution and Free Energy of Micellization;* Zana, R.; *Langmuir* **1996**, *12,* 5, 1208-1211, (c) *Fluorescence Study of Premicellar Aggregation in Cationic Gemini Surfactants; Mathias,* J. H.; Rosen, M. J.; Davenport, L.; *Langmuir* **2001**, *17,* 20, 6148-6154.
[150] *Synthesis and surface-active properties of sulfobetaine-type zwitterionic gemini surfactants;* Yoshimura, T.; Ichinokawa, T.; Kaji, M.; Esumi, K.; *Colloids Surf., A* **2006**, *273,* 1-3, 208-212.
[151] (a) *Anion receptor chemistry: highlights from 2010;* Wenzel, M.; Hiscock, J. R.; Gale, P. A.; *Chem. Soc. Rev.* **2012**, *41,* 480-520, (b) *Anion receptor chemistry: highlights from 2011 and 2012;* Gale, P. A.; Busschaert, N.; Haynes, C. J.; Karagiannidis, L. E.; Kirby, I. L.; *Chem. Soc. Rev.* **2014**, *43,* 205-241.

- *Politopic receptor*: it is composed by more than one molecular region covalently joined abled to complex two or more substrates.[152]

The selective binding of a substrate molecule (Guest) with the molecular receptor (Host) to produce a host-guest complex or supermolecule through reversible non-covalent interactions is known as molecular recognition. Supermolecules are generally formed by a guest component (smaller in size) with divergent binding sites and a host component (larger in size) with convergent binding sites. This phenomenon is also called as Host-guest chemistry or Inclusion phenomenon. The intermolecular interactions involved between the two species must follow a strong complimentary pattern in good agreement with the lock and key model of enzymatic sites proposed by Emil Fischer (Figure 21).[153]

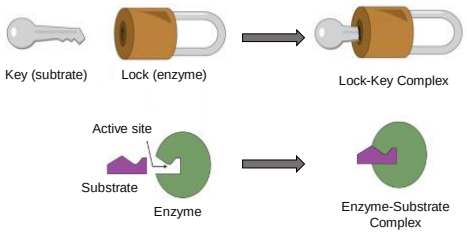

Figure 21 Representation of the Key and Lock mechanism (top) and the interaction of an enzyme with a substrate to give an enzyme-substrate complex (bottom).

Host-guest (or receptor-substrate) chemistry is mainly based upon three historical concepts. Firstly, Paul Ehrlich introduced the concept of the biological receptor.[154] Later, the idea that the binding must be selective was postulated by Emil Fischer as a part of the study of substrate binding by enzymes, and also suggested that the enzyme-substrate interactions adapt to the lock and key principle.[155] Finally, the mutual affinity between a receptor and a substrate was developed in the Alfred Werner's theory of coordination chemistry.[156]

A wide variety of molecular receptors have been synthesized and investigated since their discovery, especially macrocyclic compounds. This kind of molecular

[152] *Macrocycles as Ion Pair Receptors;* He, Q.; Vargas-Zúñiga, G. I.; Kim, S. H.; Kim, S. K.; Sessler, J. L.; Chem. Rev. **2019**, *119, 17,* 9753-9835.
[153] *The Key–Lock Theory and the Induced Fit Theory;* Koshland, D. E.; *Angew. Chem. Int. Ed. Engl.* **1995**, *33,* 2375-2378.
[154] Ehrlich, P. *Studies on immunity;* Wiley: New York., **1906**.
[155] *Einfluss der Configuration auf die Wirkung der Enzyme;* Fischer, E.; *Ber. Dtsch. Chem. Ges.* **1894**, *27,* 2985-2993.
[156] *Beitrag zur Konstitution anorganischer Verbindungen;* Werner, A.; *Zeit. anorg. Chem.* **1893**, *3,* 267-330.

receptors marked the beginning of Supramolecular chemistry. As named before, the works carried out by Pedersen[8], Cram and Lehn[1a] were crucial to develop this field. The macrocyclic compounds synthesized by them were known as "crown ethers," "spheres" and "cryptands", which are receptors capable of selectively complexing cations of different sizes depending on the size of the macrocycle.[157]

The structure and stability of inclusion complexes depends on two fundamental parameters:

1. *Substrate polarity*: The stability of the inclusion complexes is a function of the hydrophobic nature of the substrate.
2. *Geometric compatibility*: The stability of inclusion complexes also depends on the size and geometric shape of the substrate with respect to the dimensions of the receptor.

One of the most studied molecular receptors has been Cyclodextrins which consist of multiple glucose building blocks linked together in a ring.[158] They can be produced by enzymatic degradation of plant starch. Cyclodextrins are monotopic three-dimensional molecular receptors, which are formed by a central hydrophobic cavity. This cavity can trap lipophilic molecules as “guests” obtaining inclusion complexes with a wide variety of inorganic and organic compounds (Figure 22).

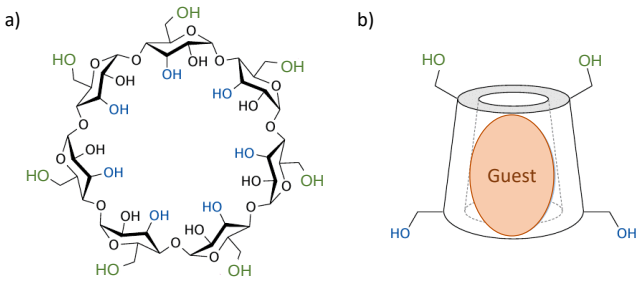

Figure 22 (a) Example of cyclodextrin and (b) Three-dimensional representation of cyclodextrin as a receptor and a general guest trapped in its cavity.

[157] (a) *The Chemistry of Macrocyclic Ligand Complexes;* Lindoy, L. F.; *Cambridge University Press,* **1989**, 1-20. DOI: https://doi.org/10.1017/CBO9780511564376.002, (b) Izatt, R. M. *Macrocyclic and Supramolecular Chemistry: How Izatt–Christensen Award Winners Shaped the Field;* John Wiley & Sons, Ltd, 2016.
[158] Wimmer, T. *Cyclodextrins.* In Ullmann’s Encyclopedia of Industrial Chemistry; American Cancer Society, **2003**. https://doi.org/10.1002/14356007.e08_e02

The receptor and the substrate should be compatible in size and shape, this is the key of molecular recognition process of substrates by cyclodextrins. In this way, they can complex bioactive substances. The hydrophilic outer surface ensures compatibility with aqueous systems. This special structure of cyclodextrins opens a wide range of applications, for instance, selective transport of substrates through biological membranes.[159]

During the last years, researchers have developed a wide variety of molecular receptors which have been investigated as compounds to vast functionalities, such as new healable coatings to use in cables and pipes,[160] catalysis processes,[161,162] medical applications[163] and so on. In summary, the processes of recognition, self-assembly, catalysis and transport make up the basic functions of supramolecular receptors.[164,165]

2 Pseudopeptidic compounds in Supramolecular Chemistry

Nature uses a limited number of structural units named amino acids to build complex systems. Although there are few types of amino acids, their multiple combinations allow to form long peptide chains to achieve the construction of an essentially infinite number of structures.[166] Hence, pseudopeptidic compounds are formed by combination of structural subunits derived from amino acids (natural components) that provides functional elements with abiotic units (non-natural components) that serves as structural scaffolds.[167] It is precisely these units that provide them specific properties, such as lability of

[159] *Cyclodextrins as Building Blocks for Supramolecular Structures and Functional Units;* Wenz, G.; *Angrit. Clitw. lnt. Ed. Enxi.* **1994**, *33,* 803-822.
[160] *Healable Polymeric Materials;* Greenland, B. W.; Hayes, W.; *R. Soc. Chem.* **2013**, ISBN: 978-1-84973-626-8.
[161] *Molecular recognition. Design of new receptors for complexation and catalysis;* Hamilton, A. D.; Fan, E.; Arman, S. V.; Vicent, C.; Tellado, F. G.; Geib, S. J.; *Supramol. Chem.* **1993**, *1*, 247-252.
[162] *Cu^{2+}, Zn^{2+}, and Ni^{2+} Complexes of C2-Symmetric Pseudopeptides with an Aromatic Central Spacer;* Gorla, L.; Martí-Centelles, V.; Freimuth, L.; Altava, B.; Burguete, M. I.; Luis, S. V.; *Inorg. Chem.* **2016**, *55,* 7617−7629.
[163] *Molecularly imprinted polymers as receptors for assays of antibiòtics;* Tarannum, N.; Hendrickson, O. D.; Khatoon, S.; Zherdev, A. V.; Dzantiev, B. B.; *Crit. Rev. Anal. Chem.* **2019**, 1–20.
[164] *Molecular recognition of N-protected dipeptides by pseudopeptidic macrocycles: a comparative study of the supramolecular complexes by ESI-MS and NMR;* Alfonso, I.; Bolte, M.; Bru, M.; Burguete, M. I.; Luis, S. V.; Vicent, C.; *Org. Biomol. Chem.* **2010**, *8,* 1329–1339.
[165] *Recognition of Free Tryptophan in Water by Synthetic Pseudopeptides: Fluorescence and Thermodynamic Studies;* Martí-Centelles, V.; Izquierdo, M. A.; Burguete, M. I.; Galindo, F.; Luis, S. V.; *Chem. Eur. J.* **2014**, *20,* 7465 – 7478.
[166] *Towards functional bionanomaterials based on self-assembling cyclic peptide nanotubes;* Brea, R. J.; Reiriz, C.; Granja, J. R.; *Chem. Soc. Rev.* **2010**, *39,* 1448-1456.
[167] (a) *Bioinspired Chemistry Based on Minimalistic Pseudopeptides;* Luis, S. V.; Alfonso, I.; *Acc. Chem. Res.* **2013**, *47*, 112-124, (b) *The synthesis of peptides and proteins containing non-natural amino acids;* Hodgson, D. R. W.; Sanderson, J. M.; *Chem. Soc. Rev.* **2004**, *33*, 422-430.

racemization, rearrangements, conformational subtleties, physical properties like solubility or stereochemical control, sheer molecular size or number of stereogenic centers.[168] However, amino acids are a type of essential building blocks due to their high functional density, their structural variability and the information associated to their conformational preferences. The combination of natural and non-natural components, designed using the knowledge gathered from natural systems, could achieve ideally the desired functionalities with low molecular weight molecules. Thus, the building of small model compounds can be argued by the fact that activity in peptides is associated with a small specific peptidic fragment and has been used for the understanding of the structural parameters and factors determining the properties of interest in proteins and peptides.[169]

Hence, during the last decades, researchers have used supramolecular interactions in order to obtain biological or biomimetic molecular architectures that are capable of performing functions of extreme complexity.[170] So that, numerous types of pseudopeptides have been reported to display important properties, being able to form ordered structures and participate in different processes, efficiently mimicking the properties of natural systems. Moreover,

---

[168] (a) Hiemstra, H. *The synthesis of optically active a-amino acids;* Williams, R. H.; Pergamon Press, Oxford, **1989**. ISBN 0-08-035939-6, (b) *Aminoacid-derived mercaptoimidazoles;* Crépin, A.; Wattier, N.; Petit, S.; Bischoff, L.; Fruit, C.; Marsais, F.; *Org. Biomol. Chem.* **2009**, 7, 128-134.
[169] *Peptidomimetics;* Wu, Y.-D; Gellman, S.; *Acc. Chem. Res.* **2008**, *41*, 1231-1232.
[170] (a) *Structural Architectures with Toughening Mechanisms in Nature: A Review of the Materials Science of Type-I Collagenous Materials;* Yang, W.; Meyers, M. A.; Ritchie, R. O.; *Prog. Mater. Sci.* **2019**, 103, 425–483, (b) *Biomimetic Architectures for Peripheral Nerve Repair: A Review of Biofabrication Strategies;* Wieringa, P. A.; Gonçalves de Pinho, A. R.; Micera, S.; Van Wezel, R. J. A.; Moroni, L.; *Adv. Healthcare Mater.* **2018**, *7*, 1701164, (c) *Tethered Membrane Architectures—Design and Applications;* Andersson, J; Köper, I; Knoll, W; *Front. Mater.* **2018**, *5*, 55, (d) *Nano/Micro-Manufacturing of Bioinspired Materials: a Review of Methods to Mimic Natural Structures;* Zhang, C.; Mcadams, D. A.; Grunlan, J. C.; *Adv. Mater.* **2016**, *28*, 6292–6321, (e) *Design and synthesis of (S)- and (R)-a-(phenyl)- ethylamine-derived NH-type ligands and their application for the chemical resolution of a-amino acids;* Takeda, R.; Kawamura, A.; Kawashima, A.; Moriwaki, H.; Sato, T.; Acena, J. L.; Soloshonok, V. A.; *Org. Biomol. Chem.* **2014**, *12*, 6239-6249, (f) *[2,3]-Sigmatropic Rearrangement of Allylic Selenimides: Strategy for the Synthesis of Peptides, Peptidomimetics, and N-Aryl Vinyl Glycines; Armstrong, A.;* Emmerson, D. P. G.; Milner, H. J.; Sheppard, R. J.; *J. Org. Chem.* **2014**, *79*, 3895-3907, (g) *Synthesis of libraries of peptidomimetic compounds containing a 2-oxopiperazine unit in the main chain;* Suwal, S.; Kodadek, T.; *Org. Biomol. Chem.* **2013**, *11*, 2088- 2092, (h) *A New Approach to the Synthesis of Peptidomimetic Renin Inhibitors: Palladium-Catalyzed Asymmetric Allylation of Acyclic Alkyl Aryl Ketones;* Hanessian, S.; Chénard, E.; *Org. Lett.* **2012**, *14*, 3222-3225, (i) *Serine Protease Inhibition by a Silanediol Peptidomimetic;* Singh, S.; Sieburth, S. M.; *Org. Lett.* **2012**, *14*, 4422-4425, (i) *Peptoid Macrocycles: Making the Rounds with Peptidomimetic Oligomers;* Yoo, B.; Shin, S. B. Y.; Huang, M. L.; Kirshenbaum, K.; *Chem. Eur. J.* **2010**, *16*, 5528-5537.

many peptidomimetics systems are able to interact selectively with different molecules of biological or environmental interest.[171]

In this regard, the Sustainable and Supramolecular chemistry group has been developing different families of pseudopeptidic systems, most of them with C_2 symmetry, prepared by combination of natural (amino acids, mainly valine and phenylalanine) and abiotic units do not present in natural peptides and proteins. One of the simplest pseudopeptides involves just two amino acids linked by a diamine spacer (Figure 23). This general structure presents a high potential of structural diversity through changes in the central spacer, the amino acid unit or via the functionalization of any of the amino groups present in the molecule.

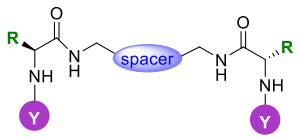

Figure 23 Schematic representation of C2 symmetric pseudopeptidic structure.

The multiple molecular diversity allows to fine tune the sites for supramolecular interactions. These compounds contain two kinds of nitrogen atoms, with different coordination capabilities, connected through a chiral backbone. The amine and amide groups allow the interaction through hydrogen bonding, while the spacer, the side chains and the groups attached to the amino acid fragment can participate in π-π or hydrophobic interactions. Furthermore, this kind of compounds provides ligands with high structural and conformational flexibility. Their properties can be easily tuned by the selection of the appropriate N-substituents, R carbon substituents and the spacer, which is involved in hydrophobic, and π-π interactions or introducing additional functionalities (Figure 24).

[171] (a) *Synthesis and study of a cyclophane displaying dual fluorescence emission: a novel ratiometric sensor for carboxylic acids in organic medium;* Galindo, F.; Becerril, J.; Burguete, M. I.; Luis S. V.; Vigara, L.; *Tetrahedron Lett.* **2004**, *45*, 1659-1662, (b) *Chiral bis(amino amides) as chiral solvating agents for enantiomeric excess determination of a-hydroxy and arylpropionic acids;* Altava, B.; Burguete, M. I.; Carbó, N.; Escorihuela, J.; Luis, S. V.; *Tetrahedron Asymm.* **2010**, *21*, 982-989, (c) *Bis(amino amides) derived from natural amino acids as chiral receptors for N-protected dicarboxylic amino acids;* Altava, B.; Burguete, M. I.; Carbó, N.; Luis, S. V.; Martí, V.; Vicent, C.; *Tetrahedron Lett.* **2013**, *54*, 72-79.

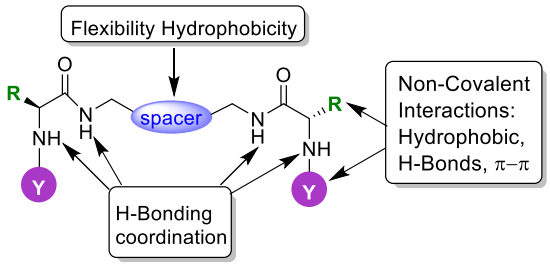

Figure 24 Schematic representation of the interactions present in C2 symmetric pseudopeptidic structures.

Initial reports in the 1990s on the supramolecular chemistry of simple C2 pseudopeptides reported by Kilburn,[172] Burrows,[173] Hamilton,[174] and others[175] involved in most cases the use of aromatic diamine spacers.[176] However, our group initially focused on systems derived from R,ω-alkyldiamines (H_2N-$(CH_2)_n$-NH_2), in order to exploit their conformational flexibility.[45]

The Sustainable and Supramolecular chemistry group not only has synthetized *C_2* symmetric open-chain pseudopeptidic structures, it is also possible to find macrocyclic structures of type I or II (Figure 25).

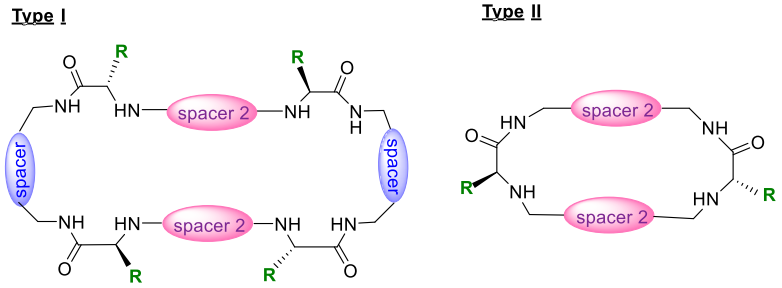

Figure 25 Schematic representation of C2 symmetric pseudopeptidic macrocycles.

For the synthesis of these macrocyclic pseudopeptides I and II, the corresponding macrocyclization processes have been based on the

---

[172] *Identification of Sequence-Selective Receptors for Peptides with a Carboxylic Acid Terminus;* Fessmann, T.; Kilburn, J. D.; *Angew. Chem.* Int. Ed. **1999**, *38*, 1993–1996.
[173] *Optically Active Difunctionalized Dioxocyclam Macrocycles: Ligands for Nickel-Catalyzed Oxidation of Alkenes;* Wagler, T. R.; Fang, Y.; Burrows, C. J.; *J. Org. Chem.* **1989**, *54*, 1584–1589.
[174] *Synthesis and Structure of Chiral Macrocycles Containing 2,20-Bipyridine Subunits;* Hopkins, R. B.; Albert, J. S.; Van Engen, D.; Hamilton, A. D.; *Bioorg. Med. Chem.* **1996**, *4*, 1121–1128.
[175] *Discovery of Sequence-Selective Peptide Binding by Synthetic Receptors Using Encoded Combinatorial Libraries;* Still, W. C.; *Acc. Chem. Res.* **1996**, *29*, 155–163.
[176] (a) *Catalysis via a Minimalist Interpretation of a Metalloprotein;* Dangel, B.; Clarke, M.; Haley, J.; Sames, D.; Polt, R.; *J. Am. Chem. Soc.* **1997**, *119*, 10865–10866, (b) *Amino Acid Containing Anion Receptors;* Kubik, S.; *Chem. Soc. Rev.* **2009**, *38*, 585–605, (c) *The Design and Evaluation of Heparin-Binding Foldamers;* Choi, S.; Clements, D. J.; Pophristic, V.; Ivanov, I.; Vemparala, S.; Bennett, J. S.; Klein, M. L.; Winkler, J. D.; DeGrado, W. F.; *Angew. Chem.* Int. Ed. **2005**, *44*, 6685–6689.

preorganization induced by conformational elements,[177] configurational factors,[178] or through the use of anionic templates.[179]

Some of those systems are able to display interesting features, behaving as organogelators[180] or acting as 'in vivo' fluorescent pH probes.[181] They are also capable to act as selective receptors for substrates of biological relevance,[182] as minimalistic molecular machines,[183] as ligands for the preparation of enantioselective catalysts or as chiral solvating agents.[184]

Due to this variety of properties, one part of the present work is focused on the preparation and study of different families of pseudopeptides derived from several amino acids, mainly Valine and Phenylalanine.

---

[177] (a) *An efficient β-turn directed cyclization of simple peptidomimetics;* Adrián, F.; Burguete, M. I.; Luis, S. V.; Miravet, J. F.; Querol, M.; García-España, E.; *Tetrahedron Lett.* **1999**, *40*, 1039-1040, (b) *Efficient Macrocyclization of U-Turn Preorganized Peptidomimetics: The Role of Intramolecular HBond and Solvophobic Effects;* Becerril, J.; Bolte, M.; Burguete, M. I.; Galindo, F.; García-España, E.; Luis, S. V.; Miravet, J. F.; *J. Am. Chem. Soc.* **2003**, *125*, 6677-6686.

[178] (a) *Efficient syntheses of new chiral peptidomimetic macrocycles through a configurationally driven preorganization;* Bru, M.; Alfonso, I.; Burguete, M. I.; Luis, S. V.; *Tetrahedron Lett.* **2005**, *46*, 7781- 7785, (b) *Designed Folding of Pseudopeptides: The Transformation of a Configurationally Driven Preorganization into a Stereoselective Multicomponent Macrocyclization Reaction;* Alfonso, I.; Bolte, M.; Bru, M.; Burguete, M. I.; Luis, S. V.; *Chem.-Eur. J.* **2008**, *14*, 8879-8891.

[179] (a) *Macrocyclization Reactions: The Importance of Conformational, Configurational, and Template-Induced Preorganization;* Martí-Centelles, V.; Pandey, M. D.; Burguete, M. I.; Luis, S. V.; *Chem. Rev.* **2015**, *115*, 8736-8834, (b) *Anion-Templated Syntheses of Pseudopeptidic Macrocycles;* Bru, M.; Alfonso, I.; Burguete, M. I.; Luis, S. V.; *Angew. Chem.* Int. Ed. **2006**, *45*, 6155-6159, (c) *Supramolecular Control for the Modular Synthesis of Pseudopeptidic Macrocycles through an Anion-Templated Reaction;* Alfonso, I.; Bolte, M.; Bru, M.; Burguete, M. I.; Luis, S. V.; Rubio, J.; *J. Am. Chem. Soc.* **2008**, *130*, 6137-6144, (d) *Macrocycle Synthesis by Chloride Templated Amide Bond Formation;* Martí-Centelles, V.; Burguete, M. I.; Luis, S. V.; *J. Org. Chem.* **2016**, *81*, 2143–2147.

[180] (a) *Minimalist peptidomimetic cyclophanes as strong organogelators;* Becerril, J.; Burguete, M. I.; Escuder, B.; Luis, S. V.; Miravet, J. F.; Querol, M.; *Chem. Commun.* **2002**, *7*, 738-739, (b) *Selfassembly of small peptidomimetic cyclophanes;* Becerril, J.; Burguete, M. I.; Escuder, B.; Galindo, F.; Gavara, R.; Miravet, J. F.; Luis, S. V.; Peris, G.; *Chem. Eur. J.* **2004**, *10*, 16, 3879-3890, (c) *Use of fluorescence spectroscopy to study polymeric materials with porous structure based on imprinting by self assembled fibrillar networks;* Burguete, M. I.; Galindo, F.; Gavara, R.; Izquierdo, M. A.; Lima, J. C.; Luis, S. V.; Parola, A. J.; Pina, F.; *Langmuir* **2008**, *24*, 17, 9795-9803, (d) *Time resolved fluorescence of naproxen in organogel medium;* Burguete, M. I.; Izquierdo, M. A.; Galindo, F.; Luis, S. V.; *Chem. Phys. Lett.* **2008**, *460*, 4-6, 503-506.

[181] *Synthetic macrocyclic peptidomimetics as tunable pH probes for the fluorescence imaging of acidic organelles in live cells;* Galindo, F.; Burguete, M. I.; Vigara, L.; Luis, S. V.; Kabir, N.; Gavrilovic, J.; Russell, D. A.; *Angew. Chem. Int. Ed.* **2005**, *44*, 40, 6504-6508.

[182] *Novel peptidomimetic macrocycles showing exciplex fluorescence;* Burguete, M. I.; Galindo, F.; Izquierdo, M. A.; Luis, S. V.; Vigara, L., *Tetrahedron* **2007**, *63*, 38, 9493-9501.

[183] *A hydrogen-bonding-modulated molecular rotor: Environmental effect in the conformational stability of peptidomimetic macrocyclic cyclophanes;* Alfonso, I.; Burguete, M. I.; Luis, S. V.; *J. Org. Chem.* **2006**, *71*, 6, 2242-2250.

[184] *Homogeneous and supported copper complexes of cyclic and open-chain polynitrogenated ligands as catalysts of cyclopropanation reactions;* Adrián, F.; Burguete, M. I.; Fraile, J. M.; García, J. I.; García, J.; García-España, E.; Luis, S. V.; Mayoral, J. A.; Royo, A. J.; Sánchez, M. C.; *Eur. J. Inorg. Chem.* **1999**, *12*, 2347-2354.

2.1 Supramolecular materials involving pseudopeptidic compounds

2.1.1 Gels

As previously mentioned, several families of pseudopeptides have shown relevant self-assembly properties.[185] The Supramolecular and Sustainable chemistry group has synthesized and studied different amphiphilic pseudopeptides containing long aliphatic tails attached to the two nitrogen atoms of the C2 symmetric pseudopeptides.[186] They have investigated how a variety of pseudopeptides of this family of compounds, similar from those presented in the following chapters, have interesting properties as organogelators and hydrogelators. For example, it was demonstrated that the intermolecular hydrogen bonding through the central amine NH group in the spacer is responsible for the formation of supramolecular aggregates leading to the generation of hydrogels (Figure 26).[187] Detailed studies of the self-association process allowed to observe that, in some instances, this process can be controlled by external stimuli and crystallographic data highlighted the key role of the amino acid side chain in the self-association process.[188]

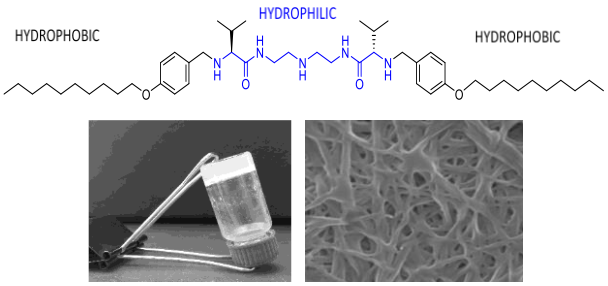

Figure 26 Chemical structure of a pseudopeptidic hydrogelator (top) and its hydrogel image and its corresponding microscopic morphology (SEM) (down).[187]

[185] *Understanding the Expression of Molecular Chirality in the Self-Assembly of a Peptidomimetic Organogelato;* Becerril, J.; Escuder, B.; Miravet, J. F.; Gavara, R.; Luis, S. V.; *Eur. J. Org. Chem.* **2005,** *3,* 481-485.
[186] *Gemini amphiphilic pseudopeptides: synthesis and preliminary study of their self-assembling properties;* Rubio, J.; Alfonso, I.; Burguete, M. I.; Luis, S. V.; *Tetrahedron Lett.* ***2010****, 51,* 5861-5867.
[187] *Synthesis and organogelating ability of bis-urea pseudopeptidic compounds;* Rubio, J.; Martí-Centelles, V.; Burguete, M. I.; Luis, S. V.; *Tetrahedron,* **2013**, *69,* 2302-2308.
[188] *Crystal structures of the HCl salts of pseudopeptidic macrocycles display "knobs into holes" hydrophobic interactions between aliphatic side chains;* Alfonso, I.; Bolte, M.; Bru, M.; Burguete, M. I.; Luis, S. V.; *CrystEngComm.* **2009**, *11,* 735-738.

The formation of the gels can be affected by different stimuli. Thus, the external pH stimulus can be useful to obtain hydrogels from amphiphilic peptides.[189] For instance, the Rajagopal group prepared a new class of peptide compounds whose hydrogelator capacity depended on the state in which the molecules in solution would be found and this state depended on the pH of the medium.[190]

Pseudopeptidic gels have been studied in the field of substances' delivery as one of the most important application.[191] In regard to perfume delivery, during the nineties, patents describing volatile species delivery technologies started to grow in number. The general objective consisted in developing devices capable of slowly dispensing fragrances to the surroundings in the long term.[192] The role of gels in the process revolves around their swelling properties that can be exploited in materials. These devices release volatile particles thanks to osmotic diffusion of the specie from the swollen gel to new water in the environment.

Similar process take place for drug release, being also one of the most relevant applications.[193] The drug is trapped into the fibres of the gel formed by the substrate capable of slowly dispensing it through a membrane to another media.[194]

---

[189] *Amphiphilic peptides and their cross-disciplinary role as building blocks for nanoscience;* Cavalli, S.; Albericio, F.; Kros, A.; *Chem. Soc. Rev.* **2010**, *39,* 1, 241-263.

[190] (a) *Probing the importance of lateral hydrophobic association in self-assembling peptide hydrogelators;* Rajagopal, K.; Ozbas, B.; Pochan, D. J.; Schneider, J. P.; *Eur. Biophys. J.* **2006**, *35,* 2, 162-169, (b) *Responsive hydrogels from the intramolecular folding and self-assembly of a designed peptide;* Schneider, J. P.; Pochan, D. J.; Ozbas, B.; Rajagopal, K.; Pakstis, L.; Kretsinger, J.; *J. Am. Chem. Soc.* **2002**, *124,* 50, 15030-15037.

[191] (a) *Head Group Modulated pH Responsive Hydrogel of Amino Acid-Based Amphiphiles: Entrapment and Release of Cytochrome c and Vitamin B12;* Shome, A.; Debnath, S.; Das, P. K.; *Langmuir* **2008**, *24,* 4280−4288, (b) *Deamidation of pseudopeptidic molecular hydrogelators and its application to controlled release,* Angulo-Pachón, C. A.; Navarro-Barreda, D.; Rueda, C. M.; Galindo, F.; Miravet, J. F.; *J. Colloid Interface Sci.* **2017**, *505,* 1111-1117.

[192] *Release of bioactive volatiles from supramolecular hydrogels: influence of reversible acylhydrazone formation on gel stability and volatile compound evaporation;* Buchs (née Levrand), B.; Fieber, W.; Vigouroux-Elie, F.; Sreenivasachary, N.; Lehn, J.-M.; Herrmann, A.; *Org. Biomol. Chem.* **2011**, *9,* 2906-2919.

[193] *Self-assembled L-alanine derivative organogel as in situ drug delivery implant: characterization, biodegradability, and biocompatibility;* Wang, K.; Jia, Q.; Han, F.; Liu, H.; Li, S.; *Drug Dev. Ind. Pharm.* **2010**, *36,* 1511–1521.

[194] *Insights into low molecular mass organic gelators: a focus on drug delivery and tissue engineering Applications;* Skilling, K. J.; Citossi, F.; Bradshaw, T. D.; Ashford, M.; Kellam, B.; Marlow, M.; *Soft Matter* **2014**, *237*, 10.

Moreover, pseudopeptidic gels have been investigated in different fields such as in cosmetics,[195] catalysis[196] or biomedical applications.[197]

2.1.2 Solid state

The selfassembly behavior of pseudopeptides can be studied in solid state using different techniques. In this regard,the Sustainable and Supramolecular chemistry group have characterized the selfassembly of open chain and macrociclic pseudopeptides using SEM, TEM, X-Ray difraction or FT-IR. For exemple, the microscopy studies revealed large differences in the morphology of the selfassembling micro/nanostructures of different pseudopeptidic macrocycles, depending on the macrocyclic chemical structures illustrated in Figure 27.[198] The presence of additional methylene groups or the change from para to meta geometry of the aromatic phenylene backbone moiety triggered self-assembly process. Also, the nature of the side chain played a fundamental role in some nanostructures, thus producing structures from long fibers to spheres which were obtained in different solvents and on different surfaces. Therefore, the chemical information for the self-assembly was contained in the molecular structure. The self-assembly of these pseudopeptidic macrocycles was dictated by a synergic action of hydrogen-bonding and π–π interactions.

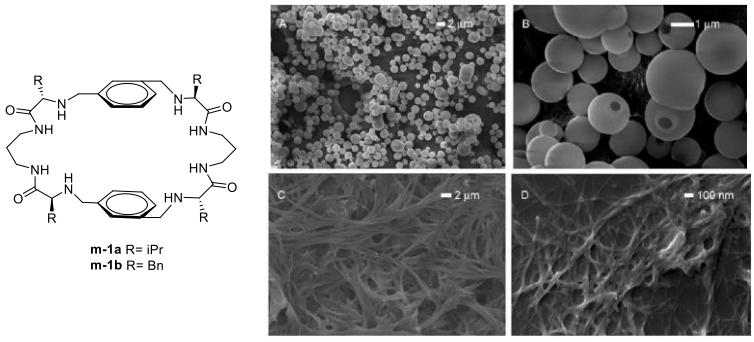

Figure 27 (a,b) SEM images of m-1b grown from $CHCl_3$/MeOH (9:1) dried onto an aluminum surface; and SEM images of m-1a grown from (c) CH_3CN/MeOH (3:1) dried onto an aluminum surface, and (d) $CHCl_3$/MeOH (9:1) dried onto a glass surface.[198]

---

[195] *Organogels for cosmetic and dermo-cosmetic applications-classification, preparation and characterization of organogel formulations-part I;* Kirilov, P.; Le cong Anh, K.; Denis, A.; Rabehi, H.; Rum, S.; Villa, C.; Haftek, M.; Pirot, F.; *Household Pers. Care Today* **2015**, *10,* 15–19.
[196] *Peptide-Based Molecular Hydrogels as Supramolecular Protein Mimics;* Singh, N.; Kumar, M.; Miravet, J. F.; Ulijn, R. V.; Escuder, B.; *Chem. Eur. J.* **2017**, *23,* 981-993.
[197] *Supramolecular Phase-Selective Gelation by Peptides Bearing Side-Chain Azobenzenes: Effect of Ultrasound and Potential for Dye Removal and Oil Spill Remediation;* Bachl, J.; Oehm, S.; Mayr, J.; Cativiela, C.; Marrero-Tellado, J. J.; Díaz, D. D.; *Int. J. Mol. Sci.* **2015**, *16,* 11766-11784.
[198] *Structural Diversity in the Self-Assembly of Pseudopeptidic Macrocycles;* Alfonso, I.; Bru, M.; Burguete, M. I.; García-Verdugo, E.; Luis, S. V.; *Chem. Eur. J.,* **2010***, 16,* 1246-1255.

Besides, the self-assembly properties of open chain bis(amino amides) with C2-symmetry have been studied by X-ray difraction as suitable crystals were obtained for X-ray diffraction (Figure 28).[199] Thus, the role of the different structural parameters as the amino acid residue, the length and nature of the spacer were studied. In regard to aminoacid residue, different behavior was observed. Polar intermolecular interactions stabilized a β-sheet-like structure for all *L*-Val pseudopeptidic compounds, while *L*-Phe pseudopeptidic compounds leaded to display folding conformation of the side chain. They also observed different behaviour depending on the aliphatic spacers of the pseudopeptidic compounds. Thus, *L*-Phe compounds with enough length in the aliphatic spacer preferred a folding conformation of the side chain stabilized by π-π intramolecular interactions. Overall, this study demonstrated the importance of the spacer and amino acid residue to form different conformations.

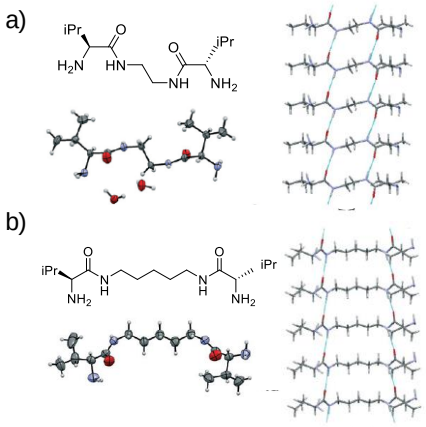

Figure 28 Molecular structure, its representation of the fully extended conformations found in the crystal structure and its hydrogen bonding network in the formation of pseudopeptidic β-sheet-like stacks for Val derivative for the molecules in (a) and (b).[200]

Moreover, the family of different amphiphilic pseudopeptides containing long aliphatic tails attached to the two nitrogen atoms of the C2 symmetric pseudopeptides[163] also showed some interesting properties in terms of their self-assembly in the solid state.[200] The family of gemini amphiphilic pseudopeptidic compounds (GAPs) synthesized presented different self-aggregation properties

[199] *The role of the side chain in the conformational and self-assembly patterns of C2-symmetric Val and Phe pseudopeptidic derivatives;* Gorla, L.; Martí-Centelles, V.; Altava, B.; Burguete, M. I.; Luis, S. V.; *Cryst.Eng.Comm.* **2019**, *21,* 2398-2408.
[200] *Stimulus responsive self-assembly of Gemini Amphiphilic Pseudopeptides;* Rubio, J.; Alfonso, I.; Burguete, M. I.; Luis S. V.; *Soft Matter* **2011**, *7*, 10737–10748.

depending on the solvent in which the experiment was carried out. The media used for the researchers were from apolar solvent (chloroform) to polar solvent (MeOH, MeOH:H_2O, using different pH). They observed the formation of a large variety of nanostructures in the solid state, rendering fibres (in polar environments at neutral or basic pH), spheres or vesicles (upon protonation at acidic pH values) or amorphous materials (in chloroform). The H-bonds with the polar solvent unfolded the GAPs leading to an extended conformation which selfassemble upon concentration through intermolecular H-bonding and van der Waals contacts producing the fibers. The vesicles were formed due to the intermolecular hydrophobic contacts between tails, in a cationic surfactant-like mode. Finally, the amorphous materials in chloroform were produced because of the ability of the GAPs to establish intramolecular H-bond interactions in a partially folded conformation. This study revealed the importance of the solvent, as well as the different stimulus (for example, pH) that can affect to the formation of the aggregate.

Therefore, although the morphology and properties of self-assembled structures obtained in the solid state depend on structural parameters, they can also be modulated through external stimuli, according to the delicate balance of structural and environmental factors. Thus, Ke and collaborators reported a smooth and reversible transition between nanofibers and vesicles from a controllable self-assembly of an amphiphilic tripeptide–bipyridine conjugate.[201]

2.1.3 Other materials in solution

As named before, nature presents complex and elegant examples of adaptive and intelligent systems created by self-assembly. Significant effort was devoted to understanding these sophisticated systems in solution. Different supramolecular compounds with high order and complexity have been created through a self-assembly process. Peptide-based self-assembling building blocks can serve as suitable platforms to construct systems showing diverse features and applications. These building blocks provide greater biocompatibility and biodegradability as well as the complex found in nature. In this regard, Ekiz and collaborators created a new family of peptide constructs with well-defined

[201] *Morphological Transformation between Nanofibers and Vesicles in a Controllable Bipyridine_Tripeptide Self-Assembly;* Ke, D.; Zhan, C.; Li, A. D. Q.; Yao, J.; *Angew. Chem. Int. Ed.* **2011**, *50,* 3715-3719.

characteristics through a self-assembly process.[202] The morphology and function of the resulting structures were manipulated at the molecular level by altering the number, type and sequence of amino acids, or exposing the system to external stimuli such as pH, temperature, electric or magnetic fields, light, and sound in solution.

On this matter, surfactants are mainly used as detergents, generating the necessity of the development of less toxic and more ecological surfactants (greater biodegradability and biocompatibility). Therefore, one of the lines of research to achieve these objectives consists in the synthesis of surfactants derived from amino acids. This class of compounds is a very efficient alternative to conventional synthetic surfactants, due to its multifunctionality and the use of renewable raw materials. For example, lipoamino acids are amphiphilic molecules which contain an amino acid as a hydrophilic part and a hydrocarbon chain as a hydrophobic part. These compounds have multifunctionality, biodegradability and low toxicity, thus being an interesting alternative to conventional surfactants.[203]

The combination of peptides or amino acids in the polar region and hydrocarbon chains of variable length in the apolar region, gived rise to amphiphilic compounds with a high surfactant capacity. Due to the great variety of amino acids and aliphatic chains that can be used, the possible number of amphiphilic compounds is very high and the surfactants derived from amino acids have been classified into three large groups.[204] They present different physicochemical and biological properties depending on their structure (Figure 29).

[202] (a) *Self-assembled peptide nanostructures for functional materials;* Ekiz, M. S.; Cinar, G.; Khalily, M. A.; O Guler, M.; *Nanotechnol.* **2016**, *27, 40,* 402002, (b) *Presentation of functional groups on selfassembled supramolecular peptide nanofibers mimicking glycosaminoglycans for directed mesenchymal stem cell differentiation;* Yasa, O.; Uysal, O.; Ekiz, M. S.; Guler, M. O.; Tekinay, A. B.; *J. Mater. Chem. B* **2017**, *5,* 48904900.

[203] *Chemical Structure/Property Relationship in Single-Chain Arginine Surfactants;* Morán, C.; Clapes, P.; Comelles, F.; Garcia, T.; Perez, L.; Vinardell, P.; Mitjans, M.; Infante, M. R.; *Langmuir* **2001**, *17,* 16, 5071-5075.

[204] *"Green" amino acid-based surfactants;* Morán, C.; Pinazo, A.; Pérez, L.; Clapés, P.; Angelet, M.; García, M. T.; Vinardell, M. P.; Infante, M. R.; *Green Chem.* **2004**, *6,* 5, 233-240.

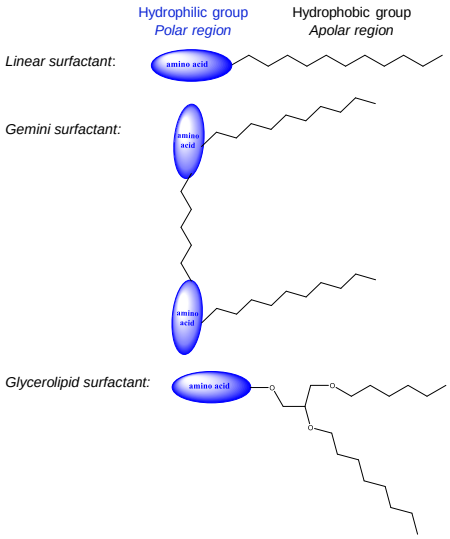

Figure 29 Structures of surfactants derived from amino acids.

The fundamental features of each of these types are:

- *Linear surfactants.* They consist in an amino acid (polar head) attached to a hydrocarbon chain (apolar region). The amino acids used can be acidic, basic or neutral, and bind to the aliphatic chain through the α-amino acid and α-COOH groups or to the functional groups of the side chain. They may contain acyl-amino acid, N-alkyl amide, and O-alkyl ester groups.[205]

- *Gemini surfactants.* As mentioned before, its structure is formed by two aliphatic chains and two hydrophilic groups (amino acids) linked together by a spacer chain.[206] These surfactants have superior surface activity properties than linear surfactants.

- *Glycerolipids.* They consist of a polar amino acid head and one or two hydrophobic portions attached to a glycerol skeleton.[207] Their emulsifying and encapsulating properties make them ideal candidates for application in food and cosmetic preparations.

---

[205] *Non-conventional Surfactants from Amino Acids and Glycolipids" Structure, Preparation and Properties;* Infante, M. R.; Pinazo, A.; Seguer, J.; *Colloids Surf A* **1997**, *123-124,* 49-70.
[206] *Dimeric (Gemini) Surfactants: Effect of the Spacer Group on the Association Behavior in Aqueous Solution;* Zana, R.; *J. Colloid Interface Sci.* **2002**, *248,* 2, 203-220.
[207] *A Novel Family of L-Amino Acid-Based Biodegradable Polymer-Lipid Conjugates for the Development of Long-Circulating Liposomes with Effective Drug-Targeting Capacity;* Metselaar, J. M.; Bruin, P.; De Boer, L. W. T.; De Vringer, T.; Snel, C.; Oussoren, C.; Wauben, M. H. M.; Crommelin, D. J. A.; Storm, G.; Hennink, W. E.; *Bioconjugate Chem.* **2003**, *14,* 6, 1156-1164.

Therefore, the 20 standard amino acids constitute a versatile tool box for synthesis of surfactants. Anionic, cationic and zwitterionic amphiphiles can be prepared and surfactants with several functional groups can be obtained by the proper choice of starting amino acid.

The Sustainable and Supramolecular chemistry group carried out studies of gemini amphiphilic pseudopeptidic compounds (GAPs) in the solution states using different techniques as NMR, UV, CD, FT-IR, optical microscopy and fluorescence spectroscopy.[208] Thus, high stability O/W emulsions have been observed using GAPs which allow the tuning of the self-assembling properties by slight modifications in the chemical structures (Figure 30).

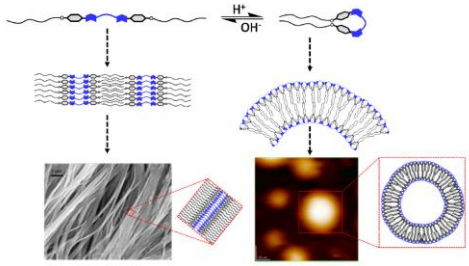

Figure 30 Representation of the dual self-assembly of Gemini pseudopeptides to form either fibers or vesicles.[208]

As mention above, it is important to determine the CAC of GAPs. Hence, the CMC values for these GAPs were ontained by fluorescence spectroscopy and compared with those obtained for other surfactants, both linear and gemini.[200] The results revealed that CMC values of the new synthesized GAPs (4-25 μM)[208] were much better than those of conventional linear surfactants (1-16 mM). This fact was to be assumed because of low CMC values which were one of the main improvement properties of geminal surfactants regarding to conventional surfactants. However, in addition, the CMC values obtained by the new synthesized GAPs were relatively good compared to the geminal surfactants described in the literature, whose CMC values are around 0.1-0.001 mM.[209]

---

[208] (a) *Structure-membrane activity relationship in a family of peptide-based gemini amphiphiles: An insight from experimental and theoretical model systems;* Korchowiec, B.; Gorczyca, M.; Korchowiec, J.; Rubio-Magnieto, J.; Lotfallah, A. H.; Luis, S. V.; Rogalska, E.; *Colloids Surf., B* **2016**, *146,* 54–62, (b) *Synthesis of second-generation self-assembling Gemini Amphiphilic Pseudopeptides;* Lotfallah, A. H.; Burguete, M. I.; Alfonso, I.; Luis, S. V.; *J. Colloid Interface Sci.* **2020**, *564,* 52–64.

[209] (a) *Gemini Surfactants;* Menger, F. M.; Keiper, J. S.; *Angew. Chem. Int. Ed.* **2000**, *39,* 11, 1906-1920, (b) *Gemini Surfactants: A New Class of Self-Assembling Molecules;* Menger, F. M.; Littau, C. A.; *J. Am. Chem. Soc.* **1993**, *115,* 22, 10083-10090.

2.1.4 Molecular receptors

Selective recognition of molecules is a common yet crucial phenomenon in nature. It is responsible for many functions, such as sensing the environment (smell, taste), communication within multicellular organisms (hormones, neurotransmitters), communication between organisms (pheromones), and immunological response (antigen–antibody).[210] The generation of a precise functional structure usually requires large individual macromolecules, for which, activity can be associated with a small specific peptidic fragment. Therefore, the building of small peptides has been used for the understanding of the structural parameters and factors determining the properties of interest in proteins and peptides.[211,212] During last years, it has been developed a lot of studies in this field to fully understand the recognition processes taking place in nature.

The Sustainable and Supramolecular chemistry group was pioneer in developing macrocyclization strategies based on the conformational, configurational and template-induced self-organization of open-chain pseudopeptidic structures as mention above.[179] This allowed the preparation of a variety of pseudopeptidic macrocycles, including cages that have been studied for the molecular recognition of anions and dipeptides and studied for the transport of chloride through lipidic membranes.[213]

Herein, it was synthesized different families of pseudopeptidic structures which demonstrated their ability for the selective recognition of a variety of targets, leading to the development of sensing systems based, for example, in the introduction of fluorescent moieties in their structure. In this regard, intracellular pH sensors were developed revealing the interest of this kind of compounds in biological applications.[181,214] It was shown that the interactions with anions were very favorable for this type of receptors, besides, in the case of

---

[210] *Supramolecular chemical biology; bioactive synthetic self-assemblies;* Petkau-Milroy, K.; Brunsveld, L.; *Org. Biomol. Chem.* **2013**, *11,* 219-232.
[211] Kubik, S. *Supramolecular Chemistry in Water,* Wiley, **2019**.
[212] *Synthetic Peptides as Protein Mimics,* Groß A.; Hashimoto, C.; Sticht, H.; Eichler, J.; *Front. Bioeng. Biotechnol.* **2016**, *(b) Peptidomimetics;* Wu, Y-D.; Gellman, S.; *Acc. Chem. Res.* **2008**, *41,* 1231-1438.
[213] (a) *Efficient Synthesis of Pseudopeptidic Molecular Cages;* Moure, A.; Luis, S. V.; Alfonso, I.; *Chem. Eur. J.* **2012**, *18,* 5496-5500, (b) *Pseudopeptidic Cages as Receptors for N-Protected Dipeptides;* Faggi, E.; Moure, A.; Bolte, M.; Vicent, C.; Luis, S. V.; Alfonso, I.; *J. Org. Chem.* **2014**, *79,* 4590-4601.
[214] *Fluorescent macrocyclic probes with pendant functional groups as markers of acidic organelles within live cells;* Wadhavane, P. D.; Izquierdo, M. A.; Lutters, D.; Burguete, M. I.; Marin, M. J.; Russell, D. A.; Galindo, F.; Luis, S. V.; *Org. Biomol. Chem.* **2014**, *12,* 823-831.

acridine derivatives, this fact allowed the selective sensing of phosphate anions (Figure 31 N).[215] Martí-Centelles *et al.* prepared one macrocyclic pseudopeptidic molecule and the respective open chain molecule, both containing an acridine unit. The fluorescence response of these receptors to a series of acids was measured in $CHCl_3$. The results concluded that receptors were selective to $H_2PO_4^-$ versus HSO_4^-, showing that the macrocyclic receptor was more selective for $H_2PO_4^-$ than the related open chain receptor.

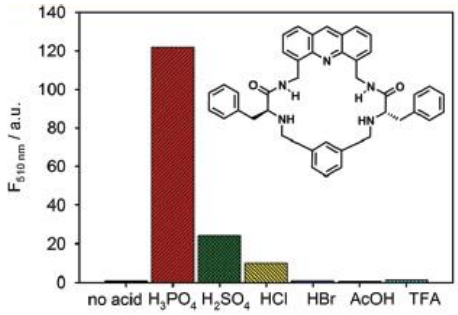

Figure 31 Normalized fluorescence intensity at 510 nm of compounds the macrocyclic compound (10 μM) upon addition of 25 equiv of each acid in $CHCl_3$. λex = 357 nm.[215]

Interaction with carboxylates was also relevant and this was exploited by developing pseudopeptides structures able to interact with amino acid derivatives,[216] including dipeptides,[164] and systems for the selective sensing of tryptophan.[165]

Moreover, different NOx sensing systems were developed by the Sustainable and Supramolecular chemistry group.[217] These receptors can also form stable complexes with metals, in particular neutral complexes formed by the complexation of divalent cations with bisdeprotonated aminoamides, their

[215] *Fluorescent Acridine-Based Receptors for $H_2PO_4^-$;* Martí-Centelles, V.; Burguete, M. I.; Galindo, F.; Izquierdo, M. A.; Kumar, D. K.; White, A. J. P.; Luis, S. V.; Vilar, R.; *J. Org. Chem.* **2012**, *77,* 490-500.

[216] (a) *Ratiometric fluorescence sensing of phenylalanine derivatives by synthetic macrocyclic receptors;* Burguete, M. I.; Galindo, F.; Luis, S. V.; Vigara, L.; *J. Photochem. Photobiol.* **2010**, *209,* 1, 61-67, (b) *Unraveling the Molecular Recognition of Amino Acid Derivatives by a Pseudopeptidic Macrocycle: ESI-MS, NMR, Fluorescence, and Modeling Studies;* Alfonso, I.; Burguete, M. I.; Galindo, F.; Luis, S. V.; Vigara, L.; *J. Org. Chem.* **2009**, *74*, 6130-6142.

[217] (a) *Nitric oxide sensitive fluorescent polymeric hydrogels showing negligible interference by dehydroascorbic acid;* Fabregat, V.; Izquierdo, M. A.; Burguete, M. I.; Galindo, F.; Luis, S. V.; *Eur. Polym. J.* **2014**, *55,* 108-113, (b) *Turn-on fluorescent probes for nitric oxide sensing based on the ortho-hydroxyamino structure showing no interference with dehydroascorbic acid;* Beltran, A.; Burguete, M. I.; Abánades, D. R.; Pérez-Sala, D.; Luis, S. V.; Galindo, F.; *Chem. Commun.* **2014**, *50,* 3579-3581.

nature and stability being affected by different structural parameters.[218] Some of these metal complexes showed interesting catalytic properties.[219]

These studies about macrocyclization strategies provided important progresses in the application of DCC (dynamic combinatorial chemistry) for the generation of new macrocyclic structures and it is also closely connected with the use of template species.[179a]

Moreover, other researchers have synthesized opened molecules derived from amino acids which adopt a tubular conformation in solution and lipid bilayer membranes.[220] The peptide-appended pillar[n]arene (n = 5, 6) derivatives synthesized were studied using the fluorescent labeling method with lipid vesicles and the kinetic measurements revealed that these molecules can efficiently mediate the transport of amino acids across lipid membranes at a very low channel-to-lipid ratio (EC_{50} = 0.002 mol %). Besides, in some cases, chiral selectivity for amino acid enantiomers was achieved, which is one of the key functions of natural amino acid channels.

2.1.5 Bioactive pseudopeptidic compounds

Cancer is the second leading cause of death globally; it means that about 1 in 6 deaths is due to this illness.[221] This disease results when cellular changes cause the uncontrolled growth and division of cells. Depend on the type of cancer, it causes rapid cell growth which some of them could result in visible growths called tumors, while others cause cells to grow and divide at a slower rate. Tumor tissues, as a result of the altered cancer-cell metabolism, are characterized by a slightly basic intracellular pH (pHi) and an acidic extracellular pH (pHe).[222] In this regard, researchers have focused on the possibility to treat cancer by changing the pH media through ions' transport

---

[218] (a) *Zinc(II) coordination polymers with pseudopeptidic ligands;* Martí-Centelles, V.; Kumar, D. K.; White, A. J. P.; Luis, S. V.; Vilar, R.; *CrytEngComm.* **2011**, *13,* 6997-7008, (b) *Copper(II) complexes of bis(amino amide) ligands: effect of changes in the amino acid residue;* Martí, I.; Ferrer, A.; Escorihuela, J.; Burguete, M. I.; Luis, S. V.; *Dalton Trans.* **2012**, *41,* 6764-6766.

[219] (a) *New chiral tetraaza ligands for the efficient enantioselective addition of dialkylzinc to aromatic aldehydes;* Burguete, M. I.; Escorihuela, J.; Luis, S. V.; Lledós, A.; Ujaque, G.; *Tetrahedron* **2008**, *64,* 9717–9724, (b) *Dual stereocontrolled alkylation of aldehydes with polystyrene-supported nickel complexes derived from alpha-amino amides;* Escorihuela, J.; Altava, B.; Burguete, M. I.; Luis, S. V.; *RSC Adv.* **2015**, *5,* 14653-14662.

[220] *Chiral Selective Transmembrane Transport of Amino Acids through Artificial Channels;* Chen, L.; Si, W.; Zhang, L.; Tang, G.; Li, Z-T.; Hou, J-L.; *J. Am. Chem. Soc.* **2013**, *135,* 2152−2155.

[221] World Health Organization, Implications of the SDGs for health monitoring-a challenge and an opportunity for all countries, World Health Statistics 2016: Monitoring Health for the SDGs Sustainable Development Goals, WHO Press, Geneva, Switzerland, **2016**.

[222] *Dysregulated pH: a perfect storm for cancer progression;* Webb, B. A.; Chimenti, M.; Jacobson, M. P.; Barber, D. L.; *Nat. Rev. Cancer* **2011**, *11,* 671 –677.

across membrane. Therefore, it was designed small peptide-like receptors for chloride that could show pH-modulated affinity and transmembrane transport abilities,[223] trying to enhance their cytotoxicity in acidic environments. Recently, it has been shown the efficacy of pseudopeptidic tripodal cages that, when protonated, selectively binded chloride and were able to transport this anion through artificial lipid bilayers.[224] This could open a new way to kill cancer cells using pH-dependent anionophores in chemotherapy.

Aside from cancer, hummankind has had to cope with other significant illness generated by microorganisms. The major groups of microorganisms are bacteria, archaea, fungi (yeasts and molds), algae, protozoa, and viruses. To understand the molecular behavior of these complex organisms, researchers tried to develop molecules with the aim of destroying them. The strategy consisted in combining natural building blocks that provide functional elements with abiotic fragments that serve as structural scaffolds. Therefore, pseudopeptidic compounds represented a crucial opportunity to explore and evaluate this approach.[225] In this regard, peptide backbone modifications were incorporated into many biologically active peptides in order to obtain active and metabolically stable analogues.[226] Hence, pseudopeptides corresponding to the antimicrobial peptide that acted on the lipid membrane of the pathogen were synthesized. In this study, it was demonstrated that most pseudopeptides exhibited a longer half-life than the peptide in the presence of serum as well as a considerable activity against test bacteria and fungi.

Recently, Gly-POX (Poly(2-oxazoline)-based glycine pseudopeptides), a host defense peptide mimic, has demonstrated to exert potent antibacterial activities

---

[223] (a) *Bis(sulfonamide) transmembrane carriers allow pH-gated inversion of ion selectivity;* Roy, A.; Biswas, O.; Talukdar, P.; *Chem. Commun.* **2017**, *53,* 3122–3125, (b) *pH-Regulated Nonelectrogenic Anion Transport by Phenylthiosemicarbazones;* Howe, E. N. W.; Busschaert, N.; Wu, X.; Berry, S. N.; Ho, J.; Light, M. E.; Czech, D. D.; Klein, H. A.; Kitchen, J. A.; Gale, P. A.; *J. Am. Chem. Soc.* **2016**, *138,* 8301–830.

[224] *pH-Dependent Chloride Transport by Pseudopeptidic Cages for the Selective Killing of Cancer Cells in Acidic Microenvironments;* Tapia, L.; Pérez, Y.; Bolte, M.; Casas, J.; Solá, J.; Quesada, R.; Alfonso, I.; *Angew. Chem. Int. Ed.* **2019**, *58,* 12465-12468.

[225] (a) *Novel Antimicrobial Agents Against Multi-drug-resistant Gram-positive Bacteria: An Overview,* Giannakaki, V.; Miyakis, S.; *Recent Pat. Anti-Infect. Drug Discovery* **2012**, *3,* 182-188, (b) *Arginine/Tryptophan-Rich Cyclic a/b-Antimicrobial Peptides: The Roles of Hydrogen Bonding and Hydrophobic/Hydrophilic Solvent-Accessible Surface Areas upon Activity and Membrane Selectivity;* Bagheri, M.; Amininasab, M.; Dathe, M.; *Chem. Eur. J.* **2018**, *24,* 14242-14253, (c) *Selectivity Modulation and Structure of a/aza-β3 Cyclic Antimicrobial Peptides;* Laurencin, M.; Simon, M.; Fleury, Y.; Baudy-Floc'h, M.; Bondon, A.; Legrand, B.; *Chem. Eur. J.* **2018**, *24,* 6191-6201, (d) *Antimicrobial peptides and plant disease control,* Montesinos, E.; *FEMS Microbiol Lett.* **2007**, *270,* 1–11.

[226] *Design, synthesis and characterization of antimicrobial pseudopeptides corresponding to membrane-active peptide;* Oh, J. E.; Hong, S. Y.; Lee, K.-H.; *J. Peptide Res.* **1999**, *54,* 129-136.

against MRSA (methicillin-resistant S. Aureus) both in vitro and in vivo.[227] S. Aureus is frequently encountered in serious nosocomial and community acquired infections and represent a severe threat to global health.[228] This bacteria presents a quick spreading of multidrug resistance, however, S. Aureus was unable to acquire resistance after repeated use of POX as the antimicrobial agent.[226]

Thus, it is noteworhy that backbone modifications can be a great tool for developing pseudopeptides with improved biological activity.[229]

3 Ionic Liquids in Supramolecular Chemistry

In the last decades, ionic liquids (ILs) have aroused great interest in the world of scientific research and among the most diverse technological and industrial sectors. Therefore, it is obvious to ask ourselves what is the meaning of ILs, from a point of chemical view, and which are the characteristics or chemical properties that have led to its great diffusion.[230]

Ionic liquids (ILs) are salts formed by very asymmetric and large ions, because of they have weaker attractive cation-anion forces than those found in conventional ionic salts, which makes them liquids in a wide range of temperatures, including room temperature in a good number of cases.[231]

The term ionic liquid is considered synonymous with "molten salt"; however, molten salts are usually liquids that consist of ions. Due to their high melting temperature, corrosion power and high viscosity, molten salts cannot be used as a liquid phase to carry out chemical reactions. Thus, the term "ionic liquids"

---

[227] *Poly(2-Oxazoline)-Based Functional Peptide Mimics: Eradicating MRSA Infections and Persisters while Alleviating Antimicrobial Resistance;* Zhou, M.; Qian, Y.; Xie, J.; Zhang, W.; Jiang, W.; Xiao, X.; Chen, S.; Dai, C.; Cong, Z.; Ji, Z.; Shao, N.; Liu, L.; Wu, Y.; Liu, R.; *Angew. Chem. Int. Ed.* **2020**, *59,* 6412–6419.

[228] *Waves of resistance: Staphylococcus aureus in the antibiotic era;* Chambers, H. F.; Deleo, F. R.; *Nat. Rev. Microbiol.* **2009**, *7,* 629-641.

[229] *Design and Synthesis of Novel Antimicrobial Pseudopeptides with Selective Membrane-Perturbation Activity;* Lee, K-H.; Oh, J-E.; *Bioorg. Med. Chem.* **2000**, *8,* 833-839.

[230] (a) *Applications of ionic liquids in the chemical industry;* Plechkova, N. V.; Seddon, K. R.; *Chem. Soc. Rev.* **2008**, *37,* 123-150, (b) *Biocompatible ionic liquids: fundamental behaviours and applications;* Gomes, J. M.; Silva, S. S.; Reis, R. L.; *Chem. Soc. Rev.* **2019**, *48,* 4317-4335, (c) *Ionic Liquids: Structure, Properties and Major Applications in Extraction/Reaction Technology;* Dupont, J.; *Chem. Inform.* **2007**, *38*, 47, (d) Poole, C. F. *Applications of ionic liquids in extraction, chromatography, and electrophoresis,* Grushka, E, Grinberg, N., Eds.; Advances in chromatography, **2007**, 45, 89-124.

[231] (a) *Ionic liquids as electrolytes;* Galínski, M.; Lewandowski, A.; Stepniak, I.; *Electrochim. Acta* **2006**, *51,* 5567–5580, (b) Rollet, A. L.; Bessada, C. *NMR Studies of Molten Salt and Room Temperature Ionic Liquids;* Webb, G. A., Eds.; Annual reports on NMR spectroscopy **2013**, 78, 149-207.

refers to other compounds that are also liquids formed exclusively by ions but with very different properties from those found in liquids from molten salts.

In this regard, ionic liquids are salts formed by organic cations and either inorganic or organic anions (Figure 32).[232] They exhibit excellent properties such as melting points lower than 100 ºC, a negligible vapor pressure and volatility, nonflammability, high ionic conductivity and ionic density and chemical and thermal stability. The potential applications of ILs are closely related to their physicochemical properties, and those depend on the interaction established between both the cation and the anion.[233] Generally for the same cation, the nature of the anion is responsible of the physical properties such as melting point or viscosity of the final IL. Thus, these properties of the ILs are lowered either by delocalizing negative charge or by increasing anion flexibility. On the other hand, elongating the cation chain length increases the viscosity of the IL, therefore increases the melting points. The nature of the ILs' components can be easily varied[234] (Figure 32) and, thus, the large structural diversity available for ILs plays an important role in our ability to define their final properties, such as electrochemical stability,[235] miscibility with water and/or organic solvents,[236] melting point[237] and viscosity.[238]

[232] *Room-Temperature Ionic Liquids: Solvents for Synthesis and Catalysis 2;* Hallet, J. P.; Welton, T.; *Chem. Rev.* **2011**, *111,* 3508-3576.
[233] (a) *Protic Ionic Liquids: Properties and Applications;* Greaves, T. L.; Drummond, C. J.; *Chem. Rev.* **2007**, *108,* 206– 237, (b) *Air and water stable ionic liquids in physical chemistry;* Endres, F.; El Abedin, S. Z.; *Phys. Chem. Chem. Phys.* **2006**, *8,* 2101–2116.
[234] *Mixtures of ionic liquids;* Niedermeyer, H.; Hallett, J. P.; Villar-Garcia, I. J.; Hunt, P. A.; Welton, T.; *Chem. Soc. Rev.* **2012**, *41,* 23, 7780-7802.
[235] *On the Solid, Liquid and Solution Structural Organization of Imidazolium Ionic Liquids;* Dupont, J.; *J. Braz. Chem. Soc.* **2004**, *15,* 341–350.
[236] *Characterization and comparison of hydrophilic and hydrophobic room temperature ionic liquids incorporating the imidazolium cation;* Huddleston, J. G.; Visser, A. E.; Reichert, W. M.; Willauer, H. D.; Broker, G. A.; Rogers, R. D.; *Green Chem.* **2001**, *3,* 156–164.
[237] (a) *Going Full Circle: Phase-Transition Thermodynamics of Ionic Liquids;* Preiss, U.; Verevkin, S. P.; Koslowski, T.; Krossing, I.; *Chem. Eur. J.* **2011**, *17,* 6508–6517, (b) *The phase behaviour of 1-alkyl-3-methylimidazolium tetrafluoroborates; ionic liquids and ionic liquid crystals;* Holbrey, J. D.; Seddon, K. R.; *J. Chem. Soc. Dalton Trans.* **1999**, 2133–2140.
[238] *Physicochemical Properties of Tungstate-Based Room-Temperature Ionic Liquids;* Qiao, Y.; Hu, J.; Li, H.; Hua, L.; Hu, Y.; Feng, B.; Hou, Z.; *J. Electrochem. Soc.* **2010**, *157,* 124–129.

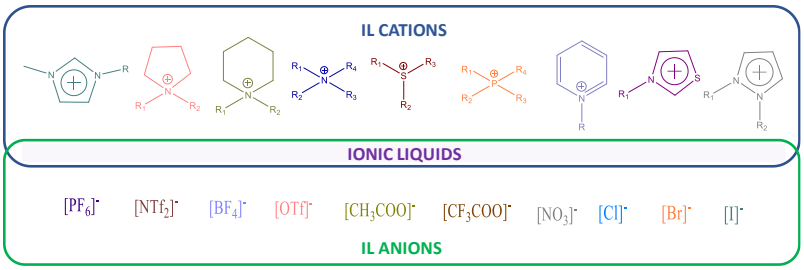

Figure 32 Most common cations and anions that form ionic liquids.

Therefore, ILs are regarded as a novel class of promising liquids, potentially applicable to multiple functions.[239] Nevertheless, some ot their properties such as their fluidity, high viscosity, and slow gas diffusivity strongly limit their applications, recyclability and separation,[240] being ILs poorly biodegradable. ILs environmental impact is strongly dependent on the structure of the cation and anion.[241]

In this regard, nowadays, ILs contain more biocompatible cations and anions, derived from relatively inexpensive, eco-friendly natural products, such as carbohydrates and amino acids.[242] Thus, Amino acid ionic liquids (AAILs) can be used as either cations or anions because they have both a carboxylic acid residue and an amino group in a single molecule providing an ability to introduce functional groups.[243] There is a wide variety of amino acids and consequently of ILs that can be prepared. Hence, the variety of functional groups present in the side chains of the amino acids enables the facile incorporation of chirality and a wide range of properties into the IL.[244] The incorporation of new functional groups into the AAIL allows considerable supramolecular interactions such as hydrogen bonding, electrostatic interactions and so on,

---

[239] *Ionic liquids for energy, materials, and medicine;* Smiglak, M.; Pringle, J. M.; Lu, X.; Han, L.; Zhang, S.; Gao, H.; MacFarlane, D. R.; Rogers, R. D.; *Chem. Commun.* **2014**, *50,* 9228-9250.
[240] *Ionic liquids and continuous flow processes: a good marriage to design sustainable processes;* García-Verdugo, E.; Altava, B.; Burguete, M. I.; Lozano, P.; Luis, S. V.; *Green Chem.* ***2015****, 17,* 2693-2713.
[241] *Ionic liquids: a pathway to environmental acceptability;* Petkovic, M.; Seddon, K. R.; Rebelo, L. P. N.; Pereira, C. S.; *Chem. Soc. Rev.* **2011**, *40,* 1383-1403.
[242] *Synthesis and Applications of Ionic Liquids Derived from Natural Sugars;* Chiappe, C.; Marra, A.; Mele, A.; *Top. Curr. Chem.* **2010**, *295,* 177-195.
[243] (a) *Amino Acid Ionic Liquids*; Ohno, H.; Fukumoto, K.; *Acc. Chem. Res.* **2007,** *40,* 1122–1129, (b) *Amino acid based ionic liquids: A green and sustainable perspective*; Kirchhecker, S.; Esposito, D.; *Curr. Opin. Green Sustainable Chem.* **2016**, *2*, 28-3, (c) *Room Temperature Ionic Liquids from 20 Natural Amino Acids*; Fukumoto, K.; Yoshizawa, M.; Ohno, H.; *J. Am. Chem. Soc.* **2005**, *127*, 2398-2399.
[244] (a) *Synthesis of chiral ionic liquids from natural amino acids;* Bao, W.; Wang, Z.; Li, Y.; *J. Org. Chem.* **2003**, *68,* 591–593, (b) *(S)-Histidine: the ideal precursor for a novel family of chiral aminoacid and peptidic ionic liquids;* Guillen, F.; Brégeon, D.; Plaquevent, J.-C.; *Tetrahedron. Lett.* **2006**, *47,* 1245–1248, (e) *Synthesis and properties of novel chiral-amine-functionalized ionic liquids;* Luo, S.; Zu, D.; Yue, H.; Wang, L.; Yang, W.; Xu, Z.; *Tetrahedron: Asymmetry* **2006**, *17,* 2028–2033.

which directly influence the IL's properties.[245] There are many advantages of amino acids, including biodegradability[246] and biological activity[247] being outstanding features to find application in all of the biological, medical, and pharmaceutical sciences.[248] The availability of amino acids as both anions and cations is another advantage, the amino acids are cheap and abundant. Therefore, these AAILs open a door to a wide range of ILs' applications.[249] In this context, ILs are attracting considerable attention as green reaction solvents,[250] catalysis,[252] energy production,[253] gas absorption,[254] new magnetic and luminescent materials[255] and electrolyte materials,[256] as well

[245] *The Relationship between the Structure and Properties of Amino Acid Ionic Liquids*; Ossowicz, P.; Klebeko, J.; Roman, B.; Janus, E.; Rozwadowski, Z.; *Molecules* **2019**, *24*, 3252.
[246] *Biodegradable ionic liquids: Part I. Concept, preliminary targets and evaluation;* Gathergood, N.; Garcia, M. T.; Scammells, P. J.; *Green Chem.* **2004***, 6,* 166–175.
[247] *Toxicity and antimicrobial activity of imidazolium and pyridinium ionic liquids.* Docherty, K. M.; Kulpa, C. F. Jr.; *Green Chem.* **2005**, *7,* 185–189.
[248] (a) *A possible means of realizing a sacrifice-free three component separation of lignocellulose rom wood biomass using an amino acid ionic liquid*; Hamada, Y.; Yoshida, K.; Asai, R-i.; Hayase, S.; Nokami, T.; *Green Chem.* **2013**, *15*, 1863, (b) *Critical Assessment of the Interaction between DNA and Choline Amino Acid Ionic Liquids: Evidences of Multimodal Binding and Stability Enhancement;* Sahoo, D. K.; Jena, S.; Dutta, J.; Chakrabarty, S.; Biswal, H. S.; *ACS Cent. Sci.* **2018**, *4*, 1642−1651.
[249] (a) *A review on nanofibers membrane with amino-based ionic liquid for heavy metal removal*; Foong, C. Y.; Wirzal, M. D. H.; Bustam, M. A.; *J. Mol. Liq.* **2020**, *297*, 111793, (b) *CO_2 absorption characteristics of amino group functionalized imidazolium-based amino acid ionic liquids;* Kang, S.; Chung, Y. G.; Kang, J. H.; Song, H.; *J. Mol. Liq.* **2020**, *297*, 111825, (c) Aggregation Behavior of Imidazolium-Based Amino Acid Ionic Liquid Surfactants in Aqueous Solution: The Effect of Amino Acid Counterions; Yang, X-J.; Zhang, P.; Lv, W.; Zhou, T.; Li, P.; Zhao, M.; *J Surfact Deterg* **2019**, *22*, 515–523.
[250] (a) *Facile N-alkylation of acridine esters with 1,3-propane sultone in ionic liquids;* Natrajan, A.; Wen, D.; *Green Chem.* **2011**, *13,* 913–921, (b) *Application of a Novel Ionic Liquid as an Alternative Green Solvent for the Extraction of Curcumin from Turmeric with Response Surface Methodology: Determination and Optimization Study*; Gokdemir, B.; Baylan, N.; Cehreli, S.; *Anal. Lett.* **2020**, *53*, 13, 2111-2121, (c) *Deep eutectic solvent an efficient reaction medium for the synthesis of chromeno pyrazolo and indazolo phthalazine derivatives*; Patil, A.; Lohar, T.; Mane, A.; Kamat, S.; Salunkhe, R.; *J. Heterocyclic Chem.* **2019**, *56*, 3145–3151.
[252] (a) *Task-specific Ionic Liquids as a Green Catalysts and Solvents for Organic Synthesis*; Padvi, S. A.; Dalal, D. S.; *Curr. Green Chem.* **2020**, *7*, 105-109, (b) *Green and efficient synthesis of pyranopyrazoles using [Bmim][OH] as an ionic liquid catalyst in water under microwave irradiation and investigation of their antioxidant activity*; Aliabadi, R. S.; Mahmoodi, N. O.; *RSC Adv.* **2016**, *6*, 85877-85884, (c) *Biocatalysis in Ionic Liquids;* van Rantwijk, F.; Sheldon, R. A.; *Biocatalysis in ionic liquids. Chem. Rev.* **2007**, *107, 6,* 2757-2785.
[253] (a) *Pretreatment methods for lignocellulosic biofuels production: current advances, challenges and future prospects*; Cheah, W. Y.; Sankaran, R.; Show, P. L.; Ibrahim, T. B. T.; Chew, K. W.; Culaba, A.; Chang, J-S.; *Biofuel Res. J.* **2020**, *7*, 1, 1115-1127, (b) *The Second Evolution of Ionic Liquids: From Solvents and Separations to Advanced Materials-Energetic Examples from the Ionic Liquid Cookbook;* Smiglak, M.; Metlen, A.; Rogers, R. D.; *Acc. Chem. Res.* **2007**, *40,* 1182-1192.
[254] (a) *Study of CO_2 removal in natural gas process using mixture of ionic liquid and MEA through process simulation*; Akinola, T. E.; Oko, E.; Wang, M. H.; *Fuel* **2019**, *236*, 135–146, (b) *Reversible physical absorption of SO_2 by ionic liquids;* Huang, J.; Riisager, A.; Wasserscheid, P.; Fehrmann, R.; *Chem. Commun.* **2006**, 4027-4029.
[255] (a) *Highly Luminescent Ionic Liquids Based on Complex Lanthanide Saccharinates*; Tang, S-F.; Mudring, A-V.; *Inorg. Chem.* **2019**, *58*, 11569−11578, (b) *Magnetic manipulation of materials in a magnetic ionic liquid;* Okuno, M.; Hamaguchi, H.; Hayashi, S.; *Appl. Phys. Lett.* **2006**, *89,* 132506.
[256] (a) *Ionic liquids as electrolytes for energy storage applications – A modelling perspective*; Jonsson, E.; *Energy Storage Materials* **2020**, *25*, 827–835, (b) *Electrodeposition of Metals and Semiconductors in Air- and Water-Stable Ionic Liquids;* Zein, S.; Abedin, E.; Endres, F.; *ChemPhysChem.* **2006**, *7,* 58–61.

as structured media for other technological applications such as their use for enhancing the sensitivity of thermal lens measurements.[257] Moreover, due to the unique properties of ILs such as their capacity to establish simultaneous polar and nonpolar interactions with the analytes, their negligible vapour pressures and wide liquid ranges or their high thermal stability, ILs have been widely used in the analytical area.[258] Regarding this, ILs exhibit a similar behaviour to polar stationary phases such as polyethylene glycol or cyanopropyl-substituted polysiloxanes due to their ability to display a high dipolar interaction and hydrogen bonding. Thus, ILs have been recently considered as good stationary phases materials for Gas Chromatography.[259] Therefore, it was used a monocationic imidazolium salt derived from *L*-phenylalanine as a stationary phase giving a coated GC column, which exhibited good thermal stability (270 °C) and good efficiency (2700 plates/m) for the separation and characterization of the different fatty acids in anhydrous milk fat (AMF).[260] The use of amino acid based ionic liquids (AAILs) allows introducing additional functional groups able to provide complementary interactions such as hydrogen bonding or hydrophobic and aromatic interactions with good potential for the separation of the different products. Hence, this column allowed the separation of geometric isomers avoiding the high column bleeding, which is one of the main disadvantages of polar capillary columns. Furthermore, recoveries from 90% and 99% were achieved in this kind of columns. Another important disadvantage that cannot be overlooked is the preparation of highly homogenous coating to obtain good peak symmetry which has been resolved by the introduction of polymerized ionic liquids (PILs).[261]

---

[257] (a) *Thermal refraction in ionic liquids induced by a train of femtosecond laser pulses;* Nóvoa-López, J. A.; López Lago, E.; Domínguez-Pérez, M.; Troncoso, J.; Varela, L. M.; de la Fuente, R.; Cabeza, O.; Michinel, H.; Rodríguez, J. R.; *Opt. Laser Technol.* **2014**, *61*, 1–7, (b) *Properties of ionic liquid solvents for catalysis;* Wilkes, J. S.; *J. Mol. Catal. A* **2004**, *214,* 11–17.

[258] *The Influence of Ionic Liquids on the Effectiveness of Analytical Methods Used in the Monitoring of Human and Veterinary Pharmaceuticals in Biological and Environmental Samples—Trends and Perspectives;* Treder, N.; *Baczek, T.; Wychodnik, K.; Rogowska; J.; Wolska, L.; Plenis, A.; Molecules* **2020**, *25,* 286-343.

[259] (a) *Ionic liquid stationary phases for multidimensional gas chromatography;* Nan, H; Anderson, J. L.; *Trends Anal. Chem.* **2018**, *105,* 367-379, (b) *Advances of ionic liquids in analytical chemistry;* Trujillo-Rodríguez, M. J; Nan, H; Varona, M; Emaus, M. N; Souza, I. D; Anderson, J. L.; *Anal Chem.* **2019**, *91,* 505–531,

[260] *Gas chromatographic analysis of fatty acid methyl esters of milk fat by an ionic liquid derived from L-phenylalanine as the stationary phase;* González Mendoza, L.; González-Álvarez, J.; Fernández Gonzalo, C.; Arias-Abrodo, P.; Altava, B.; Luis, S. V.; Burguete, M. I.; Gutiérrez-Álvarez, M. D.; *Talanta* **2015**, *143,* 212–218.

[261] *Crosslinked structurally-tuned polymeric ionic liquids as stationary phases for the analysis of hydrocarbons in kerosene and diesel fuels by comprehensive two-dimensional gas chromatography;* Zhang, C.; Park, R. A.; Anderson, J. L.; *J. Chromatogr. A* **2016**, *1440*, 160-171.

In this framework, other researchers have applied ILs as stationary phases in GC to separate simultaneously complex mixtures of isomeric and/or homologous components with similar structural and physical characteristics obtaining really good results.[262] Thus, the introduction of ILs as stationary phases for GC have opened up new interesting perspectives thanks to their exceptional selectivity and tunable properties of ILs, which can dramatically change the selectivity or the separation capacity for the analyte of interest.

As named above, one of the most interesting features of ILs is their tunable properties. These can be defined by the network of coulombic interactions formed by the anions and cations.[263] Nevertheless, in some cases, this network seems to depend not only on the cation-anion coulombic forces, but also on extended networks of additional supramolecular interactions (H-bonds, π−π, C-H···π, hydrophobic interaction and so on). They have strong implications on their three-dimensional (3D) organization and, therefore, on their properties.[264]

Dupont compared room temperature ILs, especially those based on imidazolium cations, and simple molten salts.[265] One of the main differences between them is the molecular asymmetry built into at least one of the ions. This asymmetry in modern ILs opposes the strong charge ordering due to ionic interactions that normally would cause the system to crystallize. Likewise, hydrogen bonds between the cations and anions taking part cooperatively in the network induces structural directionality. Hence, weak interactions, as well as hydrogen bonds, order the structures in modern ILs while Coulomb interactions dominate static long-range behaviour in classical molten salt systems. Meaning that modern ILs form preorganized structures that induce structural directionality, however, classical salts form aggregates only through ionic bonds. From a historical perspective, the first compound that would fit the current definition of IL would

---

[262] (a) *Properties of columns with several pydridinium and imidazolium ionic liquid stationary phases;* Shashkov, M. V.; Sidelnikov, V. N; *J. Chromatogr. A* **2013**, *1309,* 56-63, *(b) Ionic liquids as gas chromatographic stationary phases: how can they change food and natural product analyses?;* Cagliero, C.; Bicchi, C; *Anal. Bioanal. Chem.* **2020**, *412,* 17–25.

[263] (a) *The Structure of a Room-Temperature Ionic Liquid with and without Trace Amounts ofWater: The Role of C_H···O and C_H···F Interactions in 1-n-Butyl-3-Methylimidazolium Tetrafluoroborate;* Mele, A.; Tran, C. D.; de Paoli Lacerda, S. H.; *Angew. Chem. Int. Ed.* **2003**, *42,* 4364-4366, (b) *Ionic Liquids for the Convenient Synthesis of Functional Nanoparticles and Other Inorganic Nanostructures;* Antonietti, M.; Kuang, D.; Smarsly, B.; Zhou, Y.; *Angew. Chem. Int. Ed.* **2004**, *43,* 4988-4992.

[264] *The influence of hydrogen bonding on the physical properties of ionic liquids;* Fumino, K.; Peppel, T.; Geppert-Rybczynska, M.; Zaitsau, D. H.; Lehmann, J. K.; Verevkin, S. P.; Kçckerling, M.; Ludwig, R.; *Phys. Chem. Chem. Phys.* **2011**, *13,* 14064-14075.

[265] *From Molten Salts to Ionic Liquids: A "Nano" Journey;* Dupont, J.; *Acc. Chem. Res.* **2011**, *44,* 1223-1231.

correspond to the ethylammonium nitrate salt synthesized in 1914 by Paul Walden (melting point of 12 °C).[266] Subsequently, between 1970 and 1980, the first ionic liquids based on substituted alkyl imidazolium cations and pyridiniums were developed, with halides and chloroaluminate such as anions.[267] During the 1980s, Seddon[268] began using imidazolium and pyridinium chloroalumininates as polar solvents in reactions with transition metal complexes. Later, in the early 1990s, Chauvin used ILs as solvents in homogeneous catalysis reactions with transition metals.[269]

Nevertheless, the compounds synthesized until that moment had the disadvantage of being very sensitive to moisture, hydrolyzing in most cases. Thus, Mike Zaworotko and John Wilkes, workers of the US Air Force Academy, developed, synthesized and fully characterized salts with dialkylimidazolium as cation, but with stable anions in water such as tetrafluoroborate, hexafluorophosphate, nitrate, sulfate or acetate.[270] In 1994, Fuller and collaborators published the synthesis of new series of ILs with monoalkylimidazolium and trialkylimidazolium cations combined with water-stable anions and with an additional series of anions: bromide, cyanide, bisulfide, iodide, sulfonate, tosylate and tartrate.[271] Indeed, these investigations currently constitute the basis of a chemical model for the development of molten salts at room temperature or ionic liquids.

However, in 1999, when the Queen's University Ionic Liquid Laboratories (QUILL) research centre in Belfast (Northern Ireland) was opened, the interest in the field of ionic liquids started to grow up. The number of publications on ionic liquids increased around six times between 2005 and 2013, being 46000 the total number. In the same way, the number of patents involving ionic liquids

---

[266] *Molecular Weights and Electrical Conductivity of Several Fused Salts;* Walden, P.; *B. Russ. Acad. Sci.,* **1914**, 405-422.

[267] (a) *An electrochemical scrutiny of organometallic iron complexes and hexamethylbenzene in a room temperature molten salt;* Chum, H. L.; Koch, V. R.; Miller, L. L.; Osteryoung, R. A.; *J. Am. Chem. Soc.* **1975**, *97,* 11, 3264-3265, (b) *Dialkylimidazolium chloroaluminate melts: A new class of room-temperature ionic liquids for electrochemistry, spectroscopy, and Synthesis;* Wilkes, J. S.; Levisky, J. A.; Wilson, R. A.; Hussey, C. L.; *Inorg. Chem.* **1982**, *21,* 3, 1263-1264.

[268] *Molybdenum chloro complexes in room-temperature chloroaluminate ionic liquids: Stabilization of* $[MoCl_4]^{2-}$ *and* $[MoCl_6]^{3-}$*;* Scheffler, T. B.; Hussey, C. L.; Seddon, K. R.; Kear, C. M.; Armitage, P. D.; *Inorg. Chem.* **1983**, *22,* 15, 2099-2100.

[269] *Catalytic dimerization of alkenes by nickel complexes in organochloroaluminate molten salts;* Chauvin, Y.; Gilbert, B.; Guibard, I.; *J. Chem. Soc. Chem. Commun.* **1990**, *23,* 1715-1716.

[270] *Air and water stable ionic liquids in physical chemistry;* Wilkes, J. S.; Zaworotko, M. J.; *J. Chem. Soc. Chem. Commun.* **1992**, *13,* 965-967.

[271] *Structure of 1-ethyl-3-methylimidazolium hexafluorophosphate: Model for room temperature molten salts;* Fuller, J.; Carlin, R. T.; De Long, H. C.; Haworth, D.; *J. Chem. Soc. Chem. Commun.* **1994**, *3,* 299-300.

has increased about 24 times since 2005.[272] Nowadays, the catalog of cations and anions is even greater, so the possibility of creating new ILs has virtually no limitations and its applications are almost endless.

In the literature, we can find different types of ionic liquids. Priyanka, and Gardas have recently proposed aqueous biphasic systems based on monocationic and dicationic ionic liquids (MILs and DILs) (Figure 33).[273] They have used these compounds to scrutinize for their ability to extract model nonsteroidal antiinflammatory drug. In their work, they synthesized imidazolium, pyrrolidinium, morpholinium and ammonium-based MILs and corresponding DILs with bromide as common anion.

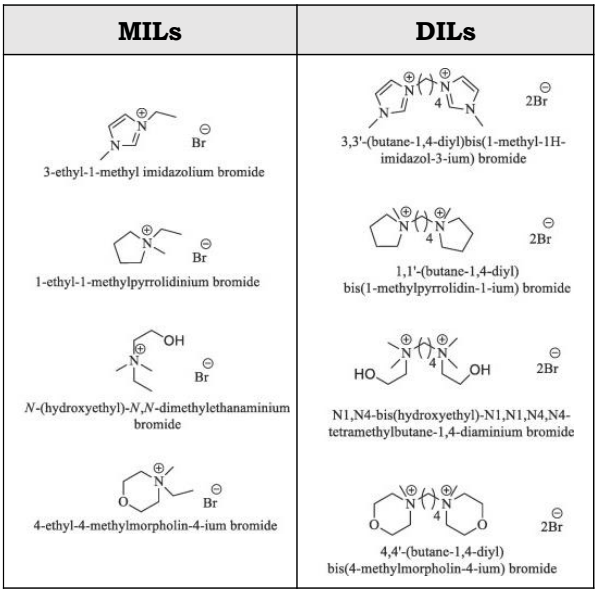

Figure 33 Monocationic and dicationic ionic liquids structures.[273]

Furthermore, it is also possible to find tricationic ionic liquids (TILs). Zincke and Lawson had already synthezised 1,2,3-triazolium salts in 1887 but without being conscious about their properties as ionic liquids.[274] Later, Yacob and Liebscher prepared 1,2,3-triazolium salts as a new class of ionic liquid with a wide scope by Cu-(I)-catalyzed cycloaddition of terminal alkynes and azides

[272] *Scopus data base.*
[273] *Mono- and di- cationic ionic liquids based aqueous biphasic systems for the extraction of diclofenac sodium;* Priyanka, V. P.; Gardas, R. L.; *Sep. Purif. Technol.* **2020**, *234,* 116048-116058.
[274] *Azo-derivatives of phenyl-^{1} -naphthylamine;* Zincke, T.; Lawson, A. T.; *Ber. deut. chem. Ges.* **1887**, *20,* 1167-1176, ISSN 0365-9496.

followed by N-alkylation and eventual salt metathesis.[275] By the other hand, besides, have been described synthesis of macrocyclic ionic liquids. In fact, Yoon and co-workers developed a new family of macrocyclic ionic liquids as receptors for different biological anions and compared the results obtained with different MILs, DILs and TILs.[276]

Although, it has been described large groups of ILs, one of the most sudied has been the ILs derived from amino acids. This is due to the chirality of the compounds. As named before, chirality plays a key role in organic chemistry and is present in many biological processes. Therefore, the design and synthesis of enantiopure ILs with the possibility of easy structural tuneability is highly attractive and a continue effort is being currently devoted to the preparation of chiral ionic liquids (CILs).[277]

Chirality can be introduced in the anion[278] or in the cation.[279] Furthermore, it was shown that the configuration of the resulting CILs played an important role in defining their final physical properties. Within this context the Supramolecular and Sustainable Chemistry group were involved in the preparation and study of new CILs prepared either from racemic materials or from enantiomerically pure materials obtained from the chiral pool.[280] CILs

[275] *1,2,3-Triazolium Salts as a Versatile New Class of Ionic Liquids;* Yacob, Z.; Liebscher, J.; *Ionic Liq.-Classes and Properties* **2011**, 1-22.
[276] *Imidazolium receptors for the recognition of anions;* Yoon, J.; Kim, S. K.; Singh, N. J.; Kim, K. S.; *Chem. Soc. Rev.* **2006**, *35,* 355-360.
[277] (a) *Ionic liquids and chirality: opportunities and challenges;* Baudequin, C.; Baudoux, J.; Levillain, J.; Cahard, D.; Gaumont, A.-C.; Plaquevent, J.-C.; *Tetrahedron: Asymmetry* **2003**, *14,* 3081–3093, (b) *Chiral ionic liquids, a renewal for the chemistry of chiral solvents? Design, synthesis and applications for chiral recognition and asymmetric synthesis;* Baudequin, C.; Brégeon, D.; Levillain, J.; Guillen, F.; Plaquevent, J.-C.; Gaumont, A.-C.; *Tetrahedron: Asymmetry* **2005**, *16,* 3921–3945, (c) *Amino Acid Ionic Liquids;* Ohno, H.; Fukumoto, K.; *Acc.Chem. Res.* **2007**, *40,* 1122–1129, (d) *The Use of Switchable Polarity Solvents for the Synthesis of 16-Arylidene Steroids via Claisen–Schmidt Condensation;* Bica, K.; Gaertner, P.; *Eur. J. Org. Chem.* **2008**, 3236–3250, (e) *Functionalized Chiral Ionic Liquids: A New Type of Asymmetric Organocatalysts and Nonclassical Chiral Ligands;* Luo, S.; Zhang, L.; Cheng, J.-P.; *Chem. Asian J.* **2009**, *4,* 1184–1195, (f) *Ephedrinium-Based Protic Chiral Ionic Liquids for Enantiomeric Recognition;* De Rooy, S. L.; Li, M.; Bwambok, D. K.; El-Zahab, B.; Challa, S.; Warner, I. M.; *Chirality* **2011**, *23,* 54–62; (g) *Ionic-Liquid-Supported (ILS) Catalysts for Asymmetric Organic Synthesis;* Ni, B.; Headley, A. D.; *Chem. Eur. J.,* **2010**, *16,* 4426–4436, (i) *Chiral Ionic Liquids: A Compendium of Syntheses and Applications (2005–2012),* Payagala, T.; Armstrong, D. W.; *Chirality* **2012**, *24,* 17–53.
[278] *Synthesis and Characterization of Chiral Imidazolium Salts;* Machado, M. Y.; Dorta, R.; *Synth.* **2005**, *15,* 2473-2475.
[279] *New chiral imidazolinic derivatives,* Génisson, Y., Lauth-De Viguerie, N., André, C., Baltas, M., Gorrichon, L., *Tetrahedron Asymmetry* **2005,** *16,* 5, 1017-1023.
[280] *Synthesis of new chiral imidazolium salts derived from amino acids: their evaluation in chiral molecular recognition;* Altava, B.; Barbosa, D. S.; Burguete, M. I.; Escorihuela, J.; Luis, S. V.; *Tetrahedron: Asymmetry* **2009**, *20,* 999–1003.

have potential as chiral solvents,[281] shift reagents,[282] or enantioselective catalysts.[283] However, researchers from this group focused on CILs as receptors for anions.

In this regard, our group has developed a variety of ionic liquids used to a wide range of applications.[284] Below in Figure 34, are shown the most common structures related with the work presented in the following chapters. These compounds are imidazolium salts derived from different aminoacids as phenylalanine, proline or valine (R) with a variety of aliphatic and aromatic as side chain (R_1, R_2) and bromide or bistriflamide as anions (X).

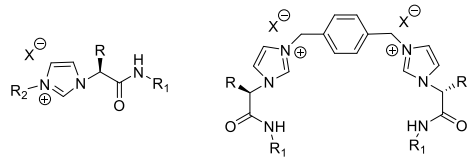

Figure 34 General structure of monocationic and dicationic imidazolium salts.[283b,285]

They observed that different structural elements dramatically affect the physicochemical properties of the ILs. For instance, the Sustainable and

[281] *Greener Solvents: Room Temperature Ionic Liquids from Biorenewable Sources;* Handy, S. T.; *Chem. Eur. J.* **2003**, *9,* 2938–2944.
[282] (a) *New chiral ionic liquids based on imidazolinium salts;* Winkel, A.; Wilhelm, R.; *Tetrahedron: Asymmetry* **2009**, *20,* 2344–2350, (b) *Design and synthesis of a novel imidazolium-based ionic liquid with planar chirality;* Ishida, Y.; Miyauchi, H.; Saigo, K.; *Chem. Commun.* **2002**, 2240– 2241, (c) *Synthesis of novel spiro imidazolium salts as chiral ionic liquids;* Patil, M. L.; Rao, C. V. L.; Takizawa, S.; Takenaka, K.; Onitsuka, K.; Sasai, H.; *Tetrahedron* **2007**, *63,* 12702–12711, (d) *Design and synthesis of imidazolinium salts derived from (L)-valine. Investigation of their potential in chiral molecular recognition;* Clavier, H.; Boulanger, L.; Audic, N.; Toupet, L.; Mauduit, M.; Guillemin, J.-C.; *Chem. Commun.* ***2004***, 1224–1225.
[283] (a) *Combinatorial synthesis of functionalized chiral and doubly chiral ionic liquids and their applications as asymmetric covalent/non-covalent bifunctional organocatalysts*; Zhang, L.; Luo, S.; Mi, X.; Liu, S.; Qiao, Y.; Xu, H.; Cheng, J.-P.; *Org. Biomol. Chem.* **2008**, *6,* 567–576, (b) *Design and synthesis of novel ionic liquid/liquid crystals (IL2Cs) with axial chirality;* Baudoux, J.; Judeinstein, P.; Cahard, D.; Plaquevent, J.-C.; *Tetrahedron Lett.* **2005**, *46,* 1137–1140.
[284] (a) *Divergent Multistep Continuous Synthetic Transformations of Allylic Alcohol Enabled by Catalysts Immobilized in Ionic Liquid Phases;* Peris, E.; Porcar, R.; García-Álvarez, J.; Burguete, M. I.; García-Verdugo, E.; Luis, S. V.; *ChemSusChem* **2019**, *12,* 1684–1691, (b) *Chiral Room Temperature Ionic Liquids as Enantioselective Promoters for the Asymmetric Aldol Reaction;* González, L.; Escorihuela, J.; Altava, B.; Burguete, M. I.; Luis, S. V.; *Eur. J. Org. Chem.* **2014**, 5356–5363, (c) *Chiral Triazolium Salts and Ionic Liquids: From the Molecular Design Vectors to Their Physical Properties through Specific Supramolecular Interactions;* Porcar, R.; Rios-Lombardia, N.; Busto, E.; Gotor-Fernandez, V.; Montejo-Bernardo, J.; Garcia-Granda, S.; Luis, S. V.; Gotor, V.; Alfonso, I.; Garcia-Verdugo, E.; *Chem. Eur. J.* **2013**, *19,* 892-904, (d) *Supported ionic liquid-like phases as organocatalysts for the solvent-free cyanosilylation of carbonyl compounds: from batch to continuous flow process;* Martín, S.; Porcar, R.; Peris, E.; Burguete, M. I.; García-Verdugo, E.; Luis, S. V.; *Green Chem.* **2014**, *16,* 1639-1647.
[285] (a) *Synthesis of Chiral Room Temperature Ionic Liquids from Amino Acids-Application in Chiral Molecular Recognition;* González, L.; Altava, B.; Bolte, M.; Burguete, M. I.; García-Verdugo, E.; Luis, S. V.; *Eur. J. Org. Chem.* **2012**, 4996–5009, (b) *Bis(imidazolium) salts derived from amino acids as receptors and transport agents for chloride anions;* González-Mendoza, L.; Altava, B.; Burguete, M. I.; Escorihuela, J.; Luis, S. V.; Hernando, E.; Quesada, R.; Vicent, C.; *RSC Adv.* **2015**, *5,* 34415–34423.

Supramolecular chemistry group developed a family of IL based on the structure shown in Figure 35.[286]

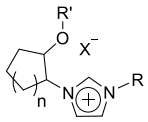

Figure 35 General structure of the family of IL synthesized, being n= ring size, R'= H or Ac, X^-= Cl^-, Br^-, BF_4^-, or NTf_2^-, R= Bn, nBu, or nOct.[286]

The microscopic interactions of the supramolecular ionic network of these imidazolium salts at the molecular level were investigated both spectroscopically (NMR, FT-IR-ATR) and theoretically. Moreover, a topological analysis of the experimental electron densities obtained by X-ray diffraction of single crystals was performed. Both experimental data and calculations strongly supported the stabilization effect of the OH···anion hydrogen-bonding interactions, although secondary inter-cationic interactions (such as additional H bonding, π-π or C-H···π bonding involving benzyl aromatic rings) were observed in the crystal structures. These interactions could also contribute significantly to the global stability of the salts. Hence, the presence of additional functionalities in the ILs, which were able to form hydrogen-bond interactions with the counterion, had a significant influence on their final macroscopic properties.[287,288]

3.1 Supramolecular materials involving ILs and their applications in Supramolecular Chemistry

3.1.1 Gels

Researchers have recently focused on ionic liquid gels and their potential roles due to their more sustainable future.[289] Supramolecular ionic liquids gels are formed by noncovalent interactions, including interactions such as hydrogen

[286] *From Salts to Ionic Liquids by Systematic Structural Modifications: A Rational Approach Towards the Efficient Modular Synthesis of Enantiopure Imidazolium Salts;* Ríos-Lombardía, N.; Busto, E.; Gotor-Fernández, V.; Gotor, V.; Porcar, R.; García-Verdugo, E.; Luis, S. V.; Alfonso, I.; García-Granda, S.; Menéndez-Velázquez, A.; *Chem. Eur. J.* **2010**, *16,* 836-847.
[287] (a) *Competitive interactions in carboxy-functionalized pyridinium salts: crossover from O–H…O to O–H…X–M contacts;* Neve, F.; Crispini, A.; *CrystEngComm* **2007**, *9,* 698–703.
[288] *A comparison of ether- and alkyl-derivatized imidazolium-based room-temperature ionic liquids: a molecular dynamics simulation study;* Smith, G. D.; Borodin, O.; Li, L.; Kim, H.; Liu, Q.; Bara, J. E.; Ginc, D. L.; Nobel, R.; *Phys. Chem. Chem. Phys.* **2008**, *10,* 6301–6312.
[289] *Gelation of Ionic Liquid-Based Electrolytes with Silica Nanoparticles for Quasi-Solid-State Dye-Sensitized Solar Cells;* Wang, P.; Zakeeruddin, S. M.; Comte, P.; Exnar, I.; Grätzel, M.; J. Am. Chem. Soc. **2003**, *125,* 1166-1167.

bonding, π–π interactions or π stacking, and van der Waals, which lead to self-assembly into a 3D network.[290] The ionic liquids can be used as media to form gels or as gelators.

Regarding to the first group, a symbiosis between the dispersed ionic liquid phase and solid continuous phase are offered by ionic liquid gel materials. Thus, an emerging trend in ILs research is their hybridization with solid matrices, named ionogels. The liquid dispersed/trapped inside a solid retains the function of the ionic liquid and therefore the gel can retain the favourable properties of ionic liquid, such as thermal stability and negligible vapour pressure, combined with the practicality of a solid. In most cases, these confined ionic liquids retain or display enhanced functional properties when contained within a gel material. Moreover, ionic liquid gels provide the ability to build functionality at every level, the solid component, the ionic liquid used as solvent, and any incorporated active functional agents. This allows materials to be custom designed for a vast assortment of applications, being mainly relevant the electrocatalysis,[291] as electrolytes in solar cells[292] and in fuel cells.[293]

Bang et al. developed a variety of polymers as smart materials allowing a simple and reversible crosslinking involving S–S bonds.[294] They were inspired by the natural phenomenon of the disulfide bond formation as a robust mechanism that nature uses for protein stabilization and crosslinking. Following this idea, the Sustainable and Supramolecular chemistry group carried out the aminolysis of different compounds in the presence of an amine which leads to a functionalized polymer with thiols as side-chain groups (Figure 36).[295] In the absence of any other reagents, it could be expected that the originally formed

---

[290] *Preparation of Supramolecular Ionic Liquid Gels Based on Host− Guest Interactions and Their Swelling and Ionic Conductive Properties;* Sinawang, G.; Kobayashi, Y.; Zheng, Y.; Takashima, Y.; Harada, A.; Yamaguchi, H.; *Macromol.* **2019**, *52,* 2932−2938.

[291] *Direct electrochemistry and electrocatalysis of myoglobin based on silica-coated gold nanorods/room temperature ionic liquid/silica sol–gel composite film;* Zhu, W.-L.; Zhou, Y.; Zhang, J. R.; Talanta **2009**, *80*, 224-230.

[292] *High efficiency dye-sensitized nanocrystalline solar cells based on ionic liquid polymer gel electrolyte;* Wang, P.; Zakeeruddin, S. M.; Exnar, I.; Grätzel, M.; Chem. Commun. **2002**, 2972-2973.

[293] *Inorganic–organic hybrid membranes with anhydrous proton conduction prepared from tetramethoxysilane/methyl-trimethoxysilane/trimethylphosphate and 1-ethyl-3methylimidazolium-bis(trifluoromethanesulfonyl)imide for H_2/O_2 fuel cells;* Lakshminarayana, G.; Nogami, M.; Electrochim. Acta **2010**, *55,* 1160-1168.

[294] *Poly(disulfide)s;* Bang, E.; Lista, M.; Sforazzini, G.; Sakai, N.; Matile, S.; *Chem. Sci.* **2012**, *3,* 1752–1763.

[295] *Poly(acrylamide-homocysteine thiolactone) as a synthetic platform for the preparation of polymeric ionic liquids by post ring-openingorthogonal modifications;* Montolio, S.; Zagorodko, O.; Porcar, R.; Burguete, M. I.; Luis, S. V.; Tenhu, H.; García-Verdugo, E.; *Polym. Chem.* **2017**, *8,* 4789–4797.

linear polymers ionic liquids (PILs) became crosslinked through the formation of intermolecular disulfide bridges, giving rise to the formation of the corresponding polymeric ionic liquid gels. Hence, a strong gelation was observed depending on the amine used. The gelation time showed a strong dependence on the pKa of the corresponding amine. The results suggested that the basicity of the amines was also key to determine disulfide crosslinking and gel formation. This polymer gel formation through sulfide bridge formation (S–S) opened the possibility of preparing ionogels by means of the corresponding amine tethered to an IL fragment using the thiolactone opening reaction. It was observed an increase in the viscosity of the mixture with bromide leading to the formation of a gel. However, when the more hydrophobic IL containing NTf_2^- was used, an increase in the viscosity of the mixture was also observed, but the system did not evolve to form a gel. This different behaviour for the two compounds showed that the nature of the anion has a significant effect on the morphology of the self-assembled nanostructures containing IL-like units. Generally, the presence of more basic anions such as bromide is likely to provide strong imidazolium/anion interactions, while hydrophobic anions led to weak electrostatic interactions not favouring the S–S bond formation.

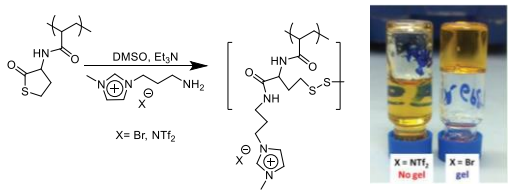

Figure 36 Ionogel formation across disulphide bridges.[294]

On the other hand, ILs have been also used as gelators. In this regard, there is a wide variety of ionic liquids that have been reported as capable of acting as molecular gelators for organic solvents. The average hydrogen bonding in normal organic compounds are weaker than the hydrogen bonds charge-assisted by organic salts,[296] this fact plays an important role in self-assembly, gel formation, morphology, strength, and longevity. D'Anna, *et al.* investigated the ability of some diimidazolium salts as LMWG for organic solvents.[297] The

[296] *Designing a simple organic salt-based supramolecular topical gel capable of displaying in vivo self-delivery application;* Majumder, J.; Deb, J.; Das, M. R.; Jana, S. S.; Dastidar, P.; Chem. Commun. **2014**, *50,* 1671-1674.
[297] *The Gelling Ability of Some Diimidazolium Salts: Effect of Isomeric Substitution of the Cation and Anion;* D'Anna, F.; Vitale, P.; Ferrante, F.; Marullo, S.; Noto, R.; ChemPlusChem **2013**, *78,* 331-342.

results concluded that the ability of an ionic liquid to gel an organic solvent seemed not to be determined by the cation structure. Nevertheless, for the obatined gels, researchers found that the overall properties and structural features of these seemed to be controlled by the anion properties, beeing the gelling ability significantly improved using dianions insted of monoanions. Therefore, depending on the components that form the ionic liquid, the properties of the gel vary substantially, and a wide range of ionic liquids gels can be found.[298]

3.1.2 Solid state

As named before, supramolecular interactions play a key role in the self-assembling abilities of several compounds to preorganize themselves to obtain well-defined structures in the solid state. In this regard,the Sustainable and Supramolecular chemistry group obtained suitable crystals for X-ray diffraction analysis of different chiral ILs salts.[299,284a]

This group synthesized a series of structurally new room temperature chiral ionic liquids based on an imidazolium group and derived from natural amino acids[285a] (Figure 37), similar than the compounds present in the following chapters. The strong interaction between the imidazolium cation and the corresponding anion through electrostatic forces and NH-anion hydrogen bonding give tightly associated ion pairs with well-defined structures, as well as defined supramolecular structures in the solid state. During the different studies carried out, it was observed that the intrinsic physical properties of these family of ILs depended on the nature of the side chain as well as the presence of additional functional groups.

[298] (a) *One-Step Synthesis of Thermosensitive Nanogels Based on Highly Cross-Linked Poly(ionic liquid)s;* Xiong, Y.; Liu, J.; Wang, Y.; Wang, H.; Wang, R.; *Angew. Chem. Int. Ed.* **2012**, *51,* 9114-9118, (b) *Thermoresponsive poly(ionic liquid) hydrogels;* Ziolkowski, B.; Diamond, D.; *Chem. Commun.* **2013**, *49,* 10308-10310, (c) *Specialist Gelator for Ionic Liquids;* Hanabusa, K.; Fukui, H.; Suzuki, M.; Shirai, H.; *Langmuir* **2005**, *21,* 10383-10390.

[299] *Simple and straightforward synthesis of novel enantiopure ionic liquids via efficient enzymatic resolution of (±)-2-(1H-imidazol-1-yl)cyclohexanol;* Busto, E.; Gotor-Fernaández, V.; Ríos-Lombardía, N.; García-Verdugo, E.; Alfonso, I.; García-Granda, S.; Menéndez-Velázquez, A.; Burguete, M. I.; Luis, S. V.; Gotor, V.; *Tetrahedron Lett.* **2007**, *48,* 5251–5254.

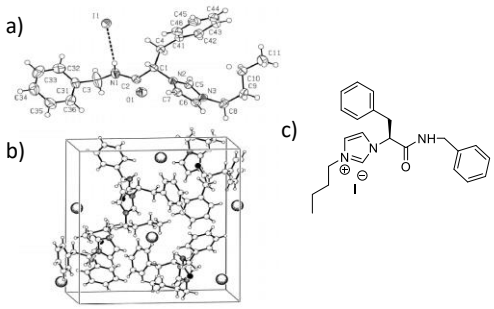

Figure 377 (a) Molecular structure and (b) crystal packing for compound represented in (c), obtained by X-ray diffraction analysis.[285a]

Secondary inter-cationic interactions (such as additional H bonding, π-stacking or C–H–π bonding involving benzyl aromatic rings) were also observed in the different crystal structures, contributing significantly the global stability of the salts in the solid state.[285a]

Moreover, X-ray analysis of the enantiopure IL shown in Figure 38, unambiguously confirmed that the chemical structure of the chiral imidazole salts consisted of layers of cations and anions, which were interconnected by a network of hydrogen bonds between OH and the anion and π-π interactions between the aromatic rings.[286]

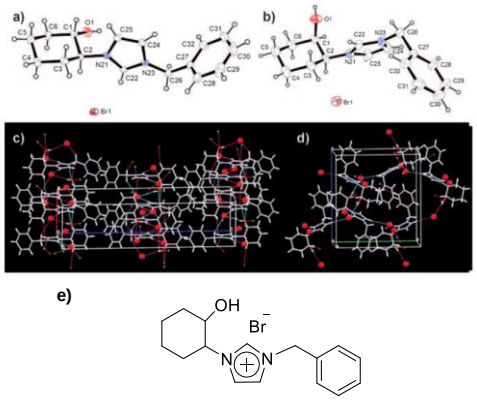

Figure 38 X-ray diffraction studies for (a) (S,S)-trans-Cy6-OH-Im-Bn-Br; (b) (R,S)-cis-Cy6-OH-Im-Bn-Br; (c) crystal packing of (S,S)-trans-Cy6-OH-Im-Bn-Br; (d) crystal packing of (R,S)-cis-Cy6-OH-Im-Bn-Br, (e) Cy6-OH-Im-Bn-Br.[286]

By the other hand, hydrogen bonding and electrostatic and hydrophobic interactions have been also observed in homogeneous polymeric ionic liquids (PILs) blends obtained by the Sustainable and Supramolecular chemistry

group.[300] The PILs were obtained using the electrospinning instrument.[301] They studied these interactions using UV-Vis and TEM and compared the results with pure PILs.[302] The differences observed, over those of the systems containing just one individual component, for the solutions containing PILs and PVP and for the morphology and performance of the final fibres were related with the nature of these supramolecular interactions. Therefore, the experimental evidence suggested that PILs and PVP were able to undergo strong supramolecular interpolymeric interactions between complementary structural elements directly or mediated by water molecules. Thus, the enhancement of these interactions low molecular weight polymers or even nonpolymeric species consists in the possibility to electrospun them. The overall properties of the compounds obtained can be easily tuned not only through a proper design of the electrospinning parameters, but through appropriate changes in the molecular vectors of the imidazolium fragments present in PILs.

The properties of ionic liquids have enabled important advances to be made in sustainable energy generation and storage.[303] In this regard, some researchers have discussed the use of ionic liquids as media for electromaterials' synthesis, for example, in the preparation of doped carbons, intercalation electrode materials and conducting polymers.[304] These materials were characterized using diferents instruments such as TGA, FT-IR, elemental analysis, among others.[305]

---

[300] *Hierarchically structured polymeric ionic liquids and polyvinylpyrrolidone mat-fibers fabricated by electrospinning;* Montolio, S.; Abarca, G.; Porcar, R.; Dupont, J.; Burguete, M. I.; García-Verdugo, E.; Luis, S. V.; *J. Mater. Chem. A* **2017**, *5,* 9733–9744.

[301] *A critique on multi-jet electrospinning: State of the art and future outlook;* El-Sayed, H.; Vineis, C.; Varesano, A.; Mowafi, S.; Carletto, R. A.; Tonetti, C.; Taleb, M. A.; *Nanotechnol. Rev.* **2019**, *8,* 236-245.

[302] *Enhancing the Electrospinnability of Low Molecular Weight Polymers Using Small Effective Cross-Linkers;* Wang, X.; Pellerin, C.; Bazuin, C. G.; *Macromol.* **2016**, *49,* 891–899.

[303] *Ionic plastic crystal-polymeric ionic liquid solid-state electrolytes with high ionic conductivity for lithium ion batteries;* Yang, K.; Liao, Z.; Zhang, Z.; Yang, L.; Hirano, S.; *Mater. Lett.* **2019**, *236,* 554–557.

[304] *Ionic liquids and their solid-state analogues as materials for energy generation and storage;* MacFarlane, D.; Forsyth, M.; Howlett, P.; Kar, M.; Passerini, S.; Pringle, J. M.; Ohno, H.; Watanabe, M.; Yan, F.; Zheng, W., Zhang, S.; Zhang, J.; *Nat. Rev. Mater.* **2016**, *1,* 15005.

[305] (a) *The electrochemical growth of highly conductive single PEDOT (conducting polymer): BMIPF6 (ionic liquid) nanowires;* Kannan, B.; Williams, D. E.; Laslauab, C.; Travas-Sejdic, J.; *J. Mater. Chem.* **2012**, *22*, 18132, (b) *A new conducting salt for high voltage propylene carbonate-basedelectrochemical double layer capacitors;* Pohlmann, S.; Balducci, A.; Electrochim. Acta **2013**, *110*, 221– 227, (c) *Easy synthesis of poly(ionic liquid) for use as a porous carbon precursor*; Liao, C.; Liu, R.; Hou, X-S.; Sun, X-G.; Dai, S.; *New Carbon Mater.* **2014**, *29*, 1, 78-80, (d) *25th Anniversary Article: "Cooking Carbon with Salt": Carbon Materials and Carbonaceous Frameworks from Ionic Liquids and Poly(ionic liquid)s*; Fellinger, T-P.; Thomas, A.; Yuan, J.; Antonietti, M.; *Adv. Mater.* **2013**, *25*, 5838–5855.

3.1.3 Other materials in solution

ILs can be used as solvents,[306] surfactants[307] or salts additives such as co-surfactants[308] or hydrotropes[309] in solution. Both co-surfactants and hydrotropes can be defined as surfactants with a hydrophilic and a hydrophobic part, however the co-surfactants contain small head groups while the hydrotropes have small hydrophobic part so they cannot cause spontaneous self-aggregation.[311] It means that the additives do not have a critical concentration above which self-aggregation spontaneously starts to occur due to their small parts respectively. Thus, when the concentration is raised above their solubility limit, they form a new phase because their respective groups are so small they cannot stop the aggregation process at a particular aggregation number. The solubility limit of the additives can therefore be considered as the CMC of them.

Hence, the addtives tend to act in addtion to another surfactant and they may either increase or decrease the solubility of a solute in a given solvent. The effect of an additive depends very much on the influence it has on the structure of water or its ability to compete with the solvent water molecules. In this regard, the hydrotropes are compounds that solubilize hydrophobic compounds in aqueous solutions by means other than micellar solubilization. Nevertheless, co-surfactants are miscible with surfactants and form mixed micelles. Because their head groups are small, the average head group area between the surfactant and the co-surfactant at the micellar surface is decreased and the packing parameter for the mixed system is increased. Addition of co-surfactants to surfactants produces more surface activity, the increase of the packing parameter, the change of the micelles from globules to worm-like micelles to bilayer phases and the decrease of the interfacial tension.

---

306 *Using ionic liquids to formulate microemulsions: Current state of affairs;* Kunz, W.; Zemb, T.; Harrar, A.; *Curr. Opin. Colloid Interface Sci.* **2012**, *17,* 205–211.
307 (a) *Phase behavior and characterization of ionic liquids based microemulsions;* Safavi, A.; Maleki, N.; Farjami, F.; *Colloids Surf., A* **2010**, *355,* 61–66.
308 *Ionic liquids in microemulsions;* Qiu, Z.; Texter, J.; *Curr. Opin. Colloid Interface Sci.* **2008**, *13,* 252–262.
309 *Composition and Concentration Gradient Induced Structural Transition from Micelles to Vesicles in the Mixed System of Ionic Liquid–Diclofenac Sodium;* Singh, O.; Kaur, R.; Aswal, V. K.; Mahajan, R. K.; *Langmuir* **2016**, *32,* 6638−6647.
311 Gräbner, D.; Hoffmann, H. *Rheology of Cosmetic Formulations; Cosmetic Science and Technology,* Theoretical Principles and Applications, 27, Elsevier, **2017**, 471-488.

Typical co-surfactants are n-alcohols and alkyl carboxylic acids,[312] while the most important hydrotropes include urea, tosylate, cumenesulfonate and xylenesulfonate.[313]

Therefore, many ILs have been designed as amphiphilic substances which contain hydrophilic and lipophilic molecular fragments, both determine their surface activity and the ability to self-organize in solutions.[314] In this regard, some authors studied the dialkylimidazolium ILs' property of self-organizing as representative molecules. Both the positively charged imidazolium rings and anions arranged polar domains supported by strong electrostatic interactions, whereas alkyl groups aggregate formed nonpolar domains anchored by van der Waals interactions. At high dilutions, the role of interactions between water molecules and polar IL groups increases carrying out the formation of aggregates in aqueous surrounding.[315] The average aggregation numbers of these compounds have been determined by techniques like fluorimetry or NMR.[316] Moreover, it has been described that the aggregation number increased with longer aliphatic alkyl chains.[317]

Some autors have focused on the influence of the alkyl chain length in the cation and anion of 1-alkyl-3-methylimidazole (mim) alkylsulfonate salts of ionic liquids type with the formula $[C_nH_{2n+1}\text{-mim}][C_mH_{2m+1}SO_3]$, where n=8, 10, or 12, m=1 and n=4 or 8, m=4 or 8, on the self-aggregation in aqueous solution.[318] These compounds are known as catanionic surfactants, that are equimolar mixtures of two oppositely charged surfactants (the parent surfactants) from which the inorganic counterions are completely removed.[319] It is necessary to distinc them from surfactants obtained by mixing two salts

[312] Vaidya, S.; Ganguli, A. K. *Microemulsion Methods for Synthesis of Nanostructured Materials;* Comprehensive Nanoscience and Nanotechnology, 2nd Edition, **2019**, *2,* 1-12.
[313] *Hydrotropes;* Kunz, W.; Holmberg, K.; Zemb, T.; *Curr. Opin. Colloid Interface Sci.* **2016**, *22,* 99–107.
[314] *Ionic Liquids as Surfactants;* Smirnova, N. A.; Safonova, E. A.; *Russ. J. Phys. Chem. A* **2010**, *84,* 1695–1704.
[315] *Molecular Dynamics Simulation of Nanostructural Organization in Ionic Liquid/Water Mixtures*; Jiang, W.; Wang, Y.; Voth, G. A.; *J. Phys. Chem. B* **2007**, *111*, 4812-4818.
[316] *On the Self-Aggregation and Fluorescence Quenching Aptitude of Surfactant Ionic Liquids*; Blesic, M.; Lopes, A.; Melo, E.; Petrovski, Z.; Plechkova, N. V.; Canongia Lopes, J. N.; Seddon, K. R.; Rebelo, L. P. N.; *J. Phys. Chem. B* **2008**, *112*, 29, 8645–8650.
[317] *Dependence of Micelle Size and Shape on Detergent Alkyl Chain Length and Head Group*; Oliver, R. C.; Lipfert, J.; Fox, D. A.; Lo, R. H.; Doniach, S.; Columbus, L.; PLos One **2013**, *8*, 5, 62488.
[318] *New catanionic surfactants based on 1-alkyl-3-methylimidazolium alkylsulfonates, $[C_nH_{2n+1}mim][C_mH_{2m+1}SO_3]$: mesomorphism and aggregation;* Blesic, M.; Swadzba-Kwasky, M.; Holbrey, J. D.; Lopes, J. N. C.; Seddon, K. R.; Rebelo, L. P. N.; *Phys. Chem. Chem. Phys.* **2009**, *11,* 4260–4268.
[319] Khan, A.; Marques, E. *Catanionic surfactants;* Robb, I. D., Eds.; Specialist Surfactants, Springer, Dordrecht, **1997**.

(mixtures of cationic and anionic surfactants, either equimolar or non-equimolar, where the inorganic counterions are also present) and gemini surfactants constituted by two or more amphiphilic groups anchored by a covalent linker. The fluorescence spectroscopy and interfacial tension measurements were used to determine the critical micelle-formation concentration, the surface activity, and to assess the effect of alkyl substitution in cations and anions on the surface properties of these salts. It was observed that when the alkyl chain length in the cation was increased, a decrease in the critical micelle-formation concentration was noticed.

Thus, in the last decade, researchers have widely studied the building blocks of the supramolecular aggregates (micelle, mixed micelle, and vesicular assemblies) not only from oppositely charged surfactant/surfactant pair but also surfactant/IL surfactant and pair IL surfactant/IL surfactant. In this regard, Dutta *et al.* synthesized a new family of IL surfactants and studied their sef-aggregation by different techniques like SEM, TEM, DLS, UV-Vis and Confocal fluorescence microscopy.[320] They observed different kind of aggregates depending on the concentration of the surfactant used (Figure 39). They detected by TEM that the addition of vitamin E generates an effect on the morphology and phase behavior of the cationic surfactant C_{16}mimCl inducing the formation of unilamellar vesicles from micellar aggregates (Figure 39b).[321] The different vesicular assemblies were used as suitable drug carriers obtained by replacement of the Na^+ ion of NaAOT (sodium 1,4-bis(2-ethylhexyl) sulfosuccinate) by the imidazolium ion containing ILs (CnmimCl, n = 8, 12, 16) which produces [Cnmim][AOT].

[320] *Ionic liquid-induced aggregate formation and their applications;* Dutta, R.; Kundu, S.; Sarkar, N.; *Biophys. Rev.* **2018**, *10,* 861-871.
[321] *Influence of bile salt on vitamin E derived vesicles involving a surface active ionic liquid and conventional cationic micelle;* Roy, A.; Kundu, S.; Dutta, R.; Sarkar, N.; *J. Colloid Interface Sci.* **2017**, *501,* 202–214.

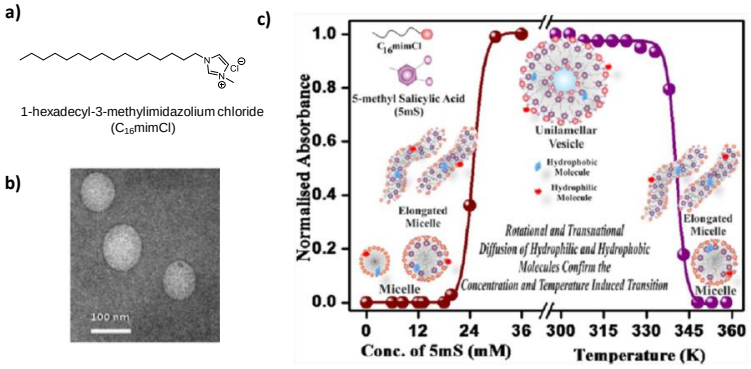

Figure 39 (a) Structure of the IL surfactant C_{16}mimCl, (b) TEM images of unilamellar vesicles of C_{16}mimCl-vitamin E and (c) Change in the turbidity of C_{16}mimCl-5-mS aggregates with change in the concentration of 5-mS and the temperature of the system. Adapted with permission from (Langmuir 2016, 32, 7127- 7137). Copyright (2016) American Chemical Society.[320]

Apart from this application, ILs surfactants have been studied in different fields, for instance, as a potential use to enhance oil recovery,[322] capillary electrophoresis,[323] and so on.[324]

3.1.4 Molecular receptors

Recently, numerous efforts have been devoted to the study of imidazolium ILs as receptors, including benzene-based tripodal systems, cyclophanes and caliximidazolium, fluorescent imidazolium, ferrocenyl imidazolium, cavitand and calixarene, and polymeric imidazolium systems.[325]

In contrast to the well-known hydrogen bonding, which is often found in amide, pyrrole, urea, ammonium or guanidinium groups, the imidazolium group can

---

[322] *Ionic liquids as novel surfactants for potential use in enhanced oil recovery;* Benzagouta, M. S.; AlNashef, I. M.; Karnanda, W.; Al-Khidir, K.; *Korean J. Chem. Eng.* **2013**, *30,* 2108-2117.

[323] *Ionic liquids in enhancing the sensitivity of capillary electrophoresis: Off-line and on-line sample preconcentration techniques;* El-Hady, D. A.; Albishri, H. M.; Watzig, H.; *Electrophoresis* **2016**, *37,* 1609–1623.

[324] (a) *Ionic liquid microemulsions and their technological applications;* Mehta, S. K.; Kaur, K.; *Indian J. Chem.* **2010**, *49,* 662-684; (b) *Ionic Liquid Surfactants;* Asadov, Z. G.; Akhmedova, G. A.; Aga-Zadeh, A. D.; Nasibova, Sh. M.; Zarbalieva, I. A.; Bagirova, A. M.; Ragimov, R. A.; *Russ. J. Gen. Chem.* **2012**, *82,* 1916–1927.

[325] (a) *Revisit to imidazolium receptors for the recognition of anions: highlighted research during 2006–2009;* Xu, Z.; Kim, S. K.; Yoon, J.; *Chem. Soc. Rev.* **2010**, *39,* 1457-1466, (b) *Imidazolium-Functionalized BINOL as a Multifunctional Receptor for Chromogenic and Chiral Anion Recognition;* Lu, Q.-S.; Dong, L.; Zhang, J.; Li, J.; Jiang, L.; Huang, Y.; Qin, S.; Hu, C.-W.; Yu, X.-Q.; *Org. Lett.* **2009**, *11,* 669-672, (c) *Synthesis and selective anion recognition of imidazolium cyclophanes;* Yuan, Y.; Gao, G.; Jiang, Z.-L.; You, J.-S.; Zhou, Z.-Y.; Yuan, D.-Q.; Xie, R.-G.; *Tetrahedron* **2002**, *58,* 8993 –8999, (d) *Synthesis of a Novel Cyclic Donor−Acceptor Conjugate for Selective Recognition of ATP;* Neelakandan, P. P.; Hariharan, M.; Ramaiah, D.; *Org. Lett.* **2005**, *7,* 5765-5768, (e) *A Supramolecular ON-OFF-ON Fluorescence Assay for Selective Recognition of GTP;* Neelakandan, P. P.; Hariharan, M.; Ramaiah, D.; *J. Am. Chem. Soc.* **2006**, *128,* 11334-11335, (f) *DNA-Assisted Long-Lived Excimer Formation in a Cyclophane;* Neelakandan, P. P.; Ramaiah, D.; *Angew. Chem., Int. Ed.* **2008**, *47,* 8407-8411, (g) *Novel Bile Acid-Based Cyclic Bisimidazolium Receptors for Anion Recognition;* Khatri, V. K.; Upreti, S.; Pandey, P. S.; *Org. Lett.* **2006**, *8,* 1755-1758.

interact with anions through the involvement of (C–H)+-anion hydrogen bonds and, usually, the recognition is dominated by charge–charge electrostatic interactions.[326]

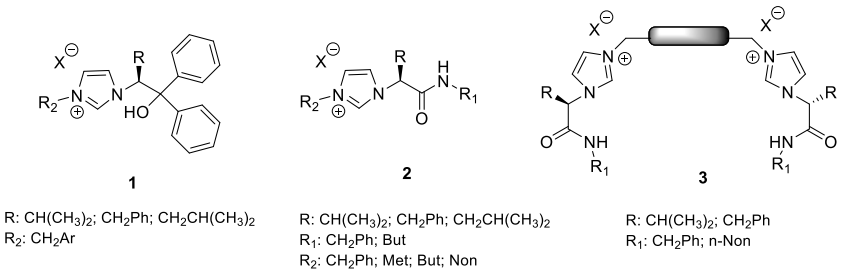

Figure 40 Structures of chiral ionic liquids used as CSAs for chiral carboxylates.

In fact, the Supramolecular and Sustainable chemistry group were involved in the preparation and study of different imidazolium receptors prepared from racemic mixtures,[171c,328] or from enantiomerically pure materials obtained from the chiral pool, as potentials receptors for anions.[171c,328b] Thus, imidazolium based receptors **1** and **2** (Figure 40) have been described as chiral shift agents (CSAs) for the enantiodiscrimination of racemic mandelate and other chiral carboxylic acids.[328b] The ditopic dicationic receptors **3** derived from amino acids with the general structure shown in Figure 40, have been used as chiral receptors for the enantiorecognition of dicarboxylic acids and as receptors and transporters for inorganic anions such as the spherical chloride, bromide and iodide anions and the trigonal NO_3^- anion.[215b]

Taking all this in account, the present thesis is based on supramolecular chemistry highlighting the self-assembly processes of the new compounds. The following chapters describe the synthesis and selfassembly behavior of new pseudopeptidic compounds and pseudopeptidic ionic liquids as well as their different applications.

---

326 (a) *Ammonium based anion receptors;* Llinares, J. M.; Powell, D.; Bowman-James, K.; *Coord. Chem. Rev.* **2003**, *240,* 57-75, (b) *Amide based receptors for anions;* Bondy, C. R.; Loeb, S. J.; *Coord. Chem. Rev.* **2003**, *240,* 77-99, (c) *N-confused calix[4]pyrroles;* Anzenbacher, P.; Nishiyabu, R.; Palacios, M. A.; *Coord. Chem. Rev.* ***2006****, 250,* 2929-2938, (d) *Influence of dimensionality and charge on anion binding in amide-based macrocyclic receptors;* Kang, S. O.; Hossain, M. A.; James, K. B.; *Coord. Chem. Rev.* **2006**, *250,* 3038-3052.

328 (a) *Chiral Imidazolium Receptors for Citrate and Malate: The Importance of the Preorganization;* Faggi, E.; Porcar, R.; Bolte, M.; Luis, S. V.; García-Verdugo, E.; Alfonso, I.; *J. Org. Chem.* **2014**, *79,* 9141-9149, (b) *Application of optically active chiral bis(imidazolium) salts as potential receptors of chiral dicarboxylate salts of biological relevance;* González-Mendoza, L.; Escorihuela, J.; Altava, B.; Burguete, M. I.; Luis, S. V.; *Org. Biomol. Chem.* **2015**, *13,* 5450-5459.

3.1.5 Bioactive ILs compounds

As named before, cancer disease kills millions of people around the world, so it is necessary to find ways to deal with this illness. The main problem is that the current treatment, which is chemotherapy, consists in chemical compounds with several toxicities to normal cells. Moreover, the low solubility and thus bioavailability of pharmaceutical compounds severely hamper the efficacy of important commercially available drugs.[329] Thereby, some poorly water-soluble drugs have been converted into lipophilic ionic liquids to facilitate incorporation into lipid-based formulations and integration into lipid absorption pathways. The resultant active pharmaceutical ingredient-ionic liquids (API–ILs) were liquids or low melting point solids and either completely miscible or highly soluble in lipid based.[330] In this regard, IL based on the association of choline with nonsteroidal anti-inflammatory drugs, ketoprofen and naproxen forming IL-APIs allowed to improve solubility up to 58 times which got the ability to interact with biological membranes. This fact can have a positive impact on drug bioavailability and ultimately on its efficacy.[331] Thus, ILs have been at the cutting edge of the most promising science and technology, so they are crucial candidates to solve these problems.[332] Hence, imidazolium based-ionic liquids have been found to be the most promising type of ionic liquids showing fascinating anticancer activities against different cancer cells.[333]

The anti-tumor activity of imidazolium salts is highly related to their lipophobicity because of the ILs' solubility and interactions with water, which is the predominant media of living beings. They are the utmost factors determining environmental/biological activity of ILs. Thus, imidazolium ILs compared with pyrrolidinium, pyridinium and piperidinium ILs containing butyl or isobutyl

---

329 *Ionic Liquids in Pharmaceutical Applications;* Marrucho, I. M.; Branco, L. C.; Rebelo, L. P. N.; *Annu. Rev. Chem. Biomol. Eng.* **2014**, *5*, 527–546.

330 *Transformation of Poorly Water-Soluble Drugs into Lipophilic Ionic Liquids Enhances Oral Drug Exposure from Lipid Based Formulations;* Sahbaz, Y.; Williams, H. D.; Nguyen, T-H.; Saunders, J.; Ford, L.; Charman, S. A.; Scammells, P. J.; Porter, C. J. H.; *Mol. Pharm.* **2015**, *12,* 1980−1991.

331 *Anti-inflammatory choline based ionic liquids: Insights into their lipophilicity, solubility and toxicity parameters;* Azevedo, A. M. O.; Costa, S. P. F.; Dias, A. F. V.; Marques, A. H. O.; Pinto, P. C. A. G.; Bica, K.; Ressmann, A. K.; Passos, M. L. C.; Araújo, A. R. T. S.; Reis, S.; Saraiva, M. L. M. F. S.; *J. Mol. Liq.* **2017**, *232,* 20-26.

332 *Ionic liquids as active pharmaceutical ingredients;* Ferraz, R.; Branco, L. C.; PrudÞncio, C.; Noronha, J. P.; Petrovski, Z.; Chem. Med. Chem. **2011**, *6*, 975-985.

333 (a) *Biological activity of ionic liquids and their application in pharmaceutics and medicine;* Egorova, K. S.; Gordeev, E. G.; Ananikov, V. P.; *Chem. Rev.* **2017**, *117,* 7132-7189, (b) *Cytotoxicity of Imidazole Ionic Liquids in Human Lung Carcinoma A549 Cell Line;* Chen, H-L.; Kao, H-F.; Wang, J-Y.; Wei, G-T.; Chin. J.; *Chem. Soc.* **2014**, *61,* 763–769, (c) *Imidazolium salts and their polymeric materials for biological Applications;* Riduan, S. N.; Zhang, Y.; *Chem. Soc. Rev.* **2013**, *42,* 9055-9070.

side chains and the bis(trifluoromethylsulfonyl)amide anion ($[NTf_2]^-$) are observed to be the most water soluble.[334] Lipophobicity can be tuned by the introduction of different hydrophobic substituents on the nitrogen atoms of the imidazolium ring of the molecule. Due to their amphiphilic character, strong interactions with biological materials can be expected. Taking this into consideration, 1-alkyl-3-methylimidazolium species showed to behave as amphipathic compounds and revealed surface activities analogous to quaternary ammonium compounds (QACs).[335] Long alkyl chain-containing imidazolium salts have been tasted against a sizable panel of cancer cell lines giving high activity.[336] Recently, researchers have started to assess a series of tripodal imidazolium salts as antibacterial and anticancer agents.[337]

Lipophilicity of compounds and their various structural modifications (existence of the aliphatic or aromatic polar group) has been proved to be related with toxicity of the compounds.[338] AlogP is a calculated lipophilic parameter useful to predict potential toxicity of the compounds. The most toxic compounds have the highest lipophilicity parameter, indicating that lipophilicity can be a good descriptor for predicting toxic effect of different compounds.

Moreover, another important factor to be considered is the CAC of the ILs. During IL-lipid membranes' interaction, ILs have the ability to self-aggregate in relation to the electrostatic or hydrophobic contributions of the isolated cation in water.[339] Lower critical micelle concentrations (CMCs) indicate easier formation of a lipid-like assembly, which could be beneficial for an incorporation

---

[334] *The effect of the cation alkyl chain branching on mutual solubilities with water and toxicities;* Kurnia, K. A.; Sintra, T. E.; Neves, C. M.; Shimizu, K.; Canongia Lopes, J. N.; Gonçalves, F.; Ventura, S. P.; Freire, M. G.; Santos, L. M.; Coutinho, J. A.; *Phys. Chem. Chem. Phys.* **2014**, *16,* 19952–19963.

[335] (a) *Biological effects of imidazolium ionic liquids with varying chain lengths in acute Vibrio fischeri and WST-1 cell viability assays;* Ranke, J.; Moelter, K.; Stock, F.; Bottin-Weber, U.; Poczobutt, J.; Hoffmann, J.; Ondruschka, B.; Filser, J.; Jastorff, B.; *Ecotoxicol. Environ. Saf.* **2004**, *58,* 396-404, (b) *Imidazole alkaloids from Lepidium meyenii;* Cui, B.; Zheng, B. L.; He, K.; Zheng, Q. Y.; *J. Nat. Prod.* **2003**, *66,* 1101-1103, (c) *Ionic liquids as pharmaceutical salts: a historical perspective;* Kumar, V.; Malhotra, S. V.; *ACS Symp. Ser.* **2010**, *1038,* 1–12.

[336] *A profile of the in vitro anti-tumor activity of imidazolium-based ionic liquids;* Malhotra, S. V.; Kumar, V.; *Bioorg. Med. Chem. Lett.* **2010**, *20,* 581-585.

[337] *Benzene centered tripodal imidazolium (BTI) system: Emerged towards multidisciplinary research and development;* Rondla, R.; *Inorg. Chim. Acta* **2018**, *477,* 183-191.

[338] *The effect of polar head group of dodecyl surfactants on the growth of wheat and cucumber;* Tot, A.; Maksimovic, I.; Putnik-Delic, M.; Danicic, M.; Gadzuric, S.; Bester-Rogac, M.; Vranes, M.; *Chemosphere* **2020**, *254,* 126918.

[339] *Self-aggregation of ionic liquids: micelle formation in aqueous solution;* Blesic, M.; Marques, M. H.; Plechkova, N. V.; Seddon, K. R.; Rebelo, L. P. N.; Lopes, A.; *Green Chem.* **2007**, *9,* 5, 481-490.

into a membrane.[340] In this regard, one recent study between RTILs based on 1-alkyl-3-methylimidazolium cations ($[C_nC_1Im]^+$) of alkyl group C_n from C_4 to C_8, in combination with a few different anions and DOPC lipid bilayer has demonstrated the effect of CMC into the cellular membrane damage.[341] The damage increases rapidly with increasing length n of the alkyl chain, proposing that long alkyl chain RTILs can act as detergents and exhibit strong lytic activity on the cell membranes. Thus, another influential factor on the toxicity of the ILs is the self-assembly process, suggesting that the micellation plays a critical role in the cellular toxicity.[342]

However, cancer is not the only significant illness that people worry about. Although it a growing problem to be faced, unfortunately others caused by microorganins are taking part in our daily basis. Nowadays, coronavirus disease (Covid-19) is an ongoing pandemic affecting 213 countries and territories around the world. It is caused by severe acute respiratory syndrome coronavirus 2 (SARS-CoV-2).[343]

Moreover, new cases of tuberculosis have recently appeared in developed countries such as Spain.[344] Tuberculosis is a bacterial infection caused by a germ called Mycobacterium tuberculosis. The bacteria usually attacks the lungs, but it can also damage other parts of the body even reaching people's death. Thus, bacterias can provoke important deadly diseases because they create biofilms as its major survival strategy in the face of environmental stresses. In this regard, a recent tangent in ionic liquids research aims to harness tuneable biological properties of these compounds in the design of novel potent antimicrobials.[345]

---

[340] *Influence of the Headgroup of Azolium-Based Lipids on their Biophysical Properties and Cytotoxicity;* Rehling, A.; Wang, D.; Ernst, J. B.; Wulff, S.; Honeker, R.; Richter, C.; Ferry, A.; Galla, H-J.; Glorius, F.; *Chem. Eur. J.* **2017**, *23,* 5920-5924.

[341] *Room-Temperature Ionic Liquids and Biomembranes: Setting the Stage for Applications in Pharmacology, Biomedicine, and Bionanotechnology;* Benedetto, A.; Ballone, P.; *Langmuir* **2018**, *34,* 9579−9597.

[342] (a) *A remarkably simple class of Imidazolium-based lipids and their biological properties;* Wang, D.; Richter, C.; Rühling, A.; Drücker, P.; Siegmund, D.; Metzler-Nolte, N.; Glorius, F.; Galla, H-J.; *Chem Eur J.* **2015**, *21,* 43, 15123-15126, (b) *Anti-tumor activity and cytotoxicity in vitro of novel 4,5-dialkylimidazolium surfactants;* Wang, D.; Richter, C.; Rühling, A.; Hüwel, S.; Glorius, F.; Galla, H-J.; *Biochem. Biophys. Res. Commun.* **2015**, *467,* 1033-1038.

[343] *"Naming the coronavirus disease (COVID-19) and the virus that causes it".* World Health Organization (WHO).

[344] *Sociedad Española de Neumología y cirugía toràcica SEPAR, https://www.separ.es/node/1081*

[345] *The antimicrobial potential of ionic liquids: A source of chemical diversity for infection and biofilm control;* Pendleton, J. N.; Gilmore, B. F.; *Int. J. Antimicrob. Agents* **2015**, *46,* 131–139.

Therefore, knowledge of the antibiofilm activity of ionic liquids is environmentally relevant. The family of 1-alkyl-3-methylimidazolium chloride ionic liquids demonstrated to have in vitro antibiofilm activity.[346] The study illustrated that antibiofilm activity of these ionic liquids was also dependent on alkyl chain length. Ionic liquids [$C_n$mim]Cl where n ≥10 exhibited broad spectrum antimicrobial activity. A range of 1-alkylquinolinium bromide ionic liquids also worked as antimicrobial and antibiofilm agents showing its dependency on the length of alkyl chain substituent, with compounds having alkyl chain lengths of 12-14 carbon atoms exhibiting greatest antimicrobial potency.[347]

Consequently, researchers have focused on ionic liquids as promising candidates of drugs due to their tuneable and physicochemical properties.[348] In this regard, imidazolium skeleton has demonstrated to be a promising type of ionic liquids with potent pharmacological properties.[349]

---

[346] *Antibiofilm activities of 1-alkyl-3-methylimidazolium chloride ionic líquids;* Carson, L.; Chau, P. K. W.; Earle, M. J.; Gilea, M. A.; Gilmore, B. F.; Gorman, S. P.; McCann, M. T.; Seddon K. R.; *Green Chem.* **2009**, *11,* 4, 492-497.

[347] *Antimicrobial and antibiofilm activities of 1-alkylquinolinium bromide ionic líquids;* Busetti, A.; Crawford, D. E.; Earle, M. J.; Gilea, M.; Gilmore, B. F.; Gorman, S. P.; Laverty, G.; Lowry, A. F.; McLaughlin, M.; Seddon, K. R.; *Green Chem.* **2010**, *12,* 420-425.

[348] (a) *Crystalline vs. ionic liquid salt forms of active pharmaceutical ingredients: a position paper;* Stoimenovski, J.; MacFarlane, D. R.; Bica, K.; Rogers, R. D.; Pharm. Res. **2010**, *27,* 521–526, (b) *Chemistry: Develop ionic liquid drugs;* Shamshina, J. L.; Kelley, S. P.; Gurau, G.; Rogers, R. D.; Nature 2015, 528, 188–189, (c) *The Use of Liquids Ionic Fluids as Pharmaceutically Active Substances Helpful in Combating Nosocomial Infections Induced by Klebsiella Pneumoniae New Delhi Strain, Acinetobacter Baumannii and Enterococcus Species;* Miskiewicz, A.; Ceranowicz, P.; Szymczak, M.; Bartus, K.; Kowalczyk, P.; *Int. J. Mol. Sci.* **2018**, *19,* 2779.

[349] (a) *Anti-microbial activities of ionic líquids;* Pernak, J.; Sobaszkiewicz, K.; Mirska, I.; *Green Chem.* **2003**, *5,* 52–56, (b) *Synthesis, characterization and the antimicrobial activity of new eco-friendly ionic líquids; M*essali, M.; Moussa, Z.; Alzahrani, A. Y.; El-Naggar, M. Y.; ElDouhaibi, A. S.; Judeh, Z. M. A.; Hammouti, B.; *Chemosphere* **2013**, *91,* 1627–1634; (c) *Dicationic imidazolium-based ionic liquids: a new strategy for non-toxic and antimicrobial materials;* Gindri, I. M.; Siddiqui, D. A.; Bhardwaj, P.; Rodriguez, L. C.; Palmer, K. L.; Frizzo, C. P.; Martinsc, M. A. P.; Rodrigues, D. C.; *RSC Adv.* **2014**, *4,* 62594, (d) *Imidazolium-Derived Ionic Salts Induce Inhibition of Cancerous Cell Growth through Apoptosis;* Malhotra, S. V.; Kumar, V.; Velez, C.; Zayas, B.; Med. Chem. Comm. 2014, 5, 1404–1409.

CHAPTER 2. General Objectives

CHAPTER 2. General Objectives

The aim of the thesis here presented is the design and development of pseudopeptidic multifunctional systems and their applications in supramolecular chemistry.

As mentioned before, this doctoral thesis includes seven scientific sections in which could be found the observations, experimental sections, and highlighted results (Chapter 3). All of them have been designed, planned, and developed to achieve the general objective proposed.

In this context, the general objectives considered for the current PhD work were as follows:

A. Designing and synthesizing a variety of new pseudopeptidic compounds derived from different amino acids as new LMWGs.

B. Designing and synthesizing a vast of new mono-, di- and tritopic imidazolium salts derived from different amino acids.

C. Characterising all the compounds synthesized using NMR, ATR-FT-IR, MS, DSC, TGA, $[\alpha]^{25}_{D}$ and elemental analysis.

D. Study some physical properties of great interest about the synthesized compounds in solution and solid state, such as supramolecular self-assembly behaviour, as well as analysing the supramolecular structures and stablish relations between its properties and structures.

E. Study the possible applications of the LMWGs as bioactive delivery systems, for example in drug delivery through skin or fragrances release.

F. Study the possible applications of the imidazolium salts as therapeutic agents, such as antibacterial or antitumoral compounds.

G. Synthesising new stationary phases based on silica-supported polymeric ionic liquid (PIL) for gas chromatography.

More concise objectives can be defined as follows:

1. Studying the preorganization of the supramolecular intermediates in the synthesis of tripodal amino acid imidazolium salts from

tris(halomethyl)benzenes and imidazoles using ^{1}H NMR spectroscopy, ESI mass spectrometry and Computational studies.

2. Testing a series of tripodal imidazolium salts derived from *L*-valine and *L*-phenylalanine containing different hydrophobic groups against different cancer cell lines at physiologic and acidic pHe (6.2).

3. Investigating the transmembrane anion transport abilities of the tripodal imidazolium salts at external physiologic and acidic pH.

4. Studying the aggregation behavior, size distributions and morphology of the aggregates formed of the different imidazolium Gemini amphiphiles derived from *L*-valine with different substitution pattern on the aromatic central spacer.

5. Investigating the emulsifying capacity of these imidazolium Gemini surfactants in different aqueous mixtures.

6. Designing of new imidazole and imidazolium salts derived from *L*-valine and *L*-phenylalanine containing different hydrophobic groups and testing their antibacterial activity.

7. Studying the aggregation behaviour of the imidazole and imidazolium salts to determine whether the monomeric or aggregate species were responsible of the observed antibacterial activity.

8. Synthesising new stationary phases for GC based on silica-supported polymeric ionic liquid (PIL) and study the effects of the amount of DVB as crosslinker on the the thermal stability and efficiency of the columns.

9. Designing new LMWGs from a new family of open chain-pseudopeptidic compounds functionalized with a pendant carboxylic group and studying them as hydrogelators for controlled drug delivery.

10. Designing low-molecular-weight organogelators derived from miminalistic pseudopeptidic structures containing alkylurea fragments and studying their gelation properties in relevant active substances.

CHAPTER 3.

3.1. Supramolecularly assisted synthesis of chiral tripodal imidazolium compounds

Supramolecularly assisted synthesis of chiral tripodal imidazolium compounds

Abstract

A strong preference for the formation of tripodal systems over the related monotopic and ditopic compounds is observed for the reaction between tris(halomethyl)benzenes and imidazoles derived from amino acids and containing an amide fragment. This preference allows the formation of the tripodal derivative as the major product even when an equimolar mixture of the tris(halomethyl)benzene and the imidazole is reacted (1 : 1 ratio instead of the stoichiometric 1 : 3 ratio). The reactions were monitored using 1H NMR spectroscopy and ESI mass spectrometry and kinetically characterized. Computational studies were also performed in order to rationalize the observed preference of the tri-substituted product. The results reveal the existence of well-defined supramolecular interactions between the imidazolium groups and the reacting imidazoles that facilitate the formation of the multitopic systems once the first imidazolium group is formed. Analysis of the different structural components shows that the presence of the amide group from the amino acid moiety is the key structural requirement for such supramolecular assistance to take place. The preorganization of the supramolecular intermediates formed through hydrogen bonding interactions involving amide-NH fragments in imidazoles and bromide anions in imidazolium groups seems to be also present at the corresponding TSs, decreasing the associated energy barriers.

1. Introduction

In nature, biomolecules are synthesized very efficiently, frequently triggered by external stimuli, through processes encompassing the appropriate supramolecular preorganization of the involved components. This is illustrated by enzymes displaying a high supramolecular preorganization.[1] Their catalytic activities depend on the presence of functional groups in the active site, often

[1] (a) *The evolution of multiple active site configurations in a designed enzyme;* Hong, N. S.; Petrović, D.; Lee, R.; Grynova, G.; Purg, M.; Saunders, J.; Bauer, P.; Carr, P. D.; Lin, C.-Y.; Mabbitt, P. D.; Zhang, W.; Altamore, T.; Easton, C.; Coote, M. L.; Kamerlin, S. C. L.; Jackson, C. J.; *Nat. Commun.* **2018**, *9*, 3900-3910, (b) *Conformational dynamics and enzyme evolution;* Petrovic, D.; Risso, V. A.; Kamerlin, S. C. L.; Sanchez-Ruiz, J. M.; *J. R. Soc. Interface* **2018**, *15*, 1742-5662, (c) *Transition States and Transition State Analogue Interactions with Enzymes;* Schramm, V. L.; *Acc. Chem. Res.* **2015**, *48*, 1032-1039.

belonging to amino acids situated far away in the peptidic sequence, located at the right distances and orientations and facilitating the proper preorganization of the substrates for the corresponding reaction.[2,3]

A suitable preorganization of the substrates assisted by supramolecular interactions can also be important in abiotic systems, particularly for synthesizing macrocyclic structures.[4] In this case, the approach of the two reactive ends is facilitated by the folding of the open-chain intermediate through hydrogen-bonding, conformational or configurational factors or by the use of templates.[5] For non-cyclic compounds, the formation of cyclic or chelate hydrogen bonds in close proximity to the target covalent bond can promote the desired reaction, facilitating the approach of the reactive elements.[6] Thus, the development of structures able to control a hierarchically ordered synthesis is an important and challenging target.

Considerable efforts have been made in developing selfreplicating systems.[7] In a model self-replicating system, the final molecule is able to selectively recognize

---

[2] Bugg, T. D. H.; *Introduction to Enzyme and Coenzyme Chemistry,* **2012***,* Wiley.

[3] *The tautomeric half-reaction of BphD, a C-C bond hydrolase. Kinetic and structural evidence supporting a key role for histidine 265 of the catalytic triad;* Horsman, G. P.; Bhowmik, S.; Seah, S. Y.; Kumar, P.; Bolin, J. T.; Eltis, L. D.; *J. Biol. Chem.* **2007**, *282*, 19894-19904.

[4] (a) *Anion-coordination-directed self-assemblies;* Yang, D.; Zhao, J.; Yang, X. J.; Wu, B.; *Org. Chem. Front.* **2018**, *5*, 662-690, (b) *Efficient active-template synthesis of calix[6]arene-based oriented pseudorotaxanes and rotaxanes;* Zanichelli, V.; Ragazzon, G.; Orlandini, G.; Venturi, M.; Credi, A.; Silvi, S.; Arduini, A.; Secchi, A.; *Org. Biomol. Chem.* **2017**, *15*, 6753-6763, (c) *Solvent driven selective pi-cation templating in dynamic assembly of interlocked molecules,* Pun, A. B.; Gagnon, K. J.; Klivansky, L. M.; Teat, S. J.; Li, Z. T.; Liu, Y.; *Org. Chem. Front.* **2014**, *1*, 167-175.

[5] (a) *Macrocycle Synthesis by Chloride-Templated Amide Bond Formation;* Martí-Centelles, V.; Burguete, M. I.; Luis, S. V.; *J. Org. Chem.* **2016**, *81*, 2143-2147, (b) *Structurally disfavoured pseudopeptidic macrocycles through anion templation;* Bru, M.; Alfonso, I.; Bolte, M.; Burguete, M. I.; Luis, S. V.; *Chem. Commun.* **2011**, *47*, 283-285, (c) *Supramolecular Control for the Modular Synthesis of Pseudopeptidic Macrocycles through an Anion-Templated Reaction;* Alfonso, I.; Bolte, M.; Bru, M.; Burguete, M. I.; Luis, S. V.; Rubio, J.; *J. Am. Chem. Soc.* **2008**, *130*, 6137, (d) *Designed Folding of Pseudopeptides: The Transformation of a Configurationally Driven Preorganization into a Stereoselective Multicomponent Macrocyclization Reaction;* Alfonso, I.; Bolte, M.; Bru, M.; Burguete, M. I.; Luis, S. V.; *Chem.–Eur. J.* **2008**, *14*, 8879, (f) *Structurally disfavoured pseudopeptidic macrocycles through anion templation;* Bru, M.; Alfonso, I.; Burguete, M. I.; Luis, S. V.; *Tetrahedron Lett.* **2005**, *46*, 7781, (e) *Efficient macrocyclization of U-turn preorganized peptidomimetics: the role of intramolecular H-bond and solvophobic effects;* Becerril, J.; Bolte, M.; Burguete, M. I.; Galindo, F.; García-España, E.; Luis, S. V.; Miravet, J. F.; *J. Am. Chem. Soc.* **2003**, *125*, 6677-6686, (g) *Polyazacyclophanes. 2,6,9,13-Tetraaza[14] paracyclophane as a cationic and anionic receptor;* Andrés, A.; Burguete, M. I.; García-España, E.; Luis, S. V.; Miravet, J. F.; Soriano, C.; *J. Chem. Soc. Perkin Trans. 2*, **1993**, 749-755.

[6] Maharramov, A. M.; Mahmudov, K. T.; Kopylovich, M. N.; Pombeiro, A. J. L.; *Non-covalent Interactions in the Synthesis and Design of New Compounds*, **2016**, Wiley.

[7] (a) *Parasitic Behavior of Self-Replicating Molecules;* Altay, M.; Altay, Y.; Otto, S.; *Angew. Chem. Int. Ed.* **2018**, *57*, 10564-10568, (b) *Exploring the emergence of complexity using synthetic replicators;* Kosikova, T.; Philp, D.; *Chem. Soc. Rev.* **2017**, *46*, 7274-7305, (c) *Towards open-ended evolution in self-replicating molecular systems;* Duim, H.; Otto, S.; *Beilstein J. Org. Chem.* **2017**, *13*, 1189-1203, (d) *Self-replicating systems;* Clixby, G.; Twyman, L.; *Org. Biomol. Chem.* **2016**, *14*, 4170-4184, (e) *A self-replicating peptide nucleic acid;* Plöger, T. A.; von Kiedrowski, G.; *Org. Biomol.*

the component fragments and preorganize them in the correct location as to promote the synthesis of a new identical molecule in a selfcatalytic process.[8,9] If several interacting replicators are combined, then complex behaviours can occur as the network of cross and autocatalytic reactions increases in size.[10,11]

In this regard, the synthesis of polytopic receptors can benefit from a proper recognition by the monotopic intermediate of one of the components, favouring the synthesis of the ditopic system. The recognition of this component by the ditopic intermediate would favour the preparation of the tritopic compound and so on, eventually leading to polytopic systems even in the presence of a limited amount of the component being recognized. In this context, polytopic supramolecular imidazolium receptors are of current relevance taking into account their properties as receptors and transporters,[12,13] with tripodal imidazolium compounds providing flexible but selective 3D environments for

Chem. **2014**, *12*, 6908-6914, (f) *Mechanisms of Autocatalysis;* Bissette, A. J.; Fletcher, S. P.; *Angew. Chem. Int. Ed.* **2013**, *52*, 12800-12826, (g) *Sigmoidal growth in a self-replicating system;* Rotello, V.; Hong, J. I.; Rebek, J.; *J. Am. Chem. Soc.* **1991**, *113*, 9422-9423.

[8] (a) *Autocatalysis and organocatalysis with synthetic structures;* Kamioka, S.; Ajami, D.; Rebek, J.; *Proc. Natl. Acad. Sci. U. S. A.* **2010**, *107*, 541-544, (b) *Making Molecules Make Themselves – the Chemistry of Artificial Replicators;* Vidonne, A.; Philp, D.; *Eur. J. Org. Chem.* **2009**, 593-610.

[9] (a) *Self-Replicating Molecules: A Second Generation;* Wintner, E. A.; Conn, M. M.; Rebek, J.; *J. Am. Chem. Soc.* **1994**, *116*, 8877-8884, (b) *New Evidence for Template Effects in a Self-Replicating System;* Conn, M. M.; Wintner, E. A.; Rebek, J.; *J. Am. Chem. Soc.* **1994**, *116*, 8823-8824, (c) *Template Effects in New Self-Replicating Molecules;* Conn, M. M.; Wintner, E. A.; Rebek, J.; *Angew. Chem. Int. Ed. Engl.* **1994**, *33*, 1577-1579, (d) *Crossover Reactions Between Synthetic Replicators Yield Active and Inactive Recombinants;* Feng, Q.; Park, T. K.;Rebek, J.; *Science* **1992**, *256*, 1179-1180, (e) *Kinetic studies and modeling of a self-replicating system;* Nowick, J. S.; Feng, Q.; Tjivikua, T.; Ballester, P.; Rebek, J.; *J. Am. Chem. Soc.* **1991**, *113*, 8831-8839.

[10] *Autocatalytic networks: the transition from molecular self-replication to molecular ecosystems;* Lee, D. H.; Severin, K.; Ghadiri, M. R.; *Curr. Opin. Chem. Biol.* **1997**, *1*, 491-496.

[11] (a) *Autocatalysis and organocatalysis with synthetic structures;* Kamioka, S.; Ajami, D.; Rebek, J. Jr.; *Proc Natl Acad Sci U S A* **2010**, *107*, 541-544, (b) *Synthetic autocatalysts show organocatalysis of other reactions;* Kamioka, S.; Ajami, D.; Rebek, J. Jr.; *Chem. Commun.* **2009**, 7324-7326, (c) *Chemistry - Amplification by compartmentalization;* Chen, J.; Korner, S.; Craig, S. L.; Rudkevich, D. M.; Rebek, J. Jr.; *Nature* **2002**, *415*, 385-386.

[12] (a) *Flexible imidazolium macrocycles: building blocks for anion-induced self-assembly,* Yang, Y. D.; Sessler, J. L.; Gong, H. Y.; *Chem. Commun.* **2017**, *53*, 9684-9696, (b) *Revisit to imidazolium receptors for the recognition of anions: highlighted research during 2006–2009;* Xu, Z.; Kim, S. K.; Yoon, J.; *Chem. Soc. Rev.* **2010**, *39*, 1457-1466.

[13] (a) *Anion Template-Directed Synthesis of Dicationic [14]Imidazoliophanes*, Alcalde, E.; Ramos, S.; Perez-García, L.; *Org. Lett.* **1999**, *1*, 1035-1038, (b) *Quantitative Evaluation of the Chloride Template Effect in the Formation of Dicationic [14]Imidazoliophanes*, Ramos, S.; Alcalde, E.; Doddi, G.; Mencarelli, P.; *J. Org. Chem.* **2002**, *67*, 8463-8468, (c) *Imidazolium-Based Dicationic Cyclophanes. Solid-State Aggregates with Unconventional (C–H)$^{+}$···Cl^{-} Hydrogen Bonding Revealed by X-ray Diffraction*, Alcalde, E.; Mesquida, N.; Vilaseca, M.; Alvarez-Rúa, C.; García-Granda, S.; *Supramolecular Chemistry* **2007**, *19*, 501-509.

anion recognition.[14] Thus, based on the previous results of our group,[15] tripodal compounds displaying the general structure shown in Figure 1f represented an interesting target, combining a well-defined 3D cavity with hydrogen bonding potential (amide and imidazolium moieties) with hydrophobic and aromatic regions playing essential roles in supramolecular recognition.[16] They integrate the supramolecular features of imidazolium compounds and those of amphiphilic pseudopeptides.[17] The synthetic approach is straightforward, involving the reaction of three equivalents of the corresponding imidazole with a tris(halomethyl) benzene. However, the accumulation of charge in the periphery of the aromatic fragments could hamper the introduction of the second and the third charged fragment. Rather surprisingly, preliminary experiments showed that even when working with a defect of the imidazole (*e.g.* equimolar mixtures) the tripodal imidazolium compound was always preferentially obtained over the related mono- and ditopic molecules.

---

[14] (a) *Benzene centered tripodal imidazolium (BTI)system: Emerged toward smulti disciplinary research and development;* Rondla, R.; *Inorg. Chim. Acta* **2018**, *477*, 183-191, (b) *Tripodal halogen bonding iodo-azolium receptors for anion recognition;* Ruiz-Botella, S.; Vidossich, P.; Ujaque, G.; Peris, E.; Beer, P. D.; *RSC Adv.* **2017**, *7*, 11253-11258, (c) *Di- and Tricationic Organic Salts: An Overview of Their Properties and Applications;* D'Anna, F.; Notto, R.; *Eur. J. Org. Chem.* **2014**, 4201-4223, (d) *Homochiral tripodal imidazolium receptors: structural and anion-receptor studies;* Alhashimy, N.; Brougham, D. J.; Howarth, J.; Farrell, A.; Quilty, B.; Nolan, K.; *Tetrahedron Lett.* **2007**, *48*, 125-128, (e) *Tripodal Nitro-Imidazolium Receptor for Anion Binding Driven by (C−H)+- - -XHydrogen Bonds;* Ihm, H.; Yun, S.; Gon Kim, H.; Kim, J. K.; Kim, K. S.; *Org. Lett.* **2002**, *4*, 2897-2900.

[15] (a) *Application of optically active chiral bis(imidazolium) salts as potential receptors of chiral dicarboxylate salts of biological relevance;* Gonzalez, L.; Escorihuela, J.; Altava, B.; Burguete, M. I.; Luis, S. V.; *Org. Biomol. Chem.* **2015**, *13*, 5450-5459, (b) *Bis(imidazolium) salts derived from amino acids as receptors and transport agents for chloride anions;* Gonzalez, L.; Altava, B.; Burguete, M. I.; Escorihuela, J.; Hernando, E.; Luis, S. V.; Quesada, R.; Vicent, C.; RSC Adv. **2015**, *5*, 34415-34423.

[16] (a) *Supramolecular forces and their interplay in stabilizing complexes of organic anions: tuning binding selectivity in water;* Savastano, M.; Bazzicalupi, C.; Garcia-Gallarin, C.; de la Torre, M. D. L.; Bianchi, A.; Melguizo, M.; *Org. Chem. Front.* **2019**, *6*, 75-86, (b) *Molecular recognition: preparation and characterization of two tripodal anion receptors;* Shokri, A.; Deng, S. H. M.; Wang, X. B.; Kass, S. R.; *Org. Chem. Front.* **2014**, *1*, 54-61, (c) *Selectivity in supramolecular host–guest complexes;* Schneider, H. J.; Yatsimirsky, A. K.; *Chem. Soc. Rev.* **2008**, *37*, 263-277, (d) *What Anions Do to N−H-Containing Receptors;* Amendola, V.; Fabbrizzi, L.; *Acc. Chem. Res.* **2006**, *39*, 343-353, (e) *Alfred Werner Revisited: The Coordination Chemistry of Anions;* Bowman-James, K.; *Acc. Chem. Res.* **2005**, *38*, 671-678, (f) Bianchi, A.; Bowman-James, K.; Garcia-España, E.; *The Supramolecular Chemistry of Anions;* Wiley-VCH, Weinheim, **1997**.

[17] (a) *Bioinspired chemistry based on minimalistic pseudopeptides;* Luis, S. V.; Alfonso, I.; *Acc. Chem. Res.* **2014**, *47*, 112, (b) *Evaluation of multivalency as an organization principle for the efficient synthesis of doubly and triply threaded amide rotaxanes;* Kaufmann, L.; Trautsen, N. L.; Springer, A.; Schroder, H. V.; Makela, T.; Rissanen, R.; Schalley, C. A.; *Organic Chemistry Frontiers* **2014**, *1*, 521-531.

In light of these initial results, this process has been studied in detail to properly understand the specific supramolecular effects favouring the formation of the tripodal imidazolium species and the influence of the different structural elements. The combination of experimental results and computational studies has been essential for understanding the effects observed.

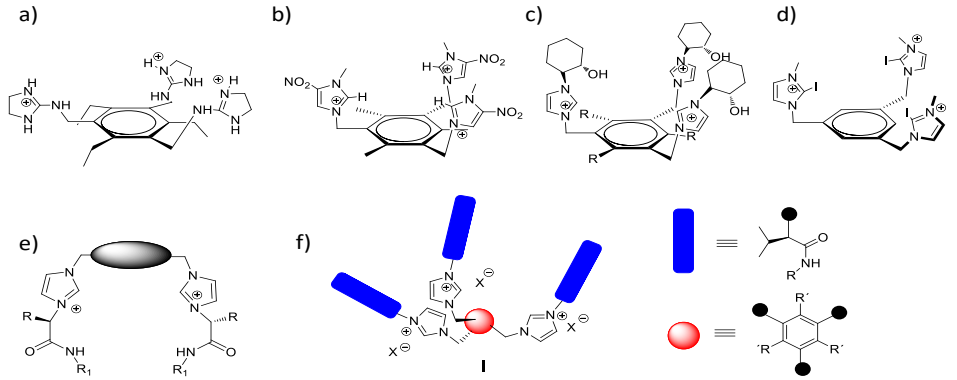

Figure 1 Polytopic supramolecular receptors based on imidazolium and relate systems: (a) citrate receptor;[18d] (b) halide recognition;[14e] (c) citrate and malate recognition;[19a] (d) anion recognition involving halogen-bonding instead of hydrogen onding;[14a] (e) transmembrane chloride transport and CSA for dicarboxylic acids;[15b] (f) tripodal receptors in this work.

2. Results and discussion

As shown in Figure 1, the general tripodal structure **I** contains three elements of diversity: the central aromatic core, the side chain of the amino acid used for the preparation of the imidazole ring and the length of the aliphatic chain attached to the amino acid moiety through an amide bond. The final synthetic step involves a [1 + 3] S_N2 process between a tris(halomethyl) benzene and an amino acid based imidazole (Scheme 1). Tris (halomethyl)benzenes are standard alkylating agents used in the synthesis of different tripodal receptors including imidazolium salts and pseudopeptic cages.[18,19]

---

[18] (a) *Template Synthesis of Three-Dimensional Hexakisimidazolium Cages;* Sun, L. Y.; Sinha, N.; Yan, T.; Wang, Y. S.; Tan, T. T. Y.; Yu, L.; Han, Y. F.; Hahn, F. E.; *Angew. Chem. Int. Ed.* **2018**, *57*, 5161-5165, (b) *Effect of counterions and central cores of tripodal imidazolium salts on palladium-catalyzed Suzuki–Miyaura cross-coupling reactions;* Zhong, R.; Wang, Y. N.; Guo, X. Q.; Hou, X. F.; *J. Organomet. Chem.* **2011**, *696*, 1703-1707, (c) *A small tris(imidazolium) cage forms an N-heterocyclic carbene complex with silver(i);* Willans, C. E.; Anderson, K. M.; Junk, P. C.; Barbour, L. J.; Steed, J. W.; *Chem. Commun.* **2007**, 3634-3636, (d) *A Chemosensor for Citrate in Beverages;* Metzger, A.; Anslyn, E. V.; *Angew. Chem. Int. Ed.* **1998**, *37*, 649-652.

[19] (a) *Chiral imidazolium receptors for citrate and malate: the importance of the preorganization;* Faggi, E.; Porcar, R.; Bolte, M.; Luis, S. V.; García-Verdugo, E.; Alfonso, I.; *J. Org. Chem.* **2014**, *79*, 9141-9149, (b) *Tuning Chloride Binding, Encapsulation, and Transport by Peripheral Substitution of Pseudopeptidic Tripodal Small Cages;* Martí, I.; Rubio, J.; Bolte, M.; Burguete, M. I.; Vicent, C.; Quesada, R.; Alfonso, I.; Luis, S. V.; *Chem.–Eur. J.* **2012**, *18*, 16728-16741, (c) *Tight and Selective Caging of Chloride Ions by a Pseudopeptidic Host;* Martí, I.; Bolte, M.; Burguete, M. I.; Vicent, C.; Alfonso, I.; Luis, S. V.; *Chem.–Eur. J.* **2014**, *20*, 7458-7464.

Moreover, the synthesis of the considered amino acid based imidazoles has been previously described.[20]

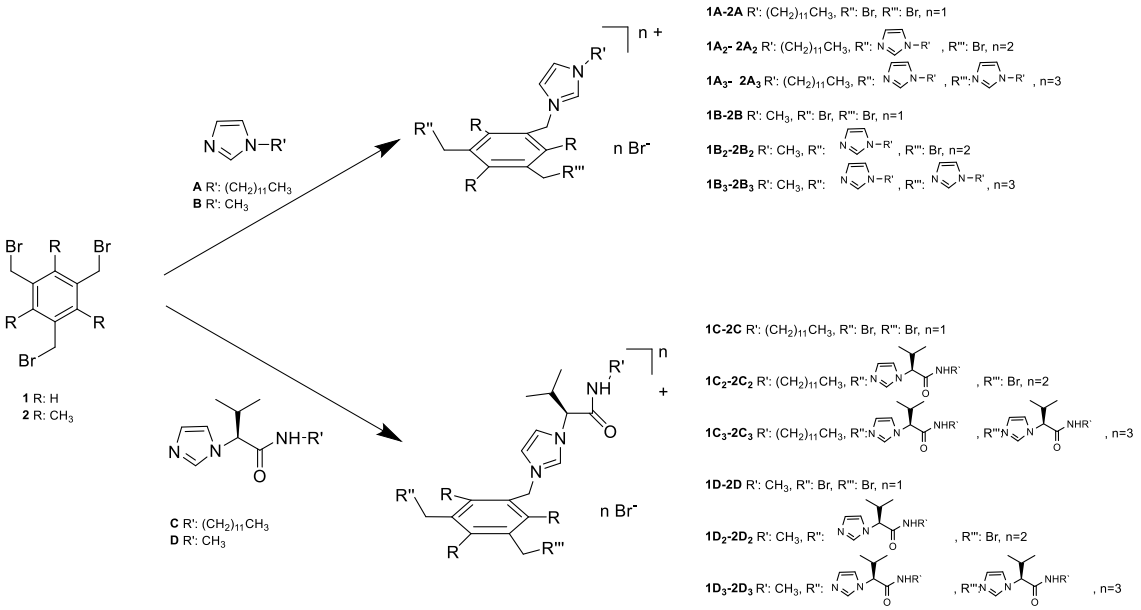

Scheme 1 Synthetic approach for the preparation of polytopic imidazolium compounds from the reaction between different imidazoles (**A**-**C**) and 1,3,5-tris(bromomethyl)benzene derivatives (**1**, **2**). The structure of each polyimidazolium compounds is denoted by three digits, the first one is a number related to the aromatic component (**1** or **2**), the second one indicates the imidazole used (**A**-**C**) and the third one, included as a subindex, defines the monoimidazolium (**NX$_1$**), bisimidazolium (**NX$_2$**) or tris(imidazolium) (**NX$_3$**) structure.

Initial experiments involving tris(bromomethyl)benzene **1** and the imidazole obtained from valine and containing a dodecyl aliphatic tail (**C**) (Scheme 1) revealed that the preparation of the corresponding tripodal trisimidazolium compound **1C$_3$** took place very efficiently. Even when a deficit of imidazole was used (equimolar **1** : **C** ratio) the tripodal derivative **1C$_3$** was the major species formed, while the monotopic (**1C**) and the ditopic (**1C$_2$**) imidazolium salts were only obtained as minor side products (**1C$_3$**: 73%, **1C$_2$**: 12% and **1C**: 5%).

In order to analyse the generality of this process and its origin, the preparation of a family of imidazolium compounds, as shown in Scheme 1, was considered. To simplify this analysis, the amino acid component was fixed to be L-valine, while the alkyl chain attached to the amide nitrogen atom was either dodecyl (long aliphatic tail, imidazole **C**) or methyl (short aliphatic tail, imidazole **D**). Finally the alkylating agents selected were 1,3,5-tris(bromomethyl)benzene (**1**)

[20] *Synthesis of Chiral Room Temperature Ionic Liquids from Amino Acids – Application in Chiral Molecular Recognition;* González, L.; Altava, B.; Bolte, M.; Burguete, M. I.; García-Verdugo, E.; Luis, S. V.; *Eur. J. Org. Chem.* **2012**, 4996-5009.

and its 2,4,6-trimethyl derivative (**2**), previously used for the synthesis of tris (imidazolium) derivatives.[18,19] Commercially available N-dodecyl (**A**) and N-methyl (**B**) imidazoles were also studied as nucleophiles to provide suitable comparison models lacking the amino acid based fragment.

2.1. ^{1}H NMR and ESI-MS experiments

Initial kinetic experiments were carried out in $CDCl_3$ by ^{1}H NMR. To ensure that aggregation processes did not interfere, it was checked that these imidazoles do not aggregate in this solvent in the 1 to 60 mM range (ESI, Figure S1‡ for imidazoles **A** and **C**). Thus, the imidazole concentration was fixed in all experiments to ca. 15 mM in $CDCl_3$ and the reactions were carried out in an NMR tube. The temperature was kept constant at 25 °C and dioxane (0.17 mM) was used as the internal standard. ^{1}H NMR spectra were obtained directly from these reaction tubes and the same reaction crudes were also analysed by ESI-MS. The reactions were monitored for up to ca. 700 h. Different tris(halomethyl)arene : imidazole molar ratios (*ca.* 1 : 3, 1 : 2 and 1 : 1) were assayed. Although some of the signals of interest could overlap at specific reaction times, ^{1}H NMR spectra allowed the determination of the concentration of the different species involved at the different time intervals.

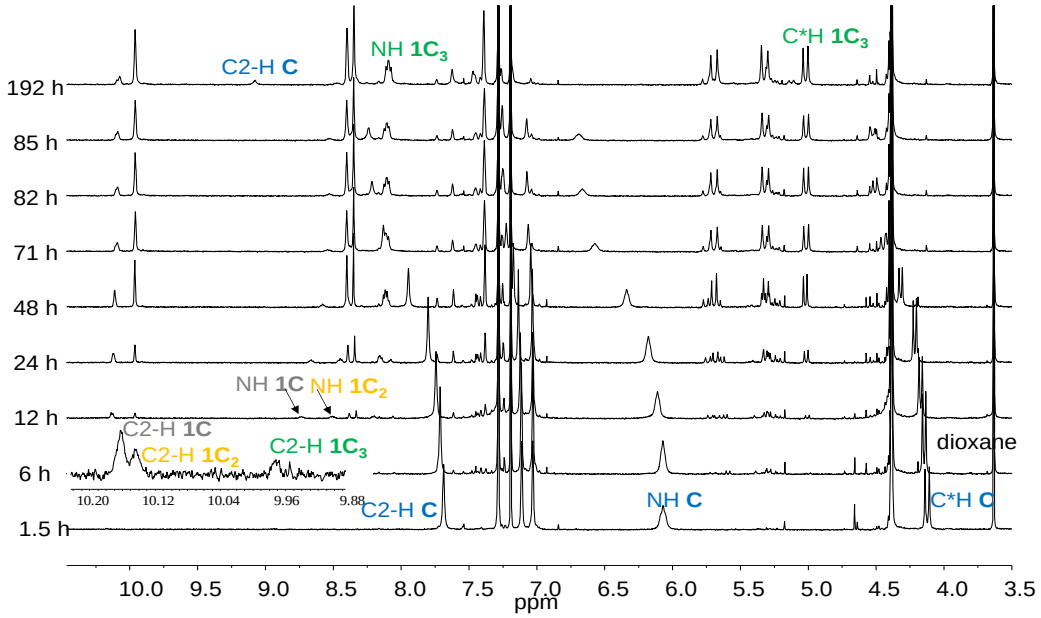

Figure 2 Partial ^{1}H NMR (400 MHz, $CDCl_3$) spectra obtained at different time intervals for the reaction of tris(bromomethyl)benzene **1** (13.8 mM) with imidazole **C** (13.8 mM) at 25°C. The region around 10 ppm corresponding to the presence of C2-H signals of the imidazolium rings has been expanded for the spectrum after 6 h of reaction.

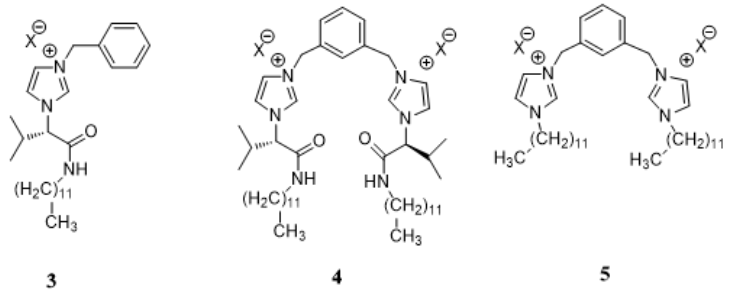

Figure 3 Model mono- and bis-imidazolium salts used for reference.

Figure 2 shows the ^{1}H NMR spectra of the process leading to **1C$_3$** when an equimolar mixture of aromatic compound **1** and imidazole **C** was used. The signal corresponding to the C2–H proton of the imidazolium ring in **1C$_3$** was observed initially at ca. 10.03 ppm, while the signals for the mono- and di-substituted products appeared at 10.22 and 10.20 ppm respectively (see the expanded region after 6 h of reaction). These chemical shifts, and others used in this study, agreed well with those obtained for the pure isolated **1C$_3$**, and for the model compounds **3** and **4** that had been prepared previously (Figure 3; ESI, Figure S2‡).[15a] The formation of **1C$_3$** could also be followed through the appearance of other characteristic signals like those for the amide NH and the proton at the stereogenic carbon atom (C*–H) initially at 8.22 and 5.08 ppm respectively. The signals originally at 7.78, 6.14 and 4.21 ppm, corresponding to the imidazole C2–H, amide NH and the C*–H of the starting imidazole **C** could be used to monitor its disappearance.

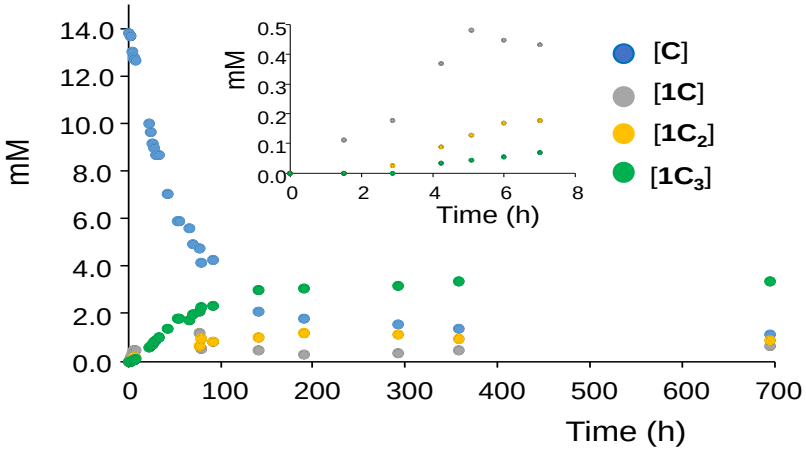

Figure 4 Variation with time of the concentration of the different species for an equimolar mixture (13.8 mM) of **1** and **C** as measured following the C2–H proton signals of the imidazolium compounds (green **1C$_3$**, yellow **1C$_2$**, grey **1C**) and those for the C*–H (blue) signal for **C**; the inset displays the formation of imidazolium species at initial times. Reaction carried out in $CDCl_3$ at 25 °C.

Figure 4 shows the kinetic profiles obtained for this reaction using these signals. Data presented in Figure 4 (top) for the equimolar mixture of **1** and **C** show clearly how the formation of the tripodal compound **1C$_3$** is significantly favoured over that of the mono- and di-substituted species **1C** and **1C$_2$**. After 77 h, the conversion of the starting imidazole **C** increased to ca. 65%, with 46% of these units incorporated into **1C$_3$**, 9% of them into **1C$_2$** and only 9% into **1C**. After this time, the concentration of **1C$_3$** continued to increase but not those of **1C$_2$** and **1C**. After 360 h, imidazole conversion reached ca. 90%, with more than 72% of the consumed imidazole groups incorporated into **1C$_3$**. The inset in Figure 4 reveals the existence of an apparent induction period for the formation of the bis- and tris-imidazolium derivatives **1C$_2$** and **1C$_3$** (ca. 3 and 4 h respectively), but not for **1C**, which has been often associated with processes involving autocatalytic steps or related processes.[7–10] Similar results were obtained when the **1** : **C** ratio was changed to 1 : 2.1 or 1 : 2.8 (ESI, Figure S3‡) with **1C$_3$** always being the major product obtained after ca. 24 h.

ESI-MS also allowed the reaction to be monitored, identifying charged species associated with the starting imidazole building block **C** and with the tri-, di- and mono-imidazolium derivatives (**1C$_3$**, **1C$_2$** and **1C**). Thus, for the reaction between 1,3,5-tris(bromomethyl)benzene **1** and the imidazole **C** in an equimolar ratio, after 48 h, ESI-MS in positive ion mode (Figure 5) contained a peak at m/z 612.4 for the monosubstituted compound [**1C**–Br]$^+$ (100% relative intensity) and a second minor peak at 434.6 (20%) associated with the bisimidazolium compound [**1C$_2$**–2Br]$^{2+}$. Species corresponding to the trisimidazolium product appeared at 374.6 and 602.0 associated with [1C3–3Br]3+ (75%) and [1C3–2Br]$^{2+}$ (80%, this peak can also contain contributions from [**1C$_2$**–2Br + **C**]$^{2+}$) and at 486.6 (10%), 598.2 (20%) and 710.2 (9%) related to the **1C$_3$** : **C** clusters [**1C$_3$**–3Br + **C**]$^{3+}$, [**1C$_3$**–3Br + 2**C**]$^{3+}$ and [**1C$_3$**–3Br + 3**C**]$^{3+}$. Moreover the peaks that appeared at 336.3 (50%) and 671.8 (16%) were associated with [**C** + H]$^+$ and [**C** + **C** + H]$^+$ species from the unreacted imidazole. After 697 h the peak at 612.4 for [**1C**–Br]$^+$ decreased significantly (20%) while the peak at 434.6 associated with [**1C$_2$**–2Br]$^{2+}$ maintained its intensity (20%); being the base peak, the one at 602.0 was associated with [**1C$_3$**–2Br]$^{2+}$. As expected, the peak at 336.5 associated with unreacted imidazole [**C** + H]$^+$ considerably decreased (18%).

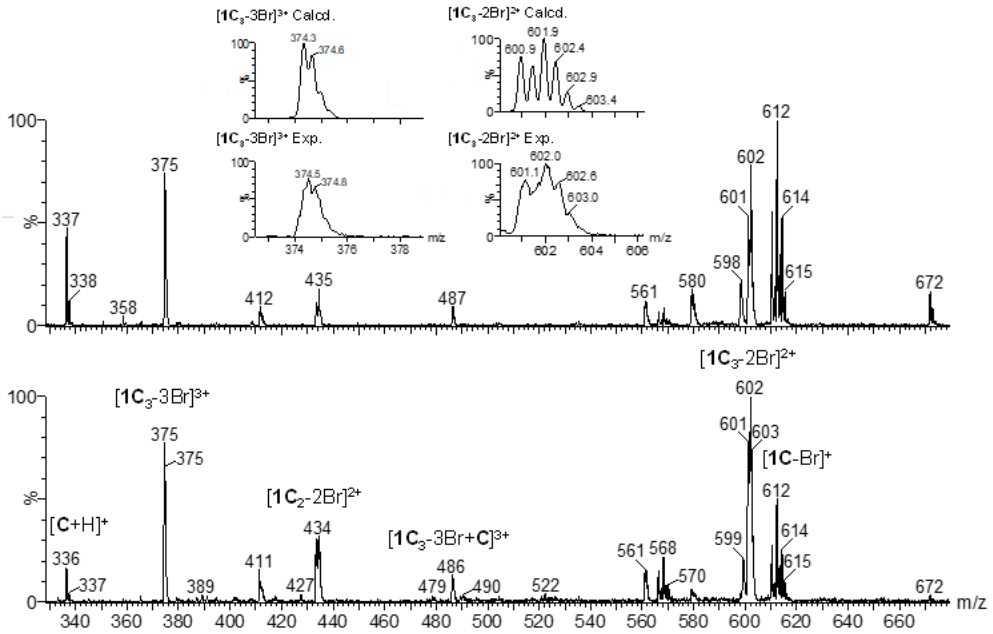

Figure 5 ESI-MS in positive ion mode obtained from an equimolar reaction mixture between tris(bromomethyl)benzene **1** and imidazole **C** after 48 h (top) and 697 h (bottom) of reaction. The initial concentration of both reactants was 13.8 mM. All the assigned peaks provided the correct isotopic pattern. The insets show the comparison of the calculated and observed isotopic patterns for the peaks at 375 and 602.

Moreover, when the **1** : **C** molar ratios were ca. 1 : 2 and 1 : 3, ESI-MS in positive ion mode after 48 h displayed the most intense peaks for the $\mathbf{1C_3}$ clusters [$\mathbf{1C_3}$–3Br + 2**C**]$^{3+}$ and [$\mathbf{1C_3}$–3Br + **C**]$^{3+}$, the abundance of peaks from mono and bisimidazolium salts being lower (ESI, Figure S4, Table S1‡). ESI-MS in positive ion mode after 697 h for the 1 : 3 molar ratio was simplified with the two most important peaks corresponding to [$\mathbf{1C_3}$–3Br]$^{3+}$ and [$\mathbf{1C_3}$–2Br]$^{2+}$ species (ESI, Figure S4‡).

Some interesting differences were observed when imidazole **A** was studied in the reaction with 1,3,5-tris(bromomethyl)benzene. Imidazole **A** is identical to **C** but lacks the amino acid moiety and accordingly the supramolecular potential associated with the peptidic bond in pseudopeptides.[15,17] Reaction progress was monitored following the C2–H (imidazolium) and benzylic methylene signals for the tripodal compound $\mathbf{1A_3}$ initially at 10.38 and 5.54 ppm respectively. For the monosubstituted **1A** and the disubstituted $\mathbf{1A_2}$ the signals appeared initially at 11.17 and 10.56 ppm respectively (imidazolium C2–H) and 5.68 and 5.63 ppm (benzylic protons). The disappearance of the signals initially at 3.94 and 7.58 ppm for the N–CH_2 and C2–H protons of imidazole **A** and at 4.45 ppm for the benzylic protons of **1** were used to determine the conversion (ESI, Figure S5‡).

These chemical shifts agreed with those for pure **1A$_3$** or for the model compound **5** (ESI, Figure S6‡).

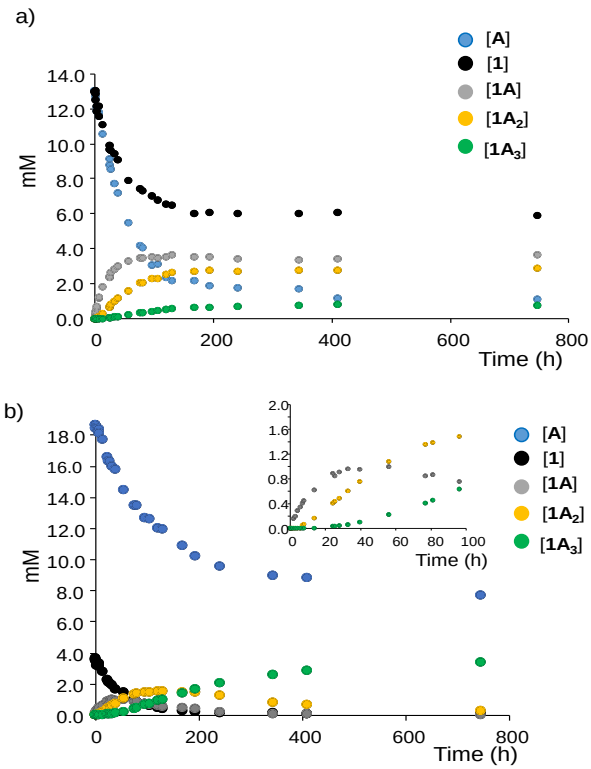

Figure 6 Kinetic profiles for the disappearance of **A** (blue) and **1** (black) and the formation of **1A** (grey), **1A$_2$** (yellow) and **1A$_3$** (green) by reaction of **1** and **A** in $CDCl_3$ at 25 °C following the C2–H protons for **A**, **1A**, **1A$_2$** and **1A$_3$** and the benzylic protons for **1**. (a) Using an equimolar ratio of 1 and imidazole **A** (13 mM). (b) Using a fivefold excess of **A** (18.6 mM) over **1** (3.6 mM).

Figure 6a shows the kinetic profiles obtained when the reaction was run with an equimolar mixture of imidazole **A** and **1** (13 mM). After 746 h at 25 °C, the conversion of the imidazole product was slightly higher than 90%, but only 17% of the consumed units were present in the tris(imidazolium) compound **1A$_3$**, with around 44% and 28% being incorporated into **1A$_2$** and **1A** species respectively. This behaviour clearly deviates from the one observed for the pseudopeptidic imidazole **C**, revealing the importance of the amino acid derived fragment in the preferential formation of the tripodal structure **1C$_3$**, which must be associated with supramolecular interactions involving the pseudopeptidic moiety.

The experiment carried out using a fivefold excess of imidazole **A** over 1,3,5-tris(bromomethyl)benzene **1** provided the expected kinetic profile in the absence of supramolecular assistance (Figure 6b, see ESI Figure S7‡ for ^{1}H NMR spectra)

with **1A** being the predominant species for the initial period, reaching a maximum yield of ca. 9% at a reaction time of 40 h.

Afterwards, the yield of **1A** starts to decrease while those of $\mathbf{1A_2}$ and $\mathbf{1A_3}$ increase, with $\mathbf{1A_2}$ being the predominant species until 170 h of reaction (up to 27% yield). Finally, after 170 h, the amount of $\mathbf{1A_2}$ also starts to decrease while the concentration of $\mathbf{1A_3}$ steadily increases to reach an essentially quantitative yield for long reaction times.

For the equimolar ratio of reagents and a reaction time of 48 h, ESI-MS in positive ion mode showed the peaks corresponding to the $[\mathbf{1A}–Br]^+$ (513.2, 100%), $[\mathbf{1A_2}–2Br]^{2+}$ (335.4, 20%) and $[\mathbf{1A_3}–3Br]^{3+}$ (275.4, 20%) species (Figure 7). At higher reaction times (747 h), the peak at 237.4 associated with $[\mathbf{A} + H]^+$ decreases (from 80% to 30%), the peaks at 335.4 and 275.4 m/z increase (40% and 28% respectively) and the peak at 513.2 m/z associated with $[\mathbf{1A}–Br]^+$ continues being the base peak (100%). When the reaction was run using an excess of **A** (3.9 mM in **1** and 19.9 mM in **A**) the peak for the unreacted imidazole was predominant at 48 h, while the one corresponding to $[\mathbf{1A_3}–3Br]^{3+}$ (275.4) became the base peak at longer reaction times (ESI, Figure S8, see also Table S2‡).

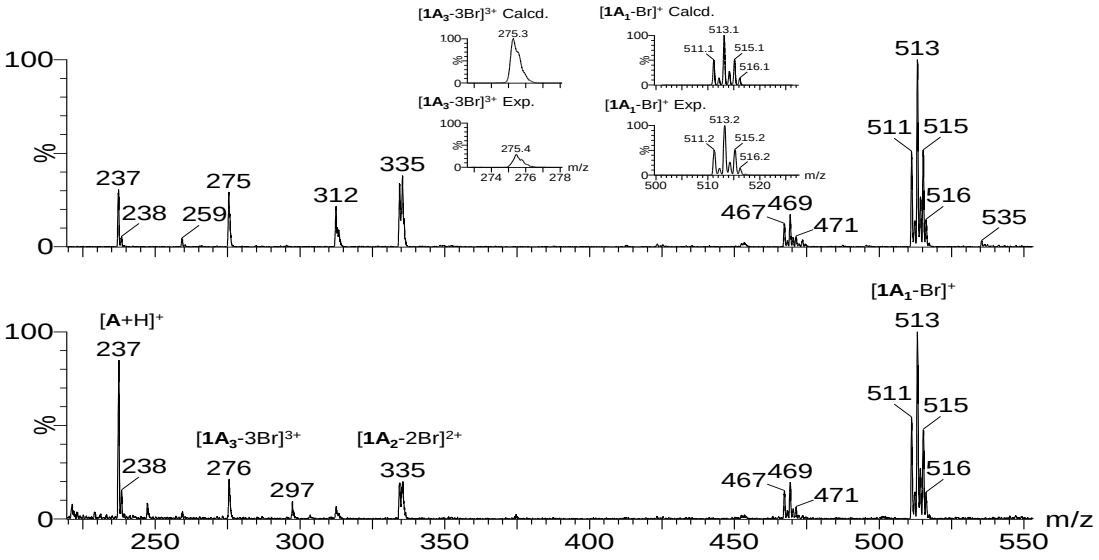

Figure 7 ESI-MS in positive ion mode obtained from an equimolar reaction mixture between tris(bromomethyl)benzene 1 and imidazole A after 48 h (bottom) and 747 h (top) of reaction in $CDCl_3$. The initial concentration of both reactants was 13 mM. All the assigned peaks provided the correct isotopic pattern. The insets show the comparison of the calculated and observed isotopic patterns for the peaks at 275 and 513.

The presence of a long aliphatic tail is also an important structural feature of imidazole **C**. Thus, the reaction between **1** and imidazole **D** having a methyl group instead of the dodecyl fragment was also studied by ^{1}H NMR and ESI-MS to obtain information on its role in the overall process (ESI, Figure S9 and S10‡). In this case, no significant differences were observed with respect to the use of imidazole **C**, revealing that the aliphatic chain does not play an important role in the observed preference towards the formation of **1C$_3$** or **1D$_3$**. Attempts to analyse the reaction of **1** with imidazole **B** lacking both the amino acid derived fragment and the long tail were unsuccessful due to the low solubility of the intermediates in $CDCl_3$. Finally, the effect of changing tris(halomethyl)arene was also studied. For the process involving imidazole **C** (14.8 mM) and 1,3,5-tris(bromomethyl)-2,4,6-trimethylbenzene **2** (15.6 mM), the conversion was monitored by following the ^{1}H NMR signals for the C2–H of the imidazole ring and the proton at the stereogenic carbon (initially at 7.81 and 4.24 ppm) in **C** along with the signal initially at 4.58 ppm for the benzylic protons of **2**. The signals for the C2–H imidazolium proton of **2C**, **2C$_3$** and **2C$_2$**, initially at 9.93, 9.80 and 9.40 ppm, were used to follow the formation of the different imidazolium species (ESI, Figure S11‡). The reaction was significantly faster than when using **1**, but again the formation of the tripodal compound **2C$_3$** was much favoured over that of **2C$_2$** and **2C**. In this case, **2C$_3$** became the major species present in the reaction mixture after 0.5 h (ESI, Figure 12a‡). ESI-MS in positive ion mode also confirmed these data, with the peaks associated with the tripodal species [**2C$_3$**–3Br]$^{3+}$ and [**2C$_3$**–2Br]$^{2+}$ being the more intense even at short reaction times (100% and 62% respectively, ESI, Figure S13a‡). Similar results were obtained for other **2** : **C** ratios (ESI, Figure S12c, d and S13c, d‡).

On the other hand, when imidazole **A** (15.7 mM) and **2** (13.8 mM) were used as starting materials, the reaction was again faster than with **1** but the formation of the monosubstituted and disubstituted imidazolium products **2A** and **2A$_2$** was favoured at all times over the formation of the tripodal compound. When a ca. 1 : 3 molar ratio (**2** : **A**) was used, **2A** and **2A$_2$** were the predominant imidazolium species up to 11 h of reaction and, later on, the concentration of these species decreased with the tripodal compound **2A$_3$** becoming predominant (ESI, Figure S14‡). The formation of the different species was also confirmed by ESI-MS (ESI, Figure S15‡). Thus, the preferential formation of tripodal species is associated with the presence of the amide group in **C** and **D**.

Some anions, and particularly bromide, are able to act as efficient catalysts in macrocyclization reactions involving S_N2 reactions and other processes of pseudopeptidic molecules.[21] The bromide anion can participate in templating a proper preorganization of the open chain precursor but also reducing the energy of the transition state through supramolecular interactions. Besides, the increase in the ionic strength of the medium has been reported to slightly increase the reaction rate in the synthesis of some dicationic imidazoliophanes through S_N2 reactions.[13] When the reaction was carried out in the presence of NEt_4Br (9 mM) employing imidazole **C** (16.6 mM) and **1** (7.6 mM) the results obtained revealed that the main effect of the presence of a bromide anion was a decrease in the overall conversion rate and in the formation of **1C$_3$**, although the tripodal compound was still the more abundant species (ESI, Figure S16‡).

2.2. Determination of kinetic constants

From the former experimental kinetic curves, a detailed kinetic analysis was carried out to determine the main kinetic parameters for each specific reaction. The fitting of the experimental data to a model considering a second order reaction for each step was carried out by means of the Levenberg–Marquardt nonlinear least-squares algorithm,[22] using the Rand the RStudio software.[23,24,25] Moreover, the Eyring equation, $k = (k_B T/h)\exp(-\Delta G‡/RT)$,[26] was employed to calculate the Gibbs free energy barrier. Table 1 summarizes the kinetic constants obtained following this approach. The calculated kinetic curves obtained from data in Table 1 show a good agreement with the experimental ones (ESI, Figure S17‡). Some deviations are observed for very long reaction times that can be associated with the difficulty in determining with enough

---

[21] (a) *The Role of the Amino Acid-Derived Side Chain in the Preorganization of C2 Symmetric Pseudopeptides: Effect on SN2 Macrocyclization Reactions;* Martí-Centelles, V.; Burguete, M. I.; Cativiela, C.; Luis, S. V.; *J. Org. Chem.* **2014**, *79*, 559-570, (b) *Fluorescent Acridine-Based Receptors for $H_2PO_4^-$;* Martí-Centelles, V.; Burguete, M. I.; Galindo, F.; Izquierdo, A. M.; Kumar, D. K.; White, A. J. P.; Luis, S. V.; Vilar, R. J.; *J. Org. Chem.* **2012**, *77*, 490-500.

[22] Elzhov, T. V.; Mullen, K. M.; Spiess, A. N.; Bolker, B.; *minpack.lm: R Interface to the Levenberg-Marquardt Nonlinear LeastSquares Algorithm Found in MINPACK, Plus Support for Bounds (R package version 1.2-0),* **2015**. https://CRAN.R-project.org/package=minpack.lm (accessedJanuary 23, 2018).

[23] R Core Team, R: *A language and environment for statistical computing, R Foundation for Statistical Computing,* Vienna, Austria, **2015**. https://www.R-project.org/ (accessed January 23, 2018).

[24] Studio Team, *RStudio: Integrated Development for R, version 0.99.892,* RStudio, Inc., Boston, MA, **2015**. http://www.rstudio.com/ (accessed January 23, 2018).

[25] *High Activity and Efficient Turnover by a Simple, Self-Assembled Artificial "Diels-Alderase";* Martí-Centelles, V.; Lawrence, A. L.; Lusby, P. J.; *J. Am. Chem. Soc.* **2018**, *140*, 2862-2868.

[26] (a) *Development of transition-state theory;* Laidler, K. J.; King, M. C.; *J. Phys. Chem.* **1983**, *87*, 2657-2664, (b) *Perspective on "The activated complex in chemical reactions";* Petersson, G. A.; *Theor. Chem. Acc.* **2000**, *103*, 190-195.

accuracy the experimental values by ^{1}H NMR for some of the species at these times and by the potential interference of the formation of unproductive supramolecular complexes between the tripodal species and the starting imidazole (*e.g.* **C·1C$_3$**).

Table 1 Kinetic parameters obtained for the different reactions studied in the synthesis of tris(imidazolium) compounds[a,b]

Tripodal final compound	k_1 (M^{-1} h^{-1})	k_2 (M^{-1} h^{-1})	k_3 (M^{-1} h^{-1})	$\Delta G_1^{\ddagger}$ (kcal/mol)	$\Delta G_2^{\ddagger}$ (kcal/mol)	$\Delta G_3^{\ddagger}$ (kcal/mol)
	Macroscopic kinetic constants[b]					
1C$_3$	0.46 ± 0.01	10.33 ± 1.04	4.43 ± 0.25	17.98 ± 0.01	16.13 ± 0.06	16.63 ± 0.03
1A$_3$	0.99 ± 0.01	1.75 ± 0.04	0.72 ± 0.04	17.53 ± 0.01	17.18 ± 0.02	17.71± 0.03
2C$_3$	9.36 ± 0.22	245.49 ±37.81	379.35 ±98.65	16.19 ± 0.01	14.24 ± 0.09	13.99 ± 0.14
2A$_3$	11.81 ± 0.35	28.96 ± 1.65	9.04 ± 0.74	16.05 ± 0.02	15.51 ± 0.03	16.21 ± 0.05
	Intrinsic kinetic constants					
1C$_3$	0.15	5.16	4.43			
1A$_3$	0.33	0.87	0.72			
2C$_3$	3.12	122.74	379.35			
2A$_3$	3.94	14.48	9.04			

[a] All the experimental data, obtained using the different studied ratios between substrates, were used for the fitting. b k1, k2 and k3 correspond to the formation of the monotopic, ditopic and tripodal compounds respectively.

Data in Table 1 show that kinetic constants obtained for 1,3,5-tris(bromomethyl)-2,4,6-trimethylbenzene **2** are significantly higher than those for 1,3,5-tris(bromomethyl)benzene **1**. When the pseudopeptidic imidazole **C** is used, k_1 is always smaller than k_2 and k_3, while k_3 is always the smaller constant when imidazole **A** is used, highlighting the role of the amide moiety in the supramolecular assistance for the preferential formation of polytopic imidazolium systems. When analysing the absolute values for the constants, it is important to bear in mind that the concentration of the bromomethyl species has been used directly for the calculations. However, compounds **1** or **2** contain three reactive sites, the monotopic species like **1C** contain two reactive sites and the ditopic species like **1C$_2$** contain just one reactive site. Thus, a statistical correction provides the corresponding microconstants describing the intrinsic reactivity of the respective bromomethyl groups. This reveals that the intrinsic constants for the formation of **1C$_2$** and **1C$_3$** are of the same order and both one order of magnitude higher than that for the formation of **1C**. The intrinsic constant for the formation of **2C$_3$** is almost two orders of magnitude higher than the one for the formation of **2C**.

2.3. Interactions studies

^{1}H NMR studies revealed significant chemical shift variations for the signals of C*H, NH and C2–H protons in the starting imidazoles **C** and **D** during the course of the reaction (Figure 2, see also ESI, Figure S9c‡). This suggests the existence of strong supramolecular interactions between the corresponding imidazole and the imidazolium species formed. This was corroborated by the ESI-MS of the reaction crudes with the observation of some clusters involving imidazolium species and the starting imidazole (Figure 5 and ESI, Figure S4‡). This should be in good agreement with the initial hypothesis regarding the formation of supramolecular complexes between **C** and **1C** or **1C$_2$** that could favour the formation of **1C$_2$** and **1C$_3$**, justifying the predominant formation of tripodal species even when using a defect of **C**. To analyse this in more detail, imidazole **C** (15 mM) was titrated with the tripodal imidazolium salt **1C$_3$**, or the analogous mono- and bis-imidazolium model compounds **3** and **4** using $CDCl_3$ as the solvent and the results were recorded by ^{1}H NMR (Figure 8 and ESI, Figure S18‡). The addition of increasing quantities of the imidazolium salts produced downfield shifts of the C2–H, amide NH and C*H proton signals of imidazole **C**, along with an upfield shift of the signal for the amide NH protons of the imidazolium salts. This agrees well with the presence of supramolecular imidazole–imidazolium species stabilized through hydrogen bonds involving the anion as the hydrogen bond acceptor and the amide N–H and the acidic hydrogen atoms of the imidazole/imidazolium ring as hydrogen bond donors. The key role played by the amide groups and their relevance for the preferential formation of tripodal species is highlighted by the lack of any significant association when imidazole **A**, for which no preferential formation of **1A$_3$** is observed, was used instead of **C**.

Titration curves also suggest that the interaction of **C** is stronger with the mono- and bisimidazolium compounds than with **1C$_3$**. This is of interest as the preferential interaction of **C** with **1C** and **1C$_2$** can also contribute to promote the preferential formation of **1C$_3$** in excellent yields even when using a limited amount of **C**, avoiding the formation of significant amounts of **C·1C$_3$**, and can be assigned to the presence of a strong intramolecular hydrogen bonding network in **1C$_3$**.

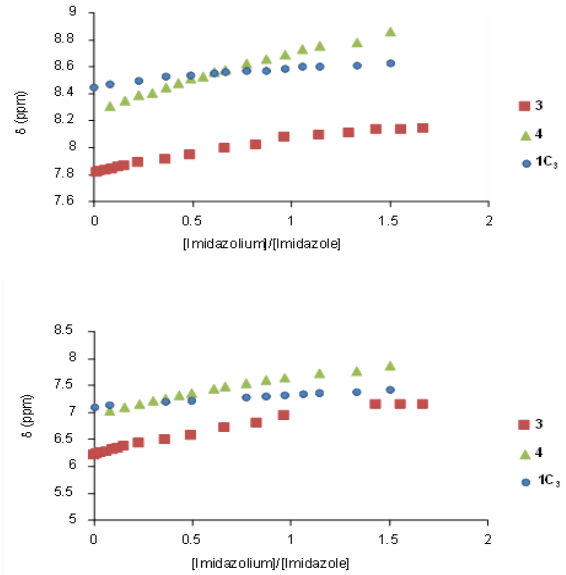

Figure 8 ^{1}H NMR titration curves (500 MHz, $CDCl_3$) following the imidazole C2–H (top) and the amide N–H (bottom) signals of **C** (15 mM) in the presence of increasing amounts of the monoimidazolium derivative (**3**, red squares), the bisimidazolium model compound (**4**, green triangles) or the tripodal derivative **1C$_3$** (blue circles).

In this regard, it must be noted that NMR data suggest the presence of a rigid conformation in **1C$_3$** with a strong nonequivalence of the two hydrogen atoms of the benzylic groups. Again the amide group is essential for this behaviour as the NMR data for **1A$_3$** are in agreement with less rigid conformations for these species (ESI, Figure S19‡). Rather surprisingly, a decrease in rigidity is observed for **2C$_3$**, as compared with **1C$_3$**, in spite of the presence of additional methyl groups in the aromatic fragment, which is usually accompanied by loss of conformational freedom in related systems.[15a] This is indicative of a stronger intramolecular hydrogen bonding network in **1C$_3$** as confirmed by the higher chemical shifts detected for the acidic hydrogen atoms in **1C$_3$** (9.96 ppm for C2–H in **1C$_3$** vs. 9.55 ppm for **2C$_3$**). Moreover, ROESY experiments and theoretical studies also supported a rigid arrangement of the three chains in **1C$_3$** with the C2–H being close to one of the benzylic protons but not to the other (ESI, Figure S20‡) and the modelling showing a higher number of H-bonds linking the bromide anions and the imidazolium groups in **1C$_3$** (ESI, Figure S21‡).

The role of the bromide anion in the formation of these supramolecular imidazole/imidazolium complexes also explains the observed reduction in reaction rates when using an excess of this anion. Thus, the addition of increasing quantities of the bromide anion produced a downfield shift of the

signals of the amide NH proton, the imidazole C2–H and the C*H for **C** while no significant changes were observed in the case of **1C$_3$** (ESI, Figure S22‡). This supramolecular association between bromide and **C** would make the formation of the supramolecular complex of this starting material with the initially formed imidazolium species that promote a more rapid reaction less favourable. In the presence of excess bromide, imidazole/imidazolium clusters were not detected in ESI-MS experiments (ESI, Figure S16‡).

Such hydrogen bonding interactions are expected to be very sensitive to polar protic solvents. Thus, the reaction between 1,3,5-tris(bromomethyl)benzene **1** (9.0 mM) and imidazole **C** (13.3 mM) was also run in CD_3OD. Following the ^1H NMR signals for C*H and C2–H of the imidazole **C**, a significant decrease in reactivity was observed (*e.g.* at 498 h only 36% conversion of C occurred) (ESI, Figure S23a‡); H/D exchange did not allow proper monitoring of C2–H signals in imidazolium species, but positive ion mode ESI-MS experiments after long reaction times (679 h, ESI, Figure S23b‡) revealed that ditopic and tritopic imidazolium compounds were very minor species, with the monoimidazolium compound being the major formed species. This again confirms the key role of the supramolecular interactions involving hydrogen bonding between imidazolium intermediates and starting imidazoles.

2.4. Self-sorting and competitive studies

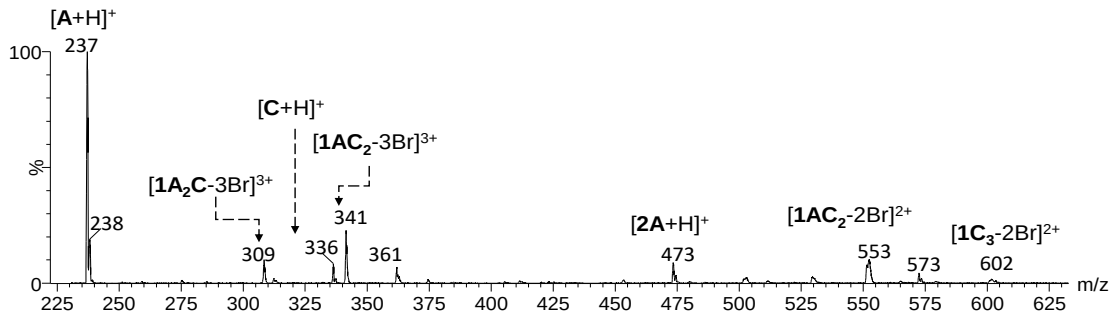

Figure 9 ESI-MS in positive ion mode for the reaction between **C** (13.9 mM) and **A** (13.7 mM) with **1** (5.5 mM) after 480 h of reaction in $CDCl_3$.

Considering the observed differences between the pseudopeptidic imidazole **C** and imidazole **A** lacking the amino acid derived fragment, additional experiments were carried out to analyse potential self-sorting when using 1,3,5-tris(bromomethyl)benzene **1** and an excess of an equimolar mixture of

imidazoles **A** (13.7 mM) and **C** (13.9 mM) (2.5 equiv. each).[27] Figure 9 shows the ESI-MS in positive ion mode obtained after 480 h of reaction. Although a full self-sorting is not observed the spectrum reveals the preferential incorporation of imidazole **C** into the polytopic imidazolium species. The unreacted imidazole **A** provides the base peak (237, [**A** + H]$^+$), while the peak at 336.4 corresponding to [**C** + H]$^+$ is very small (<5%). Mixed tripodal species [**1AC$_2$**–3Br]$^{3+}$ (m/z: 341.6, 23%) and [**1AC$_2$**–2Br]$^{2+}$ (552.4, 10%) are more important than those containing two units from A like [**1A$_2$C**–3Br]$^{3+}$ (308.5, 10%). A relatively minor peak is also observed for the homotripodal species [**1C$_3$**–2Br]$^{2+}$ at 602.1. The ^{1}H NMR spectra also showed a preferential consumption of imidazole **C** (**C**/**A** molar ratio became 0.59 after 184 h) (ESI, Figure S24‡).

To assess the effect of the length of the aliphatic chain, additional competitive studies were run using a deficit of 1,3,5-tris(bromomethyl)benzene **1** and an equimolar mixture of **C** and **D** (3 equiv.). After 120 h of reaction, ESI-MS experiments showed the presence of homo- and heterotritopic species, but with a slight preference for the incorporation of imidazole **D** (ESI, Figure S25 and Table S3‡). This confirms that, in opposition to the amide fragment, the long aliphatic tail does not participate in the recognition process favouring the formation of the tripodal species. As a matter of fact, the presence of smaller aliphatic fragments seems to better facilitate this process.

Finally, competitive studies were run mixing 1,3,5-tris(bromomethyl)benzene **1** (5 mM) and imidazoles **C** (3 equiv.), **D** (3 equiv.) and **A** (3 equiv.) (ESI, Figure S26‡). In this case, after 120 h, species containing the imidazole building block **D** seem to be favoured, with the most important species detected by ESI-MS in positive ion mode corresponding to [**1D$_3$**–3Br]$^{3+}$ (220, 23%), [**1CD^2**–3Br]$^{3+}$ (272, 25%), [**1D$_3$**–2Br]$^{2+}$ (371, 3%) and [**1CD$_2$**–2Br]$^{2+}$ (448, 3%).

2.5. Computational studies

In order to gain additional insights into the mechanisms involved, a computational study was carried out using Gaussian 16[28] by means of the

---

[27] *Self-sorting of crown ether/secondary ammonium ion hetero-[c2]daisy chain pseudorotaxanes;* Zheng, B.; Klautzsch, F.; Xue, M.; Huang, F. H.; Schalley, C. A.; *Organic Chemistry Frontiers* **2014**, *1*, 532-540.

[28] Frisch, M. J.; Trucks, G. W.; Schlegel, H. B.; Scuseria, G. E.; Robb, M. A.; Cheeseman, J. R.; Scalmani, G.; Barone, V.; Petersson, G. A.; Nakatsuji, H.; Li, X.; Caricato, M.; Marenich, A. V.; Bloino, J.; Janesko, B. G.; Gomperts, R.; Mennucci, B.; Hratchian, H. P.; Ortiz, J. V.; Izmaylov, A. F.; Sonnenberg, J. L.; Williams-Young, D.; Ding, F.; Lipparini, F.; Egidi, F.; Goings, J.; Peng, B.; Petrone, A.; Henderson, T.; Ranasinghe, D.; Zakrzewski, V. G.; Gao, J.; Rega, N.; Zheng, G.;

commonly used DFT functional (B3LYP)[29] using the 6-311+G(d,p) basis set.[30] In order to save computational time, imidazoles **B** and **D** lacking the long dodecyl aliphatic tail were selected as model compounds. This is reasonable taking into account that the change from dodecyl to methyl experimentally plays a minor role in the process. The evaluation of **B** and **D** still allows the comparison of the effect of the amide group.

For the pseudopeptidic compound **D**, the DFT study showed that formation of the monotopic derivative **1D** presents a TS with a higher activation barrier than the one for the formation of the ditopic derivative **1D$_2$**, this being higher than that for the formation of the trisubstituted compound **1D$_3$**. The computed activation free enthalpies ($\Delta H^{\ddagger}_{calc}$) were found to be 23.7, 13.5 and 11.1 kcal mol^{-1} for **1D**, **1D$_2$** and **1D$_3$**, respectively (ESI, Table S4‡). For the imidazole **B**, the DFT study showed that the formation of the monotopic compound **1B** occurs through a TS with a higher activation energy than the one required for the formation of **1B$_2$**; but this last barrier, however, was slightly lower than the one present in the formation of the tripodal derivative **1B$_3$**. The computed activation free enthalpies ($\Delta H^{\ddagger}_{calc}$) were in this case 27.0, 23.1 and 24.2 kcal mol^{-1} for **1B**, **1B$_2$** and **1B$_3$**, respectively (ESI, Table S4‡). When comparing the reaction of imidazole **D** with trisbromomethyl derivatives **1** and **2**, the computed activation barriers for the formation of species derived from **2** were always slightly lower than the ones computed for species derived from **1**. Thus, the methyl substitution on the central aromatic ring accelerates the S_N2 reaction as observed experimentally (ESI, Table S4‡). All the reactions were exergonic with free reaction energy values ranging from −5 to −15 kcal mol^{-1}.

Liang, W.; Hada, M.; Ehara, M.; Toyota, K.; Fukuda, R.; Hasegawa, J.; Ishida, M.; Nakajima, T.; Honda, Y.; Kitao, O.; Nakai, H.; Vreven, T.; Throssell, K.; Montgomery, J. A. Jr.; Peralta, J. E.; Ogliaro, F.; Bearpark, M. J.; Heyd, J. J.; Brothers, E. N.; Kudin, K. N.; Staroverov, V. N.; Keith, T. A.; Kobayashi, R.; Normand, J.; Raghavachari, K.; Rendell, A. P.; Burant, J. C.; Iyengar, S. S.; Tomasi, J.; Cossi, M.; Millam, J. M.; Klene, M.; Adamo, C.; Cammi, R.; Ochterski, J. W.; Martin, R. L.; Morokuma, K.; Farkas, O.; Foresman, J. B.; Fox, D. J.; Gaussian 16, Revision B.01, Gaussian, Inc., Wallingford CT, **2016**.

[29] (a) *Development of the Colle-Salvetti correlation-energy formula into a functional of the electron density;* Lee, C.; Yang, W.; Parr, R. G.; *Phys. Rev. B: Condens. Matter* **1988**, *37*, 785-789, (b) A *New Mixing of Hartree-Fock and Local Density-Functional Theories;* Becke, A. D.; *J. Chem. Phys.* **1993**, *98*, 1372-1377, (c) *Density-Functional Thermochemistry. III. The Role of Exact Exchange;* Becke, A. D.; *J. Chem. Phys.* **1993**, *98*, 5648-5652.

[30] *A set of d-polarization functions for pseudo-potential basis sets of the main group elements Al-Bi and f-type polarization functions for Zn, Cd, Hg;* Höllwarth, A.; Bohme, M.; Dapprich, S.; Ehlers, A.; Gobbi, A.; Jonas, V.; Köhler, K. F.; Stegmann, R.; Veldkamp, A.; Frenking, G.; *Chem. Phys. Lett.* **1993**, *208*, 237-240.

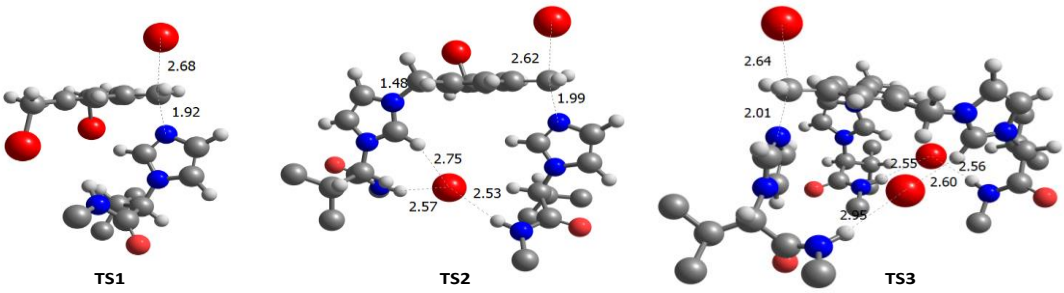

Figure 10 Structures of the calculated transition states obtained for the synthesis of **1D$_3$**.

Figure 10 shows the three consecutive transition states calculated for the reaction between **1** and **D**. As can be observed for [TS2]$^{\neq}$ and [TS3]$^{\neq}$, both TSs display intramolecular hydrogen bonds linking the imidazolium and the imidazole fragments involved in the reaction through a bromide anion. In both cases the hydrogen atom at the C2 position of the imidazolium ring participates in the hydrogen bond network, highlighting the supramolecular potential of imidazolium subunits. For [TS2]$^{\neq}$ the imidazolium fragment displays two hydrogen bonds to the bromide involving the amide N–H and the C2–H of the imidazolium ring. The smaller distance calculated for NH···Br$^-$ suggests that this hydrogen bond is stronger than the one with the C2–H, as should correspond with its higher acidity. For [TS3]$^{\neq}$ the two imidazolium subunits are hydrogen bonded to one bromide anion. One of them participates with the amide N–H and the C2–H moieties, while the second one only participates with the amide N–H fragment. Thus, the C2–H of this imidazolium group is hydrogen bonded with a second bromide displaying a hydrogen bond with the amide NH of the reacting imidazole. Interestingly, a strong hydrogen bonding of the imidazole units, significantly favouring the formation of the polytopic derivatives, takes place when the amide group is present. Thus, computational results are in excellent agreement with the experimental ones, and support the presence of supramolecular interactions, even at the TS level, of the formed imidazolium groups with the imidazole nucleophiles, particularly relevant for pseudopeptidic systems.

3. CONCLUSIONS

Supramolecular interactions associated with the presence of the peptidic bond are essential in many natural systems but also in pseudopeptidic receptors, and the results presented here show that they are also able to strongly assist the synthesis of polytopic pseudopeptidic imidazolium compounds. The

experimental data presented, in good agreement with computational calculations, reveal that in the considered trisimidazolium compounds the introduction of the first imidazolium fragments facilitates the second functionalization by establishing supramolecular interactions with the imidazole acting as the nucleophilic reagent. Once the ditopic system is formed, similar supramolecular interactions favour the formation of the tripodal imidazolium system. According to computational calculations, such supramolecular interactions are also present at the corresponding TSs ([TS2]$^{\neq}$ and [TS3]$^{\neq}$). The imidazole/imidazolium groups considered contain three different structural elements of interest for supramolecular interactions: the imidazole/imidazolium group itself, the amide group associated with the amino acid involved, and a long aliphatic tail (dodecyl group). However, the study of similar processes involving other imidazole derivatives lacking either the amide group or the long aliphatic tail has demonstrated that the combination of the imidazole/imidazolium fragments containing an amide group is playing the key role in these supramolecular interactions, while the length of the aliphatic tail does not provide a significant contribution. The importance of this supramolecular assistance is highlighted by the fact that in the case of pseudopeptidic imidazole reagents, the tripodal imidazolium compound is always obtained as the major product even when a deficit of imidazole (*e.g.* 1/3 of the stoichiometric amount) is used for the reaction. This behaviour is reminiscent of the one found in autocatalytic and selfreplicating systems.

4. Toc graphic

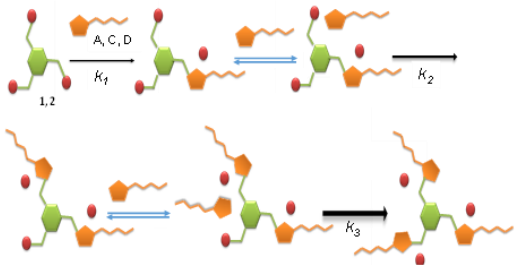

5. Supporting information

All reagents were purchased from commercial suppliers and used as received. The NMR spectroscopic experiments were carried out at the field reported, at 25 °C and using trimethylsilane as the internal standard. Microwave reactions were carried out using a Discover System Model

908010 from CEM Corporation using custom-made high purity quarts vials (capacity 10 mL). ESI-MS experiments were recorded on a Q-TOF Premier mass spectrometer with an orthogonal Z-spray electrospray interface (Micromass, Manchester, UK) by electrospray in positive or negative mode.

5.1. Synthetic Protocols and Structural Characterization

Synthesis of $1A_3$: Compound **A** (0.308 g, 1.27 mmol, 3.3 equiv.) and 1,3,5-tris(bromomethyl)benzene (0.141 g, 0.39 mmol, 1 equiv.) were dissolved in acetonitrile (3 mL) in a microwave tube and heated in a microwave instrument at 150 °C (120 W) for 1 h. The precipitate obtained was filtered, washed with cold ethyl acetate and vacuum dried. The product was a beige solid (0.38 g, 93%). M.p. (DSC): 178.2 °C. $[\alpha]_D^{25}$ = -2.51 (c = 0.021, CH_3OH). IR (ATR): 3419, 3083, 2919, 2850, 1553, 1467 cm^{-1}. ^1H NMR (300 MHz, $CDCl_3$) δ= 10.44 (s, 3H), 8.65 (s, 3H), 8.63 (s, 3H), 7.06 (s, 3H), 5.54 (s, 6H), 4.22 (q, J = 7.6, 6.2 Hz, 6H), 1.25 (s, 6H), 1.40-1.17 (m, 54H), 0.95 – 0.79 (m, 9H). ^{13}C NMR (101 MHz, $CDCl_3$): δ= 136.5, 135.5, 132.0, 124.5, 121.2, 52.1, 50.3, 31.9, 30.1, 29.6, 29.6, 29.5, 29.4, 29.3, 29.0, 26.3, 22.6, 14.1 ppm. MS (ESI^+): m/z (%) = 275 (100) $[C_{54}H_{93}N_6]^{3+}$. Calculated for $C_{54}H_{93}N_6Br_3 \cdot 3.5\ H_2O$: C 57.4, H 8.9, N 7.4; found C 57.4, H 8.4, N 7.2.

Synthesis of $2A_3$: Compound **A** (0.100 g, 0.42 mmol, 3.3 equiv.) and 1,3,5-tris(bromomethyl)-2,4,6-trimethylbenzene (0.057 g, 0.13 mmol, 1 equiv.) were dissolved in chloroform (5 mL) and stirred in a round bottom flask (25 mL) for 5 days at rt. The reaction gave a yellow solid product (0.13 g, 94%). M.p. (DSC): 297.5 °C. $[\alpha]_D^{25}$ = -0.45 (c = 0.021, CH_3OH). IR (ATR): 3432, 3067, 2921, 2852, 1559, 1465 cm^{-1}. ^1H NMR (400 MHz, $CDCl_3$) δ= 10.00 (s, 3H), 8.43 (s, 3H), 7.28 (s, 3H), 5.80 (s, 6H), 4.31 (t, J = 7.4 Hz, 6H), 2.34 (s, 9H), 2.20 (s, 6H), 1.41-1.13 (m, 54H), 0.87 (t, J= 6.8 Hz, 9H). ^{13}C NMR (101 MHz, $CDCl_3$): δ= 142.0, 135.5, 136.0, 129.0, 124.1, 121.7, 50.0, 49.3, 31.9, 30.5, 29.6, 29.6, 29.4, 29.3, 29.1, 26.3, 22.7, 17.7 14.1 ppm. MS (ESI^+): m/z (%) = 290 (100) $[C_{57}H_{99}N_6]^{3+}$, 474 (31) $[C_{57}H_{99}N_6Br]^{2+}$. Calculated for $C_{57}H_{99}N_6Br_3 \cdot 4.5\ H_2O$: C 57.6, H 9.2, N 7.1; found C 57.7, H 8.6, N 6.6.

Synthesis of $1C_3$: Compound **C** (0.299 g, 0.89 mmol, 3.3 equiv.) and 1,3,5-tris(bromomethyl)benzene (0.079 g, 0.22 mmol, 1 equiv.) were dissolved

in acetonitrile (2.23 mL) in a microwave tube and heated in a microwave instrument at 150 °C (120 W) for 1 h. The solvent was evaporated, and the residue washed with cold ethyl acetate and vacuum dried. The product was a beige solid (0.33 g, 97%). M.p. (DSC): 184.8 °C. $[\alpha]_D^{25}$ = 13.77 (c = 0.021, CH_3OH). IR (ATR): 3227, 3063, 2921, 2952, 1679 cm^{-1}. ^1H NMR (400 MHz, $CDCl_3$) δ= 9.97 (s, 3H), 8.37 (d, J = 19.4 Hz, 6H), 8.10 (s, 3H), 7.39 (s, 3H), 5.50 (dd, J = 185.7, 14.1 Hz, 6H), 5.02 (d, J = 10.7 Hz, 3H), 3.30 (m, 3H), 2.91 – 2.29 (dm, 6H), 1.59 – 1.37 (m, 6H), 1.35 – 1.08 (m, 54H), 1.01 (dd, J = 12.0 Hz, 9H), 0.81 (t, J = 6.9 Hz, 9H), 0.70 (dd, J = 6.6 Hz, 9H). ^{13}C NMR (126 MHz, $CDCl_3$): δ= 163.6, 133.3, 132.8, 129.1, 121.7, 116.9, 65.9, 49.6, 37.3, 29.3, 28.4, 27.0, 26.7, 26.5, 24.4, 20.1, 16.2, 15.7, 11.5 ppm. MS (ESI^+): m/z (%) = 374.5 (100) $[C_{69}H_{120}N_9O_3]^{3+}$, 602.0 (45) $[C_{69}H_{120}N_9O_3Br]^{2+}$. Calculated for $C_{69}H_{120}N_9O_3Br_3 \cdot H_2O$: C 60.0, H 8.9, N 9.2; found C 59.8, H 8.4, N 9.5.

Synthesis of $2C_3$: Compound **C** (0.100 g, 0.30 mmol, 3.3 equiv.) and 1,3,5-tris(bromomethyl)-2,4,6-trimethylbenzene (0.040 g, 0.10 mmol, 1 equiv.) were dissolved in dichloromethane (2.23 mL) in a microwave tube and heated in a microwave instrument at 150 °C (120 W) for 1 h. The solvent was evaporated, and the residue washed with dimethyl ether and vacuum dried. The product was a beige solid (0.099 g, 94%). M.p. (DSC): 153.2 °C. $[\alpha]_D^{25}$ = -45.89 (c = 0.021, CH_3OH). IR (ATR): 3240, 3062, 2923, 2853, 1678 cm^{-1}. ^1H NMR (400 MHz, $CDCl_3$) δ= 9.60 (s, 3H), 8.08 (s, 3H), 7.94 (s, 3H), 7.73 (d, J=20.6 Hz, 3H), 6.43-5.20 (m, 6H), 5.38 (d, J = 10.2 Hz, 3H), 3.33 (m, 3H), 3.04 (m, 3H), 2.39 (s, 6H), 2.37 (s, 9H), 1.52 (s, 3H), 1.23 (s, 54H), 1.06 (dd, J = 25.2, 6.5 Hz, 9H), 0.87 (t, J = 6.9 Hz, 9H), 0.74 (d, J = 6.1 Hz, 9H). ^{13}C NMR (101 MHz, $CDCl_3$): δ= 166.8, 142.0, 135.7, 129.0, 121.6, 67.6, 49.4, 39.9, 31.9, 29.6, 29.2, 27.0, 22.7, 18.8, 18.3, 17.5, 14.1 ppm. MS (ESI^+): m/z (%) = 623.0 (100) $[C_{72}H_{125}N_9O_3Br]^{2+}$, 388.6 (91) $[C_{72}H_{126}N_9O_3]^{3+}$. Calculated for $C_{72}H_{126}N_9O_3Br_3 \cdot H_2O$: C 60.8, H 9.1, N 8.9; found C 60.5, H 9.2, N 8.9.

Synthesis of $1D_3$: Compound **D** (0.100 g, 0.55 mmol, 3.3 equiv.) and 1,3,5-tris(bromomethyl)benzene (0.068 g, 0.19 mmol, 1 equiv.) were dissolved in chloroform (5 mL) and stirred in a round bottom flask (25 mL) for 5 days at rt. The solvent was evaporated, and the residue washed with dimethyl ether and vacuum dried. The product was a beige solid (0.053 g,

89%). $[\alpha]_D^{25}$ = 38.75 (c = 0.021, CH_3OH). IR (ATR): 3397, 3077, 2967, 1673, 1550 cm^{-1}. ^1H NMR (400 MHz, $CDCl_3$) δ= 10.01 (s, 3H), 8.43 (s, 3H), 8.41 (s, 3H), 8.19 (s, 3H), 7.48 (s, 3H), 5.57 (dd, J=122.3, 14.1 Hz, 6H), 5.08 (d, J=10.8 Hz, 3H), 2.72 (d, J = 4.6 Hz, 9H), 2.40 (m, 3H) 0.92 (dd, J = 110.8, 6.6 Hz, 18H). ^{13}C NMR (101 MHz, $CDCl_3$): δ= 166.9, 135.8, 135.4, 131.8, 124.3, 119.6, 74.5, 68.4, 52.2, 30.8, 26.2, 18.8, 18.3 ppm. MS (ESI^+): m/z (%) = 220 (100) $[C_{36}H_{54}N_9O_3]^{3+}$. Calculated for $C_{36}H_{54}N_9O_3Br_3$: C 62.0, H 8.4, N 18.1; found C 62.1, H 8.3, N 18.0.

Synthesis of $2D_3$: Compound **D** (0.100 g, 0.55 mmol, 3.3 equiv.) and 1,3,5-tris(bromomethyl)-2,4,6-trimethylbenzene (0.075 g, 0.19 mmol, 1 equiv.) were dissolved in chloroform (5 mL) and stirred in a round bottom flask (25 mL) for 5 days at rt. The solvent was evaporated, and the residue washed with dimethyl ether and vacuum dried. The product was a beige solid (0.133 g, 84%). M.p. (DSC): 362.7 °C. $[\alpha]_D^{25}$ = 2.62 (c = 0.021, CH_3OH). IR (ATR): 3395, 3232, 3073, 2967, 1673, 1546 cm^{-1}. ^1H NMR (400 MHz, $CDCl_3$) δ= 9.54 (s, 3H), 8.16 (s, 3H), 7.84 (s, 3H), 7.72 (s, 3H), 5.66 (d, J=19.7 Hz, 6H), 5.26 (d, J=10.1 Hz, 3H), 2.70 (d, J=4.2 Hz, 9H), 2.45 (s, 9H), 2.40 (s, 3H), 0.96 (d, J=6.5 Hz, 9H), 0.68 (d, J=6.5 Hz, 9H). ^{13}C NMR (101 MHz, $CDCl_3$): δ= 167.4, 142.0, 135.7, 129.07, 122.8, 121.7, 67.7, 49.5, 31.4, 26.3, 18.8, 18.3, 17.6 ppm. MS (ESI^+): m/z (%) = 234 (100) $[C_{39}H_{60}N_9O_3]^{3+}$. Calculated for $C_{39}H_{60}N_9O_3Br_3 \cdot 8H_2O$: C 43.1, H 7.1, N 11.6; found C 43.4, H 6.5, N 11.0.

5.2 Computational details

The calculations were performed with the Gaussian 16 program using the widely used DFT method based on Becke's GGA exchange functional B3LYP with standard 6-311+G(d,p) basis set. The stationary points were fully characterized by means of harmonic vibrational frequency analysis. For all of the transition structures, the normal mode related to the imaginary frequency corresponds to the nuclear motion along the reaction coordinates under study. Additionally, we carried out intrinsic reaction coordinate calculations (IRC) to verify that the transition structures were connected with reactants and products.

Supramolecularly assisted synthesis of chiral tripodal imidazolium compounds

Index

17. **Fig. S15** ESI-MS in positive ion mode and ^{1}H NMR kinetic profiles for the reaction between **1** and **C** (*ca.* 1/2 molar ratio) in $CDCl_3$ in the absence and presence of NEt_4Br
18. **Fig. S16** Experimental and calculated kinetic profiles for the reaction between imidazole **C** (13.8 mM) and **1** (1 equiv.) and between imidazole **A** (13 mM) and **1** (1 equiv.)
19. **Fig. S17** ^{1}H NMR titration of imidazole **C** with increasing amounts of **3**, **4** and **1C$_3$**
20. **Fig. S18** Partial ^{1}H NMR spectra in $CDCl_3$ for the reaction between **1** or **2** with **C** or **A** at different times (1/1 molar ratios)
21. **Fig. S19** ROESY spectra for **1C$_3$** and **2C$_3$** in $CDCl_3$ at 6 mM
22. **Fig. S20** Minimum energy structures (DFT, B3LYP) obtained for **1C$_3$** and **2C$_3$**
23. **Fig. S21** Partial ^{1}H NMR in $CDCl_3$ for imidazole **C** (15 mM), imidazole **A** (15 mM) and tripodal compound **1C$_3$** (15 mM) in the presence of increasing concentrations of bromide anion
24. **Fig. S22** ^{1}H NMR spectra and ESI-MS for the reaction between imidazole **C** (13.3 mM) and **1** (9 mM) in CD_3OD
25. **Fig. S23** Partial ^{1}H NMR spectra for the competitive reaction involving trisbromomethylbenzene **1** and imidazoles **A** and **C** at different reaction times
26. **Fig. S24** ESI-MS for the competitive reaction involving trisbromomethylbenzene **1** and imidazoles **C** and **D** after 120 h in $CDCl_3$.
27. **Table S3** Summary of ESI-MS data obtained in positive ion mode for the competitive reaction involving trisbromomethylbenzene **1** (5 mM) and imidazoles **C** (3 equiv.) and **D** (3 equiv.) after 120 h in $CDCl_3$.
28. **Fig. S25** ESI-MS for the competitive reaction involving trisbromomethylbenzene **1** and imidazoles **C**, **D** and **A** after 120h in $CDCl_3$.
29. **Table S4** Calculated relative activation energies (kcal/mol) for the diferent transition states leading to the formation of tripodal imidazolium compounds **1B$_3$**, **2B$_3$**, **1D$_3$** and **2D$_3$**

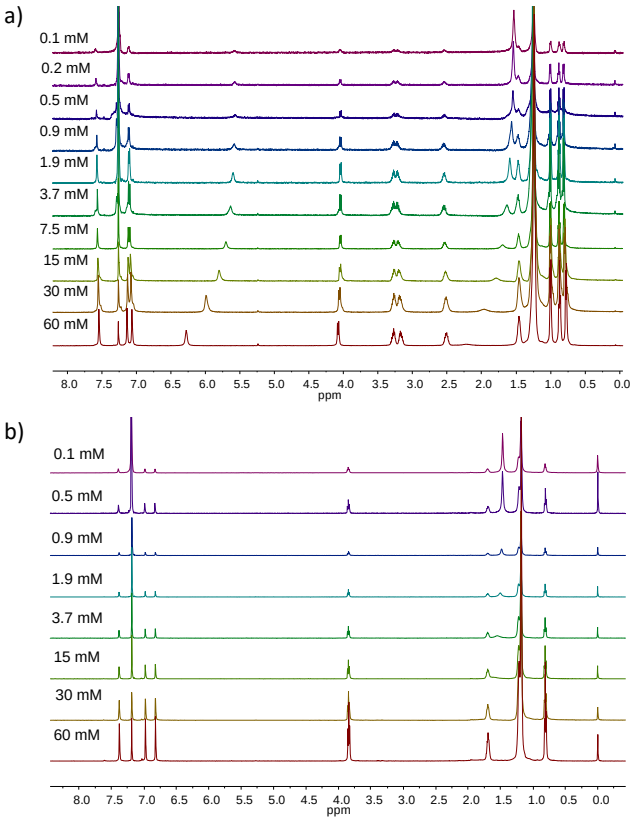

Figure S1 Aggregation studies in $CDCl_3$; a) Partial ^1H NMR (500 MHz) spectra for imidazole **C** at different concentrations; b) Partial ^1H NMR (500 MHz) spectra for imidazole **A** at different concentrations.

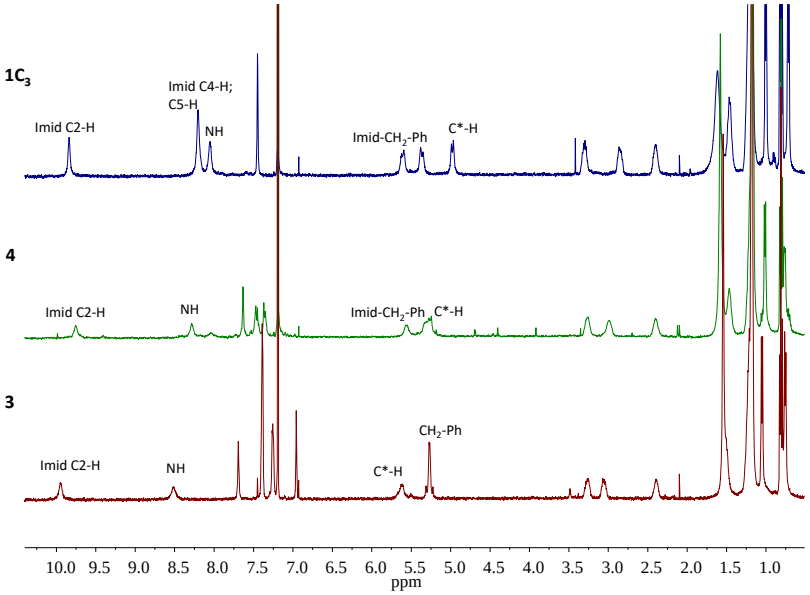

Figure S2 Partial ^1H NMR (500 MHz) spectra of **3**, **4**, and **1C₃** (4 mM in $CDCl_3$).

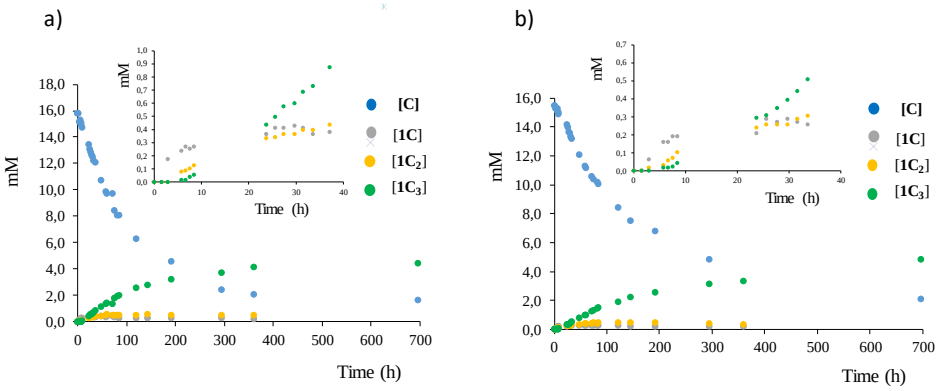

Figure S3 a) Kinetic profiles (^{1}H NMR, 300 MHz) for the reaction between imidazole **C** (15.8 mM) and **1** (7.5 mM) in $CDCl_3$; b) Kinetic profiles (^{1}H NMR, 300 MHz) for the reaction between imidazole **C** (15.5 mM) and **1** (5.5 mM) in $CDCl_3$. C2-H proton signal followed for **1C**, **1C$_2$** and **1C$_3$** and C2-H and C*H proton signals followed for **C**. The insets show an expansion of the initial period for the reaction.

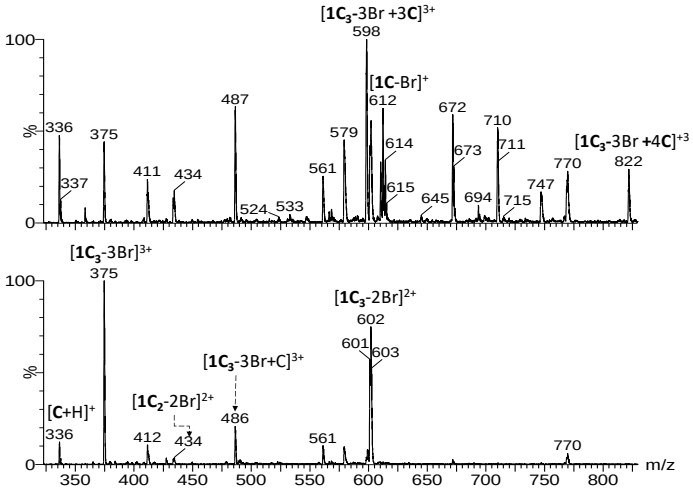

Figure S4 ESI-MS in positive ion mode from the reaction mixture between trisbromomethylbenzene **1** (5.5 mM) and imidazole **C** (15.5 mM) after 48 h (top) and after 697 h of reaction (bottom)

Table S1 Summary of ESI-MS data obtained in positive ion mode for the reaction between trisbromomethylbenzene **1** and imidazole **C** using molar ratios of 1, 2.1 and 2.8 after 48 h of reaction in $CDCl_3$

			Ratio 1/C		
		Ions m/z (%)	1/1	1/2.1	1/2.8
Compound (Mw)	$\mathbf{1C_3}$ (1363.5)	$[\mathbf{1C_3\text{-}3Br\ +4C}]^{+3}$	----	821.8 (13)	821.8 (28)
		$[\mathbf{1C_3\text{-}3Br\ +3C}]^{+3}$	710.2 (9)	710.2 (45)	710.2 (50)
		$[\mathbf{1C_3\text{-}3Br\ +2C}]^{+3}$	598.2 (20)	598.2 (100)	598.2 (100)
		$[\mathbf{1C_3\text{-}3Br\ +C}]^{+3}$	486.6 (10)	486.6 (100)	486.6 (100)
		$[\mathbf{1C_3\text{-}2Br}]^{+2}$	601.9 (77)	601.9 (73)	601.9 (53)
		$[\mathbf{1C_3\text{-}3Br}]^{+3}$	374.6 (75)	374.6 (19)	374.6 (42)
	$\mathbf{1C_2}$ (1027.9)	$[\mathbf{1C_2\text{-}2Br}]^{+2}$	434.6 (17)	434.6 (15)	434.6 (17)
	1C (692.4)	$[\mathbf{1C\text{-}Br}]^{+}$	612.4 (100)	612.4 (85)	612.4 (60)
	C (335.5)	$[\mathbf{C+C+H}]^{+}$	671.8 (16)	671.8 (53)	671.8 (60)
		$[\mathbf{C+H}]^{+}$	336.6 (48)	336.6 (50)	336.6 (48)

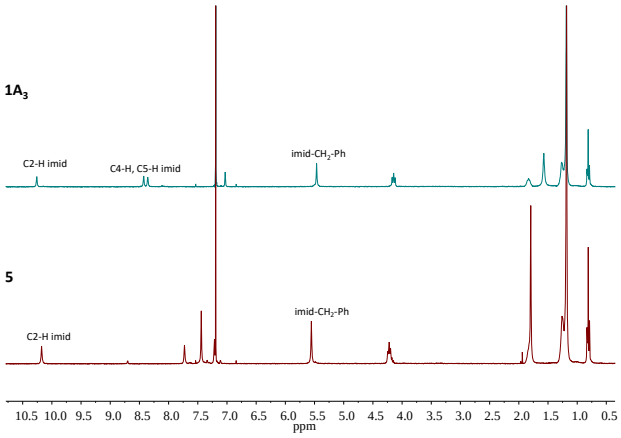

Figure S5 Partial ^{1}H NMR spectra (500 MHz) of **5** (2 mM) and $\mathbf{1A_3}$ (2 mM) in $CDCl_3$.

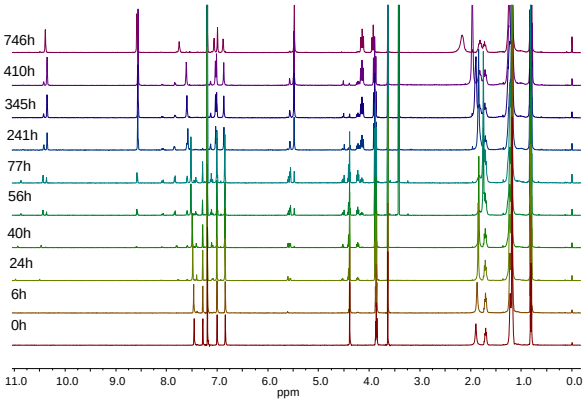

Figure S6 Evolution with time of the ^{1}H NMR (500 MHz) spectra for the reaction between **1** (3.6 mM) and imidazole **A** (18.6 mM) in $CDCl_3$.

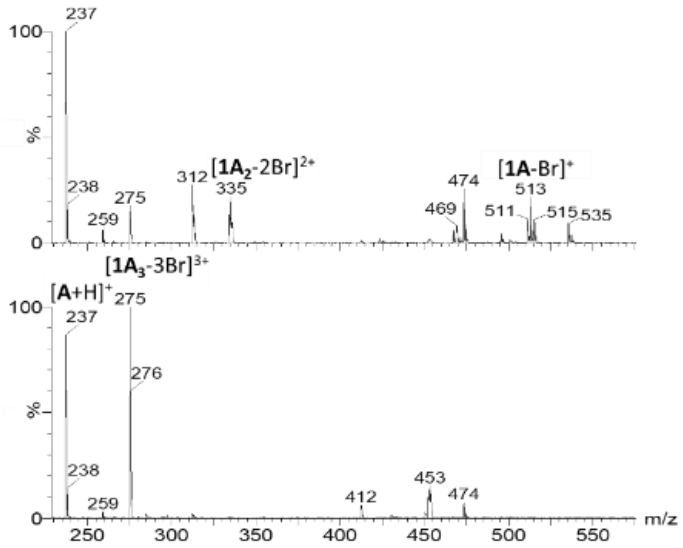

Figure S7 ESI-MS in positive ion mode for the reaction between **1** (3.6 mM) and imidazole **A** (18.6 mM) after 48 h (top) and after 747 h (bottom)

Table S2 Summary of ESI-MS data obtained in positive ion mode for the reaction between trisbromomethylbenzene **1** and imidazole **A** using molar ratios of 1 and 5.2 after 48 h of reaction in $CDCl_3$

			Ratio 1/A	
		Ions m/z (%)	1/1	1/5.2
Compound (Mw)	**1A$_3$** (1066.1)	**[1A$_3$-3Br]$^{+3}$**	275.4 (29)	275.4 (28)
	1A$_2$ (829.7)	**[1A$_2$-2Br]$^{+2}$**	335.4 (38)	335.4 (22)
	1A (593.3)	**[1A-Br]$^+$**	513.2 (100)	513.2 (20)
	A (236.4)	**[A+A+H]$^+$**	---	473.5 (25)
		[A+H]$^+$	237.4 (30)	237.4 (100)

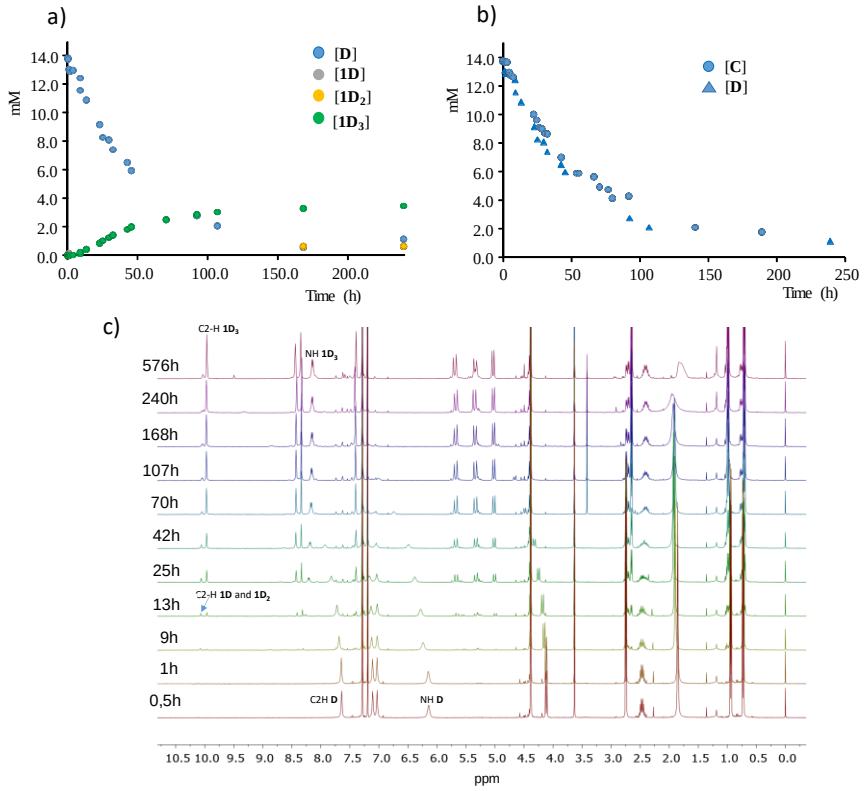

Figure S8 a) Kinetic profiles (^{1}H NMR, 400 MHz, $CDCl_3$) for the reaction between **1** (12.7 mM) and imidazole **D** (13.8 mM); b) Conversion *vs.* time of imidazoles **C** and **D** (^{1}H NMR, 400 MHz, $CDCl_3$) in their reaction with **1** (1 equiv.); The C2-H proton signal was followed for **1D**, **1D₂** and **1D₃** and the C2-H and C*H proton signals for **C** and **D**; c) Evolution of ^{1}H NMR spectra (400 MHz) with time for the reaction between imidazole **D** (13.8 mM) and **1** (12.7 mM) in $CDCl_3$.

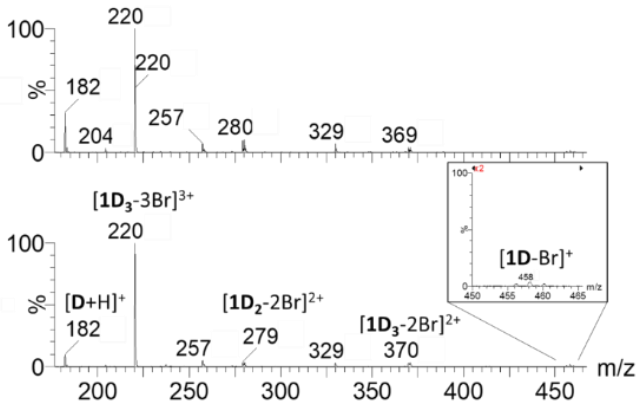

Figure S9 ESI-MS in positive ion mode for the reaction between imidazole **D** (13.8 mM) and **1** (12.7 mM) after 48 h (top) and 576 h (bottom) in $CDCl_3$.

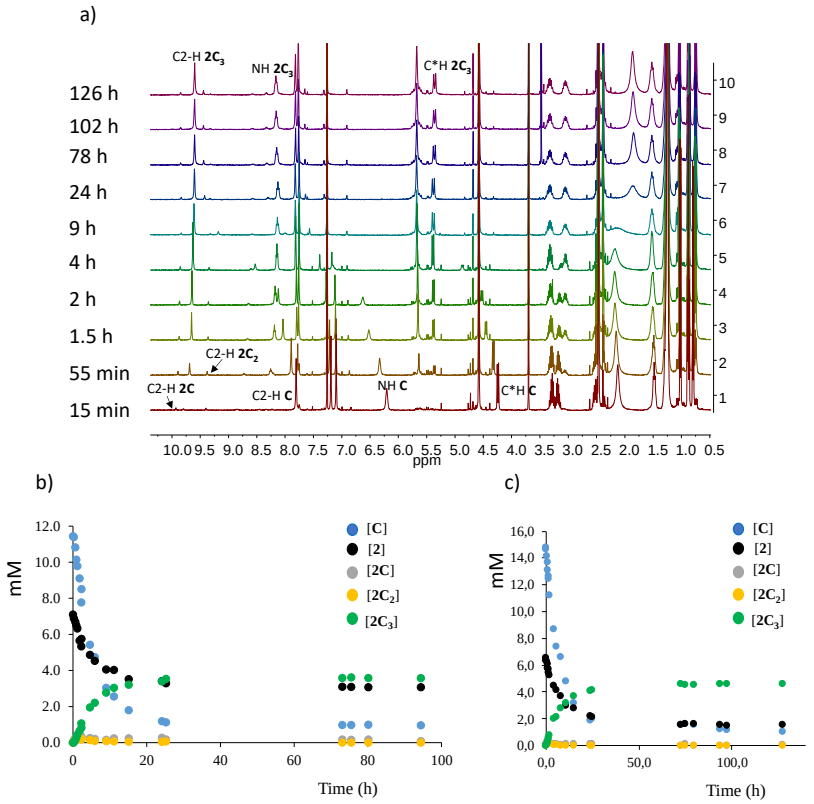

Figure S10 a) Evolution with time of ^{1}H NMR (400 MHz) partial spectra for the reaction between **C** (14.8 mM) and **2** (15.6 mM) in $CDCl_3$; b**)** Kinetic profiles for the reaction between **C** and **2** (7.1 mM) of (ratio C/2=1.6) in $CDCl_3$; c) Kinetic profiles for the reaction between C (14.8 mM) and 2 (6.5 mM) (ratio C/2= 2.3) in $CDCl_3$. The C2-H proton signal was followed for **2C**, **2C$_2$** and **2C$_3$**, the C2-H and C*H proton signals for **C** and the benzylic signal for **2**.

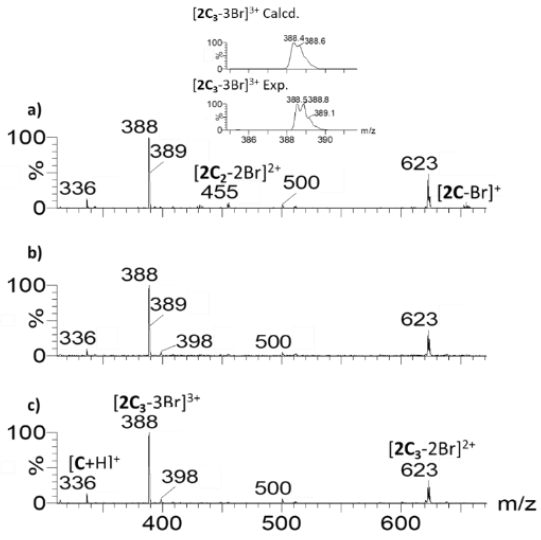

Figure S11 ESI-MS in positive ion mode for the reaction between **2** and imidazole **C** after 48 h in $CDCl_3$ using **C**/**2** molar ratios of 1/1, 1/1.6 and 1/2.3; a) 14.8 mM of **C** and 15.6 mM of **2** (ratio **C**/**2**≈1/1); b) 11.4 mM of **C** and 7.1 mM of **2** (ratio **C**/**2**=1/1.6**);** c) 14.8 mM of **C** and 6.5 mM of **2** (ratio **C**/**2**=1/2.3).

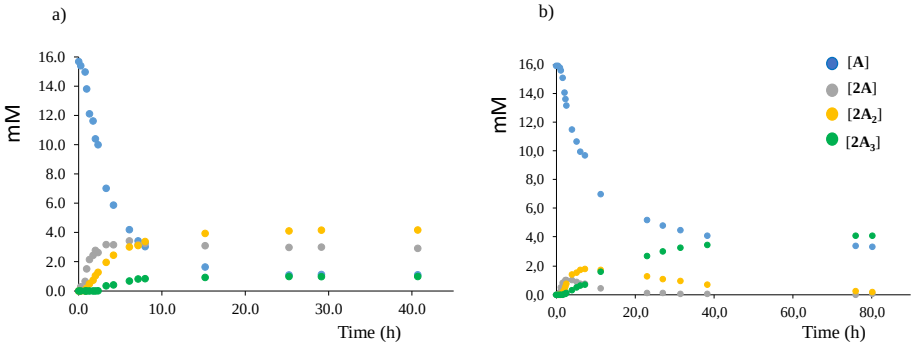

Figure S12 Kinetic profiles (^{1}H NMR, 500MHz, $CDCl_3$) for the reaction between imidazole **A** and **2**; a) 13.8 mM of **2** and 15.7 mM of **A** (ratio **A**/**2** =1.1), b) 5.2 mM of **2** and 16.0 mM of **A** (ratio **A**/**2**=3.1). The C2-H proton signal was followed for **2A**, **2A$_2$** and **2A$_3$** and the C2-H and N-CH_2 proton signals for **A**.

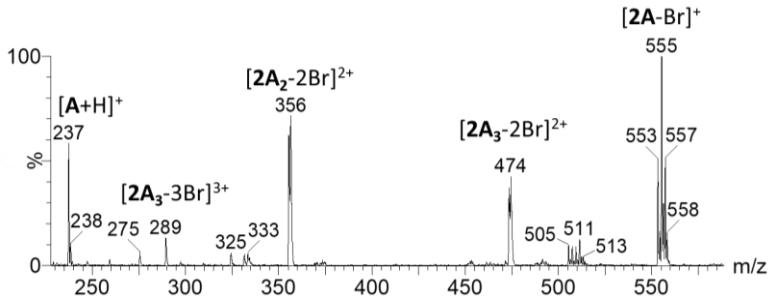

Figure S13 ESI-MS in positive ion mode for the reaction between **2** (15.7 mM) and imidazole **A** (13.8 mM) after 48 h.

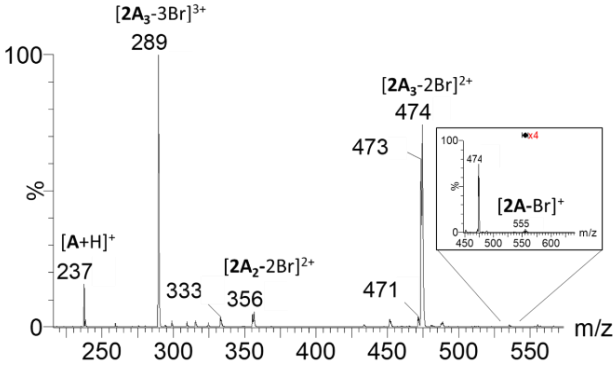

Figure S14 ESI-MS in positive ion mode for the reaction between **2** (5.2 mM) and imidazole **A** (16 mM) after 48 h.

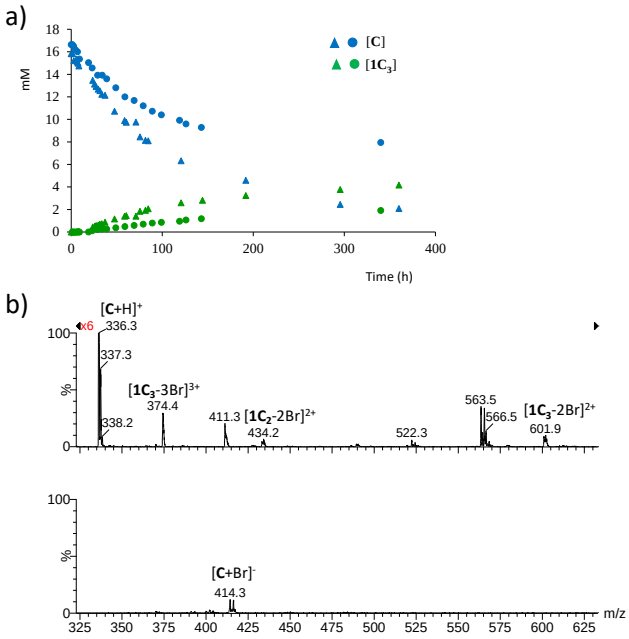

Figure S15 Reaction between **1** (*ca.* 8 mM) and **C** (*ca.* 16 mM) (*ca.* 1/2 molar ratio) in $CDCl_3$; a) kinetic profiles (^1H NMR, 400 MHz) in the absence (triangles) and presence (circles) of NEt_4Br (9 mM); b) ESI-MS after 48 h in positive ion mode (top) and in negative ion mode (bottom) of the reaction in the presence of NEt_4Br.

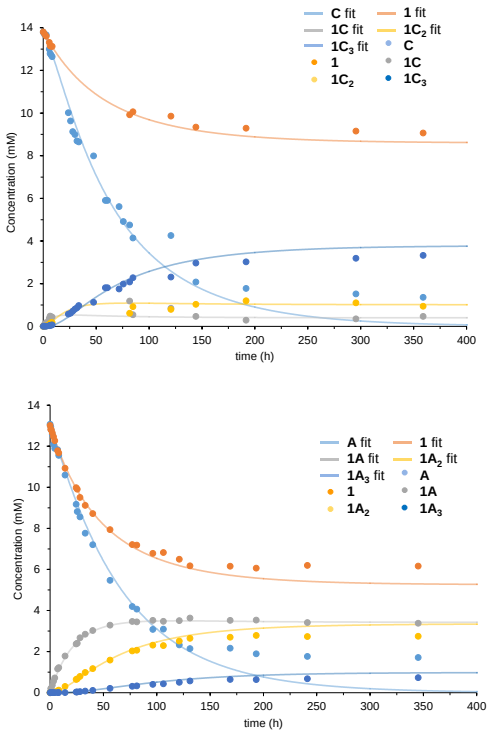

Figure S16 Experimental (solid circles, ^1H NMR, 300 MHz (**C**), 500 MHz (**A**), $CDCl_3$) and calculated (solid lines) kinetic profiles for the reaction of of **1 C** (13.8 mM) or **A** (13 mM) with **1** (1 equiv.). Left: imidazole **C** (dark blue), trisbromomethylbenzene **1** (orange), **1C** (grey), **$1C_2$** (yellow), **$1C_2$** (light blue). Right: imidazole **A** (light blue), trisbromomethylbenzene **1** (orange), **1A** (grey), **$1A_2$** (yellow), **$1A3_2$** (dark blue).

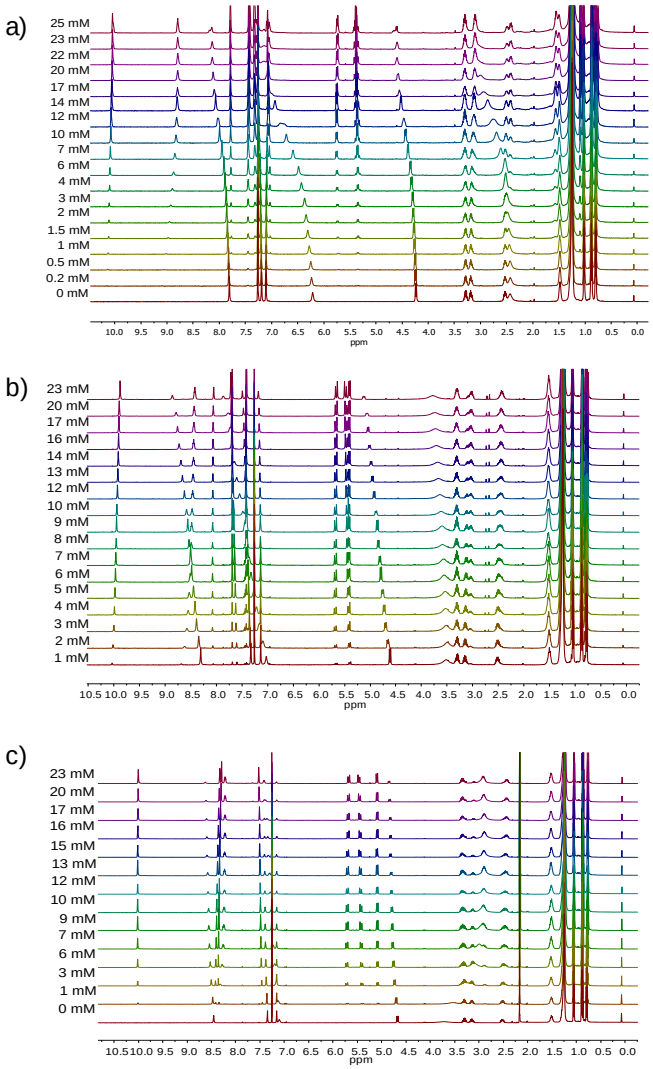

Figure S17 ^{1}H NMR titration (500 MHz, $CDCl_3$) of imidazole **C** (15 mM) with a) increasing amounts of monoimidazolium **3**; b) increasing amounts of bisimidazolium **4** and c) increasing amounts of trisimidazolium **1C$_3$**.

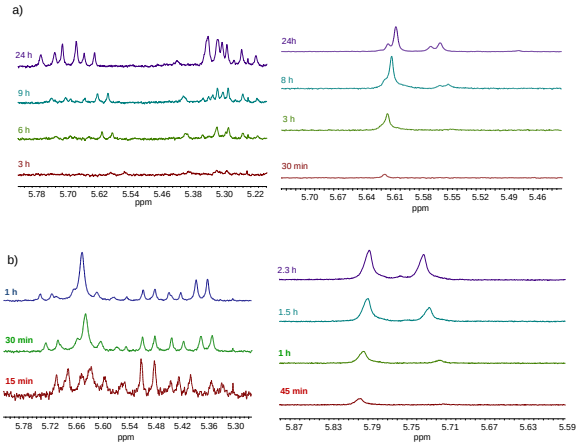

Figure S18 a) Partial ^{1}H NMR (300 MHz for **C**, 500 MHz for **A**, $CDCl_3$) spectra for the reaction between **1** and **C** (left) and between **1** and **A** (right) at different times (*ca.* 1/1 molar ratios). b) Partial ^{1}H NMR (400 MHz for **C**, 500 MHz for **A**, $CDCl_3$) spectra for the reaction between **2** and **C** (left) and between **2** and **A** (right) at different times (*ca.* 1/1 molar ratios).

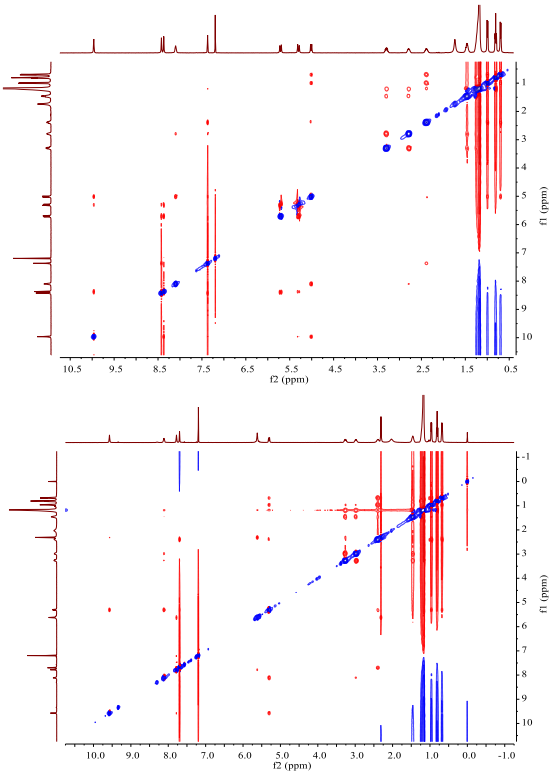

Figure S19 ROESY spectra (400 MHz, $CDCl_3$) for **1C₃** (top) and **2C₃** (botton) at 6 mM.

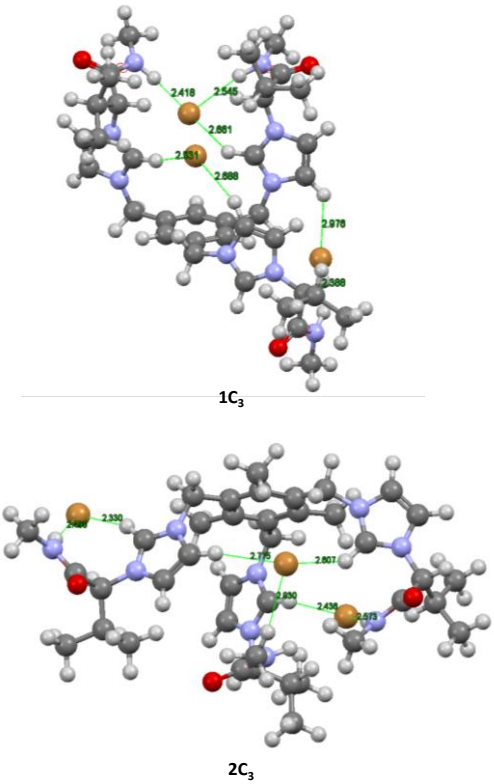

1C₃

2C₃

Figure S20 Minimum energy structures (DFT, B3LYP) obtained for **1C₃** and **2C₃**.

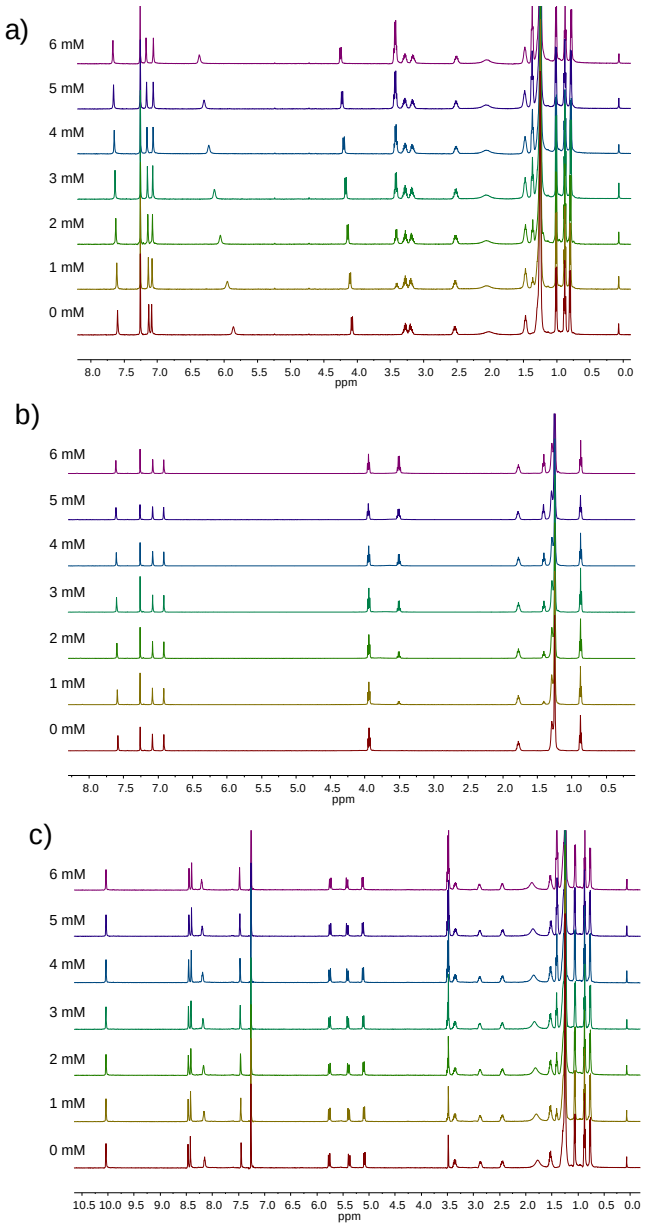

Figure S21 a) Partial ^{1}H NMR (500 MHz) spectra for imidazole **C** (15 mM, $CDCl_3$) in the presence of increasing concentrations of bromide anion; b) Partial ^{1}H NMR (500 MHz) spectra for imidazole **A** (15 mM, $CDCl_3$) in the presence of increasing concentrations of bromide anion; c) Partial ^{1}H NMR (500 MHz) for **1C$_3$** (15 mM, $CDCl_3$) in the presence of increasing concentrations of bromide anion.

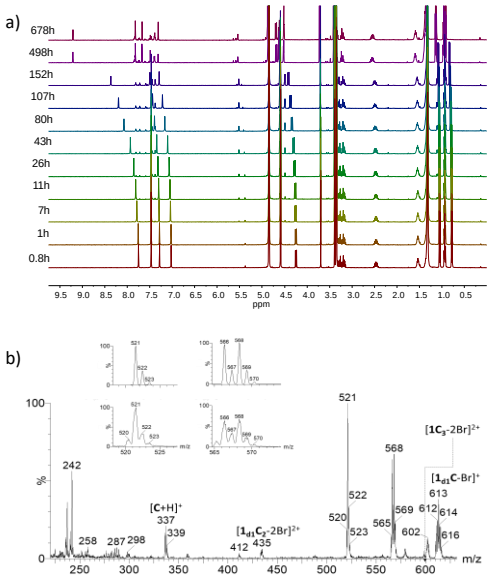

Figure S22 a) Evolution with time of the ^{1}H NMR (400 MHz) spectra for the reaction between imidazole **C** (13.3 mM) and **1** (9 mM) in CD_3OD; b) ESI-MS in positive ion mode for the reaction between imidazole **C** (13.3 mM) and **1** (9 mM) after 679 h in CD_3OD. Peaks at m/z 521 and 568 are associated to the **1C** deuterated monotopic species with one or two of the remaining -CH_2Br groups transformed into –CH_2OCD_3 groups.

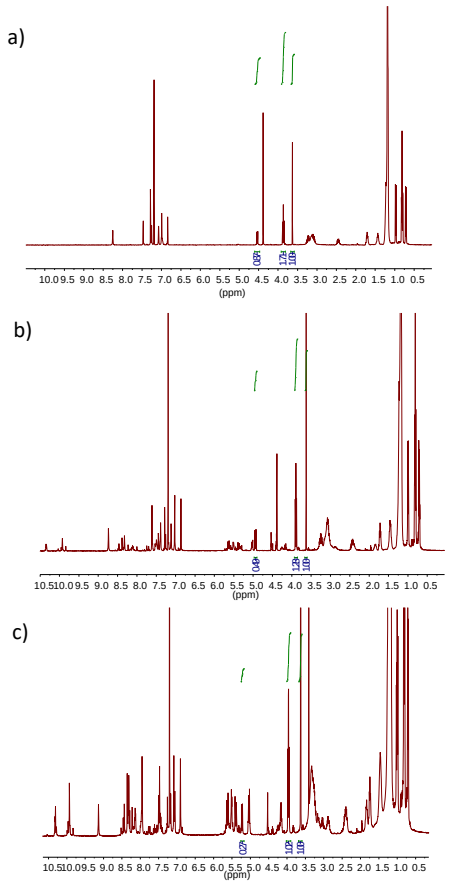

Figure S23 Partial ^{1}H NMR (400 MHz, $CDCl_3$) for the competitive reaction involving trisbromomethylbenzene **1** (5.5 mM) and imidazoles **A** (13.7 mM) and **C** (13.9 mM); a) at 0 h of reaction; b) at 90 h of reaction; c) at 184 h of reaction.

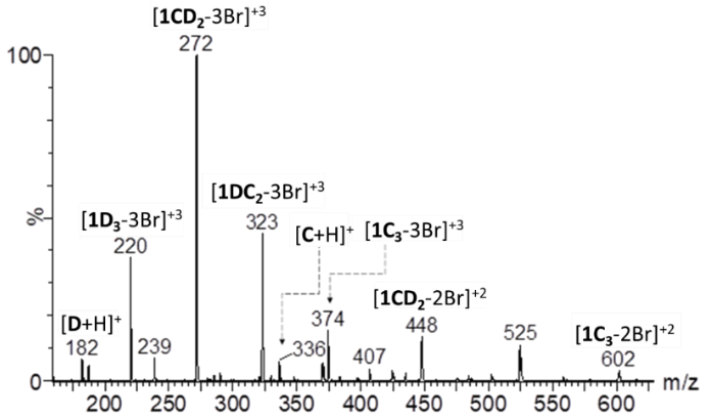

Figure S24 ESI-MS in positive ion mode for the competitive reaction involving trisbromomethylbenzene **1** (5 mM) and imidazoles **C** (3 equiv.) and **D** (3 equiv.) after 120 h in $CDCl_3$.

Table S3 Summary of ESI-MS data obtained in positive ion mode for the competitive reaction involving trisbromomethylbenzene **1** (5 mM) and imidazoles **C** (3 equiv.) and **D** (3 equiv.) after 120 h in $CDCl_3$

		Ions m/z (%)	m/z (%relative abundance)
Compound (Mw)	**1CD$_2$** (1054.9)	[**1CD$_2$**-3Br]$^{3+}$	271.7 (100)
		[**1CD$_2$**-2Br]$^{2+}$	447.9 (17)
	1DC$_2$ (1209.2)	[**1DC$_2$**-3Br]$^{3+}$	323.2 (46)
	1D$_3$ (900.6)	[**1D$_3$**-3Br]$^{3+}$	220.2 (38)
	1C$_3$ (1363.5)	[**1C$_3$**-3Br]$^{3+}$	374.4 (18)
		[**1C$_3$**-2Br]$^{2+}$	602.0 (5)
	D (181.2)	[**D**+H]$^+$	182.2 (7)
	C (335.5)	[**C**+H]$^+$	336.0 (6)

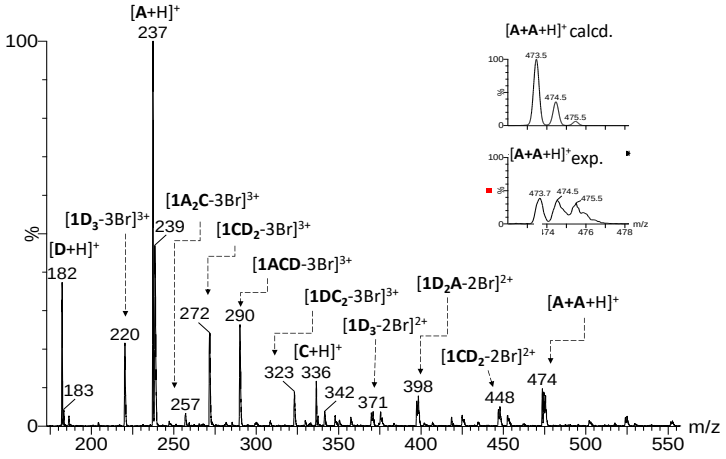

Figure S25 ESI-MS in positive ion mode for the competitive reaction involving trisbromomethylbenzene **1** (5 mM) and imidazoles **C** (3 equiv.), **D** (3 equiv.) and **A** (3 equiv.) after 120h in $CDCl_3$.

Table S4 Calculated relative activation energies (kcal/mol) for the diferent transition states leading to the formation of tripodal imidazolium compounds **$1B_3$**, **$2B_3$**, **$1D_3$** and **$2D_3$**. Imaginary frequencies are given in brackets. TS1, TS2 and TS3 correspond to the TSs for the formation of the monotopic, ditopic and tritopic imidazolium compounds

Tripodal final compound	TS1	TS2	TS3
$1B_3$	27.0 (-368.0240)	23.1 (-367.8148)	24.2 (-369.3739)
$2B_3$	25.6 (-348.3856)	20.8 (-334.6638)	19.9 (-342.3857)
$1D_3$	23.7 (-383.6526)	13.5 (-362.9522)	11.1 (-368.1623)
$2D_3$	21.4 (-366.1168)	12.8 (-343.4482)	10.6 (-340.1058)

CHAPTER 3.

3.2. Structure–Antitumor Activity Relationships of Tripodal Imidazolium-amino acid based ionic liquids. Effect of the Nature of the Amino Acid, Amide Substitution and Anion

Structure–antitumor activity relationships of tripodal imidazolium-amino acid based ionic liquids. Effect of the nature of the amino acid, amide substitution and anion

Abstract

The anti-tumor activity of imidazolium salts is highly dependent upon their lipophilicity which can be tuned by the introduction of different hydrophobic substituents on the nitrogen atoms of the imidazolium ring of the molecule. Taking this in consideration, we have synthesized and characterized a series of tripodal imidazolium salts derived from *L*-valine and *L*-phenylalanine containing different hydrophobic groups and tested them against four cancer cell lines at physiologic and acidic pHe. At acidic pHe (6.2) the anticancer activity of some of the tripodal compounds changes dramatically being this parameter crucial to control their cytotoxicity and selectivity. Moreover, several of these compounds displayed selectivities against the control healthy cell line higher than 4. The transmembrane anion transport studies revealed moderate transport abilities suggesting that the observed biological activity is likely not the result of just their transport activity. The behaviour of the biological activity at acidic pHe is mimicked by the results in the CF leakage assay. These results strongly suggest that this class of compounds can serve as potent chemotherapeutic agents.

Keywords: *antitumoral agents, imidazolium salts, amino acids, aggregation, anion transport*

1. Introduction

Cancer disease kills millions of people globally,[1] therefore, there is a great interest to fight against this illness using, chemotherapy among other treatments.[2] However, selectivity of chemical compounds used in chemotherapy

[1] (a) *Global cancer statistics 2018: GLOBOCAN estimates of incidence and mortality worldwide for 36 cancers in 185 countries*; Bray, F.; Ferlay, J.; Soerjomataram, I.; Siegel, R. L.; Torre, L. A.; Jemal, A.; *CA Cancer J. Clin.* **2018**, *68*, 394-424, (b) *World Health Organization, Implications of the SDGs for health monitoring-a challenge and an opportunity for all countries*, World Health Statistics 2016: Monitoring Health for the SDGs Sustainable Development Goals, WHO Press, Geneva, Switzerland, **2016**.

[2] (a) Thurston, D. E. *Chemistry and Pharmacology of Anticancer Drugs.,* 1st ed.; CRS Press; Taylor and Francis group: Abingdon, UK **2006**, (b) *Curcumin-I Knoevenagel's condensates and their*

is an important issue since some of them show severe toxicities to normal cells. Moreover, the solubility of the pharmacophore is another problem, restricting their use in chemotherapy.[3] Due to these problems, the development of potential new chemotherapeutic agents is an area of intense research. In this context, ionic liquids have been of great interest for their biological activity,[4] and considerable efforts have been made towards the design and synthesis of these organic salts with antibacterial, antifungal, anti-inflammatory and anticancer properties.[5,6] Imidazolium based-ionic liquids have been found to be the most promising type of ionic liquids showing intriguing anticancer activities against different cancer cells.[7] One of the first imidazolium salts displaying a high

---

Schiff's bases as anticancer agents: synthesis, pharmacological and simulation studies; Ali, I.; Haque, A.; Saleem, K.; Hsieh, M. F.; *Bioorg. & Med. Chem.* **2013**, *21*, 3808-3820, (c) *Chemotherapy for bladder cancer: treatment guidelines for neoadjuvant chemotherapy, bladder preservation, adjuvant chemotherapy, and metastatic cancer*; Sternberg, N.; Donat, S. M.; Bellmunt, J.; Millikan, R. E.; Stadler, W.; De Mulder, P.; Sherif, A.; Von Der Maase, H.; Tsukamoto, T.; Soloway, M. S.; *Urology* **2007**, *69*, 62-79, (d) *Hellenic GenitoUrinary Cancer Group. Current clinical practice guidelines on chemotherapy and radiotherapy for the treatment of non-metastatic muscle-invasive urothelial cancer: a systematic review and critical evaluation by the hellenic genito-urinary cancer group (hgucg)*; Zagouri, F.; Peroukidis, S.; Tzannis, K.; Kouloulias, V.; Bamias, A.; *Crit. Rev. Oncol. Hematol.* **2015**, *93*, 36-49.

[3] (a) *Ionic Liquids in Pharmaceutical Applications*; Marrucho, I. M.; Branco, L. C.; Rebelo, L. P. N.; *Annu. Rev. Chem. Biomol. Eng.* **2014**, *5*, 527-546, (b) *Thermoresponsive Supramolecular Chemotherapy by "V"-Shaped Armed β-Cyclodextrin Star Polymer to Overcome Drug Resistance*; Fan, X.; Cheng, H.; Wang, X.; Ye, E.; Loh, X. J.; Wu, Y.-L.; Li, Z.; *Adv. Healthcare Mater.* **2018**, *7*, 1701143.

[4] (a) *Ionic liquids as active pharmaceutical ingredients*; Ferraz, R.; Branco, L. C.; Prudencio, C.; Noronha, J. P.; Petrovski, Z.; *Chem. Med. Chem* **2011**, *6*, 975-985, (b) *Chemistry: Develop ionic liquid drugs*; Shamshina, J. L.; Kelley, S. P.; Gurau, G.; Rogers, R. D.; *Nature* **2015**, *528*, 188-189, (c) *Biological activity of ionic liquids and their application in pharmaceutics and medicine*; Egorova, K. S.; Gordeev, E. G.; Ananikov, V. P.; *Chem. Rev.* **2017**, *117*, 7132-7189.

[5] (a) *Antibacterial activities of imidazolium, pyrrolidinium and piperidinium salts*; Iwai, N.; Nakayama, K.; Kitazume, T.; *Bioorg. Med. Chem. Lett.* **2011**, *21*, 1728-173, (b) *The Use of Liquids Ionic Fluids as Pharmaceutically Active Substances Helpful in Combating Nosocomial Infections Induced by Klebsiella Pneumoniae New Delhi Strain, Acinetobacter Baumannii and Enterococcus Species*; Miskiewicz, A.; Ceranowicz, P.; Szymczak, M.; Bartus, K.; Kowalczyk, P.; *Int. J. Mol. Sci.* **2018**, *19*, 2779-2803, (c) *An Eco-Friendly Ultrasound-Assisted Synthesis of Novel Fluorinated Pyridinium Salts-Based and Antimicrobial and Antitumor Screening*; Rezki, N.; Al-Sodies, S. A.; Aouad, M. R.; Bardaweel, S. K.; Messali, M.; El Ashry, S. H.; *Inter. J. Mol. Sci.* **2016**, *17*, 766-786, (d) *Microwave-assisted synthesis of novel imidazolium, pyridinium and pyridazinium-based ionic liquids and prediction of physico-chemical properties for their toxicity and antibacterial activity*; Aljuhani, A.; El-Sayed, W. S.; Sahu, P. K.; Rezki, N.; Aouad, M. R.; Salghi, R.; Messali, M.; *J. Mol. Liq.* **2018**, *249*, 747-753, (e) *Green ultrasound-assisted three-component click synthesis of novel 1H-1,2,3-triazole carrying benzothiazoles and fluorinated-1,2,4-triazole conjugates and their antimicrobial evaluation*; Rezki, N.; Aouad, M. R.; *Acta pharmaceutica.* **2017**, *67*, 309-324, (f) *Green ultrasound synthesis, characterization and antibacterial evaluation of 1,4-disubstituted 1,2,3-triazoles tethering bioactive benzothiazole nucleus*; Rezki, N. A.; *Molecules* **2016**, *21*, 505-518.

[6] *The Anticancer Potential of Ionic Liquids*; Dias, A. R.; Costa-Rodrigues, J.; Fernandes, M. H.; Ferraz, R.; Prudencio, C.; *Chem. Med. Chem.* **2017**, *12*, 11-18.

[7] (a) *Cytotoxicity of Imidazole Ionic Liquids in Human Lung Carcinoma A549 Cell Line*; Chen, H-L.; Kao, H-F.; Wang, J-Y.; Wei, G-T.; *J. Chin. Chem. Soc.* **2014**, *61*, 763-769, (b) *Imidazolium-Derived Ionic Salts Induce Inhibition of Cancerous Cell Growth through Apoptosis*; Malhotra, S. V.; Kumar, V.; Velez, C.; Zayas, B.; *MedChemComm* **2014**, *5*, 1404-1409, (c) *Imidazolium salts and their polymeric materials for biological applications*; Riduan, S. N.; Zhang, Y.; *Chem Soc Rev* **2013**, *42*, 9055-9070, (d) *Phase I and pharmacokinetic study of YM155, a small molecule inhibitor of survivin*; Tolcher, W.; Mita, A.; Lewis, L. D.; Garrett, C. R.; Till, E.; Daud, A. I.; Patnaik, A.; Papadopoulos,

activity against a sizable panel of cancer cell lines were tested by Malhotra[8] and later 4,5-dichloro-1,3-bis(naphthalen-2-ylmethyl)imidazolium bromide was described as potential anticancer drug, although it had extremely poor water solubility, which would impair its distribution upon systemic administration.[9] By other side, and more recently a series of tripodal imidazolium salts have been evaluated as antibacterial and anticancer agents.[10] The balance between water solubility and high anticancer activity has represented a major obstacle for the potential clinical use of lipophilic imidazolium salts.

In this context, our research group has been involved in the preparation of imidazolium based compounds derived from amino acids.[11] Therefore, with the potential of imidazolium salts as anticancer agents well established and continuing with our previous work related with *L*-valine imidazolium tripodal salts,[11e] we present here the synthesis of different tripodal imidazolium salts derived from amino acids to evaluate the synergetic effects between their lipophobicity and anticancer activity. In order to tune their physicochemical and potential antitumor properties, we considered different natural amino acids (*L*-phenylalanine and *L*-valine) as well as different amide substitutions (aliphatic and aromatic) and different anion nature. Furthermore, for the amphiphilic tripodal compounds, self-aggregation studies in aqueous media have been carried out to determine their critical aggregation concentration. In addition, the

---

K.; Takimoto, C.; Bartels, P.; Keating, A.; Antonia, S. *J Clin Oncol* **2008**, *26*, 5198-5203, (e) *Novel alkyl cationic glycerolipids with a heterocyclic polar domain induce disturbances of the cell cycle and the death of human leukemia cells*; Markova, A. A.; Plyavnik, N. V.; Tatarskii, V. V. Jr.; Shtil, A. A.; Serebrennikova, G. A.; *Russ J Bioorg Chem* **2010**, *36*, 532-534.

[8] *A profile of the in vitro anti-tumor activity of imidazolium-based ionic liquids*; Malhotra, S. V.; Kumar, V.; *Bioorg Med Chem Lett* **2010**, *20*, 581-585.

[9] *Anti-tumor activity of lipophilic imidazolium salts on select NSCLC cell lines*; Wright, B. D.; Deblock, M. C.; Wagers, P. O.; Duah, E.; Robishaw, N. K.; Shelton, K. L.; Southerland, M. R.; DeBord, M. A.; Kersten, K. M.; McDonald, L. J.; Stiel, J. A.; Panzner, M. J.; Tessier, C. A.; Paruchuri, S.; *W. J. Youngs. Med Chem Res* **2015**, *24*, 2838-2861.

[10] (a) *Benzene centered tripodal imidazolium (BTI) system: Emerged towards multidisciplinary research and development*; Rondla, R.; *Inorganica Chimica Acta* **2018**, *477*, 183-191, (b) Youngs, W.; Panzner, M.; Tessier, C.; Deblock, M.; Wright, B.; Wagers, P.; Robishaw, N. *Azolium and purinium salt anticancer and antimicrobial agents* US **2014**, 0142307 A1.

[11] (a) *Synthesis of new chiral imidazolium salts derived from amino acids: their evaluation in chiral molecular recognition*; Altava, B.; Barbosa, D. S.; Burguete, M. I.; Escorihuela, J.; Luis, S. V.; *Tetrahedron:Asymmetry* **2009**, *20*, 999-1003, (b) *Application of optically active chiral bis-(imidazolium) salts as potential receptors of chiral dicarboxylate salts of biological relevance*; González-Mendoza, L.; Escorihuela, J.; Altava, B.; Burguete, M. I.; Luis, S. V.; *Org. Biomol. Chem.* **2015**, *13*, 5450-5459, (c) *Bis(imidazolium) salts derived from amino acids as receptors and transport agents for chloride anions*; Gonzalez-Mendoza, L.; Altava, B.; Burguete, M. I.; Escorihuela, J.; Hernando, E.; Luis, S. V.; Quesada, R.; Vicent, C.; *RSC Adv.* **2015**, *5*, 34415-34423, (d) *Synthesis of Chiral Room Temperature Ionic Liquids from Amino Acids – Application in Chiral Molecular Recognition*; Gonzalez-Mendoza, L.; Altava, B.; Bolte, M.; Burguete, M. I.; García-Verdugo, E.; Luis, S. V.; *Eur. J. Org. Chem.* **2012**, 4996-5009, (e) *Supramolecularly assisted synthesis of chiral tripodal imidazolium compounds*; Valls, A.; Altava, B.; Burguete, M. I.; Escorihuela, J.; Martí Centelles, V.; Luis, S. V.; *Org. Chem. Front.* **2019**, *6*, 1214-1225.

tripodal salts were evaluated as transmembrane transporters of anions with the aim of enhancing their cytotoxicity and to begin to decipher their mechanism of action.[12] The microenvironment around tumour cells is unusually acidic compared to healthy cells as a result of the altered cancer cell metabolism. This acidic microenvironment provide cancer cells with adaptative advantages. Moreover, the intracellular pH is slightly alkaline, contributing to drug resistance.[13,14] Accordingly, anticancer, self-assembly and anion transport studies were performed under physiologic and slightly acidic pH condition.[15]

2. Materials and Methods

2.1. Materials

Reagents and solvents, including NMR solvents, were purchased from commercial suppliers and were used without further purification except for pyrene, used for fluorescence studies, that was crystallized twice from ethanol. Deionized water was obtained from a MilliQ® equipment. Imidazoles **1** and **2** and imidazolium salts **3a-Br**, **3b-Br** and **5b-Br** were prepared as previously described.[11b,11e,12e] Imidazolium salts **4a-Br**, **6a-Br**, **7a-Br**, **8a-Br**, **3a-NTf$_2$**, **6a-NTf$_2$**, **7a-NTF$_2$** and **8a-NTf$_2$** were prepared following the synthetic protocols and were obtained in >70% yield by treatment of the imidazole **1** or **2** with the corresponding (tris-bromomethyl)aryl compound under Mw at 70ºC.[11e] The anion exchange was carried out by reaction of the bromide imidazolium salts

---

[12] (a) *Anion Transporters and Biological Systems*; Gale, P. A.; Pérez-Tomás, R.; Quesada, R.; *Acc. Chem. Res.* **2013**, *46*, 2801-2813, (b) *Small-molecule lipid-bilayer anion transporters for biological applications*; Busschaert, N.; Gale, P. A.; Angew. *Chem. Int. Ed.* **2013**, *52*, 1374-1382, (c) *Synthetic ion transporters can induce apoptosis by facilitating chloride anion transport into cells*; Ko, S. K.; Kim, S. K.; Share, A.; Lynch, V. M.; Park, J.; Namkung, W.; Rossom, W. V.; Busschaert, N.; Gale, P. A.; Sessler, J. L.; Shin, I.; *Nat. Chem.* **2014**, *6*, 885-892, (d) Davis, J. T. *in Topics in Heterocyclic Chemistry,* Gale, P. A.; Dehaen, W. Ed.; Springer, Berlin, Heidelberg, **2010**, vol. 24, pp. 145-176, (e) *Chiral Room Temperature Ionic Liquids as Enantioselective Promoters for the Asymmetric Aldol Reaction*; González, L.; Escorihuela, J.; Altava, B.; Burguete, M. I.; Luis, S. V.; *Eur. J. Org. Chem.* **2014**, 5356-5363.

[13] *Dysregulated pH: a perfect storm for cancer progression*; Webb, B. A.; Chimenti, M.; Jacobson, M. P.; Barber, D. L.; *Nat. Rev. Cancer* **2011**, *11*, 671-677.

[14] (a) *pH-Dependent Chloride Transport by Pseudopeptidic Cages for the Selective Killing of Cancer Cells in Acidic Microenvironments*; Tapia, L.; Pérez, Y.; Bolte, M.; Casas, J.; Sol, J.; Quesada, R.; Alfonso, I.; *Angew. Chem. Int. Ed.* **2019**, *131*, 12595-12598, (b) *A Dimeric Bis(melamine)-Substituted Bispidine for Efficient Transmembrane H+ /Cl- Cotransport*; Shinde, S. V.; Talukdar, P.; *Angew. Chem.* **2017**, *129*, 4302-4306.

[15] (a) *Bis(sulfonamide) transmembrane carriers allow pH-gated inversion of ion selectivity*; Roy, A.; Biswas, O.; Talukdar, P.; *Chem. Commun.* **2017**, *53*, 3122-3125, (b) *pH-Regulated Nonelectrogenic Anion Transport by Phenylthiosemicarbazones*; Howe, E. N. W.; Busschaert, N.; Wu, X.; Berry, S. N.; Ho, J.; Light, M. E.; Czech, D. D.; Klein, H. A.; Kitchen, J. A.; Gale, P. A.; *J. Am. Chem. Soc.* **2016**, *138*, 8301-8308, (c) *pH switchable anion transport by an oxothiosquaramide*; Elmes, R. B. P.; Busschaert, N.; Czech, D. D.; Gale, P. A.; Jolliffe, K. A.; *Chem. Commun.* **2015**, *51*, 10107-10110, (d) *Thiosquaramides: pH switchable anion transporters*; Busschaert, N.; Elmes, R. B. P.; Czech, D. D.; Wu, X.; Kirby, I. L.; Peck, E. M.; Hendzel, K. D.; Shaw, S. K.; Chan, B.; Smith, B. D.; Jolliffe, K. A.; Gale, P. A.; *Chem. Sci.* **2014**, *5*, 3617-3626.

with $LiNTf_2$ in CH_3CN leading to the corresponding NTf_2 salts in good yields (> 80%) (Scheme 1).

2.2 Chemical synthesis

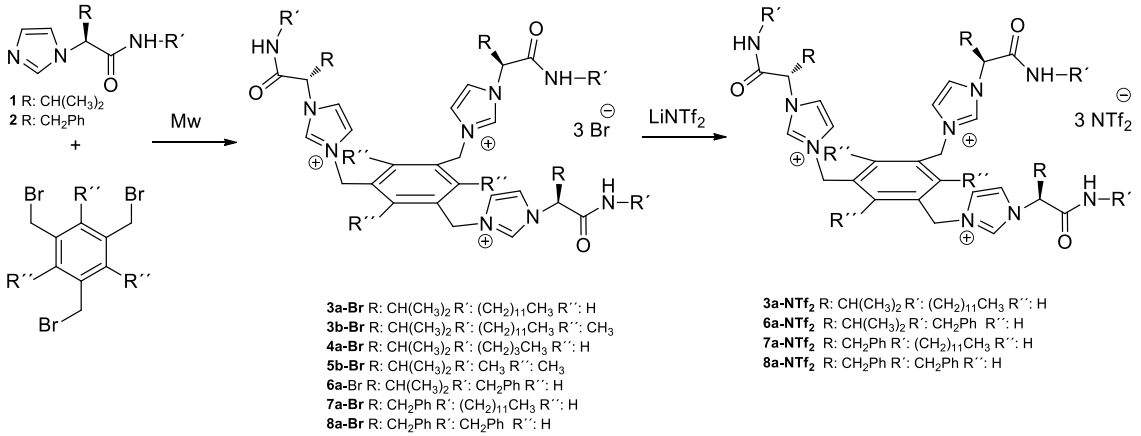

Scheme 1. Synthesis of the tripodal imidazolium salts

2.3 Anticancer and toxicity studies

Cell culture media were purchased from Gibco (Grand Island, NY). Fetal bovine serum (FBS) was obtained from HyClone (Utah, USA). Supplements and other chemicals not listed in this section were obtained from Sigma Chemical Co. (St. Louis, MO). Plastics for cell culture were supplied by Thermo Scientific BioLite (Madrid, Spain). All tested compounds were dissolved in DMSO at a concentration of 10 mM and stored at −20°C until use.

A549, HeLa, HT-29, MCF-7 and HEK-293 cell lines were maintained in Dulbecco's modified Eagle's medium (DMEM) containing glucose (1 g/L), glutamine (2 mM), penicillin (50 µg/mL), streptomycin (50 µg/mL), and amphotericin B (1.25 µg/mL), supplemented with 10% FBS. All pH 6.2 media were prepared replacing the carbonate by PIPES buffer (10 mM) and adjusting the pH with 1M HCl or 1M NaOH.

2.4 Cell proliferation assay

In 96-well plates, 3×10^3 (HeLa, A549, HT-29, MCF-7 or HEK-293) cells per well were incubated with serial dilutions of the tested compounds (from 200 µM to 0,2 µM) in a total volume of 100 µL of their growth media. The 3-(4,5-dimethylthiazol-2-yl)-2,5-diphenyltetrazolium bromide (MTT; Sigma Chemical Co.) dye reduction assay in 96-well microplates was used. After 2 days of incubation (37 °C, 5% CO_2 in a humid atmosphere), 10 µL of MTT (5 mg/mL in

phosphate-buffered saline, PBS) was added to each well, and the plate was incubated for a further 3 h (37 °C). The supernatant was discarded and replaced by 100 µL of DMSO to dissolve formazan crystals. The absorbance was then read at 540 nm by Multiskan™ FC microplate reader. For all concentrations of compound, cell viability was expressed as the percentage of the ratio between the mean absorbance of treated cells and the mean absorbance of untreated cells. Three independent experiments were performed, and the IC_{50} values (i.e., concentration half inhibiting cell proliferation) were graphically determined using GraphPad Prism 4 software.

Statistical analysis: GraphPad Prism v4.0 software (GraphPad Software Inc., La Jolla, USA) was used for statistical analysis. For all experiments, the obtained results of the triplicates were represented as means with standard deviation (SD).

2.5 ^{1}H NMR studies

The NMR experiments were carried out on a Varian INOVA 500 spectrometer (500 MHz for ^{1}H and 125 MHz for ^{13}C), on a Bruker Avance III HD 400 spectrometer (400 MHz for ^{1}H and 100 MHz for ^{13}C) or on a Bruker Avance III HD 300 spectrometer (300 MHz for ^{1}H and 75 MHz for ^{13}C). Chemical shifts are reported in ppm using TMS as a reference. Titration experiments followed by ^{1}H NMR spectroscopy were performed in CD_3CN/H_2O 8/2 v/v at 303 K and data fitting was carried out with the HypNMR 2008 version 4.0.71 software. For each ^{1}H NMR titration, the signals of the protons H_a, H_b, H_f, H_g, NH, were monitored for changes in chemical shift, which provided several data sets that were employed in the determination of the association constants K_a. The data for chloride anion was fitted satisfactorily to the 1:1 binding model.

2.6 Fluorescence spectroscopy measurements

Pyrene was used as a fluorescence probe to determine the CAC of **2a-2c** and **3a** in aqueous media at 25±1 °C. Fluorescence measurements were performed with a Spex Fluorolog 3-11 instrument equipped with a 450 W xenon lamp (right angle mode). Firstly, stock pyrene solution of $1{,}98\times10^{-4}$ mol/L was prepared in ultrapure methanol. Then, the different compounds solutions of tripodal compounds (ranging from 1×10^{-3} to 1×10^{-6} mol/L) were prepared in different vials and 5 µL of pyrene solution was transferred into the vials, where the final pyrene concentration was $9{,}89\times10^{-7}$ mol/L in each vial. Fluorescence spectra of

pyrene were recorded from 200 to 650 nm after excitation at 337 nm. The slit width was set at 5 nm for both excitation and emission. The peak intensities at 373, 382 and 470 nm were determined as I_1, I_3 and I_e, respectively. The ratios of the peak intensities at 373 and 382 nm (I_1/I_3) and 470 nm (I_e/I_1) of the emission spectra were recorded as a function of the logarithm of concentration. Samples were excited with a 337 nm NanoLED. The CAC values were taken from the break point of the plot I_1/I_3 ratio of the emission spectra against concentration.

2.7 Light scattering (LS) measurements

Light scattering measurements were performed using a Brookhaven Instruments BI-200SM goniometer, a BI-9000AT digital correlator, and a red laser operating at wavelength of 633 nm. Scattering angle was 45°. The round measurement cell was thermostated at 25 °C. A 0.6 mM solution of the compounds **3a-Br** and **3b-Br** was prepared in Milli-Q water. The solvent was filtered through a Millipore Millex syringe filter (0.22 μm). Before each measurement, the scattering cell was rinsed several times with the solution. The LS measurements started 5-10 min after the sample solutions were placed in the LS optical system to allow the sample to equilibrate. The data acquisition was carried out for 10 min and each experiment was repeated three times. The data were analyzed with the cumulant method using the software provided by the manufacturer.

2.8 Optical images

Self-assembly images were recorded with an OLYMPUS COVER-018 microscopy, BX51TF model, at 25°C. Images of cell lines were obtained by inverted microscope with Zeiss-Primovert phase contrast.

2.9 SEM images

Scanning Electron Microscopy was performed in a JEOL 7001F microscope with a digital camera. Samples were obtained by slow evaporation of a solution of the compounds (1 to 2 mg/ml) directly onto the sample holder and were conventionally coated with platinum using the sputtering technique in which microscopic particles of platinum are rejected from the surface after the material is itself bombarded by energetic particles of a plasma or gas.

2.10 Membrane transport assays

Preparation of Phospholipid Vesicles: A chloroform solution of 1-palmitoyl-2-oleoyl-sn-glycero-3-phosphocoline (POPC) (20 mg/mL) (Sigma Aldrich) was evaporated to dryness using a rotary evaporator and the resulting film was dried under high vacuum for, at least, two hours. A sodium chloride aqueous solution (489 mM and 5 mM phosphate buffer, pH 7.2, or 451 mM and 20 mM phosphate buffer, pH 7.2) was added to rehydrate the lipid film. The resulting suspension was vortexed and subjected to nine freeze-thaw cycles; subsequently, it was extruded twenty-nine times through a polycarbonate membrane (200 nm) employing a LiposoFast basic extruder (Avestin, Inc.). The resulting unilamellar vesicles were dialysed against a sodium nitrate (489 mM and 5 mM phosphate buffer, pH 7.2) or a sodium sulphate (150 mM and 20 mM phosphate buffer, pH 7.2) aqueous solutions, to remove unencapsulated chloride.

Ion selective electrode (ISE) transport assays. Chloride/Nitrate Transport Assays: Unilamellar vesicles (average diameter: 200 nm) made of POPC and containing a sodium chloride aqueous solution (489 mM and 5 mM phosphate buffer, pH 7.2, for chloride/nitrate exchange assays, or 451 mM and 20 mM phosphate buffer, pH 7.2, for chloride/bicarbonate exchange assays) were suspended in a sodium nitrate (489 mM and 5 mM phosphate buffer, pH 7.2) or a sodium sulphate (150 mM and 20 mM phosphate buffer, pH 7.2) aqueous solution, respectively, the final lipid concentration being 0.5 mM and the final volume 5 mL. A solution of the carrier in DMSO, usually 5 μL to avoid the influence of the organic solvent during the experiments, was added, and the chloride released was monitored employing a chloride-selective electrode (HACH 9652C). Once the experiment was finished, a surfactant (Triton-X, 10% dispersion in water, 20 μL) was added to lyse the vesicles and release all the encapsulated chloride. This value was regarded as 100% release and used as such. For the chloride/bicarbonate exchange assays, a sodium bicarbonate aqueous solution was added to the vesicles suspended in the sodium sulphate one (150 mM and 20 mM phosphate buffer, pH 7.2), the final bicarbonate concentration during the experiment being 40 mM. The chloride efflux was monitored for another five minutes, until the vesicles were lysed with the surfactant.

Carboxyfluorescein-based assays: POPC vesicles were loaded with a sodium chloride aqueous solution (451 mM NaCl and 20 mM phosphate buffer, 50 mM carboxyfluorescein, pH 7.2) and treated according to the procedure described above. After being subjected to extrusion, liposomes were suspended in a sodium sulphate aqueous solution (150 mM Na_2SO_4 and 20 mM phosphate buffer, pH 7.2). The unencapsulated carboxyfluorescein was removed by size-exclusion chromatography, using Sephadex G-25 as the stationary phase and the external solution as the mobile phase. The experiments were performed in 1-cm disposable cells, the final POPC concentration in the cuvette being 0.05 mM and the total volume 2.5 mL. For those experiments in which pHout = 6.2, the corresponding volume of the vesicles stock solution was suspended in a sodium sulphate aqueous solution at pH 6.2 immediately before starting the assay. At t = 60 s the anion carrier was added and the emission changes were recorded during five minutes. At t = 360 s a pulse of the detergent Triton-X (10%) was added to lyse the vesicles and release all the entrapped carboxyfluorescein. This value was regarded as 100% release and used to normalise the data.

3. Results and discussion

3.1. Anticancer and toxicity studies

The in vitro anticancer activities of the synthesized compounds were examined against four human cancer cell lines, characterizing tumours of different origins. The human lung adenocarcinoma cell line A549, the human cervix tumour cell line HeLa, the human colon adenocarcinoma cell line HT-29 and the human breast cancer cell line MCF-7. Furthermore, human embryonic kidney cell HEK-293 was used as control to evaluate the selectivity of the compounds to carcinoma cells. All the cells were incubated in culture media with varying concentrations of the examined compound and the impact of treatment was measured using the MTT assay (Figure S1).[16] We performed the experiments at different pHe values using standard DMEM medium for pHe 7.2 and using PIPES buffer to fix the pHe to 6.2. The IC_{50} values obtained for the cells under investigation are summarized in Table 1 and 2.

[16] *Tetrazolium salts and formazan products in Cell Biology: Viability assessment, fluorescence imaging, and labeling perspectives*; Stockert, J. C.; Horobin, R. W.; Colombo, L. L.; Blázquez-Castro, A.; *Acta Histochem.* **2018**, *120*, 159-167.

Table 1. (MTT cytotoxicity in A549, HeLa, HT-29, MCF-7 and HEK-293 cell lines for tripodal compounds **3-8** at physiologic pH.)

Entry	Compound	H_2O Solubility (0.5 mM)	IC_{50} (μM)[a]					α[b] (A549)	β[c] (HeLa)
			A549	HeLa	HT-29	MCF-7	HEK-293		
1	**3a-Br**	S	15.0 ± 0.5	12.9 ± 0.2	16.8 ± 1.2	19.4 ± 1.3	13.0 ± 0.9	0.9	1.0
2	**3b-Br**	S	18.9 ± 1.4	14.2 ± 0.6	16 ± 3	13 ± 3	13.5 ± 0.9	0.7	1
3	**4a-Br**	S	90 ± 9	93 ± 6	>200	>200	>200	>2.2	>2.1
4	**5b-Br**	S	>200	>200	>100	>200	>200	-	-
5	**6a-Br**	S	>100	84 ± 17	>200	>200	>200	-	>2.4
6	**7a-Br**	I	23.5 ± 0.7	2.09 ± 0.03	34.4 ± 1.3	21 ± 3	2.7 ± 0.4	0.1	1.3
7	**8a-Br**	I	23.6 ± 1.3	11.7 ± 0.8	57 ± 2	27 ± 2	15 ± 3	0.6	1.3
8	**3a-NTf_2**	I	17.1 ± 0.6	7.3 ± 0.3	99 ± 3	89 ± 3	9.7 ± 1.1	0.6	1.3
9	**6a-NTf_2**	I	93 ± 5	96 ± 12	>200	>200	42 ± 7	0.5	0.4
10	**7a-NTf_2**	I	21 ± 4	5.0 ± 0.6	45.8 ± 1.1	22.2 ± 0.6	2.8 ± 0.2	0.1	0.6
11	**8a-NTf_2**	I	4.8 ± 0.6	13 ± 5	82 ± 7	44 ± 5	12.1 ± 1.9	2.5	0.9

[a] (IC_{50} (x ± sd) average from three experiments after 48h); [b] (**α** = IC_{50} (HEK-293) / IC_{50} (A549)); [c] (**β** = IC_{50} (HEK-293) / IC_{50} (HeLa)).

When experiments were run at pH 7.2 (Table 1), the results indicate that compounds **3a-Br**, **3b-Br**, **7a-Br**, **8a-Br**, **3a-NTf_2**, **7a-NTf_2** and **8a-NTf_2** exhibited considerable cancer cell growth inhibition against the examined cancer types with IC_{50} value in the 20 μM range or lower on the four cell lines (entries 1, 2, 6, 7, 8, 10 and 11, Table 1). We believe the activity may be a result of the nature of the substituents, by one side the six benzyl groups present in compounds **8a-Br** and **8a-NTf_2**, the aromaticity and planarity of these groups are traits shared by several other anticancer agents that are efficacious due to their intercalation into the base pairs of DNA and introduce structural distortions that inhibit transcription and replication.[17] By other side compounds **3a-Br**, **3b-Br**, **7a-Br**,

[17] (a) *DNA induced DNA repair X-ray structure of a DNA-ditercalinium complex*; Gao, Q.; Williams, L. D.; Egli, M.; Rabinovich, D.; Le Chen, S.; Qugley, G.; Rich, A.; *Proc. Natl. Acad. Sci. USA.* **1991**, *88*, 2422-2431, (b) *Bis naphtalimides: a new class of antitumor agents*; Brana, M. F.; Castellano, J. M.; Moran, M.; Perez de Vega, M. J.; Romerdahl, C. R.; Qian, X. D.; Bousquet, P.; Emling, F.; Schlick, E.; Keilhauer, G.; *Anticancer Drug Des.* **1993**, *8*, 257-268, (c) *DNA-ditercalinium complex*; Villalona-Calero, M. A.; Eder, J. P.; Toppmeyer, D. L.; Allen, L. F.; Fram, R.; Velagapudi, R.; Myers,

3a-NTf$_2$ and **7a-NTf$_2$** present three long alkyl chains facilitating their interaction with the lipidic membrane and thus the observed toxicity could be related to their transmembrane transport ability. Compounds **4a-Br**, **5b-Br**, **6a-Br** and **6a-NTf$_2$** fail in the presence of such substituents.

For the tumoral cell lines HT-29 and MCF-7, none of the compounds studied offers good selectivity comparing IC_{50} with the healthy cell line HEK-293 (β <1). Nevertheless, for the cell lines A549 and HeLa compounds **4a-Br**, **6a-Br** and **8a-NTf$_2$** presented a selectivity higher than 2, having the compound **8a-NTf$_2$** the best antitumor properties for the cell line A549 with an IC_{50} of 4.8 μM and α = 2.5 (entry 11, Table 1).

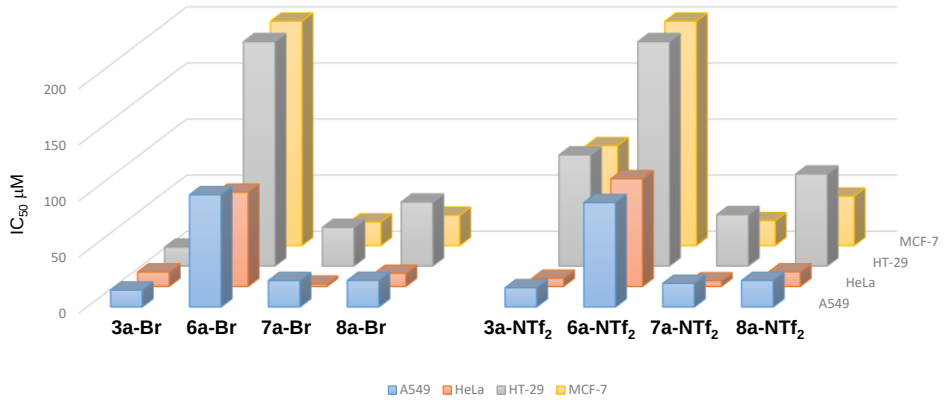

Figure 1. (Plot of IC_{50} in A549, HeLa, HT-29, MCF-7 and HEK-293 cell lines for tripodal compounds **3a, 6a, 7a, 8a** at pH 7.2).

Regarding the anion nature, as can be observed in Figure 1, the anion effect is significantly important for the four cell lines studied specially for HT-29 and MCF-7. In general, the bromide anion conferees better antitumor activities than the analogous compound with NTf_2 anion.

In Table 2 is shown the cytotoxicity of the different tripodal compounds for the cell line A549 using different external pHe: normal (7.2) and acidic (6.2). In general for bromide salts, the IC_{50} obtained at acidic external pH is relatively maintained for essentially nontoxic compounds **4a-Br, 5b-Br** and **6a-Br** (IC_{50} >100), and lowered for active ones (entries 1, 2, 6, 7), in particular for compound **7a-Br** with a IC_{50} ten times lower at pHe 6.2 (entry 6), similar results have been

M.; Amato, A.; Kagen-Hallet, K.; Razvillas, B.; Kufe, D. W.; Von Hoff, D. D.; *J. Clin. Oncol.* **2001**, *19*, 857-864.

described in the literature.[14] It has to be emphasized the high selectivity obtained for compounds **3b**-**Br** and **8a-Br** (entries 2, 7). Moreover, the results obtained for **NTf_2** salts were especially significant, since the cytotoxicity of receptors **3a-NTf_2** and **8a-NTf_2** decreased dramatically as the pH_e decreased (entries 8 and 10, Table 2), emphasising the role of the anion.

Table 2. (MTT cytotoxicity in A549 cell line for tripodal compounds **3-8** at different pHe)

Entry	Compound	IC_{50} (μM) [a]			α[b]	γ[c]
		A549 (pHe 7.2)	A549 (pHe 6.2)	HEK-293 (pHe 7.2)	(A549) (pH 7.2)	(A549) (pH 6.2)
1	**3a-Br**	15.0 ± 0.5	5.3 ± 0.4	13.0 ± 0.9	0.9	2.5
2	**3b-Br**	18.9 ± 1.4	2.8 ± 0.5	13.5 ± 0.9	0.7	4.8
3	**4a-Br**	90 ± 9	>100	>200	>2.2	-
4	**5b-Br**	>200	>100	>200	-	-
5	**6a-Br**	>100	>100	>200	-	-
6	**7a-Br**	23.5 ± 0.7	1.4 ± 0.3	2.7 ± 0.4	0.1	1.9
7	**8a-Br**	23.6 ± 1.3	4.2 ± 0.3	15 ± 3	0.6	3.5
8	**3a-NTf_2**	17.1 ± 0.6	>100	9.7 ± 1.1	0.6	<1
9	**7a-NTf_2**	21 ± 4	3.1 ± 0.6	2.8 ± 0.2	0.1	1
10	**8a-NTf_2**	4.8 ± 0.6	>100	12.1 ± 1.9	2.5	< 1

[a] (IC_{50} (x ± sd) average from three experiments); [b] (α = IC_{50} (HEK-293) / IC_{50} (A549)); [c] (γ = IC_{50} (HEK-293) / IC_{50} (A549) at pHe 6.2).

Optical microscopy images for A549 cell line after two days incubation with compound **7a-Br**, reveal a clear sign of damage, from morphological changes to disruption of the cell membrane and leakage of cytoplasmatic material (Figure S1).

Taking in consideration the results obtained, we decided to study the aggregation behaviour and anion transport properties of these compounds at different pHe to investigate the possible mechanism of action and if its mode of action depends on the level of aggregation.

3.2 Aggregation behaviour

The self-assembly behavior of the tripodal compounds in aqueous media, including the analysis of the size distributions and the morphologies of the aggregates formed, was investigated by ^{1}H-NMR, light scattering (LS), fluorescence, optical microscopy and SEM.

3.3.1. ^{1}H NMR experiments

Due to the low solubility of some of the tripodal compounds in water (< 0.5 mM, see Table 1), ^{1}H-NMR aggregation studies were run in D_2O/CD_3OD (1/1 v/v) for **3a-Br, 3b-Br**, **4a-Br, 5b-Br** and **6a-Br** from 0.1 to 4 mM, precluding an accurate analysis for compounds **7a-Br**, **8a-Br** and NTf_2 derivatives due solubility problems.

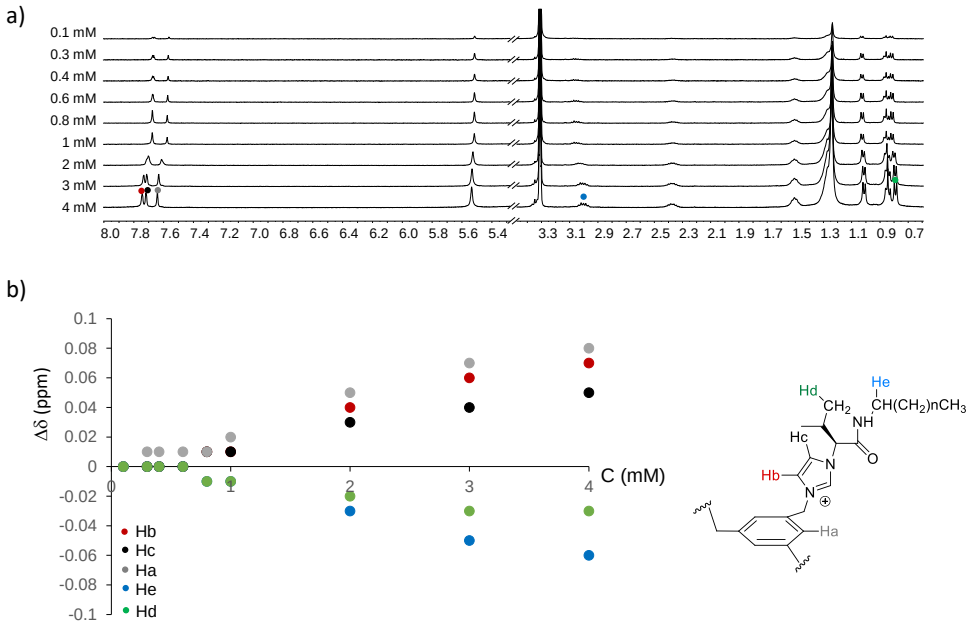

Figure 2. a) Partial ^{1}H NMR (400 MHz at 30°C) of the compound **3a-Br** in CD_3OD/D_2O (1/1 v/v) obtained for various concentrations. b) Plot of Δδ *vs.* concentration.

Figure 2 shows the partial ^{1}H NMR spectra of the compound **3a-Br** in D_2O/CD_3OD 1/1 v/v at concentrations ranging from 0.1 to 4 mM at 30 °C. When the concentration is increased, the imidazolium and aromatic protons Hb, Hc and Ha, shift downfield (Δδ= 0.06-0.08) indicating that these groups becomes slightly more involved in hydrogen bonding upon concentration, while minor changes were detected for the signals of the hydrophobic chains (Δδ ≈ 0.01), however one of the methylene protons of the alkyl chains (NH-CH_2) and the methyl protons of the valine side chain shifted upfield upon aggregation (Δδ ≈ 0.05 and 0.03 respectively) (Figure 2b). Similar trend was observed for the corresponding protons of **3b-Br** (see ESI, Figure S2a). However, for the tripodal **4a-Br** when the concentration increased from 0.1 to 4 mM, the imidazolium and aromatic protons signals shift slightly downfield (Δδ = 0.01-0.02) while no significant chemical shift variation was observed for signals of the hydrophobic chain and the methyl protons of the valine side chain (ESI, Figure S2b).

Moreover, for the tripodal **5b-Br** and **6a-Br,** when the concentration increased from 0.1 to 4 mM, no significant chemical shift variation was observed for any of the proton signals.

3.3.2. Fluorescence spectroscopy

To investigate the microenvironment of the self-assembly in water by fluorescence we use the pyrene 1:3 ratio method.[18] The plots of the pyrene 1:3 ratio as a function of the total surfactant concentration shows around the CAC, a typical sigmoidal decrease. Below the CAC the pyrene 1:3 ratio value corresponds to a polar environment and as the surfactant concentration increases the pyrene 1:3 ratio decreases rapidly, indicating that the pyrene is sensing a more hydrophobic environment. Above the CAC, the pyrene 1:3 ratio reaches a roughly constant value because of the incorporation of the probe into the hydrophobic region of the aggregates. Different approaches have been used to estimate CAC values from I_1/I_3 ratios.[18,19] The most common approach is the use of the break points, either directly or by extrapolating the values from the intersection of the two straight lines defined at the constant and variable regions of the I_1/I_3 sigmoidal curve.[20] As CAC represents the threshold of concentration at which self-aggregation starts, the corresponding value can be estimated from the break point at lower concentration.[21,22]

---

[18] (a) *Environmental effects on vibronic band intensities in pyrene monomer fluorescence and their application in studies of micellar systems*; Kalyanasundaram, K.; Thomas, J. K.; *J. Am. Chem. Soc.* **1977**, *99*, 2039-2044, (b) Kalyanasundaram, K. *Photochemistry in Microheterogeneous Systems*, Academic Press, New York, **1987**, (c) *On the determination of the critical micelle concentration by the pyrene 1:3 ratio method*; Aguiar, J.; Carpena, P.; Molina-Bolívar, J. A.; Carnero Ruiz, C.; *J. Colloid Interface Sci.* **2003**, *258*, 116–122.

[19] *Spontaneous vesicle formation and vesicle-to-micelle transition of sodium 2-ketooctanate in water*, Xu, H.; Du, N.; Song, Y.; Song, S.; Hou, W.; *J. Coll. Interf. Sci.* **2018**, *509*, 265-274.

[20] (a) *Ultrasonic Absorption Studies of Surfactant Exchange between Micelles and Bulk Phase In Aqueous Micellar Solutions of Nonionic Surfactants with Short Alkyl Chains. 1,2-Hexanedlol and 1,2,3-Octanetrlol*; Frindi, M.; Michels, B.; Zana, R.; *J. Phys. Chem.* **1991**, *95*, 4832-4837, (b) *Aggregation Behavior of Tyloxapol, a Nonionic Surfactant Oligomer in Aqueous Solution*; Regev, O.; Zana, R.; *J. Colloid Interf. Sci.* **1999**, *210*, 8-17.

[21] (a) *Fluorescence Probes for Critical Micellé Concentration*; Ananthapadmanabhan, K. P.; Goddard, E. D.; Turro, N. J.; Kuo, P. L.; *Langmuir* **1985**, *2*, 352-355, (b) *Linolenic acid-modified chitosan for formation of selfassembled nanoparticles*; Liu, C. G.; Desai, K. G. H.; Chen, X. G.; Park, H. J.; *J. Agric. Food Chem.* **2005**, *53*, 437-441, (c) *Preparation and Characterization of Self-Assembled Nanoparticles of Hyaluronic Acid-Deoxycholic Acid Conjugates*; Dong, X.; Liu, C.; *J. Nanomat.,* **2010**, Article ID 906936.

[22] *Synthesis and surface-active properties of sulfobetaine-type zwitterionic gemini surfactants*; Yoshimura, T.; Ichinokawa, T.; Kaji, M.; Esumi, K.; *Colloids Surf. A: Physicochem. Eng. Aspects* **2006,** *273*, 208-212.

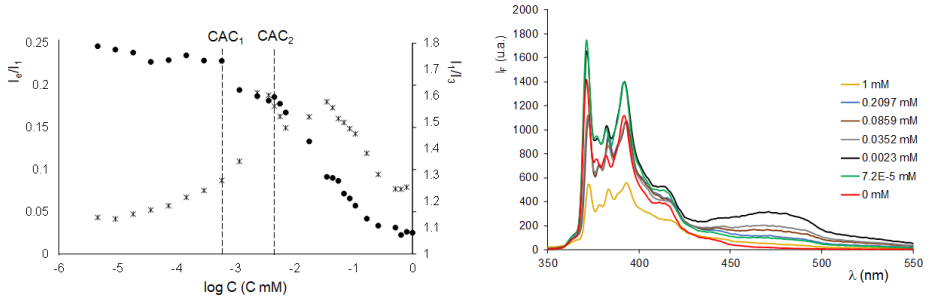

Figure 3. a) Plot of the I_1/I_3 (circles, right axes) and Ie/I_1 (stars, left axes) ratios *v* log C for **3a-Br** in H_2O at 25ºC, b) Emission spectra of pyrene in H_2O in the presence of different amounts of **3a-Br**.

Table 3. (Estimated CACs obtained in aqueous media using fluorescence studies at 25ºC)

Entry	Amphiphilic compound	Solvent	CACs[a] (μM)	
1	**3a-Br**	H_2O	0.6	4.2
2	**3a-Br**	Buffer pH 7.2	7.1	
3	**3a-Br**	Buffer pH 6.2	16.2	
4	**3b-Br**	H_2O	10.5	
5	**4a-Br**	H_2O	1387	
6	**4a-Br**	Buffer pH 7.2	1747	
7	**4a-Br**	Buffer pH 6.2	1792	
8	**5b-Br**	H_2O	120	
9	**6a-Br**	H_2O	41.6	

a) (values at the break points).

The corresponding CACs obtained by fluorescence in water are shown in Table 3. All the compounds presented CAC values in the μM range, only for compound **4a-Br** the CAC was in the mM range, being the lower CAC value for compound **3a-Br** (entry 1, table 3). The plot of the I_1/I_3 ratio for the corresponding emission spectra *vs* concentrations showed for compounds **3b-Br**, **4a-Br**, **5b-Br and 6a-Br** one single break point reaching in all cases values of $I_1/I_3 \approx 1.1$ or lower after the break point (Figure S3, and S4). However, for compound **3a-Br**, the plot of the I_1/I_3 ratios for the corresponding emission spectra *vs* concentration presented two single break point suggesting the presence of two different aggregates (Figure 3). The first break point is at 0.6 μM with values of $I_1/I_3 \approx 1.6$, affording aggregates with an appreciable pyrene solvent exposed, while the second break point is located at higher concentration region (4.5 μM) reaching I_1/I_3 values ≈ 1.1 and leading to aggregates with a low polarity microenvironment to pyrene.

Moreover, it has been described that pyrene can show a broad excimer emission band around 470 nm in dilute water surfactant solution containing vesicles or bilayer structures.[23] In this regard, compounds **3a-Br** and **3b-Br** presented a broad emission band (I_e) around 470 nm. For **3a-Br** the I_e/I_1 ratio increases at concentrations higher than CACs, reaching two maxima at *ca.* 2.3 μM and 35 μM, decreasing the I_e/I_1 ratio sharply until concentrations where no further change in the the I_1/I_3 ratio is observed (Figure 3). However, for **3b-Br**, the I_e/I_1 ratio reached two maxima at ca. 11 μM and 102 μM corresponding the CAC to the first maximum when the I_1/I_3 ratio start to decrease sharply, being the second maximum at concentrations where no further change in the the I_1/I_3 ratio is observed (Figure S3).

To study the role of the pH in the aggregation behaviour, fluorescence studies for **3a-Br** and **4a-Br** were measured at normal and acidic pH using the corresponding phosphate buffer solution (10 mM). For tripodal compound **3a-Br,** the acidic pH increases the CAC and difficulties the formation of aggregates (Table 3 entries 2 and 3, Figure S5a), however for compound **4a-Br** the CAC did not increase significantly form pH 7.2 to pH 6.2 (Table 3 entries 6 and 7, Figure S5b). It must be mention than the CAC increases from water to buffer pH 7.2 for **4a-Br** and **3a-Br** (Table 3 entries 1, 2 and entries 5, 6).

Comparing the CAC values in water and the IC_{50} for cell line A549 for the tripodal compounds **3a-Br, 4a-Br, 6a-Br, 3b-Br** and **5b-Br**, the IC_{50} is above the CAC for **3a-Br**, **3b-Br**, **5b-Br** and **6a-Br**, implying that the compounds are aggregated in some extend at the antitumoral response concentration. However, for compounds **4a-Br**, the IC_{50} is 15 times below the CAC, indicating the compound is not aggregated at the antitumoral response concentration and that monomeric specie is mainly the responsible of its moderate cytotoxicity.

Interestingly, for **3a-Br** at acidic pH, the CAC value is above the IC_{50}, implying that the compound is not aggregated at the antitumoral response concentration, this is in accordance with the decrease of the IC_{50} at pHe 6.2 (table 2, entry 1).

[23] (a) *Thermodynamically stable vesicle formation and vesicle-to-micelle transition of single-tailed anionic surfactant in water*; Sakai, T.; Ikoshi, R.; Toshida, N.; Kagaya, M.; *J. Phys. Chem. B* **2013**, *117*, 5081-5089, (b) *Strong effect of NaBr on self-assembly of quaternary ammonium gemini surfactants at air/water interface and in aqueous solution studied by surface tension and fluorescence techniques*; You, Y.; Zhao, J.; Jiang, R.; Cao, J.; *Colloid Polym. Sci.* **2009**, *287*, 839-846, (c) *Fluorescence Emission of Pyrene in Surfactant Solutions*; Piñeiro, L.; Novo, M.; Al-Souf, W.; *Advances in Colloid and Interface Science* **2015**, *205*, 1-12.

Thus, the monomeric specie is the main responsible of the cytotoxic activity, leading to higher concentration of biactive specie as its CAC increases.

3.3.3. LS measurements

The hydrodynamic size distributions of the aggregates were investigated by means of dynamic light scattering (DLS) deducing the apparent hydrodynamic diameters D_h from the diffusion coefficients. Experiments could not be performed in pure water at concentration range between 0.01 to 0.5 mM as at such low concentrations the results could not be achieved properly, thus the experiments were performed on compounds **3a-Br, 3b-Br**, **5b-Br** and **6a-B** in CH_3OH/H_2O 1/1 v/v within the 0.1 - 6 mM concentration range at 25 °C. For **4a-Br** the experiment was not achieved properly in CH_3OH/H_2O 1/1 v/v.

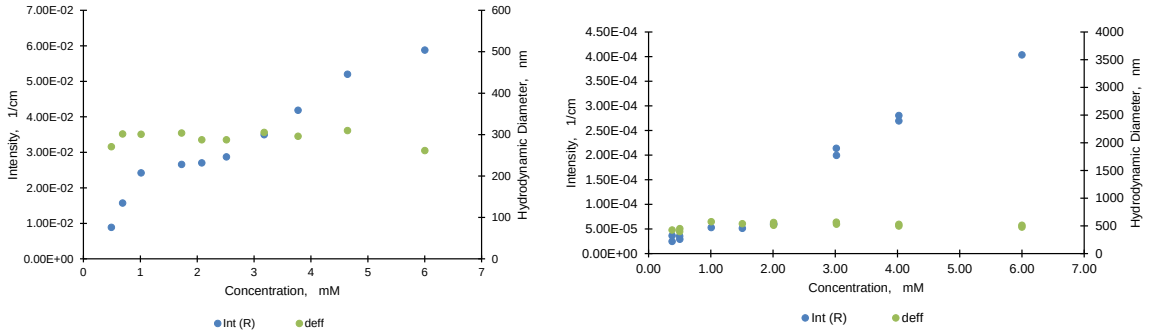

Figure 4. Hydrodynamic diameter (green circles, right axes) and intensity of the scattered light in absolute units (1/cm) (blue circles, left axes) obtained with DLS for a) **3a-Br** and b) **3b-Br**, in CH_3OH/H_2O (1/1 v/v) and presented as a function of the surfactant concentration.

Figure 4 and Figure S6 shows the results obtained for **3a-Br**/**3b-Br** and **5b-Br**/**6a-Br** respectively. The total intensity of scattered light as a function of the total surfactant concentration, increases almost linearly with concentration, suggesting that the aggregates increase in number when concentration increases, keeping their average size constant. For **3a-Br** the hydrodynamic diameter is around 300 nm while it increases to 500 nm for **3b-Br** and **6a-Br**, reaching 700 nm for **5b-Br**.

3.3.4. Optical microscopy and SEM

The formation of aggregates in H_2O and H_2O/CH_3OH 1/1 v/v for **3a-Br, 3b-Br**, **4a-Br, 5b-Br** and **6a-Br** were studied by optical microscopy and SEM. Optical microscopy in H_2O/CH_3OH 1/1 v/v, allowed to observe for compounds **3a-Br, 3b-Br** and **4a-Br** the formation of spherical aggregates at 6 mM concentrations

with sizes between 0.5-5 μm (Figure S7). However, for tripodal compounds **5b-Br** and **6a-Br** only a homogeneous solution was observed. Furthermore, in the case of compound **4a-Br** dendritic structures from spherical aggregates were observed. Moreover, SEM images in H_2O for **3a-Br** (0.1 mM) and **6a-Br** (0.4 mM) allowed to observe the formation of distorted spherical aggregates lower than 2 μm and 0.5 μm size respectively (Figure S8).

3.3 Anion transport studies

In order to investigate the origin of the cytotoxicity of these compounds, their transmembrane transport activity and their potential to disturb the membrane integrity were explored in model POPC liposomes. First, the ability of these compounds to facilitate chloride efflux from chloride-loaded vesicles was monitored using a chloride-selective electrode (ISE). The liposome suspension was placed in an isotonic, chloride-free medium and the studied tripodal imidazolium salts were added as aliquots of stock DMSO solutions. Release of all encapsulated chloride by addition of a detergent allowed the normalization of the chloride leakage and facilitated chloride efflux was monitored over time for each compound. For these experiments, NTf_2 salts were employed and different external anions tested (Table 4, ESI Figure S9-S20). In order to provide the appropriate basic data for chloride transport studies, ^{1}H NMR anion-binding studies were also conducted for the NTf_2 salts in aqueous acetonitrile (Table 4, ESI Figure S21-S24). The corresponding stability constants, K_{ass}, were determined, by following the shift of the ^{1}H NMR signals of five protons from the receptor and fitting the data to 1:1 and 1:2 receptor:anion binding isotherms using HypNMR (ESI, Figure S25-28). Interestingly, as is shown in Table 4, we observed their ability to bind only one chloride anion with very different binding constants for the corresponding 1:1 complex (entries 1-4, Table 4), the higher binding constants were obtained for compounds **3a-NTf$_2$** and **7a-NTf$_2$** both containing dodecyl alkyl chains (entries 1 and 3).

The NTf_2 salts showed moderate chloride-transport abilities, being compounds **6a-NTf$_2$** and **8a-NTf$_2$** the most active ones (Table 4, entries 2 and 4). Little differences were observed in the chloride efflux activity when different anions such as nitrate or sulphate/carbonate were used as the external anions (Table 4 and ESI Figure S9-S20). These results suggested the possibility of these compounds promoting an unspecific transmembrane transport and acting as membrane disrupting agents. In order to confirm this possibility,

carboxyfluorescein (CF) release assays were carried out. In this assay, CF is loaded at high concentration inside the liposomes. At this concentration, CF is non-emissive because of self-quenching processes. Leakage from the interior of the vesicles result in an immediate dilution and recovering of the CF fluorescence. Addition of detergent at the end of the experiment lyse the vesicles and allows normalization of the data for comparison purposes. The results at pH = 7.2 and pH = 6.2 are shown in ESI Figure S29-S40 for each studied compound and the normalised intensity at λ = 520 nm vs time is represented in Figure S41-S42. The most active derivative in all assays is compound **8a-Br/NTf$_2$**, compounds **4a-Br** and **6a-Br/NTf$_2$** were also found to form large non-selective pores in the lipid membrane. The maximum leakage detected for these compounds was 25%/36%, 22% and 15%/28% respectively, being NTf_2 salts more active in these assays. When these experiments were carried out at pH = 6.2 using the bromide salts the main difference is the lack of activity showed by compound **4a-Br** under these conditions, whereas the leakage of CF promoted by **8a-Br** increased to 32% in the time frame of these experiments.

Table 4. (Chloride affinity (logK 1:1, BC_{50}), chloride-efflux rates in model liposomes (% Cl s^{-1}, at pHi/pHe 7.2) using different external anion)

Entry	Compound	log β[a,b]	Chloride efflux rate (%Cl·s^{-1})[c]		
			NO_3^-	HCO_3^- /SO_4^{2-}	SO_4^{2-}
1	**3a-NTf$_2$**	1.76 (± 0.04)	13.6 [d]	12.8	13
2	**6a-NTf$_2$**	1.43 (± 0.03)	16.4[d]	21.7	20
3	**7a-NTf$_2$**	1.74 (± 0.02)	17.0[d]	15.5	16
4	**8a-NTf$_2$**	1.62 (± 0.02)	25.1 [d]	23.4	24

[a] (Obtained by simultaneous non-linear regression fitting of all the available ^{1}H NMR signals), [b] (log β is defined as the formation constant for the 1:1 receptor/substrate complex in M^{-1}); [c] (10% imidazolium salt to POPC molar ratio).

These assays suggested that the observed biological activity is likely not the result of just their transport activity. For instance, compounds **3a-Br/NTf$_2$**, **3b-Br, 7a-Br/NTf$_2$ and 5b-Br** did not act as detergents although **3a-Br/NTf$_2$**, **3b-Br, 7a-Br/NTf$_2$** presented high cytotoxic activities (Table 1). On the other hand, compound **8a-Br/NTf$_2$**, the most active in liposomes displays a significant cytotoxicity which is enhanced at acidic pH. This behaviour is mimicked by the results of **8a-Br** in the CF leakage assay. Loss of activity of **4a-Br** at acidic pH is also in agreement with the results discussed in cytotoxicity studies.

4. Conclusions

A series of novel tripodal pseudopeptides derived from *L*-valine and *L*-phenylalanine containing different hydrophobic groups have been synthetized, showing good cancer cell growth inhibition against different cancer cell lines, with IC_{50} values in the 20 μM range or lower. Results demonstrate that an optimum lipophilicity of the tail is needed for an efficient cytotoxicity being compound **3a-Br** the most bioactive. Moreover, when the anticancer activity is studied at pHe 6.2 the cell growth inhibition and selectivity against HEK-293, changes dramatically increasing the inhibition in some cases more than 10 orders of magnitude. Interestingly, compounds **3a-NTf$_2$** and **8a-NTf$_2$** presented loss of antitumor activity at acidic pHe. The transmembrane anion transport studies at normal pH revealed compound **8a-NTf$_2$** as the most active for chloride and carboxyfluorescein (CF) release assays with a leakage of 25% and 36% respectively. When carboxyfluorescein (CF) release assays were carried out at pHe = 6.2 using the bromide salts, the main difference is the lack of activity showed by compound **4a-Br** which is in agreement with the decrease in cytotoxicity activity at this pHe.

Finally, aggregation studies have been carried out using different techniques and the results have revealed that spherical aggregates are formed in aqueous media. Furthermore, compounds with long alkyl chains have CAC values in the μM range being aggregated in some extent at their cytotoxicity concentration. The observed increase of the CAC at acidic pH, suggest the presence of higher amount of active monomeric specie, which is in accordance with the increase of the antitumoral activity at acidic pHe for **3a-Br**, indicating that the monomeric species is mainly the responsible for the antitumoral activity.

5. Supporting information

5.1. Synthetic Protocols and Structural Characterization

Synthesis of 4a-Br. (*S*)-N-butyl-2-(1H-imidazol-1-yl)-3-methylbutanamide (0.201 g, 0.914 mmol, 3.3 equiv) and 1,3,5-tris(bromomethyl)benzene (0.097 g, 0.273 mmol, 1 equiv) were dissolved in acetronitrile (0.4 M, 2.65 mL) in a microwave tube. The conditions of this reaction in the Microwave instrument were: 150 ºC, 1h and 120W. The liquid obtained was evaporated and washed with ether at the vaccum and then with ethyl acetate. The reaction gave a brown solid product (0.27 g, 97.7%): mp 99 °C; $[\alpha]_D^{25}$ = 10.8 (c = 0.011, CH_3OH). IR (ATR): ν˜max = 3228, 3067, 2961, 2933, 2872, 1672, 1549, 1463, 1369, 1154

cm^{-1}. ^{1}H NMR (400 MHz, CD_3OD, δ): 9.30 (s, 3H), 8.67 (s, NH), 7.74 (t, *J* = 1.8 Hz, 3H), 7.65 (t, *J* = 1.8 Hz, 3H), 7.60 (s, 3H), 5.55 (s, 6H), 4.69 (d, *J* = 10.0 Hz, 3H), 3.40-3.24 (m, 6H), 2.44 (m, *J* = 9.7, 6.5 Hz, 3H), 1.51 (m, 6H), 1.33 (m, 6H), 1.06 (m, 9H), 0.97-0.82 (m, 18H) ppm; ^{13}C NMR (101 MHz, CD_3OD, δ): 167.2, 167.1, 136.3, 129.7, 122.6, 122.5, 122.4, 68.9, 68.9, 52.1, 39.3, 39.1, 31.8, 31.8, 30.8, 30.8, 19.7, 17.9, 17.5, 12.6.ppm; MS (TOF MS ES^+): m/z (%) = 433.75 (100) $[C_{45}H_{72}N_9O_3Br]^{2+}$, 946.42 (45) $[C_{45}H_{72}N_9O_3Br_2]^+$, 262.19 (70) $[C_{45}H_{72}N_9O_3]^{3+}$. Anal. calcd for $C_{42}H_{72}N_9O_3Br_3$: C 68.67, H 9.22, N 16.02 found C 67.42, H 9.43, N 16.24.

Synthesis of 6a-Br. (*S*)-N-Benzyl-2-(1H-imidazol-1-yl)-3-methylbutanamide (0.273 g, 1.06 mmol, 4 equiv) and 1,3,5-tris(bromomethyl)benzene (0.98 g, 0.27 mmol, 1 equiv) were dissolved in acetronitrile (0.4 M, 2.65 mL) in a microwave tube. The conditions of this reaction in the Microwave instrument were: 150 ºC, 1h and 120W. The liquid obtained was evaporated and washed with ether at the vaccum and then, with ethyl acetate. The reaction gave a brown solid product (0.27 g, 98.9%): mp 239 ºC; $[\alpha]_D^{25}$ = 26.5 (c = 0.011, CH_3OH). IR (ATR): ν˜max = 3225, 3055.66, 2967, 1676, 1548 cm^{-1}. ^{1}H NMR (500 MHz, $CDCl_3$, δ):10.00 (s, 3H), 8.60 (s, 3H), 8.31 (s, 6H), 7.29 (s, 3H), 7.24-7.04 (m, 15H), 5.65 (d, *J* = 14.3 Hz, 3H), 5.28 (d, *J* = 14.1 Hz, 3H), 5.12 (d, *J* = 10.8 Hz, 3H), 4.44 (dd, *J*=15.0, 6.6 Hz, 3H), 4.07 (dd, *J*=15.0, 5.2 Hz, 3H), 2.48-2.29 (m, 3H), 0.97 (d, *J*=6.4 Hz, 9H), 0.70 (d, *J*=6.6 Hz, 9H); ^{13}C NMR (75 MHz, 30 °C, $CDCl_3$, δ): 166.4, 137.3, 135.8, 135.5, 131.5, 128.5, 127.5, 127.3, 124.2, 119.4, 68.3, 52.0, 43.5, 30.8, 18.8, 18.3 ppm; MS (ESI^+): m/z (%) = 296.4 (100) $[C_{54}H_{66}N_9O_3]^{3+}$, 484.9 (20) $[C_{54}H_{66}N_9O_3Br]^{2+}$. Anal. calcd for $C_{54}H_{66}N_9O_3$: C 72.59, H 6.41, N 13.37; found C 72.2, H 6.6, N 13.0.

Synthesis of 7a-Br. (*S*)-N-dodecyl-2-(1H-imidazol-1-yl)-3-phenylpropanamide (0.25 g, 0.64 mmol, 3.3 equiv) and 1,3,5-tris(bromomethyl)benzene (0.07 g, 0.19 mmol, 1 equiv) were dissolved in acetronitrile (0.4 M, 2.65 mL) in a microwave tube. The conditions of this reaction in the Microwave instrument were: 150 ºC, 1h and 120W. The liquid obtained was evaporated and washed with ether at the vaccum and, then, with ethyl acetate. The reaction gave a brown solid product (0.25 g, 86.8%): mp 179 ºC; $[\alpha]_D^{25}$ = 2.3 (c = 0.011, CH_3OH). IR (ATR): ν˜max = 3398, 3289, 3063, 2955, 2922, 2852, 1656, 1556, 1466, 1156 cm^{-1}. ^{1}H NMR (400 MHz, $CDCl_3$, δ): 9.35 (s, 3H), 8.35 (s, 3H), 8.10 (s, 3H), 8.09 (s, 3H), 7.43 (s, 3H), 7.23 – 6.97 (m, 30H), 5.74 (t, *J* = 8.2 Hz, 3H), 5.52 (d, *J* = 14.1 Hz, 3H),

4.98 (d, *J* = 13.9 Hz, 3H), 3.31 – 3.11 (m, 6H), 2.80 (d, *J* = 8.4 Hz, 3H), 1.60 (s, 6H),1.42– 1.02 (m, 42H), 0.85 – 0.76 (m, 9H) ppm; ^{13}C NMR (101 MHz, $CDCl_3$, δ): 165.8, 135.8, 135.2, 134.3, 131.4, 129.1, 128.9, 127.7, 124.1, 119.4, 63.1, 51.8, 40.0, 38.9, 31.9, 29.7, 29.4, 29.0, 26.9, 22.7, 14.1 ppm. MS (TOF MS ES$^+$): m/z (%) = 673.93 (100) $[C_{81}H_{120}N_9O_3Br]^{2+}$, 422.31 (70) $[C_{81}H_{120}N_9O_3]^{3+}$, 1426.78 (80) $[C_{81}H_{120}N_9O_3Br_2]^+$. Anal. calcd for $C_{81}H_{120}N_9O_3Br_3$: C 76.73, H 9.54, N 9.99 found C 75.9, H 9.67, N 9.80.

Synthesis of 8a-Br. (*S*)-N-Benzyl-2-(1H-imidazol-1-yl)-3-phenylpropanamide (0.192 g, 0.63 mmol, 4 equiv) and 1,3,5-tris(bromomethyl)benzene (0.056 g, 0.157 mmol, 1 equiv) were dissolved in acetronitrile (0.4 M, 1.57 mL) in a microwave tube. The conditions of this reaction in the Microwave instrument were: 150 ºC, 1h and 120W. The yellow liquid obtained was evaporated to dryness and washed with ethyl acetate at the vacuum. Finally, the product obtained was evaporated under reduce pressure. The reaction gave a brown solid product (0.14 g, 70.3%): mp 327 ºC; $[\alpha]_D^{25}$ = 2.1 (c = 0.013, CH_3OH). IR (ATR): ν˜max = 3216, 3058, 2968, 1679, 1549 cm^{-1}. ^{1}H NMR (400 MHz, CD_3OD-$CDCl_3$, δ): 9.37 (s, 3H), 7.68-7.52 (m, 6H), 7.41 (s, 3H), 7.23-6.95 (m, 30H), 5.40-5.29 (m, 9H), 4.33 (d, *J* = 14.9 Hz, 3H), 4.15 (d, *J* = 14.9 Hz, 3H), 3.45 (dd, *J* = 13.7, 7.1 Hz, 3H), 3.38-3.24 (m, 3H); ^{13}C NMR (75 MHz, CD_3OD-$CDCl_3$, δ): 166.9, 135.7, 135.5, 134.0, 131.1, 128.9, 128.8, 127.6, 123.4, 120.6, 63.0, 51.9, 39.1, 26.1; MS (ESI$^+$): m/z (%) = 344.5 (100) $[C_{66}H_{66}N_9O_3]^{3+}$, 556.8 (20) $[C_{66}H_{66}BrN_9O_3]^{2+}$. Anal. calcd for $C_{66}H_{66}N_9O_3Br_3$: C 76.72, H 6.44, N 12.20; found C 77.80, H 6.99, N 12.10.

Synthesis of 3a-NTf$_2$. 3,3',3"-(benzene-1,3,5-triyltris(methylene))tris(1-((*S*)-1-(dodecylamino)-3-methyl-1-oxobutan-2-yl)-1H-imidazol-3-ium) bromide(0.09 g, $6.64\cdot10^{-2}$ mmol, 1 equiv) and lithium bis((trifluoromethyl)sulfonyl)amide (0.064 g, 0.22 mmol, 3.3 equiv) were dissolved in methanol in a round bottom flask (50 ml). The reaction mixture was stirred at room temperature for 24 h. The solvent was evaporated under reduced pressure and the resulting crude residue was extracted with CH_2Cl_2 (3x), dried with anhydrous $MgSO_4$, filtered, and concentrated. The reaction gave a yellow liquid product (0.09 g, 66%): mp 15 ºC; $[\alpha]_D^{25}$ = 10.4 (c = 0.021, CH_3OH). IR (ATR): ν˜max = 3379, 3147, 2924, 2855, 1679, 1186 cm^{-1}. ^{1}H NMR (500 MHz, $CDCl_3$, δ): 8.95 (s, 3H), 7.77 (s, 6H), 7.70 (s, 3H), 6.84-6.74 (m, NH), 5.48-5.30 (m, 6H), 4.53 (d, *J* = 10.3 Hz, 3H), 3.36 (m, 3H), 3.04 (m, 3H), 2.39 (m, 3H), 1.49 (m, 6H), 1.36-1.16 (m, 54H), 1.05 (d, *J* =

6.6 Hz, 9H), 0.88 (t, *J* = 6.9 Hz, 9H), 0.75 (d, *J* = 6.7 Hz, 9H) ppm; ^{13}C NMR (126 MHz, 30 °C, $CDCl_3$, δ): 166.1, 135.7, 135.0, 131.4, 123.4, 121.7, 120.9 (CF_3), 118.3 (CF_3), 69.0, 52.7, 40.0, 31.9, 29.6, 29.5, 29.4, 29.3, 29.1, 28.8, 26.8, 22.6, 18.7, 18.2, 14.1 ppm; MS (TOF MS ES$^+$): m/z (%)= 701.4 (100) $[C_{71}H_{120}F_6N_{10}O_7S_2]^{2+}$, 374.3 (48) $[C_{69}H_{120}N_9O_3]^{3+}$, 1682.8 (20) $[C_{73}H_{120}F_{12}N_{11}O_{11}S_4]^+$. Anal. calcd for $C_{75}H_{120}N_{12}O_{15}F_{18}S_6$.: C 45.86, H 6.44, N 8.56, S 9.79; found C 44.97, H 6.38, N 8.74, S 10.05.

Synthesis of 6a-NTf$_2$. 3,3',3"-(benzene-1,3,5-triyltris(methylene))tris(1-((*S*)-1-(benzylamino)-3-methyl-1-oxobutan-2-yl)-1H-imidazol-3-ium) bromide(0.07 g, $6.16\cdot10^{-2}$ mmol, 1 equiv) and lithium bis((trifluoromethyl)sulfonyl)amide (0.06 g, 0.21 mmol, 3.3 equiv) were dissolved in methanol in a round bottom flask (50 ml). The reaction mixture was stirred at room temperature for 24 h. The solvent was evaporated under reduced pressure and the resulting crude residue was extracted with CH_2Cl_2 (3x), dried with anhydrous $MgSO_4$, filtered, and concentrated. The reaction gave a beige solid product (0.10 g, 90.0%): mp 40 ºC; $[\alpha]_D^{25}$ = 17.9 (c = 0.032, CH_3OH). IR (ATR): ν˜max = 3373, 3146, 2972, 1679, 1181 cm^{-1}. ^{1}H NMR (400 MHz, CD_3CN, δ): 8.97 (s, 3H), 7.55 (s, 3H), 7.37 (m, 6H), 7.32-7.20 (m, 15H), 5.36 (s, 6H), 4.56 (d, *J* = 9.6 Hz, 3H), 4.40 (d, *J* = 14.9 Hz, 3H), 4.25 (d, *J* = 14.9 Hz, 3H), 2.31 (m, 3H), 0.92 (d, *J* = 6.6 Hz, 9H), 0.75 (d, *J* = 6.6 Hz, 9H) ppm; ^{13}C NMR (75 MHz, $CDCl_3$ δ): 166.3, 137.0, 135.5, 135.1, 131.1, 128.7, 127.8, 127.7, 123.2, 121.6 (CF_3), 117.5 (CF_3), 68.8, 52.6, 43.9, 31.9, 18.6, 18.1 ppm; MS (ESI$^+$): m/z (%) = 296.4 (100) $[C_{54}H_{66}N_9O_3]^{3+}$, 584.8 (54) $[C_{56}H_{66}F_6N_{10}O_7S_2]^{2+}$. Anal. calcd for $C_{60}H_{66}N_{12}O_{15}F_{18}S_6$: C 41.67, H 3.85, N 9.72, S 11.12; found C 41.15, H 3.54, N 9.56, S 10.64.

Synthesis of 7a-NTf$_2$. 3,3',3"-(benzene-1,3,5-triyltris(methylene))tris(1-((*S*)-1-(dodecylamino)- -1-oxo-3-phenylpropan-2-yl)-1H-imidazol-3-ium) bromide (0.10 g, $6.44\cdot10^{-2}$ mmol, 1 equiv) and lithium bis((trifluoromethyl)sulfonyl)amide (0.06 g, 0.22 mmol, 3.3 equiv) were dissolved in methanol in a round bottom flask (50 ml). The reaction mixture was stirred at room temperature for 24 h. The solvent was evaporated under reduced pressure and the resulting crude residue was extracted with CH_2Cl_2 (3x), dried with anhydrous $MgSO_4$, filtered, and concentrated. The reaction gave a yellow liquid product (0.11 g, 79%): mp 24 ºC; $[\alpha]_D^{25}$ = -1.3 (c = 0.011, CH_3OH). IR (ATR): ν˜max = 3378, 3148, 2925, 2856, 1678, 1551, 1457, 1346, 1187, 1137, 1054 cm^{-1}. ^{1}H NMR (400 MHz, $CDCl_3$, δ): 8.54 (s, 3H), 7.75 (s, 3H), 7.56 (s, 3H), 7.49 (s, 3H), 7.22-7.10 (m,

12H), 7.08-6.97 (m, 3H), 6.47 (m, NH), 5.13 (d, *J* = 9.7 Hz, 6H), 3.30 (dd, *J* = 13.6, 7.3 Hz, 3H), 3.16 (m, 6H), 2.91 (m, 3H), 1.17 (m, 64H), 0.81 (t, *J* = 6.7 Hz, 9H); ^{13}C NMR (101 MHz, $CDCl_3$, δ): 165.6, 135.4, 134.8, 133.7, 131.0, 129.0, 128.9, 127.8, 123.1, 121.5, 121.2 (CF_3), 118.0 (CF_3), 63.8, 52.3, 40.0, 39.9, 31.9, 29.6, 29.4, 29.3, 29.1, 28.7, 26.6, 22.7, 14.1; MS (TOF MS ES$^+$): m/z (%) = 773.44 (100) $[C_{83}H_{120}F_6N_{10}O_7S_2]^{2+}$, 422.31 (20) $[C_{81}H_{120}N_9O_3]^{3+}$. Anal. calcd for $C_{87}H_{120}N_{12}O_{15}F_{18}S_6$: C 49.56, H 5.74, N 7.97, S 9.12; found C 49.35, H 5.98, N 7.52, S 9.74.

Synthesis of 8a-NTf$_2$. 3,3',3"-(benzene-1,3,5-triyltris(methylene))tris(1-((*S*)-1-(benzylamino)-1- oxo-3-phenylpropan-2-yl)-1H-imidazol-3-ium) bromide (0.05 g, $3.5 \cdot 10^{-2}$ mmol, 1 equiv) and lithium bis((trifluoromethyl)sulfonyl)amide (0.03 g, 0.12 mmol, 3.3 equiv) were dissolved in methanol in a round bottom flask (50 mL). The reaction mixture was stirred at room temperature for 24 h. The solvent was evaporated under reduced pressure and the resulting crude residue was extracted with CH_2Cl_2 (3x), dried with anhydrous $MgSO_4$, filtered, and concentrated. The reaction gave a beige solid product (0.047 g, 70.2%): mp 46ºC; $[\alpha]_D^{25}$ = -1.9 (c = 0.013, CH_3OH). IR (ATR): ν˜max = 3371, 3147, 2926, 1679, 1182 cm^{-1}. ^{1}H NMR (400 MHz, $CDCl_3$, δ): 8.53 (s, 3H), 7.68 (s, 3H), 7.48 (s, 3H), 7.42 (s, 3H), 7.24-6.79 (m, 33H), 5.29-5.05 (m, 9H), 4.38 (dd, *J* = 14.7, 6.6 Hz, 3H), 4.05 (dt, *J* = 15.8, 5.8 Hz, 3H), 3.31 (dd, *J* = 13.5, 7.6 Hz, 3H), 3.14 (dd, *J* = 13.6, 8.0 Hz, 3H) ppm; ^{13}C NMR (126 MHz, $CDCl_3$, δ): 165.8, 136.6, 135.4, 135.0, 133.6, 130.9, 129.1, 128.9, 128.6, 127.8, 127.6, 123.2, 121.6, 120.9 (CF_3), 118.3 (CF_3), 63.7, 52.4, 43.8, 39.7 ppm; MS (ESI$^+$): m/z (%) = 656.4 (100) $[C_{68}H_{66}F_6N_{10}O_7S_2]^{2+}$, 344.5 (68) $[C_{66}H_{66}N_9O_3]^{3+}$, 1592.6 (10) $[C_{70}H_{66}F_{12}N_{11}O_{11}S_4]^+$. Anal. calcd for $C_{72}H_{66}N_{12}O_{15}F_{18}S_6$: C 46.15, H 3.55, N 8.97, S 10.27; found C 46.34, H 3.36, N 8.82, S 9.72.

Structure–antitumor activity relationships of tripodal imidazolium-amino acid based ionic liquids. Effect of the nature of the amino acid, amide substitution and anion

Index

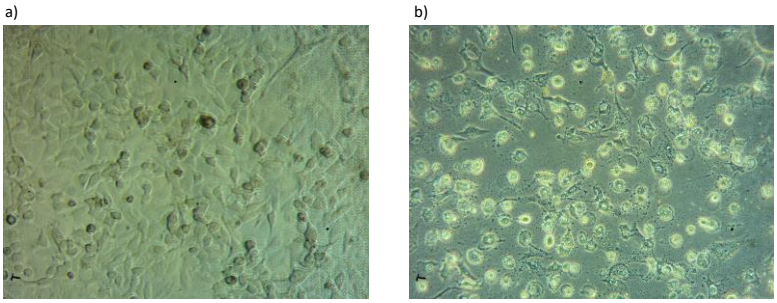

Figure S1. Microscopic appearance of A549 cell line in DMEM medium a) under white light and b) incubated with **7a-Br** (5 μM) after 2 days under fluorescence light. Magnification 20×, phase contrast, Inverted microscope with Zeiss-Primovert phase contrast.

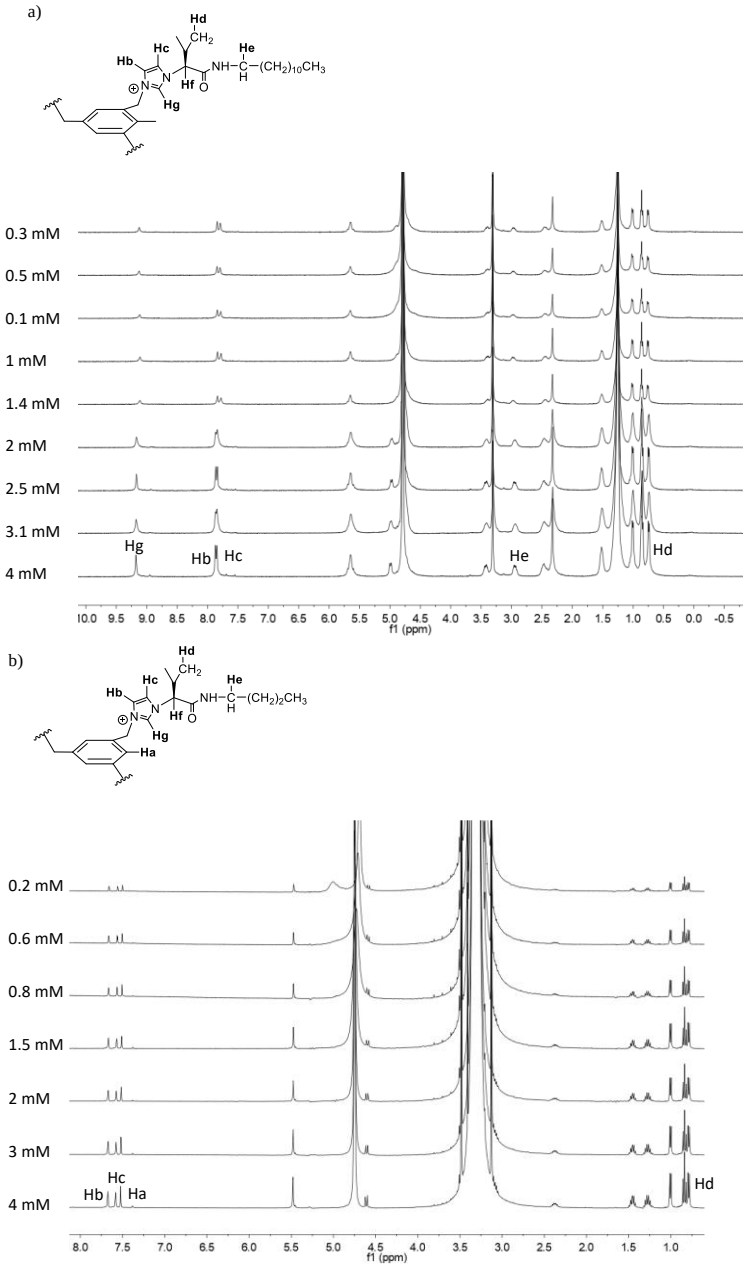

Figure S2 Partial ^{1}H NMR of tripodal compounds at different concentrations in CD_3OD/D_2O 1/1 v/v (400 MHz): a) **3b-Br** b) **4a-Br**.

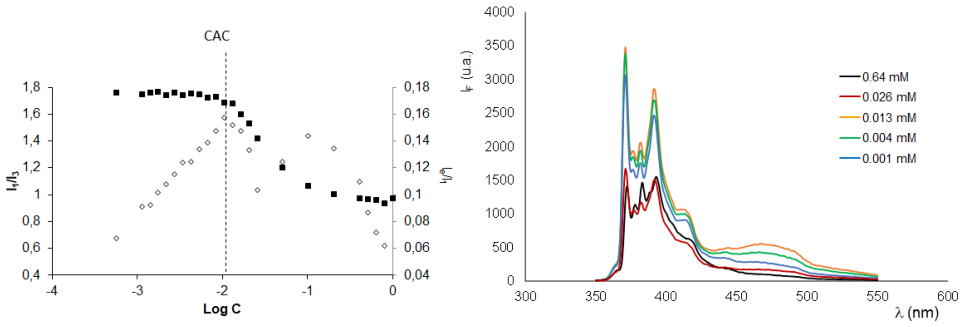

Figure S3. a) Plot of polarity ratio I_1/I_3 (orange, left axes) and Ie/I_1 (blue, right axes) *υ* log C (C mM) for **3b-Br** in H_2O at 25ºC, b) Emission spectra of pyrene in H_2O in the presence of different amounts of **3b-Br**.

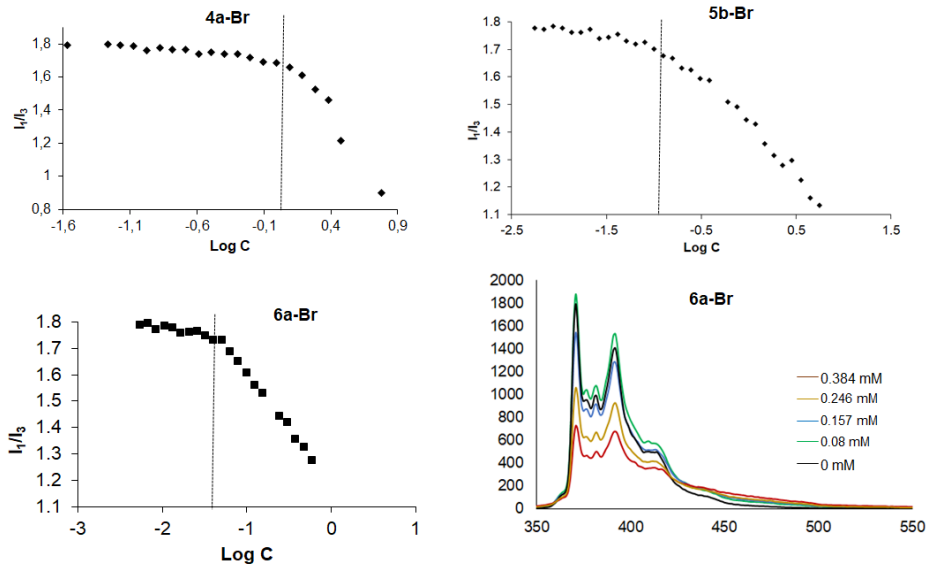

Figure S4. Plot of polarity ratio I_1/I_3 *υ* log C (C mM) in H_2O at 25ºC for: **4a-Br**, **6a-Br** and **5b-Br.** Emission spectra of pyrene in H_2O in the presence of different amounts of **6a-Br**.

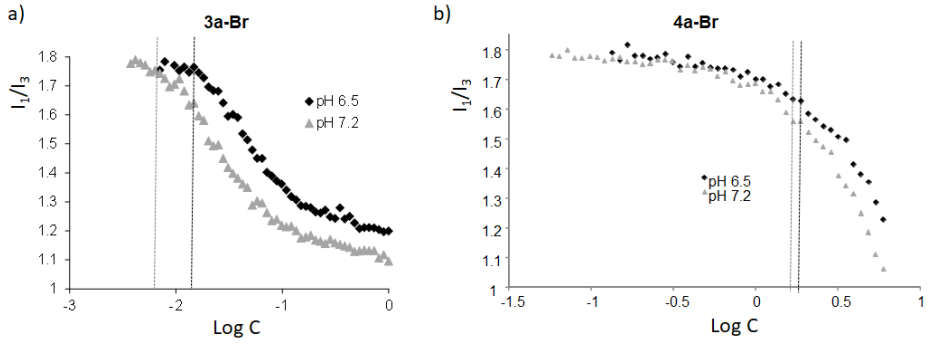

Figure S5. Plot of polarity ratio I_1/I_3 *υ* log C (C mM) in buffer at different pHs at 25ºC for: a) **3a-Br** and b) **4a-Br**.

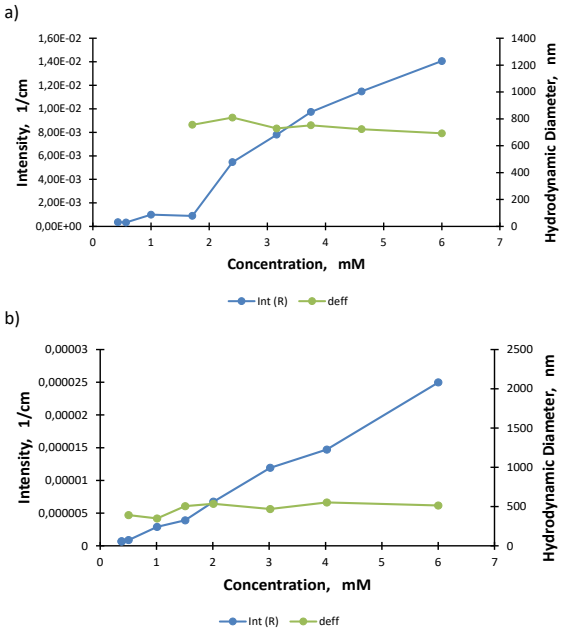

Figure S6. Hydrodynamic diameter (green circles, right axes) and intensity of the scattered light in absolute units (1/cm) (blue circles, left axes) obtained with DLS in CH_3OH/H_2O and presented as a function of the surfactant concentration for (a) **5b-Br** and (b) **6a-Br.**

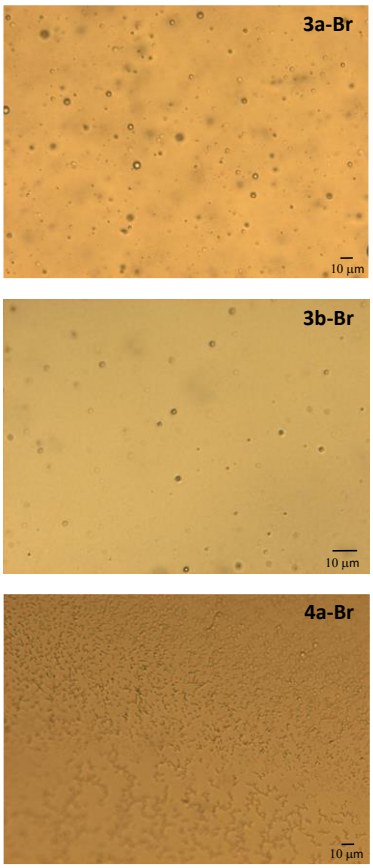

Figure S7. Optical microscopy images for tripodal compounds (6 mM in H_2O/CH_3OH 1/1 v/v).

a)

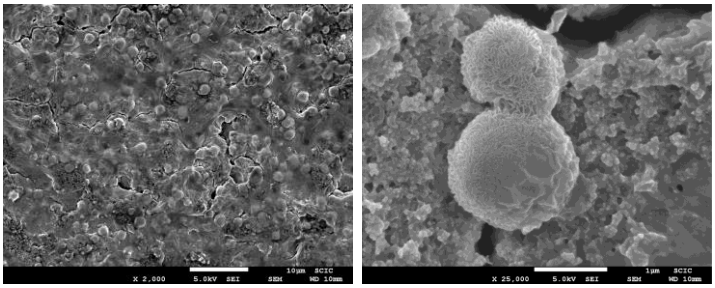

b)

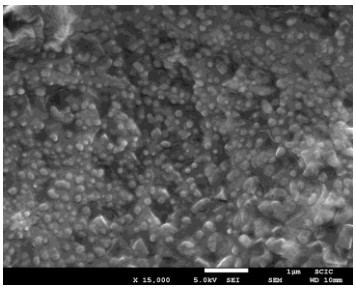

Figure S8. SEM images for tripodal compounds in H_2O: a) **3a-Br** 0.1 mM and b) **6a-Br** 0.4 mM.

Nitrate outside the vesicles

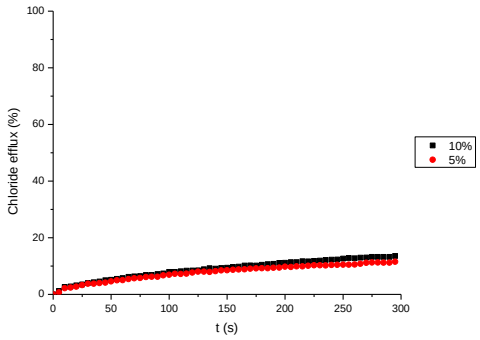

Figure S9. Chloride efflux promoted by **3a-NTf$_2$** (50 μM - 10%; 25 μM - 5% mol carrier to lipid concentration) in unilamellar POPC vesicles. Vesicles loaded with 489 mM NaCl were buffered at pH 7.2 with 5 mM phosphate and dispersed in 489 mM $NaNO_3$ buffered at pH 7.2. Each trace represents the average of at least three trials.

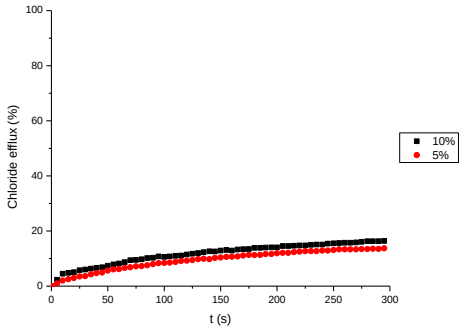

Figure S10. Chloride efflux promoted by **6a-NTf$_2$** (50 μM - 10%; 25 μM - 5% mol carrier to lipid concentration) in unilamellar POPC vesicles. Vesicles loaded with 489 mM NaCl were buffered at pH 7.2 with 5 mM phosphate and dispersed in 489 mM $NaNO_3$ buffered at pH 7.2. Each trace represents the average of at least three trials.

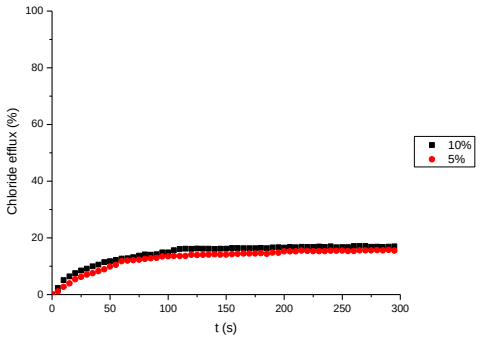

Figure S11. Chloride efflux promoted by **7a-NTf$_2$** (50 μM - 10%; 25 μM - 5% mol carrier to lipid concentration) in unilamellar POPC vesicles. Vesicles loaded with 489 mM NaCl were buffered at pH 7.2 with 5 mM phosphate and dispersed in 489 mM $NaNO_3$ buffered at pH 7.2. Each trace represents the average of at least three trials.

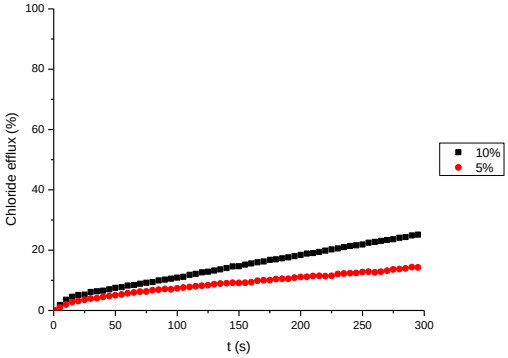

Figure S12. Chloride efflux promoted by **8a-NTf$_2$** (50 μM - 10%; 25 μM - 5% mol carrier to lipid concentration) in unilamellar POPC vesicles. Vesicles loaded with 489 mM NaCl were buffered at pH 7.2 with 5 mM phosphate and dispersed in 489 mM $NaNO_3$ buffered at pH 7.2. Each trace represents the average of at least three trials.

Sulfate and bicarbonate outside the vesicles

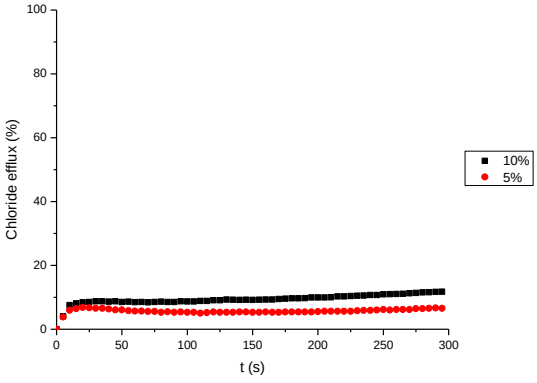

Figure S13. Chloride efflux promoted by **3a-NTf$_2$** (50 μM - 10%; 25 μM - 5% mol carrier to lipid concentration) in unilamellar POPC vesicles. The vesicles, which contained NaCl (451 mM NaCl and 20 mM phosphate buffer, pH 7.2), were immersed in Na_2SO_4 (150 mM Na_2SO_4, 40 mM HCO_3^- and 20 mM phosphate buffer, pH 7.2). Each trace represents an average of at least three different experiments.

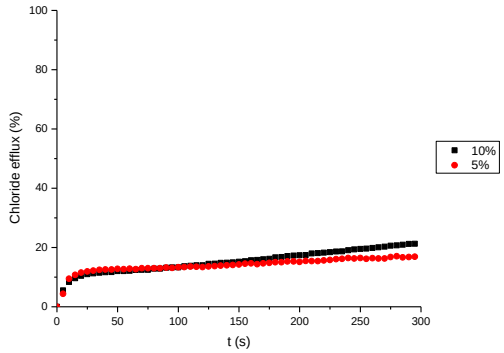

Figure S14. Chloride efflux promoted by **6a-NTf$_2$** (50 μM - 10%; 25 μM - 5% mol carrier to lipid concentration) in unilamellar POPC vesicles. The vesicles, which contained NaCl (451 mM NaCl and 20 mM phosphate buffer, pH 7.2), were immersed in Na_2SO_4 (150 mM Na_2SO_4, 40 mM HCO_3^- and 20 mM phosphate buffer, pH 7.2). Each trace represents an average of at least three different experiments.

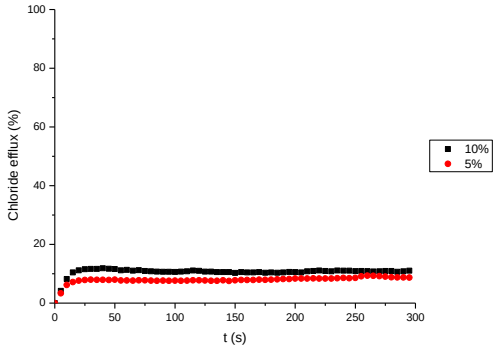

Figure S15. Chloride efflux promoted by **7a-NTf$_2$** (50 μM - 10%; 25 μM - 5% mol carrier to lipid concentration) in unilamellar POPC vesicles. The vesicles, which contained NaCl (451 mM NaCl and 20 mM phosphate buffer, pH 7.2), were immersed in Na_2SO_4 (150 mM Na_2SO_4, 40 mM HCO_3^- and 20 mM phosphate buffer, pH 7.2). Each trace represents an average of at least three different experiments.

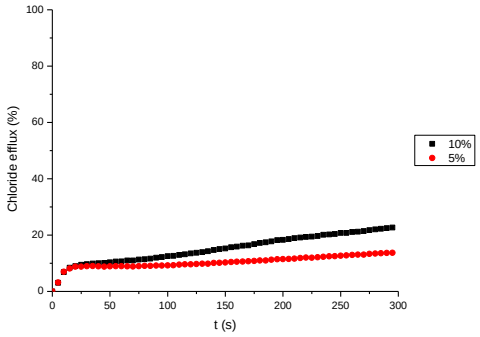

Figure S16. Chloride efflux promoted by **8a-NTf$_2$** (50 μM - 10%; 25 μM - 5% mol carrier to lipid concentration) in unilamellar POPC vesicles. The vesicles, which contained NaCl (451 mM NaCl and 20 mM phosphate buffer, pH 7.2), were immersed in Na_2SO_4 (150 mM Na_2SO_4, 40 mM HCO_3^- and 20 mM phosphate buffer, pH 7.2). Each trace represents an average of at least three different experiments.

Sulfate outside the vesicles

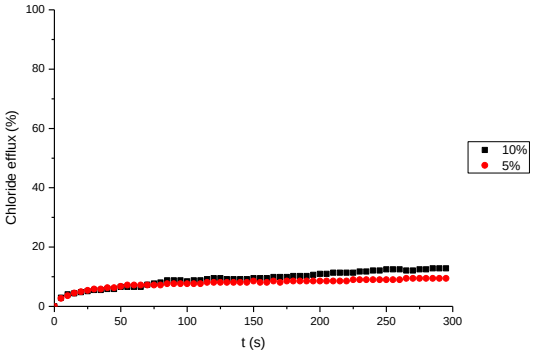

Figure S17. Chloride efflux promoted by **3a-NTf₂** (50 μM - 10%; 25 μM - 5% mol carrier to lipid concentration) in unilamellar POPC vesicles. The vesicles, which contained NaCl (451 mM NaCl and 20 mM phosphate buffer, pH 7.2), were immersed in Na_2SO_4 (150 mM Na_2SO_4 and 20 mM phosphate buffer, pH 7.2). Each trace corresponds to one experiment.

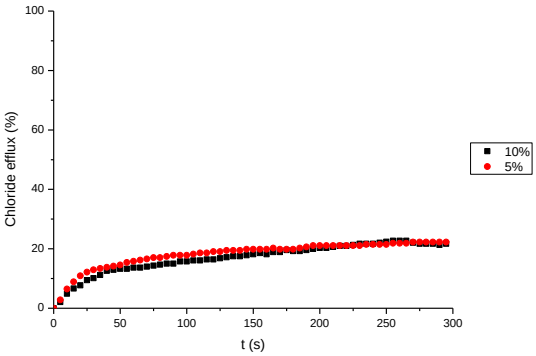

Figure S18. Chloride efflux promoted by **6a-NTf₂** (50 μM - 10%; 25 μM - 5% mol carrier to lipid concentration) in unilamellar POPC vesicles. The vesicles, which contained NaCl (451 mM NaCl and 20 mM phosphate buffer, pH 7.2), were immersed in Na_2SO_4 (150 mM Na_2SO_4 and 20 mM phosphate buffer, pH 7.2). Each trace corresponds to one experiment.

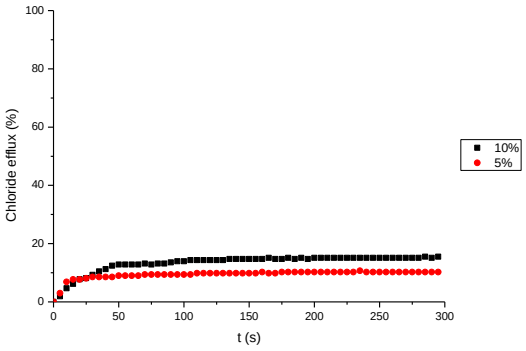

Figure S19. Chloride efflux promoted by **7a-NTf₂** (50 μM - 10%; 25 μM - 5% mol carrier to lipid concentration) in unilamellar POPC vesicles. The vesicles, which contained NaCl (451 mM NaCl and 20 mM phosphate buffer, pH 7.2), were immersed in Na_2SO_4 (150 mM Na_2SO_4 and 20 mM phosphate buffer, pH 7.2). Each trace corresponds to one experiment.

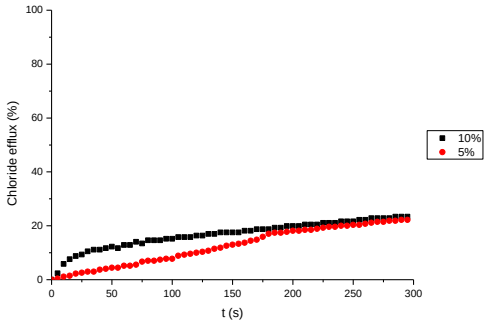

Figure S20. Chloride efflux promoted by **8a-NTf$_2$** (50 μM - 10%; 25 μM - 5% mol carrier to lipid concentration) in unilamellar POPC vesicles. The vesicles, which contained NaCl (451 mM NaCl and 20 mM phosphate buffer, pH 7.2), were immersed in Na_2SO_4 (150 mM Na_2SO_4 and 20 mM phosphate buffer, pH 7.2). Each trace corresponds to one experiment.

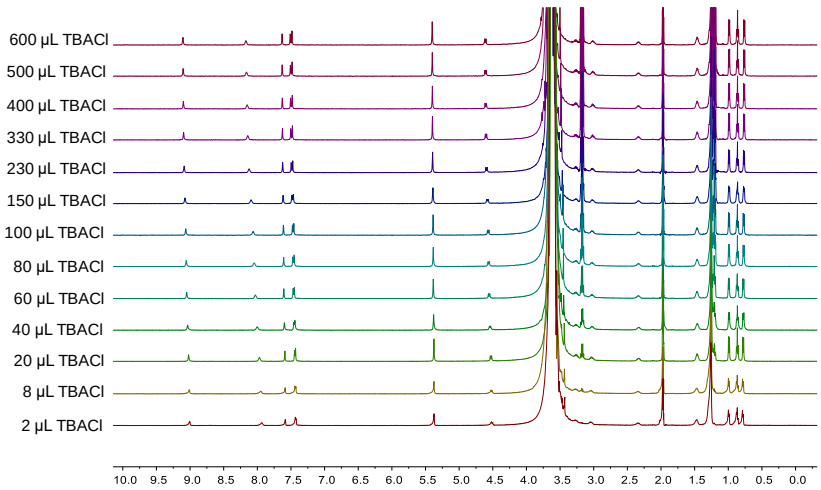

Figure S21. ^{1}H NMR spectra (400 MHz, CD_3CN/D_2O 8/2 v/v) for **3a-NTf$_2$** (6 mM) obtained upon addition of different aliquots of a 60 mM solution of TBACl.

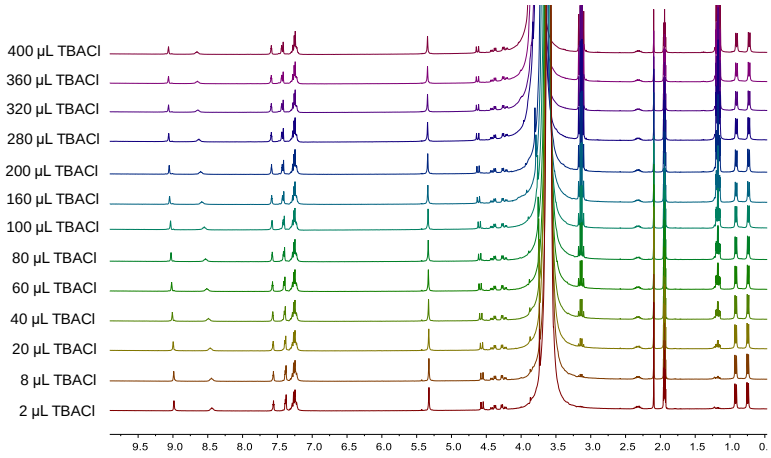

Figure S22. ^{1}H NMR spectra (300 MHz, CD_3CN/D_2O 8/2 v/v) for **6a-NTf$_2$** (6 mM) obtained upon addition of different aliquots of a 60 mM solution of TBACl.

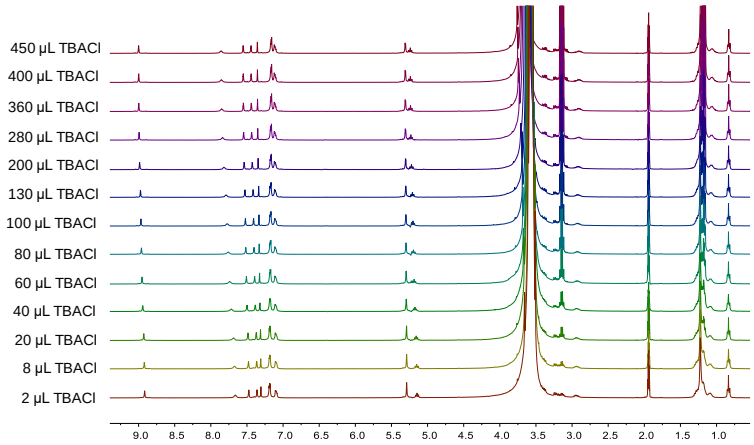

Figure S23. ^{1}H NMR spectra (400 MHz, CD_3CN/D_2O 8/2 v/v) for **7a-NTf$_2$** (6 mM) obtained upon addition of different aliquots of a 60 mM solution of TBACl.

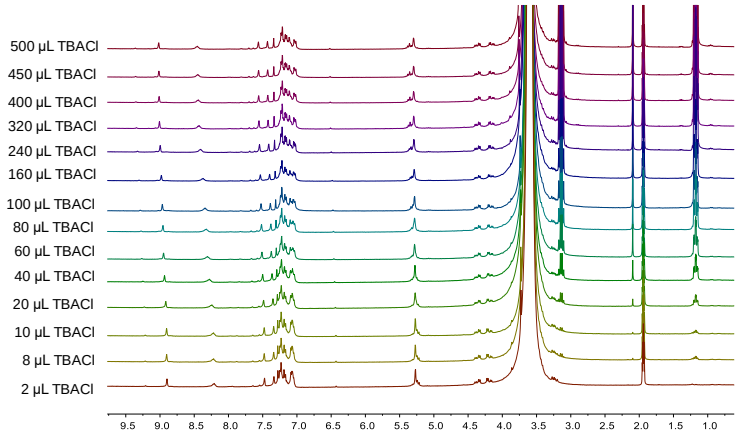

Figure S24. ^{1}H NMR spectra (300 MHz, CD_3CN/D_2O 8/2 v/v) for **8a-NTf$_2$** (6 mM) obtained upon addition of different aliquots of a 60 mM solution of TBACl.

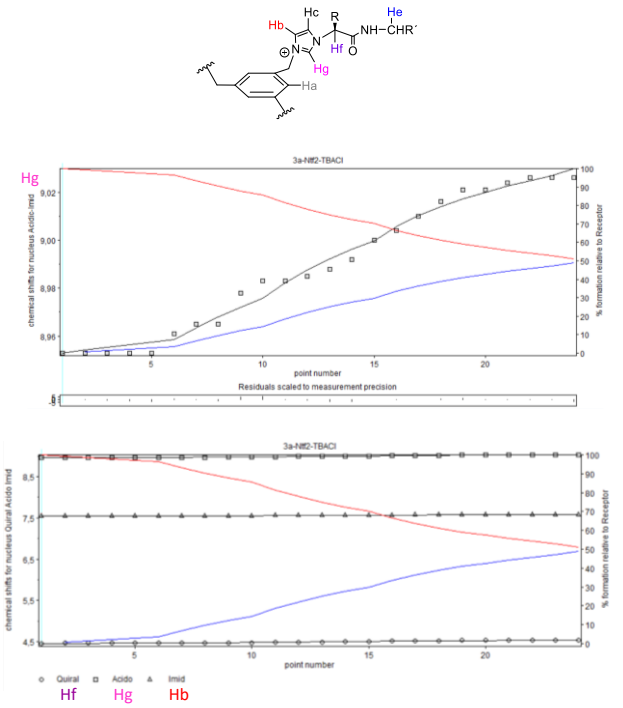

Figure S25. Fitted binding isotherm obtained for the titration of a 6 mM solution of compound **3a-NTf$_2$** with a 60 mM solution of TBACl (CD_3CN/D_2O 8/2 v/v). In order to avoid the dilution effect, the latter was prepared with the former. The graph shows the change in chemical shift of the signals due imidazolium H_g, H_f, H_b protons of the molecule, fitted to the 1:1 binding model.

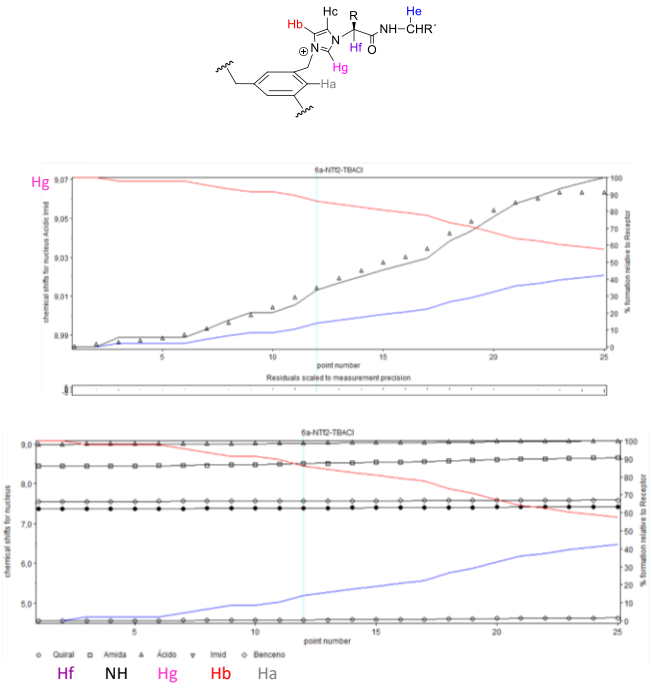

Figure S26. Fitted binding isotherm obtained for the titration of a 6 mM solution of compound **6a-NTf$_2$** with a 60 mM solution of TBACl (CD_3CN/D_2O 8/2 v/v). In order to avoid the dilution effect, the latter was prepared with the former. The graph shows the change in chemical shift of the signals due imidazolium H_g, H_f, NH, H_b, H_a protons of the molecule, fitted to the 1:1 binding model.

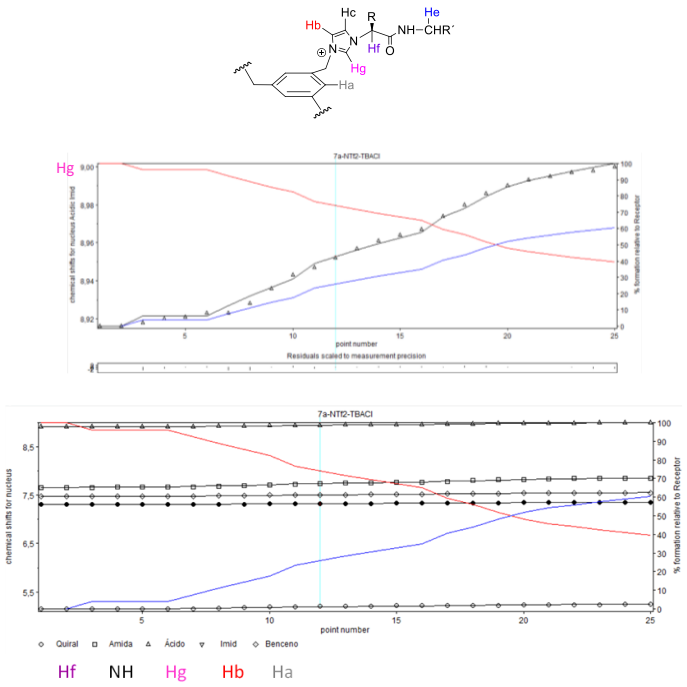

Figure S27. Fitted binding isotherm obtained for the titration of a 6 mM solution of compound **7a-NTf$_2$** with a 60 mM solution of TBACl (CD_3CN/D_2O 8/2 v/v). In order to avoid the dilution effect, the latter was prepared with the former. The graph shows the change in chemical shift of the signals due imidazolium H_g, H_f, NH, H_b, H_a protons of the molecule, fitted to the 1:1 binding model.

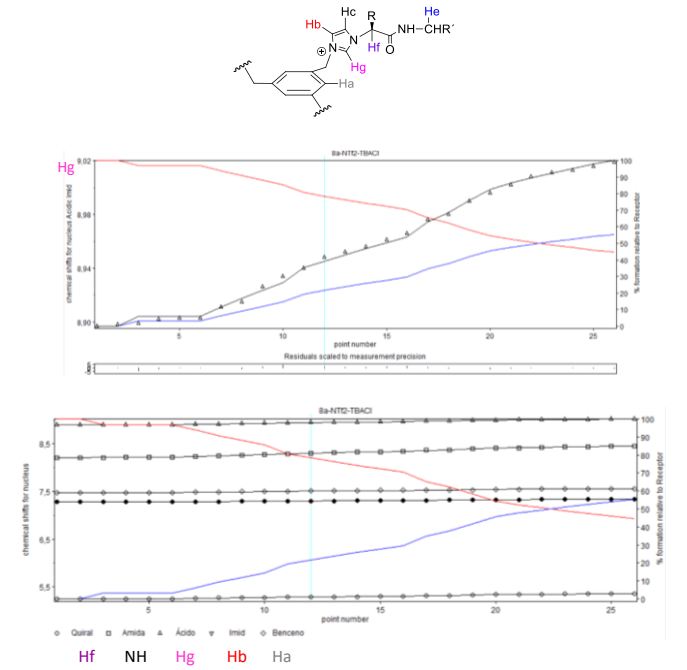

Figure S28. Fitted binding isotherm obtained for the titration of a 6 mM solution of compound **8a-NTf$_2$** with a 60 mM solution of TBACl (CD_3CN/D_2O 8/2 v/v). In order to avoid the dilution effect, the latter was prepared with the former. The graph shows the change in chemical shift of the signals due imidazolium H_g, H_f, NH, H_b, H_a protons of the molecule, fitted to the 1:1 binding model.

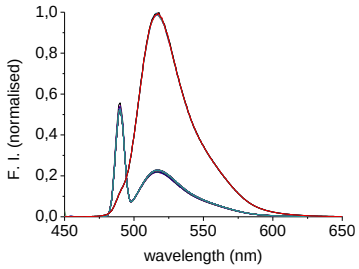

Figure S29. Carboxyfluorescein normalised fluorescence intensity recorded upon addition of **DMSO**, the blank, to POPC vesicles (0.05 mM). Vesicles (loaded with 451 mM NaCl buffered at pH 7.2 with 20 mM phosphate and containing 50 mM CF; I.S. 500 mM) were suspended in Na_2SO_4 (150 mM, buffered at pH 7.2 with 20 mM phosphate; I.S. 500 mM). At t = 60 s DMSO was added (10 μL), while at t = 360 s the detergent (20 μL) was added. Each spectrum represents the average of six trials, carried out with three different batches of vesicles.

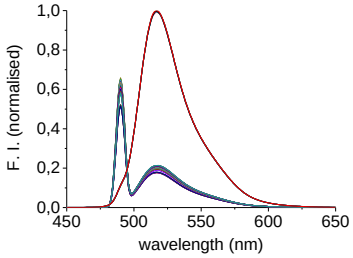

Figure S30. Carboxyfluorescein normalised fluorescence intensity recorded upon addition of **3a-NTf₂** to POPC vesicles (0.05 mM). Vesicles (loaded with 451 mM NaCl buffered at pH 7.2 with 20 mM phosphate and containing 50 mM CF; I.S. 500 mM) were suspended in Na_2SO_4 (150 mM, buffered at pH 7.2 with 20 mM phosphate; I.S. 500 mM). At t = 60 s the compound was added (10% mol carrier to lipid), while at t = 360 s the detergent (20 μL) was added. Each spectrum represents the average of three trials.

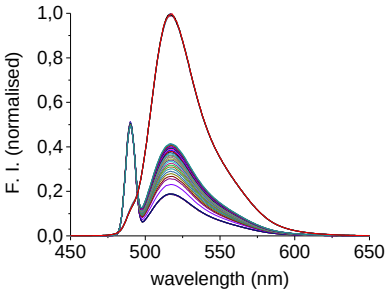

Figure S31. Carboxyfluorescein normalised fluorescence intensity recorded upon addition of **6a-NTf₂** to POPC vesicles (0.05 mM). Vesicles (loaded with 451 mM NaCl buffered at pH 7.2 with 20 mM phosphate and containing 50 mM CF; I.S. 500 mM) were suspended in Na_2SO_4 (150 mM, buffered at pH 7.2 with 20 mM phosphate; I.S. 500 mM). At t = 60 s the compound was added (10% mol carrier to lipid), while at t = 360 s the detergent (20 μL) was added. Each spectrum represents the average of three trials.

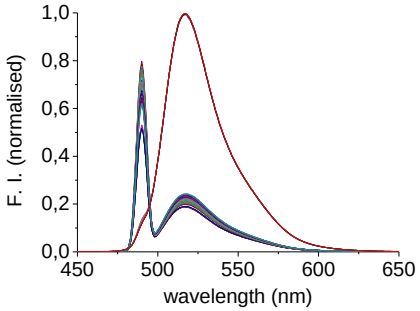

Figure S32. Carboxyfluorescein normalised fluorescence intensity recorded upon addition of **7a-NTf$_2$** to POPC vesicles (0.05 mM). Vesicles (loaded with 451 mM NaCl buffered at pH 7.2 with 20 mM phosphate and containing 50 mM CF; I.S. 500 mM) were suspended in Na_2SO_4 (150 mM, buffered at pH 7.2 with 20 mM phosphate; I.S. 500 mM). At t = 60 s the compound was added (10% mol carrier to lipid), while at t = 360 s the detergent (20 μL) was added. Each spectrum represents the average of three trials.

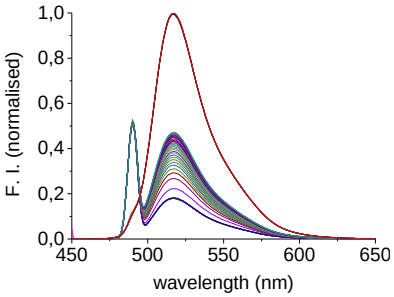

Figure S33. Carboxyfluorescein normalised fluorescence intensity recorded upon addition of **8a-NTf$_2$** to POPC vesicles (0.05 mM). Vesicles (loaded with 451 mM NaCl buffered at pH 7.2 with 20 mM phosphate and containing 50 mM CF; I.S. 500 mM) were suspended in Na_2SO_4 (150 mM, buffered at pH 7.2 with 20 mM phosphate; I.S. 500 mM). At t = 60 s the compound was added (10% mol carrier to lipid), while at t = 360 s the detergent (20 μL) was added. Each spectrum represents the average of three trials.

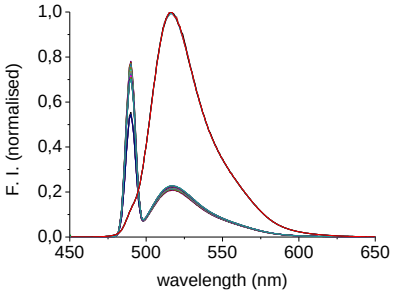

Figure S34. Carboxyfluorescein normalised fluorescence intensity recorded upon addition of **3a-Br** to POPC vesicles (0.05 mM). Vesicles (loaded with 451 mM NaCl buffered at pH 7.2 with 20 mM phosphate and containing 50 mM CF; I.S. 500 mM) were suspended in Na_2SO_4 (150 mM, buffered at pH 7.2 with 20 mM phosphate; I.S. 500 mM). At t = 60 s the compound was added (10% mol carrier to lipid), while at t = 360 s the detergent (20 μL) was added. Each spectrum represents the average of six trials, carried out with three different batches of vesicles.

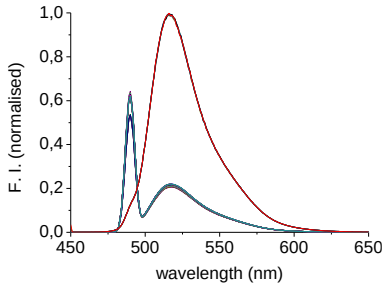

Figure S35. Carboxyfluorescein normalised fluorescence intensity recorded upon addition of **3b-Br** to POPC vesicles (0.05 mM). Vesicles (loaded with 451 mM NaCl buffered at pH 7.2 with 20 mM phosphate and containing 50 mM CF; I.S. 500 mM) were suspended in Na_2SO_4 (150 mM, buffered at pH 7.2 with 20 mM phosphate; I.S. 500 mM). At t = 60 s the compound was added (10% mol carrier to lipid), while at t = 360 s the detergent (20 μL) was added. Each spectrum represents the average of six trials, carried out with three different batches of vesicles.

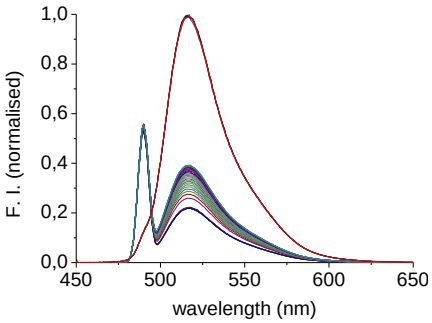

Figure S36. Carboxyfluorescein normalised fluorescence intensity recorded upon addition of **4a-Br** to POPC vesicles (0.05 mM). Vesicles (loaded with 451 mM NaCl buffered at pH 7.2 with 20 mM phosphate and containing 50 mM CF; I.S. 500 mM) were suspended in Na_2SO_4 (150 mM, buffered at pH 7.2 with 20 mM phosphate; I.S. 500 mM). At t = 60 s the compound was added (10% mol carrier to lipid), while at t = 360 s the detergent (20 μL) was added. Each spectrum represents the average of six trials, carried out with three different batches of vesicles.

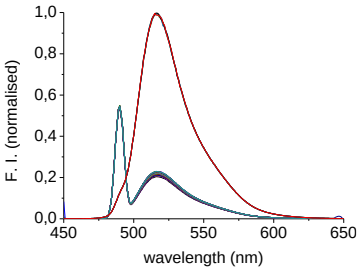

Figure S37. Carboxyfluorescein normalised fluorescence intensity recorded upon addition of **5a-Br** to POPC vesicles (0.05 mM). Vesicles (loaded with 451 mM NaCl buffered at pH 7.2 with 20 mM phosphate and containing 50 mM CF; I.S. 500 mM) were suspended in Na_2SO_4 (150 mM, buffered at pH 7.2 with 20 mM phosphate; I.S. 500 mM). At t = 60 s the compound was added (10% mol carrier to lipid), while at t = 360 s the detergent (20 μL) was added. Each spectrum represents the average of six trials, carried out with three different batches of vesicles.

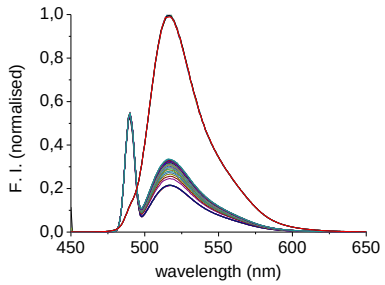

Figure S38. Carboxyfluorescein normalised fluorescence intensity recorded upon addition of **6a-Br** to POPC vesicles (0.05 mM). Vesicles (loaded with 451 mM NaCl buffered at pH 7.2 with 20 mM phosphate and containing 50 mM CF; I.S. 500 mM) were suspended in Na_2SO_4 (150 mM, buffered at pH 7.2 with 20 mM phosphate; I.S. 500 mM). At t = 60 s the compound was added (10% mol carrier to lipid), while at t = 360 s the detergent (20 μL) was added. Each spectrum represents the average of six trials, carried out with three different batches of vesicles.

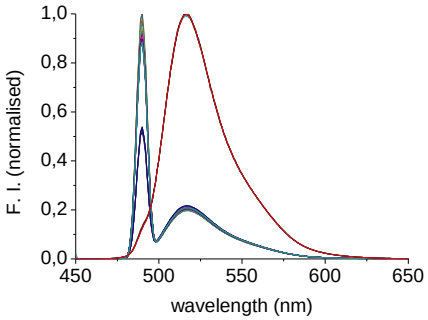

Figure S39. Carboxyfluorescein normalised fluorescence intensity recorded upon addition of **7a-Br** to POPC vesicles (0.05 mM). Vesicles (loaded with 451 mM NaCl buffered at pH 7.2 with 20 mM phosphate and containing 50 mM CF; I.S. 500 mM) were suspended in Na_2SO_4 (150 mM, buffered at pH 7.2 with 20 mM phosphate; I.S. 500 mM). At t = 60 s the compound was added (10% mol carrier to lipid), while at t = 360 s the detergent (20 μL) was added. Each spectrum represents the average of six trials, carried out with three different batches of vesicles.

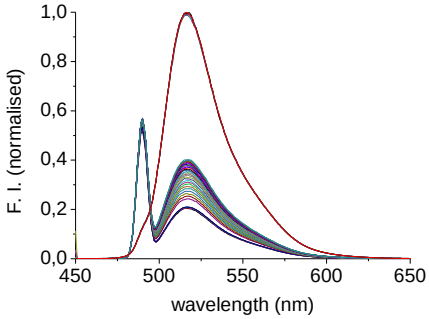

Figure S40. Carboxyfluorescein normalised fluorescence intensity recorded upon addition of **8a-Br** to POPC vesicles (0.05 mM). Vesicles (loaded with 451 mM NaCl buffered at pH 7.2 with 20 mM phosphate and containing 50 mM CF; I.S. 500 mM) were suspended in Na_2SO_4 (150 mM, buffered at pH 7.2 with 20 mM phosphate; I.S. 500 mM). At t = 60 s the compound was added (10% mol carrier to lipid), while at t = 360 s the detergent (20 μL) was added. Each spectrum represents the average of six trials, carried out with three different batches of vesicles.

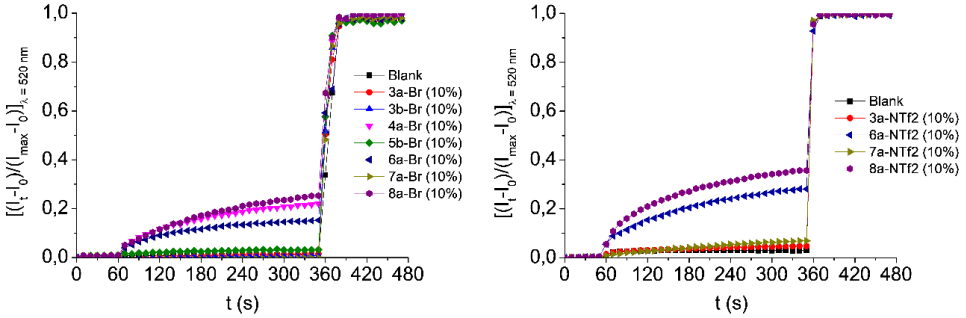

Figure S41. Carboxyfluorescein leakage observed upon addition of the studied compounds to POPC vesicles (0.05 mM). Vesicles (loaded with 451 mM NaCl buffered at pH 7.2 with 20 mM phosphate and containing 50 mM CF; I.S. 500 mM) were suspended in Na_2SO_4 (150 mM, buffered at pH 7.2 with 20 mM phosphate; I.S. 500 mM). At t = 60 s the compound was added (10% mol carrier to lipid), while at t = 360 s the detergent (20 μL) was added. The blank is DMSO (10 μL). Each trace represents the average of six trials, carried out with three different batches of vesicles.

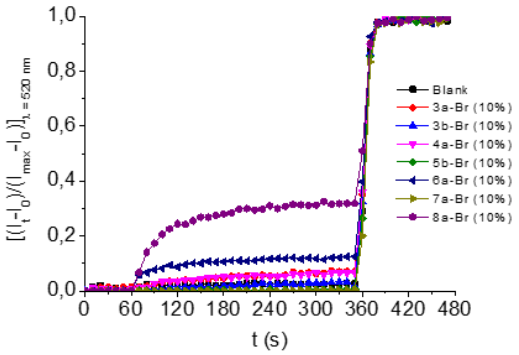

Figure S42. Carboxyfluorescein leakage observed upon addition of **3a-Br** (red trace), **3b-Br** (light blue trace), **4a-Br** (pink trace), **5b-Br** (green trace), **6a-Br** (dark blue trace), **7a-Br** (gold trace) and **8a-Br** (purple trace) to POPC vesicles (0.05 mM). Vesicles (loaded with 451 mM NaCl buffered at pH 7.2 with 20 mM phosphate and containing 50 mM CF; I.S. 500 mM) were suspended in Na_2SO_4 (150 mM, buffered at pH 6.2 with 20 mM phosphate; I.S. 500 mM). At t = 60 s the compound was added (10% mol carrier to lipid), while at t = 360 s the detergent (20 μL) was added. The blank is DMSO (10 μL). Each trace represents the average of six trials, carried out with three different batches of vesicles.

Work in progress

The Universitat Jaume I of Castellón, where I have been developing my phD, recently has acquired an ElectroSpray Ionization-Travelling Wave Ion Mobility-Mass Spectrometry (ESI-TWIM-MS).[1] This state-of-the-art technique allows the separation of isomeric compounds in gas phase of the molecules according to their charge state, shape, and size. The technic provide access to three-dimensional (3D) analytical information, namely shape, mass, and abundance. The combination of ESI-TWIM with MS results in two-dimensional plots of drift time (t_D) versus *m/z*. This technic allows to obtain drift time measurements that lead to the calculation of collision cross sections (CCSs) for low- and high–molecular-weight molecules.[2] Thus, we decided to study the conformation behaviour of some of the tripodal imidazolium compounds by ESI-TWIM-MS. All the compounds shown in Scheme 1 were previously synthesized as described before except **9a-Br** compound which is a new one.

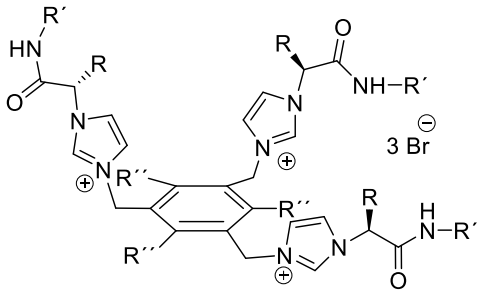

3a-Br R: $CH(CH_3)_2$ R´: $(CH_2)_{11}CH_3$ R´´: H
3b-Br R: $CH(CH_3)_2$ R´: $(CH_2)_{11}CH_3$ R´´: CH_3
4a-Br R: $CH(CH_3)_2$ R´: $(CH_2)_3CH_3$ R´´: H
5b-Br R: $CH(CH_3)_2$ R´: CH_3 R´´: CH_3
7a-Br R: CH_2Ph R´: $(CH_2)_{11}CH_3$ R´´: H
9a-Br R: CH_2Ph R´: CH_3 R´´: H

Scheme 1. Tripodal imidazolium salts

The t_D and CCS values for compounds **3a-Br**, **3b-Br** and **7a-Br** are shown in Table 1:

[1] *Applications of a travelling wave-based radio-frequency-only stacked ring ion guide*; Giles, K.; Pringle, S. D.; Worthington, K. R.; Little, D.; Wildgoose, J. L.; Bateman, R. H.; *Rapid Commun. Mass Spectrom.* **2004**, *18*, 2401-2414.

[2] (a) *Sites of metabolic substitution: investigating metabolite structures utilising ion mobility and molecular modelling*; Dear, G. J.; Munoz-Muriedas, J.; Beaumont, C.; Roberts, A.; Kirk, J.; Williams, J. P.; Campuzano, I.; *Rapid Commun Mass Spectrom.* **2010**, *24*, 3157–3162, (b) *Product ion mobility as a promising tool for assignment of positional isomers of drug metabolites*; Cuyckens, F.; Wassvik, C.; Mortishire-Smith, R. J.; Tresadern, G.; Campuzano, I.; Claereboudt, J.; *Rapid Commun Mass Spectrom.* **2011**, *25*, 3497–3503.

Table 1. Drift time and CCS values obtained for **3a-Br**, **3b-Br** and **7a-Br** compounds by ESI-TWIM-MS.

Compound	Ionic specie	t_D (ms)	^{TW}CCS(Å^2)
3a-Br (M_1)	$[M_1]^{3+}$	2.68	**470**
	$[M_1 + Br]^{2+}$	4.31	**396**
	$[M_1 - H]^{2+}$	4.37	**400**
3b-Br (M_2)	$[M_2]^{3+}$	2.73	**473**
	$[M_2 + Br]^{2+}$	4.51	**406**
	$[M_2 - H]^{2+}$	4.53	**408**
7a-Br (M_3)	$[M_3]^{3+}$	2.90	**486**
	$[M_3 + Br]^{2+}$	4.69	**415**
	$[M_3 - H]^{2+}$	4.94	**429**

The main species observed were $[M]^{3+}$, $[M + Br]^{2+}$ and $[M - H]^{2+}$, being the first one the most predominant. The structural differences between **3a-Br** and **3b-Br** remains in the methylenes of the aromatic ring, so it is expected to have similar CCS values for the different ionic species being slightly higher for **3b-Br**. Moreover, **7a-Br** contains phenylalanine which is a bulky group compared to valine, obtaining higher CCS values than **3a-Br** for the corresponding ion species. Comparing three-charged and double-charged ions for the same compound lower CCS values were obtained for the double-charged ions, this could be due to the reduction of charge that makes less repulsion between the imidazolium cations. Moreover, the $[M + Br]^{2+}$ species presented lower CCS values than $[M_3 - H]^{2+}$ species, specially **7a-Br**, this could be ascribe to the participation of the bromide anion in intramolecular hydrogen bonding interactions leading to folded structures (Figure 1).

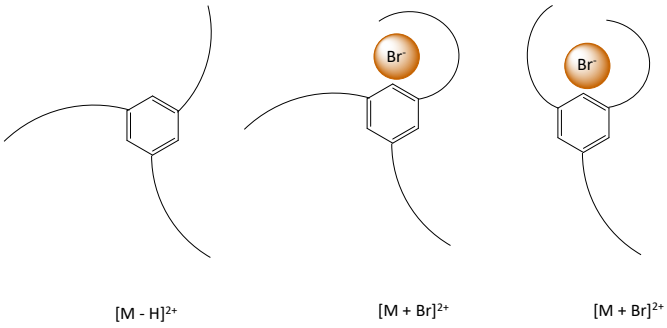

Figure 1. Possible hypothesis of the folded structured.

Next, the studies were performed in the presence of different halide anions using tripodal compound **5b-Br**, **4a-Br** and **9b-Br**. The CCS results for the different species are shown in table 2.

Table 2. CSS values of the different cation for **5b-Br**, **4a-Br** and **9b-Br** species in the presence of halide anions

Compound	**Ionic specie**	**^{TW}CCS(Å^2)**
5b-Br (M_4)	$[M_4\text{-}H]^{2+}$	**302**
	$[M_4 + Cl]^{2+}$	**288**
	$[M_4 + Br]^{2+}$	**295**
	$[M_4 + I]^{2+}$	**297**
4a-Br (M_5)	$[M_5\text{-}H]^{2+}$	**330**
	$[M_5 + Cl]^{2+}$	**316**
	$[M_5 + Br]^{2+}$	**320**
	$[M_5 + I]^{2+}$	**324**
9b-Br (M_6)	$[M_6\text{-}H]^{2+}$	**323**
	$[M_6 + Cl]^{2+}$	**301**
	$[M_6 + Br]^{2+}$	**307**
	$[M_6 + I]^{2+}$	**312**

The CCS values for $[M - H]^{2+}$ species were lower than values for the different halide species $[M + X]^{2+}$. Comparing CCS values between halide species, it can be observed as the anion electronegativity and size increases, higher is the CCS value observed (table 2).

DFT calculations are now being carried out for $[M_1]^{3+}$, $[M_1 + Br]^{2+}$ and $[M_1 – H]^{2+}$ species to get the theoretical CCS values and more information about the folded structures.

CHAPTER 3.

3.3. Imidazolium based Gemini Amphiphiles derived from *L*-valine. Structural elements and surfactant properties.

Imidazolium based Gemini amphiphiles derived from *L*-valine. Structural elements and surfactant properties

Abstract

Hypothesis: Imidazolium Gemini amphiphiles have been found to have excellent surfactants properties. On the other hand, amide functionalities and chirality are structural features of interest in order to implement the self-assembly behavior in surfactant molecules. Hence, the introduction of these additional functionalities in imidazolium Gemini amphiphiles is expected to allow tuning their aggregation properties leading to a higher emulsifying capacity that can be of interest for industrial applications. Furthermore, the structure of the central aromatic spacer can also be used to fine tune their properties.

***Experiments*:** After preparation of the desired Gemini surfactants derived from *L*-valine, their aggregation behavior, including the size distributions and morphology of the aggregates formed were investigated using different techniques. Moreover, the emulsifying capacity of these compounds in different oil/water mixtures has been analyzed as well as their potential application for the controlled release of active substances such as (*R*)-limonene.

***Findings*:** The synthetized imidazolium Gemini amphiphiles derived from *L*-valine have been found to present excellent surfactant properties. Differences on their aggregation behavior have been observed according to the substitution pattern of the aromatic central spacer. Remarkably, two different critical aggregation concentrations (CACs) were observed by fluorescence studies in aqueous media using pyrene as probe. The large apparent hydrodynamic radii obtained through dynamic LS suggest that the amphiphiles form large aggregates in diluted aqueous solutions. Furthermore, SEM images revealed the formation of vesicles at higher concentrations. Finally, the fragrance delivery studies carried out using (*R*)-limonene as a benchmark volatile compound, showed as these Gemini surfactants can be potential emulsifiers for aqueous emulsions.

1. Introduction

Gemini surfactants are amphiphilic molecules consisting of two hydrophobic tails and two hydrophilic head groups, which are connected through a rigid or flexible spacer.[1] In comparison to conventional monomeric surfactants, Gemini amphiphiles typically present significantly improved physicochemical properties, such as higher surface activity, remarkably lower critical aggregation concentration (CAC) and Krafft point (which is the minimum temperature at which a surfactant can form micelles),[2] higher solubilization capacity, as well as better wetting, detergency and emulsifying capacity.[3,4] Due to these unique properties, Gemini surfactants have important applications in various fields, such as washing, sterilization, emulsification, dispersion, cosmetics, antibacterial and antifungal preparations, tertiary oil recovery, synthesis of ordered mesoporous materials, *etc.*[5] Moreover, Gemini surfactants derived from natural amino acids are often biodegradable surfactants that meet the requirements of both biological and ecological compatibilities[6] becoming very

---

[1] (a) *Mixed aggregate formation in Gemini surfactant/1,2-dialkyl-sn-glycero-3-phosphoethanolamine systems*; Akbar, J.; Tavakoli, N.; Marangoni, D. G.; Wettig, S. D.; *J. Colloid Interface Sci.* **2012**, *377*, 237-243, (b) *Gemini surfactants: a new class of self-assembling molecules*; Menger, F. M.; Littau, C. A.; *J. Am. Chem. Soc.* **1993**, *115*, 10083-10090, (c) *Phase behaviors of Gemini cationic surfactants/*n*-butanol/water systems*; Wei, X.; Fu, S.; Yin, B.; Sang, Q.; Sun, D.; Dou, J.; Wang, Z.; Chen, L.; *Fluid Phase Equilib.* **2010**, *287*, 146-150.

[2] *Hysteresis of conductivity in a micellar surfactant solution near the Krafft point*; Manojlovic, J. Z.; *J. Serb. Chem. Soc.* **2020**, *85*, 67-68.

[3] (a) *Gemini surfactants*; Menger, F. M.; Keiper, J. S.; *Angew. Chem., Int. Ed.* **2000**, *39*, 1906-1920, (b) *Dimeric and oligomeric surfactants. Behavior at interfaces and in aqueous solution: a review*; Zana, R.; *Adv. Colloid Interface Sci.* **2002**, *97*, 205-253, (c) Ultrastable mesostructured silica vesicles; Kim, S. S.; Zhang, W. Z.; Pinnavaia, T. J.; *Science* **1998**, *282*, 1302-1305, (d) *Alkanediyl-.alpha.,.omega.-bis(dimethylalkylammonium bromide) surfactants. 2. Structure of the lyotropic mesophases in the presence of water*; Alami, E.; Levy, H.; Zana, R.; *Langmuir* **1993**, *9*, 940-944.

[4] (a) *Polymerisation of styrene in microemulsion with catanionic surfactant mixtures*; Bernd, T.; *Colloid Polym. Sci.* **2005**, *283*, 421-430, (b) *Transfection Mediated by Gemini Surfactants: Engineered Escape from the Endosomal Compartment*; Bell, P. C.; Bergsma, M.; Dolbnya, I. P.; Bras, W.; Stuart, M. C. A.; Rowan, A. E.; Feiters, M. C.; Engberts, J. B. F. N.; *J. Am. Chem. Soc.* **2003**, *125*, 1551-1558, (c) *Aggregation behaviours and bactericidal activities of novel cationic surfactants functionalized with amides and ether groups*; Cao, G.; Guo, X.; Jia, L.; Tian, X.; *RSC Adv.* **2015**, *5*, 27197-27204, (d) *Aggregation Behavior of Surface Active Dialkylimidazolium Ionic Liquids [$C_{12}C_n$im]Br (n = 1–4) in Aqueous Solutions*; Liu, X.; Hu, J.; Huang, Y.; Fang, Y.; *J. Surf. Deterg.* **2012**, *16*, 539-546, (e) *Empirical correlations between Krafft temperature and tail length for amidosulfobetaine surfactants in the presence of inorganic salt*; Chu, Z.; Feng, Y.; *Langmuir* **2012**, *28*, 1175-1181, (f) *Synthesis, surface active and thermal properties of novel imidazolium cationic monomeric surfactants*; Patial, P.; Shaheen, A.; Ahmad, I.; *J. Ind. Eng. Chem.* **2014**, *20*, 4267-4275.

[5] (a) *Thermodynamic Studies of Aqueous m–s–m Gemini Surfactant Systems*; Wettig, S. D.; Verrall, R. E.; *J. Colloid Interface Sci.* **2001**, *235*, 310-316, (b) *Polymerizable semi-fluorinated Gemini surfactants designed for antimicrobial materials*; Caillier, L.; Taffin de Givenchy, E.; Levy, R.; Vandenberghe, Y.; Geribaldi, S.; Guittard, F.; *J. Colloid Interface Sci.* **2009**, *332*, 201-207.

[6] (a) Amino acids as raw material for biocompatible surfactants; Pinazo, A.; Pons, R.; Pérez, L.; Infante, M. R.; *Ind. Eng. Chem. Res.* **2011**, *50*, 4805-4817, (b) *Green amino acid-based surfactants*; Morán, M. C.; Pinazo, A.; Pérez, L.; Clapés, P.; Angelet, M.; Garcia, M. T.; Vinardell, M. P.; Infante, M. R.; *Green Chem.* **2004**, *6*, 233-240, (c) *Gemini surfactants from natural amino acids*; Pérez, L.; Pinazo, A.; Pons, R.; Infante, M. R.; *Adv. Colloid Interface Sci.* **2014**, *205*, 134-155.

attractive for biomedical applications including drug and gene delivery.[7] In this regard, previous studies on the synthesis and characterization of Gemini amphiphilic pseudopeptides (GAPs) have shown how they are able to self-assemble into different nanostructures depending on the environment, and even to respond to different stimuli.[8]

In this field, cationic Gemini surfactants are among the most widely studied Gemini surfactants due their superior performances in industrial applications.[9] In this regard, ionic liquid-related surfactants based on imidazolium structures demonstrate a stronger tendency towards self-aggregation owing to the distinct polarizability of their imidazolium head group.[10,11] Much work has been done to modify and control the solution properties of Gemini surfactants by a rational design of their structural components like the type of the head groups, the

---

[7] (a) *Drug solubilisation and in vitro toxicity evaluation of lipoamino acid surfactants*; Ménard, N.; Tsapis, N.; Poirier, C.; Arnauld, T.; Moine, L.; Lefoulon, F.; Péan, J.-M.; Fattal, E.; *Int. J. Pharm.* **2012**, *423*, 312-320, (b) *Amino acid-substituted Gemini surfactant-based nanoparticles as safety and versatile gene delivery agents*; Singh, J.; Yang, P.; Michel, D.; Verrall, R. E.; Foldvari, M.; Baeda, I.; *Curr. Drug Deliv.* **2011**, *8*, 299-306, (c) *Enhanced gene expression in epithelial cells transfected with amino acid-substituted Gemini nanoparticles*; Yang, P.; Singh, J.; Wettig, S.; Foldvari, M.; Verrall, R. E.; Baeda, I.; *Eur. J. Pharm. Biopharm.* **2010**, *75*, 311-320.

[8] (a) *Gemini amphiphilic pseudopeptides: synthesis and preliminary study of their self-assembling properties*; Rubio, J.; Alfonso, I.; Bru, M.; Burguete, M. I.; Luis, S. V.; *Tetrahedron Lett.* **2010**, *51*, 5861–5867, (b) *Stimulus responsive self-assembly of Gemini Amphiphilic Pseudopeptides*; Rubio, J.; Alfonso, I.; Burguete, M. I.; Luis, S. V.; *Soft Matter* **2011**, *7*, 10737–10748, (c) *Interplay between hydrophilic and hydrophobic interactions in the self-assembly of a Gemini Amphiphilic Pseudopeptide: from vesicles to room temperature hydrogels*; Rubio, J.; Alfonso, I.; Burguete, M. I.; Luis, S. V.; *Chem. Commun.* **2012**, *48*, 2210-2212, (d) *Effects of Gemini amphiphilic pseudopeptides on model lipid membranes: A Langmuir monolayer study*; Rubio-Magnieto, J.; Luis, S. V.; Orlof, M.; Korchowiec, B.; Sautrey, G.; Rogalska, E.; *Colloids Surf. B.* **2013**, *102*, 659-666, (e) *Synthesis of second-generation self-assembling Gemini Amphiphilic Pseudopeptides*; Lotfallah, A. H.; Burguete, M. I.; Alfonso, I.; Luis, S. V.; *J. Colloid Interface Sci.* **2020**, *564*, 52-64.

[9] (a) *Structural and Functional Stability of Cellulase in Aqueous-Biamphiphilic Ionic Liquid Surfactant Solution*; Bharmoria, P.; Mehta, M. J.; Pancha, I.; Kumar, A.; *J. Phys. Chem. B.* **2014**, *118*, 9890-9899, (b) *Synthesis and evaluation of novel cationic Gemini surfactants based on Guava crude fat as petroleum-collecting and dispersing agents*; Abo-Riya, M.; Tantawy, A. H.; El-Dougdoug, W.; J. Mol. Liq. **2016**, *221*, 642-650, (c) *Synthesis, surface activity and aggregation behavior of Gemini imidazolium surfactants 1,3-bis(3-alkylimidazolium-1-yl) propane bromide*; Ren, C.; Wang, F.; Zhang, Z.; Nie, H.; Li, N.; Cui, M.; *Colloids Surf A: Physicochem Eng Asp* **2015**, *467*, 1-8, (d) *Structure membrane activity relationship in a family of peptide-based Gemini amphiphiles: An insight from experimental and theoretical model systems*; Korchowiec, B.; Gorczyca, M.; Korchowiec, J.; Rubio-Magnieto, J.; Lotfallah, A. H.; Luis, S. V.; Rogalska, E.; *Colloids Surf., B,* **2016**, *146*, 54-62.

[10] (a) *Synthesis and Properties of Thioether Spacer Containing Gemini Imidazolium Surfactants*; Bhadani, A.; Singh, S.; *Langmuir* **2011**, *27*, 14033-14044, (b) *Synthesis, characterization and properties of geminal imidazolium ionic liquids*; Ding, Y. S.; Zha, M.; Zhang, J.; Wang, S. S.; *Colloids Surf. A* **2007**, *298*, 201-205, (c) *Synthesis and properties of ionic liquid-type Gemini imidazolium surfactants*; Ao, M. Q.; Xu, G. Y.; Zhu, Y.; Bai, Y.; *J. Colloid Interface Sci.* **2008**, *326*, 490–495.

[11] (a) *Gemini Imidazolium Surfactants: Synthesis and Their Biophysiochemical Study*; Kamboj, R.; Singh, S.; Bhadani, A.; Kataria, H.; Kaur, G.; *Langmuir* **2012**, *28*, 11969–11978, (b) *Interfacial and micellar properties of imidazolium-based monocationic and dicationic ionic liquids*, Baltazar, Q. Q.; Chandawalla, J.; Sawyer, K.; Anderson, J. L.; *Colloids Surf., A* **2007**, *302*, 150-156.

length of the hydrophobic chains and the nature of the spacer.[12,13] For instance, the aggregation of ionic surfactants can be easily tuned by varying the charge density or the spontaneous curvature along with the concentration or the temperature, leading to different aggregates morphologies like rod like micelles, vesicles etc.[14,15] It must be noted that most of the vesicles reported in the literature derived from ionic liquid surfactants were formed in the presence of co-surfactants.[16] There are only a few reports on vesicles formed by pure imidazolium surfactants.[17]

The presence of amide functionalities in cationic surfactants has been reported to increase their biodegradability and improve their surfactant properties.[18]

---

[12] (a) *Aggregation behavior of long-chain N-aryl imidazolium bromide in aqueous solution*; Shi, L.; Li, N.; Yan, H.; Gao, Y. A.; Zheng, L.; *Langmuir* **2011**, *27*, 1618-1625, (b) *Effect of ethylene glycol and propylene glycol on the aggregation of alkanediyl-α,ω-bis(tetradecyldimethylammonium bromide) (14–s–14; s = 4–6) Gemini surfactants*; Koya, P. A.; Wagay, T. A.; Ismail, K.; *J. Mol. Liq.* **2016**, *219*, 505-512, (c) *The effect of alkyl chain length on synergistic effects in micellization and surface tension reduction in nonionic Gemini (S-10) and anionic surfactants mixtures*; Trawinska, A.; Hallmann, E.; Medrzycka, K.; *Colloids Surf A: Physicochem Eng Asp* **2016**, *506*, 114-126.

[13] (a) *Alkanediyl-α,ω-Bis(dimethylalkylammonium Bromide) Surfactants: 9. Effect of the Spacer Carbon Number and Temperature on the Enthalpy of Micellization*; Grosmaire, L.; Chorro, M.; Chorro, C.; Partyka, S.; Zana, R.; *J. Colloid Interface Sci.* **2002**, *246*, 175-181, (b) *Adsorption and micellization of Gemini surfactants with pyrrolidinium head groups: effect of the spacer length*; Cai, B.; Dong, J.; Cheng, L.; Jiang, Z.; Yang, Y.; Li, X.; *Soft Matter* **2013**, *9*, 7637-7646, (c) *The effect of the spacer rigidity on the aggregation behavior of two ester-containing Gemini surfactants*; Zhang, Z.; Zheng, P.; Guo, Y.; Yang, Y.; Chen, Z.; Wang, X.; An, X.; Shen, Z.; *J. Colloid Interface Sci.* **2012**, *379*, 64-71, (d) *Aggregation and thermodynamic properties of ionic liquid-type Gemini imidazolium surfactants with different spacer length*; Ao, M.; Huang, P.; Xu, G.; Yang. X.; Wang, Y.; *Colloid Polym. Sci.* **2009**, *287*, 395-402.

[14] (a) *Theory of self-assembly of hydrocarbon amphiphiles into micelles and bilayers*; Israelachvili, J.; Mitchell, D.; Ninham, B.; *J. Chem. Soc. Faraday Trans.* **1976**, *2* (72), 1525−1568, (b) *Molecular Packing Parameter and Surfactant SelfAssembly. The neglected role of the surfactant tail*; Nagarajan, R.; *Langmuir* **2002**, *18*, 31-38, (c) *Calculating the 'Chain Splay' of Amphiphilic Molecules: Towards Quantifying the Molecular Shapes*; Chandrashekhar, K.; *Chem. Phys. Lipids* **2019**, *218*, 16-21, (d) *Lipid Self-Assemblies and Nanostructured Emulsions for Cosmetic Formulations*; Chandrashekhar, K.; *Cosmetics* **2016**, *3*, 37-52.

[15] (a) *Spontaneous vesicle formation in aqueous mixtures of single-tailed surfactants*; Kaler, E. W.; Murthy, K. A.; Rodriguez, B. E.; Zasadzinski, J. A. N.; *Science* **1989**, *245*, 1371-1374, (b) *Self-assembly of flat nanodiscs in salt-free catanionic surfactant solutions*; Zemb, T.; Dubois, M.; Deme, B.; Gulik-Kryzwicki, T.; *Science* **1999**, *283*, 816-819, (c) *Synergism and polymorphism in mixed surfactant systems*; Khan, A.; Marques, E. F.; *Curr. Opin. Colloid Interface Sci.* **2000**, *4*, 402-410.

[16] (a) *Ultrafast FRET to study spontaneous micelle-to-vesicle transitions in an aqueous mixed surface-active ionic-liquid system*; Mandal, S.; Kuchlyan, J.; Banik, D.; Ghosh, S.; Banerjee, C.; Khorwal, V.; Sarkar, N.; *Chemphyschem.* **2014**, *15* (16), 3544-3553, (b) *Micelle-vesicle-micelle transition in aqueous solution of anionic surfactant and cationic imidazolium surfactants: Alteration of the location of different fluorophores*; Dutta, R.; Ghosh, S.; Banerjee, P.; Kundu, S.; Sarkar, N.; *J Colloid Interface Sci.* **2017**, *490*, 762-773, (c) *Spontaneous vesicle formation of an industrial single-chain surfactant at acidic pH and at room-temperature*; Renoncourt, A.; Bauduin, P.; Nicholl, E.; Touraud, D.; Verbavatz, J-M.; Dubois, M.; Drechsler, M.; Kunz, W.; *ChemPhysChem* **2006**, *7*, 1892-1896, (d) *Two distinct mechanisms of vesicle-to-micelle and micelle-to-vesicle transition are mediated by the packing parameter of phospholipid-detergent systems*; Stuart, M. C. A.; Boekema, E. J.; *Biochim. Biophys. Acta, Biomembr.* **2007**, *1768*, 2681-2689.

[17] *Supramolecular "Big Bang" in a Single-Ionic Surfactant/Water System Driven by Electrostatic Repulsion: From Vesicles to Micelles*; Leclercq, L.; Bauduin, P.; Nardello-Rataj. V.; *Langmuir* **2017**, *33*, 3395-3403.

[18] (a) *An interplay between spacer nature and alkyl chain length on aqueous micellar properties of cationic Gemini surfactants: A multi-technique approach*; Parikh, K.; Singh, S.; Desai, A.; Kumar,

Furthermore, enantiomerically pure surfactants have been shown to form more stable aggregates and provide lower CAC values as compared to their racemic mixtures.[19] In this context, our research group has been involved in the preparation of imidazolium based receptors derived from enantiomerically pure materials obtained from the chiral pool,[20] and ditopic imidazolium derivatives containing amino acid fragments behaved as receptors for the recognition of the chiral anions from dicarboxylic acids and as transmembrane chloride anion transporters.[21]

In the light of these former results, here we report the synthesis of a family of bisimidazolium Gemini surfactants derived from *L*-valine (**2a-c** in Figure 1) and the study of their aggregation in different media with the objective to determine the effect on their aggregation behavior of structural factors like the substitution in the aromatic spacer and the presence of the amino acid derived amide moiety, which can be of significance for the in depth understanding of structure-property relationships in Gemini surfactants.[22] Moreover, the properties of these compounds as surfactants for the stabilization of oil/water (O/W) emulsions and their ability for controlled fragrance release.

S.; *J. Mol. Liq.* **2019**, *278*, 290-298, (b) *Synthesis and Antibacterial Activity of Novel Amido-Amine-Based Cationic Gemini Surfactants*, Ghumare, A. K.; Pawar, B. V.; Bhagwat, S. S.; *J. Surfactants Deterg.* **2013**, *16*, 85-93, (c) *Preparation of a novel class of cationic Gemini imidazolium surfactants containing amide groups as the spacer: their surface properties and antimicrobial activity*; Wang, L.; Qin, H.; Ding, L.; Huo, S.; Deng, Q.; Zhao, B.; Meng, L.; Yan, T.; *J. Surfactants Deterg.* **2014**, *17*, 1099–106.

[19] (a) *Chiral discrimination of a Gemini type surfactant with rigid spacer at the air–water interface*; Shankar, B. V.; Patnaik, A.; *J Phys Chem B* **2007**, *111*, 11419-11427, (b) *pH-dependent chiral vesicles from enantiomeric sodium 2,3-bis(decyloxy) succinate in aqueous solution*; Shankar, B. V.; Patnaik, A.; *Langmuir* **2007**, *23*, 3523-3529, (c) *A new pH and thermo-responsive chiral hydrogel for stimulated release*; Shankar, B.V.; Patnaik, A.; *J Phys Chem B* **2007**, *111*, 9294-9300.

[20] (a) *Chiral Room Temperature Ionic Liquids as Enantioselective Promoters for the Asymmetric Aldol Reaction*; González, L.; Escorihuela, J.; Altava, B.; Burguete, M. I.; Luis, S. V.; *Eur. J. Org. Chem.* **2014**, 5356-5363, (b) *Synthesis of Chiral Room Temperature Ionic Liquids from Amino Acids – Application in Chiral Molecular Recognition*; González, L.; Altava, B.; Bolte, M.; Burguete, M. I.; García-Verdugo, E.; Luis, S. V.; *Eur. J. Org. Chem.* **2012**, 4996-5009, (c) *Synthesis of new chiral imidazolium salts derived from amino acids: their evaluation in chiral molecular recognition*; Altava, B.; Barbosa, D. S.; Burguete, M. I.; Escorihuela, J.; Luis, S. V.; *Tetrahedron: Asymm.* **2009**, *20*, 999-1003.

[21] (a) *Application of optically active chiral bis(imidazolium) salts as potential receptors of chiral dicarboxylate salts of biological relevance*; González-Mendoza, L.; Escorihuela, J.; Altava, B.; Burguete, M. I.; Luis, S.V.; *Org. Biomol. Chem.* **2015**, *13*, 5450-5459, (b) *Bis(imidazolium) salts derived from amino acids as receptors and transport agents for chloride anions*; González-Mendoza, L.; Escorihuela, J.; Altava, B.; Burguete, M. I.; Hernando, E.; Luis, S. V.; Quesada, R.; Vicent, C.; *RSC Adv.* **2015**, *5*, 34415-34423.

[22] (a) *Gemini Imidazolium Amphiphiles for the Synthesis, Stabilization, and Drug Delivery from Gold Nanoparticles*; Casal-Dujat, L.; Rodrigues, M.; Yague, A.; Calpena, A. C.; Amabilino, D. B.; Gonzalez-Linares, J.; Borras, M.; Perez-García, L.; *Langmuir* **2012**, *28*, 2368–2381, (b) *Synthesis, characterization and comparative evaluation of phenoxy ring containing long chain Gemini imidazolium and pyridinium amphiphiles*; Bhadani, A.; Kataria, H.; Singh, S.; *J. Colloid Interface Sci.,* **2011**, *361*, 33-41.

2. Materials and Methods

2.1 Materials

Reagents and solvents, including NMR solvents, were purchased from commercial suppliers and were used without further purification. Deionized water was obtained from a MilliQ® equipment. Imidazole **1** was prepared as previously described.[20a] Gemini amphiphiles **2** were prepared following the synthetic protocols reported for **2b**[21] and the preparation of compounds **3** has been reported elsewhere.[23]

2.2 NMR spectroscopy

NMR experiments were carried out on a Varian INOVA 500 spectrometer (500 MHz for ^{1}H and 125 MHz for ^{13}C), on a Bruker Advance III HD 400 spectrometer (400 MHz for ^{1}H and 100 MHz for ^{13}C) or on a Bruker Advance III HD 300 spectrometer (300 MHz for ^{1}H and 75 MHz for ^{13}C) at 25 ºC. Chemical shifts are reported in ppm using TMS as the reference.

2.2.1. CAC determination using NMR

Firstly, different solutions of **2a-2c** and **3a** ranging from 0.5 to 20 mol/L in CD_3OD/D_2O (except for **2a**+Et_4NBr ranging from 0.25 to 15 mol/L and for **3a** ranging from 0.3 to 20 mol/L), from 0.2 to 25 mol/L in $CDCl_3$ and from 2.5 to 20 mol/L in CD_3OD/H_2O for **2a** were prepared in NMR tubes and secondly, were measured at 25ºC. CAC is the cross point of the two straight lines obtained through the changes in chemical shift as a function of the inverse of the concentration.

2.3 CAC determination using fluorescence spectroscopy

Fluorescence measurements were performed with a Spex Fluorolog 3-11 instrument equipped with a 450 W xenon lamp (right angle mode). Pyrene was used as a fluorescence probe to determine the CAC of **2a-2c** and **3a** in aqueous media at 25±1 °C. Firstly, a stock pyrene solution ($1{,}98\times10^{-4}$ mol/L) was prepared in ultrapure methanol. Then, different solutions of **2a-2c** and **3a** (ranging from 3×10^{-3} to 7×10^{-6} mol/L for CH_3OH/H_2O and H_2O) were prepared in different vials (1 mL) and 5 µL of the pyrene solution were added to each vial, achieving a final pyrene concentration of 9.89×10^{-7} mol/L. The fluorescence

[23] *Insights into the Formation and Structures of Molecular Gels by Diimidazolium Salt Gelators in Ionic Liquids or "Normal" Solvents*; Rizzo, C.; D'Anna, F.; Noto, R.; Zhang, M.; Weiss, R. G.; *Chem. Eur. J.* **2016**, *22*, 11269-11282.

spectra of pyrene were recorded for all the samples from 200 to 650 nm after excitation at 337 nm. The slit width was set at 5 nm for both excitation and emission. The peak intensities at 373 and 392 nm were determined as I1 and I3, respectively. The ratios of the peak intensities at 373 and 392 nm (I1/I3) of the emission spectra were recorded as a function of the logarithm of concentration. The CAC values were taken from the break point using the intersection of the best fit straight lines. The CAC was obtained from the average of three measurements for each compound.

2.4 Light scattering (LS) measurements

Light scattering measurements were performed using a Brookhaven Instruments BI-200SM goniometer, a BI-9000AT digital correlator, and a red laser operating at a wavelength of 633 nm. The scattering angle was 45°. The round measurement cell was thermostated at 25 °C. A 6.0 mM solution of compounds **2a-2c** and **3a** was prepared in CH_3OH:Milli-Q® water 1/1 v/v or Milli-Q® water. The solution was filtered directly into the scattering cell through a Millipore Millex syringe filter (0.22 μm). Before each measurement, the scattering cell was rinsed several times with the filtered solution. The LS measurements started 5-10 min after the sample solutions were placed in the LS optical system to allow the sample to equilibrate. The data acquisition was carried out for 10 min and each experiment was repeated three times. The data were analyzed with the cumulant method using the software provided by the manufacturer.

2.5 SEM images

Scanning Electron Microscopy was performed in a JEOL 7001F microscope with a digital camera. Samples were obtained by slow evaporation of a solution of the compounds (1 to 2 mg/ml) directly onto the sample aluminium holder, and were conventionally coated previous to the measurement, using the sputtering technic in which microscopic particles of platinum are rejected from the surface after the material is itself bombarded by energetic particles of a plasma or gas.

2.6 Optical images

Images were recorded with an OLYMPUS COVER-018 microscopy, BX51TF model, at RT (25°C).

2.7 CD measurements

CD spectra were recorded with a JASCO J-810 spectropolarimeter at RT (25°C). The normalized CD spectra were obtained by transforming the molar circular dichroic absorption data (Δε, cm^2/mmol) using the formula: $\Delta\varepsilon = \theta/(32980 \times C \times l)$, in which θ is the measured ellipticity (in mdeg), C is the concentration (in mol/L) and l is the path length (in cm).

2.8 UV measurements

UV/Vis absorption spectra were recorded on a Hewlett-Packard 8453 spectrophotometer at 25 °C. Molar extinction coefficients of the UV spectra were obtained by linear regression between the measured absorbance and the sample concentration).

2.9 Release studies. Determination of the release profiles

To a emulsion containing 4 mL of H_2O/EtOH 1/1 v/v and 10% of limonene the corresponding surfactant was added, the mixture was kept at 30 °C in a closed 10 mL vial connected to a second one containing 2 mL of toluene and the internal standard (Acetophenone 0,43 M) via a Teflon tubing (10 cm) passing through the septa closing both vials. To avoid the generation of over pressure the septum on second vial was punctured with a needle (0,8 mm). Experiments were repeated twice. Limonene release was analyzed by taking aliquots (100 μL), at different times, of the toluene phase in the second vial and using GC for the determination. The method used in a VARIAN 3900 instrument was: Analysis time: 60 min. Column SUPELCO BETA DEX 120, Pressure: 45.00 Psi, Oven Temperature: T: 100 °C. Detector: T: 300 °C, Injector: T: 250 °C, Helium flow: 25 mL/min, Hydrogen flow: 30 mL/min, Air flow: 300 mL/min.

3. Results and discussion

3.1 Synthesis of bis-imidazolium surfactants

Amphiphilic bis-imidazolium salts **2a-c** derived from *L*-valine were obtained in >80% yield by reaction of the compound **1** with the corresponding (bisbromomethyl)benzene (Figure 1). The starting imidazole **1** was obtained from the corresponding α-amino amide as described previously.[20a] Compounds **3a** and **3b**, used as analogues lacking the *L*-valine fragment, were prepared in a similar way from N-dodecyl imidazole.

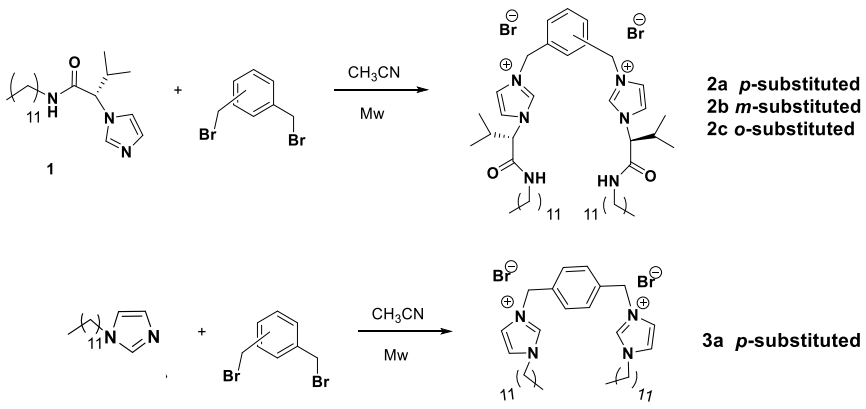

Figure 1. Synthesis of bisimidazolium gemini surfactants **2** and **3**.

3.2 Aggregation behaviour

The self-assembly behavior of the Gemini surfactants **2a-c** in chloroform and in aqueous media (water and water/methanol), including the analysis of the size distributions and the morphologies of the aggregates formed, was investigated by ^{1}H-NMR, circular dichroism (CD), light scattering (LS), fluorescence, attenuated total reflection-fourier-transform infrared (ATR-FTIR), optical microscopy and scanning electron microscopy (SEM).

3.2.1. ^{1}H NMR experiments

Figure 2 shows the ^{1}H NMR spectra of **2a** in D_2O/CD_3OD 1/1 v/v at concentrations ranging from 0.5 to *ca.* 20 mM and at 25 ^{o}C. In comparison with the spectra in $CDCl_3$ (ESI, Figure S1) some significant changes are observed that indicate the presence of rather different conformations in both media for all the range of concentrations studied. Thus, at 0.6 mM, the benzylic protons in deuterated chloroform appear as two doublets ($\Delta\delta$ = 0.05 ppm), while in the aqueous solvent an apparent singlet is observed. This suggests the presence in $CDCl_3$ of very rigid conformations most likely associated to strong hydrogen bond networks involving the basic anions and the acidic hydrogen atoms of the amide and imidazolium ring (C2-H and at a lower extent C4-H or C5-H). This should preclude the free rotation of the C-C and C-N bonds at the benzylic position as observed in some related compounds.[21a] Such rigid hydrogen bond networks should be weakened in aqueous media through an efficient solvation of cations and anions, facilitating free rotation and making the two benzylic protons equivalent. This agrees with the significant upfield shift observed in the aqueous medium for the C2-H signal ($\Delta\delta$ = 0.60 ppm) and to a lower extent for

C4-H/C5-H, which is indicative of the presence of a very strong imidazolium/chloride ion pair in $CDCl_3$. The conformational changes affect mostly to the amino acid derive moiety. The splitting of the two valine CH_3 signals is reduced from 0.28 to 0.16 ppm in D_2O/CD_3OD as occurs for the non-equivalent geminal hydrogen atoms in the NH-CH_2 group (from 0.34 to 0.14 ppm). Finally, a remarkable upfield chemical shift is detected for the C*-H signal ($\Delta\delta$ = 0.97 ppm). When the ^{1}H NMR spectrum of **2a** was recorded in H_2O/CD_3OD to detect the NH signal (ESI, Figure S2, for ca. 2mM spectra) a downfield shift of 0.42 ppm was observed relative to the same signal in $CDCl_3$, indicating than in the aqueous media the amide group is exposed to the solvent and strongly hydrogen bonded.

When the concentration of **2a** was increased in D_2O/CD_3OD, only very minor changes were detected for the signals of the hydrophobic chains ($\Delta\delta \approx$ -0.02 ppm for the central methylene groups and $\Delta\delta$ = -0.02 ppm for the methyl group). The signals for the imidazolium protons experienced small downfield shifts ($\Delta\delta$= 0.07-0.09) indicating that this group becomes slightly more involved in hydrogen bonding upon concentration. Interestingly, at the lower concentration studied (0.5 mM) the signal for C2-H disappears through H/D exchange, which suggests that this acidic position is much less exposed in the aggregates formed. Surprisingly, $\Delta\delta$ for the amide NH was very small when changing the concentration in H_2O/CD_3OD from 2.5 to 20 mM (-0.01 ppm, ESI, Figure S2), supporting that it is strongly hydrogen bonded in the solution and in the aggregates. While one of the methylene protons of the alkyl chains (NH-CH_2) shifted upfield upon aggregation the second one remained essentially in the same position, giving place to an increase in the observed splitting of these geminal protons (from 0.12 to ca. 0.26 ppm). This can be ascribed to the conformational changes involving rotation around the C-N bond and a higher rigidity of the aliphatic tails in the aggregates.[24] Similar trends were observed for **2b**. However, the changes for **2c** were much smaller (ESI, Table S1, Figure

[24] (a) *Aggregation Behavior of Nitrophenoxy-Tailed Quaternary Ammonium Surfactants*; Huang, X.; Han, Y.; Wang, Y.; Wang, Y.; *J Phys Chem B* **2007**, *111*, 12439-12446; (b) *Aggregation Behavior of Ionic Liquids in Aqueous Solutions: Effect of Alkyl Chain Length, Cations, and Anions*; Singh, T.; Kumar, A.; *J. Phys. Chem. B* **2007**, *111*, 7843-7851, (c) *Aggregation of Ionic Liquids [C$_n$mim]Br (n = 4, 6, 8, 10, 12) in D$_2$O: A NMR Study*; Zhao, Y.; Jian, S. G.; Tang, W. J.; *J. Phys. Chem. B.* **2008**, *1127*, 2031-2039, (d) *Conformational Analysis of (Phenylenedimethylene)bis(n-octylammonium)dibromides in Aqueous Solution. Conformational Change upon Micellization*; Hattori, N.; Yoshino, A.; Okabayashi, H.; O'Connor, C. J.; *J. Phys. Chem. B* **1998**, *102*, 8965-8973.

S3-S4). The δ_{diff} values observed for the different protons in general follow the order: **2a**>**2b**>**2c** (see Table S1), indicating their dependence on the relative geometric disposition to the aromatic central substitution.

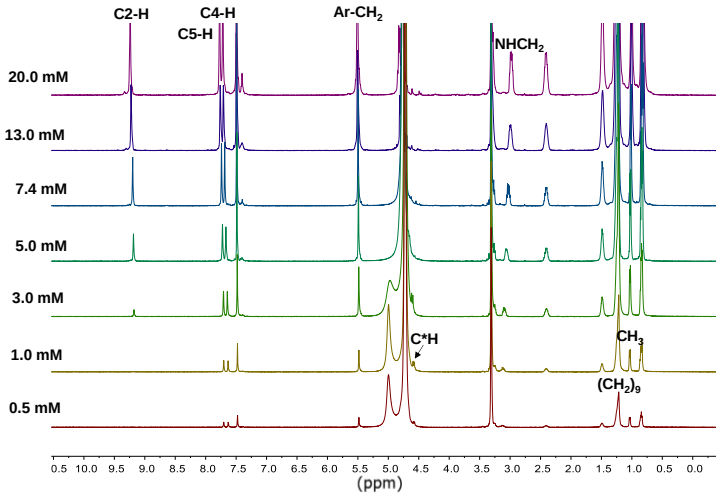

Figure 2. ^{1}H NMR spectra (400 MHz, 25 °C) of **2a** in CD_3OD/D_2O (1/1 v/v) at different concentrations.

As the aggregation behavior in aqueous media can be affected by the ionic strength,[25] compound **2a** was also studied in D_2O/CD_3OD 1/1 v/v containing an added salt. In this regard, no appreciable changes were observed in the former trends when using a 2/1 molar ratio **2a**/Et_4NBr, for the 0.25 to 15 mM concentration range (ESI, Table S1, Figure S5a). Only very minor changes were observed in chemical shifts in the presence and absence of the salt at a given concentration (ESI, Figure S5b).

Aggregation studies for **2a-2c** were also carried out in $CDCl_3$ for concentrations ranging from 0.2 to 25 mM. For **2a**, the imidazolium C2-H protons of the head group shifted upfield ($\Delta\delta$ = -0.16 ppm), while the opposite was found for C5-H protons ($\Delta\delta$ = 0.27ppm) upon increasing concentration as well as for the benzylic protons (C*H*$_2$)Ar ($\Delta\delta$ = 0.17 ppm). On the contrary, only minute upfield shifts ($\Delta\delta$ = -0.02 ppm) were detected for the protons of the aliphatic tails (ESI, Figure S1 and S6). This suggests that aggregation in this medium involves mainly, as could be expected, polar and hydrogen bonding interactions associated to a weakening of the strong ion pair for the anion and the acidic C2-H and, concomitantly, to the strengthening of intermolecular hydrogen bonds with participation of other imidazolium protons. The hydrogen bonding of the amide

[25] *Molecular packing parameter in bolaamphiphile solutions: Adjustment of aggregate morphology by modifying the solution conditions*; Yan, Y.; Xiong, W.; Li, X.; Lu, T.; Huang, J.; Li, Z.; Fu, H.; *J. Phys. Chem. B.* **2007**, *111*, 2225-2230.

N-H also changes in this process. Initially, from 0.2 to ca 2 mM an upfield shift is observed ($\Delta\delta$ = -0.09 ppm) and then a small downfield shift is seen at higher concentrations. Thus, the conformational changes associated to the initial steps of aggregation encompass a small weakening of the hydrogen bonding of the amide N-H groups, while the formation of more compact aggregates leads to slightly stronger H-bonds. The substitution pattern at the benzene ring is relevant for this process. Similar trends were observed for **2c**, except for the signal of the amide NH that constantly shifts downfield upon concentration (ESI, Figure S7). The situation is quite different for **2b**, for which the signals for C2-H, C*H and amide N-H shift downfield until *ca.* 1.8 mM and then shift upfield at higher concentrations (ESI, Figure S8). Table S1 shows the corresponding $\Delta\delta$ obtained from ca. 0.5 to 25 mM for the different protons of **2a-2c** in D_2O/CD_3OD and $CDCl_3$.

As chirality can play an important role in self-assembly,[20c] the aggregation for the analogous non chiral imidazolium surfactant **3a** was also studied in CD_3OD/D_2O 1/1 v/v (0.3 - 20 mM) (ESI, Table S1, Figure S10). In general, the observed changes in chemical shifts upon concentration were appreciably smaller than for **2a**, indicating a less tight packing in the absence of the amino acid moiety.

Taking into account the former data, Figure 3a shows the change in the chemical shift $\Delta\delta$ as a function of the concentration for the different protons of **2a** in CD_3OD/D_2O 1/1 v/v.[26] It is important to note that when the exchange rate of an amphiphilic molecule between the bulk solution and the aggregates is fast on the NMR time scale, the observed chemical shift (δ_{obs}) can be expressed as a weighted average of the chemical shifts of the monomer (δ_{mon}) and the aggregates (δ_{aggr}).[27] This plot shows two well differentiated areas. Chemical shift changes are very minor below concentration A, while shifts change significantly above this point. Similar graphs were obtained for **2b** and **2c** (ESI, Figure S4).

[26] $\Delta\delta = (\delta_{obs} - \delta_{mon})$, where δ_{mon} (chemical shift for the fully unaggregated monomer) was obtained by extrapolation to zero concentration of the initial values of from the lineal plot of δ_{obs} against concentration.

[27] (a) *^{1}H NMR Studies on Aggregation-Induced Conformational Changes in Linear Alkylbenzenesulfonates;* Goon, P.; Das, S.; Clemett, C. J.; Tiddy, G. J. T.; Kumar, V. V.; *Langmuir* **1997**, *13*, 5577-5582, (b) *Aggregation Behavior of Surface Active Imidazolium Ionic Liquids in Ethylammonium Nitrate: Effect of Alkyl Chain Length, Cations, and Counterions*; Shi, L.; Zheng, L.; *J. Phys. Chem. B.* **2012**, *116*, 2162-2172, (c) *Aggregation behavior of imidazolium-based chiral surfactant in aqueous solution*; Gao, H.; Shi, L.; Zhang, S.; Li, J.; Wang, X.; Zheng, L.; *Colloid Polym Sci* **2013**, *291*, 1077-1084.

This concentration (A) can be assimilated qualitatively with the point at which aggregation starts to be relevant. In a quantitative analysis, representing the changes in chemical shift as a function of the inverse of the concentration facilitates obtaining more accurate values of the critical aggregation concentration (CAC) at the cross point of the two observed straight lines.[27] Figure 3b shows the corresponding graph for the C4-H of **2a** allowing to estimate a value of 3 mM for its CAC in this medium. The full set of graphs for the different protons of compounds **2a-c** in CD_3OD/D_2O 1/1 v/v can be found at the ESI (Figures S10 and S11).

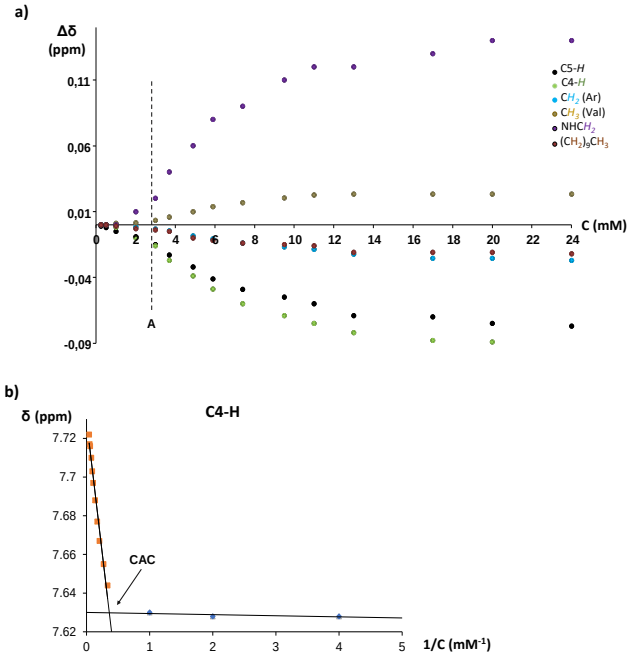

Figure 3. Chemical shifts changes observed with concentration in the ^{1}H NMR of **2a** in CD_3OD/D_2O (1/1 v/v) at 25 ^{o}C: a) Plot of Δδ *vs.* concentration, b) Plot of δ_{obs} *vs.* the inverse of concentration for C4-H.

The CAC values estimated by ^{1}H NMR for **2a-c** in CD_3OD/D_2O 1/1 v/v, assuming that the monomer concentration is constant above the CAC, have been included in Table 1. In all cases, the values were in the mM range (ca. 3-5 mM). Structural changes affected CAC values following the trends qualitatively discussed above. CAC values for **2a** and **2b** (*para*- and *meta*-substitution at the benzene ring) were very similar (≈ 3 mM) while the one for **2c** (*orto*-substitution) was larger (4.5 mM). Compound **3a** lacking the chiral valine derived fragment presented a CAC value even larger (5.3 mM). The presence of some added salt only had a minor effect, although, as expected, slightly reduced the CAC value. It must be noted that structural changes also played a role on the solubility of the aggregates formed. While for **2a** and **2b** some turbidity was observed at

concentrations over 20 mM, for **2c** this started to be present concentrations over 10 mM. It must be noted that CAC values in $CDCl_3$ were slightly lower for compounds **2a-c** (Table 1, entries 6-8), with the lower value displayed by **2b** in this case (1.7 mM) (ESI, Figure S6-S8 and S12).

Table 1. Estimated CAC values obtained in $CHCl_3$ and aqueous media for **2a-c** and **3a** using ^{1}H-NMR, LS and fluorescence studies at 25 ^{o}C.

Entry	Amphiphilic compound	Solvent	CAC NMR[a] (mM)	CAC LS (mM)	CAC Fluorescence[b] (mM)	
					CAC1	CAC2
1	**2a**	CH_3OH/H_2O	3.0	3.1	0.026	3
2	**2b**	CH_3OH/H_2O	3.1	3.1	0.29	2[c]
3	**2c**	CH_3OH/H_2O	4.5	4.8	0.5	
4	**2a**/NEt_4Br (2/1 molar ratio)	CH_3OH/H_2O	2.7	3.4	3.0	
5	**3a**	CH_3OH/H_2O	5.3	--	2	15
6	**2a**	$CHCl_3$	2.3	2.2	--	
7	**2b**	$CHCl_3$	1.7	2.7	--	
8	**2c**	$CHCl_3$	2.2	1.7	--	
9	**2a**	H_2O	--	0.27	0.0075	
10	**2b**	H_2O	--	0.42	0.0098	0.2
11	**2c**	H_2O	--	0.42	0.00069	0.0075
12	**3a**	H_2O	--	--	0.03	
13	**3b**	H_2O	--	--	0.3[b,28]	
14	**SDS**	H_2O	--	--	7.6 [307c]	

[a] Deuterated solvents used for the NMR measurements. CAC values obtained as the average from three different proton signals.
[b] CAC values from the break point at lower concentrations.
[c] A third self-aggregation process is observed starting at 6 mM

Spin-lattice relaxation time (T_1) measurements can be used to monitor mobility of protons. Being sensitive to longitudinal diffusion, T_1 provides information about motions in a wide range of frequencies. Changes in T_1 values for proton signals help to understand the change in the molecular environment and are very sensitive to the aggregation state.[29] Figure 4 shows the variation in longitudinal relaxation times (T_1) with concentration for different protons of **2a**. For all of them, T_1 values decrease at concentrations above 2 mM. This implies the motion of the corresponding fragments is severely limited when increasing

[28] *Nanocarriers from dicationic bis-imidazolium amphiphiles and their interaction with anionic drugs*; Casal-Dujat, L.; Griffiths, P. C.; Rodríguez-Abreu, C.; Solans, C.; Rogere, S.; Pérez-García, L.; *J. Mater. Chem. B* **2013**, 1, 4963-4971.
[29] *^{1}H NMR study on premicellation of quaternary ammonium Gemini surfactants*; Jiang, Y.; Chen, H.; Cui, X-H.; Mao, S-Z.; Liu, M-L.; Luo, P-Y.; Du, Y-R.; *Langmuir* **2008**, *24*, 3118-3121.

the concentration above this value, which agrees well with the observed aggregation process and with the importance of aromatic and imidazolium fragments in the packing of the aggregates as the signals from those fragments are the most affected.

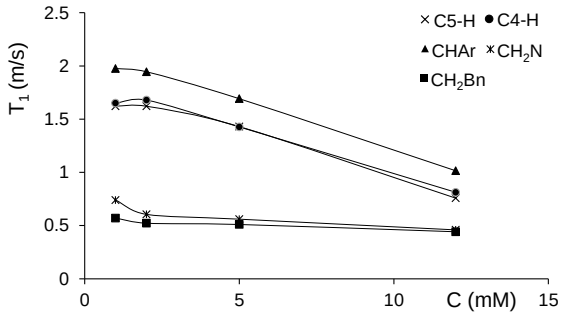

Figure 4. Variations of the longitudinal relaxation times (T_1) of different protons with the surfactant concentrations for **2a** in D_2O/CD_3OD 1/1 v/v at 30 °C.

3.2.2. Fluorescence experiments

The high sensitivity of fluorescence allows exploring the self-assembly at much lower concentrations. Taking into account the environmental effects on the intensity ratio of the fluorescence bands of pyrene, the ratio of the intensity of two of the peaks (I_1/I_3) of the pyrene fluorescence spectrum has been often used to investigate the self-assembly of amphiphilic molecules.[30] Plots of the pyrene I_1/I_3 ratio as a function of the total surfactant concentration show a typical sigmoidal decrease in the region where self-assembly takes place. At low concentrations, this ratio is larger as corresponds to a polar environment for pyrene. When the surfactant concentration increases this ratio decreases rapidly, as the self-assembly favours the location of pyrene in a more hydrophobic environment, until reaching a roughly constant value because of the full incorporation of the probe into the hydrophobic region of the aggregates. Different approaches have been used to estimate CAC and CMC values from I_1/I_3 ratios,[30] and in some instances from the intensity of the excimer band.[31] The most common approach is the use of the break points, either directly or by extrapolating the values from the intersection of the two straight lines defined

[30] (a) *Environmental effects on vibronic band intensities in pyrene monomer fluorescence and their application in studies of micellar systems*; Kalyanasundaram, K.; Thomas, J. K.; *J. Am. Chem. Soc.* **1977**, *99*, 2039-2044, (b) Kalyanasundaram, K. *Photochemistry in Microheterogeneous Systems*, Academic Press, New York, **1987**, (c) *On the determination of the critical micelle concentration by the pyrene 1:3 ratio method*; Aguiar, J.; Carpena, P.; Molina-Bolívar, J. A.; Carnero Ruiz, C.; *J. Colloid Interface Sci.* **2003**, *258*, 116-122.

[31] *Spontaneous vesicle formation and vesicle-to-micelle transition of sodium 2-ketooctanate in water*; Xu, H.; Du, N.; Song, Y.; Song, S.; Hou, W.; *J. Coll. Interf. Sci.* **2018**, *509*, 265–274.

at the constant and variable regions of the I_1/I_3 sigmoidal curve.[30,31,32] As CAC represents the threshold of concentration at which self-aggregation starts, the corresponding value can be estimated from the break point at lower concentration.[33,34]

Fluorescence data revealed some complex patterns for the self-aggregation behavior of compounds **2** in the mixed solvent CH_3OH/H_2O 1/1 v/v (see Table 1 for estimated CAC values). This is illustrated in Figure 5a for the case of **2a**. The plot of the I_1/I_3 ratios *vs* **2a** concentration suggests the presence of two different processes. The first one takes place at the micromolar range (CAC1 = 26 ± 2 μM). The second one is observed at the millimolar range (CAC2 = 3 mM). At concentrations lower than 26 μM (CAC1) I_1/I_3 = 1.66. This value essentially replicates the value of 1.67 obtained for pyrene in the absence of surfactant using this 1/1 v/v mixture of CH_3OH (I_1/I_3 = 1.33) and water (I_1/I_3 = 1.81) and reveals that pyrene is fully exposed to the polar solvent mixture. After the first aggregation step, at concentration around 0.5 mM, this ratio reaches a value of 1.47, suggesting the formation in this region of aggregates in which the probe molecule is partly solvent exposed. At concentrations higher than 3 mM, the I_1/I_3 ratio further decreases to values of 1.3 of lower, compatible with the formation of more ordered spherical aggregates.[35] A similar behavior was presented by **2b**, although the first break point (CAC1) was observed at concentrations one order of magnitude larger (0.29±0.03 mM) (ESI, Figure S13a). However, for **2c** one single break point was observed around 0.5 mM (ESI, Figure S13b), though solubility problems preclude an accurate analysis at concentrations above 9 mM. In the presence of **2a** and 0.5 eq. of Et_4NBr in CH_3OH/H_2O 1/1 v/v the first preaggregation step at the micromolar range was essentially not present, and the only well-defined CAC was observed around 3

---

[32] (a) *Ultrasonic Absorption Studies of Surfactant Exchange between Micelles and Bulk Phase In Aqueous Micellar Solutions of Nonionic Surfactants with Short Alkyl Chains. 1,2-Hexanedlol and 1,2,3-Octanetrlol*; Frindi, M.; Michels, B.; Zana, R.; *J. Phys. Chem.* **1991**, *95*, 4832-4837, (b) *Aggregation Behavior of Tyloxapol, a Nonionic Surfactant Oligomer, in Aqueous Solution*; Regev, O.; Zana, R.; *J. Colloid Interf. Sci.* **1999**, *210*, 8-17.

[33] (a) *Fluorescence Probes for Critical Micellé Concentration*; Ananthapadmanabhan, K. P.; Goddard, E. D.; Turro, N. J.; Kuo, P. L.; *Langmuir* **1985**, *2*, 352-355, (b) *Linolenic acid-modified chitosan for formation of selfassembled nanoparticles*; Liu, C. G.; Desai, K. G. H.; Chen, X. G.; Park, H. J.; *J. Agric. Food Chem.* **2005**, *53*, 437-441, (c) *Preparation and Characterization of Self-Assembled Nanoparticles of Hyaluronic Acid-Deoxycholic Acid Conjugates*; Dong, X.; Liu, C.; *J. Nanomat.* **2010**, Article ID 906936.

[34] *Synthesis and surface-active properties of sulfobetaine-type zwitterionic Gemini surfactants*; Yoshimura, T.; Ichinokawa, T.; Kaji, M.; Esumi, K.; *Colloids Surf. A: Physicochem. Eng. Aspects* **2006**, *273*, 208–212.

[35] *Spontaneously Formed Vesicles of Sodium N-(11-Acrylamidoundecanoyl)-glycinate and L-Alaninate in Water*; Roy, S.; Dey, J.; *Langmuir* **2005**, *21*, 10362-10369.

mM (ESI, Figure S13d,e). The final value of the I_1/I_3 ratio obtained after this aggregation step (1.45) suggests again the formation of aggregates where the probe is solvent exposed.

Interesting differences were observed in pure water, with CAC values significatively lower, which is reasonable for the structures considered.[36] For **2a,** in the μM range, only one single aggregation step was observed displaying a CAC value of 7.5 μM (Figure 5b). Moreover, a broad excimer emission band around 470 nm is observed during this aggregation process. The I_e/I_1 ratio increases continuously at concentrations higher than CAC, reaches a maximum at ca. 0.25 mM and decreases sharply to zero at concentrations where no further change in the the I_1/I_3 ratio is observed (ca. 0.4 mM) (Figure 5c). This has been often associated to the transformation of premicellar aggregates (i.e. vesicles or bilayer structures) into micelles, with the maximum being associate to the CMC.[31,37] The low micropolarity experienced by the probe after completion of this aggregation process (I_1/I_3 < 1) suggests the formation of strongly ordered spherical aggregates compatible with the formation of vesicles.[35] On the contrary, for **2b** the observed CAC was 9.8 μM, with the micropolarity of these initial aggregates being higher (I_1/I_3 > 1.3) and an additional aggregation process developing at concentrations above 0.2 mM (ESI, Figure S14a). A two steps aggregation was clearly visible for **2c** with the first break point at 0.69 μM leading to aggregates with an appreciable solvent exposed probe (I_1/I_3 > 1.3) and the second process starting at ca. 1 μM affording aggregates providing a low polarity microenvironment to pyrene (I_1/I_3 ≈ 1) (ESI, Figure S14a).

According to the former, the substitution pattern at the central aromatic spacer is important in defining the aggregation behavior of compounds **2**. The *para*-substituted compound (**2a**) provides the best-defined self-assembly processes, taking place in water at the μM region. For comparison, compound **3a** lacking

---

[36] (a) *Effect of Ethanol on the Aggregation Properties of Cetyltrimethylammonium Bromide Surfactant*; Li, W.; Han, Y.-C.; Zhang, J.-L.; Wang, B.-G.; *Colloid J.* **2005**, *67*, 159-163, (b) *Fluorescence Probe Study of Oil-In-Water Microemulsions. 1. Effect of Pentanol and Dodecane or Toluene on Some Properties of Sodium Dodecyl Sulfate Micelles*; Llanos, P.; Lang, J.; Strazlelle, C.; Zana, R.; *J. Phys. Chem.* **1982**, *86*, 1019-1025.

[37] (a) *Thermodynamically stable vesicle formation and vesicle-to-micelle transition of single-tailed anionic surfactant in water*; Sakai, T.; Ikoshi, R.; Toshida, N.; Kagaya, M.; *J. Phys. Chem. B* **2013**, *117*, 5081-5089, (b) *Strong effect of NaBr on self-assembly of quaternary ammonium Gemini surfactants at air/water interface and in aqueous solution studied by surface tension and fluorescence techniques*; You, Y.; Zhao, J.; Jiang, R.; Cao, J.; *Colloid Polym. Sci.* **2009**, *287*, 839–846, (c) *Fluorescence Emission of Pyrene in Surfactant Solutions*; Piñeiro, L.; Novo, M.; Al-Souf, W.; *Adv. Colloid Interface Sci.* **2015**, *215*, 1-12.

the amino acid moiety was also studied (Table 1, entries 5 and 12; ESI, Figures S13c, S14b) confirming the importance of this fragment, as the CAC values in both media were one order of magnitude higher than for **2a**. In the mixed solvent, CAC values estimated by NMR are in the same range than one of the values obtained by fluorescence for **2a**, **2b** and **3a**, but not for **2c**. Nevertheless, it is worth mentioning that important differences are sometimes found when such parameters are calculated using different techniques,[38] and that deuterated solvents can also influence them.[39]

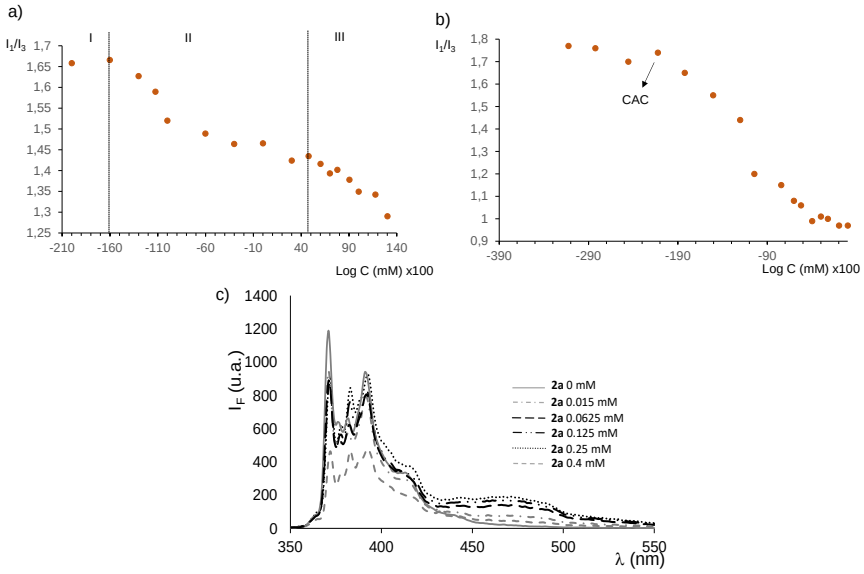

Figure 5. a) Plot of the I_1/I_3 ratio *vs.* log C for **2a** in CH_3OH/H_2O (1:1, v/v) at 25 ºC, b) Plot of the I_1/I_3 ratio *vs.* log C for **2a** in H_2O at 25 ºC, c) Emission spectra of pyrene in H_2O in the presence of different amounts of **2a**.

3.2.3 Light scattering (LS) experiments

LS intensity measurements were also used to study CAC and the hydrodynamic size distributions of the aggregates. Experiments were performed on **2a-c** in CH_3OH/H_2O 1/1 v/v and in $CHCl_3$ within the 0.1 - 6 mM concentration range at 25 ºC. LS experiments at lower concentrations could not be achieved properly. The measured scattering intensity is expected to increase with the size and number of the aggregates formed. Their apparent hydrodynamic diameters D_h can be deduced from the diffusion coefficients. These coefficients are influenced

[38] *Discrepancies over the onset of surfactant monomer aggregation interpreted by fluorescence, conductivity and surface tension methods*; Costa, M. F. C.; Froehner, S. J.; Ruzza, A. A.; Santos, S.; Zanette, D.; *Química Nova* **1998**, *21*, 1678-7064.
[39] *Didodecyldimethylammonium Bromide Vesicles and Lamellar Liquid Crystals. A Multinuclear NMR and Optical Microscopy Study*; Caboi, F.; Monduzzi, M.; *Langmuir* **1996**, *12*, 3548-3556.

by the repulsion among the highly charged aggregates,[40] and, therefore, the apparent average size determined from LS can differ from that observed by the optical microscopy or SEM. In general, the estimated CAC values (CAC_{LS}) were in good agreement with those from NMR (CAC_{NMR}) and fluorescence (CAC_{fluor}) studies (Table 1).

Figure 6 shows the results obtained for **2a-c** in H_2O/CH_3OH 1/1 v/v. For **2a**, the hydrodynamic diameter increases slightly with concentration from 400 to 450 nm. The total intensity of the scattered light initially increases almost linearly with concentration, at low surfactant concentration. This constant slope suggests an increase in the number of aggregates, keeping their size constant and indicates, as confirmed by hydrodynamic diameter data, the formation of aggregates at lower concentrations. A maximum of intensity is reached at ca. 3 mM and then intensity decreases until *ca.* 5 mM. Above this concentration, changes in intensity are minor. This trend can be interpreted as the progressive transformation of one type of aggregate structure into a second one being more uniform and much less in number density than the former one.[41] For **2b** the hydrodynamic size initially increased with concentration (from 360 to 475 nm) and then decreased (from 450 nm to 320 nm), showing a maximal apparent average diameter of 475 nm at 3.0 mM. The intensity of the scattered light also increased linearly with concentration at low surfactant concentration but, after the maximum at ca. 3.0 mM, decreased until nearly zero. This process, again in agreement with fluorescence data for this region, is comparable with the one for **2a**, although the transformation affords aggregates with a lower apparent average diameter. In both cases, CAC_{NMR} and CAC_{fluor} values were in this concentration range. As in other techniques, amphiphilic compound **2c** behaves differently. The hydrodynamic diameter increases slightly with concentration from 280 to 325 nm. The LS intensity monotonically increases with increasing concentration and shows a slope change at ca. 4.5 mM, close to the CAC_{NMR},

---

[40] (a) *Dynamic light scattering from cetyltrimethylammonium bromide micelles. Intermicellar interactions at low ionic strengths*; Dorshow, R.; Briggs, J.; Bunton, C. A.; Nicoli, D. F.; *J. Phys. Chem.* **1982**, *86*, 2388–2395, (b) *Comparative study of intermicellar interactions using dynamic light scattering*; Dorshow, R. B.; Bunton, C. A.; Nicoli, D. F.; *J. Phys. Chem.* **1983**, *87*, 1409-1416, (c) *Dynamic light scattering study of a micellar system of low fractional ionization: cetyltrimethylammonium sulfate $(CTA)_2SO_4$ + sodium sulfate*; Biresaw, G.; McKenzie, D. C.; Bunton, C. A.; Nicoli, D. F.; Nicoli, D.; *J. Phys. Chem.* **1985**, *89*, 5144-5146.

[41] (a) *Structural Transitions in a Bicationic Amphiphile System Studied by Light-Scattering, Conductivity, and Surface Tension Measurements*; Viseu, M. I.; Velazquez, M. M.; Campos, C. S.; Garcıa-Mateos, I.; Costa, S. M. B.; *Langmuir* **2000**, *16*, 4882-4889, (b) *Spontaneous Vesicles Formed in Aqueous Mixtures of Two Cationic Amphiphiles*; Viseu, M. I.; Edwards, K.; Campos, C. S.; Costa, S. M. B.; *Langmuir* **2000**, *16*, 2105-2114.

indicating the possible transition between two different types of aggregate with an increase in number and size.

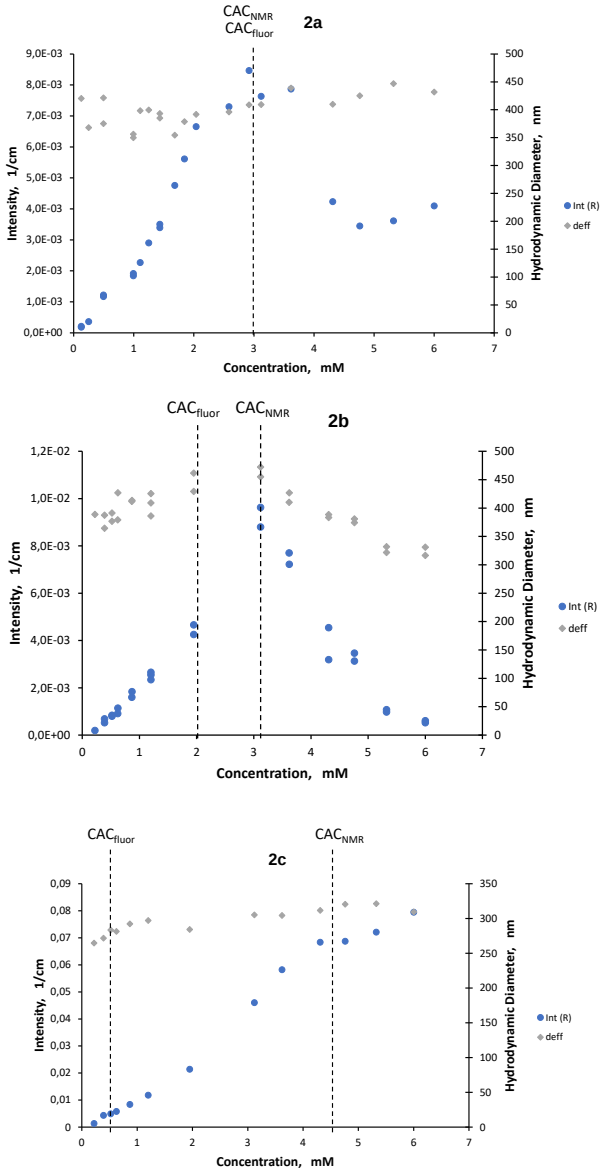

Figure 6. Hydrodynamic diameter (grey diamonds, right axes) and intensity of the scattered light in absolute units (1/cm) (blue circles, left axes) obtained with LS for **2a-c** in CH_3OH/H_2O 1/1 v/v and presented as a function of the **2a-c** concentration.

LS results show that the apparent average diameter of the aggregates in the concentration range studied qualitatively follows the order **2c**<**2b**≈**2a**. As mentioned above, the particle average diameter increases slightly with concentration for **2a** and **2c**, while the dependence for **2b** has a maximum. This suggests that aggregates formed by **2a** and **2c** molecules is better organized and steady than those from **2b**. At the studied concentration range, the different

hydrodynamic diameters estimated are big for all compounds, indicating the presence of large aggregates in solution.[42,43]

LS experiments were also run for **2a** in the presence of 0.5 eq. of Et_4NBr in CH_3OH/H_2O 1/1 v/v. The intensity of the scattered light followed a similar pattern than in its absence, displaying a maximum at ca. 3 mM, although the apparent average diameter over this concentration was higher (ESI, Figure S15).[44] As mentioned above, addition of salts causes the reduction of electrostatic repulsion among the surfactant head-groups and is a key factor to influence the morphology of aggregates in ionic surfactant solutions.

When LS experiments were run in H_2O for **2a-c** from 0.05 to 0.6 mM, the hydrodynamic diameter obtained for the aggregates was essentially constant and slightly higher than the ones observed in CH_3OH/H_2O 1/1 v/v, following the order (**2a > 2b ≈ 2c**). For **2a**: the intensity of the scattered light initially increased with the concentration reaching a maximum at 0.27 mM, in the region related to the second process observed by fluorescence, and then decreased. On the contrary, for **2b** and **2c** the intensity increased with concentration though observing a slope change at the concentration range related to the same second process (ESI, Figure S16).

In the case $CHCl_3$, LS experiments were carried out from 0.3 to 6 mM (Figure S17). For **2a** the hydrodynamic diameter of the aggregates constantly increased with the concentration up to ca. 50 nm at 2 mM and then sharply became larger, remaining constant (ca. 425 nm) above 2.2 mM. The intensity of the scattered light increases continuously with concentration, but a sharp discontinuity was also observed at a concentration close to that of CAC_{NMR} (2.3 mM). For **2b**, the hydrodynamic diameter estimated for the aggregates remained constant from 1 to 6 mM (ca. 701 nm), whilst the intensity of the scattered light decreased with the concentration showing a slope change at around 2 mM (CAC_{NMR} = 1.7 mM). For **2c**, the average particle size increased initially with concentration (from ca.

---

[42] *Surface Tension and Aggregation Properties of Novel Cationic Gemini Surfactants with Diethylammonium Headgroups and a Diamido Spacer*; Zhang, Q.; Xu, Z. G. F.; Tai, S.; Liu, X.; Mo, S.; Niu, F.; *Langmuir* **2012**, *2833*, 11979-11987.

[43] (a) *Formation of Polymerlike Mixed Micelles and Vesicles in Lecithin-Bile Salt Solutions: A Small-Angle Neutron-Scattering Study*; Pedersen, J. S.; Egelhaaf, S. U.; Schurtenberger, P.; J. *Phys. Chem.* **1995**, *994*, 1299-1305, (b) *Synthesis and properties of novel ester-containing Gemini imidazolium surfactants*; Zhuang, L-H.; Yu, K-H.; Wang, G-W.; Yao, C.; *J. Colloid Interface Sci.* **2013**, *408*, 94-100.

[44] *Cationic vesicles of a carnitine-derived single-tailed surfactant:Physicochemical characterization and evaluation of in vitro genetransfection efficiency*; Patra, T.; Ghosh, S.; Dey, J.; *J. Colloid Interface Sci.* **2014**, *436*, 138-145.

500 to 700 nm) and then experienced a sudden change around 1.8 mM (CAC_{NMR} = 2.2), being then constant from 2 to 6 mM (ca. 356 nm). The intensity of the scattered light increased continuously for all the concentration range studied, showing again a slope change at 1.8 mM.

3.2.4 UV-Vis and CD studies

The presence of the chiral fragment derived from *L*-valine in the structure of compounds **2** allows their study by Circular Dichroism (CD), a technique that is very sensible to conformational changes in chiral molecules and has been very useful in the study of amino acid derived molecules.[45] The UV-visible spectrum of **2a** in $CHCl_3$ is characterized by two bands (ESI, Figure 7a). The first one is more intense and displays a maximum at ca. 240 nm and must contain contributions from π–π* and n-π* transitions of the amide chromophore. The position of this amide band is significantly red shifted in comparison with the average positions observed in peptides and other amides,[46] including short and charged peptidic and pseudopeptidic structures.[8e,47,48,49,50] This must be attributed to the influence of the imidazolium rings. The second band, less intense and with the fine structure partly observed, appears in the 255-280 nm region and is associated to the substituted benzene ring of the spacer. CD spectroscopy provides two sets of important information. Changes in the CD spectral pattern can be used to identify conformational changes taking place upon aggregation. On the other hand, changes in the intensity of the bands (molar ellipticity) are often associated to the degree of chiral ordering, the so-

[45] (a) Berova, N.; Ellestad, G. A.; Harada, N. *Modern Methods in Natural Product Chemistry: Characterization by Circular Dichroism Spectroscopy, In Comprehensive Natural Products II Chemistry and Biology*; Mander, L., Lui, H.-W, Eds.; Elsevier: Oxford, **2010**, vol. 9, pp. 91-147, (b) Berova, N.; Harada, N.; Nakanishi, K. *Exciton Coupling, In Encyclopedia of Spectroscopy and Spectrometry*; Lindon, J. C.; Tranter, G. E.; Koppenaal, D. W. Eds.; 3rd Edition, Academic Press: **2017**, pp. 539-557, (c) Banerjee, B.; Misra, G.; Ashraf, M. T. *Circular dichroism, In Data Processing Handbook for Complex Biological Data Sources*; G. Misra, Ed.; Academic Press: **2019**, pp. 21-30, (d) *Using circular dichroism spectra to estimate protein secondary structure*; Greenfield, N. J.; *Nat. Protoc.* **2006**, *1*, 2876-2890.

[46] (a) *The Absorption Spectra of Simple Amides and Peptides*; Nielsen, E. B.; Schellman, J. A.; *J. Phys. Chem.* **1967**, *71* (7), 2297–2304, (b) *Rotatory Properties of Molecules Containing Two Peptide Groups: Experimental and Theoretical Results*; Nielsen, E. B.; Schellman, J. A.; *Biopolymers* **1971**, *10*, 1559-1581.

[47] *Water-Mediated Electronic Structure of Oligopeptides Probed by Their UV Circular Dichroism, Absorption Spectra, and Time-Dependent DFT Calculations*; Kumar, A.; Toal, S. E.; DiGuiseppi, D.; Schweitzer-Stenner, R.; Wong, B. M.; *J. Phys. Chem. B* **2020**, *124*, 2579−2590.

[48] *Tuning the Handedness: Role of Chiral Component in Peptide-Appended Bolaamphiphile-Based Coassembled Hydrogels*; Biswas, S.; Das, A. K.; *Langmuir* **2019**, *35*, 2383−2391.

[49] *Aggregation behavior of a Gemini surfactant with a tripeptide spacer*; Wang, M.; Han, Y.; Qiao, F.; Wang, Y.; *Soft Matter* **2015**, *11*, 1517–1524.

[50] *Self-Assembly of Aβ-Based Peptide Amphiphiles with Double Hydrophobic Chains*; He, C.; Han, Y.; Fan, Y.; Deng, M.; Wang, Y.; *Langmuir* **2012**, *28*, 3391-3396.

called super asymmetry, in the assemblies formed. Thus, for instance, an enhancement of CD signals is often observed for fibrillar aggregates hierarchically organized into helical assemblies, as found for some gelator systems.[49,50,51] On the contrary, the aggregation into low-order assemblies not displaying chiral superstructures if associated to a decrease in the intensity of the corresponding CD signals.[52,53,54]

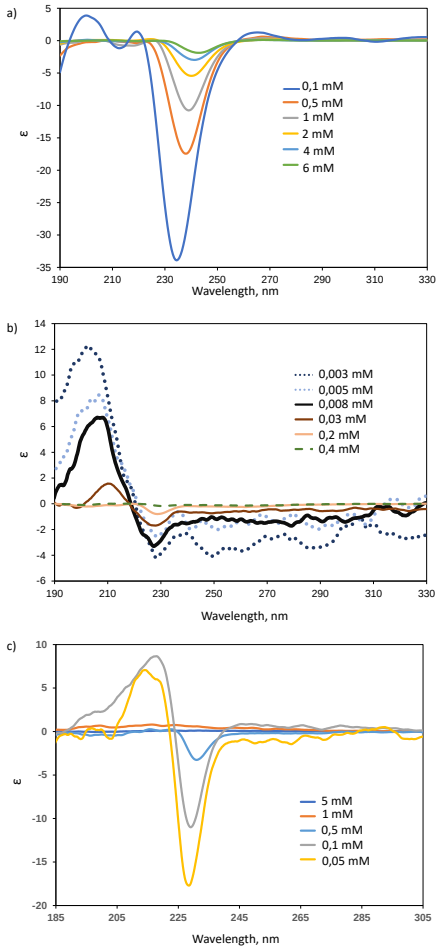

Figure 7. Partial CD spectra for **2a** a) in $CHCl_3$, b) in H_2O and c) H_2O/CH_3OH 1/1 v/v in at different concentrations.

---

51 *Exploring the thermal reversibility and tunability of a low molecular weight gelator using vibrational and electronic spectroscopy and rheology*; DiGuiseppi, D.; Thursch, L.; Alvarez, N. J.; Schweitzer-Stenner, R.; *Soft Matter* **2019**, *15*, 3418-3431.

52 (a) *Light Scattering and Cryo-Transmission Electron Microscopy Investigation of the Self-Assembling Behavior of Di-C12P-Nucleosides in Solution*; Bombelli, F. B.; Berti, D.; Almgren, M.; Karlsson, G.; Baglioni, P.; *J. Phys. Chem. B* **2006**, *110*, 17627-17637, (b) *Chiroptical Aggregates from Block Copolymer Bearing Amino Acid Moieties in Aqueous Solution*; Zhao, F.; Liu, Z.; Feng, L.; Sun, J.; Hu, J.; *J. of Polymer Sci.: Part B: Polymer Physics* **2009**, *47*, 1345-1355.

53 *Evaluation of Molecular Ordering in Bicelle Bilayer Membranes Based on Induced Circular Dichroism Spectra*; Suga, K.; Kitagawa, K.; Taguchi, S.; Okamoto, Y.; Umakoshi, H.; *Langmuir* **2020**, *36*, 3242−3250.

54 *Temperature-Dependent Reversible Morphological Transformations in N-Oleoyl α-D-Galactopyranosylamine*; Johnson, M.; Bhattacharya, A.; Brea, R. J.; Podolsky, K. A.; Devaraj, N. K.; *J. Phys. Chem. B* **2020**, *124*, 5426-5433.

Compound **2a** in CCl_3 displays at low concentrations (0.1 mM) and intense negative CD signal ($\Delta\varepsilon$ = -34) at 237 nm related to the red-shifted amide band observed in UV at 239 nm. This CD pattern can be associated to the presence of extended conformations for the amide group related to those found in random coils or pPII (polyproline) conformations in peptides.[45,46,55] No conformational changes are detected upon increasing the concentration (Figure 7a), even above the estimated CAC values, but the intensity of the signal significantly decreases ($\Delta\varepsilon$ = -2.8 for 6 mM). According to NMR data, aggregation in this solvent is mainly associated to intermolecular coulombic and hydrogen bonding interactions, and must occur leading to low order aggregates (as confirmed by SEM, see below) maintaining a strong solvation of the aliphatic tails by the apolar solvent. A small red shift (7 nm) is detected that can be associated to the location of additional aliphatic tails in the environment of the amide functions in the aggregates.[47]

In water, the UV-Vis spectra are characterized again by two bands, although the one corresponding to the aromatic chromophore lacks a fine structure (Figure 7b). Both bands are appreciably blue shifted as compared with the spectrum in chloroform under similar conditions ($\Delta\lambda \approx$ -16 nm). Blue shifts are usually reported for n-π^* transitions of amides when changing the solvent from apolar to polar.[46] The amide band experiences a ca. 20 nm blue shift when increasing the concentration, while the opposite is found for the aromatic band. This agrees with the location of the molecule in a more apolar environment in the aggregates formed. The CD spectrum at concentrations below the first CAC detected by fluorescence (< 10 μM) shows a relatively intense positive band ($\Delta\varepsilon$ = 12) at a position very close to that of the maximum of the amide UV absorption band (ca. 205 nm) but also a much weaker negative CD band centered around 230 nm ($\lambda_{zero} \approx$ 220 nm, Figure 7b). In water, it is expected that molecules like **2a** will adopt folded conformations in order to minimize the solvent exposed surface of the hydrophobic regions. In such conformations, a *trans* disposition of the amide groups seems to predominate, giving place to a CD pattern similar to that found in antiparallel β-sheet arrangements in proteins.[45] During the aggregation process detected by fluorescence (CAC = 8 μM), the intensity of both bands

[55] (a) *The Circular Dichroism Spectrum and Structure of Unordered Polypeptides and Proteins*; Krimm, S.; Tiffany, M. L.; *Isr. J. Chem.,* **1974**, *12*, 189-200, (b) *Polyproline-II Helix in Proteins: Structure and Function*; Adzhubei, A. A.; Sternberg, M. J. E.; Makarov, A. A.; *J. Mol. Biol.* **2013**, *425*, 2100–2132.

decreases, indicating the formation of low-order assemblies, but this effect is more relevant for the (+) CD band. The red shift observed in both bands at increasing concentrations is also more important for the positive band. Finally, after the finalization of this process (CAC = 0.3-0.4 mM) both CD signals are essentially lost.

The CD spectra of **2a** in $CHCl_3$ and CH_3OH/H_2O 1/1 v/v showed an intense negative peak at ca. 235 nm below CAC, that decreases and shift to higher wavelength upon aggregation (Figure 7c).

In the mixed solvent (CH_3OH/H_2O 1/1 v/v) the observed wavelengths for **2a**, both in UV-Vis and CD spectra, are, as expected, intermediate between those in pure water and those in $CHCl_3$. CD spectra (Figure 7c) at low concentrations show again a negatively biased bisigned signal with the maximum centred around 215 nm and the more intense negative extreme appearing at ca. 230 nm. The higher intensity of the negative component suggests the coexistence of extended and folded conformations. At concentrations above CAC1, the rotational strength of the CD signals decreases that finally disappear at the end of this aggregation process ([**2a**] > 0.5 mM). It is interesting to note that at 0.5 mM only the negative CD band is observed, which suggests that folded conformations are preferentially incorporated into low-order aggregates. At the concentrations related to the second process detected by fluorescence or LS, the CD spectrum is fully silent, indicating that this change is not accompanied by further conformational changes. Thus, it is to be attributed, most likely, to processes involving morphological changes in the aggregates that could include their fusion or crosslinking.[522,53] Only minimal changes were observed when the same study was carried out in the presence of Et_4NBr (ESI, Figure S18). Similar trends were observed for compounds **2b** and **2c** in the different solvents (ESI, Figure S19).

3.2.5 SEM and optical microscopy studies

The morphology of the aggregates formed was also studied by optical microscopy and SEM. Optical microscopy allowed to observe for all the bisimidazolium pseudopeptides **2a**-**c** the formation of spherical aggregates (vesicles) in water at mM concentrations (well above CAC2 in this medium). In the case of **2a**, in water, Figure 8a shows that spherical aggregates (vesicles) were formed by **2a** in H_2O/CH_3OH 1/1 v/v at concentrations above CAC2 (20 mM). Vesicle sizes range from 1 to 3 μm. In the presence of 1 eq. of $BrNEt_4$ the aggregates increase

in size (2-4 μm) (Figure 8b).[56] The formation of vesicles could also be easily monitored under fluorescence optical microscopy (1% fluorescein) as this fluorescent probe was efficiently incorporated the aggregates (Figure S20). Moreover, distorted spherical aggregates (< 0.4 μm) were observed by SEM when using $CHCl_3$ as solvent (ESI, Figure S21).

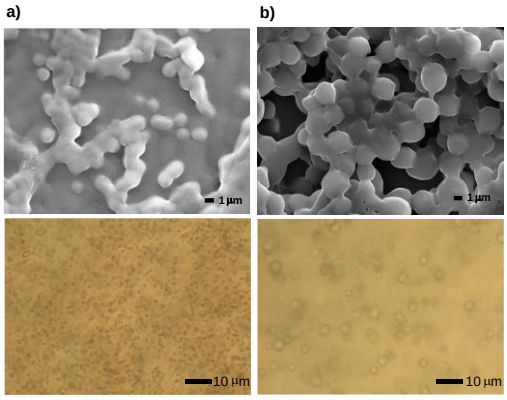

Figure 8. Optical microscopy (bottom) and SEM (top) images for **2a** (20 mM in H_2O/CH_3OH 1/1) in the absence (a) and in the presence (b) of 1 eq. of $BrNEt_4$.

Usually, surfactants first form small aggregates at low concentrations, then the aggregates become larger with the increase of the surfactant concentration. However, the results obtained above confirms the existence of different type of large aggregates in solution. Furthermore, the supramolecular arrangement at concentrations higher than CC in aqueous media can be explained by the existence of hydrophilic/lipophilic, electrostatic, van der Waals and H-bonding interactions between the surfactant molecules in a bilayer arrangement (Figure 9a). The first region on either side of the bilayer is the hydrophilic head-group formed by the imidazolium group and hence, this portion of the membrane is completely hydrated and facing toward the inner aqueous core of the aggregate. Near to the hydrated region is an intermediate region having polar amide groups. It can be assumed that the NH group may be involved in intermolecular H-bonding with neighboring molecules.[45]

Moreover, it has been described the formation of cross-linked vesicles associated to configuration change from trans into the *cis* configuration involving the

[56] (a) *Synthesis and physiochemical properties of novel Gemini surfactants with phenyl-1,4-bis(carbamoylmethyl) spacer*; Wang, L.; Zhang, Y.; Ding, L.; Liu, J.; Zhao, B.; Deng, Q.; Yan, T.; *RSC Adv.* **2015**, *5*, 74764-74773, (b) *Synthesis, physiochemical property and antibacterial activity of Gemini quaternary ammonium salts with a rigid spacer*; Fu, S. Q.; Guo, J. W.; Zhong, X.; Yang, Z.; Lai, X. F.; *RSC Adv.* **2016**, *6*, 16507-16515.

spacer group.[45a] The *trans* configuration causes the formation of vesicles network as is observed for more concentrated solutions (Figure 9b).

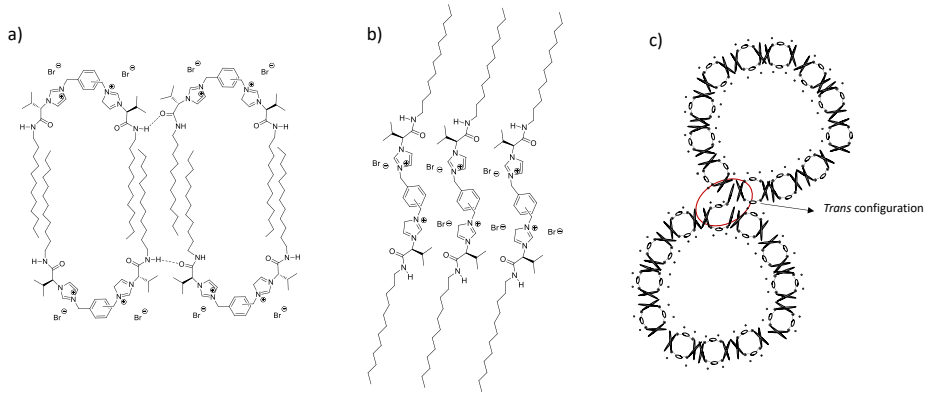

Figure 9. a) Schematic representation of spherical self-aggregation between different surfactant molecules in water; b) Schematic representation of self-aggregation between different surfactant molecules in $CHCl_3$, c) Schematic representation of cross-linked vesicles by *trans* configurations involving the methylene groups of the spacer.

3.3 Emulsification and controlled release studies

3.3.1 Stability of water emulsions

The stability of emulsions generated using compound **2a** in different water mixtures were studied visually and by UV-Vis spectroscopy at a determined frequency of 600 cm^{-1}.[57] Therefore, compound **2a** was studied as surfactant using different O/W emulsions (water/1-methyl-THF (20%), water/methyl laureate (1%) and water/hexane (20%)) and the stability of these emulsions were compared using the analogous non-chiral Gemini surfactant **3a** and the commercial surfactant SDS, the concentration of surfactants was fixed to 1 mM, and all surfactants have an hydrophilic character, tend to be water soluble.[58]

As can be observed in Figure S22, the stability of the different o/w emulsions at 25 ^{o}C in the presence of surfactant **2a** were higher than when **3a** or SDS were used. Water/ methyl laureate (1%) emulsions were stable until 11 days when **2a** was used while using SDS the emulsion is broken after 2 days (Figure S22a and Figure S23). Moreover, for water/hexane (20%), surfactants SDS and **3a** were not able to form emulsions, observing two phases all the time while a stable

[57] (a) Monitoring particle aggregation processes; Gregory, J.; *Adv. in Colloid and Interf. Sci.* **2009**, *147–148*, 109–123, (b) *Controlled and Reversible Aggregation of Biotinylated Gold Nanoparticles with Streptavidin*; Aslan, K; Luhrs, C. C.; Pérez-Luna, V. H.; *J. Phys. Chem. B,* **2004**, *108*, 15631–15639.
[58] *Classification of Surface-Active Agents by "HLB"*; Griffin, W. C.; *J. Cosmetic Sci.* **1949**, *1*, 311-326.

emulsion was observed using **2a** until 15 min (Figure S22c). The optical images for the hexane emulsion using **2a** showed the formation of a multiple emulsion w/o/w (Figure S24).[59] Finally, for water/methyl-THF (20%) the stability of the emulsion containing **2a** as surfactant was longer-time (Figure S22b and S25). All the emulsions underwent creaming with time as is observed in Figure S22 and all the emulsions could be recovered after sacking.

The stability of water/Me-THF and methyl laureate emulsions were also studied by UV-vis measuring the absorbance at 600 cm^{-1} at 25ºC. As is shown in Figure S22e the stability of the water/Me-THF were three times longer time when **2a** were used instead of **3a** and SDS. The stability of the methyl laureate emulsions in the presence of **2a** or **3a** were similar (> 90 hr) and higher than when SDS (< 24 hr) was used (Figure S22d). As previously stated, one of the drawbacks of some naturally occurring surfactants is their low long-term stability, specially under non-natural stress inputs, such high temperatures or extreme pH values. We decided to test the stability of the water/Me-THF emulsion at 40 ºC, as can be seen in Figure S26 big differences in the stability of the emulsions were observed decreasing in all cases at 40ºC.

3.3.2 Controlled release studies

In order to understand better the different Gemini amphiphilic aggregates formed in ethanolic solutions, controlled release studies of volatiles were run, using (*R*)-limonene as model fragrance. Thus first a 10% of (*R*)-limonene (b.p. 176 ºC) in 5 mL of H_2O/EtOH 1/1 v/v using 3.5 mM of the different surfactants **2a**, **3a** and **SDS** at 30ºC was used.[60] The release active substance was entrapped on a toluene solution containing acetophenone as internal standard (Figure 10c) and was followed by GC (ESI Figure S28). In Figure 10a is shown the release profile for (*S*)-Limonene in the absence (blank) and presence of surfactants, following the release rate the order **blank** >**SDS**>**3a**>**2a**. Thus, in the absence of surfactant, a 50% of limonene release was observed after 3hr, while in the presence of surfactants the release of ca. 50% of the limonene was observed after 4.5h, 5h and 6hr for SDS, **3a** and **2a** respectively. Furthermore, while the release rate is constant in the absence of surfactant (blank), as observed in

[59] *Some Stability Criteria for Double Emulsions*; Ficheux, M.-F.; Bonakdar, L.; Leal-Calderon, F.; Bibette, J.; *Langmuir* **1998**, *14*, 2702-2706.
[60] *Controlled Release of Volatile Fragrance Molecules from PEO-b-PPO-b-PEO Block Copolymer Micelles in Ethanol-Water Mixtures*; Berthier, D. L.; Schmidt, I.; Fieber, W.; Schatz, C.; Furrer, A.; Wong, K.; Lecommandoux, S.; *Langmuir* **2010**, *26*, 7953–7961.

Figure 10a in the presence of SDS, **2a** and **3a** two disappearance rates of limonene are present, below ca. 4 hr the realized rate was slower than over 4 hr, the first fragrance release curve could be associated to the release of limonene mostly entrapped inside the aggregates, while the second fragrance release curve could indicates the release of limonene due the emulsion bleakness. Images of the emulsion containing surfactant **2a** at ca. 2h and 5h are shown (inset in Figure 10a) observing at 5hr separation of two phases. It has to be highlighted that the ethanol is evaporated together with the fragrance (^{1}H NMR of the emulsion at 0 hr and 5 hr showed the disappearance of ethanol, Figure S29, ESI),[61] thus the properties of the continuous phase in the emulsion is changing and this can favor the separation of the two phases.

Assuming that the release of (*R*)-Limonene from the micelles over time follows zero-order kinetics, the sets of data points in Figure 10 in the first part of the fragrance release curve were fitted to Eq. (1)

$$Q = Kt \quad (1)$$

Where Q is % of the limonene released, at a time t and k is the zero-order constant, values are given in Table 3.

We compare the responsiveness of (*R*)-Limonene control release using the different Gemini surfactants **2a-c** for a 3.5 mM surfactant concentration, in order to understand better the different aggregates formed in the ethanolic emulsions (Figure S30). In the presence of **2a** and **2b**, a 20% of limonene release was observed up to 4hr, while the release was slightly higher using surfactant **2c** (30%). In table 3 kinetic release rate constants are shown, using data for the first part of the fragrance release curve, following the release rate the order **2b<2a<2c**.

[61] *Investigation of the Release of Bioactive Volatiles from Amphiphilic Multiarm Star-Block Copolymers by Thermogravimetry and Dynamic Headspace Analysis*; Ternat, C.; Ouali, L.; Sommer, H.; Fieber, W.; Velazco, M. I.; Plummer, C. J. G.; Kreutzer, G.; Klok, H-A.; Manson, J-A. E.; Herrmann, A.; *Macromolecules* **2008**, *41*, 7079-7089.

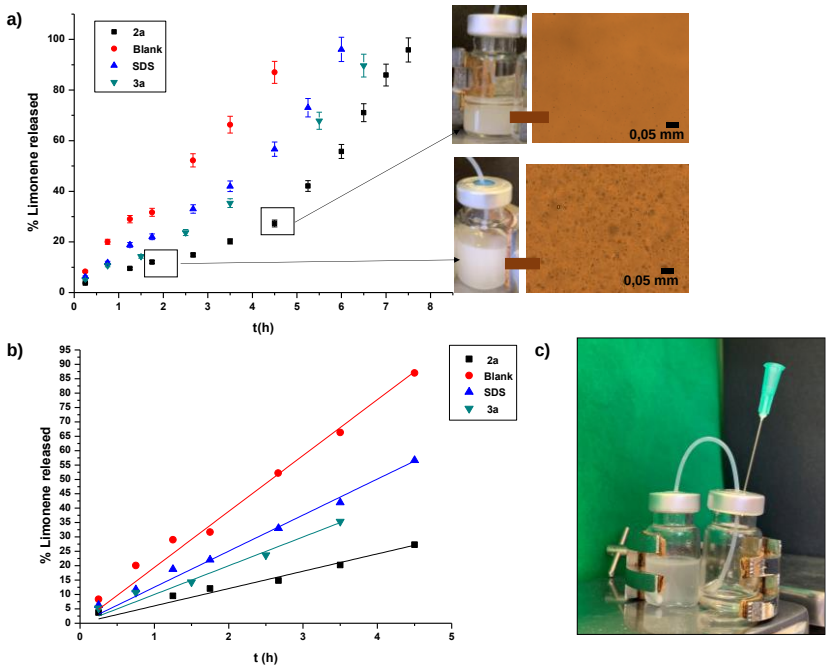

Figure 10. (*R*)-Limonene realise studies in water/ethanol 1/1 at 30ºC. a) (*R*)-Limonene realise profile in the absence and presence of different surfactants (surfactant concentration 3.5 mM). b) Values for the best-fit evaporation rates (slopes) are the lines of the plots, values are given in Table 3. c) System used. Data points represent averages of two samples.

As mention above, some naturally occurring surfactants display low long-term stability under extreme pH values. Thus, the effect of the pH was also studied for **2a** ethanoic emulsion by addition of either HCl or NaOH to the pre-formed emulsions. As can be shown in Figure S30a, at pH 3 and pH 12 after 4 h, the release profile was similar, however up to 4hr the release in acid and basic media decreases. This could be related with an increase of the ionic straight in the medium stabilizing the aggregates, concluding that the emulsions remained stable up to 6 hr in strong acidic and basic media.

The controlled release responsiveness studies toward a biochemically meaningful stimulus was also studied. After adding 1.5 mg mL^{-1} of thermolysin to our emulsions, we observed that this protease was able to destroy the emulsions leading to a faster limonene realise (ESI Figure S30b).

We studied the controlled release responsiveness of (*R*)-Limonene using 15 mM of surfactants **2a**, **3a** and **SDS** (concentration used over the CAC of **3a**). The release rate of (*R*)-Limonene decreases in all the cases, comparing with the data obtained at 3.5 mM (Figure S31), thus the release of around 50% of the limonene

was observed after ca. 5.5h, 6.5h and 9hr for SDS, **3a** and **2a** respectively. Furthermore, a release lag time was observed in all the cases.

Finally, we studied the controlled release responsiveness of (*R*)-Limonene using 1 mM of surfactants **2a** in water (Figure S32). A constant release was observed during all the period time studied, being the rate kinetic constant lower than when using EtOH/H_2O 1/1 v/v (table 3).

Table 3. Release rate kinetic constants for an emulsion containing 10% of (*R*)-limonene in 5 mL EtOH/H_2O 1/1 v/v at 30ºC using a surfactant concentration of 3.5 mM

	Surfactant					
	None	**SDS**	**3a**	**2a**	**2b**	**2c**
k **(h^{-1})**	19.06 (R^2 0.989)	12.53 (R^2 0.985)	9.99 (R^2 0.982)	6.03 (R^2 0.961) 4.16 (R^2 0.992) (pH 3) 5.54 (R^2 0.977) (pH 12) 15.08 (R^2 0.973) (termolisin)	5.17 (R^2 0.973)	8.53 (R^2 0.99)
k **(h^{-1})**[a]		7.20 (R^2 0.99) L=0.44 h	6.53 (R^2 0.973) L= 0.6hr	4.32 (R^2 0.97) L= 1h		
k **(h^{-1})**[c]				2.92 (R^2 0.984) L= 0h		

[a] Surfactant concentration 15 mM. [c] Surfactant concentration 1 mM in pure water

4. Conclusions

Imidazolium *L*-valine Gemini amphiphilic compounds have been synthetized and their aggregation behaviour have been studied by ^{1}H NMR, fluorescence and CD spectroscopy in aqueous and $CDCl_3$ media. Moreover, the morphology and hydrodynamic radius of the aggregates have been studied by SEM, optical microscopy and LS. The large apparent hydrodynamic radius obtained from LS measurements suggests that the amphiphiles form large aggregates (300- 600 nm) which are mostly invariant with the total surfactant concentration.[41a] Two critical aggregation concentrations have been observed in aqueous media by fluorescence pyrene method studies. The first, that is the lowest, can corresponds to the formation of large, disordered bilayer structures, and the second due to the formation of spherical vesicles. Differences in the hydrodynamic radius of the aggregates and CCs were observed between **2a-c** substituted Gemini surfactants in aqueous media and $CHCl_3$.

Moreover, the vesicles formed in concentrated solutions can lead to network aggregates as has been described in the literature.[56a] The SEM pictures of the

aqueous solutions of surfactants confirmed the formation of these network vesicle aggregates. The data obtained from ^{1}H NMR and FT-IR suggest that one of the driving forces for the vesicle formation is the conformational change of the hydrophobic part. Furthermore, the CD spectral features suggested the loss of chirality in the aggregates as has been described with other chiral surfactant molecules.[52]

The emulsifying ability observed in different o/w emulsions using the Gemini surfactant **2a**, containing the amide functionality, were always better than when using the analogous Gemini surfactant **3a** or the commercial surfactant SDS, highlighting the role of the amide moiety. The encapsulation of (*R*)-Limonene inside the aggregates in EtOH/water leads to two different release rates due the loss of the emulsion after ca. 4 hr, however in water a constant release rate was observed for the (*R*)-Limonene encapsulated leading a ca. 30% of release after 9hr.

5. Supporting information

5.1 Synthetic Protocols and Structural Characterization

Synthesis of 2a. Compound **1** (0.15 g, 0.44 mmol) and 1, 4-(bisbromomethyl)benzene (0.06 g, 0.21 mmol) were dissolved in acetonitrile (5 mL). The mixture was subjected to microwave irradiation (120 W, 250 psi, 150 °C) for 1 hour. After solvent evaporation, the remaining solid was washed with diethyl ether (x3) to afford compound **2a**. Yield (0.20 g, 98%, white solid); m.p. 136 ºC; $[\alpha]_D^{25}$= +20.66 (c = 0.01, CH_3OH). IR (ATR)= 3400, 3224, 3066, 2924, 2854, 1679, 1550, 1462, 1370, 1222, 1155 cm^{-1}. ^{1}H NMR (400 MHz, $CDCl_3$) δ (ppm)= 9.48 (s, 2H), 8.12 (t, *J* = 4.8 Hz, 2H), 7.82 (s, 2H), 7.64 (s, 2H), 7.46 (s, 4H), 5.55 (dd, *J* = 36.0, 14.5 Hz, 4H), 5.47 (d, *J* = 10.8 Hz, 2H), 3.32-3.20 (m, 2H), 3.00-2.87 (m, 2H), 2.45-2.33 (m, 2H), 1.53-1.39 (m, 4H), 1.17 (s, 36H), 0.99 (d, J = 6.5 Hz, 6H), 0.81 (t, J=6.6 Hz, 6H), 0.72 (d, J=6.6 Hz, 6H); ^{13}C NMR (101 MHz, $CDCl_3$) δ(ppm)= 166.9, 135.6, 133.6, 130.7, 122.9, 121.2, 67.8, 53.2, 39.9, 31.9, 31.2, 29.6, 29.7, 29.6, 29.5, 29.3, 29.0, 27.0, 22.7, 18.8, 18.5, 14.1; LRMS (ESI, m/z)= 387.7 (M^{2+}, 100%). $C_{48}H_{82}Br_2N_6O_2$: calcd. C 61.66, H 8.84, N 8.99; found C 61.93, H 8.57, N 9.08.

Synthesis of 2c. Compound **1** (0.17 g, 0.50 mmol) and 1, 3-(bis-bromomethyl)benzene (0.07 g, 0.25 mmol) were dissolved in acetonitrile (5 mL). The mixture was subjected to microwave irradiation (120 W, 250 psi, 150 ºC)

for 1 hour. After solvent evaporation, the remaining solid was washed with diethyl ether (x3) to afford compound **2c**. Yield (0.22 g, 92%, white solid); m.p. 133 °C; $[\alpha]_D^{25}$= -7.88 (CH_3OH). IR (ATR)= 3412, 3231, 3068, 2924, 2854, 1677 cm^{-1}. ^1H NMR(400 MHz, $CDCl_3$) δ(ppm)= 9.64 (s, 2H), 8.37 (t, J = 5.7 Hz, 2H), 7.58 (s, 2H), 7.53 (s, 2H), 7.43 (dd, J =5.7, 3.3 Hz, 2H), 7.27 (dd, J= 7.4, 4.1 Hz, 2H), 5.92 (s, 4H), 5.29 (d, J =10.4 Hz, 2H), 3.35–3.19 (m, 2H), 3.04-2.99 (m, 2H), 2.41-2.29 (m, 2H), 1.54-1.40 (m, 4H), 1.23 (s, 36H), 0.97 (d, J =6.5 Hz, 6H), 0.81 (t, J= 6.7 Hz, 6H), 0.73 (d, J= 6.7 Hz, 6H); ^{13}C NMR (101 MHz, $CDCl_3$) δ(ppm)= 166.7, 136.0, 131.9, 130.9, 122.1, 121.4, 68.3, 51.1, 39.9, 31.9, 31.7, 29.6, 29.6, 29.6, 29.3, 29.2, 29.1, 27.0, 22.7, 18.8, 18.5, 14.1; LRMS (ESI, m/z) = 387.8 (100%); $C_{48}H_{82}Br_2N_6O_2$: calcd. C 61.66, H 8.84, N 8.99; found C 61.84, H 8.62, N 9.14.

Imidazolium based Gemini amphiphiles derived from *L*-valine. Structural elements and surfactant properties

Index

16. **Fig. S18-S19.** CD spectra for different compounds.
17. **Fig. S20.** Optical microscopy (a) and fluorescence microscopy (b) images for **2a** in CH_3OH/H_2O 1/1 v/v in the presence of $BrNEt_4$ (1 eq.) and fluorescein (1%).
18. **Fig. S21.** a) SEM images for **2c** in $CHCl_3$, b) Optical microscopy images for **2c** in $CHCl_3$, c) Optical microscopy images for **2b** in $CHCl_3$.
19. **Fig. S22.** Water emulsions in the presence of surfactant **2a**, **3a** and **SDS** (1 mM).
20. **Fig. S23.** Optical images of the methyl laureate (1%) water emulsion.
21. **Fig. S24.** Optical images of the hexane (20%) water emulsions.
22. **Fig. S25.** Optical images of the Me-THF (20%) water emulsions.
23. **Fig. S26.** Absorbance at 600 nm for 20% methyl-THF/water emulsions.
24. **Fig. S27.** Optical images of the limonene (10%) water emulsions.
25. **Fig. S28.** GC chromatogram of limonene release in the presence of internal standard.
26. **Fig. S29.** Limonene release profile when surfactant **2a-c** were used in H_2O/EtOH 1/1 v/v (10% limonene).
27. **Fig. S30.** Limonene release profile when surfactant **2a** was used (10% limonene).
28. **Fig. S31.** Limonene release profile when surfactants **2a, 3a** and **SDS** were used (10% limonene, H_2O/EtOH 1/1 v/v).
29. **Fig. S32.** Limonene release profile when surfactants **2a** was used (10% limonene).

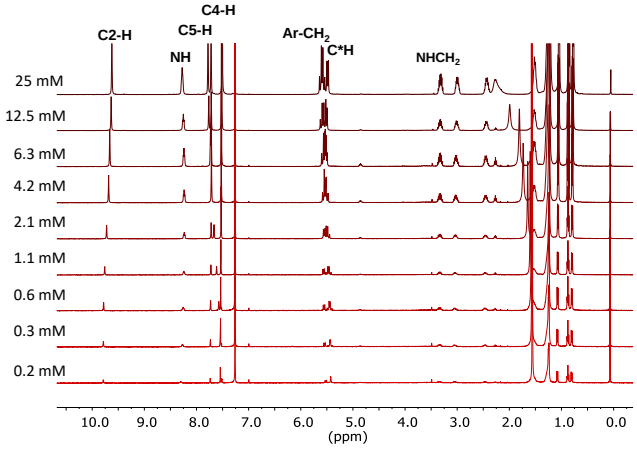

Figure S1. ^{1}H NMR spectra (400 MHz) of compound **2a** at different concentrations in $CDCl_3$.

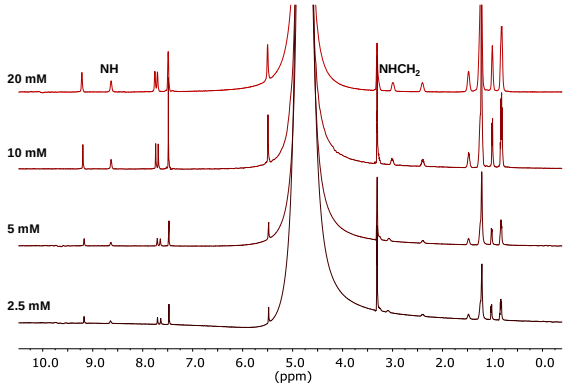

Figure S2. ^{1}H NMR spectra (400 MHz) of compound **2a** at different concentrations in CD_3OD/H_2O 1/1 v/v.

Table S1. Maximum Δδ values observed upon concentration for the different protons of **2a**, **2b** and **2c** in D_2O/CD_3OD and $CDCl_3$ at 25 ºC.

		Δδ								
	Solvent	C2-*H*	C4-*H*	C5-*H*	N*H*	C*H*$_2$Ar	C*H*$_2$ NH	(C*H*$_2$)$_9$	C*H*$_3$ (Val)	C*H*$_3$ (dodecyl)
2a	D_2O/ CD_3OD	0.03	0.09	0.07	--	0.03	0.03 -0.16	0.02	-0.02 -0.03	-0.02
2a[a]	H_2O/ CD_3OD	0.05	0.06	0.05	-0.01	0.02	0.03 -0.09	0.02	-0.02 -0.02	-0.02
2a/ NEt_4Br (1/2)[b]	D_2O/ CD_3OD	--	0.07	0.06	--	0.02	-0.12	0.03	-0.02	-0.02
2b	D_2O/ CD_3OD	0.07	0.09	0.06	--	0.04	-0.09	0.02	-0.03 -0.03	-0.02
2c	D_2O/ CD_3OD	--	0.03	0.03	--	0.07	-0.09	0.02	-0.02	-0.02 -0.02
3a[c]	D_2O/ CD_3OD	0.03	0.01	-0.01	--	0.01	--	0.00	--	-0.02
2a	$CDCl_3$	-0.16	0.30	0.27	0.03	0.17	-0.02 -0.05	-0.02	-0.04 -0.04	-0.01
2b	$CDCl_3$	-0.12	0.22	-0.01	0.03	--	-0.02 -0.04	-0.02	-0.04 -0.04	-0.03
2c	$CDCl_3$	-0.16	0.13	-0.04	0.11	0.13	-0.03 -0.03	-0.01	-0.04 -0.03	-0.02

[a] Δδ from 2.5 to 20 mM in H_2O/CD_3OD.[b] Δδ from 0.25 to 15 mM in D_2O/CD_3OD. [c] Δδ from 0.3 to 20 mM in D_2O/CD_3OD.

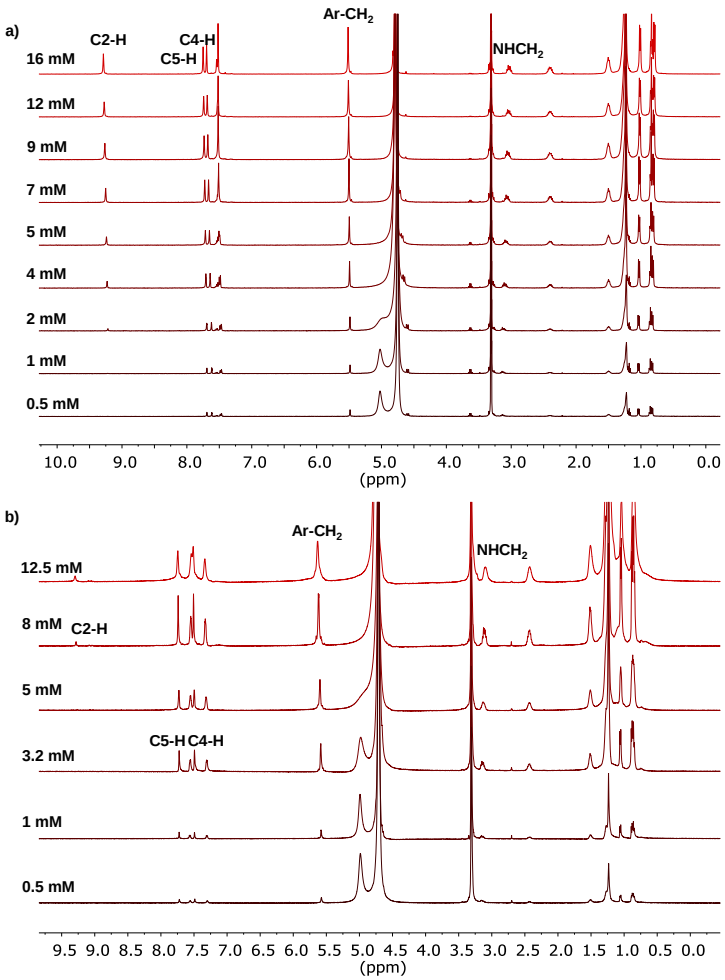

Figure S3. a) ^{1}H NMR (400 MHz) of compound **2b** at different concentrations in CD_3OD/D_2O 1/1 v/v, b) ^{1}H NMR (400 MHz) of compound **2c** at different concentrations in CD_3OD/D_2O 1/1 v/v.

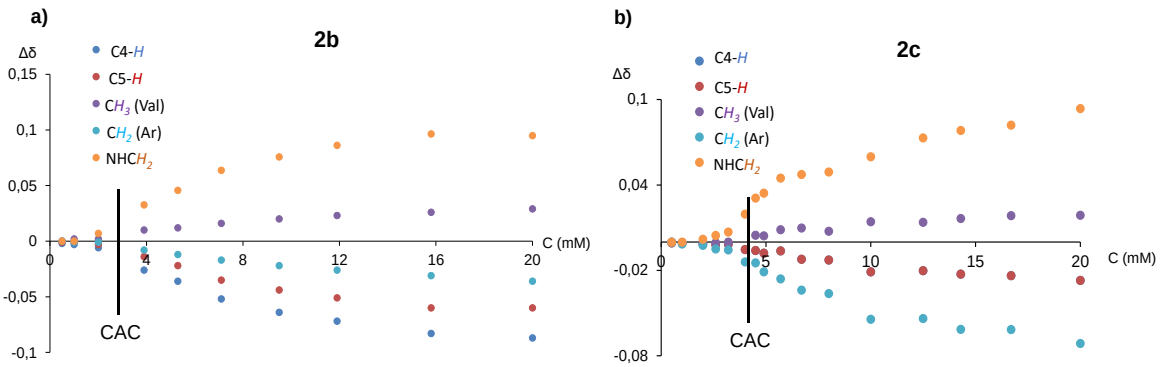

Figure S4. Plot of Δδ against concentration for **2b** and **2c** in CD_3OD/D_2O 1/1 v/v.

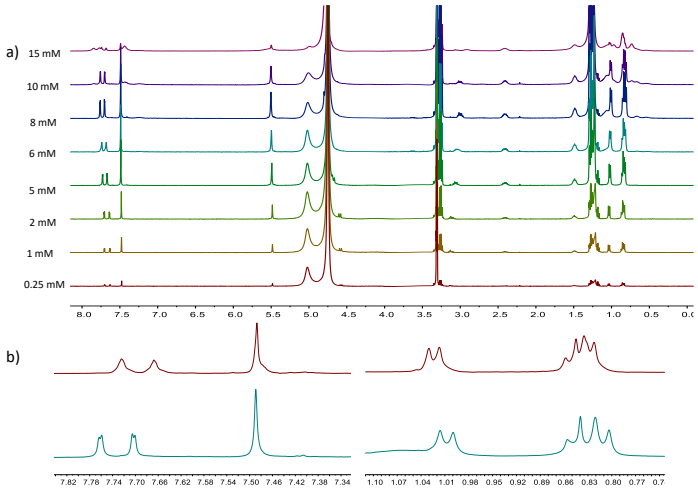

Figure S5. a) ^{1}H NMR (400 MHz) of compound **2a** at different concentrations in CD_3OD/D_2O 1/1 v/v in the presence of 2 equiv. of Et_4NBr, b) Partial ^{1}H NMR (400 MHz) of compound **2a** (9 mM in CD_3OD/D_2O 1/1 v/v) in the absence (above) and presence (below) of 2 equiv. of Et_4NBr.

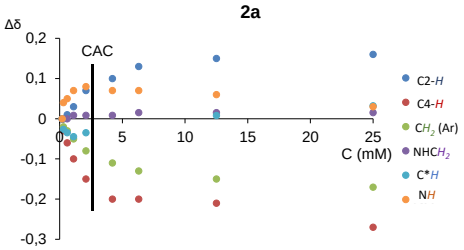

Figure S6. Plot of Δδ against concentration for the different signals of **2a** in $CDCl_3$.

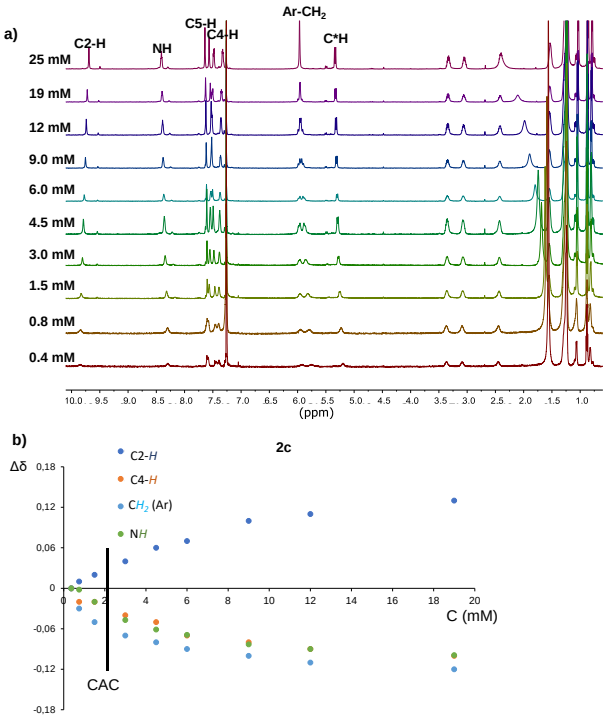

Figure S7. a) ^{1}H NMR (500 MHz) of **2c** at different concentrations in $CDCl_3$, b) Plot of Δδ against concentration for the different signals of **2c** in $CDCl_3$.

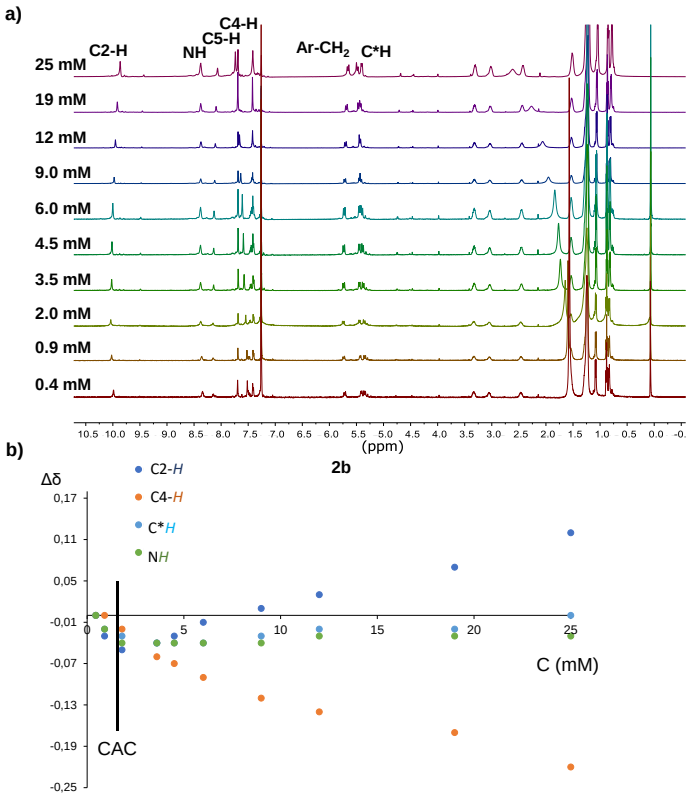

Figure S8. a) ^{1}H NMR (400 MHz) of **2b** at different concentrations in $CDCl_3$, b) Plot of Δδ against concentration for the different signals of **2b** in $CDCl_3$.

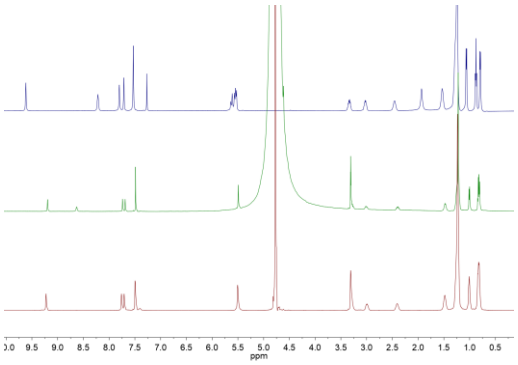

Figure S9. ^{1}H NMR (500 MHz) of **2a** (13 mM) in $CDCl_3$ (bottom), H_2O/CD_3OD 1/1 v/v (middle) and D_2O/CD_3OD (top).

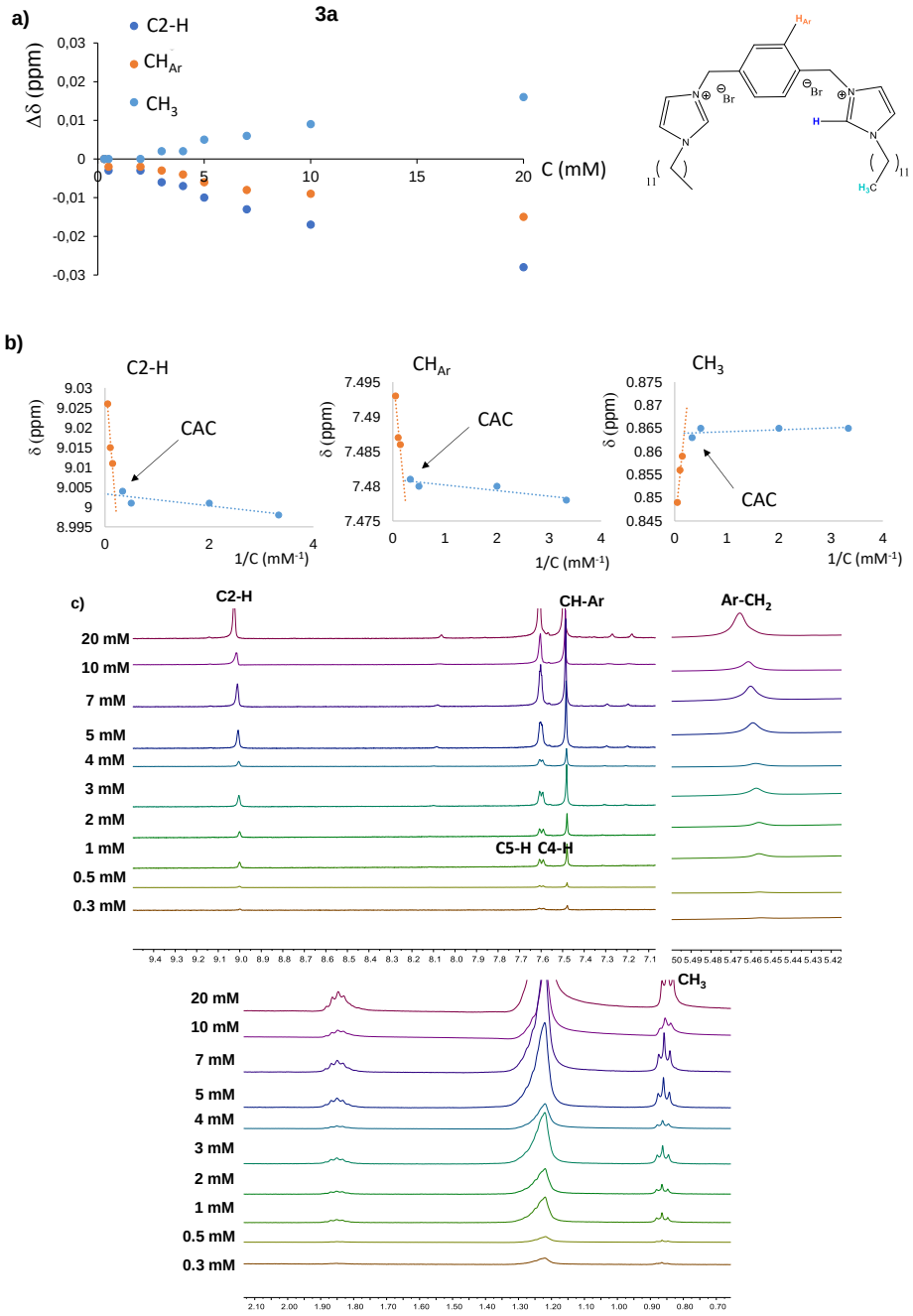

Figure S10. Variation of the ^{1}H NMR signals of **3a** with the concentration in CD_3OD/D_2O 1/1: a) Plot of Δδ against concentration for the signals from CH-Ar, C2-H and CH_3, b) plot of δ against 1/C for **3a** for the same signals, c) partial ^{1}H NMR spectra of **3a** in different concentrations in CD_3OD/D_2O 1/1 v/v.

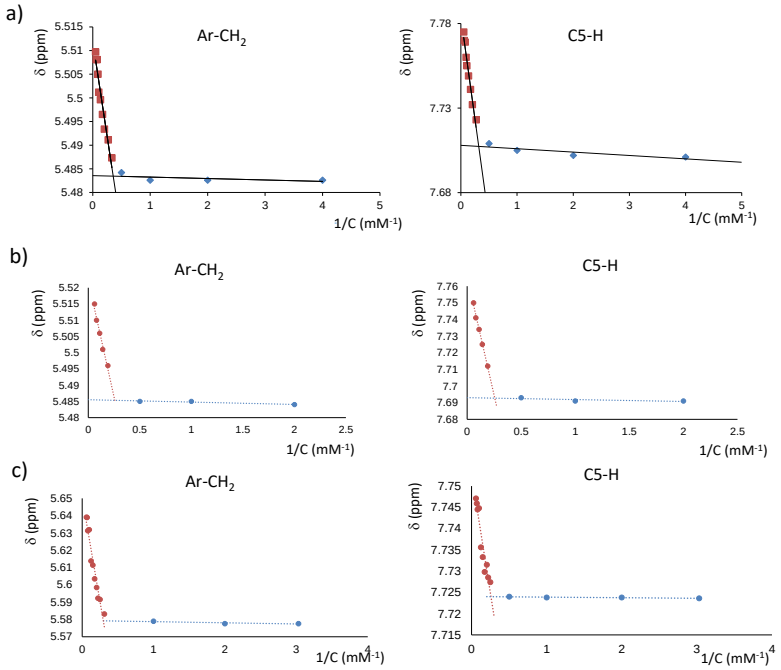

Figure S11. Plot of δ_{obs} against 1/C for a) **2a**; b) **2b**; c) **2c** in CD_3OD/D_2O 1/1 v/v for the signals corresponding to the benzylic protons Ar-CH_2 and C5-H of the imidazolium ring.

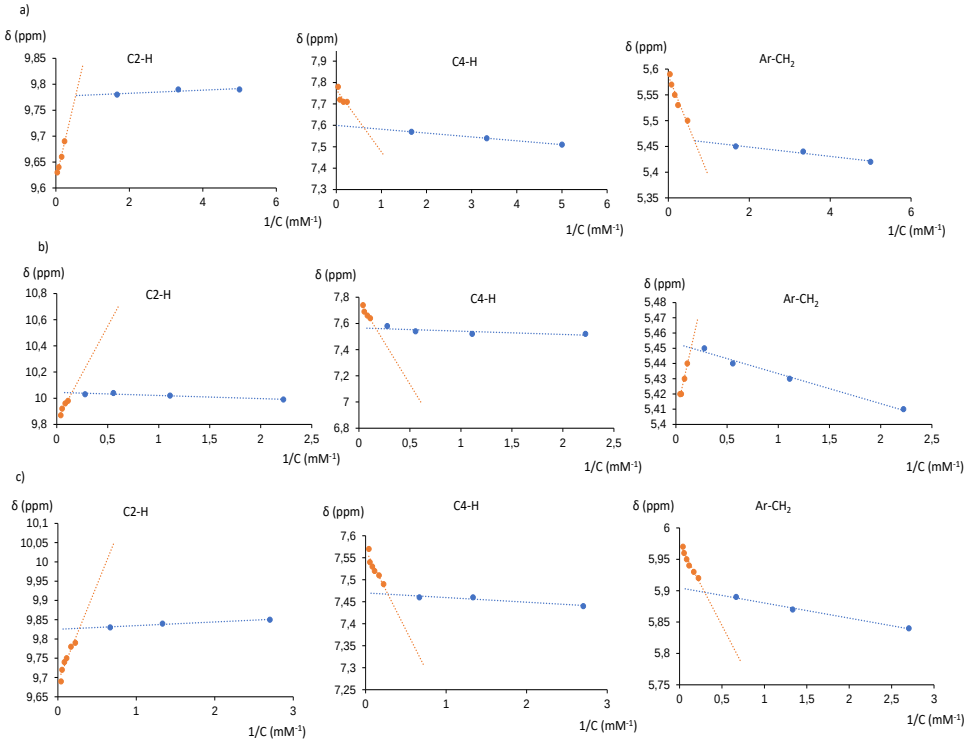

Figure S12. Plot of δ_{obs} against 1/C for a) **2a**; b) **2b**; c) **2c** in $CDCl_3$ for the signals corresponding to the benzylic protons CH_2-Ar and the C2-H and C4-H of the imidazolium ring.

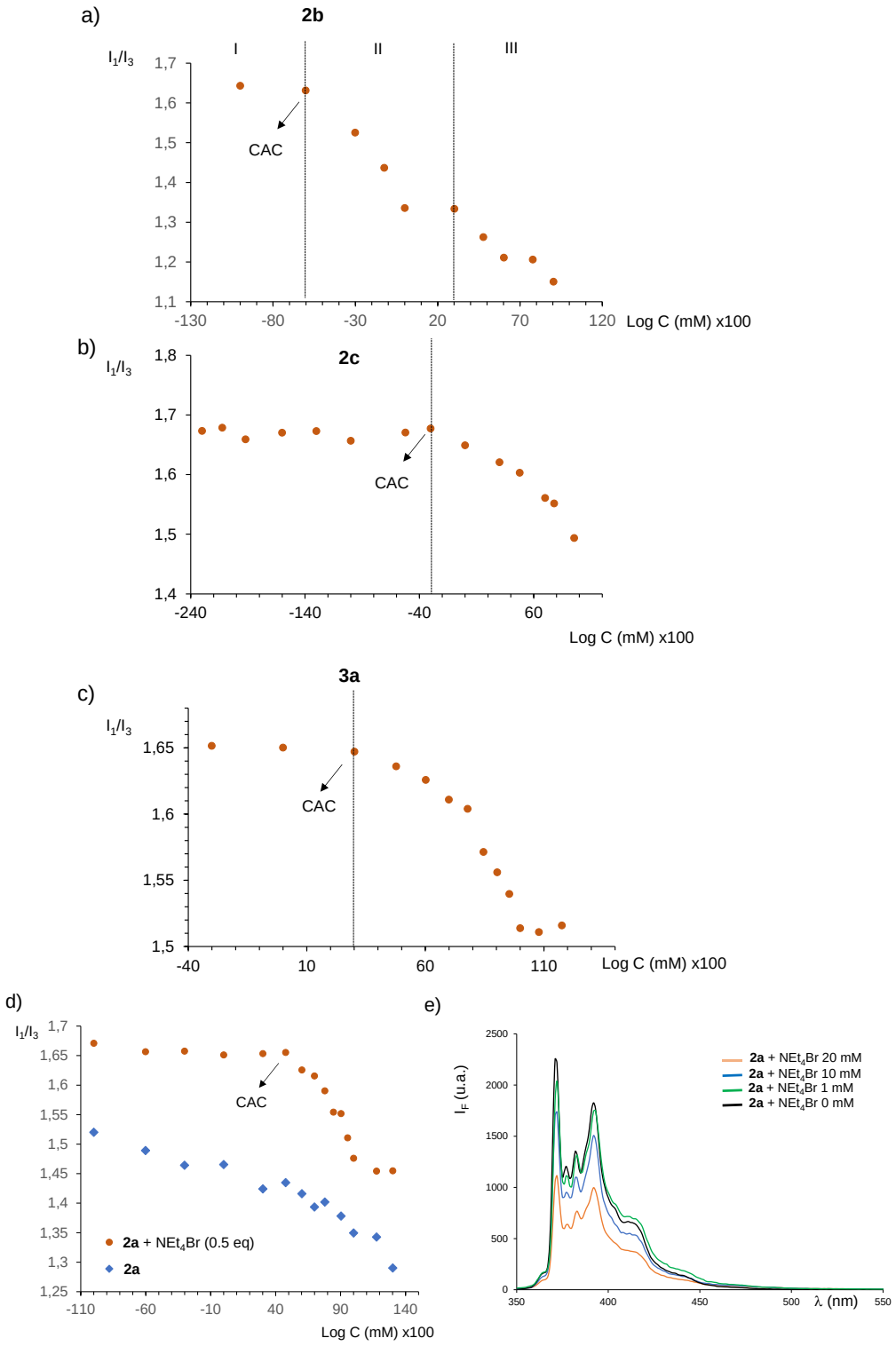

Figure S13. Plot of I_1/I_3 against log C for **2b** (a), **2c** (b), **3a** (c), and **2a** + Et_4NBr (0.5 eq.) (d) using CH_3OH/H_2O 1/1 v/v, (e) Emission spectra of pyrene in CH_3OH/H_2O 1/1 v/v in the presence of different amounts of **2a** + Et_4NBr (0.5 eq.).

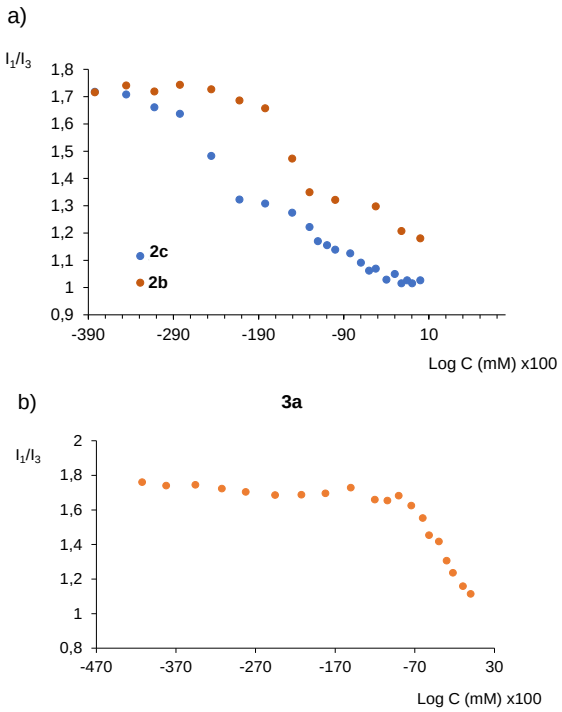

Figure S14. Plot of I_1/I_3 against log C for **2b, 2c** and **3a** in H_2O.

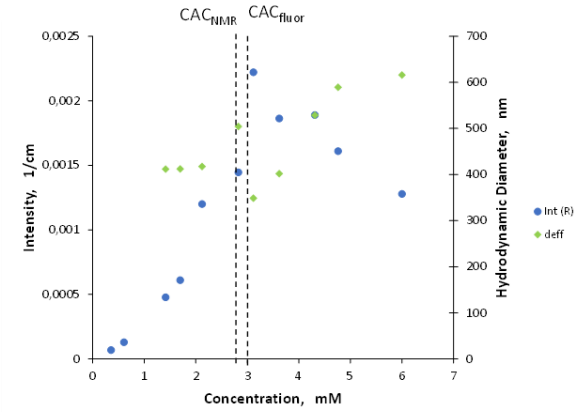

Figure S15. Hydrodynamic Diameter and Scattered Light Intensity obtained by LS for **2a** in the presence of NEt_4Br (0.5 equiv.) in H_2O/CH_3OH 1/1 v/v at different concentrations.

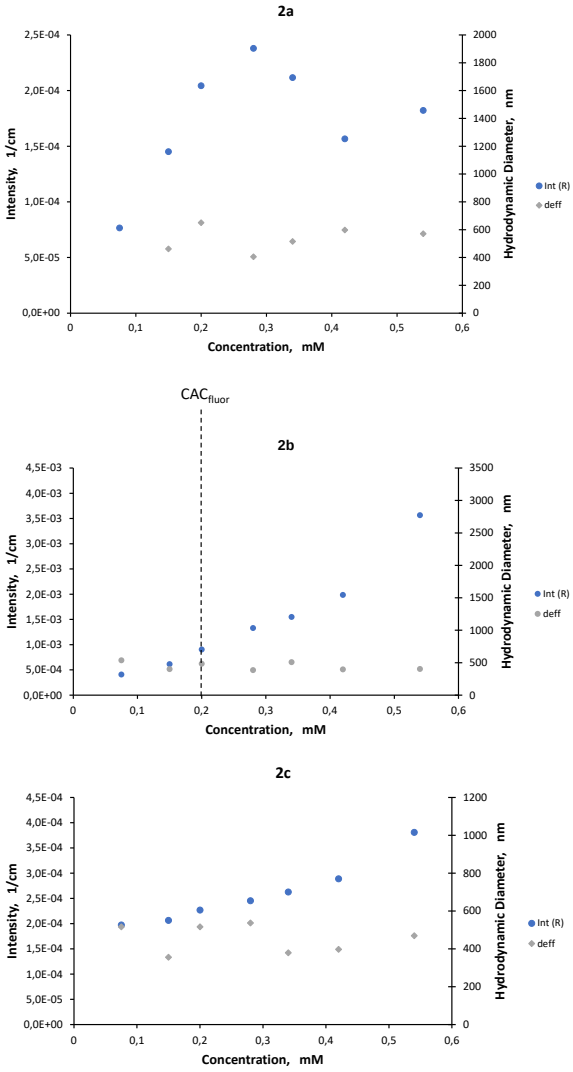

Figure S16. Hydrodynamic Diameter and Scattered Light Intensity obtained by LS for **2a-c** in H_2O at different concentrations.

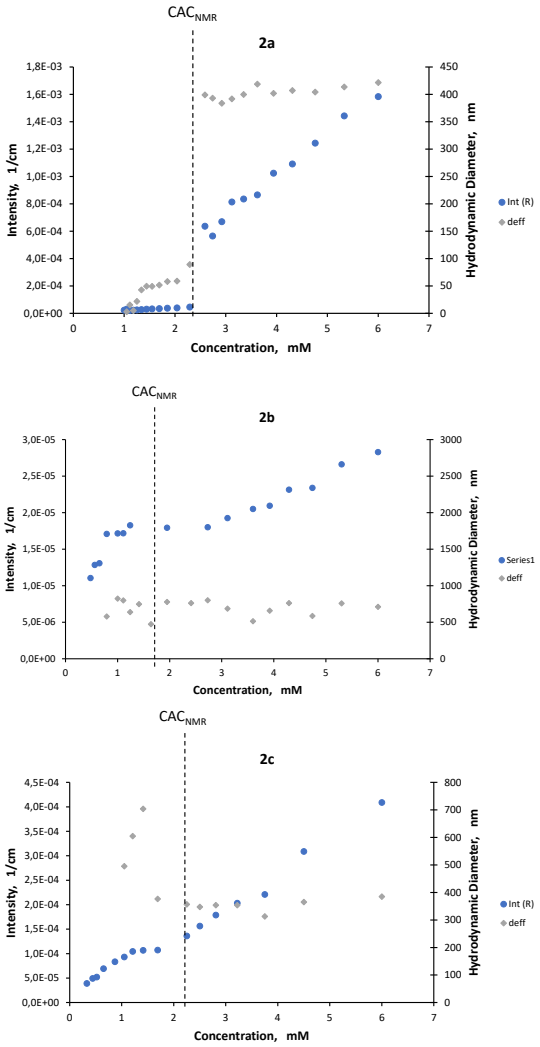

Figure S17. Hydrodynamic diameter (grey points, right axes) and the scattered light intensity in absolute units (1/cm) (blue points, left axes) obtained by LS for **2a-c** in $CHCl_3$ at different concentrations.

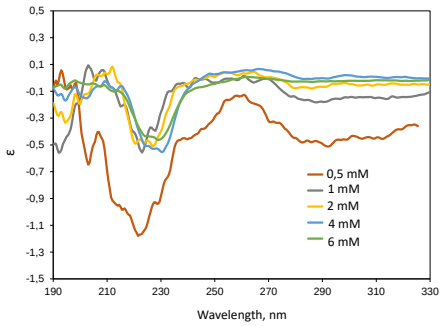

Figure S18. CD spectra for **2a** in the presence of NEt_4Br (0.5 equiv.) in H_2O/CH_3OH 1/1 v/v at different concentrations.

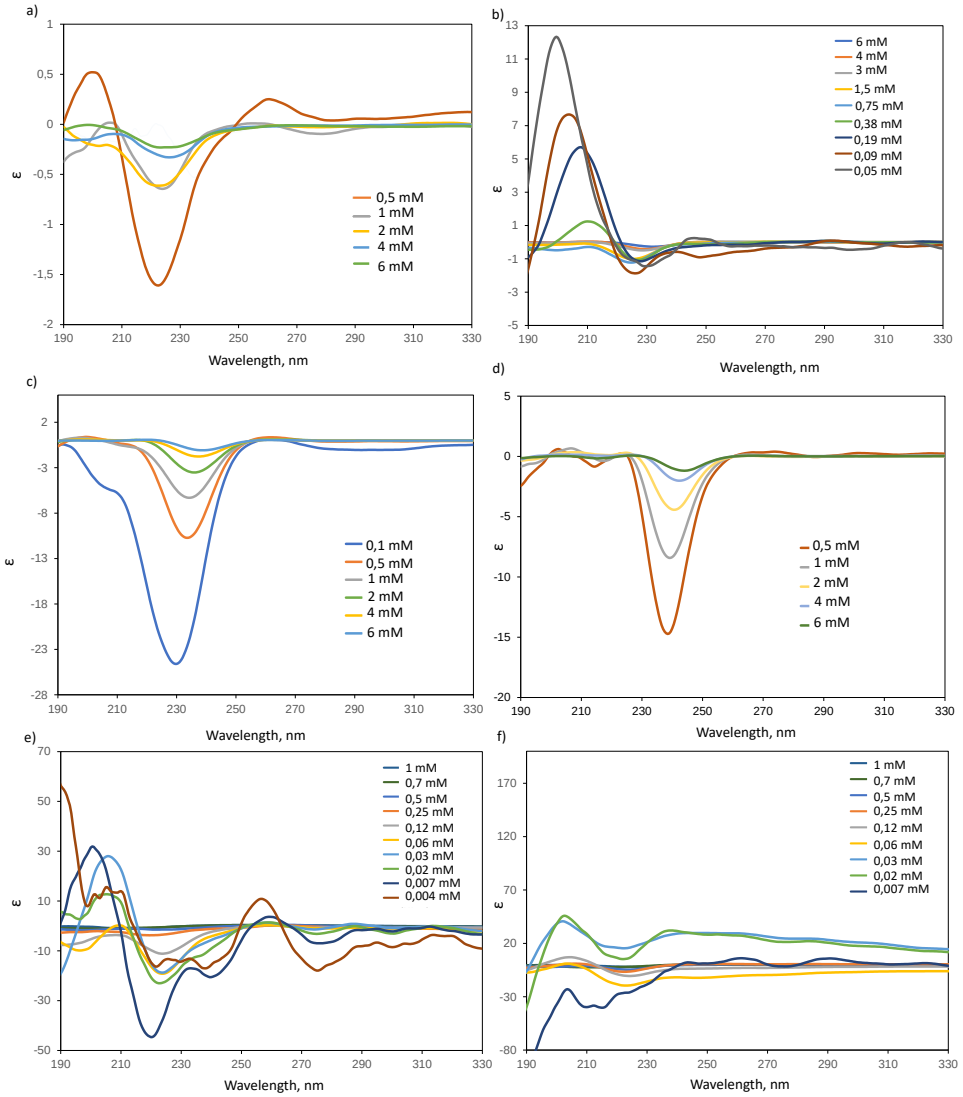

Figure S19. CD spectra a) for **2b** in H_2O/CH_3OH 1/1 (v/v), b) for **2c** in H_2O/CH_3OH 1/1 (v/v), c) for **2b** in $CHCl_3$, d) for **2c** in $CHCl_3$, e) for **2b** in H_2O and f) for **2c** in H_2O at different concentrations.

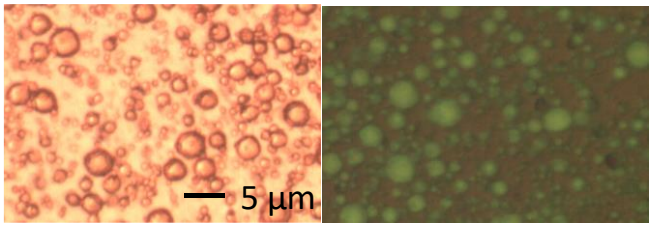

Figure S20. Optical microscopy (a) and fluorescence microscopy (b) images for **2a** (20 mM) in CH_3OH/H_2O 1/1 (v/v) in the presence of $BrNEt_4$ (1 eq.) and fluorescein (1%).

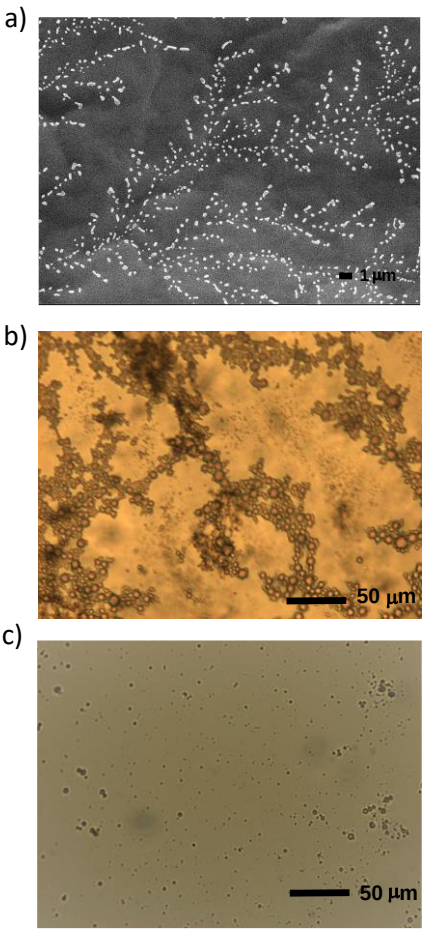

Figure S21. a) SEM images for **2c** (6 mM) in $CHCl_3$, b) Optical microscopy images for **2c** (6 mM) in $CHCl_3$, c) Optical microscopy images for **2b** (5 mM) in $CHCl_3$.

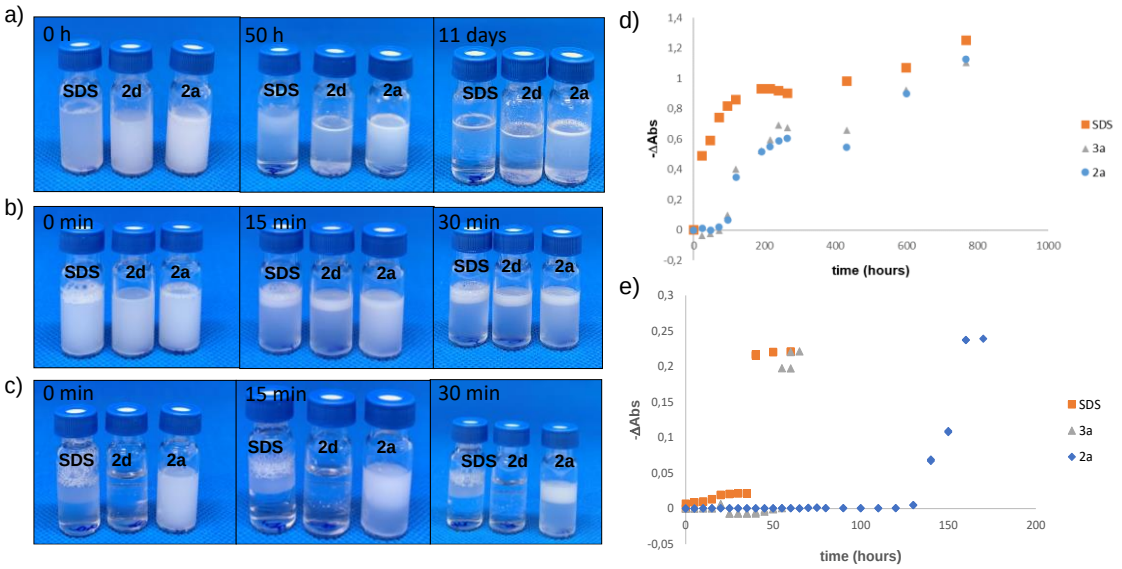

Figure S22. Water emulsions in the presence of surfactant **2a, 3a** and **SDS** (1 mM): a) 1% methyl laureate, b) 20% methyl-THF, c) 20% hexane, d) Absorbance variation at 600 nm for 1% methyl laureate/water emulsions, e) Absorbance variation at 600 nm for 20% methyl-THF/water emulsions.

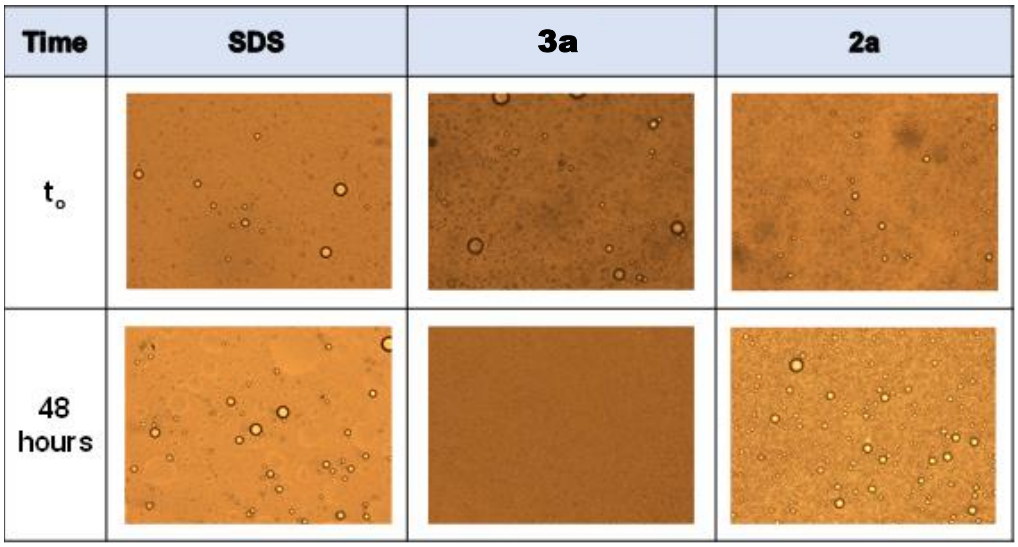

Figure S23. Optical images of the methyl laureate (1%) water emulsion (10x1).

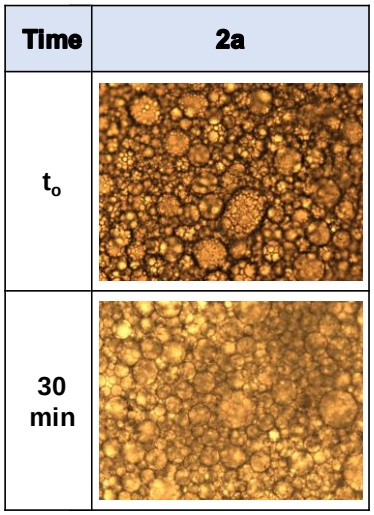

Figure S24. Optical images of the hexane (20%) water emulsions (10x1).

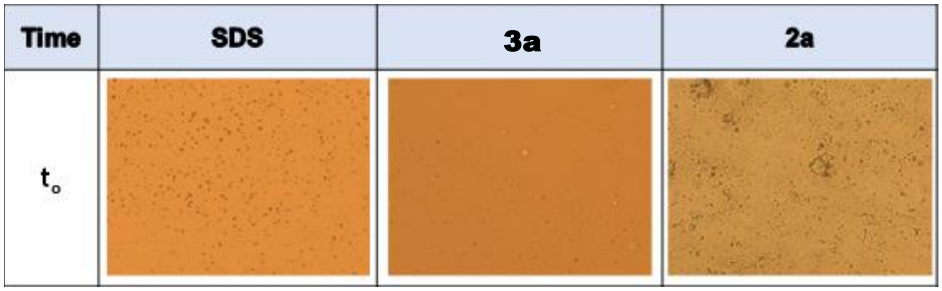

Figure S25. Optical images of the Me-THF (20%) water emulsions (10x1).

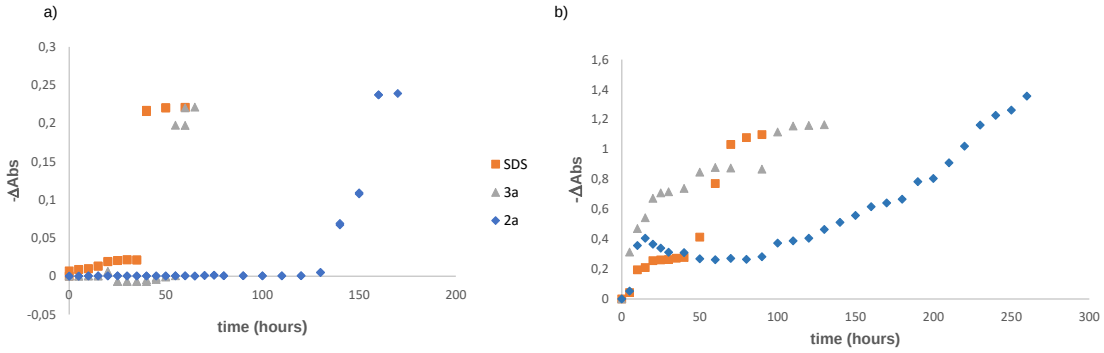

Figure S26. Absorbance variation at 600 nm for 20% methyl-THF/water emulsions in the presence of **3a** (grey)**, 2a** (blue) and **SDS** (orange) (3.5 mM): a) 25ºC; b) 40ºC.

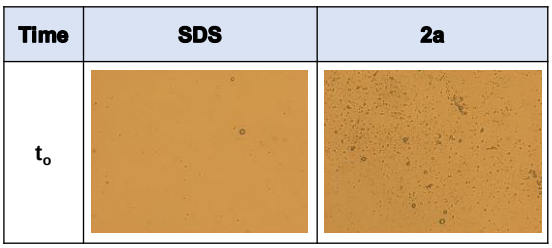

Figure S27. Optical images of the limonene (10%) water emulsions (10x1).

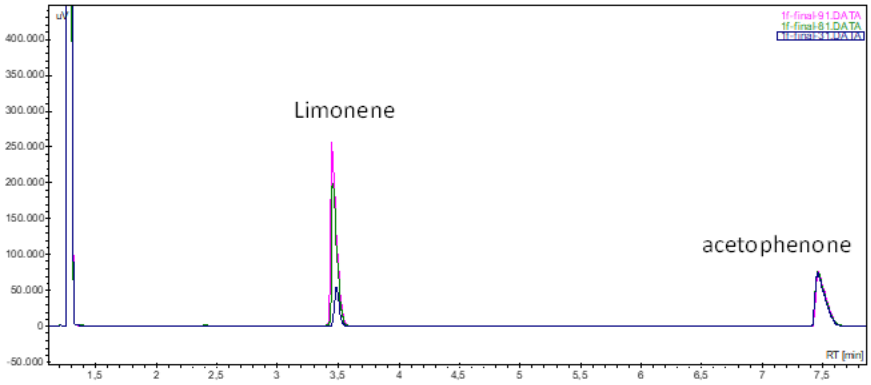

Figure S28. GC chromatogram of limonene release in the presence of internal standard.

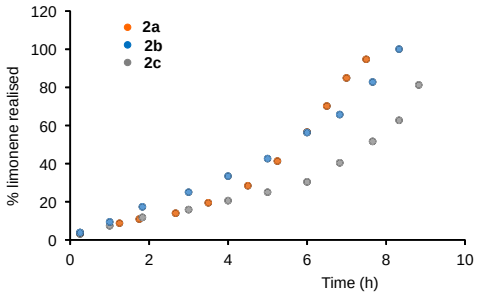

Figure S29. Limonene realise profile when surfactant **2a-c** (3.5 mM) were used in H_2O/EtOH 1/1 v/v (10% limonene).

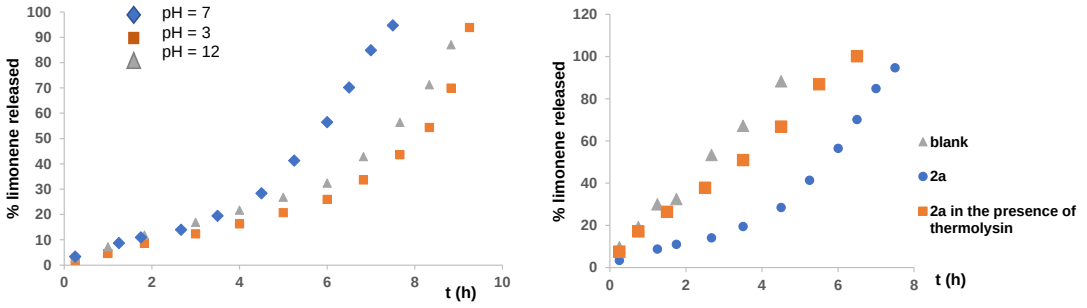

Figure S30. Limonene release profile when surfactant **2a** was used (10% limonene, 3.5 mM **2a**).

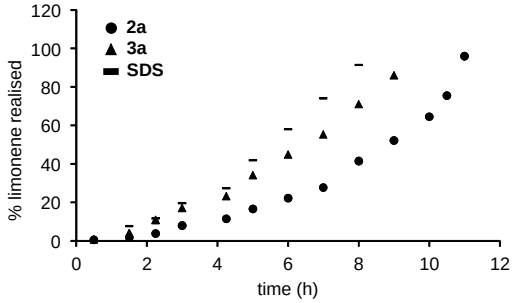

Figure S31. Limonene release profile when surfactants **2a, 3a** and **SDS** were used (10% limonene, 15 mM surfactant, H_2O/EtOH 1/1 v/v).

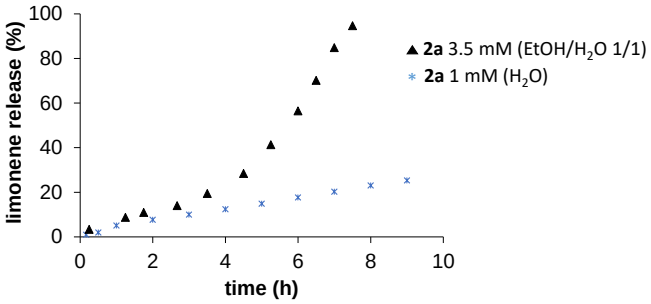

Figure S32. Limonene realise profile when surfactants **2a** was used (10% limonene).

CHAPTER 3.

3.4. Imidazole and Imidazolium Antibacterial Drugs Derived from Amino Acids

Imidazole and imidazolium antibacterial drugs derived from amino acids

Abstract

The antibacterial activity of imidazole and imidazolium salts is highly dependent upon their lipophilicity, which can be tuned through the introduction of different hydrophobic substituents on the nitrogen atoms of the imidazole or imidazolium ring of the molecule. Taking this into consideration, we have synthesized and characterized a series of imidazole and imidazolium salts derived from *L*-valine and *L*-phenylalanine containing different hydrophobic groups and tested their antibacterial activity against two model bacterial strains, Gram-negative *E. coli* and Gram-positive *B. subtilis*. Importantly, the results demonstrate that the minimum bactericidal concentration (MBC) of these derivatives can be tuned to fall close to the cytotoxicity values in eukaryotic cell lines. The MBC value of one of these compounds toward *B. subtilis* was found to be lower than the IC_{50} cytotoxicity value for the control cell line HEK-293. Furthermore, the aggregation behavior of these compounds has been studied in pure water, in cell culture media, and in mixtures thereof, in order to determine if the compounds formed self-assembled aggregates at their bioactive concentrations with the aim of determining whether the monomeric species were in fact responsible for the observed antibacterial activity. Overall, these results indicate that such imidazole and imidazolium compounds derived from *L*-valine and *L*-phenylalanine - with different alkyl lengths in the amide substitution - can serve as potent antibacterial agents with low cytotoxicity to human cell lines.

Keywords: *imidazole and imidazolium salts, amino acid, antibacterial agents, aggregation, lipophilicity*

1. Introduction

Aromatic heterocycles, particularly the imidazole ring, have been used in the last decades as structural skeletons to obtain different types of bioactive compounds with antibacterial, antifungal, anticancer, antiviral, antidiabetic

and other properties.[1,2,3,4] The search for new potent drug molecules derived from imidazole continues to be an intense area of investigation in medicinal chemistry.[5,6,7] Moreover, pharmaceutical research, manufacture and regulation are enhancing the development of solid active ingredients, delivered as powders or tablets; however, many solid drugs which perform well in in vitro evaluation remain too insoluble for the body to absorb.[8,9] Most of the bioactive agents sold for pharmaceutical or food industries are salts[10,11] and in this context ionic liquids (ILs) represent a promising class of drug candidates whose physicochemical and pharmaceutical properties can be easily tuned.[12,13,14,15,16,17] In this regard, the imidazolium skeleton can be transformed

[1] *Imidazoles as Promising Scaffolds for Antibacterial Activity: A Review. Mini-Rev*; Rani, N.; Sharma, A.; Singh, R.; *Med. Chem.* **2013**, *13*, 1812-1835.
[2] *Exploration of Structure-Based on Imidazole Core as Antibacterial Agents*; Duan, Y. T.; Wang, Z. C.; Sang, Y. L.; Tao, X. X.; Zhu, H. L.; *Curr. Top. Med. Chem.* **2013**, *13*, 3118-3130.
[3] *Synthesis, Fungicidal Activity, and Sterol 14a-Demethylase BindingInteraction of 2-Azolyl-3,4-dihydroquinazolines on Penicillium digitatum*; Li, W. J.; Li, Q.; Liu, D.; Ding, M. W.; *J. Agric. Food Chem.* **2013**, *61*, 1419-1426.
[4] *Synthesis of Novel 3,4-Chloroisothiazole-Based Imidazoles as Fungicides and Evaluation of Their Mode of Action*; Chen, L.; Zhao, B.; Fan, Z. J.; Liu, X. M.; Wu, Q. F.; Li, H. P.; Wang, H. X.; *J. Agric. Food Chem.* **2018**, *66*, 7319-7327.
[5] *Synthesis and biological evaluation of coumarin derivatives containing imidazole skeleton as potential antibacterial agents*; Hu, Y.; Shen, Y. F.; Wu, X. H.; Tu, X.; Wang, G. X.; *Eur. J. Med. Chem.* **2018**, *143*, 958-969.
[6] *Rational Optimization and Action Mechanism of Novel Imidazole (or Imidazolium)-Labeled 1,3,4 Oxadiazole Thioethers as Promising Antibacterial Agents against Plant Bacterial Diseases*; Wang, P-Y.; Wang, M-W.; Zeng, D.; Xiang, M.; Rao, J-R.; Liu, Q-Q.; Liu, L-W.; Wu, Z-B.; Li, Z.; Song, B. A.; Yang, S. *J. Agric. Food Chem.* **2019**, *67*, 3535-3545.
[7] *An Updated Review on the Synthesis and Antibacterial Activity of Molecular Hybrids and Conjugates Bearing Imidazole Moiety*; Rossi, R.; Ciofalo, M.; *Molecules* **2020**, *25* (21), 5133-5238.
[8] *Chemistry: Develop ionic liquid drugs*; Shamshina, J. L.; Kelley, S. P.; Gurau, G.; Rogers, R. D.; *Nature* **2015**, *528*, 188-189.
[9] *Oral lipid-based formulations*; Hauss, D.; *J. Adv. Drug Deliv. Rev.* **2007**, *59*, 667–676.
[10] Guillory, J. K. *Pharmaceutical Salts: Properties, Selection, and Use,* 2nd ed.; Stahl, P.H.; Wermuth, C.G. Eds.; Wiley-VCH, VHCA: Weinheim, Germany, **2002**.
[11] *Encapsulation Systems for Antimicrobial Food Packaging Components: An Update*; Becerril, R.; Nerín, C.; Silva, F.; *Molecules* **2020**, 25, 1134-1174.
[12] *Crystalline vs. ionic liquid salt forms of active pharmaceutical ingredients: a position paper*; Stoimenovski, J.; MacFarlane, D. R.; Bica, K.; Rogers, R. D.; *Pharm. Res.* **2010**, *27*, 521–526.
[13] *Sulfasalazine in ionic liquid form with improved solubility and exposure*; Shadid, M.; Gurau, G.; Shamshina, J. L.; Chuang, B.-C.; Hailu, S.; Guan, E.; Chowdhury, S. K.; Wu, J. T.; Rizvi, S. A. A.; Griffin, R. J.; Rogers, R. D.; *Med. Chemç. Comm.* **2015**, *6*, 1837-1841.
[14] *Biological activity of ionic liquids and their application in pharmaceutics and medicine*; Egorova, K. S.; Gordeev, E. G.; Ananikov, V. P.; *Chem. Rev.* **2017**, *117*, 7132–7189.
[15] *Ionic liquids as active pharmaceutical ingredients*; Ferraz, R.; Branco, L. C.; Prudencio, C.; Noronha, J. P.; Petrovski, Z.; *Chem. Med. Chem.* **2011**, *6*, 975–985.
[16] *The Use of Liquids Ionic Fluids as Pharmaceutically Active Substances Helpful in Combating Nosocomial Infections Induced by Klebsiella Pneumoniae New Delhi Strain, Acinetobacter Baumannii and Enterococcus Species*; Miskiewicz, A.; Ceranowicz, P.; Szymczak, M.; Bartus, K.; Kowalczyk, P.; *Int. J. Mol. Sci.* **2018**, *19*, 2779.
[17] *A Novel Simple Approach to Material Parameters from Commonly Accessible Rheometer Data*; Schrüfer, S.; Sonnleitner, D.; Lang, G.; Schubert, D. W.; *Polymers* **2020**, *12*, 1276-1300.

into ionic liquids with promisingly potent pharmacological properties.[18,19,20,21] Consequently, monoimidazolium[22,23,24] and bisimidazolium[25,26,27,28] salts have been explored as a new generation of antibacterial agents. In this context, amino acid based monoimidazolium salts with good bacterial toxicity have been reported in the literature.[29]

Our research group has an ongoing interest in the biomimetic and bioactive capacity of imidazole or imidazolium amino acid derivatives.[30,31,32,33] Herein, imidazole, monotopic and ditopic imidazolium salts derived from *L*-valine and

---

[18] *Synthesis, characterization and the antimicrobial activity of new eco-friendly ionic liquids*; Messali, M.; Moussa, Z.; Alzahrani, A. Y.; El-Naggar, M. Y.; ElDouhaibi, A. S.; Judeh, Z. M. A.; Hammouti, B.; *Chemosphere*, **2013**, *91*, 1627–1634.

[19] *A Remarkably Simple Class of Imidazolium-Based Lipids and Their Biological Properties*; Wang, D.; Richter, C.; Rühling, A.; Drücker, P.; Siegmund, D.; Metzler-Nolte, N.; Glorius, F.; Galla, H-J.; *Chem. Eur. J.* **2015**, *21*, 15123–15126.

[20] *Cytotoxicity of Imidazole Ionic Liquids in Human Lung Carcinoma A549 Cell Line*; Chen, H-L.; Kao, H-F.; Wang, J-Y.; Wei, G-T.; *J. Chin. Chem. Soc.* **2014**, *61*, 763–769.

[21] *Imidazolium-Derived Ionic Salts Induce Inhibition of Cancerous Cell Growth through Apoptosis*; Malhotra, S. V.; Kumar, V.; Velez, C.; Zayas, B.; *MedChemComm* **2014**, *5*, 1404–1409.

[22] *Anti-microbial activities of ionic liquids*; Pernak, J.; Sobaszkiewicz, K.; Mirska, I.; *Green Chemistry,* **2003**, *5*, 52–56.

[23] *Supramolecular systems based on cationic imidazole-containing amphiphiles bearing hydroxyethyl fragment: aggregation properties and functional activity*; Kuznetsova, D. A.; Gabdrakhmanov, D. R.; Lukashenko, S. S.; Voloshina, A. D.; Sapunova, A. S.; Kulik, N. V.; Nizameev, I. R.; Kadirov, M. K.; Kashapov, R. R.; Ya Zakharova, L.; *J. Mol. Liq.* **2019**, *289*, 111058-1110065.

[24] *Micellization and antimicrobial properties of surface-active ionic liquids containing cleavable carbonate linkages*; Garcia, M. T.; Ribosa, I.; Perez, L.; Manresa, A.; *Langmuir* **2017**, 33 (26), 6511–6520.

[25] *Dicationic imidazolium-based ionic liquids: a new strategy for non-toxic and antimicrobial materials;* Gindri, I. M.; Siddiqui, D. A.; Bhardwaj, P.; Rodriguez, L. C.; Palmer, K. L.; Frizzo, C. P.; Martinsc, M. A. P.; Rodrigues, D. C.; *RSC Adv.*, **2014**, *4*, 62594-62602.

[26] *Antimicrobial activity and SAR study of new gemini imidazolium-based chlorides*; Pałkowski, Ł.; Błaszczyński, J.; Skrzypczak, A.; Błaszczak, J.; Kozakowska, K.; Wróblewska, J.; Kożuszko, S.; Gospodarek, E.; Krysiński, J.; Słowiński, R.; *J. Chem. Biol. Drug Design.* **2014**, *83*, 278–288.

[27] *The structure – Activity correlation in the family of dicationic imidazolium surfactants: Antimicrobial properties and cytotoxic effect*; Voloshina, A. D.; Gumerova, S. K.; Sapunova, A. S.; Kulik, N. V.; Mirgorodskaya, A. B.; Kotenko, A. A.; Prokopyeva, T. M.; Mikhailov, V. A.; Zakharova, L. Y.; Sinyashin, O. G.; *BBA* **2020**, *1864*, 129728-129737.

[28] *Preparation of a novel class of cationic gemini imidazolium surfactants containing amide groups as the spacer: their surface properties and antimicrobial activity*; Wang, L.; Qin, H.; Ding, L.; Huo, S.; Deng, Q.; Zhao, B.; Meng, L.; Yan, T.; *J. Surfactant Deterg.* **2014**, *17*, 1099–1106.

[29] *Synthesis, self-assembly, bacterial and fungal toxicity, and preliminary biodegradation studies of a series of L-phenylalanine-derived surface-active ionic liquids*; Kapitanov, I. V.; Jordan, A.; Karpichev, Y.; Spulak, M.; Perez, L.; Kellett, A.; Kümmerer K.; Gathergood N.; *Green Chem.* **2019**, *21*, 1777–1794.

[30] *Chiral Room Temperature Ionic Liquids as Enantioselective Promoters for the Asymmetric Aldol Reaction*; González, L.; Escorihuela, J.; Altava, B.; Burguete, M. I.; Luis, S.V.; *Eur. J. Org. Chem.* **2014**, 5356-5363.

[31] *Synthesis of Chiral Room Temperature Ionic Liquids from Amino Acids–Application in Chiral Molecular Recognition*; González, L.; Altava, B.; Bolte, M.; Burguete, M. I.; García-Verdugo, E.; Luis, S. V.; *Eur. J. Org. Chem.* **2012**, 4996-5009.

[32] *Application of optically active chiral bis(imidazolium) salts as potential receptors of chiral dicarboxylate salts of biological relevance*; González-Mendoza, L.; Escorihuela, J.; Altava, B.; Burguete, M. I.; Luis, S. V.; *Org. Biomol. Chem.* **2015**, *13*, 5450-5459.

[33] *Bis(imidazolium) salts derived from amino acids as receptors and transport agents for chloride anions*; González-Mendoza, L.; Escorihuela, J.; Altava, B.; Burguete, M. I.; Hernando, E.; Luis, S. V.; Quesada, R.; Vicent, C.; *RSC Adv.* **2015**, *5*, 34415-34423.

L-phenylalanine with different alkyl lengths in the amide substitution were synthesized and characterized comprehensively. The antibacterial activity of these amino acid-based imidazolium salts against Gram-negative *Escherichia coli* DH5-α (herein *E. coli*) and Gram-positive *Bacillus subtilis* 1904-E (herein *B. subtilis*) were evaluated and their cytotoxicity was also studied using a human embryonic kidney cell line (HEK-293). Finally, due to the amphiphilic character of these compounds and the strong tendency towards self-aggregation of ionic liquid-related surfactants based on imidazolium salts,[34,35,36,37] we investigated the spontaneous aggregation behavior of these compounds in water and in bacterial cell culture medium. Through optical and scanning electron microscopy, as well as UV-vis and fluorescence spectroscopy, we have extracted structure-property relationships between the degree of aggregation/self-assembly of the *L*-valine and *L*-phenylalanine derivatives and their corresponding antibacterial activity and cytotoxicity.[38]

2. Results

2.1. Synthesis

The imidazole-amino acid derivatives **1a**, **2a** and **3a** were obtained from the corresponding α-amino amide as previously described.[31] Monotopic and ditopic -imidazolium salts **1b-3b** and **1c-3c** were obtained in high yield by treatment of the corresponding imidazole with benzyl bromide or 1,3-bromomethylbenzene, respectively, as described in our previous publication (Scheme 1).

[34] *Interfacial and micellar properties of imidazolium-based monocationic and dicationic ionic liquids*; Baltazar, Q. Q.; Chandawalla, J.; Sawyer, K.; Anderson, J. L.; *Colloids Surf., A* **2007**, *302*, 150–156.
[35] *Gemini Imidazolium Surfactants: Synthesis and Their Biophysiochemical Study*; Kamboj, R.; Singh, S.; Bhadani, A.; Kataria, H.; Kaur, G.; *Langmuir* **2012**, *28*, 11969–11978.
[36] *Synthesis and properties of novel ester-containing gemini imidazolium surfactants*; Zhuang, L.-H. *J. Colloid Interface Sci.* **2013**, *408*, 94–100.
[37] *Structural diversity, physicochemical properties and application of imidazolium surfactants: Recent advances*; Bhadani, A.; Singh, T. M. S.; Sakai, K.; Sakai, H; Abe, M.; *Adv. Colloid Interface Sci.* **2016**, *231*, 36–58.
[38] *Membrane interactions of ionic liquids and imidazolium salts*; Wang, D.; Galla, H-J.; Drücker, P.; *Biophys. Rev.* **2018**, *10*, 735–746.

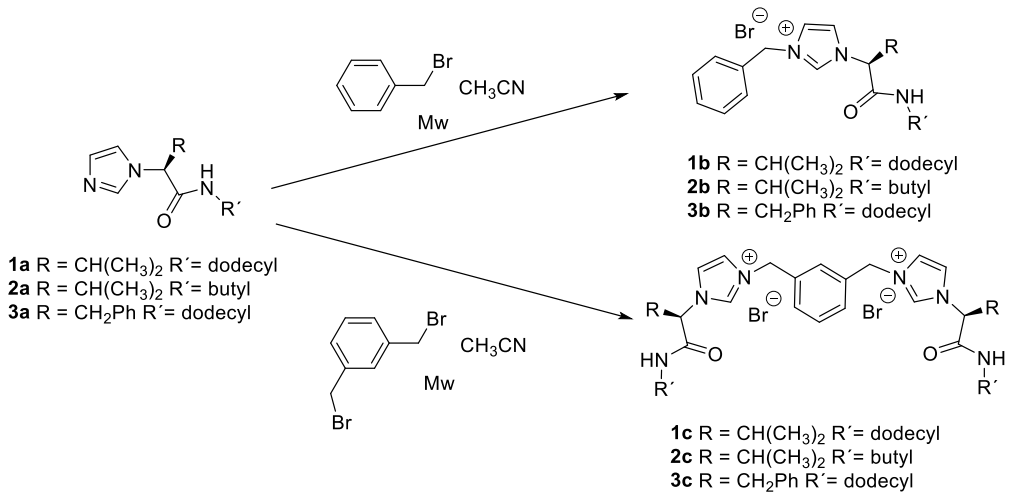

Scheme 1. Synthesis of the amino acid-based imidazolium salts in this report.

2.2. Antibacterial and cytotoxicity studies

The *in vitro* antibacterial activities of the synthesized compounds were examined against *E. coli* and *B. subtilis*. Bacteria were incubated in culture media with varying concentrations of the examined compound and the antibacterial properties were determined by observation of the optical density at 560 nm (bacteriostatic activity) and by the Resazurin cell viability assay (bactericidal activity). The corresponding Minimal Bactericidal Concentration (MBC) and Minimum Inhibitory Concentration (MIC) values obtained are summarized in Table 1 (see also Table S1 for MIC and MBC values in µM).

The outer membrane of Gram-negative bacteria such as *E. coli* includes porins, which allow the passage of small hydrophilic molecules across the membrane, and lipopolysaccharide molecules that extend into extracellular space. Thus, the observed trend in the activity results could be explained by the relative lipophilicity of the compounds combined with their capacity to disrupt the cell membrane.[39,40]

The relative lipophilicity of the compounds was determined theoretically using VCCLab and Molinspiration softwares (LogP values Table 1) and experimentally (retention time values from HPLC, Table 1, Figure S3-S8). The HPLC method used was first validated using different lipophilic commercial compounds with

[39] *QSAR analysis of substituent effects on tambjamine anion transporters*; Knight, N. J.; Hernando, E.; Haynes, C. J. E.; Busschaert, M.; Clarke, H. J.; Takimoto, K.; García-Valverde, M.; Frey, J. G.; Quesada, R.; Gale, P. A.; *Chem. Sci.* **2016**, *7*, 1600–1608.

[40] *A Study of the Interaction between a Family of Gemini Amphiphilic Pseudopeptides and Model Monomolecular Film Membranes Formed with a Cardiolipin*; Gorczyca, M.; Korchowiec, B.; Korchowiec, J.; Trojan, S.; Rubio-Magnieto, J.; Luis, S. V.; Rogalska, E.; J. Phys. Chem. B **2015**, *119*, 6668-6679.

LogP values from 1 to 4.5 (Figure S3a). The structure-activity relationships of the compounds will be further discussed in Section 3.

Table 1. Minimum Inhibitory Concentration (MIC, μg/mL), Minimal Bactericidal Concentration (MBC, μg/mL), the half maximal inhibitory concentration IC50 (μg/mL) values and the partition coefficient logP values and HPLC retention times for the different compounds.

Entry	Compound	LogP[a]	Retention time[b] (min)	*E. coli*		*B. subtilis*		HEK-293
				MIC[e] μg/mL	MBC[e] μg/mL	MIC[e] μg/mL	MBC[e] μg/mL	IC_{50} μg/mL
1	**1a**	3.01[c]	6.1	>2000	>2000	16	16	3.2 ± 0.5
2	**1b**	3.63[d]	6.2	128	256	4	8	0.8 ± 0.2
3	**1c**	4.83 [d]	7.7	256	256	16	32	18 ± 4
4	**2a**	-0.67[c]	3.4	>2000	>2000	>2000	>2000	>45
5	**2b**	-0.20 [d]	3.7	>2000	>2000	>1000	>1000	>79
6	**2c**	-1.34 [d]	3.1	1000	>2000	128	256	>142
7	**3a**	3.50[c]	6.7	1000	>2000	16	16	7.3 ± 1.2
8	**3b**	4.26 [d]	8.8	32	128	4	4	61 ± 6
9	**3c**	5.96 [d]	10.0	2000	2000	64	64	37 ± 5
11	1-butylimidazole[f,41]	--	--	99	198	--	--	--
12	1-dodecylimidazole[f,41]	--	--	>10000	>10000	--	--	--
10	Alamethicin[42]	--	--			16	--	62.5[g,43]

[a] Average of values calculated using VCCLab and Molinspiration software. [b] Retention time in HPLC C18 reverse phase, CH_3CN/H_2O 70/30 (0.1% HCO_2H). [c] Value for the protonated forms. [d] Calculated for the imidazolium cations. [e] MIC/MBC values were obtained from a minimum of three separate experiments. Please refer to Supporting Information for MIC/MBC/IC_{50} values in μM. [f] Disk diffusion method [g] Cytotoxicity against MRC-5 cells.

Electron microscopy is a powerful tool to further assess the effect on bacterial cell growth, inhibition, and death caused by the imidazole derivatives and imidazolium salts. Two compounds which showed from moderate to good antibacterial activity - the bisimidazolium salt **1c** and the monoimidazolium salt **3b**, respectively – were chosen for electron microscopy characterization. For these studies *E. coli* and *B. subtilis* were inoculated for 20 h with each compound

[41] *Synthesis of N-Alkylated derivatives of imidazole as antibacterial agents*; Khabnadideh, S.; Rezaei, Z.; Khalafi-Nezhad, A.; Bahrinajafi, R.; Mohamadi, R.; Farrokhroz, A. A.; *Bioorg. Med. Chem. Lett.* **2003**, *13*, 2863–2865.

[42] *Single-cell, time-resolved study of the effects of the antimicrobial peptide alamethicin on Bacillus subtilis*; Barns, K. J.; Weisshaar, J. C.; *Biochim. Biophys. Acta,* **2016**, *1858*, 725–732.

[43] *In vitro and in vivo antitrypanosomal activities of three peptide antibiotics: leucinostatin A and B, alamethicin I and tsushimycin*; Ishiyama, A.; Otoguro, K.; Iwatsuki, M.; Namatame, M.; Nishihara, A.; Nonaka, K.; Kinoshita, Y.; Takahashi, Y.; Masuma, R.; Shiomi, K.; Yamada, H.; Omura, S.; *J. Antibiot.* **2009**, *62*, 303–308.

at their corresponding MIC (Figure 1) and ½ MIC (Figure S1 & S2) concentrations and fixed with glutaraldehyde.

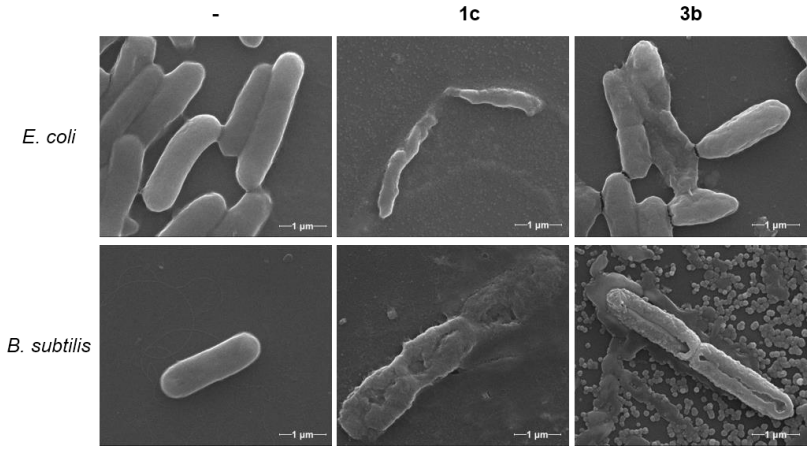

Figure 1. Scanning Electron Microscopy (SEM) images of *E. coli* and *B. subtilis* without treatment (-) and after incubation with compounds **1c** and **3b** at their corresponding MIC (60000 x). See supporting information for additional SEM images.

2.3. Aggregation studies

The self-assembly of the compounds in aqueous medium and in the culture cell medium, was investigated by optical and scanning electron microscopy, as well as UV-vis and fluorescence spectroscopy.

2.3.1 Fluorescence spectroscopy

To investigate the microenvironment of the critical aggregation concentration (CAC) for self-assembly in water and in the bacterial cell culture medium by fluorescence the intensity ratio of two of the peaks (I_1/I_3) of the pyrene fluorescence spectrum was used.[44,45,46] Plots of the pyrene I_1/I_3 ratio as a function of the total surfactant concentration show a typical sigmoidal decrease in the region where self-assembly takes place. At low concentrations, this ratio is larger as corresponds to a polar environment for pyrene. When the surfactant concentration increases this ratio decreases rapidly, as the self-assembly favors the location of pyrene in a more hydrophobic environment, until reaching a roughly constant value because of the full incorporation of the probe into the hydrophobic region of the aggregates. Different approaches have been used to

[44] *Environmental effects on vibronic band intensities in pyrene monomer fluorescence and their application in studies of micellar Systems*; Kalyanasundaram, K.; Thomas, J. K.; *J. Am. Chem. Soc.* **1977**, *99*, 2039-2044.
[45] Kalyanasundaram, K. *Photochemistry in Microheterogeneous Systems*, 1st ed.; Academic Press, New York, **1987**.
[46] *On the determination of the critical micelle concentrationby the pyrene 1:3 ratio method*; Aguiar, J.; Carpena, P.; Molina-Bolívar, J.A.; Carnero Ruiz, C.; *J. Colloid Interface Sci.* **2003**, *258*, 116–122.

estimate CAC values from I_1/I_3 ratios.[47] The most common approach is the use of the break points, either directly or by extrapolating the values from the intersection of the two straight lines defined at the constant and variable regions of the I_1/I_3 sigmoidal curve.[44,47,48,49] As CAC represents the threshold of concentration at which self-aggregation starts, the corresponding value can be estimated from the break point at lower concentration (see Figure S9-S14).[50,51,52,53]

Table 2. Estimated critical aggregation concentration (CAC) values obtained in aqueous and culture cell medium using fluorescence spectroscopy at 25 °C.

Entry	Amphiphilic compound	CAC Fluorescence (mM)[a]		
		W[b]	CCM:W[c]	
			CAC1	CAC2
1	1a	0.085	0.004	0.045
2	1b	0.084	0.006	0.048
3	1c	0.010	0.016	0.21
4	2a	4.31	2.89	5.4
5	2b	4.57	3.46	8.4
6	2c	2.34	2.25	3.54
7	3a	0.033	0.018	0.325
8	3b	0.098	0.063	0.33
9	3c	nd[d]	nd[d]	

[a] CAC values from the break point. [b] In water. [c] In the 1/1 bacterial cell culture medium/water. [d] low solubility.

Fluorescence studies were carried out using MilliQ® water and 1/1 MilliQ® water/ bacterial cell culture medium, because with the pure cell culture medium, a strong broad fluorescence emission band was observed precluding an accurate analysis. Furthermore, compound **3c** could not be studied due to

[47] *Tetrazolium salts and formazan products in Cell Biology: Viability assessment, fluorescence imaging, and labeling perspectives*; Stockert, J.C.; Horobin, R.W.; Colombo, L.L.; Blázquez-Castro, A.; *Acta Histochem.* **2018**, *120*, 159–167.
[48] *Ultrasonic Absorption Studies of Surfactant Exchange between Micelles and Bulk Phase In Aqueous Micellar Solutions of Nonionic Surfactants with Short Alkyl Chains. 1,2-Hexanedlol and 1,2,3-Octanetrlol*; Frindi, M.; Michels, B.; Zana, R.*; J. Phys. Chem.* **1991**, *95,* 4832-4837.
[49] *Aggregation Behavior of Tyloxapol, a Nonionic Surfactant Oligomer, in Aqueous Solution*; Regev, O.; Zana, R.; *J. Colloid Interf. Sci.* **1999**, *210*, 8–17.
[50] *Fluorescence Probes for Critical Micelle Concentration*; Ananthapadmanabhan, K. P.; Goddard, E. D.; Turro, N. J.; Kuo, P. L.; *Langmuir* **1985**, *2*, 352-355.
[51] *Linolenic acid-modified chitosan for formation of selfassembled nanoparticles*; Liu, C. G.; Desai, K. G. H.; Chen, X. G.; Park, H. J.; *J. Agric. Food Chem.* **2005**, *53*, 437–441.
[52] *Preparation and Characterization of Self-Assembled Nanoparticles of Hyaluronic Acid-Deoxycholic Acid Conjugates*; Dong, X.; Liu, C.; *J. Nanomat.*, **2010**, *2010*, 1-9.
[53] *Synthesis and surface-active properties of sulfobetaine-type zwitterionic gemini surfactants*; Yoshimura, T.; Ichinokawa, T.; Kaji, M.; Esumi, K.; *Colloids Surf. A: Physicochem. Eng. Aspects,* **2006**, *273*, 208–212.

solubility problems. The corresponding CACs obtained in water and in the 1/1 mixture of water/ bacterial cell culture medium, by fluorescence are shown in Table 2.

2.3.2. Optical microscopy and scanning electron microscopy (SEM)

The morphology of the aggregates in water, in 1/1 water/bacterial cell culture medium and in the cell culture medium at concentrations above the CAC, were studied by optical microscopy (Figures S15-17) and SEM (Figure 2 and S18).

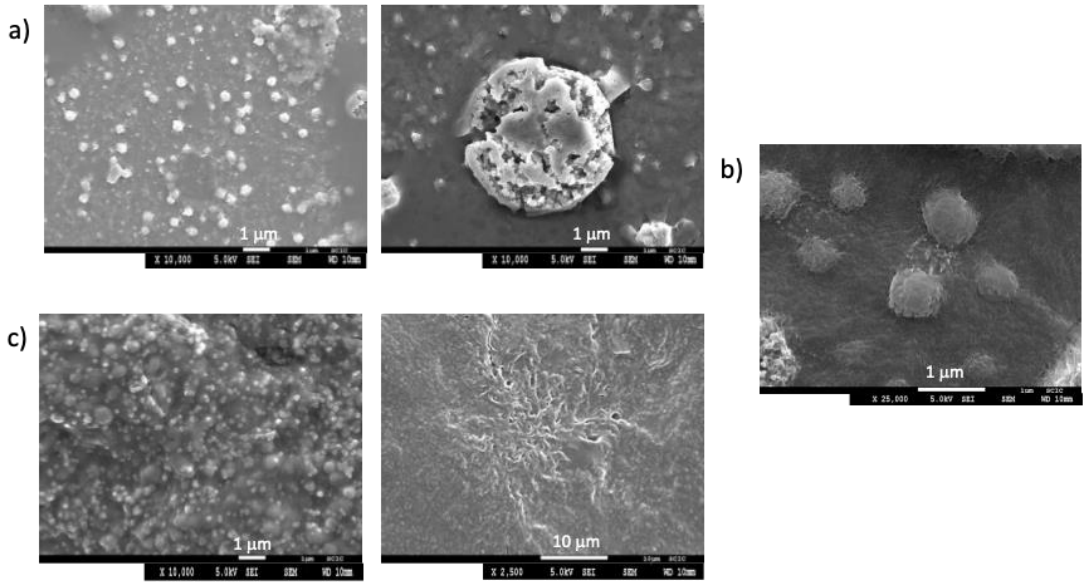

Figure 2. SEM images for **3b** a) 0.5 mM in water; b) 0.7 mM in 1/1 water/bacterial cell culture medium and c) 0.7 mM in the bacterial cell culture medium.

2.3.3. UV-vis spectroscopy

The aggregation and stability of the aggregates in the different solvents, water, 1/1 water/bacterial cell culture and bacterial cell culture medium for **1a-c** were studied by UV-vis at 25 ºC measuring the absorbance at 600 nm, for 1 mM colloidal solutions (Figure 3 and Figure S19-S20).[54,55]

[54] *Monitoring particle aggregation processes*; Gregory, J.; *Adv. in Colloid and Interf. Sci,*.**2009**, *147–148*, 109–123.
[55] *Controlled and Reversible Aggregation of Biotinylated Gold Nanoparticles with Streptavidin*; Aslan, K; Luhrs, C. C.; Pérez-Luna, V. H.; *J. Phys. Chem. B,* **2004**, *108*, 15631–15639.

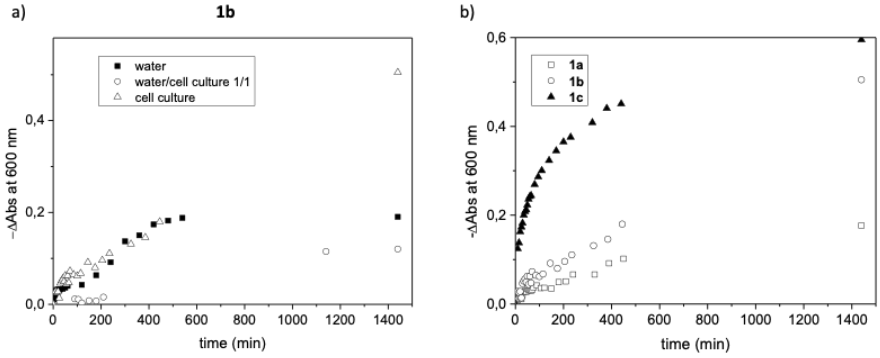

Figure 3. a) Change in absorbance at 600 nm with respect to time for **1b** at 1 mM in different media. b) Change in absorbance at 600 nm with respect to time for **1a-1c** at 1 mM in the bacterial cell culture medium.

3. Discussion

The Gram-positive cell wall is composed of a thick, multilayered peptidoglycan sheath outside of the cytoplasmic membrane, while the Gram-negative cell wall is composed of an outer membrane linked by lipoproteins to thin, mainly single-layered peptidoglycan. The peptidoglycan is located within the periplasmic space that is created between the outer and inner membranes.[56] It therefore follows that all the tested compounds were more active against *B. subtilis* (Gram-positive) than *E. coli* (Gram-negative) (i.e., see Table 1, entries 1 and 7). Compound **3b** (entry 8) proved to be the most active antibacterial agent possessing an MBC as low as 4 and 128 μg/mL against *B. subtilis* and *E. coli* respectively; while those compounds with shorter alkyl chains presented the lowest activity. Some of the compounds (Table 1, entries 2, 3, 6, 7 and 8) presented MIC values lower than MBC values. An antimicrobial compound is considered as bactericidal whenever its MBC to MIC ratio is less than or equal to 4. Otherwise, if its MBC is greater than four times its MIC, the compound would present bacteriostatic activity.[57] In all the cases we could obtain exact MBC and MIC values, their ratio was equal or minor than four. Therefore, compounds 1b, 1c, 3b and 3c present bactericidal activity.

The structural element which clearly relates to a better activity is the use of longer alkyl chains (compounds 1 and 3) in contrast to shorter alkyl chains (compounds 2), probably due to an increased lipophilicity. The toxicity towards miscellaneous bacterial strains of alkyl imidazolium salts have been reported to

[56] *Through the wall: Extracellular vesicles in gram-positive bacteria, mycobacteria and fungi*; Brown, L.; Wolf, J. M.; Prados-Rosales, R.; Casadevall, A.; *Nat. Rev. Microbiol.* **2015**, *13*, 620–630.
[57] Bury-Moné, S.; Antibacterial Therapeutic Agents: Antibiotics and Bacteriophages. In Reference Module in Biomedical Sciences, 3rd ed.; Elsevier, **2014**; pp. 1-13. ISBN 9780128012383

increase with the length of the alkyl chain.[58] The monoimidazolium salts with these longer alkyl chains (**1a-b** and **3a-b**) were more active against *B. subtilis* and *E. coli* than the bisimidazolium counterparts, with the monotopic salt **3b** showing the lowest MIC and MBC values (entries 2 and 8, Table 1), this indicates that the introduction of two hydrophobic alkyl chains contributes greatly to decrease the activity, opposite to the trends observed in the literature.[27]

Regarding amino acid nature, phenylalanine monotopic salt with long alkyl chain (**3b**) presented higher activities for *E. coli*– lower MIC & MBC values - than the analogous valine compound (**1b**) (entries 2 and 8, Table 1), however for ditopic salts the behavior is the opposite, **3c** presented lower activities than **1c** (entries 3 and 9, Table 1).

Although a similar biological activity for the Gram-positive and Gram-negative organisms is preferred, it is not always the case with different strains of microorganisms. Some authors have described that Gram-positive organisms preferred a more lipophilic molecule than the Gram-negative ones.[59] This has been attributed to the difference in the cell outer membrane between bacterial types and strains: while Gram-positive bacteria have a very simple cell wall, the outer membrane of Gram-negative bacteria contains lipopolysaccharides which are cross-bridged by divalent cations, adding strength to the membrane and impermeability to lipophilic molecules. This agreed with the results obtained in Table 1 where the more lipophilic compounds showed less activity against *E. coli*.

A good correlation was obtained between the theoretical logP, calculated using the average values from VCCLab software and Molinspiration, and the retention time observed from HPLC (Figure S1). The activity observed against *B. subtilis* increases for compounds with logP > 3 with MBC ≤ 64 mg/mL. However, MBC values greater than 2000 μg/mL were obtained for both lipophilic and lipophobic compounds, with the exception of the lipophilic compounds **1b**, **1c** and **3b** which present lower MBC values (Figure 4).

---

[58] *Effect of imidazolium-based ionic liquids on bacterial growth inhibition investigated via experimental and QSAR modelling studies*; Ghanema, O. B.; Mutaliba, M. J. A.; El-Harbawi, M.; Gonfaa, G.; Kait, C. F.; Alitheend, N. B. M.; Leveque, J. M.; *J. Hazard. Mater.* **2015**, *297*, 198–206.

[59] *Structure-activity correlations for antibacterial agents on gram-positive and gram-negative cells*; Lien, E.; Hansch, C.; Anderson, S.; *J. Med. Chem.* **1968**, *11*, 430–441.

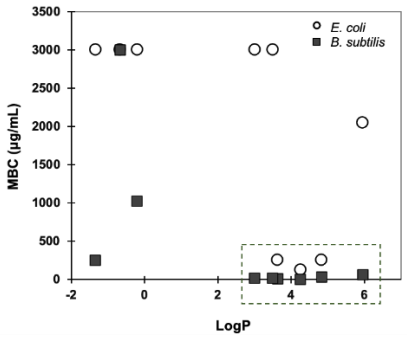

Figure 4. Plot of Log P vs. MBC. *For the sake of clarity, MBC values > 2000 µg/mL are given the value of 3000 µg/mL.

From the SEM images in Figure 1, both bacteria strains incubated with compounds **1c** and **3b** show clear signs of damage: from morphological changes to disruption of the cell membrane and leakage of cytoplasmatic material, ending with the disintegration of the bacteria into small fragments. Most images, especially of *B. subtilis*, show an "implosion" of bacteria, with a marked depression in the middle of the cell (also refer to Figure S1 and Figure S2). In some of the images, aggregates of the compounds can be seen surrounding the bacteria, many of which are attached to the cell membrane.

Human embryonic kidney cells, HEK-293, were chosen as a cell model to evaluate the cytotoxicity of the compounds. The HEK-293 cells were incubated in the cell culture medium with varying concentrations of the examined compound and the impact of treatment was measured using the MTT cell viability assay.[47] The results indicated that compounds **1a-1c, 3a** and **3c** were considerably toxic with IC_{50} values lower than 36 µM (Tables 1 and S1). Surprisingly, compound **3b** derived from phenylalanine was less toxic to the HEK-293 cell line at concentrations 15 times lower than the MIC and MBC for the *B. subtilis* strain (Table 1, entry 8).[60]

Comparing results with the non-chiral 1-butylimidazole, although MIC and MBC values were determined using disk diffusion method,[41] the non-chiral compound is more active against *E. coli* than the analogous amino acid derivative **2a** (MBC 198 µg/mL and >2000 µg/mL, respectively). However, 1-dodecylimidazole is less active than the chiral compound **3a** (MBC 14 mg/mL vs. 1 mg/mL, respectively) (see Table 1), highlighting the role of the amino acid

[60] *Antimicrobial toxicity studies of ionic liquids leading to a 'hit' MRSA selective antibacterial imidazolium salt*; Coleman, D.; Špulák, S.; Garcia, M.T.; Gathergood, N.; *Green Chem.* **2012**, *14*, 1350–1356.

moiety. Furthermore, comparing with commercial alamethicin, (Table 1, entry 10), the inhibition response for *B. subtilis* is in the same range and lower than **3b**,[42] being its toxicity against MRC-5 human cells similar than the cytotoxicity of the imidazolium salt **3b** against HEK-293 line.[43]

To gain a more detailed understanding on the mechanism of cytotoxicity of these imidazole and imidazolium salts on bacteria, we studied the possible structure-activity relationship between their biological activities and their aggregation behavior in culture cell medium.[23,38]

From pyrene fluorescence studies in pure water, the plot of the I_1/I_3 ratio for the corresponding emission spectra *vs* concentrations showed one single break point (Figure S9, S11 and S13) reaching in all cases values of $I_1/I_3 \approx 1.3$ or lower after the break point. However, in the bacterial culture cell medium, the plot of the I_1/I_3 ratios for the corresponding emission spectra *vs* concentration presented two single break point and, in some cases, even three points**.** The two break points observed for all the compounds, suggest the presence of two different processes. The first one takes place at I_1/I_3 values observed for pyrene in the absence of compounds (I_1/I_3 = 1.16 in water 1/1 bacterial culture cell medium) and reveals that pyrene is fully exposed to the polar solvent mixture in this first aggregation step. At the second break point, at higher concentrations, this ratio reaches lower values suggesting the formation in this region of aggregates in which the probe molecule is less solvent exposed.[61] For example, for compound **1b** the first break point at 6 µM leads to aggregates with an appreciable solvent exposed probe ($I_1/I_3 \approx 1.1$) and the second process starts at *ca.* 48 µM affording aggregates providing a low polarity microenvironment to pyrene reaching I_1/I_3 values ≈ 0.8 for 1 mM concentration.

The CAC values obtained for compounds with long alkyl chain were in the µM range while for compounds **2a-c** with short alkyl chains the CAC values obtained were in the mM range (i.e., entries 1 and 4, Table 2), being in water the lower CAC values for the ditopic salts. When the medium change from water to water/culture cell medium in general for imidazole and monotopic salts the CAC values decrease (i.e Table 2, entries 1 and 2), however for ditopic salts the CAC values do not change significantly (Table 2, entries 3 and 6).

---

[61] *Spontaneously Formed Vesicles of Sodium N-(11-Acrylamidoundecanoyl)-glycinate and l-Alaninate in Water*; Roy, S.; Dey, J.; *Langmuir* **2005**, *21*, 10362-10369.

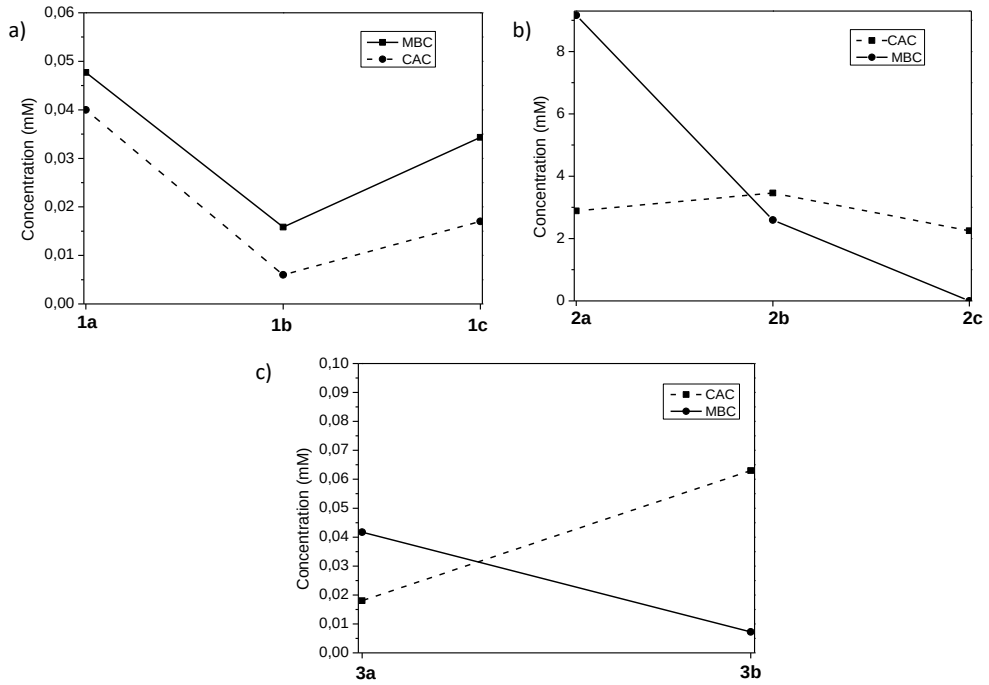

Figure 5. Correlation of MBC for *B. subtilis* and CAC for the different series of compounds in the culture cell medium: a) valine derivatives with long alkyl chain; b) valine derivatives with long short chain; and c) phenylalanine derivatives with long alkyl chain.

Comparing the first CAC values obtained in 1/1 water/bacterial culture cell medium and the MBC for *B. subtilis* for the different series of compounds in Figure 5, it can be observed as compounds **1a-1c** presented the CAC below the MBC, implying that these compounds exist in an aggregated form at the MBC concentration, meaning fewer imidazolium monomers will be present at these concentrations, less than is needed to produce a significant biologic effect, thus increased overall concentrations are needed to obtain the desired bactericidal effects if the monomeric form is the responsible of the corresponding bioactivity. However, different behavior was observed for the series **3a-3b** derived from phenylalanine, it is observed in Figure 5b as the linear CAC line intersects the MBC line, being the CAC lower and above the MBC line for **3a** and **3b** respectively, indicating compound **3b** is not aggregated at the antimicrobial response concentration decreasing its concentration for a significant biologic effect as observed in Table 2 (entry 8). Finally, for **2a-2c** series, the CAC is below the MBC for **2a** while is above for **2b** and **2c,** being its monomeric form the main responsible of the corresponding moderate bioactivity (Table 2, entry 6).

In addition to the results above, the compounds containing dodecyl chains can easily align with lipids and hence accumulate within the cell membrane. In this regard, compounds with longer alkyl tails have CACs in μM range in the

bacterial culture cell medium and thus easily self-assemble, leading to an easy accumulation within cell membrane. Therefore, being its effective concentration at the site of action within the cellular cytoplasm lower. This accumulation could lead to membrane destabilization or disruption,[38] being a possible biocide mechanism, as is observed in Figure 1. Furthermore, it appears that the shorter chain length results in reduced membrane interaction as well as provided an energetically unfavorable micelle formation, meaning low self-assembling capability, leading to lower bacterial cytotoxicity as seen from the corresponding MIC and MBC values (Table 1).

Overall, by comparing the MBC for *B. subtilis* and CAC of the imidazole and imidazolium series, this study has provided a better understanding of the relationship between the biological activities of these compounds correlated with their aggregation capabilities. It was shown that the compounds with longer alkyl chains provide excellent antimicrobial activity although most of them are aggregated at the antimicrobial response concentration, with only compound **3b** being in its monomeric form.

Optical microscopy confirmed the formation of spherical aggregates between 0.5-20 μm diameter in size in the three different media (Figure S15-S17). Regarding the medium, in general in the culture medium the dispersity of the aggregates decreases for compounds with longer alkyl chains (see Figure S15 and S17). Furthermore, in the bacterial culture medium compounds **2a-c** and **3b** were able to form worm-like aggregates at the studied concentrations (Figure S16 and S17).

Furthermore, SEM images for **1c** and **3b** in water, in 1/1 water/bacterial cell culture medium and in the bacterial cell culture medium revealed the formation of different aggregates morphologies. Compound **1c** showed spherical aggregates with < 3 μm diameter size in the three media, being more distorted the aggregates in water (Figure S18). Compound **3b** was able to form spherical aggregates in water and water/culture cell medium (Figure 2a-2b), while in the culture medium different morphologies were observed, spherical aggregates with sizes < 1 μm coexisting with fibrillary aggregates (Figure 2c). When viewed at higher magnification, it is observed that the bigger spherical aggregates consist of several smaller aggregates or dendritic fibrillary aggregates for **3b** and **1c** respectively (Figure 2 and S18).

Regarding the stability of the aggregates formed, studies by UV-vis spectroscopy for **1a-c** are gathered in Figure 3. Figure 3a shows the change in absorbance ($-\Delta A_{600}$) of compound **1b** (1 mM) at 600 nm with respect to time in the different media. The initial rate for the change in absorbance associated to the destabilization of the aggregates is defined by the slope of the linear region of the initial $-\Delta A_{600}$ versus time plot. The slope and the total change in the absorbance was the smallest when using the water/bacterial culture cell medium, being the rate at the initial region for pure water and culture cell medium in the same ranges. However, it must be highlighted that the absorbance decreases until reaching a zero value after 500 min for pure water. A different behavior was obtained for **1a** and **1c** (see Figure S19 and S20). For compound **1a**, the absorbance at 600 nm decreased with time in the three media with similar rates, while for **1c** the rate followed the order water > bacterial culture cell medium > 1/1 water/bacterial culture cell medium, reaching almost zero values in the tree media after 24 h.

Overall, the results obtained show that in the pure culture medium the stability of the aggregates follows the order **1a** > **1b** > **1c** (Figure 3b), indicating that the introduction of two headgroups and hydrophobic alkyl chains in **1c** contributes to a minor stabilization of the aggregates in this medium.

4. Materials and methods

4.1. Materials

4.1.1. Reagents and culture media

Resazurin sodium salt and dimethyl sulfoxide (DMSO) were bought from Sigma-Aldrich. Luria-Bertani (LB) liquid broth (Miller's formulation) and Nutrient Broth (NB) were freshly prepared and sterilized by autoclave. Broth powders were bought from Scharlab. Tryptone Soy Agar plates were purchased from Thermo Scientific. Glutaraldehyde was purchased in solution at 25% in H_2O and Grade II from Sigma Aldrich and used as provided. Phosphate buffer was prepared from the solid salts NaH_2PO_4 and Na_2HPO_4, both purchased from Aldrich at qualities 99% and 99.5% respectively, by dissolving them in MilliQ® water and adjusting pH with NaOH and HCl solutions.

Cell culture media for cytotoxicity studies were purchased from Gibco (Grand Island, NY). Fetal bovine serum (FBS) was obtained from HyClone (Utah USA). Supplements and other chemicals not listed in this section were obtained from

Sigma Chemical Co. (St. Louis, MO). Plastics for cell culture were supplied by Thermo Scientific BioLite (Madrid, Spain). All tested compounds were dissolved in DMSO at a concentration of 10 mM and stored at -20 °C until use. HEK-293 cell llines were maintained in Dulbecco's modified Eagle's medium (DMEM) containing glucose (1 g/L), glutamine (2 mM), penicillin (50 μg/mL), streptomycin (50 μg/mL) and amphotericin B (1.25 μg/mL) supplemented with 10% FBS.

Reagents and solvents, including NMR solvents, were purchased from commercial suppliers and were used without further purification except for pyrene, used for fluorescence studies, that was crystallized twice from ethanol. Deionized water was obtained from a MilliQ® equipment. Imidazoles **1a** and **2a** and imidazolium salts **1b** and **1c** were prepared as previously described.[30,32]

4.1.2. Microorganisms and growth conditions

Two bacterial strains were used in the antibacterial assays: *Escherichia coli* DH5α as a Gram-negative model and *Bacillus subtilis* 1904-E as a Gram-positive model. Both bacteria strains were incubated at 37 °C and the pre-inoculum incubation time was of 24 h. Liquid Luria-Bertani (LB) medium was used for *E. coli* DH5α and Nutrient Broth (NB) for *B. subtilis*.

4.2. Methods

4.2.1 Bacterial proliferation assay in presence of imidazole derivatives

The bacteria cell bank suspensions were thawed and inoculated in the appropriate liquid broth for 24 h at 37 °C with mild agitation. A dilution from these culture solutions was used for the following tests, corresponding to an inoculum of $1x10^7$ CFU/mL. Stock solutions of all the tested compounds were prepared in DMSO at a concentration of 100 mg/mL, aliquoted and stored at -20 °C.

A) Bacterial growth inhibition assay

Conditions here described are for testing 6 different concentrations of the compounds, with triplicates of each condition. Therefore, 4 compounds were tested per plate. An adapted version of the microdilution method was used. Firstly, the imidazole derivatives were dissolved in the corresponding broth at 2X the highest tested concentration. 100 μL of the 2X solutions were added to the first (A) and second (B) row wells of a 96-well plate. 100 μL of liquid medium

had been previously added to rows B to F. Subsequent dilutions at 1:2 are prepared in rows B to F, by withdrawal of 100 µL from the previous row (more concentrated) to the next row (half diluted), mixing well. 100 µL were discarded from the last row (F). By now, there are 100 µL in each well, and 100 µL of bacterial suspension at 10^7 CFU/mL were added to each well. Then, the 96-well plates were incubated for 24 h at 37 °C under mild agitation. Bacterial growth was controlled both by visual observation of the turbidity in each well and by measuring the optical density (OD) at 560 nm at time 0 h and 24 h. Results are recorded as the lowest concentration of antimicrobial agent that inhibits visible growth of the bacteria and were compared with the OD variation of a control culture containing *E. coli* or *B. subtilis* (+ control) and of solution of the tested compounds without bacteria (- control).

B) Bacterial cell viability assay

Cell viability was analyzed using a Resazurin (7-Hydroxy-3H-phenoxazin-3-one 10-oxide) assay in a 96-well plate. Once the bacterial cultures of growth inhibition assay had been grown for a total of 24 h, 25 µL of a 0.1 mg/mL Resazurin (prepared in LB or NB medium) were added to each well and incubated in the dark at 37 °C for 1 h under stirring. Resazurin has a blue color at the testing pH and turns pink when reduced by the viable bacteria to Resorufin. Therefore, pink wells indicate metabolizing bacteria, while blue wells are indicative of bacteria that have lost their ability to convert Resazurin to Resorufin. Different controls were made in order to corroborate the MBC value obtained by the Resazurin assay. The change of color was confirmed at 1 h, 4 h, and 24 h after its addition. The viability of bacteria was verified (either confirmed or rejected) by the colony plate-counting method, by seeding 10 µL from the cell culture onto Tryptone Soy Agar plates and observing the presence or absence of bacterial growth after 24 h at 37 °C.

4.2.2. LogP calculation and retention time determination

LogP values for the different compounds were calculated using VCCLab (ALOGPS 2.1) and Molinspiration (miLogP2.2) softwares. We used LogP as the average of these values. The protonated forms for the imidazole derivatives were considered. Reverse phase HPLC (equipment: Agilent technologies 1100 series, column: Xterra MS C18 4.6x150 mm (5 µmol/L)) was also used for measuring the relative lipophilicity of these compounds, since the retention time of each molecule on the reverse phase column is related to its lipophilicity. All the

products were dissolved in CH_3OH at 2 mmol/L concentration and eluted using 70/30 acetonitrile/water and 0.1 % of formic acid for 15 min and flow rate 0.2 mL/min at 25 °C. λ used was 254, 280 and 220 nm taking the corresponding chromatogram with higher mAU (see Supporting Information).

4.2.3. H NMR studies

NMR experiments were carried out on a Varian INOVA 500 spectrometer (500 MHz for ^{1}H and 125 MHz for ^{13}C), on a Bruker Avance III HD 400 spectrometer (400 MHz for ^{1}H and 100 MHz for ^{13}C) or on a Bruker Avance III HD 300 spectrometer (300 MHz for ^{1}H and 75 MHz for ^{13}C) at 25 °C. Chemical shifts are reported in ppm using TMS as the reference.

4.2.4. Fluorescence spectroscopy measurements

Pyrene was used as a fluorescence probe to determine the CAC of the compounds in water and 1/1 water/bacterial cell culture medium at 25±1 °C. Fluorescence measurements were performed with a Spex Fluorolog 3-11 instrument equipped with a 450 W xenon lamp (right angle mode). Firstly, a stock pyrene solution of 1.98×10^{-4} mol/L was prepared in ultrapure methanol. Then, solutions of the imidazole and imidazolium salt compounds (ranging from 6 to 3×10^{-3} mmol/L) were prepared in different vials and 5 µL of pyrene solution was transferred into the vials, reaching a final pyrene concentration of 9.89×10^{-7} mol/L in each vial. Fluorescence spectra of pyrene were recorded from 200 to 650 nm after excitation at 337 nm, and the spectra were not corrected for the Xe lamp spectral response. The slit width was set at 5 nm for both excitation and emission. The peak intensities at 373 and 385 nm were determined as I_1 and I_3 respectively. The ratios of the peak intensities at 373 and 385 nm (I_1/I_3) for the emission spectra were recorded as a function of the logarithm of concentration. The CAC values were taken from the break point. Samples were excited with a 337 nm NanoLED.

4.2.5. Optical images

Images were recorded with OLYMPUS COVER-018 microscopy, BX51TF model, at 25 °C. Experiments were carried out in water, 1/1 water/bacterial cell culture medium and in bacterial cell culture medium.

4.2.6. Scanning Electron Microscopy (SEM)

SEM images of the compounds were obtained using a JEOL 7001F microscope with a digital camera; while SEM images of the incubated bacteria were obtained using an Inspect F50 microscope, at 10 kV and spot size of 3.0, with a digital camera. Bacteria solutions at *ca.* $0.5x10^7$ CFU/mL were incubated overnight without and with compounds **1c** and **3b** at their ½ MIC and MIC. After this, bacteria were washed with sterile PBS and fixed by incubation for 2 h in a 2.5% glutaraldehyde solution in phosphate buffer 10 mmol/L at pH 7.2. The fixed bacteria were subsequently washed once with phosphate buffer saline solution and four times with MilliQ water to remove any residual salts and glutaraldehyde. Finally, bacteria were resuspended in MilliQ water and 10 µL of these solutions were placed on silicon wafers and allowed to dry by evaporation overnight. Samples were coated with platinum using the sputtering technique in which microscopic particles of platinum are rejected from the surface after the material is itself bombarded by energetic particles of a plasma or gas. Experiments were carried out in water, 1/1 water/bacterial culture cell medium and in bacterial cell culture medium.

4.2.7. UV-vis spectroscopy

UV-Vis absorption spectra of the colloidal solutions were recorded on a Hewlett-Packard 8453 spectrophotometer at 25 °C. Experiments were carried out in water, 1/1 water/bacterial cell culture medium and in bacterial cell culture medium.

4.2.8. Cell proliferation assay for cytoxicity studies

In 96-well plates, 3×10^3 HEK-293 cells per well were seeded and incubated with serial dilutions of the tested compounds (from 200 mM to 0.2 mM) to a total volume of 100 µL of their growth media. The 3-(4,5-dimethylthiazol-2-yl)-2,5-diphenyltetrazolium bromide (MTT; Sigma Chemical Co.) dye reduction assay in 96-well microplates was used, as previously described.[18] After 2 days of incubation (37 °C, 5% CO_2 in a humid atmosphere), 10 µL of MTT (5 mg/mL in phosphate-buffered saline, PBS) was added to each well, and the plate was incubated for a further 3 h (37 °C). The supernatant was discarded and replaced by 100 µL of DMSO to dissolve formazan crystals. The absorbance was then read at 540 nm by Multiskan™ FC microplate reader. For all concentrations of compound, cell viability was expressed as the percentage of the ratio between

the mean absorbance of treated cells and the mean absorbance of untreated cells. Three independent experiments were performed, and the IC_{50} values (i.e., concentration half inhibiting cell proliferation) were graphically determined using GraphPad Prism 4 software.

Statistical analysis: GraphPad Prism v4.0 software (GraphPad Software Inc., La Jolla, USA) was used for statistical analysis. For all experiments, the obtained results of the triplicates were represented as means with standard deviation (SD).

5. Conclusions

A series of novel imidazole and imidazolium salts derived from *L*-valine and *L*-phenylalanine containing different hydrophobic groups have been synthesized and their antibacterial activity studied against *E. coli* and *B. subtilis*. The results demonstrate that an optimum lipophilicity of the alkyl chain and the amino acid side chain is needed to achieve antibacterial activity. The compounds presented better antibacterial activity against *B. subtilis* than *E. coli*, where compound **1a-1b** and **3a-3b** were the most active against *B. subtilis*, showing MBC values corresponding to 16 µg/mL or lower. Monotopic compound **3b** was 15 times less active against human embryonic kidney cells HEK-293 than toward *B. subtilis,* thus demonstrating its potential as an effective antibacterial agent with good biocompatibility. Aqueous aggregation studies revealed CAC values for compounds **1a-1c** and **3a-3c** in the µM range in water alone, and these CAC values decreased for imidazole and monotopic species when the culture cell medium was used instead of water. Optical microscopy and SEM images confirm the formation of these spherical aggregates. It is important to note that most of the bioactive compounds were aggregated to some extent at their MIC/MBC concentrations, while compound **3b** was not aggregated at its minimum bactericidal concentration, suggesting that the monomeric species was responsible for the antibacterial activity.

6. Supporting Information

6.1. Synthetic Protocols and Structural Characterization

Imidazole **3a** and compounds **2b-c** and **3b-c** were prepared following the synthetic protocols.

General procedure for compound 3a: To a mixture of glyoxal (40% aq., 1.1 equiv, 2.6 mL) and formaldehyde (37% aq., 5.0 equiv, 7.7 mL), the (*S*)-2- amino-N-dodecyl-3- phenylpropanamide compound (1.0 equiv, 6.9 g, 20.8 mmol) and ammonium acetate (1.1 equiv, 1.8 g, 23.4 mmol) were dissolved previously in methanol and added. The reaction mixture was stirred at room temperature for 48 h. The solvent was evaporated under reduced pressure and the resulting crude residue was treated with saturated Na_2CO_3 solution, extracted with CH_2Cl_2 (3x), dried with anhydrous $MgSO_4$, filtered, and concentrated.

Synthesis of 3a. Yellow liquid (7 g, 88%), $[\alpha]_D^{25}$= -7.11 (CH_3OH); m.p= 56.1 ºC. ^{1}H NMR (400 MHz, $CDCl_3$ and CD_3OD) δ 7.26 – 7.07 (m, 4H), 7.00 (m, 1H), 6.97 – 6.89 (m, 3H), 6.48 (t, J = 5.7 Hz, NH), 4.67 (dd, J = 9.1, 6.0 Hz, 1H), 3.46 (dd, J = 14.0, 6.0 Hz, 1H), 3.19 – 3.00 (m, 3H), 1.30 (m, 2H), 1.26 – 1.04 (m, 18H), 0.85 – 0.77 (m, 3H). ^{13}C NMR (101 MHz, $CDCl_3$) δ 168.3, 134.0, 136.3, 129.6, 128.8, 128.7, 127.2, 118.0, 62.9, 39.8, 39.3, 31.9, 29.6, 29.6, 29.5, 29.3, 29.2, 26.8, 22.7, 14.1. MS (ESI) (m/z) calcd. for $C_{24}H_{37}N_3O$ $[M+H]^+$ = 384.3; found 383.4 (100%), 767.7 (35%, $[M+M+H]^+$). IR (ATR)= 3309, 2953, 2919, 2850, 1656, 1549, 1493, 1469, 1454 cm^{-1}. Calculated for $C_{24}H_{37}N_3O{\cdot}4H_2O$: C 63.27, H 9.96, N 9.22; found C 62.97, H 9.74, N 9.58.

General procedure for compounds 2b-3b: To a mixture of compound **2a-3a** (1.1 eqiv) and bromomethylbencene (1.0 equiv) were dissolved in acetonitrile (5 mL). The reaction was carried out under microwave irradiation using 120 W, 1.72x10^6 Pa, 150ºC and 1 hour. After solvent evaporation, the remaining solid was washed with diethyl ether (x3) to afford the desired compound.

Synthesis of 2b. Yellow oil (150 mg, 93%); $[\alpha]_D^{25}$= 41.07 (CH_3OH); m.p. 33ºC. ^{1}H NMR (400 MHz, $CDCl_3$) δ 9.93 (s, 1H), 8.62 (t, J = 5.7 Hz, 1H), 7.75 (t, J = 1.8 Hz, 1H), 7.38 – 7.21 (m, 5H), 7.11 (s, 1H), 5.66 (d, J = 10.6 Hz, 1H), 5.47 – 5.27 (dd, J = 10.6, 2.2 Hz, 2H), 3.34 – 3.17 (m, 1H), 3.12 – 2.96 (m, 1H), 2.45 - 2.37 (m, 1H), 1.54 – 1.40 (m, 2H), 1.32 - 1.21 (m, 2H), 1.03 (d, J = 6.5 Hz, 3H), 0.81 (t, J = 7.3 Hz, 3H), 0.76 (d, J = 6.6 Hz, 3H). ^{13}C NMR (101 MHz, $CDCl_3$) δ 167.0, 136.1, 131.8, 130.1, 129.8, 128.6, 121.8, 120.9, 67.7, 53.9, 39.6, 31.2, 31.0, 20.2, 18.8, 18.3, 13.7. MS (ESI) (m/z) calcd. for $C_{19}H_{28}N_3O$ $[M]^+$ = 314.2; found 314.5 (100%); IR (ATR)= 3220, 3063, 2962, 2933, 2873, 1672, 1550, 1497, 1456, 1327, 1225, 1152 cm^{-1}. Calculated for $C_{19}H_{28}N_3OBr$: C 57.87, H 7.16, N 10.66; found C 57.80, H 6.98, N 11.01.

Synthesis of 3b. Yellow viscous solid (129 mg, 90%); $[\alpha]_D^{25}$= -31.07 (CH_3OH); m.p= 16 ºC. ^1H NMR (300 MHz, $CDCl_3$) δ 9.53 (s, 1H), 8.59 (t, J = 5.5 Hz, NH), 7.74 (s, 1H), 7.41 – 7.14 (m, 7H), 7.04 – 6.95 (m, 2H), 6.92 (s, 1H), 6.55 (m, 1H), 5.14 (q, J = 14.7 Hz, 2H), 3.51 – 2.95 (m, 4H), 1.83 (s, 3H), 1.44 (m, 2H), 1.17 (s, 16H), 0.92 – 0.70 (m, 3H). ^{13}C NMR (101 MHz, $CDCl_3$) δ 166.6, 136.1, 134.3, 131.9, 129.8, 129.7, 129.1, 129.0, 128.2, 127.5, 121.8, 120.9, 62.3, 53.6, 40.0, 39.0, 31.9, 29.7, 29.6, 29.5, 29.4, 29.2, 28.9, 27.0, 22.7, 14.1. MS (ESI) (m/z) calcd. for $C_{31}H_{44}N_3O$ $[M]^+$ = 474.4; found 474.7 (100%); IR (ATR)= 3297, 3061, 2966, 2922, 2851, 1654, 1557, 1495, 1453 cm^{-1}. Calculated for $C_{31}H_{44}N_3OBr{\cdot}H_2O$: C 65.02, H 8.10, N 7.34; found C 65.46, H 8.24, N 7.68.

General procedure for compounds 2c-3c: To a mixture of compound **2a-3a** (2.2 equiv) and 1, 3-(bis-bromomethyl)bencene (1.0 equiv) were dissolved in acetonitrile (5 mL). The reaction was carried out under microwave irradiation using 120 W, $1.72x10^6$ Pa, 150ºC and 1 hour. After solvent evaporation, the remaining solid was washed with diethyl ether (x3) to afford the desired compound.

Synthesis of 2c. Yellow oil (104 mg, 90%); $[\alpha]_D^{25}$= 6.93 (CH_3OH); m.p.= 85ºC. ^1H NMR (500 MHz, $CDCl_3$) δ 10.01 (s, 2H), 8.40 (t, J = 5.6 Hz, 2H), 8.12 (s, 2H), 7.68 (d, J = 1.3 Hz, 2H), 7.47 – 7.36 (m, 2H), 7.34 – 7.23 (m, 2H), 5.73 (d, J = 14.4 Hz, 2H), 5.55 – 5.38 (dd, J = 10.7 Hz, J = 3.5 Hz, 4H), 3.37 – 3.25 (m, 2H), 3.15 – 3.00 (m, 2H), 2.53 – 2.38 (m, 2H), 1.64 – 1.43 (m, 4H), 1.39 – 1.20 (m, 4H), 1.08 (d, J = 6.6 Hz, 6H), 0.87 (t, J = 7.3 Hz, 6H), 0.82 (d, J = 6.7 Hz, 6H). 13C NMR (126 MHz, $CDCl_3$) δ 206.8, 166.7, 136.5, 134.1, 130.6, 130.5, 129.9, 122.4, 120.8, 77.3, 77.0, 76.8, 68.1, 53.2, 39.5, 31.1, 30.9, 30.9, 20.1, 18.8, 18.4, 13.6. MS (ESI) (m/z) calcd. for $C_{32}H_{50}N_6O_2$ $[M]^{2+}$ = 275.2; found 275.3 (100%); IR (ATR)= 3412, 3228, 3125, 3066, 2962, 2933, 2873, 1671, 1550, 1465, 1360, 1298, 1226, 1152 cm^{-1}. Calculated for $C_{32}H_{50}N_6O_2Br_2{\cdot}2H_2O$: C 51.48, H 7.29, N 11.26; found C 50.84, H 7.32, N 11.46.

Synthesis of 3c. Yellow viscous solid (126 mg, 82%); $[\alpha]_D^{25}$= 17.33 (CH_3OH); m.p.= 60ºC. ^1H NMR (300 MHz, $CDCl_3$) δ 9.47 (s, 2H), 8.21 (t, J = 5.7 Hz, NH), 7.81 – 7.51 (m, 6H), 7.29 – 7.06 (m, 16H), 6.13 (t, J = 8.0 Hz, 2H), 5.31 (s, 4H), 3.37 (dd, J = 13.6, 7.2 Hz, 2H), 3.25-3.10 (m, 4H), 3.00 – 2.84 (m, 2H), 1.41-1.29 (m, 4H), 1.23 – 1.05 (m, 32H), 0.80 (m, 6H). ^{13}C NMR (101 MHz, $CDCl_3$) δ 166.3, 136.3, 134.3, 133.6, 130.6, 130.3, 129.7, 129.2, 128.9, 127.5, 122.3,

121.0, 62.6, 53.0, 39.9, 38.9, 31.9, 29.7, 29.7, 29.6, 29.5, 29.4, 29.2, 28.9, 26.9, 22.7, 14.1. MS (ESI) (m/z) calcd. for $C_{56}H_{82}N_6O_2$ $[M]^{2+}$ = 435.3; found 435.7 (100%); IR (ATR)= 3294, 3063, 2923, 2852, 1656, 1554, 1495, 1454, 1362 cm^{-1}. Calculated for $C_{56}H_{82}N_6O_2Br_2$: C 65.23, H 8.02, N 8.15; found C 65.76, H 8.57, N 8.34.

Imidazole and imidazolium antibacterial drugs derived from amino acids

Index

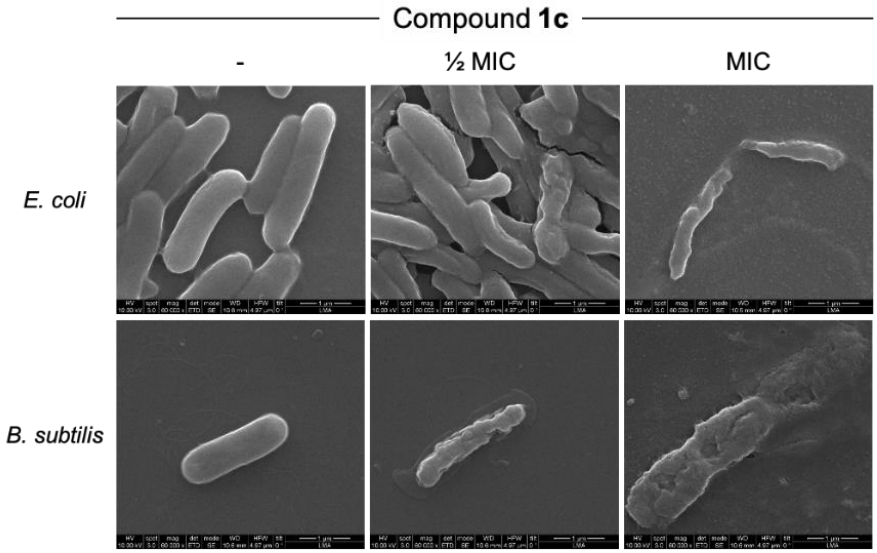

Figure S1 Scanning Electron Microscopy (SEM) images of *E. coli* and *B. subtilis* bacteria without treatment (-) and after incubation with compound **1c** at its ½ MIC and MIC (60000 x).

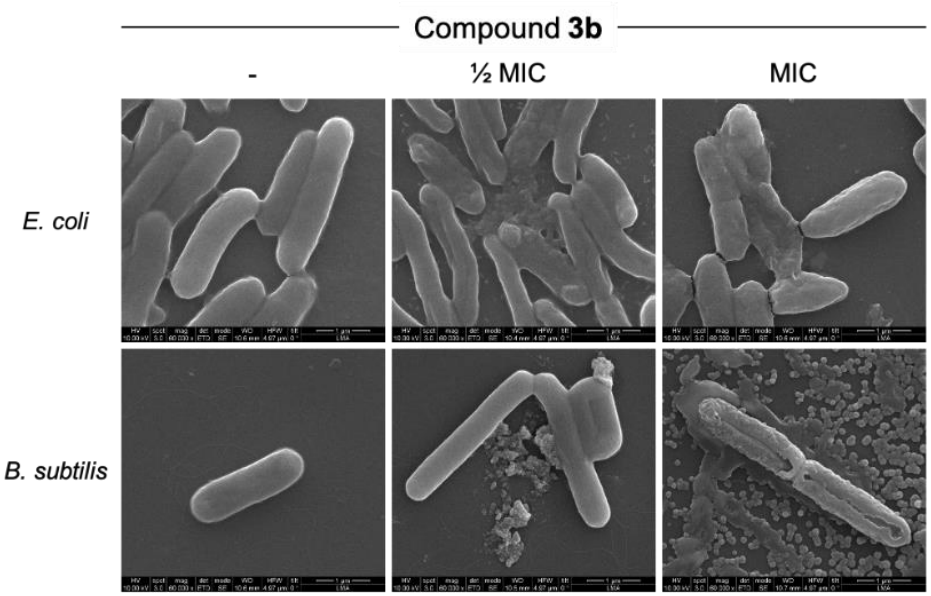

Figure S2 Scanning Electron Microscopy (SEM) images of *E. coli* and *B. subtilis* bacteria without treatment (-) and after incubation with compound **3b** at its ½ MIC and MIC (60000 x).

Table S1 Minimum Inhibitory Concentration (MIC, µM), Minimal Bactericidal Concentration (MBC, µM) and the half maximal inhibitory concentration IC_{50} (µM) values for the different compounds.

Entry	Compound	*E. coli*		*B. subtilis*		HEK-293 IC_{50} µM
		MIC[a] µM	MBC[a] µM	MIC[a] µM	MBC[a] µM	
1	**1a**	>6000	>6000	48	48	9.6 ± 1.6
2	**1b**	288	581	9	18	1.8 ± 0.4
3	**1c**	269	269	19	34	19 ± 4
4	**2a**	>9000	>9000	>9000	>9000	>200
5	**2b**	>5000	>5000	2591	2591	>200
6	**2c**	1444	>2900	180	361	>200
7	**3a**	2662	>5000	42	42	19 ± 3
8	**3b**	57	229	7	7	109 ± 10
9	**3c**	1986	1986	62	62	36 ± 5

[a] Mode – most frequent value - of MIC and MBC values from at least three experiments (when obtaining the same values) or at least five experiments (when the values obtained are different).

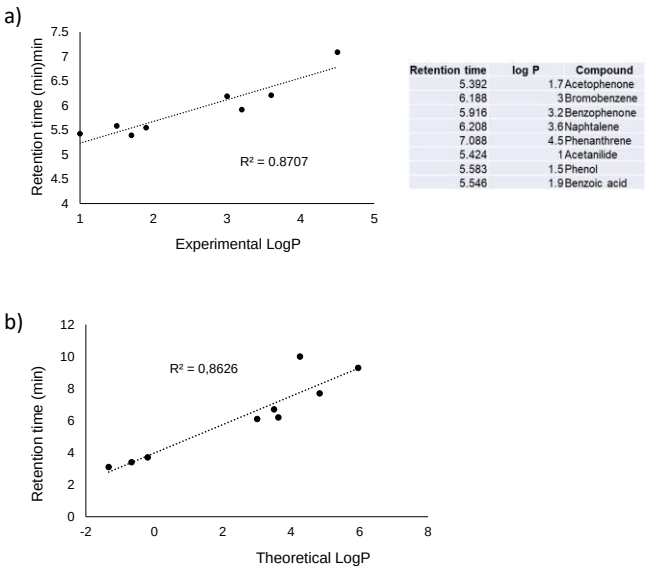

Retention time	log P	Compound
5.392	1.7	Acetophenone
6.188	3	Bromobenzene
5.916	3.2	Benzophenone
6.208	3.6	Naphtalene
7.088	4.5	Phenanthrene
5.424	1	Acetanilide
5.583	1.5	Phenol
5.546	1.9	Benzoic acid

Figure S3 a) Correlation between experimental LogP values and experimental retention time for different commercial compounds, b) Correlation between LogP and the retention time for the different compounds **1**, **2**, **3**.

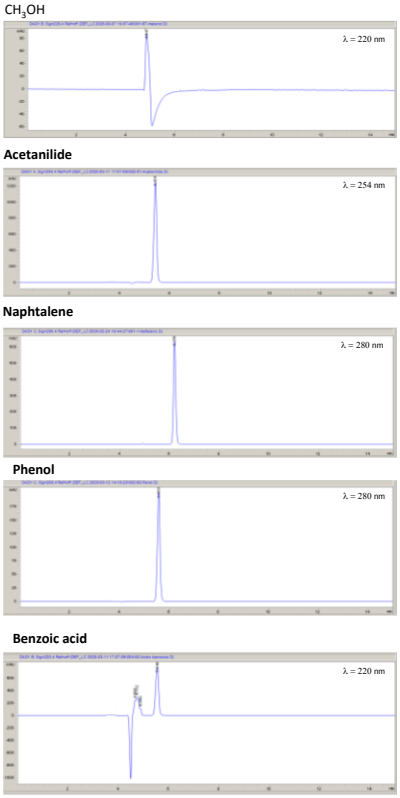

Figure S4 HPLC chromatograms for methanol, acetanilide, naphthalene, phenol and benzoic acid. Mobile phase water/CH_3CN 30/70 v/v (0.1% HCO_2H), 25 °C and flow 0.2 mL/min.

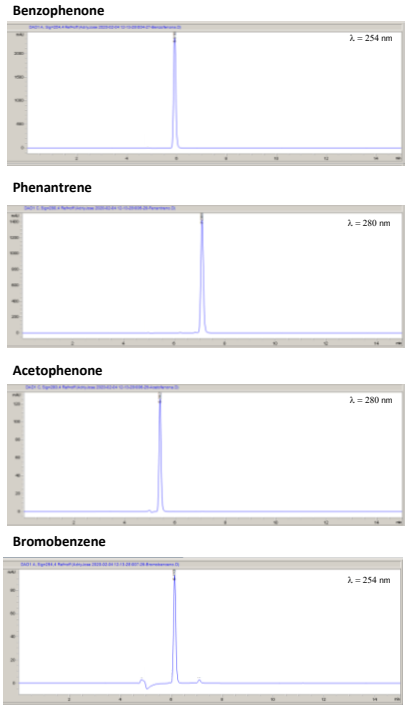

Figure S5 HPLC chromatograms for benzophenone, phenantrene, acetophenone and bromobenzene. Mobile phase water/CH_3CN 30/70 v/v (0.1% HCO_2H), 25 °C and flow 0.2 mL/min.

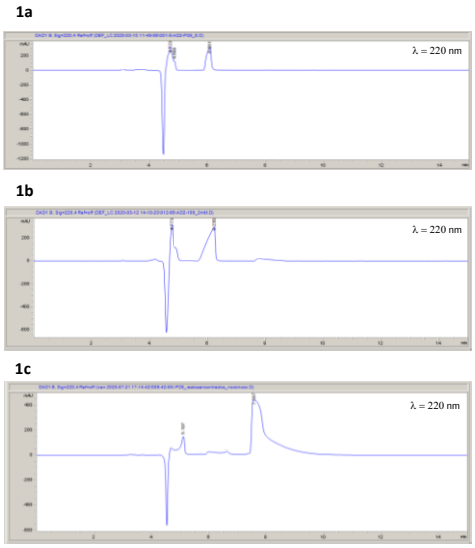

Figure S6 HPLC chromatograms for compounds **1a-c**. Mobile phase water/CH_3CN 30/70 v/v (0.1% HCO_2H), 25 °C and flow 0.2 mL/min.

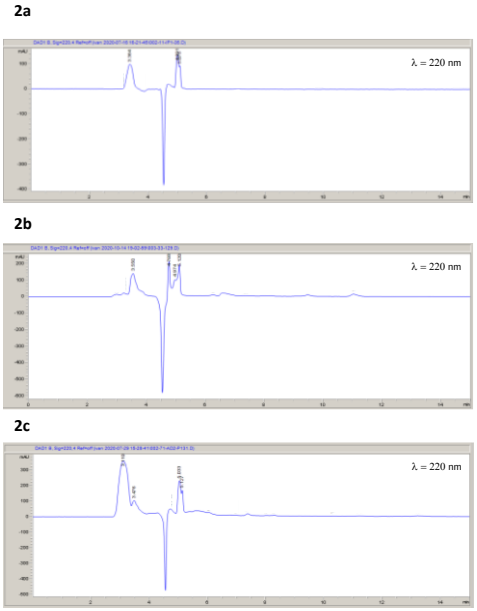

Figure S7 HPLC chromatograms for compounds **2a-c**. Mobile phase water/CH_3CN 30/70 v/v (0.1% HCO_2H), 25 °C and flow 0.2 mL/min.

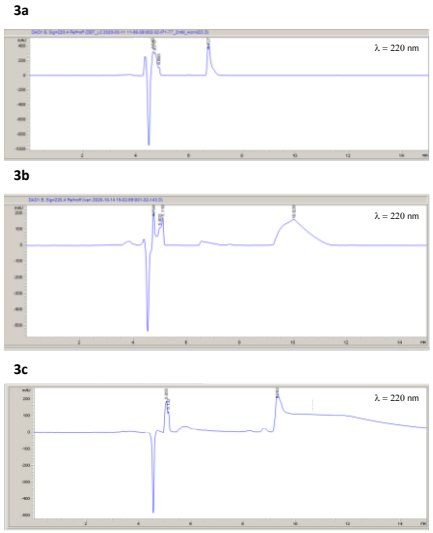

Figure S8 HPLC chromatograms for compounds **3a-c**. Mobile phase water/CH_3CN 30/70 (0.1% HCO_2H), 25 °C and flow 0.2 mL/min.

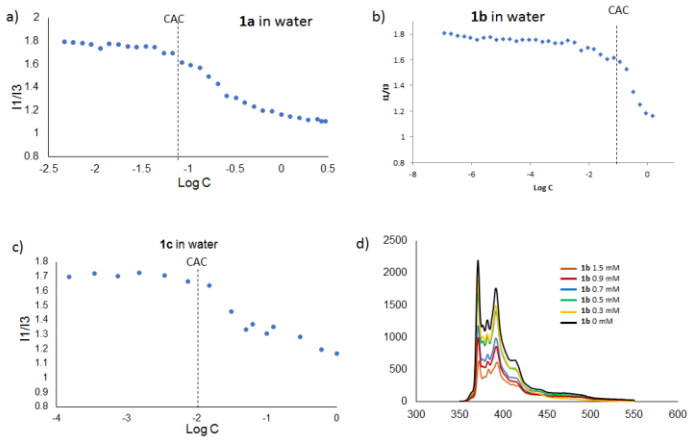

Figure S9 a) - c) Plots of the I_1/I_3 ratios *v* log C for **1a-1c** in H_2O at 25 °C, d) Emission spectra of pyrene in H_2O at 25 °C in the presence of different amounts of **1b**.

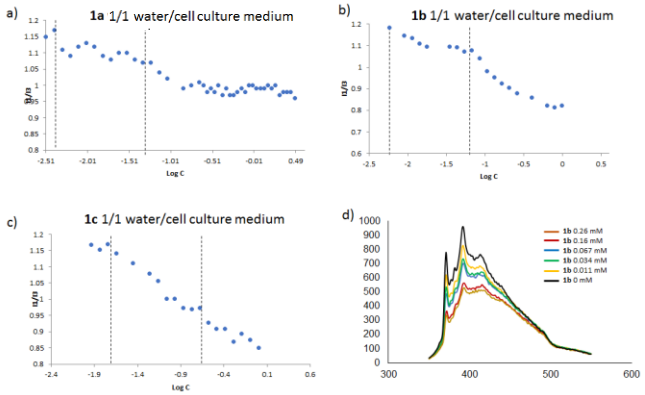

Figure S10 a) - c) Plots of the I_1/I_3 ratios *v* log C for **1a-1c** in water/bacterial culture medium 1/1 v/v at 25 °C, d) Emission spectra of pyrene in water/bacterial culture medium1/1 v/v at 25 °C in the presence of different amounts of **1b**.

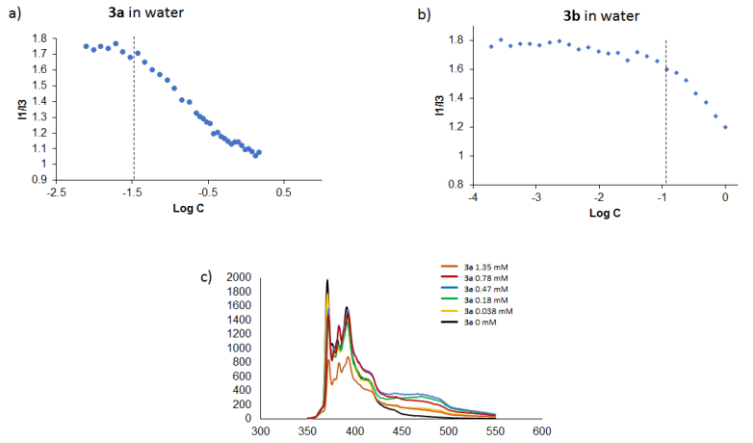

Figure S11 a)-b) Plots of the I_1/I_3 ratios *v* log C for **3a-3b** in H_2O at 25 °C, d) Emission spectra of pyrene in H_2O at 25 °C in the presence of different amounts of **3a**.

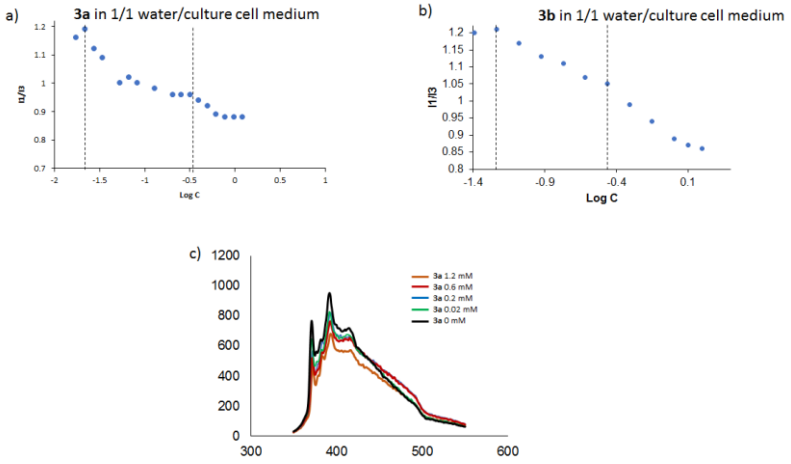

Figure S12 a)-b) Plots of the I_1/I_3 ratios *v* log C for **3a-3b** in water/bacterial culture medium 1/1 v/v at 25 °C, d) Emission spectra of pyrene in water/bacterial culture medium 1/1 v/v at 25 °C in the presence of different amounts of **3a**.

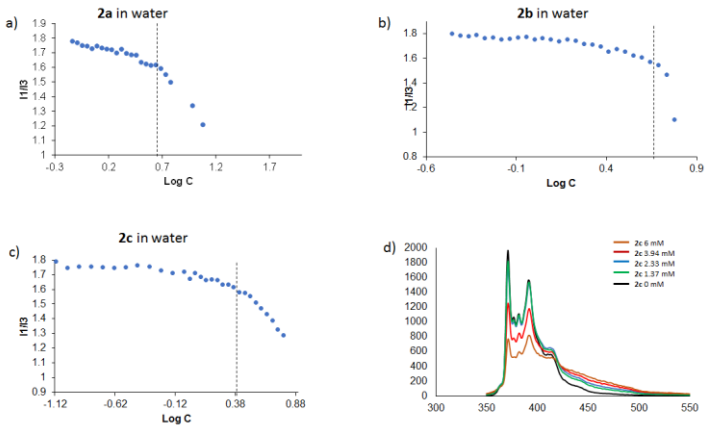

Figure S13 a) - c) Plots of the I_1/I_3 ratios *v* log C for **2a-2c** in H_2O at 25 °C, d) Emission spectra of pyrene in H_2O at 25 °C in the presence of different amounts of **2c**.

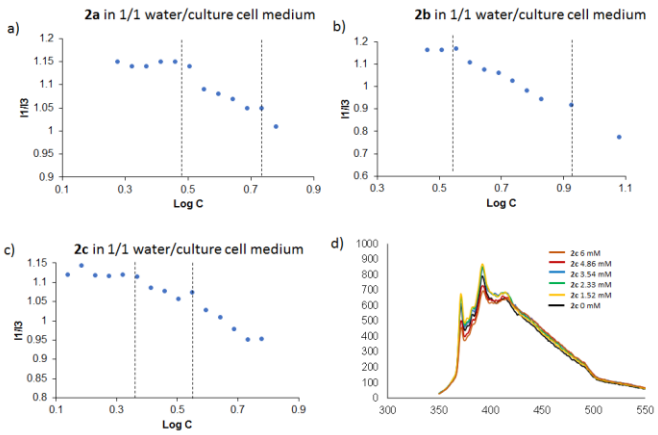

Figure S14 a) - c) Plots of the I_1/I_3 ratios υ log C for **2a-2c** in water/bacterial culture medium 1/1 v/v at 25 °C, d) Emission spectra of pyrene in water/bacterial culture medium1/1 v/v at 25 °C in the presence of different amounts of **2c**.

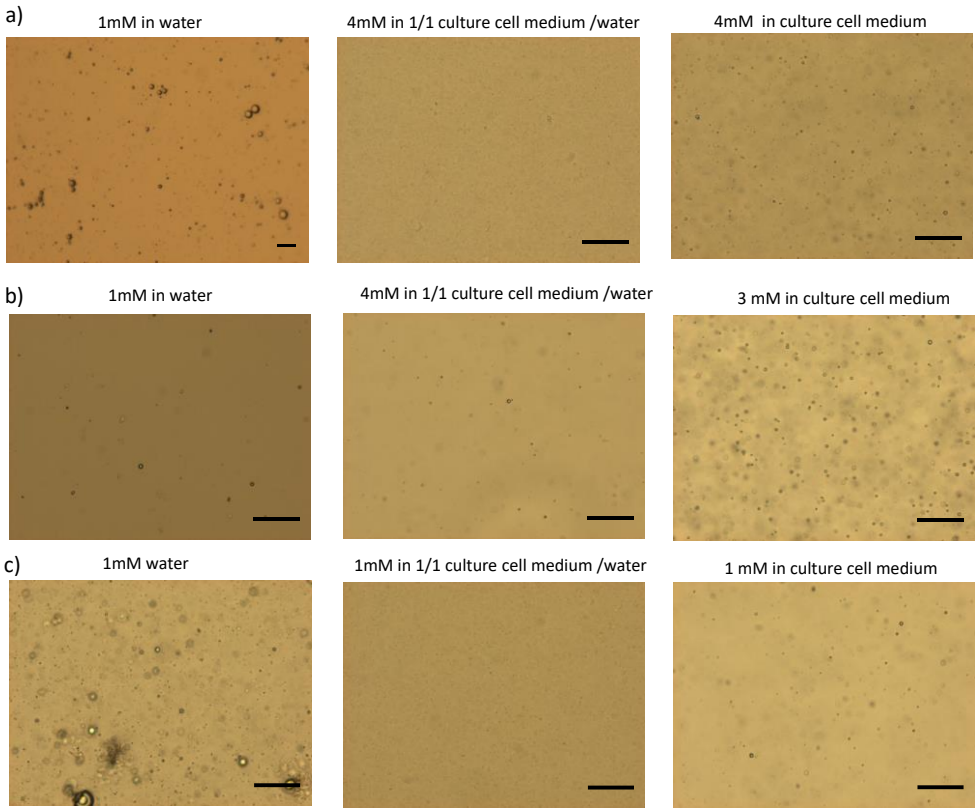

Figure S15 Optical microscopy images for a) **1a** b) **1b** and c) **1c** at 25 °C in water, 1/1 water/bacterial culture medium and bacterial culture medium. Scale bar 50 μm.

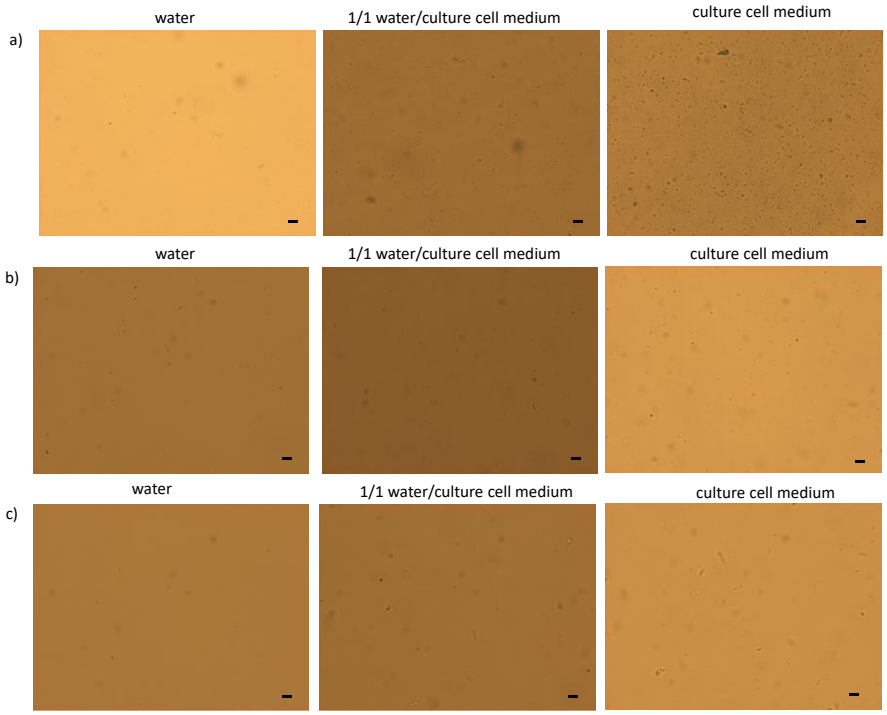

Figure S16 Optical microscopy images for a) **2a** b) **2b** and c) **2c** 4 mM at 25 °C in water, 1/1 water/bacterial culture medium and bacterial culture medium. Scale bar 10 μM.

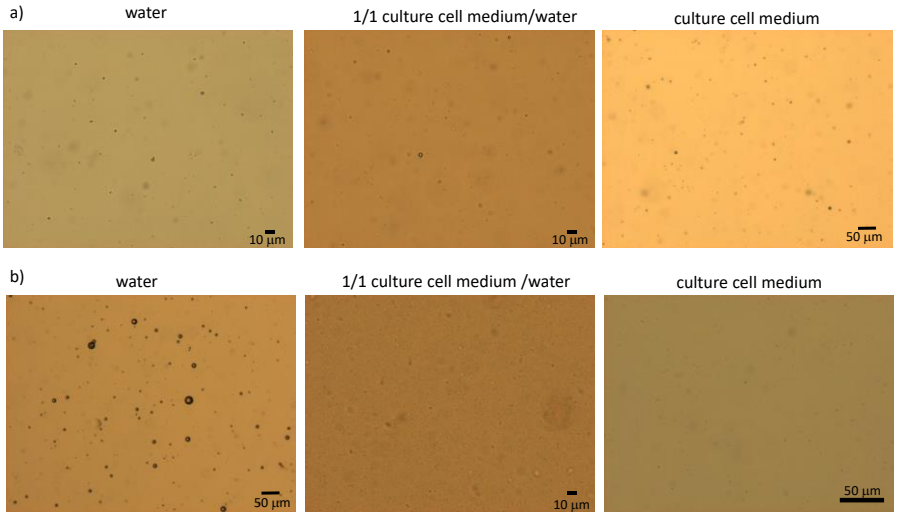

Figure S17 Optical microscopy images for a) **3a** 0.5 mM and b) **3b** 0.5 mM at 25 °C in water, 1/1 water/bacterial culture medium and bacterial culture medium.

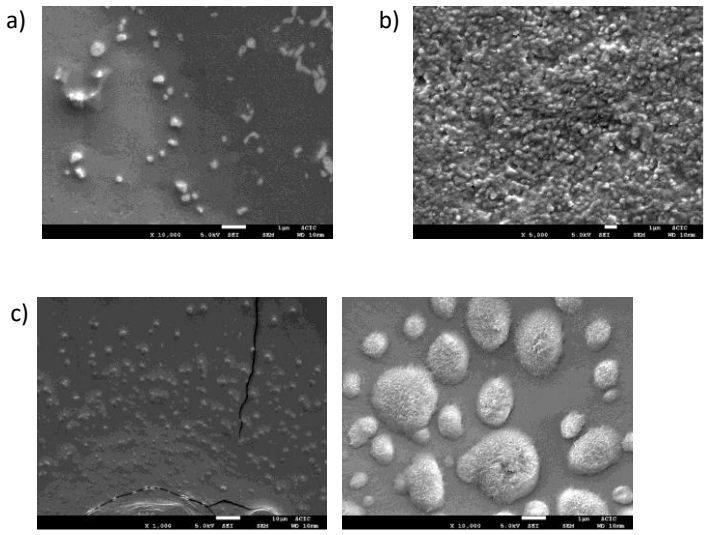

Figure S18 SEM images for **1c** a) 0.5 mM in water; b) 1 mM in water/bacterial culture cell medium1/1 v/v and c) 1 mM in bacterial culture cell medium.

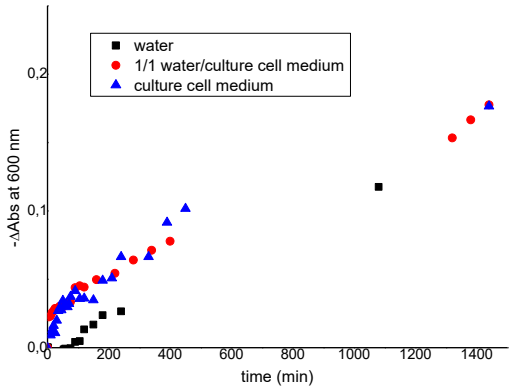

Figure S19 Absorbance variation at 600 nm against time for **1a** (1 mM) in water, water/bacterial cell culture1/1 v/v, and bacterial cell culture media.

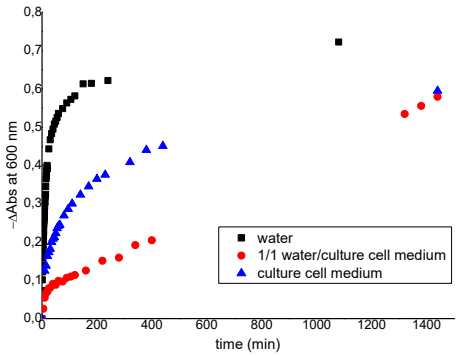

Figure S20 Absorbance variation at 600 nm against time for **1c** (1mM) in water, water/bacterial culture cell 1/1 v/v and bacterial culture cell medium.

Work in progress

Regarding the outstanding antibactericidal activity of compound **3b** and the results obtained for the tripodal imidazolium compounds as antitumoral agents, we decided to check the chemotherapeutic activity of this family of compounds (See Scheme 1) with two tumoral cell lines previously studied (A-549 and HT-29). The results are shown in Table 1.

Table 1. (MTT cytotoxicity in A549, HT-29 and HEK-293 cell lines for compounds **1a-c**, **2a-c** and **3a-c** at physiologic pH and at acidic external pH).

	IC_{50} (μM)[a]						
	A-549 (μM)		HT-29 (μM)		HEK-293 (μM)	α[b]	β[c]
	pH 7.2	pH 6.2	pH 7.2	pH 6.2	pH 7.2	pH 7.2	pH 7.2
1a	87 ± 10	-	-	-	9.6 ± 1.6	0.1	--
1b	44 ± 8 nM	9 ± 2 nM	9,5 ± 0,4 nM	6,9 ± 0,1 nM	1,8 ± 0,4	41	190
1c	11 ± 2	2,1 ± 0,3	24 ± 2	3,4 ± 0.5	19 ± 4	1.7	0.8
2a	>200	-	-	-	>200	--	--
2b	150 ± 20	6,3 ± 0,2	120 ± 22	18 ± 5	>200	--	--
2c	68 ± 4	12 ± 1	176 ± 35	14 ± 3	>200	--	--
3a	>100	-	-	-	19 ± 3	--	--
3b	48 ± 7	22 ± 6	75 ± 8	18 ± 4	109 ± 10	2.3	1.5
3c	12 ± 3	98 ± 15 nM	14 ± 1	8,5 ± 2	36 ± 5	3	2.6

[a] (IC_{50} (x ± sd) average from three experiments); [b] (α = IC_{50} (HEK-293) / IC_{50} (A549)); [c] (β = IC_{50} (HEK-293) / IC_{50} (HT-29)).

All the compounds presented chemotherapeutic activity against both tumoral cell lines. Compounds with long alkyl chains were more effective as chemotherapeutic agents than the ones with short alkyl chains. On the other hand, bisimidazolium salts **1c** and **3c** shown good antitumoral activity which was increased at acidic pHe, this increase was significantly important for **3c** with selectivity α values increasing from 3 to 37 for A-549 cell line.

Surprisingly, monoimidazolium salt **1b** could inhibit A-549 and HT-29 cell growth at nanomolar concentrations with selectivities of 41 and 190 respectively at normal pHe, increasing to 200 and 260 at acidic pHe. However, for the analogous ditopic salts **3b** derived from phenylalanine, moderate chemotherapeutic activities were observed for both tumor cell lines at normal pHe.

Optical microscopy images for A-549 cell line after two days incubation with the different compounds at concentrations over IC50, reveal for compound **1b**, **1c,**

3c and **3b** clear signs of cell damage, from the images it seems a leakage of the cytoplasmatic material, keeping the nuclei and the cell membrane in some of the cells (Figure 1 and 3). This cell damage behaviour was not observed for compounds **2b** and **2c** (Figure 2).

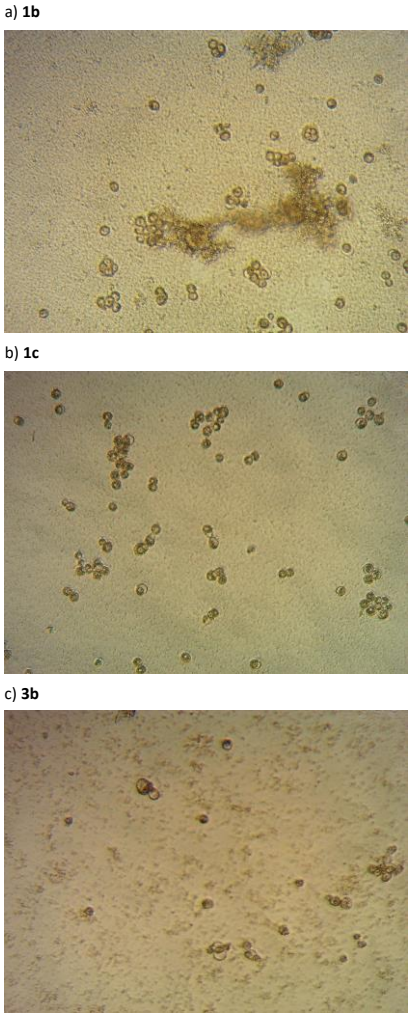

Figure 1. Optical microscopy images for A540 cell line after 2 days incubation with **1b**, **1c** and **3b** at 200 μM (Magnification 20×, phase contrast, Inverted microscope with Zeiss-Primovert phase contrast).

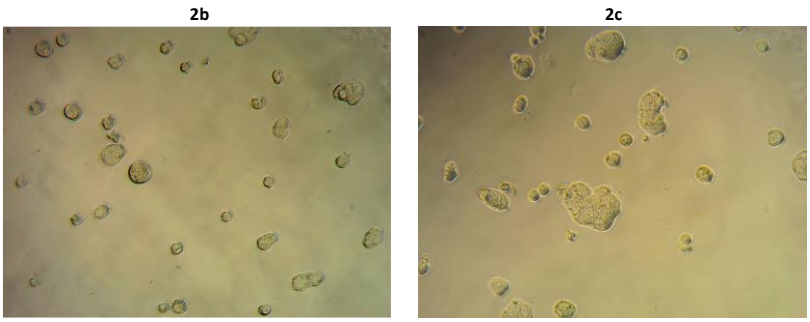

Figure 2. Optical microscopy images for A540 cell line after 2 days incubation with **2b**, and **2c** at 200 μM (Magnification 20×, phase contrast, Inverted microscope with Zeiss-Primovert phase contrast).

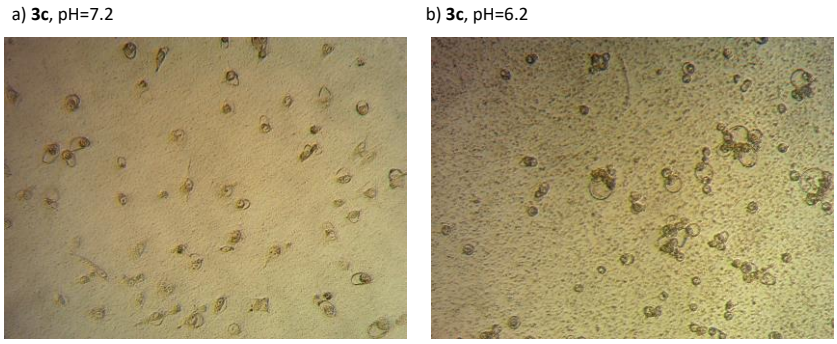

Figure 3. Optical microscopy images for A540 cell line after 2 days incubation with **3c** (100 μM) at phisyological pH (pH=7.2) and at acidic pH (pH=6.2) (Magnification 20×, phase contrast, Inverted microscope with Zeiss-Primovert phase contrast).

Therefore, following these outstanding results, we decided to synthesize a new family of compounds based in monoimidazolium salts with dodecyl chain by tunning the amino acid side chain (see Scheme 2).

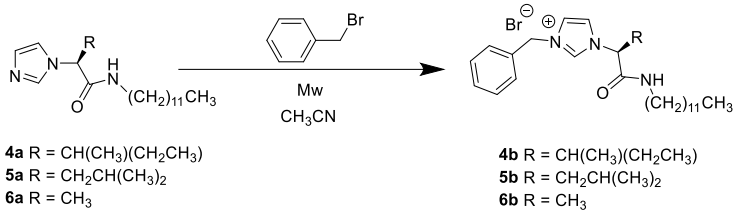

Scheme 2. Synthesis of a new family of amino acid-based monoimidazolium salts.

Furthermore, to have knowledge on the mechanism of action, we also have proposed to synthetized compound **7b** with a fluorescent group (see Figure 4) which could allow us to observe by fluorescence optical microscopy if the compound crosses the cell membrane or is mainly located within the cell membrane leading to big channels.

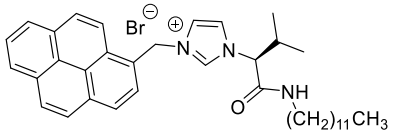

7b

Figure 4. Fluorescent pseudopeptidic monoimidazolium compound **7b**.

CHAPTER 3.

3.5. Polymeric ionic liquids derived from *L*-valine for the preparation of highly selective silica-supported stationary phases in gas chromatography

Polymeric ionic liquids derived from *L*-valine for the preparation of highly selective silica-supported stationary phases in gas chromatography

Abstract

A series of silica-supported polymeric ionic liquid (PIL)-based stationary phases derived from a vinylic *L*-valine ionic liquid monomer and divinylbenzene (DVB) as the crosslinking agent have been prepared and studied as gas chromatographic stationary phases. These coated gas chromatographic columns exhibited good thermal stabilities (230-300 ºC) and high efficiencies (1700-2700 plates/m) and were characterized using a linear solvation parameter model in order to understand the effects of the amount of DVB on the features of the resulting composite systems. Their retention behaviour and separation efficiencies were demonstrated using the Grob test. By tuning the crosslinking degree for the IL-derived stationary phase, the separation selectivity and resolution of different compounds were improved. The different retention behaviour observed for many analytes indicates that these stationary phases may be applicable as a new type of GC stationary phases.

Keywords: *Gas chromatography, Ionic liquids, Cross-linked stationary phases, Solvation parameter model*

1. Introduction

Ionic Liquids (ILs) present unique features that along with their structural modularity favour their efficient use for a variety of applications and chemical processes.[1,2,3] However, toxicological or environmental concerns,[4] as well as some of their physico-chemical properties (like high viscosities) or their high cost have often hampered their practical application. Many of those limitations

[1] Anastas, P.T.; Leitner; W.; Jessop, P.G.; Li, C.-J.; Wasserscheid, P.; Stark, A. Handbook of Green Chemistry - Green Solvents. *Wiley-VCH Verlag GmbH*, New York, **2010**.
[2] *Structure and Nanostructure in Ionic Liquids;* Hayes, R.; Warr, G.G.; Atkin, R.; *Chem. Rev.* **2015**, *115*, 6357-6426.
[3] Wasserscheid, P.; Welton, T.; *Ionic Liquids in Synthesis,* **2008**, Wiley-VCH, Weinheim.
[4] *Biodegradation of ionic liquids - a critical review;* Jordan, A.; Gathergood, N.; *Chem. Soc. Rev.* **2015**, *44*, 8200-8237.

can be overcome with the use of materials based on ILs.[5] In this context, polymeric ionic liquids (PILs) have been shown to present remarkable properties and applications,[6,7,8,9,10,11,12] enabling new and interesting separation processes.[13,14,15]

In the search of improved properties like negligible vapor pressure and better symmetry peaks, new types of stationary phases in gas chromatography (GC) are constantly being explored. In this context, ionic liquids (ILs) have drawn much attention in recent years as materials for stationary phases in GC, due to properties like their capacity to establish simultaneous polar and nonpolar interactions with the analytes, their high thermal stability, or their negligible vapor pressures and wide liquid ranges.[16,17,18,19,20] Besides, it is worth

---

[5] Montolio, S.; Altava, B.; García-Verdugo, E.; Luis, S.V. *Supported ILs / Materials based on ILs for developing Green Synthetic Processes and Procedures, in Green Synthetic Processes and Procedures,* R. Ballini Ed., Green Chemistry Series No. 61, Royal Society of Chemistry, **2019**, Chapter 13, pp 289-318.

[6] *Poly(ionic liquid)s: an update;* Yuan, J. Y.; Mecerreyes, D.; Antonietti, M.; *Prog. Polym. Sci.* **2013**, 38, 1009-1036.

[7] *Poly(ionic liquid)s with engineered nanopores for energy and environmental applications;* Lin, H.; Zhang, S.; Sun, J.-K.; Antonietti, M.; Yuan, J.; *Polymer* **2020**, *202*, 122640-122654.

[8] *Polymeric ionic liquids for CO_2 capture and separation: potential, progress and challenges;* Zulfiqar, S.; Sarwar, M.I.; Mecerreyes, D.; *Polym. Chem.* **2015**, *36*, 6435-6451.

[9] *Synthesis of Monodisperse Silica Particles Grafted with Concentrated Ionic Liquid-Type Polymer Brushes by Surface-Initiated Atom Transfer Radical Polymerization for Use as a Solid State Polymer Electrolyte;* Morinaga, T.; Honma, S.; Ishizuka, T.; Kamijo, T.; Sato, T.; Tsujii, Y.; *Polymers* **2016**, *8*, 146-159.

[10] *Thermally responsive ionic liquids and polymeric ionic liquids:emergingtrends and possibilities;* Gupta, N.; Liang, Y. N.; Hu, X.; *Curr. Opin. Chem. Eng.* **2019**, *25*, 43-50

[11] *Ionic liquids and continuous flow processes: A good marriage to design sustainable processes*; García-Verdugo, E.; Altava, B.; Burguete, M. I.; Lozano, P.; Luis, S. V.; *Green Chem.* **2015**, *17*, 2693-2713.

[12] *Recent Progress in the Development of Composite Membranes Based on Polybenzimidazole for High Temperature Proton Exchange Membrane (PEM) Fuel Cell Applications;* Escorihuela, J.; Olvera-Mancilla, J.; Alexandrova, L.; Del Castillo, L. F.; Compan, V.; *Polymers* **2020**, *12*, 1861-1902.

[13] *Ionic liquids as an enabling tool to integrate reaction and separation processes;* Villa, R.; Alvarez, E.; Porcar, R.; Garcia-Verdugo, E.; Luis, S.V.; Lozano, P.; *Green Chem.* **2019**, 21, 6527-6544.

[14] *Thin Porous Poly(ionic liquid) Coatings for Enhanced Headspace Solid Phase Microextraction;* Patinha, D. J. S.; Wang, H.; Yuan, J.; Rocha, S. M.; Silvestre, A. J. D.; Marrucho, I. M. *Polymers* **2020**, *12*, 1909-1921.

[15] *Determination of Volatile Water Pollutants Using Cross-Linked Polymeric Ionic Liquid as Solid Phase Micro-Extraction Coatings;* Tian, Y.; Feng, X. L.; Zhang, Y. P.; Yu, Q.; Wang, X. H.; Tian, M. K.; *Polymers* **2020**, *12*, 292-305.

[16] *Ionic liquid stationary phases for multidimensional gas chromatography;* Nan, H.; Anderson, J. L. *Trends Anal. Chem.* **2018**, *105*, 367-379.

[17] *Advances of ionic liquids in analytical chemistry;* Trujillo-Rodríguez, M. J.; Nan, H.; Varona, M.; Emaus, M. N.; Souza, I. D.; Anderson, J. L.; *Anal Chem.* **2019**, *91*, 505–531.

[18] *Polymeric imidazolium ionic liquids as valuable stationary phases in gas chromatography: Chemical synthesis and full characterization;* Gónzalez-Álvarez, J.; Blanco-Gomis,D.; Arias-Abrodo, P.; Díaz-Llorente, D.; Busto, E.; Ríos-Lombardía, N.; Gotor-Fernández, V.; Gutierrez-Álvarez, M. D.; *Anal. Chim. Acta* **2012**, 721, 173-181.

[19] *Ionic liquid stationary phases for gas chromatography;* Poole, C. F.; Poole, S. W.; *J. Sep. Sci.* **2011**, *34,* 880-900.

[20] *Can the selectivity of phosphonium based ionic liquids be exploited as stationary phase for routine gas chromatography? A case study: The use of trihexyl(tetradecyl) phosphonium chloride in the*

mentioning that these properties can be easily fine-tuned through small changes in the structure of both the cation or the anion, which, besides, can dramatically change the selectivity or the separation capacity for the analyte of interest.[21,22,23,24]

Thus, for instance, the increase in the nucleophilicity of the anion can decrease the thermal stability of the corresponding ionic liquids, while its coordinating capacity can define the quality of the chromatographic separation. In this regard, stationary phases based on ionic liquids with anion halides, tend to strongly retain analytes displaying hydrogen bonding donor abilities (for example, alcohols and acids), resulting in long retention times and peak asymmetry. Conversely, ILs-based stationary phases containing non-coordinating anions such as hexafluorophosphate in the IL structure often result in poor separations and overlapping peaks. In the case of ILs containing the bis[(trifluoromethyl)sulfonyl]imide (NTf_2^-) anion, the resulting stationary phases have been shown to exhibit higher thermal stability and lower surface tension as compared to ILs encompassing other anions such as tetrafluoroborate or hexafluorophosphate.[25,26,27]

This modular character of ILs allows for a tailor-made design of new structures intending to achieve specific properties (task-specific ILs-TSILS).[28] This can be illustrated by amino acid based ionic liquids (AAILs). The preparation of a variety of AAILs has been reported in the literature, which allows introducing additional

---

flavor, fragrance and natural product fields; Cagliero, C.; Mazzucotelli, M.; Rubiolo. P.; Marengo, A.; Galli, S.; Anderson, J. L.; Sgorbini, B.; Bicchi, C.; *J. Chromatogr., A* **2020**, *1619*, 460969-460979.

[21] *Evaluating the solvation properties of functionalized ionic liquids with varied cation/anion composition using the solvation parameter model;* Twu, P.; Zhao, Q.; Pitner, W. R.;. Acree, W. E.; Baker, G. A.; Anderson, J. L.; *J. Chromatogr., A* **2011**, *1218*, 5311-5338.

[22] *Use of ionic liquids as stationary phases in hyphenated gas chromatography techniques;* Ragonese, C.; Sciarrone, D.; Tranchida, P. Q.; Dugo, P.; Mondello, L.; *J. Chromatogr., A* **2012**, *1255*, 130-144.

[23] *Characterization by the solvation parameter model of the retention properties of commercial ionic liquid columns for gas chromatography;* Rodríguez-Sánchez, S.; Galindo-Iranzo, P.; Soria, A. C.; Sanz, M. L.; Quintanilla-López, J. E.; Lebrón-Aguilar, R.; *J. Chromatogr., A* **2014**, *1326*, 96–102.

[24] *Orthogonality and Quality of GC×GC Separations for Complex Samples with Ionic Liquid Stationary Phases in First Dimension;* Shashkov, M.V.; Sidelnikov, V. N.; *Chromatographia* **2019**, *82,* 615–624.

[25] *Ionic liquids in separation techniques;* Berthod, A.; Ruíz-Ángel, M.; Carda-Broch, S.; *J. Chromatogr., A* **2008**, *1184,* 6-18.

[26] *PEG-linked germinal dicationic ionic liquids as selective, high-stability gas chromatography stationary phases;* Huang, K.; Han, X.; Zhang, X.; Armstrong, D. W.; *Anal. Bioanal. Chem.* **2007**, *389*, 2265-2275.

[27] *Variation of anionic moieties of dicationic ionic liquid GC stationary phases: Effect on stability and selectivity;* Talebi, M.; Patil, R. A.; Sidisky, L. M.; Berthod, A.; Armstrong, D. W.; *Anal. Chim. Acta* **2018**, *1042*, 155-164.

[28] *Task-specific ionic liquids;* Giernoth, R.; *Angew. Chem. Int. Ed.* **2010**, *49*, 2834-2839.

functionalities like carboxylic acid, amino, amide or alcohol groups in the IL structure.[29,30,31,32] These AAILs have additional functional groups able to provide complementary interactions such as hydrogen bonding or hydrophobic and aromatic interactions that make them interesting molecules in Supramolecular Chemistry being used as selective receptors or transport agents through pseudobiological membranes.[33,34] These features also provide a strong potential for their use as stationary phases in GC, leading to the recent preparation and characterization of some new AAILs-based gas chromatography stationary phases, with good potential for the separation of the fatty acid derivatives.[35]

The interest on IL-coated GC columns has increased after their commercial introduction in 2008 and, nowadays, several IL-coated columns with different characteristics are commercially available. However, one major challenge for the development of stationary phases based on ILs is the preparation of highly homogenous coatings, which would favour good peak symmetries and highly effective compound separations and, concomitantly, provide high thermal stabilities for the resulting GC columns.[36,37,38] At high temperatures, uniform IL-coated silica columns can experience film disruption leading to a decrease in the analyte retention times and efficiency. In this regard, polymerized ionic liquids (PILs) can provide the required answers, maintaining the excellent

---

[29] *Room temperature ionic liquids from 20 natural aminoacids;* Fukumoto, K. M.; Yoshiziwa, M.; Ohno, H.; *J. Am. Chem. Soc.* **2005**, *127*, 2398-2399.

[30] *Synthesis of new chiral imidazolium salts derived from amino acids: their evaluation in chiral molecular recognition;* Altava, B.; Barbosa, D. S.; Burguete, M. I.; Escorihuela, J.; Luis, S. V.; *Tetrahedron: Asymm.* **2009**, *20*, 999-1003.

[31] *Chiral Room Temperature Ionic Liquids as Enantioselective Promoters for the Asymmetric Aldol Reaction;* Gonzalez, L.; Escorihuela, J.; Altava, B.; Burguete, M. I.; Luis, S. V.; *Eur. J. Org. Chem.* **2014,** *24*, 5356-5363.

[32] *The Relationship between the Structure and Properties of Amino Acid Ionic Liquids;* Ossowicz, P.; Klebeko, J.; Roman, R.; Janus, E.; Rozwadowski, Z.; *Molecules* **2019**, *24*, 3252-3277.

[33] *Bis(imidazolium) salts derived from amino acids as receptors and transport agents for chloride anions;* Gonzalez, L.; Altava, B.; Burguete, M. I.; Escorihuela, J.; Hernando, E.; Luis, S. V.; Quesada, R.; Vicent, C.; *RSC Adv.* **2015**, *5*, 34415-34423.

[34] *Application of optically active chiral bis-(imidazolium) salts as potential receptors of chiraldicarboxylate salts of biological relevance;* Gonzalez, L.; Escorihuela, J. ;Altava, B.; Burguete, M. I.; Luis, S. V.; Quesada, R.; Vicent ,C. *Org. Biomol. Chem.* **2015**, *13,* 5450-5459.

[35] *Gas Chromatographic Analysis of Fatty Acid Methyl Esters of Milk Fat by an Ionic Liquid Derived From L-Phenylalanine as the Stationary Phase;* Gonzalez, L.; Alvarez, J. G.; Fernandez, C.; Arias, P.; Altava, B.; Burguete, M. I.; Luis, S. V.; Gutiérrez M. D.; *Talanta* **2015**, *143,* 212-218.

[36] *Gas chromatography on wall-coated open-tubular columns with ionic liquid stationary phases;* Poole, C. F.; Lenca, N.; *J. Chromatogr. A* **2014**, *1357,* 87–109.

[37] *Ultra-high thermal stability perarylated ionic liquids as gas chromatographic stationary phases for the selective separation of polyaromatic hydrocarbons and polychlorinated biphenyls*; Odugbesi, G. A.; Nana, H.; Soltani, M.; Davis Jr., J. H.; Anderson, J. L.; *J. Chromatogr. A* **2019**, *1604,* 460-466.

[38] *Ionic liquids as gas chromatographic stationary phases: how can they change food and natural product analyses?;* Cagliero, C.; Bicchi, C.; *Anal. Bioanal. Chem.* **2020,** *412*, 17–25.

thermal stability of the columns, and combining the main features of an ionic liquid and the typical polymer properties such as improved mechanical stability and processability.[39,40,41,42] Furthermore, in recent years, Anderson et al have reported the development of cross-linked polymeric ionic liquids stationary phases for GC with higher thermal stability (up to 380 °C)[43] than the columns coated with the monocationic or dicationic ILs with similar structures.[44] More recently, this research group developed different crosslinked PILs in order to better understand the effects of the crosslinker on the efficiency, selectivity, and thermal stability of PILs-based stationary phases.[45] These studies have focused in the use of dicationic ILs as the crosslinker agent. However, the use of a simple, cheap and commercially available crosslinker like divinylbenzene (DVB) can provide significant advantages, as the use of functional crosslinkers can be of lower efficiency considering the reduced accessibility associated to functional moieties in the crosslinked regions. Thus, the use of the DVB crosslinker can be used as a simple design element to tune the morphological properties of the resulting polymeric matrices. Up to our knowledge, the use of crosslinked PILs-based stationary phases for GC using DVB as crosslinker agent has not been studied.

In this work, a series of silica-supported polymeric ionic liquid (PIL)-based stationary phases have been prepared using as monomer a vinylic *L*-valine ionic liquid derivative (AAIL) and divinylbenzene (DVB) as a crosslinking agent in order to provide an homogeneous coating of the silica surface and improve the column efficiency. The thermal stabilities of these stationary phases based on

---

[39] *Comparison between polymerized ionic liquids synthesized using chain-growth and step-growth mechanisms used as stationary phase in gas chromatography;* Roeleveld, K.; David, F.; Lynen, F.; *J. Chromatogr. A* **2016,** *1451,*135–144.

[40] *Highly selective GC stationary phases consisting of binary mixtures of polymeric ionic liquids;* Zhao, Q.; Anderson, J. L.; *J. Sep. Sci.* **2010**, *33*, 79–87.

[41] *High temperature imidazolium ionic polymer for gas chromatography;* Ho, W-Y.; Hsieh, Y-N.; Lin, W-C.; Kao, C. L.; Huang, P-C.; Yeh, C-F.; Pane, C-Y.; Kuei, C-H.; *Anal. Methods* **2010**, *2*, 455–457.

[42] *Polymerized phosphonium-based ionic liquids as stationary phases in gas chromatography: performance improvements by addition of graphene oxide;* González-Álvarez, J.; Arias-Abrodo, P.; Puerto, M.; Espinal Viguri. M.; Pérez, J.; Gutiérrez-Álvarez, M. D.; *New J. Chem.* **2015,** *39,* 8560-8568.

[43] *Immobilized ionic liquids as high-selectivity/ high- temperature/ high-stability gas chromatography stationary phases;* Anderson, J. L.; Armstrong, D. W.; *Anal. Chem.* **2005**, 77, 6453-6462.

[44] *Identifying important structural features of ionic liquid stationary phases for the selective separation of nonpolar analytes by comprehensive two-dimensional gas chromatography;* Zhang, C.; Ingram, I. C.; Hantao, L. W.; Anderson, J. L.; *J. Chromatogr. A* **2015**, *1386,* 89–97.

[45] *Crosslinked structurally-tuned polymeric ionic liquids as stationary phases for the analysis of hydrocarbons in kerosene and diesel fuels by comprehensive two-dimensional gas chromatography;* Zhang, C.; Park, R. A.; Anderson, J. L.; *J. Chromatogr. A* **2016**, *1440,* 160-171.

AAIL-DVB were evaluated and the Abraham model was used in order to determine their solvation parameters. Furthermore, the effect of the amount of the AAIL and the crosslinker were analysed and carefully optimized to improve the retention, selectivity and resolution of the columns using the Grob test.

2. Materials and Methods

2.1. Reagents, materials and instrumentation

Divinylbenzene and all reagents used for the synthesis of the monomeric AAIL, as well as the Grob mixture, were purchased from Sigma-Aldrich (Madrid, Spain). Methanol and dichloromethane were obtained from Merck (Darmstadt, Germany) and untreated fused silica capillaries (0.25 mm i.d.) were purchased from Supelco (Madrid, Spain). Imidazole **2** was synthesized as previously described starting from the corresponding amino amide 1 (Figure 1).[46]

NMR spectra were recorded on a Varian INOVA 500 spectrometer (500 and 125 MHz for ^{1}H and ^{13}C NMR, respectively) at 30 °C. The solvent signal was used as a reference standard and the chemical shifts are reported in ppm. FT-IR spectra were obtained at 4 cm^{-1} resolution for the 4000 to 600 cm^{-1} spectral range using a spectrometer (JASCO FT/IR-6200) equipped with an ATR (MIRacle single-reflection ATR diamond/ZnSe). Melting points were measured using a differential scanning calorimeter (DSC) (DSC6, Perkin Elmer). The instrument was calibrated for temperature and heat flow with zinc and indium reference samples. Samples were placed in a hermetically sealed aluminium pan with a pinhole in the top. An empty aluminium pan was used as the reference. Samples were exposed to a flowing N_2 atmosphere. Before the DSC test, samples were dried at 60 °C in a vacuum oven for 12 h. Melting transition temperatures (M.p.) were determined by multiple cycles (typically three) involving heating the sample from –70 to 125 °C followed by cooling from 125 to –70 °C, both at a rate of 5 °C min^{-1}. The melting temperatures were determined at the onset of the transition. Mass spectra were recorded on a Q-TOF Premier mass spectrometer with an orthogonal Z-spray electrospray interface (Micromass, Manchester, UK) by electrospray positive mode (ES^{+}). Sample solutions were infused via syringe pump directly connected to the ESI source at a flow rate of 10 mL min^{-1}. Microanalyses were performed on an elemental analyser equipped with an

[46] *Synthesis of Chiral Room Temperature Ionic Liquids (RTCILs) derived from Amino Acids. Application in Chiral Molecular Recognition;* González, L.; Altava, B.; Bolte, M.; Burguete, M. I.; García-Verdugo, E.; Luis, S. V.; *Eur. J. Org. Chem.* **2012**, 4996–5009.

oxygen module (CHN EuroEA3000). Optical rotations were measured in a JASCO instrument DIP-1000.

2.2. Chemical synthesis

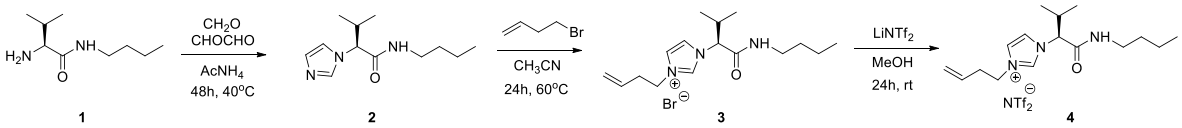

Scheme 1. Synthesis of amino acid based ionic liquid **4** (AAIL).

2.3. Column preparation

Ten-meters capillary columns were coated using the static method at 40 °C, using solutions containing AAIL 4 (0.36%, w/v) and divinylbenzene (0%, 10%, 20%, 30% and 40% of the amount of IL used) in dichloromethane. Prior to adding the solvent to the mixtures 3 mg of AIBN [2,2'-azobis(2-methylpropionitrile)] were added. Capillaries were filled with the solution of the crosslinker, the monomeric ionic liquid and the initiator. After coating, the ends of capillaries were sealed, and the capillaries were introduced in a GC oven at 80 °C for 5 h in order to ensure complete polymerization. Helium gas was then flushed through the capillaries at a rate of 1 mL min^{-1} and the capillaries were conditioned overnight from 50 °C to 120 °C at 3 °C/min. Each column was prepared in triplicate and the efficiencies of the columns were tested with naphthalene at 100 °C. All columns showed efficiencies of 1700 plates/m or better.

The method used for the evaluation of AAIL columns was the Abraham solvation parameter model as this is the most comprehensive method available today.[47,48]

This model is described by Eq (1).

$$Log\ k = c + eE + sS + aA + bB + lL \qquad (1)$$

Here, the higher case letters *E, S, A, B* and *L* are solute descriptors and are defined as *E* for the excess molar refraction, *S* for the solute dipolarity/polarizability index, *A* and *B* for the solute H-bond acidity and basicity respectively and *L* for the gas-hexadecane partition coefficient. The

[47] *The chemical interpretation and practice of linear solvation energy relationships in chromatography;* Vitha, M.; Carr, P. W.; *J. Chromatogr. A* **2006**, *1126*, 143-194.
[48] *Classification of stationary phases and other material by gas chromatography;* Abraham, M. H.; Poole, C. F.; Poole, S. K.; *J. Chromatogr. A* **1999**, *842*, 79-114.

system constants (*e, s, a, b, l*), are used to describe the solvation properties of the stationary phase and are defined as follows: the *e* term represents π and non-bonding electron interactions, *s* the ability of the phase to interact with dipolar/polarizable solutes, *a* and *b* define the solvent hydrogen bond basicity and acidity, respectively, *l* includes dispersion forces (positive contribution) and a cavity term (negative contribution), and *c* is the system constant.

In order to evaluate the capillary columns, each individual probe molecule (dissolved in dichloromethane) was injected into the columns at three different temperatures: 60 °C, 90 °C and 120 °C. The probe molecules shown in Table 1 were used for this purpose.

Multiple linear regression analysis and statistical calculations were performed using the Statgraphics Centurion XV version 15.2.06.

All characterization and separation experiments were performed using a Shimadzu GC-2010 Gas Chromatograph (Shimadzu, Kyoto, Japan) equipped with a flame ionization detector. Analysis of the Grob test was performed with helium as carrier gas at a flow of 1 mL min^{-1} and a split ratio 100/1. The inlet temperature was maintained at 250 °C and the FID was held at 280 °C. The temperature was programmed as follows: 45 °C for 1 min, increased at a rate of 10 °C min^{-1} to 160 °C and then held at this temperature for 2 min.

Table 1: Probe molecules and values of solute descriptors used in the characterization of PILs based on AAIL and DVB stationary phases.

Probe molecules	E	S	A	B	L
1-Hexanol	0.21	0.44	0.344	0.52	3.643
Anisole	0.712	0.768	0	0.311	3.808
Cyclohexanone	0.403	0.895	0	0.53	3.759
1,2-Dichlorobenzene	0.872	0.771	0	0.054	4.516
Butyl benzene	0.595	0.499	0	0.139	4.734
1-Nonanal	0.121	0.636	0	0.414	4.838
Butyl Acetate	0.079	0.57	0	0.438	3.409
Iodobencene	1.182	0.784	0	0.135	4.548
1-Nitropropane	0.243	0.925	0.049	0.27	2.878
1-Pentanol	0.219	0.44	0.344	0.52	3.128
Pyridine	0.635	0.843	0	0.532	3.006
Benzonitrile	0.742	1.135	0	0.331	4.04
Nitrobenzene	0.846	1.138	0	0.269	4.539
Naphthalene	1.24	0.906	0	0.193	5.154
2-Heptanone	0.123	0.662	0	0.496	3.781
1-Phenyl ethanol	0.823	0.819	0.351	0.648	4.424
Benzaldehyde	0.813	1.025	0	0.394	4.005
1-Octanol	0.199	0.44	0.344	0.52	4.648
1-Chloronaphthalene	1.419	0.951	0	0.135	6.175
Aniline	0.955	1.003	0.249	0.425	3.956
Fluorene	1.664	1.12	0	0.252	6.921
4-Chloroaniline	1.017	1.128	0.366	0.309	4.972
Benzyl Alcohol	0.803	0.882	0.4	0.557	4.244
Cinnamyl Alcohol	1.119	0.971	0.451	0.606	5.475
Phenol	0.769	0.759	0.716	0.319	3.844
Acetophenone	0.806	1.026	0	0.503	4.533
3-Methyl-1-butanol	0.198	0.423	0.351	0.501	2.963
1-Butanol	0.224	0.44	0.344	0.52	2.578
Ethyl Benzoate	0.694	0.886	0	0.444	5.032
2-Phenyl ethanol	0.787	0.797	0.39	0.636	4.741
1-Decanol	0.191	0.44	0.344	0.52	5.589
Undecane	0	0	0	0	5.185
Styrene	0.849	0.671	0	0.177	3.860
2-Chlorophenol	0.882	0.668	0.538	0.342	4.118
4-Chlorophenol	1.016	0.794	0.886	0.205	4.802
3,5-Dimethylphenol	0.768	0.764	0.669	0.347	4.792

3. Results and discussion

3.1. Optimization of film thickness capillary columns

A series of silica-supported polymeric ionic liquids-based stationary phases were prepared as capillary columns (see experimental section) using the polymerization of the *L*-valine derived monomer AAIL 4 and DVB as the crosslinker for the coating of the silica surface (Figure 1). Column efficiency was evaluated using naphthalene as a soluble probe. Initially, several columns were

prepared varying the percentage of AAIL 4 in the absence of any crosslinking agent to form the corresponding linear PILs for the coating. As can be seen in Figure 2a, a percentage of 0.36% w/v AAIL provided the best separation efficiency. This percentage corresponds to a linear PIL film thickness of 0.23 microns. Therefore, capillary columns were prepared with 0.36% w/v of AAIL 4 for all subsequent studies.

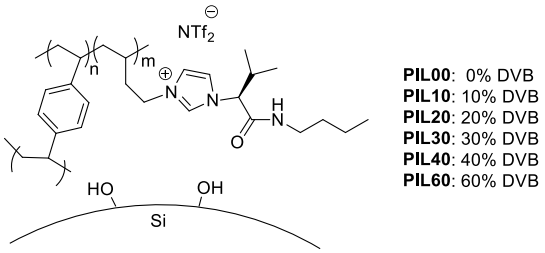

Figure 1. Silica capillaries coated with cross-linked PILs

In order to better understand the effects of the cross-linker on the efficiency of PIL-based stationary phases, PILs with varying amounts of DVB as the cross-linker (i.e., 0, 10, 20, 30, 40 and 60% w/w, Figure 1) were prepared and their efficiency compared. The efficiencies obtained are shown in Figure 2b.

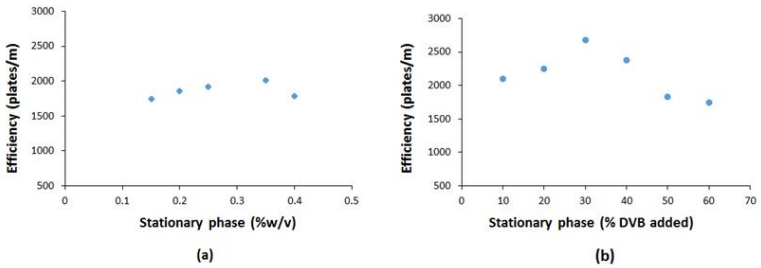

Figure 2. Representation of the efficiency variation of: (a) PIL-coated column as a function of the AAIL **4** concentration (non-crosslinked polymers). (b) PIL-coated columns with AAIL **4**-DVB as a function of the DVB added (using 0.36% w/v AAIL **4**).

As can be seen, all coated PIL columns possessed efficiencies of at least 1700 plates per meter. Moreover, the resulting columns were more efficient in the presence of the crosslinker and the efficiency increased with the amount of divinylbenzene added up to 20% w/w of DVB (DVB:AAIL ratio) with an efficiency of 2700 plates per meter at 20% DVB that compares well with efficiencies shown by other IL-based GC columns.[35,36,37,38,39,40,41,42,43,44,45,46,47,48,49] From this point, the number of plates per meter decreased significantly. This can be ascribed to the fact that for crosslinking degrees higher than 20% DVB, the interaction sites

[49] *Binary ionic liquids mixtures as gas chromatography stationary phases for improving the separation of selectivity of alcohols and aromatic compounds;* Baltazar, Q. Q.; Leininger, S. K.; Anderson, J. L.; *J. Chromatogr. A.* **2008**, *1182,* 119-127.

from AAIL located at the highly crosslinked regions become less accessible for the interaction with the analytes. Thus, some crosslinking is favorable to stablish structurally well-defined and cooperative interaction sites, but polymerization with high crosslinking degrees not only can contribute to generate diffusional problems in the polymeric matrix but also to force less well-structured interaction sites, as has been demonstrated in polymer-supported catalysts.[50,51]

3.2. Thermal stability

Thermal stability determines the operation column temperature range and the lifetime of the GC columns. It is well known that the use of crosslinker agents can affect the thermal stability of PILs-based stationary phases.[52] Thus, the thermal stability of the prepared PILs-based columns was evaluated using two different methods. The first approach was a temperature programmed GC method that can provide a rough idea of the thermal stability of the PILs-based columns studied.[53] In this case, 5-m x 0.25 mm fused silica capillaries were coated and subjected to increasing temperatures (from 50 to 400 °C at 3 °C min^{-1}) and the column bleeding was measured until decomposition was observed. As can be seen in Figure 3, different behaviours were detected. For PILs containing very low crosslinking levels (**PIL00** and **PIL10**), bleeding was observed at temperatures below 250 °C, which suggests some limitations for their application in GC. On the contrary, PILs with crosslinking degrees ≥30% displayed a similar behaviour with very good thermal stability and no bleeding below 275 °C, As a matter of fact, the non-crosslinked PIL column (**PIL00**) showed the lowest thermal stability (bleeding starting at 225 °C) and, although not linearly, the incorporation of the crosslinker increased the thermal stability of the PIL-based stationary phases, reaching a maximum for the columns containing a higher degree of DVB (lack of bleeding up to 285 °C). It must be noted, however, that the efficiency decreases significantly, as mentioned above

---

[50] *Supported Chiral Catalysts: The Role of the Polymeric Network;* Altava, B.; Burguete, M. I.; García-Verdugo, E.; Luis, S. V.; Vicent, M. J.; Mayoral, J. A.; *React. Funct. Polym.* **2001**, *48,* 25-35.

[51] *Chiral catalysts immobilized on achiral polymers: effect of the polymer support on the performance of the catalyst;* Altava, B.; Burguete, M. I.; Garcia-Verdugo, E.; Luis, S. V.; *Chem. Soc. Rev.* **2018**, *47*, 2722-2771.

[52] *Lipidic ionic liquid stationary phases for the separation of aliphatic hydrocarbons by comprehensive two-dimensional gas chromathography;* Nan, H.; Zhang, C.; O'Brien, R. A.; Benchea, A.; Davis, J. H.; Anderson, J. L.; *J. Chromatogr. A* **2017,** *1481,* 127-136.

[53] *High-stability ionic liquids. A new class of stationary phases for gas chromatography;* Anderson, J. L.; Armstrong, D. W.; *Anal. Chem.* **2003**, 75, 4851-4858.

(see Figure 2b), for crosslinking degrees higher than 20% w/w. In this regard, the column based on the polymer **PIL20**, with 20% DVB, and displaying the higher efficiency, was thermally stable up to ca. 260 °C indicating good thermal stability for standard GG applications. This method only gives a rough idea of the thermal stability of the columns studied. Thus, to properly evaluate the thermal stability of the columns, a second alternative set of experiments was carried out using an isothermal method.

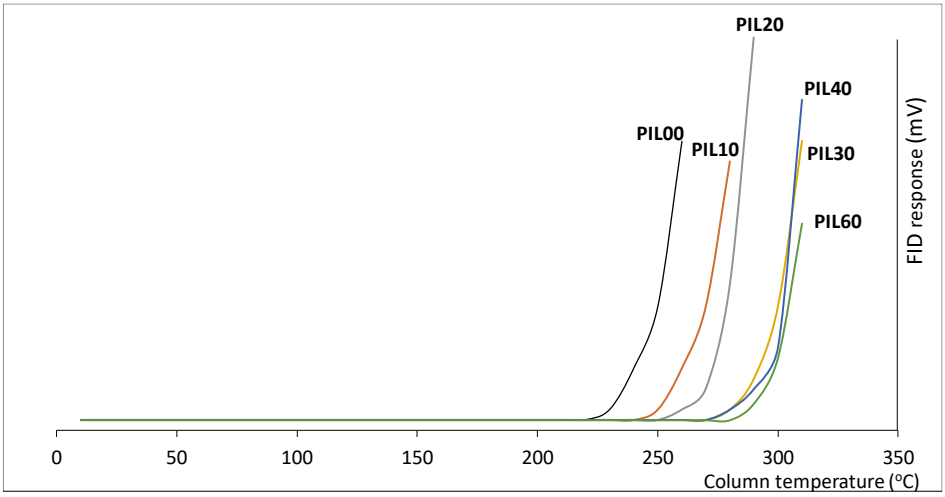

Figure 3. Column bleeding for the PIL-based stationary phases.

Table 2. Variation of naphthalene retention factor using PIL columns with different mixtures of AAIL and DVB using the isothermal method

T(°C)	PIL00	PIL10	PIL20	PIL30	PIL40	PIL60
100	0.31	0.94	1.34	1.40	1.87	2.16
150	0.26	0.91	1.32	1.37	1.79	2.10
200	0.24	0.86	1.27	1.31	1.70	2.01
230	0.29[a]	0.80	1.20	1.25	1.58	1.84
250	[b]	0.88[a]	1.16	1.24	1.53	1.75
280		[b]	1.24[a]	1.19	1.46	1.62
300			[b]	1.23[a]	1.52[a]	1.59
320				[b]	[b]	1.83[a]
340						[b]

a Peaks tailing was observed
b No retention was observed for naphthalene

Thus, the second approach was an isothermal method using naphthalene in the 100 - 350 °C temperature range. This method is based on holding the GC column at a series of constant temperatures for 12 h and measuring the retention of a well retained probe compound at a lower temperature, before and after the isothermal conditioning. Table 2 shows the isothermal measurements of naphthalene at different temperatures with the six PIL-GC columns assayed. As can be seen, the retention factor for naphthalene was smaller for the column

based on the non-crosslinked linear PIL (**PIL00**) increasing with the increase of the % of DVB for a given temperature. Furthermore, the results confirmed that an increase in the percentage of crosslinker led to an improvement of the thermal stability of the column, with an increase from 230 °C to 300 °C for columns with 10% to 60% of DVB respectively.

3.3. Comparison of interaction parameters of PILs-based stationary phases

The six different columns prepared were studied using the Abraham model to determine their solvation parameters, and to obtain information on the specific interactions that can be provided.[47,48] Although the resulting properties must be assigned to the two components of the composite, the fused silica and the polymeric ionic liquid, changes on those properties must be ascribed to changes in the PIL and more specifically to the modification in the crosslinking degree, which represents the most relevant structural change. It must be noted that the stationary phase containing 60% of DVB (**PIL60**) could not be properly characterized due to the lack of elution of most of the compounds at 60 °C and 90 °C and for the excessive asymmetry of the peaks observed, which generated large errors in the Abraham's model. The values of all the solvation parameters calculated for the other stationary phases are shown in Table 3. As can be seen, a slight decrease in the system constants was observed when increasing the temperature for all stationary phases, as usually occurs in gas chromatography analysis.[47,48,52,54] In all cases, the hydrogen bond basicity (a-term) and the dipole interactions (s-term) are the dominant system constants, followed by the hydrogen bond acidity (b-term) and the term involving dispersion forces (l). In imidazolium ILs the structure of the cation and anion involved determine their acid / basic properties as well as the values obtained for other parameters.[54] As the nature of both the cation and the anion in the PIL component remain constant for all the columns studied, the differences observed must be assigned to the crosslinking of the polymers, most likely associated to changes in the mobility and accessibility of the functional groups in the PIL coating, and to the possible generation, for the higher crosslinking degrees, of polymer domains with different polarities, which could also contribute to the low performance of **PIL60**.

[54] *Characterizing ionic liquids on the bases of multiple solvation interaction;* Anderson, J. L.; Ding, J.; Welthon, T.; Armstrong, D. W.; *J. Am. Chem. Soc.* **2002**, *124*, 14247-14254.

The hydrogen bond basicity (a-term) in imidazolium ILs has been shown to be essentially dependent on the nature of the anion. The value of this parameter for the 5 different columns is relatively similar as they share the NTf_2 anion for the imidazolium cation (*ca.* 1.77 ± 0.13 at 60 °C) and is also similar to the value calculated for ILs containing this anion (*i.e.* 1.752 for BMIM-NTf_2 at 70 °C).[54] A value of 1.377 has been reported for a commercial IL-based column (1,9-di(3-vinylimidazolium) nonane bis(trifluoromethyl sulfonyl)imide at 120 °C,[23] a value close to the one found in our case (1.23 ± 0.22), The hydrogen bond acidity (b-term), on the other hand, is different from zero for all stationary phases studied. This is relevant in comparison to most commercial stationary phases (*i.e.* HP-5 and ZB-WAX), where the b-term is practically zero,[47,48,55] and represents a clear competitive advantage of these columns containing composite materials based on polymeric ionic liquids from AAILs. The presence of acidic hydrogen atoms at the positions 2, 4 and 5 of the imidazolium ring contributes to the acidity observed in this family of ILs. In the present case, however, the value observed is significantly higher (0.66-0.90 at 60 °C) than the one reported for BMIM-NTf_2 (0.378 at 70 °C).[54] The presence in AAIL **4** of an amide functionality providing an additional hydrogen bond donor group and preserved in all prepared PILs can explain this fact. A similar value for the b-term has been reported for an imidazolium bistriflamide salt displaying a hydroxyl group,[55] and for the commercial 1,9-di(3-vinylimidazolium) nonane bis(trifluoromethyl sulfonyl)imide based column displaying ditopic bisimidazolium units.[23] It is interesting to note that the value for this parameter (b-term) initially decreased with the crosslinking (for 10 and 20% DVB), which can be attributed to the limitation in mobility and accessibility of the acidic sites in the crosslinked polymeric matrix. However, for higher degrees of crosslinking (30 and 40%) the value of the b-term increased significantly at low temperatures (up to 0.90 at 60 °C for 40% DVB). The partial generation of polymer domains with different polarities upon increasing at those levels the DVB content can be responsible of this phenomenon. At higher temperatures, the b-term always decreased with the crosslinking, as the increased chains mobility will reduce domain separation. In all cases, the value of this parameter decreased with temperature,

[55] *Properties of columns with several pydridinium and imidazolium ionic liquid stationary phases;* Shashkov, M. V.; Sidelnikov, V. N.; *J. Chromatogr. A* **2013**, *1309*, 56-63.

and at 120 °C fully inversely correlated with the DVB content, as could be expected.

Table 3. Regression parameter coefficients for PIL-based stationary phases.

PIL	T	c	e	s	a	b	l	R^2	n	SE	F
PIL00	60	−4.10 (0.09)	−0.12 (0.12)	1.69 (0.11)	1.72 (0.19)	0.75 (0.14)	0.45 (0.03)	0.98	23	0.06	192
	90	−3.89 (0.08)	0.00 (0.11)	1.55 (0.10)	1.34 (0.12)	0.61 (0.15)	0.42 (0.04)	0.97	21	0.06	109
	120	−4.26 (0.12)	−0.20 (0.17)	1.31 (0.09)	1.23 (0.11)	0.46 (0.08)	0.40 (0.02)	0.99	21	0.04	299
PIL10	60	−4.43 (0.10)	−0.18 (0.09)	1.81 (0.14)	1.87 (0.10)	0.70 (0.08)	0.62 (0.02)	0.99	23	0.02	736
	90	−4.52 (0.10)	−0.40 (0.12)	1.77 (0.16)	1.59 (0.17)	0.55 (0.12)	0.56 (0.03)	0.99	23	0.04	242
	120	−4.66 (0.09)	−0.41 (0.10)	1.53 (0.12)	1.52 (0.09)	0.39 (0.18)	0.45 (0.02)	0.99	20	0.04	221
PIL20	60	−3.81 (0.13)	0.06 (0.09)	1.43 (0.14)	1.61 (0.14)	0.66 (0.09)	0.67 (0.05)	0.99	22	0.03	393
	90	−3.85 (0.10)	0.01 (0.07)	1.40 (0.10)	1.24 (0.13)	0.52 (0.10)	0.51 (0.04)	0.98	28	0.02	677
	120	−3.90 (0.11)	−0.11 (0.06)	1.35 (0.09)	1.15 (0.13)	0.30 (0.09)	0.43 (0.03)	0.99	30	0.02	959
PIL30	60	−4.21 (0.11)	−0.12 (0.09)	1.88 (0.12)	1.84 (0.10)	0.85 (0.12)	0.60 (0.03	0.99	23	0.02	624
	90	−4.42 (0.13)	−0.15 (0.16)	1.53 (0.18)	1.59 (0.11)	0.76 (0.14)	0.56 (0.04)	0.98	22	0.04	129
	120	−4.24 (0.12)	−0.37 (0.11)	1.41 (0.14)	1.32 (0.12)	0.28 (0.13)	0.45 (0.06)	0.99	21	0.03	347
PIL40	60	−4.38 (0.16)	−0.11 (0.12)	1.62 (0.09)	1.83 (0.11)	0.90 (0.08)	0.54 (0.07)	0.98	27	0.02	395
	90	−4.00 (0.15)	−0.13 (0.12)	1.34 (0.11)	1.42 (0.10)	0.27 (0.09)	0.50 (0.05)	0.98	23	0.05	131
	120	−3.40 (0.19)	−0.40 (0.14)	0.49 (0.12)	0.91 (0.09)	0.11 (0.16)	0.47 (0.06)	0.98	21	0.07	112

R^2 = Multiple correlation coefficient, n = number of compounds included in the model, F = Fischer parameter. The numbers in parentheses are the standard deviations of the system constants. T displayed in degrees centigrade.

The e-term shows the ability of the PIL-silica composites to interact with solutes through π- and non-bonding electron interactions, being positive when the stationary phase interacts with the solutes through the electron lone pairs of the present heteroatoms and / or the π- cloud of the aromatic rings present. For all the columns studied, the e-term was very small or slightly negative, indicating that there is no appreciable interaction between the probe solutes and the stationary phases through π- or n- electrons. A value of zero has been calculated for this term in the case of BMIM derivatives not containing electron donating substituents at the imidazolium ring nor strongly coordinating anions.[54] In the present case, this indicates that the aromatic rings of the

polymeric matrix (from DVB units) do not significantly contribute to this kind of interactions. **PIL20** containing 20% of DVB and showing slightly positive values at 60 °C is the stationary phase displaying the lowest variation of this parameter with temperature, suggesting again a high degree of homogeneity in the polymers formed. In the case of the l-term, the stationary phases studied had l > 0 coefficients, implying that positive dispersion interactions dominate. As can be seen from the higher values obtained for the crosslinked stationary phases, the structural components originated by the polymerization of DVB provide a clear component for this term.

3.4. Chromatographic performance of the mono and cross-linked ionic liquid stationary phase

In order to obtain additional information on the morphologies and physical chemical properties of the PIL-based columns prepared, as well as on their potential for efficient chromatographic separations, the Grob test was injected to each of the prepared stationary phases and the results obtained were analyzed. The Grob test contains a mixture of compounds of different nature, and is used to evaluate the separation efficiencies, the acid and basic characteristics and the relative polarity of chromatographic columns.[56,57] The mix contains various types of organic compounds including hydrocarbons, fatty acids methyl esters, acids, bases and alcohols and each peak gives specific information on the column. Alkanes (n-decane and n-undecane) represent a 100% recovery marker and should be symmetrical peaks if the column was correctly prepared. Alcohols (1-octanol and 2,3-butanediol) are used to measure the adsorption caused by hydrogen bonding mechanisms. The acid / base interactions are shown by the behavior of 2,6-dimethylaniline, 2,6-dimethylphenol, dicyclohexylamine and 2-ethylhexanoic acid. Fatty acids methyl esters (methyl decanoate, methyl undecanoate and methyl dodecanoate) are a homologous series of fatty acids methyl esters used to determine the separation efficiency of the column. Thus, the use of this mixture of compounds of different nature can allow determining the influence of the DVB content in

[56] *Comprehensive standarized quality test for glass capillary columns;* Grob Jr., K.; Grob, G.; Grob, K.; *J. Chromatogr.* **1978**, *156*, 1-20.
[57] *Testing capillary gas chromatography columns;* Grob, K.; Grob, G.; Grob Jr., K.; *J. Chromatogr.* **981**, *219*. 13-20.

the polymerization mixtures on the general properties of the column and also to assess their suitability as GC columns for analytes of different nature.

The chromatograms obtained with columns **PIL40** and **PIL60**, based on mixtures of the vinylic AAIL and 40% of DVB and 60% of DVB respectively, are not shown and will not be discussed as an appropriate separation of the compounds was not observed. Figure 4 shows the results obtained for the other PILs. For a proper comparison, the chromatograms have been represented at the same scale. Figures 4a and 4b, display the results for the stationary phases prepared in the absence of crosslinking (**PIL00**) and with just 10% of DVB (**PIL10**) respectively, and reveal that all compounds exhibited high peak tailing. This indicates that the coating films generated throughout the silica capillary are not homogeneous, and that non-specific adsorptions with residual accessible silanols can be present. Furthermore, 1-nonanal and 1-octanol show both peak tailing and reduced peak heights, which implies that these stationary phases are highly polar with H-bond accepting capabilities.

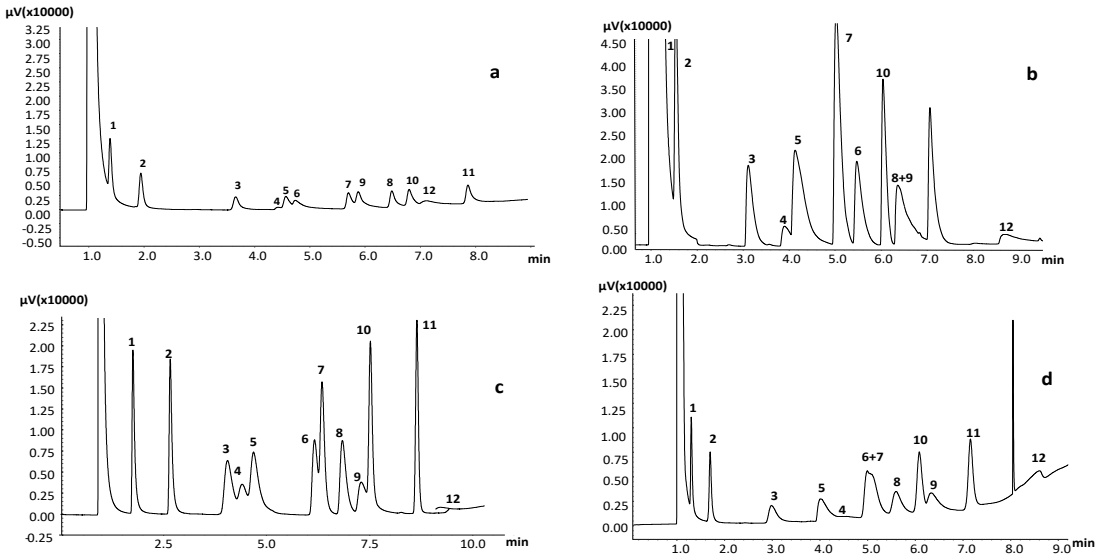

Figure 4. Separation of Grob test: 1. decane, 2. undecane, 3. 2,3-butanediol, 4. 2-ethylhexanoic acid, 5. 1-octanol, 6. 2,6 dimethylphenol, 7. methyl decanoate, 8. dicyclohexylamine, 9. 2,6 dimethylaniline, 10. methyl undecanoate, 11. methyl laurate, 12. 1-nonanal. PIL-based stationaty phases: a) **PIL00**; b) **PIL10**; c) **PIL20**; d) **PIL30**.

Figure 4c, representing the results for the stationary phase prepared with 20% DVB (**PIL20**), shows the best peak symmetries and less mass transfer losses, which is in agreement with the previously discussed solvation parameter

coefficients results and with the results for the calculation of the theoretical plates number. In this column, the alkanes were better separated from the solvent peak as compared with the other columns studied, and the fatty acid methyl esters were separated with good symmetries and good separation efficiencies. Moreover, better peak symmetries and lower mass transfer losses were also observed for 2,3-butanediol, 2-ethylhexanoic acid and dicyclohexylamine using the **PIL20** column than using the commercial imidazolium **IL82** and IL100 columns.[23] This suggests that this column can be of practical application to quantify low levels of compounds with a high capability to interact through H-bonding. It must be noted that the results were again worse when a higher crosslinking degree was used (**PIL30**, 30% DVB, Figure 4d), the corresponding chromatogram displaying lower separations and less symmetric peaks.

Although not all the analytes were separated using these PIL columns, it should be noted that in all columns studied, 2,3-butanediol and 1-octanol eluted after decane and undecane. This indicates that the interactions through hydrogen bonds between such PILs-DVB stationary phases and the analytes play an important role in the chromatographic separation. Another notable fact is that 2,6-dimethylphenol always eluted after 2,6-dimethylaniline, indicating that these stationary phases retain acidic analytes more strongly than basic analytes as suggested by the values of the corresponding Abraham parameters. Similar behavior was observed with the commercial imidazolium IL82 and IL100 columns, although 1-octanol eluted before 2,3-butandiol using these commercial stationary phases.[23] Finally, it should be emphasized that 2-ethylhexanoic acid always eluted before FAMES, opposite to commercial IL82 and IL100 stationary phases.

4. Conclusions

In this study, five stationary phases containing polymeric ionic liquids based on the AAIL **4** and variable amounts of DVB as the crosslinker were prepared and their thermal stabilities and chromatographic properties for GC analysis were evaluated. The results obtained demonstrate that DVB is an excellent modulator of the properties of the resulting polymeric phases and the degree of crosslinking represents a key parameter to define the overall chromatographic efficiency of the resulting silica coated columns. In this study, best results were obtained for a 20% crosslinking (DVB content, **PIL20**). The thermal stabilities observed for

the cross-linked stationary phases were always higher than that for the stationary phase just containing the linear AAIL **4**-based PIL (**PIL00**). Moreover, the introduction of a crosslinker such as DVB was able to improve the separation properties, most likely due to the formation of a more homogeneous film along the capillary. However, the amount of crosslinker needs to be carefully adjusted. DVB amounts over 20% led to a loss of the dual behavior of the stationary phases most probably due to a reduction in the homogeneity of the polymeric phase with generation of separate domains (apolar /polar) and to a reduction in the accessibility to the analytes of the AAIL subunits through a reduction in mobility and diffusional properties.

The solvation parameters calculated show that the dominant interactions are the hydrogen bond basicity (a-term) and the dipole interactions (s-term), with some contributions from the hydrogen bond acidity (b-term) and the dispersion forces (l-term), a trend that has also observed for other imidazolium ILs. It must be noted that the l-term for the stationary phases based on the crosslinked PILs was greater than those for the linear polymeric coating exclusively based on the AAIL monomer (**PIL00**). This constant decreased with the increase in the amount of DVB. The highest values of the b term as compared with other commercial columns provides a significant potential for developing stationary phases with selectivities different from those currently available.

5. Toc graphic

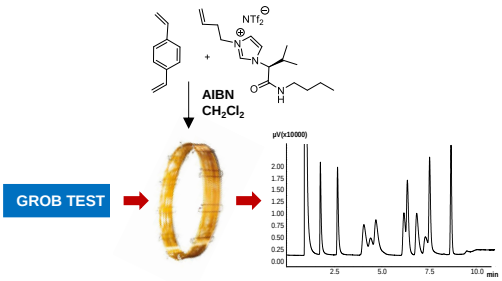

Crosslinked PILs amino acid based stationary phases in GC

6. Supporting information

6.1. Synthetic Protocols and Structural Characterization

Synthesis of (S)-3-(but-3-en-1-yl)-1-(1-(butylamino)-3-methyl-1-oxobutan-2-yl)-1H-imidazol-3-ium bromide 3: Compound **2** (0.10 g, $4.43 \cdot 10^{-4}$ mol, 1 equiv) obtained as previously described[46] and 4-bromo-1-butene (0.93 mL, $4.43 \cdot 10^{-4}$ mol, 10 equiv) were dissolved in dry acetonitrile (1 mL) in a round bottom flask (25 mL). The reaction mixture was stirred and heated at 60 °C for 24 h under a

N_2 atmosphere. The solvent was evaporated under reduced pressure and the resulting crude residue was washed with hexane:ether (2:1) affording compound **3** as a yellow oil (0.0775 g, 47.2%). M.p. 9 °C. $[\alpha]_D^{25}$= +27.64 (c = 0.033, MeOH). IR (ATR): ν_{max} = 3413, 3227, 3068, 2962, 2933, 2872, 1673, 1550, 1463, 1159 cm^{-1}. ^1H NMR ($CDCl_3$) δ= 9.84 (s, 1H), 8.55 (s, 1H), 7.77 (s, 1H), 7.15 (s, 1H), 5.80-5.62 (m, 2H), 5.17-4.94 (m, 2H), 4.33-4.17 (m, 2H), 3.31-3.20 (m, 1H), 3.15-3.03 (m, 1H), 2.70-2.54 (m, 2H), 2.46-2.34 (m, 1H), 1.58-1.41 (m, 2H), 1.38-1.22 (m, 2H), 1.03 (d, *J*=6.6 Hz, 3H), 0.83 (t, *J*=7.3 Hz, 3H), 0.73 (d, *J*=6.7 Hz, 3H).^{13}C NMR ($CDCl_3$): δ= 167.0, 136.1, 131.5, 121.6, 121.0, 120.3, 67.6, 49.5, 39.6, 34.2, 31.3, 31.0, 20.2, 18.7, 18.2, 13.6 ppm. MS (ESI+): 278.4 [$M+H^+$, 100]. $C_{16}H_{28}BrN_3O{\cdot}1.5\ H_2O$: calcd. C 53.63, H 7.88, N 11.73; found C 53.16, H 8.04, N 11.17.

Synthesis of (S)-3-(but-3-en-1-yl)-1-(1-(butylamino)-3-methyl-1-oxobutan-2-yl)-1H-imidazol-3-ium triflamide 4: Compound **3** (0.12 g, $2.76{\cdot}10^{-4}$ mol, 1 equiv) and lithium bis((trifluoromethyl)sulfonyl)amide (0.09 g, $2.76{\cdot}10^{-4}$ mol, 1.1 equiv) were dissolved in methanol in a round bottom flask (50 mL). The reaction mixture was stirred at room temperature for 24 h. The solvent was evaporated under reduced pressure and the resulting crude residue was extracted with CH_2Cl_2 (3x), dried with anhydrous $MgSO_4$, filtered and concentrated leading to compound **4** as a yellow oil (0.10 g, 62.45%). M.p. -36 °C. $[\alpha]_D^{25}$=== +23.15 (c = 0.034, MeOH). IR (ATR): ν_{max} = 3381, 3147, 3111, 2966, 2938, 2876, 1677, 1548, 1348, 1184, 1134, 1053 cm^{-1}. ^1H NMR ($CDCl_3$) δ= 8.95 (s, 1H), 7.74 (s, 1H), 7.11 (s, 1H), 7.08 (s, 1H), 5.73-5.66 (m, 1H), 5.08 (d, *J*=10.2 Hz, 1H), 4.97 (d, *J*= 17.1 Hz, 1H), 4.65 (d, *J*=10.4 Hz, 1H), 4.30-4.08 (m, 2H), 3.27-3.19 (m, 1H), 3.16-3.03 (m, 1H), 2.68-2.44 (m, 2H), 2.39-2.21 (m, 1H), 1.46-1.39 (m, 2H), 1.33-1.20 (m, 2H), 1.00 (d, *J*=6.6 Hz, 3H), 0.87-0.79 (m, 3H), 0.69 (d, *J*=6.7 Hz, 3H).^{13}C NMR ($CDCl_3$): δ= 166.5, 135.5, 131.5, 123.6, 122.0, 121.5, 121.0, 120.3, 118.5, 115.9, 68.7, 49.5, 39.7, 34.3, 32.3, 30.8, 19.9, 18.6, 18.0, 13.5 ppm. MS (ESI+): 278.4 [$M+H^+$, 100]. MS (ESI-): m/z (%) = 280.2 [NTf_2^-, 100]. $C_{18}H_{28}F_6N_4O_5S_2$: calcd. C 38.71, H 5.05, N 10.03, S 11.48; found C 39.07, H 5.31, N 9.70, S 11.03.

CHAPTER 3.

3.6. Open chain pseudopeptides as hydrogelators with reversible and dynamic responsiveness to pH, temperature and sonication as vehicles for controlled drug delivery

Open chain pseudopeptides as hydrogelators with reversible and dynamic responsiveness to pH, temperature and sonication as vehicles for controlled drug delivery

Abstract

A new family of open chain-pseudopeptidic compounds functionalized with a pendant carboxylic group have been prepared with excellent yields. Their self-assembly has been studied under different conditions and using different media. Some of the compounds obtained have revealed to act as very efficient hydrogelators at low concentrations (CGC 1 mg mL^{-1}). The resulting hydrogels provide some interesting properties, including a high thermal stability, with the hydrogels maintaining their structure at temperatures above 65 ºC, and their reversible dynamic sol-gel behavior being responsive to thermal and sonochemical inputs and to changes in the basic/acidic properties of the medium. Preliminary studies for controlled drug delivery have been carried out using a Franz Cell and employing a skin pig membrane, confirming that these Low Molecular Weight Gelators (LMWGs) can be appropriate vehicles for the controlled transdermal delivery of small-molecule drugs.

Keywords: *controlled release, pseudopeptides, hydrogels, self-assembly, transdermal delivery*

1. Introduction

Self-assembly refers to the process of spontaneous organization of biotic and synthetic molecules into higher order structures due to the participation of supramolecular interactions.[1] In this context, gelators are generally defined as chemical species that in a given solvent self-assemble to form cross-linked networks able to immobilize the corresponding solvent, giving place to the formation of a gel. Although a variety of natural and synthetic polymers are

[1] (a) *Self-assembly in natural and unnatural systems*; Philp, D.; Stoddart, J. F.; *Angew. Chem. Int. Ed. Engl.* **1996**, *35*, 1154-1196, (b) *Architectonics: Design of Molecular Architecture for Functional Applications*; Avinash, M. B.; Govindaraju, T.; *Acc. Chem. Res.* **2018**, *51*, 414-426, (c) *Self-assembly of anisotropic nanoparticles into functional superstructures*; Deng. K. R.; Luo, Z. S.; Tan, L.; Quan, Z. W.; *Chem. Soc. Rev.* **2020**, *49*, 6002-6038, (d) *Biomimetic peptide self-assembly for functional materials;* Levin, A.; Hakala, T. A.; Schnaider, L.; Bernardes, G. J. L.; Gazit, E.; Knowles, T. P. J.; *Nat. Rev. Chem.* **2020**.

known to act as efficient gelators, low-molecular weight gelators (LMWGs) continue attracting a growing attention as they present some interesting features including their well-defined molecular weights, their easy modification, the abundance of structural patterns achievable or the relatively regular nanostructures that can be formed.[2] As for other self-assembly processes, LMWGs rely on the involvement of different supramolecular forces such as hydrogen bonding, electrostatic, π–π and hydrophobic interactions to form the gels.[2,3] Hydrogels formed in aqueous systems are of special interest due to the wide variety of their potential applications ranging from tissue engineering and controlled drug delivery to nanoscale electronics.[4,5,6,7] Some of them have shown their potential as stimuli-responsive materials,[8] which properties, including their formation and disruption, can be controlled by different stimuli: from changes in temperature, which is the more obvious input, to pH changes,[9]

---

[2] (a) *Supramolecular gelling agents: Can they be designed?;* Dastidar, P.; *Chem. Soc. Rev.* **2008**, *37*, 2699-2715, (b) *Supramolecular gels formed from multi-component low molecular weight species;* Buerkle, L. E.; Rowan, S.; *J. Chem. Soc. Rev.* **2012**, *41*, 6089-6102, (c) *How should multicomponent supramolecular gels be characterised?*; Draper, E. R.; Adams, D. J.; *Chem. Soc. Rev.* **2018**, *47*, 3395-3405, (d) *Shaping and Structuring Supramolecular Gels;* Chivers, P. R. A.; Smith, D. K.; *Nature Rev. Mat.* **2019**, *4*, 463-478.

[3] (a) *Functional π-Gelators and Their Applications;* Babu, S. S.; Praveen, V. K.; Ajayaghosh, A.; *Chem. Rev.* **2014**, *114*, 1973-2129, (b) *Gelation induced supramolecular chirality: chirality transfer, amplification and application;* Duan, P.; Cao, H.; Zhang, L.; Liu, M.; *Soft Matter* **2014**, *10*, 5428–5448, (c) *Exploring Anion-pi lnteractions and Their Applications in Supramolecular Chemistry*; Wang, D. X.; Wang, M. X.; *Acc. Chem. Res.* **2020**, *53*, 1364-1380, (d) *Role of aromatic amino acids in amyloid self-assembly*; Stankovic, I. M.; Niu, S. Q.; Hall, M. B.; Zaric, S. O.; *Int. J. Biol. Macromol.* **2020**, *156*, 949-959.

[4] (a) *Water Gelation by Small Organic Molecules*; Estroff, L. A.; Hamilton, A. D.; *Chem. Rev.* **2004**, *104*, 1201−1218, (b) *Tailoring Gelation Mechanisms for Advanced Hydrogel Applications*; Nele, V.; Wojciechowski, J. P.; Armstrong, J. P. K.; Stevens, M. M.; *Adv. Funct. Mat.* **2020**, 2002759.

[5] (a) *Sugar-derived phase-selective molecular gelators as model solidifiers for oil spills*; Jadhav, S. R.; Vemula, P. K.; Kumar, R.; Raghavan, S. R.; John, G.; *Angew. Chem. Int. Ed.* **2010**, *49*, 7695-7698, (b) *Hydrogels and Hydrogel-Derived Materials for Energy and Water Sustainability*; Guo, V. H.; Bae, J.; Fang, Z. W.; Li, P. P.; Zhao, F.; Vu, G. H.; *Chem. Rev.* **2020**, *120*, 7642-7707.

[6] (a) *Hydrogels for biomedical applications*; Hoffman, A. S.; *Adv. Drug Delivery Rev.* **2012**, *64*, 18–23, (b) *The development of low-molecular weight hydrogels for applications in cancer therapy;* Tian, R.; Chen, J.; Niu, R.; *Nanoscale* **2014**, *6*, 3474–3482, (c) *From Simple to Architecturally Complex Hydrogel Scaffolds for Cell and Tissue Engineering Applications: Opportunities Presented by Two-Photon Polymerization*, Song, J.; Michas, C.; Chen, C. S.; White, A. E.; Grinstaff, M. W.; *Adv. Healthcare Mater.* **2020,** *9*, 1901217.

[7] (a) *Physical hydrogels with self-assembled nanostructures as drug delivery systems*; Tang, Y.; Heaysman, C. L.; Willis, S.; Lewis, A. L.; *Expert Opin. Drug Delivery* **2011**, *8*, 1141–1159, (b) *Release of small bioactive molecules from physical gels;* Mayr, J.; Saldias, C.; Diaz, D. D.; *Chem. Soc. Rev.* **2018**, *47*, 1484-1515.

[8] (a) *Control of molecular gelation by chemical stimuli*; Segarra-Maset, M. D.; Nebot, V. J.; Miravet, J. F.; Escuder, B.; *Chem. Soc. Rev.* **2013**, *42*, 7086-7098, (b) *Gels with sense: supramolecular materials that respond to heat, light and sound*; Jones, C. D.; Steed, J. W.; *Chem. Soc. Rev.* **2016**, *45*, 6546-6596, (c) *Stimuli-Responsive Hydrogels with Antibacterial Activity Assembled from Guanosine, Aminoglycoside, and a Bifunctional Anchor*; Hu, J.; Hu, Q.; He, X.; Liu, C.; Kong, Y.; Cheng, Y.; Zhang, Y.; *Adv. Healthcare Mater.* **2020**, *9*, 1901329.

[9] (a) *A Fast pH-Switchable and Self-Healing Supramolecular Hydrogel Carrier for Guided, Local Catheter Injection in the Infarcted Myocardium*; Bastings, M. M. C.; Koudstaal, S.; Kieltyka, R. E.; Nakano, Y.; Pape, A. C. H.; Feyen, D. A. M.; van Slochteren, F. J.; Doevendans, P. A.; Sluijter, J. P. G.; Meijer, E. W.; Chamuleau, S. A. J.; Dankers, P. Y. W.; *Adv. Healthcare Mater.* **2014**, *3*, 70–

irradiation at a variety of wavelengths,[10] or by the presence of a variety of biomolecules.[11] Exhibiting tunable, reversible and dynamic gel-sol transitions, they become specially desirable for applications in fields like smart materials and on-demand release.[12] Thus, for instance, polypeptide based thermosensitive hydrogels have been reported to provide targeted and controlled delivery of drugs to tumor microenvironments,[13] while a variety of systems have been used as injectable hydrogels to encapsulate substrates in vivo.[14]

As highlighted by some of the former examples, hydrogelators based on amino acids, their derivatives and peptides are very attractive because of the highly tuneable character of the amino acid fragments, their natural origin and, accordingly, their potential for biocompatibility and biodegradability.[15] Minimalistic pseudopeptidic systems combining structural elements derived from amino acids and simple abiotic fragments are very attractive for this

78, (b) *Dual thermal- and pH-responsive polypeptide-based hydrogels*; Meng, F.; Ni, F.; Ji, S.; Fu, X.; Wei, Y.; *Chin. J. Polym Sci.* **2017**, *35*, 1243–1252.

[10] (a) *Multistimuli Responsive Organogels Based on a New Gelator Featuring Tetrathiafulvalene and Azobenzene Groups: Reversible Tuning of the Gel−Sol Transition by Redox Reactions and Light Irradiation*; Wang, C.; Chen, Q.; Sun, F.; Zhang, D.; Zhang, G.; Huang, Y.; Zhao, R.; Zhu, D.; *J. Am. Chem. Soc.* **2010**, *13*, 3092–3096, (b) *Dipeptide hydrogelation triggered via ultraviolet light*; Raeburn, J.; McDonald, T. O.; Adams, D. J.; *Chem. Commun.* **2012**, *48*, 9355-9357, (c) *γ-Ray-responsive supramolecular hydrogel based on a diselenide-containing polymer and a peptide*; Cao, W.; Zhang, X.; Miao, X.; Yang, Z.; Xu, H.; *Angew. Chem. Int. Ed.* **2013**, *52*, 6233–6237.

[11] (a) *Enzyme-Instructed Molecular Self-assembly Confers Nanofibers and a Supramolecular Hydrogel of Taxol Derivative*; Gao, Y.; Kuang, Y.; Guo, Z. F.; Guo, Z.; Krauss, I. J.; Xu, B.; *J. Am. Chem. Soc.* **2009**, *131*, 13576–13577, (b) *Bioresponsive hydrogels*; Wilson, A. N.; Guiseppi-Elie, A.; *Adv. Healthcare Mater.* **2013**, *2*, 520-532, (c) *Supramolecular fluorescent hydrogelators as bio-imaging probes*; Mehwish, N.; Dou, X.; Zhao, Y.; Feng, C.-L.; *Mater. Horizons*. **2019**, *6*, 14-44.

[12] (a) *Supramolecular gels: Functions and uses*; Sangeetha, N. M.; Maitra, U.; *Chem. Soc. Rev.* **2005**, *34*, 821–836, (b) *Cytocompatible click-based hydrogels with dynamically tunable properties through orthogonal photoconjugation and photocleavage reactions*; Deforest, C. A.; Anseth, K. S.; *Nat. Chem.* **2011**, *3*, 925–931, (c) *A Self-Assembled Delivery Platform with Post-production Tunable Release Rate*; Boekhoven, J.; Koot, M.; Wezendonk, T. A.; Eelkema, R.; van Esch, J. H.; *J. Am. Chem. Soc.* **2012**, *134*, 12908–12911.

[13] *Thermosensitive hydrogels based on polypeptides for localized and sustained delivery of anticancer drugs*; Cheng, Y.; He, C.; Ding, J.; Xiao, C.; Zhuang, X.; Chen, X.; *Biomaterials* **2013**, *34*, 10338–10347.

[14] (a) *Injectable bioadhesive hydrogels with innate antibacterial properties*; Giano, M. C.; Ibrahim, Z.; Medina, S. H.; Sarhane, K. A.; Christensen, J. M.; Yamada, Y.; Brandacher, G.; Schneider, J. P.; *Nat. Commun.* **2014**, *5*, 4095-4104, (b) *Astrocyte scar formation aids central nervous system axon regeneration*, Anderson, M. A.; Burda, J. E.; Ren, Y.; Ao, Y.; O'Shea, T. M.; Kawaguchi, R.; Coppola, G.; Khakh, B. S.; Deming, T. J.; Sofroniew, M. V.; *Nature* **2016**, *532*, 195–200, (c) *An Injectable Strong Hydrogel for Bone Reconstruction*; Zhao, Y.; Cui, Z.; Liu, B.; Xiang, J.; Qiu, D.; Tian, Y.; Qu, X.; Yang, Z.; *Adv. Healthcare Mater.* **2019**, *8*, 1900709.

[15] (a) *Design of nanostructures based on aromatic peptide amphiphiles*; Fleming, S.; Ulijn, R. V.; *Chem. Soc. Rev.* **2014**, *43*, 8150–8177, (b) *Amino Acids and Peptide-Based Supramolecular Hydrogels for Three-Dimensional Cell Culture*; Dou, X-Q.; Feng, C-L.; *Adv. Mater.* **2017**, *29*, 1604062, (c) *Phenylalanine and derivatives as versatile low molecular- weight gelators: design, structure and tailored function*; Das, T.; Häring, M.; Haldar, D.; Díaz Díaz, D.; *Biomater. Sci.* **2018**, *6*, 38-59, (d) *Gelatin Templated Polypeptide Co-Cross-Linked Hydrogel for Bone Regeneration*; Qiao, Y.; Liu, X.; Zhou, X.; Zhang, H.; Zhang, W.; Xiao, W.; Pan, G.; Cui, W.; Santos, H. A.; Shi, Q.; *Adv. Healthcare Mater.* **2020**, *9*, 1901239.

purpose.[16] In this regard, carbamate protected amino acids and derivatives have been reported as very effective hydrogelators,[17] while C_2-symmetry pseudopeptidic compounds displaying apolar spacers have shown remarkable organogelating behavior in different solvents,[18] with the presence of urea fragments increasing significantly the stability of the resulting gels.[19] This has allowed, for instance, to develop tripodal trisurea pseudopeptidic organogelators able to gelate essential oils for natural flavors and fragrances and to modulate their controlled release.[20] Substitution of the apolar spacers in these C_2-symmetry pseudopeptides by spacers containing polar functionalities, like secondary amino groups, leads to pseudopeptides acting as hydrogelators which self-assembly can be controlled by pH changes.[21] Taking this into account, herein we report on the preparation of open chain C_2-symmetry pseudopeptides containing a carboxylic pendant group in the spacer that can be used to generate stable hydrogels possessing responsiveness to different stimuli including temperature and pH and are promising materials for transdermal controlled delivery of small-molecule drugs.

2. Results and discussion

2.1. Synthesis of the pseudopeptidic compounds as LMWGs

The synthesis of the different C_2-symmetry pseudopeptides **2a-c** is shown in Scheme 1.

---

[16] *Bioinspired Chemistry Based on Minimalistic Pseudopeptides*; Luis, S. V.; Alfonso, I.; *Acc. Chem. Res.* **2014**, *47*, 112-124.

[17] (a) *Hydrogels formed from Fmoc amino acids*; Draper, E. R.; Morris, K. L.; Little, M. A.; Raeburn, J.; Colquhoun, C.; Cross, E. R.; McDonald, T. O.; Serpell, L. C.; Adams, D. J.; *CrystEngComm* **2015**, *17*, 8047-8057, (b) *Pseudopeptide-Based Hydrogels Trapping Methylene Blue and Eosin*; Milli, Y. L.; Zanna, N.; Merlettini, A.; Giosia, M. D.; Calvaresi, M.; Focarete, M. L.; Tomasini, C.; *Chem-Eur. J.* **2016**, *22*, 12106–12112, (c) *Self-Assembly, Hydrogelation, and Nanotube Formation by Cation-Modified Phenylalanine Derivatives*; Rajbhandary, A.; Raymond, D. M.; Nilsson, B. L.; *Langmuir* **2017**, *33*, 5803–5813.

[18] (a) *Refining hydrogelator design: soft materials with improved gelation ability, biocompatibility and matrix for in situ synthesis of specific shaped GNP*; Das, D.; Maiti, S.; Brahmachari, S.; Das, P. K.; *Soft Matter* **2011**, *7*, 7291–7303, (b) *Self-healing hydrogels triggered by amino acids*; Zanna, N.; Merlettini, A.; Tomasini, C.; *Org. Chem. Front.* **2016**, *3*, 1699-1704.

[19] (a) *Anion-tuned supramolecular gels: a natural evolution from urea supramolecular chemistry*; Steed, J. W.; *Chem. Soc. Rev.* **2010**, *39*, 3686-3699, (b) *Urea derivatives as low-molecular-weight gelators*; Masamichi, Y.; *J. Incl. Phenom. Macro.* **2013**, *77*, 33-48.

[20] *Urea-Based Low-Molecular-Weight Pseudopeptidic Organogelators for the Encapsulation and Slow Release of (R)-Limonene*, Valls, A.; Castillo, A.; Porcar, R.; Hietala, S.; Altava, B.; Garcıá - Verdugo, E.; Luis, S. V.; *J. Agric. Food Chem.* **2020**, *68*, 7051-7061.

[21] *Interplay between hydrophilic and hydrophobic interactions in the self-assembly of a gemini amphiphilic pseudopepeptide: from nano-spheres to hydrogels*; Rubio, J.; Alfonso, I.; Burguete, M. I.; Luis, S. V.; *Chem. Commun.* **2012**, *48*, 2210–2212.

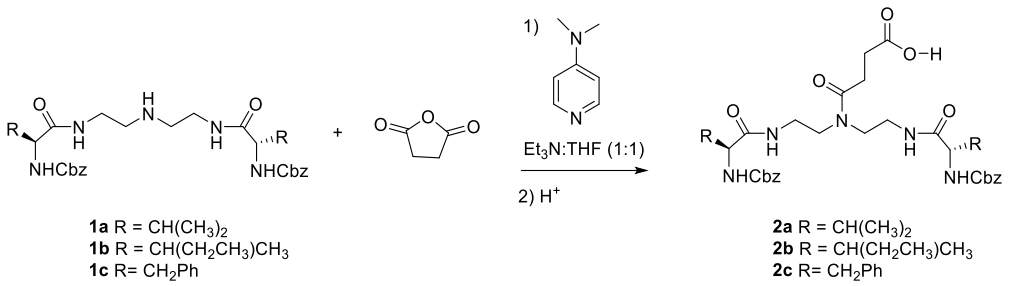

Scheme 1. Synthesis of LMWGs **2a-c**.

Compounds **1a-c** were obtained following the previously reported general synthetic procedure.[22] For the synthesis of compounds **2a-c**, the corresponding compound **1** was reacted with succinic anhydride in THF : Et_3N (1:1) in the presence of 4-(dimethylamino)pyridine.[23] The further acidification of the resulting products afforded the desired compounds **2a-c** as white solids in good yields. The presence of the additional amide group and the carboxylic fragment were expected to increase the polarity of the hydrophilic fragment, with the acidic group allowing a pH regulated control of the properties.

Pseudopeptidic compounds **2a-c** were assayed as LMWGs. As mentioned earlier, the development of the corresponding supramolecular interactions leading to gel formation depends on the participating molecules, solvent type, pH, temperature and other variables.[8-12,18,21] Thus, their gelation properties were studied in water and in different aqueous mixtures and also in some organic solvents (Table 1). In all cases, the same standard protocol was used, involving the initial sonification of the mixture and the analysis of the sample after resting for 24 h.

[22] *Coordination behaviour of new open chain and macrocyclic peptidomimetic compounds with copper(II)*; Wadhavane, P. D.; Gorla, L.; Ferrer, A.; Altava, B.; Burguete, M. I.; Izquierdo, M. A.; Luis, S. V.; *RSC Adv.* **2015**, *5*, 72579-72589.
[23] *New CSPs based on peptidomimetics: efficient chiral selectors in enantioselective separations*; Burguete, M. I.; Fréchet, J. M. J.; García-Verdugo, E.; Janco, M.; Luis, S. V.; Svec, F.; Vicent, M. J.; Xu, M.; *Polym. Bull.* **2002**, *48*, 9-15.

Table 1. Gelation properties of compounds **2a-c** (5.5 mg mL^{-1}) as a function of the solvent used.

Entry	Solvent	2a	2b	2c
1	H_2O	wG	I	I
2	90% H2O - 10% EtOH	G	wG	I
3	80% H2O - 20% EtOH	G	wG	I
4	90% H2O - 10% DMSO	G	wG	I
5	DMSO	S	S	S
6	EtOH	S	S	S
7	$CHCl_3$	S	S	I
8	Glycerol[a]	G	G	I

a) 42h. G: gel; wG(s): weak gel; I: insoluble; S: soluble

Interestingly, none of the pseudopeptides was able to form gels (5.5 mg mL^{-1}) in traditional organic solvents like DMSO, EtOH or $CHCl_3$ (entries 5-7, Table 1) and only **2a** could form a hydrogel in pure water (entry 1, Table 1). However, **2a** and **2b** formed gels in hydroalcoholic mixtures and in water : DMSO mixtures (entries 2-4, Table 1). Finally, **2a** and **2b** could also gelate glycerol using a different protocol involving the heating of the mixture at 80 ºC and a resting period of 42 h (entry 8, Table 1). The more stable hydrogels were formed by **2a**, and the results in Table 1 highlight the importance of a delicate hydrophobic / hydrophylic balance in the properties of these compounds as LMWGs, with changes in the side chain of the amino acid providing important perturbations of their self-assembly behavior.[24] Hydrogels at this concentration (5.5 mg mL^{-1}) were slightly turbid while the organogels were translucid (Figure S2). Compound **2a** formed homogeneous and stable gels, for hydroalcoholic mixtures, in the concentration range of 1-10 mg mL^{-1} and for the lower concentrations the hydrogels were also translucid (Figure S2b).

2.2. Thermal Stability of the Hydrogels

Initial assessment of the stability of the hydrogels formed was carried out using the vial inversion test, and the same was used for a first analysis of their thermal

[24] *The role of the side chain in the conformational and self-assembly patterns of C2-symmetric Val and Phe pseudopeptidic derivatives*; Gorla, L.; Marti-Centelles, V.; Altava, B.; Burguete, M. I.; Luis, S. V.; *CrystEngComm* **2019**, *21*, 2398-2408.

stability.[25] For the range of concentrations giving place to homogenous gels, increasing the concentration of the gelator is known to increase the thermal stability of the gel, leading to an increase of the Tg value.[26]

Table 2. Gelation properties of **2a** as a function of gelator content (mg mL^{-1}) in water/EtOH (9:1, v/v).

Entry	mg mL^{-1}		Tg (°C)[a]
1	1	wG	--
2	2.5	G	33
3	5.1	G	52
4	7.1	G	60
5	9.2	G	65
6	15	wG	--
7	5.5	G[b]	54
8	5.5	G[c]	60 (55[e])
9	5.5	G[d]	69

[a] Temperature of gel disassembly obtained with the inverted vial test; [b] H_2O/EtOH (8:2, v/v); [c] Glycerol as solvent; [d] H_2O/DMSO (9:1, v/v) as solvent; [e] the value in brackets corresponds to **2b**.

This is in agreement with the data gathered in Table 2 for hydrogels formed by **2a** that display Tg values in H_2O/EtOH (9:1, v/v) ranging from 33 °C (2.5 mg mL^{-1}) to 69 °C (9.2 mg mL^{-1}). Above these temperatures the gel started to flow and changed to a sol. These transitions were further supported by UV-vis and rheological studies discussed below. At concentrations of 1 and 15 mg mL^{-1}, **2a** formed weaker and / or less homogeneous hydrogels in the same medium, precluding an accurate determination of the corresponding Tg values. Furthermore, the increase in LMWG concentration was always accompanied by a slight increase in turbidity (Figure S2b).

[25] Raghavan, S. R.; Cipriano, B. H. *Gel formation: phase diagrams using tabletop rheology and calorimetry, in Molecular Gels: Materials with Self-Assembled Fibrillar Networks*; Weiss, R. G.; Terech, P. Eds.; Springer: Berlin, Heidelberg, **2005**; pp 233-244.
[26] *The rheological and structural properties of Fmoc-peptide-based hydrogels: the effect of aromatic molecular architecture on self-assembly and physical characteristics*; Orbach, R.; Mironi-Harpaz, I.; Adler-Abramovich, L.; Mossou, E.; Mitchell, E. P.; Forsyth, V. T.; Gazit, E.; Seliktar, D.; *Langmuir* **2012**, *28*, 2015–2022.

The increase in the content of EtOH of the medium essentially did not affect the observed Tg value (entries 3 and 7, Table 2), while the substitution of EtOH by DMSO (H_2O/DMSO, 9:1 v/v) produced an appreciable increase in Tg (69 ºC, entry 9, Table 2) at *ca.* 5 mg mL^{-1} concentration of **2a**. The steric hindrance of the amino acid side chain seems to produce a decrease in the melting temperature of the organogel, associated to a less efficient self-assembly, as suggested by the comparison of Tg values for **2a** and **2b** in glycerol (entry 8, Table 2).

The thermal stability of the hydrogels was also investigated by ^{1}H NMR spectroscopy (Figure S3). The ^{1}H-NMR spectra of the **2a**-hydrogel (5.5 mg mL^{-1}, D_2O/CD_3OD 9:1 v/v) in the 30-40 ºC region did not allow to observe any signal assignable to **2a**, which is in agreement with a polymeric self-associated structure, while in the 50-60 ºC region two broad peaks at 0.9 and 7.4 ppm start to be observed, corresponding to the methyl groups and the aromatic protons of **2a** as corresponds to the disassembly of the polymeric structure. The process is fully reversible, and the gel was completely reformed after 10 min when cooling back the sample to 30 ºC.

Data presented in Table 2 allowed to assign a "critical gelator concentration" (CGC) for **2a**, which is defined as the minimum amount of gelator required to gelate 1 mL of solvent at a given temperature,[2c] of 1 mg/mL, a value that compares well with those reported for other amino acid derived hydrogelators.[27]

As hydrogel formation is based in establishing appropriate supramolecular interactions like hydrogen bonding, coulombic forces and others, both changes in the pH of the medium and the presence of additional species can be key in determining hydrogel properties. Thus, the effect of pH on hydrogel formation was studied using different buffers (phosphate or acetate 10 mM) to cover a wide range of pH values (from 4.0 to 8.0) and initially using a **2a** content of 2.5 mg mL^{-1}, being relatively close to the CGC determined. Of particular interest can be the results obtained with the phosphate buffers given the biological relevance of related media.

[27] (a) *New low-molecular weight gelators based on l-valine and l-isoleucine with various terminal groups*; Suzuki, M.; Sato, T.; Kurose, A.; Shirai, H.; Hanabusa, K.; *Tetrahedron Lett.* **2005**, *46*, 2741-2745, (b) *Head Group Modulated pH-Responsive Hydrogel of Amino Acid-Based Amphiphiles: Entrapment and Release of Cytochrome c and Vitamin B12*; Shome, A.; Debnath, S.; Das, P. K.; *Langmuir* **2008**, *24*, 4280-4288.

Table 3. Gelation properties as a function of pH and buffer in water/EtOH (9:1) for **2a**[a]

Entry	pH	Buffer[b]	2a	T_g (°C)[f]
1	5.8	KH_2PO_4/K_2HPO_4	G	43 (40)
2	5.8	KH_2PO_4/K_2HPO_4[c]	G	44
3	6.7	KH_2PO_4/K_2HPO_4	S	---
4	6.7	KH_2PO_4/K_2HPO_4[d]	G	55
5	7.0	KH_2PO_4/K_2HPO_4	S	--
6	7.0	KH_2PO_4/K_2HPO_4[e]	S	--
7	8.0	KH_2PO_4/K_2HPO_4	S	--
8	4.2	AcOH/AcONa	G	45
9	5.0	AcOH/AcONa	G	45
10	5.6	AcOH/AcONa	G	44

a) 2.5 mg mL^{-1} gelator unless otherwise stated; b) 10 mM; c) 5 mM; d) 6 mg mL^{-1} gelator concentration; e) 7 mg mL^{-1} gelator concentration; f) Gel disassembly temperature obtained in the vial inversion test; in brackets T_g obtained from UV experiments (600 nm).

Main results are gathered in Table 3, suggesting that hydrogel formation is always favored in the pH < 7 regions. Although in the initial experiments no gelation took place at pH = 6.7 for a 10 mM phosphate buffer when 2.5 mg mL^{-1} LMWG concentration was used (entry 3, Table 3), a strong hydrogel was formed at a higher gelator content (6 mg mL^{-1}, entry 4, Table 3).[28] However, for the same buffer, no gel was formed at pH = 7 employing different gelator contents (entries 5 and 6, Table 3). The pKa of **2a** is predicted to be around 4-5,[22] and, therefore, the results suggest that hydrogel formation is facilitated when the carboxylic is, at least, partially protonated. At pH = 7.0, an essentially full deprotonation of the carboxylic group in **2a** must take place and this seems to inhibit the self-assembly, most likely by significantly increasing the solubility in water. The comparison of entries 1 and 2 in Table 3 shows that no significant effect was observed when reducing the concentration of the buffer from 10 M to 5 mM (pH = 5.8).

[28] *Variable gelation time and stiffness of low-molecular-weight hydrogels through catalytic control over self-assembly*; Poolman, J. M.; Boekhoven, J.; Besselink, A.; Olive, A. G. L.; H.van Esch, J.; Eelkema, R.; *Nat. Protoc.* **2014**, *9*, 977–988.

In the same way, no appreciable differences were observed when the phosphate buffer was substituted by an acetate buffer (10 mM) allowing to study gel formation in the 4-6 pH region (entries 8-10, Table 3). At acidic pH values and a gelator content of 2.5 mg mL^{-1}, gel disassembly temperatures were essentially constant (44±1 °C, vial inversion test) irrespective of the buffer nature and the exact pH value, but results shown in the entry 4 of Table 3 suggested that the value of T_g significantly increases with the amount of **2a** (entries 4, Table 3). A more detailed study using the phosphate buffer at pH = 5.8 in H_2O/EtOH (9/1, v/v) revealed an almost direct lineal correlation between the gelator content in the gel and the T_g value as shown in Figure 1.

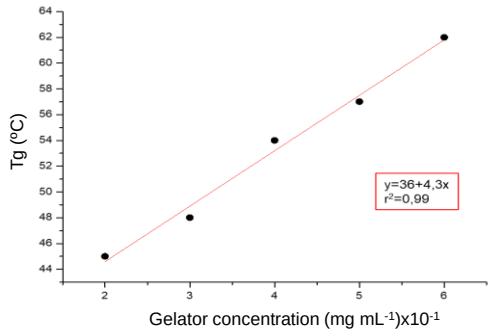

Figure 1. Variation of the T_g values as a function of the concentration of **2a** in H_2O : EtOH (9/1, v/v) using a 10 mM phosphate buffer (pH 5.8).

The T_g value was also studied by UV-vis spectroscopy for a 2.5 mg mL^{-1} gelator content at pH 5.8 (phosphate buffer, 10 mM, Figure 2a), as the formation of the gel is accompanied by changes in the absorption at 600 nm, with the absorbance at this wavelength decreasing as the gel is broken. This allowed estimating a temperature of ca. 40 °C for the sol-gel transition.[29] This methodology also confirmed the appreciable enhancement in thermal stability when the gelator content was increased to 5 mg mL^{-1} in the same medium (pH = 5.8) with the disassembly of the gel taking place at a temperature of ca. 60 °C (Figure 2b).

[29] *Effect of slight structural changes on the gelation properties of N-phenylstearamide supramolecular gels*; Meyer, A. R.; Bender, C. R.; dos Santos, D. M.; Ziembowicz, F. I.; Frizzo, C. P.; Villetti, M. A.; Reichert, J. M.; Zanatta, N.; Bonacorso, H. G.; Martins, M. A. P.; *Soft Matter* **2018**, *14*, 6716-727.

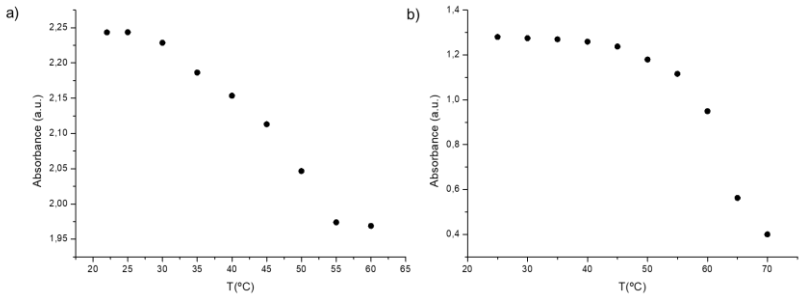

Figure 2. UV absorption at 600 nm at different temperatures for **2a** at a) 2.5 mg mL^{-1} gelator content in phosphate buffer 10 mM (pH 5.8)/EtOH (9/1, v/v); b) 5 mg mL^{-1} gelator content in the same medium.

It must be noted that when using H_2O/EtOH (9/1, v/v) with a 10 mM phosphate buffer (pH = 5.8) the CGC value determined was as low as 1 mg mL^{-1} (ESI, Table S1), though the resulting gel was a weak material, barely stable to vial inversion. Thus, the CGC values were very similar in pure H_2O/EtOH (9/1, v/v) and in the buffered medium, but the thermal stability of the gel formed in the buffered medium was always higher: for instance, for a 2 mg mL^{-1} gelator content T_g = 40 °C (entry 2, Table S1) for the buffered system, while T_g = 33 °C for a 2.5 mg mL^{-1} gelator content in the absence of buffer (entry 2, Table 2).

SEM experiments provided additional insights into the microstructure of the self-assembly produced in the hydrogels from **2a** and **2b**. Thus, SEM images for the dried gels obtained from H_2O/EtOH (9:1, v/v) allowed to observe the presence of a well-defined interpenetrated network of regular nanofibers displaying diameters of *ca.* 35 nm (Figure 3b for **2a** and S7 for **2b**). In the presence of the phosphate buffer and at acidic pH (5.8) more complex morphologies are observed with the assembly of the fibers into bundles exhibiting diameters higher than 1 µm (Figure 3d for **2a**). It is worth mentioning that although **2a** is fully soluble in EtOH in the concentrations considered here, the evaporation of the solvent also allowed to observe by SEM the tendency to form small nanofibrils (*ca.* 25 nm diameter, Figure 3a) visible on rather amorphous regions. On the contrary, the solid assemblies observed upon evaporation of the solvent when using H_2O/EtOH (9:1, v/v) in the presence of the phosphate buffer at basic pH (pH = 8) displayed a morphology related to that of supramolecular dendronized polymers (Figure 3c).[30] All these experiments

[30] (a) *Dendronized Polymers: Synthesis, Characterization, Assembly at Interfaces, and Manipulation*; Schlüter, A. D.; Rabe, J. P.; *Angew. Chem. Int. Ed.* **2000**, *39*, 864-883, (b) *Dendrimers Designed for Functions: From Physical, Photophysical, and Supramolecular Properties*

confirm the strong self-assembly potential of the considered pseudopeptidic structures in a variety of media.

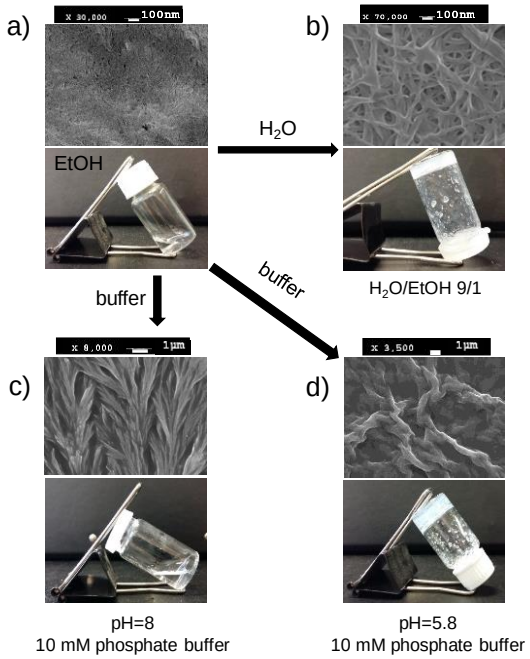

Figure 3. Vial pictures (bottom) and SEM images of the corresponding dried solids (top) for the EtOH solution of **2a** (a); the gel formed in H_2O/EtOH (9:1, v/v, 5 mg mL^{-1} in **2a**) (b), the sol formed in H_2O/EtOH (9:1, v/v, 5 mg mL^{-1} in **2a**) using a 10 mM phosphate buffer at pH = 8 (c); the gel formed in H_2O/EtOH (9:1, v/v, 5 mg mL^{-1} in **2a**) using a 10 mM phosphate buffer at pH = 5.8 (d).

2.3. ^{1}H NMR and FT-IR spectroscopic studies

In order to obtain information on the supramolecular interactions present in these systems, a series of ^{1}H NMR and FT-IR experiments were carried out. In this regard, the comparison of the ^{1}H NMR spectra of **2a** (4 mM) in CD_3OD and $CDCl_3$ is illustrative. As shown in Figure 4, in CD_3OD the aliphatic region of the spectrum displays a relatively simple set of signals confirming the presence of a C_2-symmetry and a high conformational flexibility. However, in $CDCl_3$ the spectrum indicates a complete loss of the C_2-symmetry with the observation, for instance, of two different signals for the proton at the stereogenic center (H_f) and for the signal of the methine of the isopropyl group (H_g). More relevant, even, is the observation of the loss of equivalence for the two protons of different methylene groups, in particular those closer to the amide group linking the side arm to the spacer: two pair of signals are clearly visible for H_a ($\Delta\delta$ = 0.5 and 0.3

to Applications in Sensing, Catalysis, Molecular Electronics, Photonics, and Nanomedicine; Astruc, D.; Boisselier, E.; Ornelas, C.; *Chem. Rev.* **2010**, *110*, 1857-1959.

ppm) and two signals for H_c ($\Delta\delta$ = 0.25). The same splitting is observed for amide and carbamate N-H signals (Figure S1). This suggests the prevalence of a rigid conformation associated to hydrogen bonding intramolecular interactions between the oxygen of the carbonyl group of the central amide and the acidic hydrogen of one of the amide groups derived from valine (H_e). The use of a polar protic solvent like CD_3OD precludes the formation of such intramolecular hydrogen bonds, competing efficiently for hydrogen bonding, and would also inhibit intermolecular association through these interactions, as shown for studies in the 26 to 4 mM range (ESI, Figure S4). Accordingly, hydrophobic and aromatic interactions can be key in the formation of hydrogels from **2a**. When aggregation studies were run in $CDCl_3$ (from 30 to 2 mM) some chemical shift changes with concentration were observed (ESI, Figure S5) particularly relevant for the amide and carbamate N-H signals. This indicates that the intramolecular hydrogen bonding observed in this solvent competes efficiently at low concentration with the intermolecular association, but this is possible at higher concentrations. Thus, organogels are not formed in such non-protic organic solvents at the low concentrations of relevance, but some nanofibers can be observed by SEM upon drying a solution from $CHCl_3$ (ESI, Figure S8).

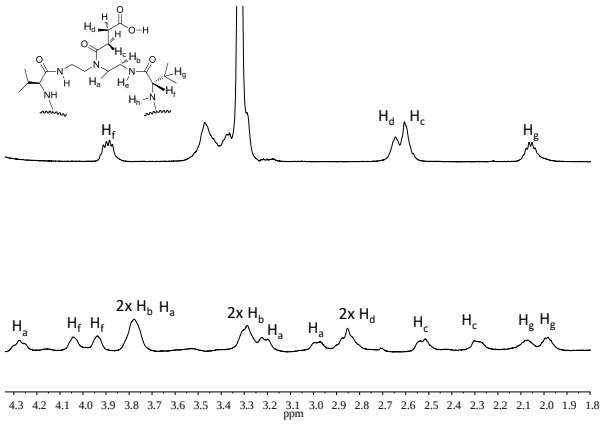

Figure 4. Partial ^{1}H-NMR spectra of **2a** (4 mM) in CD_3OD (top) and $CDCl_3$ (bottom).

The formation of gels in water / alcohol mixtures is accompanied by minor changes in the chemical shifts of the signals for **2a** and, more significantly, by a general broadening and lack of resolution of the signal with an important decrease in their intensity. It must be noted that in the gels there is a dynamic equilibrium between molecules in the solution and in the self-assembled polymeric fibrils. This is highlighted in the ^{1}H NMR of the weak gel obtained using a 5 mg mL^{-1} of **2a** in D_2O/CD_3OD 7/3 v/v (ESI, Figure S6). Interestingly,

in the presence of 2 equivalents of NaOH, leading to gel disassembly, the signal corresponding to the methylene group next to the carboxyl group (H_d) shifts slightly to higher fields, indicating the formation of the carboxylate group, and, simultaneously, the intensity of all the signals increase as corresponds to the growth in the percentage of molecules present in solution and not in the polymeric self-assemblies.

The comparison between the IR spectra of **2a** samples in the crystalline state and in the xerogel obtained drying the hydrogel highlights the rather different assemblies present in both states (Figure 5a). In the fibrillar structure from the hydrogel, the most intense $C{=}O_{st}$ band shifts from 1649 to 1641 cm^{-1}, while the other signals in this region remain essentially unaltered; besides, the complex band in the amide II region shifts from 1533 to 1539 cm^{-1} and significantly decreases its relative intensity, while the intensity of the band at 1433 cm^{-1} associated to C-O-H bending increases in the dried gel. Significant changes are also observed in the position and intensity of the bands in the 1200-1300 cm^{-1} region corresponding to amide III $C{-}O_{st}$ for the carboxyl and carbamate groups. This indicates the presence of important differences between both samples in terms hydrogen bonding and conformational preferences.[31,32] When the FT-IR spectra were obtained in the hydrogel, after subtraction the contribution of the solvent (Figure 5b) some relevant differences were observed relative to the xerogel, in particular in the intensity of the bands in the amide II and $C{-}O_{st}$ regions, which can be attributed to the additional hydrogen bonding associated to the solvation in protic solvents of the molecules in the outer shell of the fibrils. Interestingly, the study by FT-IR of the hydrogels at different temperatures also confirms the disassembly taking place at around 60 ºC, in agreement with results from other techniques.

[31] (a) *The Strength of Hydrogen Bonding: Infrared Spectroscopy;* Susi, H.; Meth. H.; *Enzymol.* **1972**, *26*, 381-391, (b) *Infrared Spectroscopic Studies of Biomembranes and Model Membranes*; Lee, D. C.; Chapman, D.; *Bioscience Rep.,* **1986**, *6*, 235-256.
[32] (a) *Hydrogen bonding in ethyl carbamate studied by IR spectroscopy*; Furer, V. L.; *J. Mol. Struct.* **1998**, *449*, 53-59, (b) *Calculation of the IR spectra of toluene-2,4-bis (methyl) carbamate*; Furer, V. L.; *J. Mol. Struct.* **1999**, *476*, 215–222.

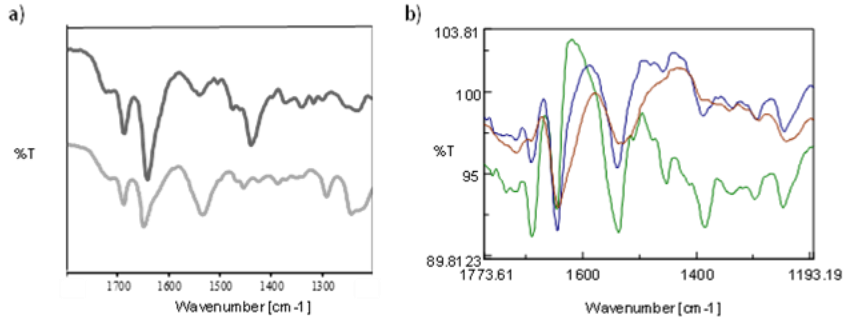

Figure 5. a) Partial ATR-FT-IR spectra of **2a** as crystalline powder (grey line) and dried hydrogel (5 mg mL^{-1}, H_2O/EtOH 9/1, v/v) (black line). b) Partial ATR-FT-IR spectra of hydrogel **2a** (5 mg mL^{-1}, H_2O/EtOH 9/1, v/v) at different temperatures (green line 25 °C; blue line 40 °C; red line 60 °C) using as background the spectrum of H_2O/EtOH 9/1, v/v.

2.4. Rheological measurements

To obtain more information on the mechanical properties of these hydrogels, rheological measurements were performed.[33] A typical LMWG will have a storage and a loss modulus (G´ and G´´, respectively), which are frequency independent, and will break at relatively low strain.[33a] Moreover, from the rheological data, the effect of temperature and concentration can be seen directly. In this regard, it is generally expected that increasing the concentration will lead to the formation of more self-assembled structures and hence, most likely, more cross-linking. Therefore, increasing the concentration of LMWG should lead to an increase in the rheological properties. Figure 6 shows the viscoelastic properties of the hydrogel in phosphate buffer (pH 5.8, 10 mM)/EtOH (9/1 v/v). The storage modulus (G') of the gel was much higher than the loss modulus (G") over the whole range of frequency swept (Figure 6), which is a characteristic feature of gelation. Moreover, the storage modulus (G') obtained for the gel at 5 mg mL^{-1} was higher than the storage modulus (G') of the gel at 2.5 mg mL^{-1}. The strain sweep measurement (Figure S9) for hydrogels containing 5 and 2.5 mg mL^{-1} of gelator showed that both the storage and loss moduli of the gel stayed constant up to 1% strain, the so-called linear viscoelastic region (LVER); beyond this region, the storage modulus began to plunge down as the strain increased.

[33] (a) *Rheological properties of peptide-based hydrogels for biomedical and other applications*; Yan, C.; Pochan, D.; *Chem. Soc. Rev.* **2010**, *39*, 3528–3540, (b) Tanaka, F. *Theory of Molecular Association and Thermoreversible Gelation*; Weiss, R. G.; Terech, P. Eds.; in Molecular Gels Materials with Self-Assembled Fibrillar Networks; Springer: Berlin, Heidelberg, **2005**; pp 17-77.

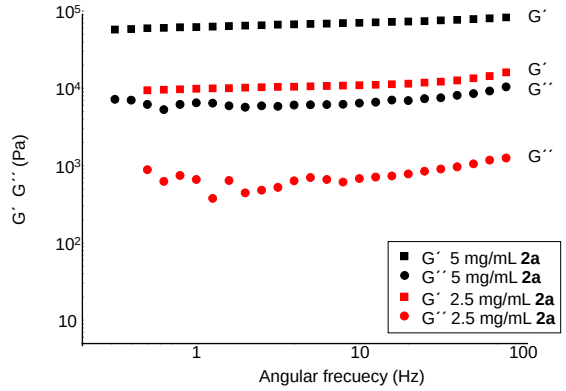

Figure 6. Frequency sweeps with 0.1% strain at 25 ºC for the hydrogels from **2a** in phosphate buffer (pH 5.8, 10 mM)/EtOH (9/1 v/v) using two different gelator contents.

Figure 7 displays the rheological results for the gels obtained from **2a** (5 mg mL^{-1}), using phosphate buffer (pH 5.8, 10 mM)/DMSO (9/1 v/v) as the medium. No significant differences were observed in the frequency sweep measurements for the storage modulus G´ and the loss modulus G´´ of the hydrogel when DMSO was used as co-solvent instead of EtOH, being the linear viscoelastic region (LVER) up to 1% strain (inset Figure 7a). However, the organogel obtained in glycerol displayed lower G´ and G´´ parameters than the corresponding hydrogels and at frequencies higher than 50 Hz the organogel properties were lost (Figure S10). Furthermore, the rheological properties of the gels were studied as a function of temperature, though for the hydrogel formed in phosphate buffer (pH 5.8, 10 mM)/EtOH (9/1 v/v) no reliable data could be obtained, presumably due to EtOH evaporation during the measurement. Figure 7b presents the results for the gel obtained in phosphate buffer (pH 5.8, 10 mM)/DMSO (9/1 v/v) allowing a larger temperature range. The temperature was varied from 25 to 80 ºC at a frequency of 1 Hz and 0.1% strain. The values for G´ decreased with the increase in temperature, allowing to determine a gelation temperature of 75 ºC (transition temperature at which G´ is equal to G´´). A similar behaviour was obtained for the organogel in glycerol, with the gelation temperature being 60 ºC. It has to be noted that the storage modulus started to decrease after 40 ºC and the oscillation strain was maintained constant up to *ca.* 40 ºC, and after this temperature started to increase significantly (ESI, Figure S11).

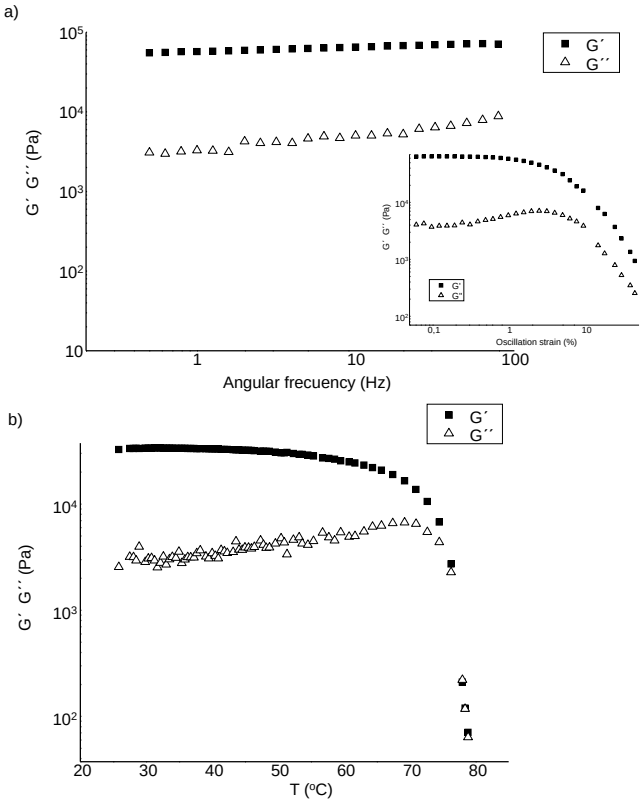

Figure 7. Rheological measurements for the hydrogels from **2a** (5 mg mL^{-1}) in phosphate buffer (pH 5.8, 10 mM)/DMSO (9/1 v/v). a) Frequency sweeps with 0.1% strain and 1 Hz amplitude sweeps at 25 ºC. b) Dependence of storage and loss modulus with the temperature using a heating rate of 0.1 ºC/min and a constant frequency of 1 Hz and 0.1% strain.

2.5. Stimuli-responsiveness and self-healing behavior

Spectroscopic studies revealed the presence of dynamic equilibria in the hydrogels formed by **2a**. This opens the way to potential stimuli-responsive and self-healing behaviors. Thus, the different results obtained as a function of pH suggested this stimulus for the initial studies that demonstrated a reversible and dynamic responsiveness to pH. Starting from the gel formed using 5 mg mL^{-1} of **2a** in H_2O/EtOH (9:1, v/v) the addition on the top of gel of 2 equiv. of NaOH from a 1 M solution, led to the gradual transformation of the gel into a fluid solution. Further addition of 2 equiv. of HCl from a 1 M solution led to the rapid conversion (less than 10 min) of the solution back into a stable gel (Figure 8). Moreover, this gel-sol transition was fully reversible and could be observed for at least four cycles involving successive additions of equimolecular amounts of NaOH and HCl (ESI, Figure S12).

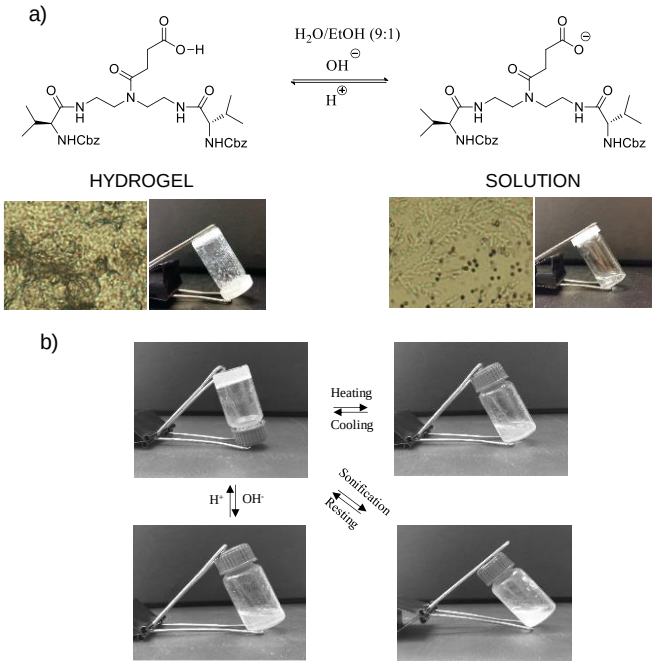

Figure 8. a) Reversible pH-responsive gel-sol transition (**2a** 5 mg mL^{-1} in H_2O/EtOH (9:1 v/v)) and the corresponding optical microscopic morphology, b) Reversible sol-hydrogel transition triggered by temperature, pH and sonication.

As is common in gels, the reversible sol-gel transition for the hydrogels prepared from **2a** was also triggered by temperature and stable gels could be obtained after several cycles of heating above T_g and further cooling. More remarkable was their responsiveness to ultrasounds that can allow for a self-healing behavior.[34] Thus, under sonication the gel changed into solution immediately with the gel reformed again in less than 10 min after suppression of this input. Finally, these dynamic equilibria allowed a simple self-healing behavior. When a piece of hydrogel was cut into two separate pieces (ESI, Figure S13a) self-healing with the reconstitution of a single piece took place almost immediately (in seconds) just after joining the two pieces (ESI, Figure S13b).

2.6. Drug Delivery Studies

As mentioned above, the controlled delivery of active substances in particular in the biomedical realm, represents one key application of hydrogels.[6-8] Such materials seem particularly well suited for transdermal drug delivery, for which the use of viscous matrices (i.e. ionic liquids or DESs) have been shown to provide interesting features.[35] In this regard, the potential of the hydrogel

[34] *Low-molecular-mass gels responding to ultrasound and mechanical stress: towards self-healing materials*; Yu, X.; Chen, L.; Zhang, M.; Yi, T.; *Chem. Soc. Rev.* **2014**, *43*, 5346-5371.
[35] (a) *Transdermal Protein Delivery Using Choline and Geranate (CAGE) Deep Eutectic Solvent*; Banerjee, A.; Ibsen, K.; Iwao, Y.; Zakrewsky, M.; Mitragotri, S.; *Adv. Healthcare Mat.* **2017**, *6*, 1601411, (b) *Design Principles of Ionic Liquids for Transdermal Drug Delivery*; Tanner, E. E. L.;

matrices based on **2a** for drug release was explored selecting (*S*)-Naproxen and caffeine as low molecular weight model drugs presenting very different chemical features (ESI, Figure S14). While (*S*)-Naproxen is a carboxylic acid (hydrogen bond donor) with low solubility in water, caffeine presents some solubility in both water and alcohol, is weakly basic and contains several functional groups able to participate in supramolecular interactions as hydrogen bond acceptors. The loaded hydrogel was prepared by mixing the gelator **2a** and the drug and dissolving the mixture in 0.2 mL of DMSO and adding then 1.8 mL of phosphate buffer (10 mM, pH = 5.8). The mixture was sonicated and left for 24 h to obtain the stable hydrogel which contained 5 mg mL^{-1} of **2a** and 0.16 mg mL^{-1} of the corresponding active substance (*ca.* 0.4 mM for caffeine, for instance).

In vitro transdermal drug release studies were performed using a Franz diffusion Cell having a permeation orifice of 10 mm and a receiver chamber volume of 5 mL. A skin ear pig membrane of 1 mm thickness was used (Figure 9b). This skin membrane prepared following a protocol previously reported,[36] was then hydrated with miliQ® water and the receiver volume filled with 5 mL of a biocompatible phosphate buffer (10 mM, pH = 7.3). Drug release was monitored during *ca.* 24 h with the receptor compartment containing phosphate buffer (pH 7.3) immersed in a water bath at 35 ± 0.5 °C. Over this period, neither shrinkage, swelling or degradation of the gel was visually perceptible.

The release was analyzed in the receiving phase following the increase in the UV-visible absorption bands associated to the drugs (ESI, Figure S15 and S16). For comparison, drug release profiles were also obtained for similar solutions of the drug, in the same solvent mixture, but in the absence of the LMWG **2a**. As shown in Figure 9a, the drug molecules were released from the hydrogel in a slow and continuous manner without any burst release up to 8 h. In the case of (*S*)-Naproxen, this release pattern was maintained after 24 h, although for caffeine an increased release was observe at this time, most likely associated to the partial loss observed for the properties of this gel (Figure S17).

Curreri, A. M.; Balkaran, J. P. R.; Selig-Wober, N. C.; Yang, A. B.; Kendig, C.; Fluhr, M. P.; Kim, N.; Mitragotri, S.; *Adv. Mat.* **2019**, *31*, 1901103, (c) *Comparison of Ionic Liquids and Chemical Permeation Enhancers for Transdermal Drug Delivery*; Qi, Q. M.; Duffy, M.; Curreri, A. M.; Balkaran, J. P. R.; Tanner, E. E. L.; Mitragotri, S.; *Adv. Funct. Mat.* **2020**, 2004257.

[36] (a) *Relationships between skin's electrical impedance and permeability in thepresence of chemical enhancers*; Karande, P.; Jain, A.; Mitragotri, S.; *J. Control. Release* **2006**, *110*, 307-313, (b) *Percutaneous release of caffeine from microemulsion, emulsion and gel dosage forms*; Bolzinger, M.-A.; Briançon, S.; Pelletier, J.; Fessi, H.; Chevalier, Y.; *Eur. J. Pharm. Biopharm.* **2008**, *68*, 446-451.

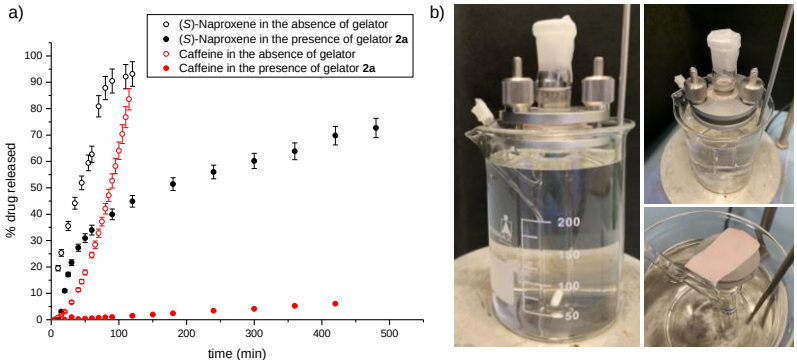

Figure 9. a) Drug release profile in the absence and presence of gelator. Data points represent averages of two samples in the absence of LMWG and three samples in the presence of **2a**. b) Image of the Franz Cell and the pig skin membrane.

The presence of the hydrogel matrix significantly reduces the release of both drugs in comparison with the use of the similar solution as the source. This was particularly important in the case of caffeine. After the first hour, the release of (*S*)-Naproxen from the hydrogel was *ca.* half of that released from the solution and a similar ratio was observed after 2 h, while the release of caffeine from the hydrogel was about 20 times smaller than the release from the solution, becoming *ca.* 40 times smaller when a period of 2 h was considered. The caffeine release rate was slower than that of (*S*)-Naproxen, both from the solution and from the gel. When the drugs were entrapped in the hydrogel matrix the release after 8 h reached *ca.* 10% for caffeine and *ca.* 70 % for (*S*)-Naproxen.

Furthermore, after 24 h the drug content in both the gel and the membrane was also determined. The membrane was sonicated in the corresponding buffer solution (phosphate buffer 10 mM pH 8 for Naproxene and pH 5.8 for caffeine) to determine the drug retained. Thus, in the presence of hydrogel, the drug retained inside the membrane was 23% and 13% for caffeine and (*S*)-Naproxen respectively, and 31% and 0% the drug remained in the hydrogel for caffeine and (*S*)-Naproxen respectively. The sum of the drug released, retained in the membrane and in the hydrogel matrix accounted for 94-95% of the total amount of drug used.

Different drug transport mechanisms have been reported and evaluated using the kinetics observed experimentally.[37] In the present case, the zero-order,

[37] (a) *Drug transport mechanisms and release kinetics from molecularly designed poly(acrylic acid-g-ethylene glycol) hydrogels*; Serra, L.; Domenech, J.; Peppas, N. A.; *Biomaterials* **2006**, *27*, 5440–5451, (b) *Strategies to Modify the Drug Release from Pharmaceutical Systems*; Bruschi, M. L. Ed. Elsevier **2015**, pp. 37-62, (c) *Biocompatible hydrogels for the controlled delivery of anti-hypertensive agent: development, characterization and in vitro evaluation*; Nawaz, S.; Khan, S.;

Higuchi,[38,39] Alfrey,[40] Ritger-Peppas[41] and Peppas-Shalin,[42,43] models were used after linearization to obtain additional information on the mechanisms of drug release involved.[44] The r^2 and Akaike Information Criterion (AICc)[45,46] values were used as goodness of fit parameters as they are indicators of the model suitability for a given data set. From the former models, the Ritger-Peppas model provided the best fitting (Tables 4 and 5; ESI, Figure S18-S22). The empirical equation in this model analyzes both the Fickian and the non-Fickian release of drug, with the equation being: $M_t/M_\infty = k(t-l)^n$, where, M_t/M_∞ is the fraction of drug released at time t, l is the lag time and n is a diffusional exponent indicating the mechanism of drug transport. For cylindrical systems and when $0.45 < n < 0.89$, more than one mechanism controls the release; for $n < 0.45$ the Fickian diffusion controls the release and for $n \geq 1$ anomalous transport occurs.[47] Finally, k is a kinetic constant (having units of t^{-n}) incorporating structural and

---

Farooq, U.; Haider, M. S.; Ranjha, N. M.; Rasul, A.; Nawaz, A.; Arshad, N.; Hameed, R.; *Des. Monomers Polym.* **2018**, *21*, 18-32.

[38] *Investigation of the influence of mean HPMC particle size and number of polymer particles on the release of aspirin from swellable hydrophilic matrix tablets*; Heng, P. W. S.; Chan, L. W.; Easterbrook, M. G.; Li, X.; *J. Control. Release* **2001**, *76*, 39-49.

[39] (a) *Rate of release of medicaments from ointment bases containing drugs in suspension*; Higuchi, T.; *J. Pharm. Sci.* **1961**, *50*, 874–875, (b) *Mechanism of sustained-action medication*; Higuchi, T.; *J. Pharm. Sci.* **1963**, *52*, 1145–1149, (c) *Diffusion in HPMC gels:II. Prediction of drug release rates from hydrophilic matrix extended-release dosage forms*; Gao, P.; Nixon, P. R.; Skoug, J. W.; *Pharm. Res.* **1995**, *12*, 965–971.

[40] *Diffusion in glassy polymers*; Alfrey, T.; Gurnee, E. F.; Lloyd, W. G.; *J. Polym. Sci. C Polym. Symp.* **1966**, *12*, 249-261.

[41] (a) *Solute and penetrant diffusion in swellable polymers. III. Drug release from glassy poly (HEMA-co-NVP) copolymers*; Korsmeyer, R. W.; Peppas, N. A.; *J. Control. Release* **1984**, *1*, 89-98, (b) *A simple equation for description of solute release I. Fickian and non-Fickian release from non-swellable devices in form of slabs, sphere, cylinders or discs*; Ritger, P. L.; Peppas, N. A.; *J. Control. Release* **1987**, *5*, 23–36, (b) *Molecular analysis of drug delivery systems controlled by dissolution of the polymer carrier*; Narasimhan, B.; Peppas, N. A.; *J. Pharm. Sci.* **1997**, *86*, 297-304.

[42] *A simple equation for the description of solute release III. Coupling of diffusion and relaxation*; Peppas, N. A.; Sahlin, J. J.; *Int. J. Pharm.* **1989**, *57*, 169–72.

[43] (a) *Solute and penetrant diffusion in swellable polymers. I. Mathematical modeling*; Korsmeyer, R. W.; Lustig, S. R.; Peppas, N. A.; *J. Polym. Sci. B Polym. Phys.* **1986**, *24*, 395–408, (b) *Solute and penetrant diffusion in swellable polymers. II. Verification of theoretical models;* Korsmeyer, R. W.; Von Meerwall, E.; Peppas, N. A.; *J. Polym. Sci. B Polym. Phys.* **1986**, *24*, 409–434, (c) *Solute and penetrant diffusion in swellable polymers. VII. A free volume-based model with mechanical relaxation*; Lustig, S. R.; Peppas, N. A.; *J. Appl. Polym. Sci.* **1987**, *33*, 533–549, (d) Peppas, N. A.; Korsmeyer, R. W. *Dynamically swelling hydrogels in controlled release applications* in *Hydrogels in Medicine and Pharmacy*; vol. *3* Properties and Applications; Peppas, N. A., Ed.; CRC Press: Boca Raton, **1987**, pp 109–136.

[44] (a) *Methods to compare dissolution profiles and a rationale for wide dissolution specifications for metoprolol tartrate tablets*; Polli, J. E.; Rekhi, G. S.; Augsburger, L. L.; Shah, V. P.; *J. Pharm. Sci.* **1997**, *86*, 690-700, (b) *Modeling and comparison of dissolution profiles*; Costa, P.; Lobo, J. M. S.; *Eur. J. Pharm. Sci.* **2001**, *13*,123-133.

[45] *Prediction of in vitro Drug Release Mechanisms from Extended Release Matrix Tablets using SSR/R2 Technique;* Singh, J.; Gupta, S.; Kaur, H.; *Trends Appl. Sci. Res.* **2011**, *6,* 400-409.

[46] (a) *Application of the Akaike Information Criterion (AIC) in the evaluation of linear pharmacokinetics equations*; Yamoaka, K.; Nakagawa, T.; Uno, T.; *J. Pharmacokinet. Biopharm.* **1978**, *6*, 165–175, (b) *Model selection fortime-activity curves: The corrected Akaike information criterion and the F-test;* Kletting, P.; Glatting, G.; *Z. Med. Phys.* **2009**, *19*, 200–206.

[47] *Designing hydrogels for controlled drug delivery*; Li, J.; Mooney, D. J.; *Nat. Rev. Mater.* **2016**, *1,* 16071.

geometric characteristics of the delivery system. This equation can be used to analyze only the first 60% of release, regardless of geometric shapes.

Table 4. Caffeine and (*S*)-Naproxen kinetic release parameters obtained by fitting to the different models selected using a phosphate buffer/DMSO solution as the source[a].

Model	(*S*)-Naproxen[b]			Caffeine[c]		
	k (k_2)	n	r^2 (AICc)	k (k_2)	n	r^2 (AICc)
Zero-order	0.011±0.001	1	0.853	$58.3E^{-4}$±$2.8E^{-4}$	1	0.883
Higuchi	0.085±0.013	0.5	$10E^{-16}$	0.068±0.012	0.5	$10\ E^{-16}$
Alfrey	0.0103±0.0025 (0.01)	0.5	-249.0	0.0052±0.0044 (0.001)	0.5	0.7854
Peppas-Shalin	0.039±0.006 (0.015±0.004)	0.41±0.22	0.996 (65.11)	$0.798E^{-3}$±$0.118E^{-3}$ ($0.258E^{-5}$±$0.2104E^{-5}$)	1.3± 0.7	0.978 (99.7)
Ritger-Peppas	0.043±0.003	0.66±0.02	0.997 (34.3)	$1.081E^{-4}$±$0.312E^{-4}$	1.88± 0.06	0.992 (116)

[a] Phosphate buffer (pH 5.8, 10 mM)/DMSO (9/1, v/v). k and k_2 represent kinetic constants and n is a diffusional exponent; [b] 0.31 mM; [c] 0.33 mM.

Data in Table 4 indicate that the mechanism of (*S*)-Naproxen release from the phosphate buffer (pH 5.8, 10 mM)/DMSO (9/1, v/v) solution was controlled by both Fickian and non-Fickian diffusion (n = 0.66), whilst for caffeine the transport mechanism observed was anomalous (n = 1.88). In the case of the hydrogels, data in Table 5 show that the release was controlled by the Fickian diffusion (n = 0.3) for (*S*)-Naproxen and by an anomalous drug transport mechanism in the case of caffeine, leading to a zero order release (n ≈ 1).

Table 5. Caffeine and (*S*)-Naproxen kinetic release parameters obtained by fitting to the different models selected using the hydrogel as the source[a].

Model	(*S*)-Naproxen[b]			Caffeine[c]		
	k (k_2)	n	r^2 (AICc)	k (k_2)	n	r^2 (AICc)
Zero-order	$13.78E^{-4}$±$1.64E^{-4}$	1	0.813	$15.06E^{-5}$±$0.23E^{-5}$	1	0.985
Higuchi	0.071±0.012	0.5	-0.067	0.003±0.001	0.5	-0.067
Alfrey	0.001±$1.701E^{-4}$ (0.01)	0.5	0.799	$15.06E^{-4}$±$0.26E^{-5}$ (0.01)	0.5	0.945 (-17)
Peppas-Shalin	0.084±0.015 (-0.001±$1.35E^{-3}$)	0.37±0 .07	0.963 (111)	$22.84E^{-3}$±$2.46E^{-3}$ ($1.853E^{-4}$±$4.238E^{-4}$)	0.49±0 .14	0.997 (42)
Ritger-Peppas	0.115±0.021	0.3±0. 03	0.976 (107)	$1.494E^{-4}$±$0.388E^{-4}$	1.01±0 .04	0.997 (-31)

a) Hydrogel composition: Phosphate buffer (pH 5.8, 10 mM)/DMSO (9/1, v/v), k and k_2 represent kinetic constants and n is a diffusional exponent; [b] 0.31 mM; [c] 0.33 mM.

Using a non-steady-state diffusion model, with the equation for the early-time being: $M_t/M_o = 4(D_E*(t-l)/h^2\pi)^{1/2}$ and the one for the late-time being: $M_t/M_o = 1 - 8/\pi^2(\exp -\pi^2 D_L(t-l)/h^2)$, where M_t is the total amount of molecules released

during the measurement, M_o is the total amount of molecules kept in the hydrogel matrix, h represents the hydrogel thickness, t is the time of measurement, and D is the diffusion constant of the molecule, the relative diffusion coefficients of the drug molecules through the gel could be calculated.[48] Considering constant the amount of drug entrapped inside the membrane after a saturation period l (lag time 24 min and 21 min for caffeine and Naproxen respectively), the diffusion coefficient values determined were D_E = 3.06 10^{-8} m^2/s (r^2 = 0.976) for (*S*)-Naproxen and D_L = 1.64 10^{-10} m^2/s (r^2 = 0.908) for caffeine. Thus, caffeine was held more tightly by the gel resulting in their slower release.[49] This is likely to be due to the presence of electrostatic and hydrophilic interactions between the drug and gel matrix that will be particularly prevalent in the case of caffeine containing hydrogen bond acceptor functionalities complementary of the hydrogen bond donor sites in the molecule of the the LMWG.[50] D values are comparable to those of small model drugs in other LMW gelling systems.[48,51]

To analyze the contribution to the different release of both drugs from their interaction with the membrane, the drug flux at steady state (Jss, μg cm^2/h) across the membrane was calculated, in the absence of gelator, from the slope of the linear portion of the cumulative drug permeation through the membrane per unit of area versus time. The Jss values determined were 291 and 77 μg cm^2/h for (*S*)-Naproxen and caffeine respectively. This indicates that caffeine also interacts stronger with the membrane than (*S*)-Naproxen affording a reduced flux, although, according to the data presented in Figure 9, the main factor affecting the slower release of caffeine must be associated to the supramolecular interactions between this drug and the hydrogel matrix.

---

[48] (a) *Tailoring drug release profile of low-molecular-weight hydrogels by supramolecular co-assembly and thiol–ene orthogonal coupling*; Díaz, D. D.; Morin, E.; Schön, E. M.; Budin, G.; Wagner, A.; Remy, J. S.; *J. Mat. Chem.* **2011**, *21*, 641–644, (b) *A novel highly stable and injectable hydrogel based on a conformationally restricted ultrashort peptide*; Thota, C. K.; Yadav, N.; Chauhan, V. S.; *Sci. Rep.* **2016**, *6*, 31167.

[49] *Stimuli Responsive Self-Assembled Hydrogel of a Low Molecular Weight Free Dipeptide with Potential for Tunable Drug Delivery*; Panda, J. J.; Mishra, A.; Basu, A.; Chauhan, V. S.; *Biomacromolecules* **2008**, *9*, 2244–2250.

[50] *Entrapment and release of quinoline derivatives using ahydrogel of a low molecular weight gelator*; Friggeri, A.; Feringab, B. L.; Esch, J. V.; *J. Control. Release* **2004**, *97*, 241–248.

[51] *Macromolecular diffusion and release from self-assembled b-hairpin peptide hydrogels*; Branco, M. C.; Pochan, D. J.; Wagner, N. J.; Schneider, J. P.; *Biomaterials* **2009**, *30*, 1339–1347.

3. Conclusion

In conclusion, a series of novel pseudopeptidic hydrogelators showing a rapid and reversible, ultrasound, pH and thermal responsiveness and displaying self-healing properties have been prepared and studied. Results demonstrate that an optimum lipophilicity of the amino acid residue is needed for an efficient gelation process. Thus, gelator **2a** was able to form stable gels in a wide range of solvents with a CGC value of 1 mg mL^{-1} in H_2O:EtOH (9:1, v/v), while compound **2c**, in which the aliphatic side chain was substituted by an aromatic one, was unable to form gels in any solvent studied at 5 mg mL^{-1}. An intermediate situation was found for **2b** differing from **2a** just by the presence of an additional methylene in the side chain, forming much weaker gels than **2a**. The resulting hydrogel from **2a** (0.5 mg mL^{-1}) displayed thermal stability up to 60 ºC in H_2O:EtOH (9:1, v/v), while the hydrogel formed in H_2O/DMSO (9:1, v/v) was stable up to 70 ºC. Stable hydrogels were also obtained in H_2O:EtOH (9:1, v/v) in the presence of a variety of buffers, including biologically relevant phosphate buffers, but were unstable in basic conditions. Preliminary drug delivery studies, using a Franz Diffusion Cell with a pig skin membrane, were carried out with caffeine and (*S*)-Naproxen as model drugs with very different features for supramolecular interactions. The results have revealed that the hydrogels allow for a continuous and significantly slower release of the drugs, which is particularly relevant for caffeine. The release process could be fitted to different mechanism models, with the best fitting achieved for the Ritger-Peppas model. The results from this model, in combination with the observation of quite different diffusion coefficients, drug fluxes at steady state and release rates, defined the presence of different drug release mechanisms for both drugs entrapped in the hydrogel matrix. The significantly slower release rate for caffeine when using the hydrogel as the source phase must be assigned to the higher complementarity, in terms of supramolecular interactions, between the drug and the LMWG, highlighting the potential of this complementarity as a design vector for the development of specific LMWGs for the focused and controlled release of active substances and drugs.

4. Experimental section

General: Reagents and solvents were purchased from commercial suppliers and were used without further purification. The C_2-symmetrical N-protected bis(amidoamines) **1** were prepared as previously described.[22]

Electron microscopy: Scanning Electron Microscopy was performed either in a LEO 440I or in a JEOL 7001F microscope with a digital camera. Samples were obtained by slow evaporation of a solution of the compounds (5 mg mL^{-1}) directly onto the sample holder, and were conventionally coated previous to the measurement.

NMR spectroscopy: NMR experiments were carried out on a Varian INOVA 500 spectrometer (500 MHz for ^{1}H and 125 MHz for ^{13}C) or on a Varian UNITY 400 (400 MHz for ^{1}H and 101 MHz for ^{13}C). Chemical shifts are reported in parts per million using the solvent residual peak as the reference.

Infrared spectroscopy: ATR FT-IR spectra were acquired in a JASCO 6200 equipment having a MIRacle Single Reflection ATR Diamond/ZnSe accessory. Samples in solution, in the gel state or in solid state were directly deposited onto the ATR sample holder, and the FT-IR spectra were collected. The raw IR data were processed with the JASCO spectral manager software.

UV-vis spectroscopy: UV-vis absorption measurements were made using a Hewlett-Packard 8453 spectrophotometer, equipped with a controlled temperature system.

Preparation of buffer solutions:

- Phosphate buffers: Buffers were prepared by dissolving the corresponding amount of KH_2PO_4 and K_2HPO_4 in 100 mL of miliQ® water. The pH was then adjusted with small additions of 1 M HCl and/or 1 M NaOH.

- Acetate buffers: Buffers were prepared using the corresponding amount of AcOH 10 mM and NaAcO 10 mM in miliQ® water. The pH was then adjusted with additions of AcOH or NaAcO 10 mM.

Gelation experiments: In a typical experiment, a weighted amount of LMWG was mixed with 2 mL of the selected solvent in a 12 mL glass vial and ultrasonicated for 1 minute. Gelation was considered to have occurred when a homogeneous substance was obtained, which exhibited no gravitational flow upon inversion of the vial. In the case of solvent mixtures (organic/water), the LMWG was first dissolved in the corresponding amount of the organic solvent (DMSO or EtOH) and later miliQ® water or the appropriate aqueous buffer was added.

Rheological characterization: The different gels were characterized using a controlled stress AR-2000 rheometer from TA Instruments. A Peltier holder with

a plate geometry (60 mm diameter, 500 μm gap) was used for all samples. Frequency sweeps were performed in the angular frequency range 0.1–100 rad s^{-1} with the instrument in oscillatory mode at 25 °C. Strain sweeps were performed using a frequency of 1 rad s^{-1} in a amplitude sweep range of 0.01% - 80% with the instrument in oscillatory mode at 25 °C.

Release studies: The appropriate amounts of gelator and drug were weighted and mixed with the corresponding solvent mixture to obtain the desired gels as described before. The experiments were conducted in a Franz Diffusion Cell where the gel was formed *in situ* on the donor compartment cell. The acceptor compartment was filled with 5 mL of phosphate buffer (10 mM, pH = 7.3) maintaining a mild magnetic stirring, and the porcine skin was placed in the diffusion area. The system was closed to avoid solvent evaporation. The experiments were conducted in duplicate or triplicate, at 35 ºC for up to 24 h. Aliquots (100 μL) from the acceptor compartment were taken at different times and evaluated using a Hewlett-Packard 8453 spectrophotometer (UV-vis spectroscopy) equipped with a control temperature system to determine the amount of caffeine or (*S*)-Naproxen released. For this purpose, the corresponding aliquot was diluted with 1 mL of phosphate buffer (10 mM, pH = 8).

Data Analysis: The cumulative amount (Q, μg/cm^2) of caffeine and (*S*)-Naproxen penetrating through an area of 1.3 cm^2 was plotted against time (t). The steady-state flux J_{SS} (g/cm^2h) was determined from the slope of the linear portion of the cumulative amount (Q μg/cm^2) versus time (t) plot.

The diffusion coefficients through the gel were calculated based on a non-steady-state diffusion model with the equation for the early-time being: $M_t/M_o = 4(D_E*(t-l)/h^2\pi)^{1/2}$ and the one for the late-time being: $M_t/M_o = 1 - 8/\pi^2(\exp - \pi^2 D_L(t-l)/h^2)$.

In order to study the drug transport mechanisms from the hydrogels, five diffusion models were considered to which the experimental data were fitted:

Higuchi equation: $M_t/M_\infty = k\, t^{1/2}$, where M_t/M_∞ is the fraction of drug released, k is a kinetic constant and t is the release time.

Ritger–Peppas equation: $M_t/M_\infty = kt^n$, where, M_t/M_∞ is the fraction of drug released, k is a kinetic constant, n represents the diffusional exponent and is indicator of the mechanism of transport of drug and t is the release time.

Peppas–Sahlin equation: $M_t/M_\infty = k_1 t^n + k_2 t^{2n}$, where M_t/M_∞ is the fraction of drug released, the first term of the equation represents the contribution of Fickian diffusion and the second term refers to the macromolecular relaxation contribution on the overall release mechanism.

Alfrey equation: $M_t/M_\infty = k_1 t^{0.5} + k_2 t$, described also by the Peppas–Sahlin equation, but with the exponent n fixed to 0.5:

Zero order equation: $M_t/M_\infty = kt$, where M_t/M_∞ is the fraction of drug released, k represents the constant for zero order release and t is the release time.

These equations were used to analyze only first 60% of release.

4. Supporting information

4.1. Synthetic Protocols and Structural Characterization

General synthesis for compounds 2a-c: The corresponding pseudopeptidic N-protected bis(aminoamide) precursor **1a-c** (4 mmoles), 4-(dimethylamino)pyridine (0.8 mmoles) and succinic anhydride (8 mmol) were dissolved in Et_3N-THF 1:1 (50 mL). The reaction mixture was stirred and heated at 70 ºC during 24 h. The solvent was vacuum evaporated, the crude was dissolved in acidic water and extracted with CH_2Cl_2 (3x), the organic layer was washed with water and then dried with anhydrous $MgSO_4$. The organic solvent was vacuum evaporated and the white solid obtained was purified by column chromatography (CH_2Cl_2:MeOH, 10:1).

Synthesis of 2a. White solid. 70% Yield. m.p. = 114 ºC, $[\alpha]_D^{25}$ = - 6.24 (c = 0.005, CH_3OH). ^{1}H-NMR (400 MHz, CD_3OD, δ): 7.42-7.21 (m, 10H), 5.16-5.03 (m, 4H), 3.89 (t, *J* = 9.3 Hz, 2H), 3.55-3.32 (m, 8H), 2.68-2.56 (m, 4H), 2.12-1.95 (m, 2H), 0.92 (dd, *J* = 10.6, 6.8 Hz, 12H); ESI$^+$, m/z (%): 670.3 $[M + H]^+$, 692.3 $[M + Na]^+$; ESI$^-$, m/z (%): 668.3 [M – H]-; ^{13}C NMR (126 MHz, CD_3OD, δ): 173.4, 173.1, 157.2, 136.8, 128.1, 127.6, 127.5, 66.4, 60.9, 45.0, 37.3, 37.1, 30.3, 28.9, 27.6, 18.4, 17.0; DEPT (101 MHz, $CDCl_3$, δ): 175.53, 174.66, 172.4, 171.9, 157.4, 156.5, 136.3, 136.1, 128.5, 128.2, 128.0, 67.3, 67.0, 60.2, 49.0, 45.7, 40.0, 38.6, 32.0, 31.0, 29.4, 27.9, 19.3, 17.8, 17.4; FT-IR (ATR) (cm^{-1}): 3290, 3202, 3105, 2968, 1709, 1648, 1528, 1237, 1022; Anal. Calcld. for $C_{34}H_{47}N_5O_9$. 2 H_2O: C, 57.86; H, 7.28; N, 9.92. found: C, 57.85, H, 6.88, N, 10.22.

Synthesis of 2b. White solid, 85% yield. m.p. = 117 ºC, $[\alpha]_D^{25}$ = - 4.93 (c = 0.005, CH_3OH). ^{1}H-RMN (500 MHz, CD_3OD, δ): 7.27-7.41 (m, 10H), 5.03-5.18 (m, 4H),

3.94 (dd, *J* = 10.5, 7.2 Hz, 2H), 3.56-3.27 (m, 8H), 2.54-2.72 (m, 4H), 1.83 (s, 2H), 1.51 (s, 2H), 1.1-1.25 (m, 2H), 0.87-0.95 (m, 12H); ^{1}H NMR (500 MHz, $CDCl_3$, δ): 7.26 (s, 10H), 6.71 (s, NH), 5.79 (s, NH), 5.35 (s, NH), 5.20-4.85 (m, 4H), 4.19 – 3.86 (m, 3H), 3.67 (s, 2H), 3.29-3.10 (m, 3H), 2.94 (s, 1H), 2.78 (s, 2H), 2.51–2.43 (m, 1H), 2.24 (s, 1H), 1.85-1.57 (s, 3H), 1.38 (s, 2H), 1.18 (s, 1H), 1.00 (s, 2H), 0.80 (s, 12H); ESI^{+}, m/z(%): 698,4 $[M + H]^{+}$; 720.5 $[M + Na]^{+}$; ESI^{-}, m/z (%): 696.2 $[M-H]^{-}$; ^{13}C NMR (101 MHz, $CDCl_3$, δ): 175.4, 174.9, 172.4, 171.7, 157.3, 156.4, 136.3, 136.0, 128.5, 128.15, 128.0, 67.3, 67.0, 59.6, 59.5, 49.2, 45.7, 40.3, 38.7, 37.3, 29.5, 27.9, 24.7, 24.51, 15.5, 11.5, 11.3; Anal. Calcld. for $C_{36}H_{51}N_5O_9$. H_2O: C, 60.40; H, 7.46; N, 9.78. found: C, 60.55, H, 7.23, N, 9.71.

Synthesis of 2c. White solid, yield 59%. m.p. = 108 °C, $[\alpha]_D^{25}$ = - 2.10 (c = 0.008, CH_3OH). ^{1}H-RMN (101 MHz, CD_3OD, δ): 7.37-7.14 (m, 20H), 5.20-4.90 (m, 4H), 4.42-4.25 (m, 2H), 3.50-3.25 (m, 8H), 3.25-3.03 (m, 2H), 2.96-2.75 (m, 2H), 2.65 (s, 4H); ESI^{+} m/z (%): 766.3 $[M + H]^{+}$; ESI^{-} m/z (%): 764.5 [M – H]-; ^{13}C-RMN (101 MHz, CD_3OD /$CDCl_3$, δ): 175.4, 173.4, 172.7, 172.5, 156.5, 136.7, 136.3, 129.1, 128.3, 127.9, 127.6, 126.7, 66.7, 56.4, 47.1, 45.2, 38.2, 37.7, 29.0, 27.6; DEPT (101 MHz, CD_3OD, δ): δ 173.5, 173.1, 172.9, 156.8, 137.3, 137.2, 128.9, 128.1, 127.5, 127.3, 126.4, 66.2, 45.1, 37.7, 37.4, 37.3, 28.7, 27.6.; IR (ATR) (cm^{-1}): 3313, 3282, 2952, 2361, 2338, 1731, 1690, 1652, 1532, 1452, 1429, 1383, 1287, 1260, 1241,1179, 1141, 1053; Anal. calcld. for $C_{42}H_{47}N_5O_9$: C, 60.40; H, 6.30; N, 8.93, found: C, 59.95; H, 6.19; N, 9.14.

Open chain pseudopeptides as hydrogelators with reversible and dynamic responsiveness to pH, temperature and sonication as vehicles for controlled drug delivery

Index

16. **Fig. S15.** UV-vis spectra of caffeine in phosphate buffer and delivered from the gel matrix at different concentrations and the corresponding linear fitting using the absorbance at 273 nm.
17. **Fig. S16.** UV-vis spectra of (*S*)-Naproxen in phosphate buffer and delivered from the gel matrix at different concentrations and the corresponding linear fitting using the absorbance at 333 nm.
18. **Fig. S17.** Drug release profile in the presence of gelator **2a** using a Franz Cell at 35 ^{o}C.
19. **Fig. S18.** Fitting of the experimental data up to 60% of drug delivery, considering the Ritger-Peppas diffusion model for (*S*)-Naproxen and caffeine in the absence and presence of the gelator.
20. **Fig. S19.** Fitting of the experimental data up to 60% of drug delivery, considering the Peppas-Sahlin diffusion model for (*S*)-Naproxen and caffeine in the absence and presence of the gelator.
21. **Fig. S20.** Fitting of the experimental data up to 60% of drug delivery, considering the Higuchi diffusion model for (*S*)-Naproxen and caffeine in the absence and presence of the gelator.
22. **Fig. S21.** Fitting of the experimental data up to 60% of drug delivery, considering the Alfrey diffusion model for (*S*)-Naproxen and caffeine in the absence and presence of the gelator.
23. **Fig. S22.** Fitting of the experimental data up to 60% of drug delivery, considering the Zero Order diffusion model for (*S*)-Naproxen and caffeine in the absence and presence of the gelator.

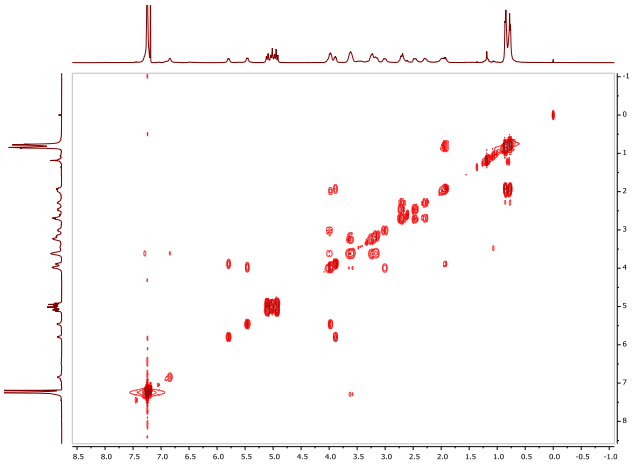

Figure S1. COSY of **2a** (15 mM in $CDCl_3$).

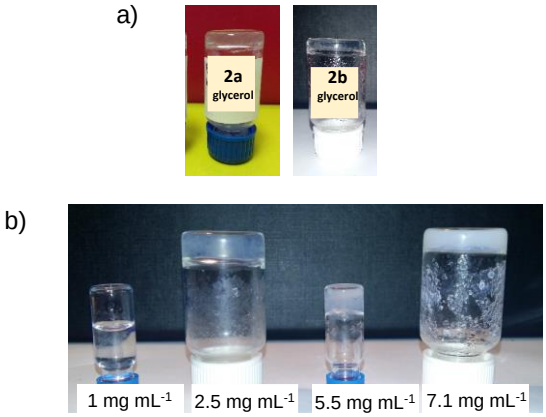

Figure S2. a) Organogels (glycerol) obtained from **2a** and **2b** (5.5 mg mL^{-1}). b) Hydrogels obtained from **2a** in H_2O/EtOH (9:1, v/v) at different concentrations.

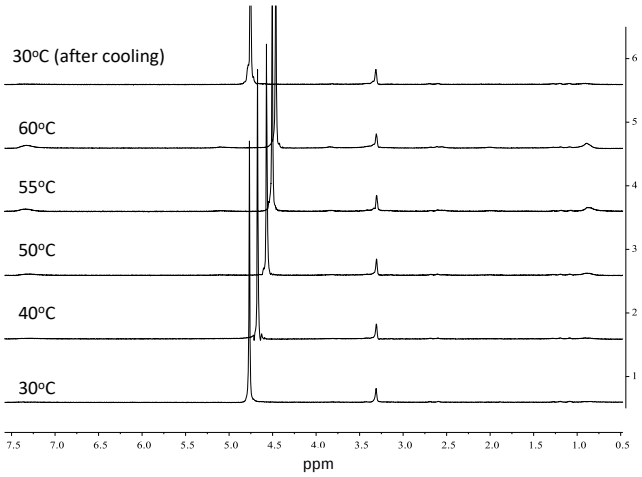

Figure S3. ^{1}H-NMR spectra of **2a** (5.5 mg mL^{-1}) in D_2O/CD_3OD 9:1 at different temperatures.

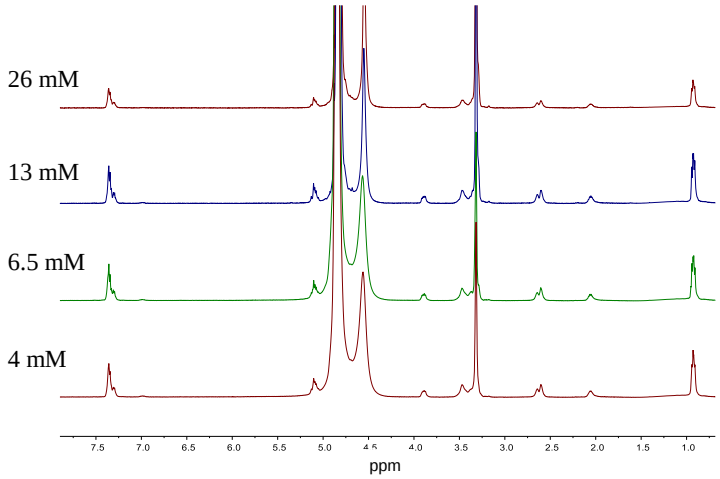

Figure S4. ^{1}H NMR of **2a** in CD_3OD at different concentrations.

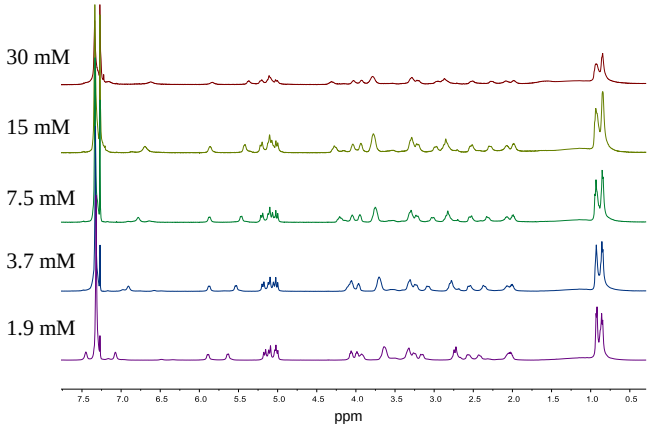

Figure S5. ^{1}H NMR spectra of **2a** in $CDCl_3$ at different concentrations at different concentrations.

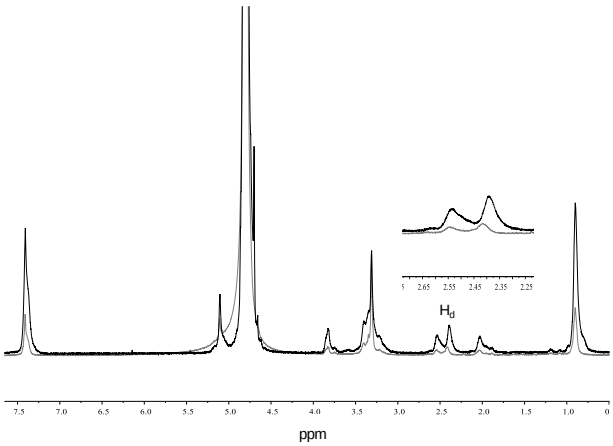

Figure S6. ^{1}H-NMR spectra of **2a** (5 mg mL^{-1}) at 40 °C in pure D_2O/CD_3OD (7:3, v/v) alone (grey line) and in the presence of 2 equiv. of NaOH (black line).

Table S1. Temperature of hydrogel disassembly for **2a** at pH 5.8 (phosphate buffer 10 mM in H_2O/EtOH (9:1, v/v)) as a function of gelator content as determined by the vial inversion method.

Entry	Gelator content mg mL^{-1}	T_g (°C)
1	1.0	--
2	2.0	40
3	3.0	45
4	4.0	50
5	5.0	55
6	6.0	60

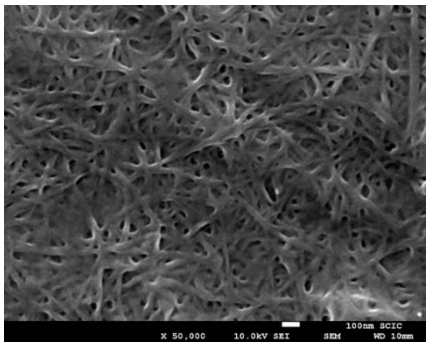

Figure S7. SEM images for the dried hydrogel from **2b**, 5 mg mL^{-1} in H_2O/EtOH (9/1, v/v).

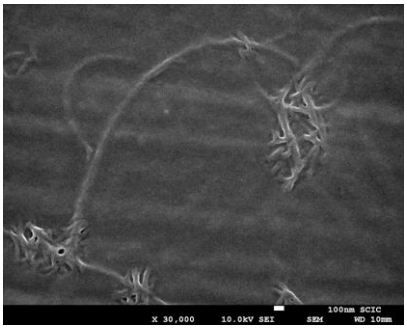

Figure S8. SEM images for the solid obtained by drying a solution of **2a** 5 mg mL^{-1} in $CHCl_3$.

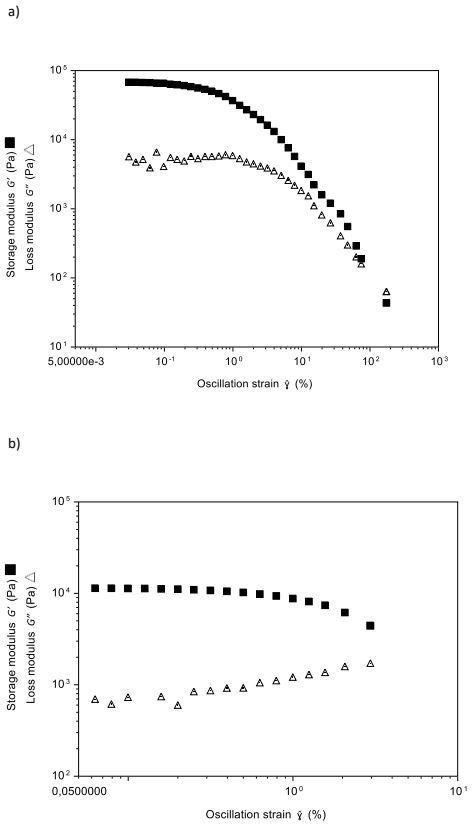

Figure S9. Amplitude sweeps with constant frequency of 1 Hz at 25 ºC for the hydrogels from **2a** in phosphate buffer (pH 5.8, 10 mM)/EtOH (9/1 v/v)) at different concentrations a) 5 mg mL^{-1}. b) 2.5 mg mL^{-1}.

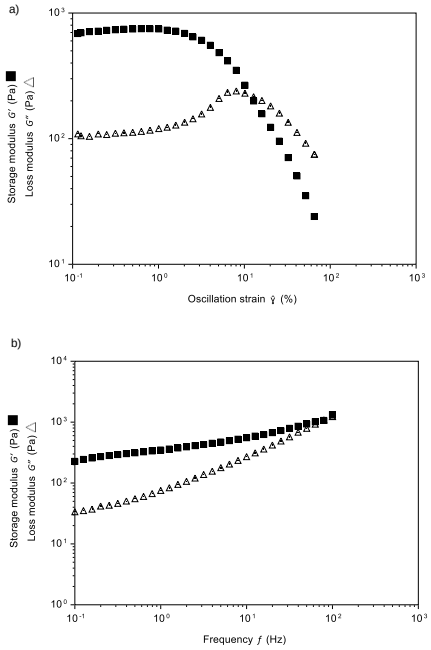

Figure S10. Rheological analysis at 25 ºC of gels from **2a** at concentrations of 5 mg mL^{-1} in glycerol. a) Strain sweep with constant frequency of 1 Hz. b) Frequency sweep with 0.3% strain.

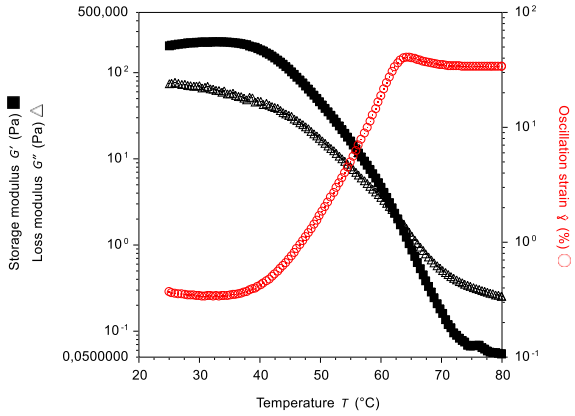

Figure S11. Dependence of storage and loss modulus with the temperature for a **2a** gelator content of 5 mg mL^{-1} in glycerol. All measurements were carried out at a heating rate of 0.1 ºC/min, a constant frequency of 1 Hz and 0.3% strain.

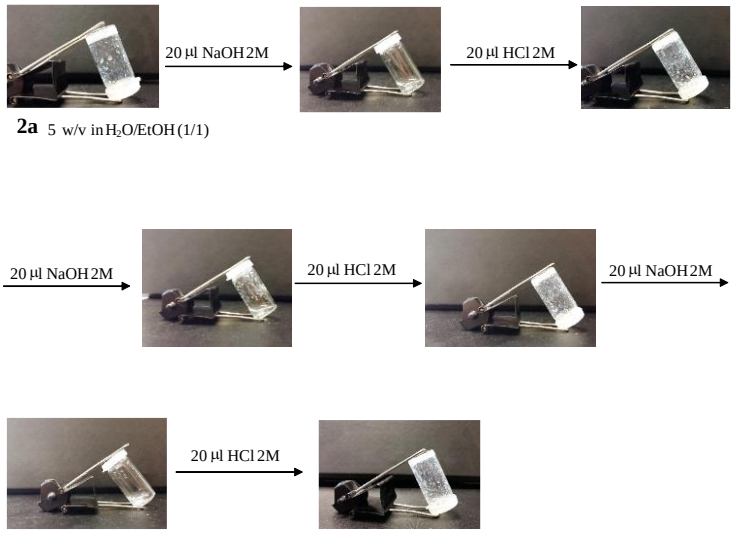

Figure S12. Reversible acid-base stimuli-responsiveness.

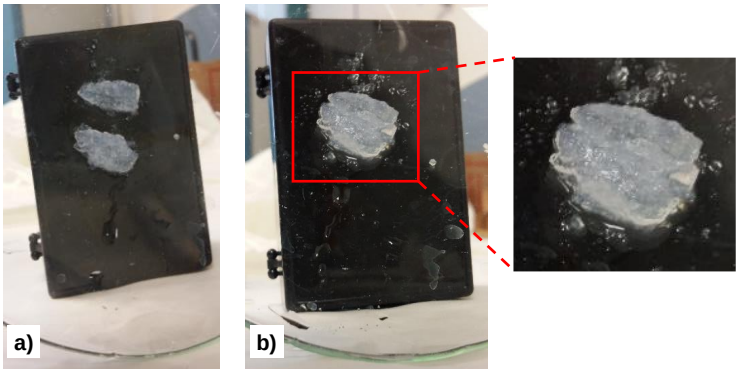

Figure S13. Self-healing of the hydrogel prepared with 5 mg mL^{-1} **2a** in H_2O/EtOH (9:1 v/v). a) hydrogel cut into two pieces; b) self-healed hydrogel.

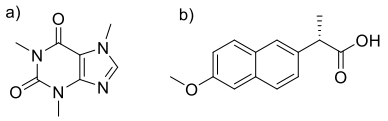

Figure S14. Molecular structures of a) caffeine and b) (*S*)-Naproxen.

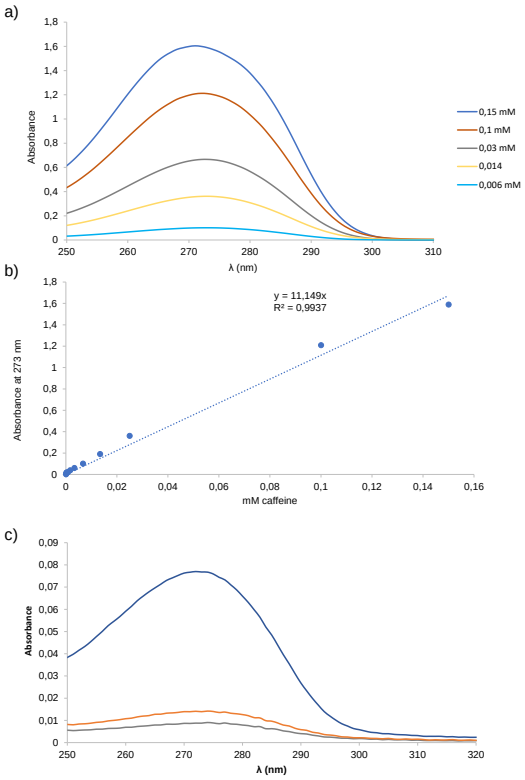

Figure S15. a) UV-vis spectra of caffeine in phosphate buffer (pH 5.8, 10 mM) at different concentrations and b) the corresponding linear fitting using the absorbance at 273 nm. c) UV-vis spectra of caffeine delivered from the gel matrix (phosphate buffer 10 mM, pH = 5.8/DMSO (9/1, v/v), 5 mg mL^{-1} of gelator and 0.16 mg mL^{-1} of drug) at 35 ºC obtained at 3 h (grey line), 5 h (orange line) and 9 h (blue line) after adding 1 mL of phosphate buffer (pH 5.8, 10 mM).

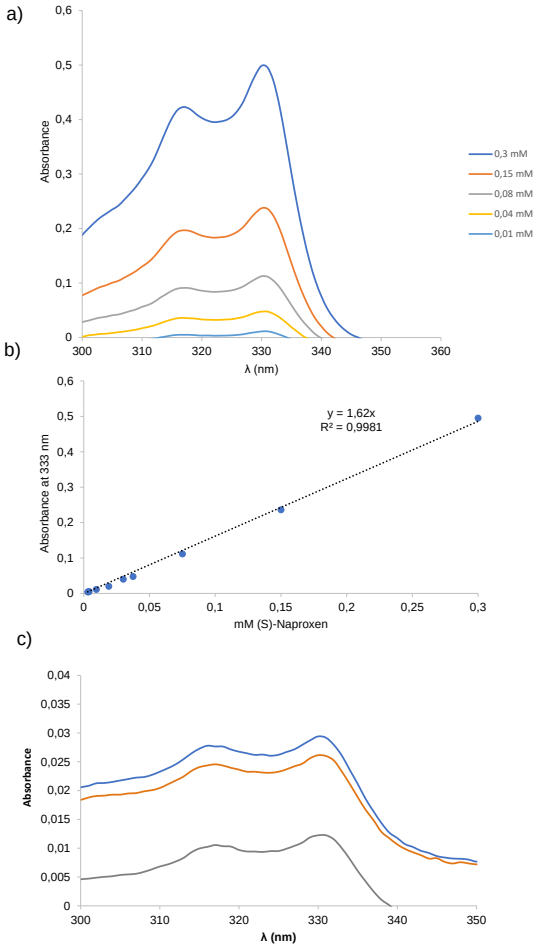

Figure S16. a) UV-vis spectra of (*S*)-Naproxen in phosphate buffer (pH 8, 10 mM) at different concentrations and b) the corresponding linear fitting obtained using the absorbance at 333 nm. c) UV-vis spectra of (*S*)-Naproxen delivered from gel matrix (phosphate buffer 10 mM, pH = 5.8/DMSO (9/1, v/v), 5 mg mL^{-1} of gelator and 0.17 mg mL^{-1} of drug) at 35 ºC obtained at 0.5 h (grey line), 3 h (orange line) and 5 h (blue line) after adding 1 mL phosphate buffer (pH 8, 10 mM).

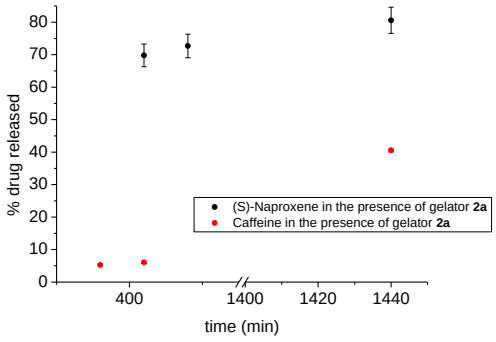

Figure S17. Drug release profile in the presence of gelator **2a** using a Franz Cell at 35 ºC. Data points represent averages of three samples in the presence of gelator.

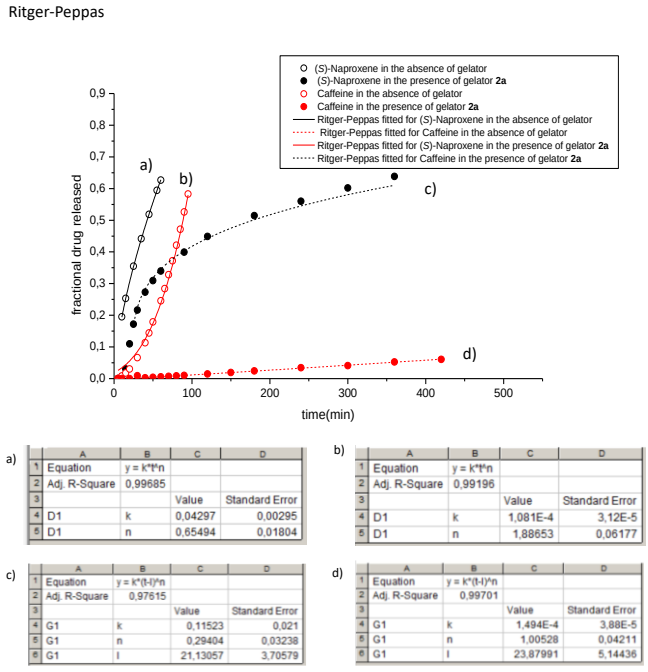

a)

	A	B	C	D
1	Equation	y = k*t^n		
2	Adj. R-Square	0,99685		
3			Value	Standard Error
4	D1	k	0,04297	0,00295
5	D1	n	0,65494	0,01804

b)

	A	B	C	D
1	Equation	y = k*t^n		
2	Adj. R-Square	0,99196		
3			Value	Standard Error
4	D1	k	1,081E-4	3,12E-5
5	D1	n	1,88653	0,06177

c)

	A	B	C	D
1	Equation	y = k*(t-l)^n		
2	Adj. R-Square	0,97615		
3			Value	Standard Error
4	G1	k	0,11523	0,021
5	G1	n	0,29404	0,03238
6	G1	l	21,13057	3,70579

d)

	A	B	C	D
1	Equation	y = k*(t-l)^n		
2	Adj. R-Square	0,99701		
3			Value	Standard Error
4	G1	k	1,494E-4	3,88E-5
5	G1	n	1,00528	0,04211
6	G1	l	23,87991	5,14436

Figure S18. Fitting of the experimental data up to 60% of drug delivery, considering the Ritger-Peppas diffusion model. a) (*S*)-Naproxen in the absence of the gelator, b) caffeine in the absence of the gelator, c) (*S*)-Naproxen in the hydrogel, d) caffeine in the hydrogel.

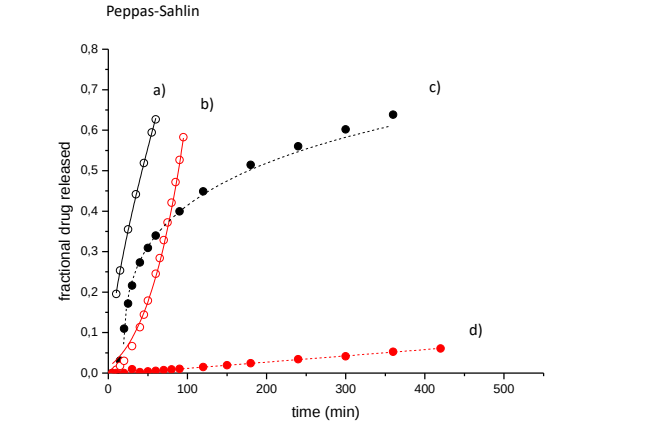

a)

	A	B	C	D
1	Equation	y = (k*t^n)+(z*t^(2*n))		
2	Adj. R-Square	0,99641		
3			Value	Standard Error
4	D1	k	0,03915	0,00563
5	D1	z	0,01477	0,00437
6	D1	n	0,40905	0,21889

b)

	A	B	C	D
1	Equation	y = (k*t^n)+(z*t^(2*n))		
2	Adj. R-Square	0,9784		
3			Value	Standard Error
4	D1	k	7,979E-4	1,1838E-4
5	D1	z	2,58119E-6	2,1E-6
6	D1	n	1,28184	0,69857

c)

	A	B	C	D
1	Equation	y = (k*(t-l)^n)+(z*(t-l)^(2*n))		
2	Adj. R-Square	0,9634		
3			Value	Standard Error
4	F1	k	0,08367	0,01455
5	F1	z	-0,00121	0,00135
6	F1	n	0,37224	0,0675
7	F1	l	14,93809	0,07388

d)

	A	B	C	D
1	Equation	y = (k*(t-l)^n)+(z*(t-l)^(2*n))		
2	Adj. R-Square	0,99687		
3			Value	Standard Error
4	B	k	2,28464E-4	0,00245
5	B	z	1,85219E-4	4,23635E-4
6	B	n	0,48959	0,14278
7	B	l	20	37,66572

Figure S19. Fitting of the experimental data up to 60% of drug delivery, considering the Peppas-Sahlin diffusion model. a) (*S*)-Naproxen in the absence of the gelator, b) caffeine in the absence of the gelator, c) (*S*)-Naproxen in the hydrogel, d) caffeine in the hydrogel.

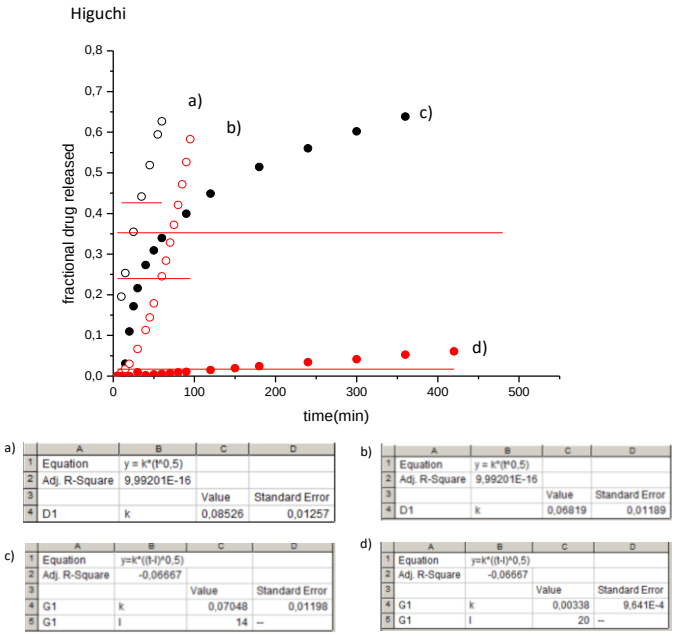

a)

	A	B	C	D
1	Equation	y = k*(t^0,5)		
2	Adj. R-Square	9,99201E-16		
3			Value	Standard Error
4	D1	k	0,08526	0,01257

b)

	A	B	C	D
1	Equation	y = k*(t^0,5)		
2	Adj. R-Square	9,99201E-16		
3			Value	Standard Error
4	D1	k	0,06819	0,01189

c)

	A	B	C	D
1	Equation	y=k*((t-l)^0,5)		
2	Adj. R-Square	-0,06667		
3			Value	Standard Error
4	G1	k	0,07048	0,01198
5	G1	l	14	--

d)

	A	B	C	D
1	Equation	y=k*((t-l)^0,5)		
2	Adj. R-Square	-0,06667		
3			Value	Standard Error
4	G1	k	0,00338	9,641E-4
5	G1	l	20	--

Figure S20. Fitting of the experimental data up to 60% of drug delivery, considering the Higuchi diffusion model. a) (*S*)-Naproxen in the absence of the gelator, b) caffeine in the absence of the gelator, c) (*S*)-Naproxen in the hydrogel, d) caffeine in the hydrogel.

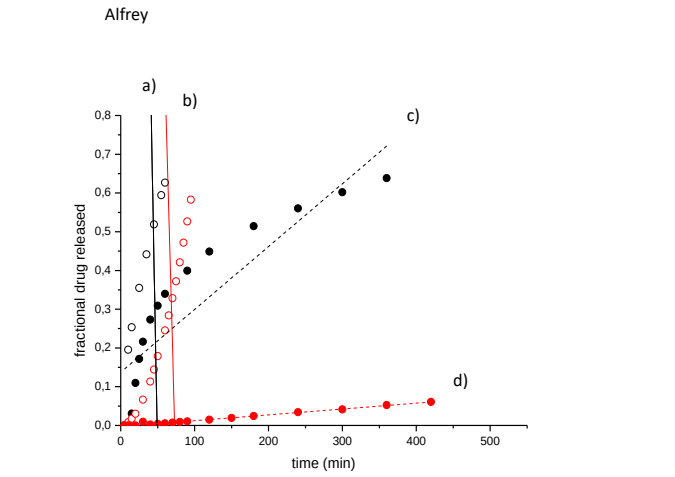

a)

	A	B	C	D
1	Equation	y = (k*t)+(z*t^0,5)		
2	Adj. R-Square	-249,0104		
3			Value	Standard Error
4	D1	k	0,0103	0,00253
5	D1	z	0,01	--

b)

	A	B	C	D
1	Equation	y = (k*t)+(z*t^0,5)		
2	Adj. R-Square	0,7854		
3			Value	Standard Error
4	B	k	0,00522	0,00438
5	B	z	1E-3	--

c)

	A	B	C	D
1	Equation	y = (k*(t-l))+(z*(t-l)^0,5)		
2	Adj. R-Square	0,79915		
3			Value	Standard Error
4	G1	k	0,00138	1,701E-4
5	G1	z	0,01	--
6	G1	l	-75,6036	33,00184

d)

	A	B	C	D
1	Equation	y = (k*(t-l))+(z*(t-l)^0,5)		
2	Adj. R-Square	0,9452		
3			Value	Standard Error
4	F1	k	0,00151	2,52387E-4
5	F1	z	0,01	--
6	F1	l	350,692	450,85257

Figure S21. Fitting of the experimental data up to 60% of drug delivery, considering the Alfrey diffusion model. a) (*S*)-Naproxen in the absence of the gelator, b) caffeine in the absence of the gelator, c) (*S*)-Naproxen in the hydrogel, d) caffeine in the hydrogel.

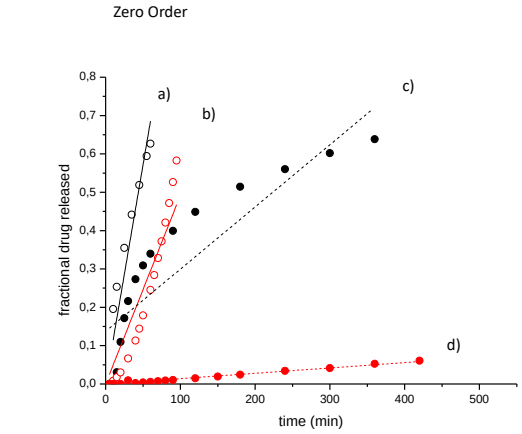

a)

	A	B	C	D
1	Equation	y = k*t		
2	Adj. R-Square	0,85328		
3			Value	Standard Error
4	D1	k	0,01143	6,12097E-4

b)

	A	B	C	D
1	Equation	y = k*t		
2	Adj. R-Square	0,88278		
3			Value	Standard Error
4	G1	k	0,00583	2,834E-4

c)

	A	B	C	D
1	Equation	y = k*(t-l)		
2	Adj. R-Square	0,81254		
3			Value	Standard Error
4	F1	k	0,00138	1,643E-4
5	F1	l	-111,8860	35,51832

d)

	A	B	C	D
1	Equation	y = k*(t-l)		
2	Adj. R-Square	0,98542		
3			Value	Standard Error
4	F1	k	1,506E-4	2,55394E-6
5	F1	l	18,62797	2,83351

Figure S22. Fitting of the experimental data up to 60% of drug delivery, considering the Zero Order diffusion model. a) (*S*)-Naproxen in the absence of the gelator, b) caffeine in the absence of the gelator, c) (*S*)-Naproxen in the hydrogel, d) caffeine in the hydrogel.

CHAPTER 3.

3.7. Urea based low molecular weight pseudopeptidic organogelators for the encapsulation and slow release of (*R*)-limonene

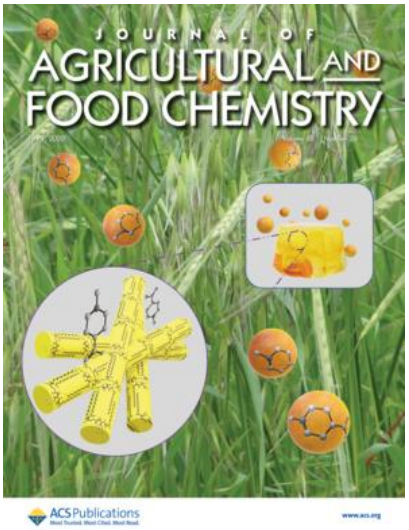

Urea based low molecular weight pseudopeptidic organogelators for the encapsulation and slow release of *(R)*-limonene

Abstract

Low-molecular-weight compounds containing alkylurea fragments attached to the amino end of different miminalistic pseudopeptidic structures have been shown to be excellent organogelators in a variety of organic solvents and liquid organic compounds of different nature. The formation of gels in this work is defined through rheological measurements for those cases where G′ > G″. Both the topology and the symmetry of the corresponding urea compounds play a role in defining their organogelator behavior. This can also be tuned by the presence of additional supramolecular guests, as is the case for suberic acid. These compounds also achieve the gelation of relevant active substances such as terpene natural oils and complex mixtures of flavors and fragrances. This provides a simple and mass-efficient supramolecular system for the quantitative encapsulation of active substances, without the need for any additional solvent or complex processes, and their consequent controlled release.

Keywords: *low-molecular-weight gelators (LMWGs), tripodal pseudopeptides, urea derivatives, flavor and fragrance release, (R)-limonene*

1. Introduction

Microencapsulation is an important tool for the cosmetic, food, agriculture, and pharmaceutical industries.[1,2] By encapsulation of a specific substance (drug, pesticide, or cosmetic active agent) an enhancement in its stability against degradation and, at the same time, its controlled release to the medium can be achieved. Further, encapsulation may also provide the benefits of easier handling (a solid like encapsulated product instead of an unstable volatile

[1] *Application of microencapsulated essential oils in cosmetic and personal healthcare products - a review;* Carvalho, I. T.; Estevinho, B. N.; Santos, L.*; Int. J. Cosmetic Science* **2016**, *38*, 109-119.
[2] *Nutraceutical delivery systems: Resveratrol encapsulation in grape seed oil nanoemulsions formed by spontaneous emulsification;* Davidov-Pardo, G.; McClements, D. J.; *Food Chemistry* **2015**, *167*, 205–212.

liquid) or improved safety (e.g., reduced flammability).[3,4,5] This is often carried out using a variety of microcapsules, which are small particles with sizes between 1 and 1000 μm comprising an active agent surrounded by a natural or synthetic polymeric membrane.[6] Large numbers of microencapsulation methods have been developed involving different types of active agents and shell materials. This has resulted in particles with a variable range of sizes, shell thicknesses, and permeabilities, thus providing a toolbox to modulate the release rate of the active principle.[7,8,9,10]

In this regard, encapsulation of essential oils for flavors and fragrances is of great interest. They are volatile compounds synthesized by plants and having strong odors. Different natural flavor oils have been described to have antimicrobial, antioxidant, antifungal, anticancer, antiviral, insecticidal, and anti-inflamatory properties.[11,12,13,14] Their encapsulation is a good strategy to avoid fast volatilization and degradation during storage, with their controlled release allowing a longer activity for the same amount of active substance.[15] *(R)-*

---

[3] *Handbook of Encapsulation and Controlled Release,* Mishra, M. Ed.; *CRC Press,* **2015***, ISBN 978-1482232325.*

[4] *Applications of Encapsulation and Controlled Release,* Mishra, M. K. Ed.; *CRC Press,* **2019***, ISBN 978-* 1138118782.

[5] *Development of Organogel-Derived Capsaicin Nanoemulsion with Improved Bioaccessibility and Reduced Gastric Mucosa Irritation;* Lu, M.; Cao, Y.; Ho, C-T.; Huang, Q.; *J. Agric. Food Chem.* **2016**, *64*, 4735−4741.

[6] *Polymeric Encapsulates of Essential Oils and Their Constituents: A Review of Preparation Techniques, Characterization, and Sustainable Release Mechanisms;* Vishwakarma, G. S.; Gautam, N.; Babu, J. N.; Mittal, S.; Jaitak, V.; *Polymer Reviews* **2016**, *56*, 668-701.

[7] *Microencapsulation of essential oils with biodegradable polymeric carriers for cosmetic applications;* Martins, I. M.; Barreiro, M. F.; Coelho, M.; Rodrigues, A. E.; *Chem. Eng. J.* **2014**, 245, 191-200.

[8] *Colloidosomes: Synthesis, properties and applications;* Thompson, K. L.; Williams, M.; Armes, S. P.; *J. Colloid Interf. Sci.* **2015**, *447*, 217–228.

[9] *Stability of monoterpenes encapsulated in gum arabic by spray-drying;* Bertolini, A. C.; Siani, A. C.; Grosso, C. R. F.; *J. Agric. Food Chem.* **2001**, *49* (2), 780−785.

[10] *Development of β-Carotene-Loaded Organogel-Based Nanoemulsion with Improved In Vitro and In Vivo Bioaccessibility;* Fan, Y.; Gao, L.; Yi, J.; Zhang, Y.; Yokoyama, W.; *J. Agric. Food Chem.* **2017**, *65*, 6188−6194.

[11] *Tetraclinis articulata (Vahl) Masters essential oils: Chemical composition and biological activities;* Chikhoune, A.; Hazzit, M.; Kerbouche, L.; Baaliouamer, A.; Aissat, K.; *J. Essent. Oil Res.* **2013**, *25* (4), 300-307.

[12] *Inhibition of food borne pathogen` bacteria by essential oils extracted from citrus fruits cultivated in Sicily;* Settanni, L.; Palazzolo, E.; Guarrasi, V.; Aleo, A.; Mammina, C.; Moschetti, G.; Germana, M. A.; *Food Control* **2012**, *26* (2), 326-330.

[13] *Antimicrobial, Insecticidal, and Medicinal Properties of Natural Product Flavors and Fragrances;* Cutler, H. G.; Hill, R. A.; Ward, B. G.; Rohitha, B. H.; Stewart, A.; *Biotechnology for Improved Foods and Flavors.* Chapter 5, pp 51-66. ACS Symposium Series vol. 637.

[14] *Physical and antimicrobial properties of peppermint oil nanoemulsions;* Liang, R.; Xu, S.; Shoemaker, C. F.; Li, Y.; Zhong, F.; Huang, Q.; *J. Agric. Food Chem.* **2012**, *60*, 7548-7555.

[15] *Encapsulation and Enhanced Retention of Fragrance in Polymer Microcapsules;* Lee, H.; Choi, C-H.; Abbaspourrad, A.; Wesner, C.; Caggioni, M.; Zhu, T.; Weitz, D. A.; *ACS Appl. Mater. Interfaces.* **2016**, *8*, 4007-4013.

Limonene, a monocyclic terpene flavor oil comprising two isoprene units, is abundantly produced in nature as a secondary plant metabolite. It has many applications and is often used as a versatile alternative to toxic solvents generally obtained from fossil fuel sources.[16] A variety of products for food and cosmetic industries and for household purposes originally represented the largest market for limonene.[17,18] Numerous biological and pharmacological activities have been reported for this compound,[19,20,21,22] being among the first natural pesticide ingredients used for environmentally friendly pest control[23] and providing an excellent penetration enhancement for transdermal drug delivery (TDD) when various transdermal formulations are applied as gels.[24,25] Therefore, the encapsulation of this flavor oil is of great interest for different applications.[26,27,28,29]

Gel formulations are of clear interest in this regard. Hydrogels are defined as those formed by gelators in aqueous media, while organogels are defined as

---

[16] *Limonene: a versatile chemical of the bioeconomy;* Ciriminna, R.; Lomeli-Rodriguez, M.; Carà, P. D.; Lopez-Sanchez, J. A.; Pagliaro, M.; *Chem. Commun.* **2014**, *50*, 15288-15296.

[17] *D-limonene: Safety and clinical applications;* Sun, J.; *Altern. Med. Rev.* **2007**, *12* (3), 259-264.

[18] *Limonene encapsulation in freeze dried gellan systems;* Evageliou, V.; Saliari, D.; *Food Chemistry* **2017**, *223*, 72-75.

[19] *Antimicrobial activity of limonene enantiomers and 1,8-cineole alone and in combination;* Van Vuuren, S. F.; Viljoen, A. M.; *Flavour Fragrance J.* **2007**, *22* (6), 540-544.

[20] *Chemoprevention and therapy of cancer by D-limonene;* Crowell, P. L.; Gould, M. N.; *Crit. Rev. Oncog.* **1994**, *5* (1), 1-22.

[21] *Chemoprevention of mammary carcinogenesis by hydroxylated derivatives of D-limonene;* Crowell, P. L.; Kennan, W. S.; Haag, J. D.; Ahmad, S.; Vedejs, E.; Gould, M. N.; *Carcinogenesis* **1992**, *13* (7), 1261-1264.

[22] *Fast-Dissolvong, Prolonged Release, and Antibacterial Cyclodestrin/Limonene-Inclusion complex Nanofibrous Webs via Polymer-Free Electrospining;* Aytac, Z.; Yildiz, Z. I.; Kayaci-Senirmak, F.; Keskin, N. O. S.; Kusku, S. I.; Durgun, E.; Tekinay, T.; Uyar, T.; *J. Agric. Food Chem.* **2016**, *64*, 39, 7325-7334.

[23] *Commercial opportunities for pesticides based on plant essential oils in agriculture, industry and consumer products;* Isman, M. B.; Miresmailli, S.; Machial, C.; *Phytochem. Rev.* **2011**, *10*, 197-204.

[24] *The electrostatic advantages of cross-linked polystyrene organogels swollen with limonene for selective adsorption and storage of hydrophobic drugs;* Charoensumran, P.; Ajiro, H.; *Polym. J.* **2018**, *50,* 1021–1028.

[25] *Cationic Moieties in Polystyrene Gels Swollen with D-Limonene Improved Transdermal Delivery System;* Charoensumran, P.; Ajiro, H.; *Polymers* **2018**, *10*, 1200-1213.

[26] *Development and characterization of electrosprayed Alyssum homo-locarpum seed gum nanoparticles for encapsulation of D-limonene;* Khoshakhlagh, K.; Koocheki, A.; Mohebbi, M.; Allafchian, A.; *J. Colloid and Interface Science* **2017**, *490*, 562–575.

[27] *Solubilization and location of phenethylalcohol, benzaldehyde, and limonene in lamellar liquid crystal formed with block copolymer and water;* Kayali, I.; Khan, A.; Lindman, B.; *J. Colloid Interf. Sci.* **2006**, *297*, 792–796.

[28] *Release behavior and stability of encapsulated D-limonene from emulsion-based edible films;* Marcuzzo, E.; Debeaufort, F.; Sensidoni, A.; Tat, L.; Beney, L.; Hambleton, A.; Peressini, D.; Voilley, A.; *J. Agric. Food Chem.* **2012**, *60* (49), 12177-12185.

[29] *Formation and Stability of D-limonene Organogel-Based Nanoemulsion Prepared by a High-Pressure Homogenizer;* Zahi, M. R.; Wan, P.; Liang, H.; Yuan, Q.; *J. Agric. Food Chem.* **2014**, *62*, 12563-12569.

those formed in organic liquids. In this context, supramolecular organogels based on low-molecular-weight gelators (LMWGs) have attracted considerable interest due to their potential applications in nanomaterials, shape memories, drug carriers, and templated synthesis.[30,31,32,33] LMWGs form gels via the creation of a network of weak noncovalent interactions such as ion−ion, H-bonding, π−π stacking, or van der Waals.[34] These driving forces facilitate the formation of 3D supramolecular structures that immobilize the liquid within the entangled supramolecular network to form the gel. In this sense, LMWGs provide a simple method for the entrapment of a given liquid phase onto a self-organized network, and accordingly, they also represent a promising approach for the controlled release of active substances.[35,36,37,38]

Between the functional groups able to participate in the development of such supramolecular interactions, urea groups have played a relevant role according to their potential to develop topologically well defined hydrogen-bond networks.[39,40,41,42] This has allowed the development of a number of LMWGs based on bis-, tris-, and even tetrakis-urea derivatives, often based on the

---

[30] *Low molecular mass gelators of organic liquids and the properties of their gels;* Terech, P.; Weiss, R. G.; *Chem. Rev.* **1997**, *97*, 3133-3159.
[31] *Water gelation by small organic molecules;* Estroff, L. A.; Hamilton, A. D.; *Chem. Rev.* **2004**, *104*, 1201-1217.
[32] *Low-Molecular-Weight Gels: The State of the Art;* Draper, E. R.; Adams, D. J.; *Chem.* **2017**, *3*, 390-410.
[33] *High-tech applications of self-assembling supramolecular nanostructured gel-phase materials: from regenerative medicine to electronic devices;* Hirst, A. R.; Escuder, B.; Miravet, J. F.; Smith, D. K.; *Angew. Chem. Int. Ed.* **2008**, *47*, 8002-8018.
[34] *Supramolecular gelling agents: Can they be designed?;* Dastidar, P.; *Chemical Society Reviews.* **2008**, *37*, 2699-2715.
[35] *Release of bioactive volatiles from supramolecular hydrogels: influence of reversible acylhydrazone formation on gel stability and volatile compound evaporation;* Buchs (née Levrand), B.; Fieber, W.; Vigouroux-Elie, F.; Sreenivasachary, N.; Lehn, J.-M.; Herrmann, A.; *Org. Biomol. Chem.* **2011**, *9*, 2906-2919.
[36] *The effects of intermolecular interactions on the physical properties of organogels in edible oils;* Lupi, F. R.; Greco, V.; Baldino, N.; de Cindio, B.; Fischer, P.; Gabriele, D.; *J. Colloid Interf. Sci.* **2016**, *483*, 154-164.
[37] *Release of small bioactive molecules from physical gels;* Mayr, J.; Saldias, C.; Diaz, D. D.; *Chem. Soc. Rev.* **2018**, *47*, 1484-1515.
[38] *Controlled release of flavor oil nanoemulsions encapsulated in filled soluble hydrogels;* Kwana, A.; Davidov-Pardo, G.; *Food Chemistry*, **2018**, *250*, 46–53.
[39] *Urea derivatives as low-molecular-weight gelators;* Yamanaka, M.; *J. Incl. Phenom. Macrocycl. Chem.* **2013**, *77*, 33-48.
[40] *Functional Supra-molecular Gels Self-Assembled by Hydrogen Bonding Among Urea-Based Gelators;* Wang, S.; Wu, B.; Duan, J. F.; Fang, J. L.; Chen, D. Z.; *Progress in chemistry* **2014**, *26*, 125-139.
[41] *Supramolecular ionogel lubricants with imidazolium-based ionic liquids bearing the urea group as gelator;* Yu, Q.; Wu, Y.; Li, D.-M.; Cai, M.; Zhou, F.; Liu, W.; *J. Colloid Interf. Sci.* **2017**, *487*, 130-140.
[42] *Braiding, branching and chiral amplification of nanofibres in supramolecular gels;* Jones, C. D.; Simmons, H. T. D.; Horner, K. E.; Liu, K.; Thompson, R. L.; Steed, J. W.; *Nat Chem* **2019**, *11*, 375-381.

presence of a central polysubstituted aromatic core. In these systems the increasing number of urea functionalities was designed to modify the strength and morphology of the gels on the basis of the increased number of hydrogen-bonding sites.[43,44,45,46,47,48,49,50]

Furthermore, the materials used for encapsulation in pharmaceutical, cosmetic, and food applications have to be nontoxic, biocompatible, biodegradable, and low cost.[51] In this regard, pseudopeptidic compounds based on natural amino acids and other natural components have a great potential in this field, with a high molecular diversity achievable through relatively simple and efficient synthetic approaches.[52,53] In this context, C_2-symmetric minimalistic pseudopeptides have shown interesting self-assembly properties,[54] including the formation of stable organogels,[55] some of them providing helical structures with a macromolecular chirality associated with the configuration of the amino acid structural components[56,57] or displaying a symbiotic behavior with

[43] *Tripodal tris-urea derivatives as gelators for organic solvents;* de Loos, M.; Ligtenbarg, A. G. J.; van Esch, J.; Kooijman, H.; Spek, A. L.; Hage, R.; Kellogg, R. M.; Feringa, B. L.; *Eur. J. Org. Chem.* **2000**, 3675–3678.
[44] *Anion binding inhibition of the formation of a helical organogel;* Stanley, C. E.; Clarke, N.; Anderson, K. M.; Elder, J. A.; Lenthall, J. T.; Steed, J. W.; *Chem. Commun.* **2006**, 3199–3201.
[45] *C_3-Symmetrical supramolecular architectures: fibers and organic gels from discotic trisamides and trisureas;* van Gorp, J. J.; Vekemans, J. A. J. M.; Meijer, E. W.; *J. Am. Chem. Soc.* **2002**, *124*, 14759–14769.
[46] *Chloroalkane gel formations by tris-urea low molecular weight gelator under various conditions;* Yamanaka, M.; Fujii, H.; *J. Org. Chem.* **2009**, *74, 5390–5394.*
[47] *Synthesis and estimation of gelation ability of* C*3-symmetry tris-urea compounds;* Yamanaka, M.; Nakagawa, T.; Aoyama, R.; Nakamura, T.; *Tetrahedron* **2008**, *64*, 11558–11567.
[48] *Development of C_3-Symmetric Tris-Urea Low-Molecular-Weight Gelators;* Yamanaka, M.; *The Chemical Record*. **2016**, *16*, 768-782.
[49] *Synthesis of a Bis-Urea Dimer and Its Effects on the Physical Properties of an Amphiphilic Tris-Urea Supramolecular Hydrogel;* Sawada, H.; Yamanaka, M.; *Chem. Asian J.* **2018**, *13*, 929-933.
[50] *Urea and Thiourea Derivatives as Low Molecular-Mass Organogelators;* George, M., Tan, G., John, V. T., Weiss, R. G.; *Chem Euro J* **2005**, *11*, 3243-3254.
[51] *Encapsulation Perfomance of Proteins and Tradicinal Materials for Spray Dried Flavors;* Charve, K.; Reineccius, G.; *J. Agric. Food Chem.* **2009**, *57*, 2486−2492.
[52] *Efficient Macrocyclization of U-Turn Preorganized Peptidomimetics: The Role of Intramolecular HBond and Solvophobic Effects;* Becerril, J.; Bolte, M.; Burguete, M. I.; Galindo, F.; García-España, E.; Luis, S. V.; Miravet, J. F.; *J. Am. Chem. Soc.* **2003**, *125*, 6677-6686.
[53] *Pseudopeptidic Compounds for Biocompatible Gels: A Review;* Luis, S. V.; Burguete, M. I.; Martí-Centelles, V.; Rubio, J.; *Cosmetic and toiletries* **2012**, *127* (4), 282-288.
[54] *Bioinspired Chemistry Based on Minimalistic Pseudopeptides;* Luis, S. V.; Alfonso, I.; *Acc. Chem. Res.* **2014**, *47*, 112-124.
[55] *Minimalist peptidomimetic cyclophanes as strong organogelators;* Becerril, J.; Burguete, M. I.; Escuder, B.; Luis, S. V.; Miravet, J. F.; Querol, M.; *Chem. Commun.* **2002**, 738-739.
[56] *Self-Assembly of small peptidomimetic cyclophanes;* Becerril, J.; Burguete, M. I.; Escuder, B.; Galindo, F.; Gavara, R.; Luis, S. V.; Miravet, J. F.; Peris, G.; *Chem. Eur. J.* **2004**, 3879-3890.
[57] *Understanding the Expression of Molecular Chirality in the Self-assembly of a Peptidomimetic Organogelator;* Becerril, J.; Escuder, B.; Gavara, R.; Luis, S. V.; Miravet, J. F.; *Eur. J. Org. Chem.* **2005**, 481-485.

quantum dots (QDs).[58,59] In a few instances, pseudopeptidic structures containing urea groups as linkers between the different structural units have also been reported as strong organogelators.[60,61]

In C_2-symmetry pseudopeptides, the introduction of a secondary nitrogen atom in the central aliphatic spacers provides new self-assembly patterns.[62,63,64] This also opens the way for the preparation of new tripodal systems lacking the C_3 symmetry associated with the use of 2,2′,2″-triaminotriethylamine (TAEA) or trisubstituted aromatic derivatives as central spacers.[65] Here, we present the development of a new family of multifunctional amphiphilic pseudopeptides derived from diethylenetriamine (DEA) or TAEA incorporating long aliphatic chains through urea linkages and displaying dipodal or tripodal character. These compounds show interesting selfassembly capabilities, providing a new family of strong organogelators with improved properties and an enhanced potential for hydrogen bonding and other polar and nonpolar intermolecular interactions and leading to mechanically and thermally stronger supramolecular gels in a variety of solvents of different polarities. Further, these novel organogelators were studied to control the encapsulation and release of a commercially important compound such as *(R)*-limonene.

---

[58] *Organogel-quantum dots hybrid materials displaying fluorescence sensitivity and structural stability towards nitric oxide;* Wadhavane, P. D.; Izquierdo, M. A.; Galindo, F.; Burguete, M. I.; Luis, S. V. *Soft. Matter*, **2012**, *8*, 4373-4381.

[59] *Photoluminescence Enhancement of CdSe Quantum Dots: A Case of Organogel−Nanoparticle Symbiosis;* Wadhavane, P. D.; Galian, R. E.; Izquierdo, M. A.; Sigalat, J.; Galindo, F.; Schmidt, L.; Burguete, M. I.; Pérez-Prieto, J.; Luis, S. V. *J. Am. Chem. Soc.* **2012**, *134*, 20554–20563.

[60] *C_3-Symmetric, amino acid based organogelators and thickeners: a systematic study of structure–property relations;* de Loos, M.; van Esch, J. H.; Kellogg, R. M.; Feringa, B. L.*; Tetrahedron* **2007**, *63,* 7285–7301.

[61] *Synthesis and organogelating ability of bis-urea pseudopeptidic Compounds.* Rubio, J; Martí-Centelles, V.; Burguete, M. I.; Luis, S. V.; *Tetrahedron* **2013**, *69*, 2302-2308.

[62] *Interplay between hydrophilic and hidrophobic interactions in the self-assembly of a gemini amphiphilic pseudopepeptide: from nano-spheres to hydrogels.* Rubio, J.; Alfonso, I.; Burguete, M. I.; Luis, S. V.; *Chem. Commun.* **2012**, *48*, 2210-2212.

[63] *Structure-membrane activity relationship in a family of peptide-based gemini amphiphiles: An insight from experimental and theorical model systems;* Korchowiec, B.; Gorczyca, M.; Korchowiec, J.; Rubio-Magnieto, J.; Lotfallah, A. H.; Luis, S. V.; Rogalska, E.; *Colloid. Surface. B* **2016**, *146*, 54-62.

[64] *Synthesis of second-generation self-assembling Gemini Amphiphilic Pseudopeptides;* Lotfallah, A. H.; Burguete, M. I.; Alfonso, I.; Luis, S. V.; *J. Colloid Interf. Sci.* **2020**, *564*, 52-64.

[65] *Fluorescent macrocyclic probes with pendant functional groups as markers of acidic organelles within live cells;* Wadhavane, P. D.; Izquierdo, M. A.; Lutters, D.; Burguete, M. I.; Marin, M. J.; Russell, D. A.; Galindo, F.; Luis, S. V. *Org. Biomol. Chem.* **2014**, *12*, 823-831.

2. Materials and methods

2.1. Materials

Reagents and solvents, including NMR solvents, were purchased from commercial suppliers and were used without further purification. Deionized water was obtained from a Milli-Q equipment. The C_2- and C_3-symmetrical bis- and tris(amidoamines) were prepared as previously described.[64,52]

2.2. General Characterization Protocols

Elemental analyses were obtained with a CHN Euro EA 3000 elementary analyzer, melting points were determined with a Stuart SMP10 apparatus and are uncorrected, and rotatory powers were obtained with a Jasco DIP-1000 instrument using a cylindrical glass cell (d, 3.5 mm; l, 50 mm). Mass spectra were obtained on a Micromass Quattro LC spectrometer (electrospray ionization source and a triple-quadrupole analyzer), while high-resolution mass spectra (HRMS) were obtained on a hybrid QTOF I instrument (Micromass, Z-spray-electrospray interface, quadrupole−hexapole−TOP). Scanning Electron Microscopy (SEM) was performed with either a LEO 440I or a JEOL 7001F microscope with a digital camera. Samples were obtained by supercritical drying of the organogels (as an example, the gel obtained with 1 wt % of **2b** in *(R)*-limonene was dried under a continuous flow of CO_2 of 0.5 mL/min at 80 °C and 80 bar) and were conventionally Pd coated before the measurement (Polaron SC7610 metalizing Fisons instrument). ATR FT-IR spectra were acquired with a JASCO 6200 instrument equipped with a MIRacle Single Reflection ATR Diamond/ZnSe accessory. Samples of the corresponding pseudopeptide at different concentrations and in the solid state were prepared and seeded onto the ATR sample holder, and the FT-IR spectra were collected. The raw IR data were processed with the JASCO spectral manager software. Molecular modeling was performed with the Spartan '08 software using the MMFF (Merck molecular force field) level of theory for the geometry optimizations.[66]

2.3. Rheology Experiments

Rheological measurements were carried out with a TA Instruments DHR-2 rheometer using a 20 mm diameter stainless steel plate and Petri dishes fixed

[66] Deppmeier, B. J.; Driessen, A. J.; Hehre, T. S.; Hehre, W. J.; Johnson, J. A.; Klunzinger, P. E.; Leonard, J. M.; Pham, I. N.; Pietro, W. J.; Jianguo, Y. *Spartan08, build 132 (Mar 27 2009),* Wavefunction Inc.: Irvine CA, **2009**.

on a Peltier heated plate. Prior to the sample preparation each Petri dish was fixed to the Peltier plate of the instrument and the gap zeroed. Then weighed amounts of the compounds and solvents were heated until complete dissolution, poured into the Petri dish, and cooled to room temperature. The measurements were made in strain-controlled mode at 20 °C using a gap of 1 mm and temperature ramps from 20 to 160 °C at a heating rate of 2 °C/min. The frequency sweeps were measured in the linear viscoelastic range, with either 0.01% or 0.1% strain. The amplitude sweeps were performed with a fixed frequency of 1 Hz. The temperature ramps were performed with a fixed 0.1% strain and a frequency of 1 Hz. Moduli values from the frequency sweeps with 0.1% strain were taken at 1 Hz. Representative examples of strain and frequency sweeps and temperature ramps are shown in Figures 2 and Figures S2–S5.

2.4. Vial Inversion Tests

Vial inversion tests were carried out in screw-capped glass vials of 6 mm diameter (R = 0.6 cm), using 1 mL of solvent (L = 0.88 cm) and 1 wt % of LMWG for the initial screening. The mixture was heated and then cooled to room temperature. The formation of a strong gel was confirmed when it did not flow under its own weight upon vial inversion.

2.4.1. Thermogravimetric Analysis (TGA)

The data were recorded with a TG-STDA Mettler Toledo Model TGA/SDTA851e/LF/1600 instrument using the following heating program: (i) heating from 25 °C to 120 °C at 10 °C/min under N_2 and holding the sample at this temperature for 25 min; (ii) cooling from 120 to 25 °C, at 10 °C/min; (iii) measuring the weight loss from 25 to 700 °C at 10 °C/min under N_2.

2.4.2. Release Studies under Ambient Conditions

The experiments were performed with a magnetic stirrer hot plate at 30 °C using a 12 mL glass vial (55 × 23 mm, height and external diameter). Gels were formed with 1 wt % of the corresponding gelator (**2b** or **2c**) in 3 mL of *(R)*-limonene. The release of the fragrance was evaluated by monitoring the weight loss at regular time intervals using a laboratory balance that was previously calibrated. These experiments were carried out for at least three times. The different measurements showed a good reproducibility. The experimental data were adjusted by exponential regression to a first order model $1 - f = e^{-kft}$ using the equation $y = A1 \exp(-x/t_1) + y_0$, with k_f (release rate constant) $= 1/t_1$.

2.5. NMR Experiments

NMR experiments were carried out on a Varian INOVA 500 spectrometer (500 MHz for ^{1}H NMR and 125 MHz for ^{13}C NMR) or on a Varian UNITY 300 spectrometer (300 MHz for ^{1}H NMR and 75 MHz for ^{13}C NMR). Chemical shifts are reported in parts per million using the solvent residual peak as the reference.

Variable-temperature ^{1}H NMR experiments were carried out with a Varian INOVA 500 spectrometer (500 MHz for ^{1}H NMR). Heated solutions of **2b** and **2c** were prepared in DMSO-d_6 (4 mg/mL) and introduced into high-quality 5 mm NMR glass tubes. Samples were cooled to room temperature (23 °C), and the corresponding spectrum was acquired. The temperature of the probe was then sequentially increased to 25, 30, 35, 40, 50, 60, 70, 80, 90, 100, 110, and 120 °C and then cooled back again to 50 and 23 °C, with one spectrum being acquired for each step.

3. Results and discussion

3.1. Synthesis of LMWGs

The general structure of the studied gelators contains two or three amino acid moieties derived from *L*-valine, connected through their acid ends by a flexible polyamine spacer. The amino ends have been functionalized with long alkyl chains via urea linkages (Scheme 1).

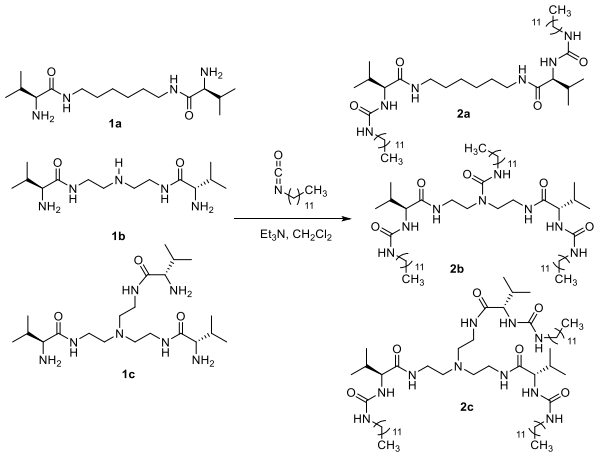

Scheme 1. Synthesis of the urea based LMWGs

The C_2-symmetric molecule 1a was obtained as previously reported.[52] Compounds 1b,c were prepared using a similar synthetic protocol by reaction

of *L*-valine with either DEA or TAEA (Scheme 1).[64] The alkylurea fragments, derived from lauric acid, were introduced by the reaction of the corresponding isocyanate with the free amino groups of 1a–c, rendering the amphiphilic compounds 2a–c.[61,67] This structural design allows evaluating the effect of the geometry in optimizing the potential for intermolecular interactions via H bonds and dipolar and hydrophobic interactions, comparing bifunctional vs trifunctional systems and C_3-symmetry tripodal systems vs those lacking such C_3 symmetry. Additionally, the selected components maximize the number of structural elements of biogenic and biocompatible nature.

3.2. Gel Formation

The dissolution and gelation abilities of compounds **2a–c** were examined in different organic solvents, including polar and apolar solvents, and water. The results obtained are summarized in Table 1. In general, all compounds showed low solubility in the studied solvents at room temperature, which stems from their strong tendency for intermolecular association via hydrogen bonds. For most of the pseudopeptide–solvent combinations only heating under sonication led to dissolution. With cooling, the formation of gels was observed in many of the solvents (indicated as G in Table 1). All of the LMWGs were insoluble in water and diethyl ether. To facilitate a qualitative (less accurate) discussion, strong and weak gels are differentiated in Table 1 according to the vial inversion test,[68] with strong gels being those that do not fall upon inversion of the vial and weak gels those that show some minor evidence of downward flow upon vial inversion.

Bifunctional compound **2a** was not soluble in *(R)*-limonene, though it formed strong organogels in DMF and toluene, while the tripodal compounds **2b,c** formed organogels in the three solvents. However, when the vial inversion test was applied, the gel formed by **2b** in DMF was shown to be slightly weaker.[68] Some additional interesting differences could also be observed in their gelation ability, as summarized in Table 1. Thus, **2c** was insoluble in MeOH while **2a,b** provided gels. In contrast, **2b** was soluble in $CHCl_3$ and geraniol, while **2a,c**

[67] *Acyclic Pseudopeptidic Hosts as Molecular Receptors and Transporters for Anions;* Martí, I.; Burguete, M. I.; Gale, P. A.; Luis, S. V.; *Eur. J. Org. Chem.* **2015**, *2015*, 5150-5158.
[68] *Gel formation: phase diagrams using tabletop rheology and calorimetry;* Raghavan, S. R.; Cipriano, B. H.; *In Molecular Gels: Materials with Self-Assembled Fibrillar Networks,* R. G. Weiss, P. Terech Eds., *Springer*, **2005**, pp 233-244.

formed gels in both. Thus, the considered structural changes allow tuning the properties of the resulting urea-functionalized pseudopeptides as LMWGs. The lack of C_3 symmetry in **2b** does not lead to a significant loss of the organogelating ability shown by **2c**. It should be noted that these gelators also formed gels in pure orange essential oil obtained from orange peels and using commercial preparations based on *(R)*-limonene. These gels formed in *(R)*-limonene displayed very good mechanical stability and could be kept in a closed vial, without observable changes in their properties, for more than 1 year. Thus, this initial screening suggested that ureas **2b,c** are potential LMWGs for natural oils such as *(R)*-limonene. In light of these results, their ability to gel complex mixtures of flavors and fragrances was evaluated. For simplicity, three easily available commercial samples currently used as air home fresheners (indicated as vanilla, orchid, and lavender in Table 1) were selected. They contain mixtures of different essential oils (see Figure S1 for composition). Only in the case of the C_3-symmetry tripodal LMWG **2c** were strong organogels obtained for all of the different air fresheners tested, while **2b** was only able to gel the vanilla air home freshener.

Table 1 Gelation behavior of compounds 2a-c in different solvents[a]

Solvent	**2a**	**2b**	**2c**
H_2O	I	I	I
DMSO	G(w)	G(w)	G(w)
DMF	G(s)	G(w)	G(s)
MeOH	G(w)	G(w)	I
EtOH	G(w)	G(w)	G(w)
2-Propanol	G(w)	G(w)	G(w)
Et_2O	I	I	I
Toluene	G(s)	G(s)	G(s)
$CHCl_3$	G(w)	S	G(w)
(*R*)-Limonene	I	G(s)	G(s)
Geraniol	G(w)	S	G(w)
Vanilla*	-	G(s)	G(s)
Orchid*	-	S	G(s)
Lavender*	-	S	G(s)

[a] Gelation tests were performed by heating 10 mg mL^{-1} of the compound in the corresponding solvent until fully dissolved and recording the results upon cooling. Abbreviations used: Gels obtained at room temperature are denoted as "G" (gel) and classified according to the vial inversion test as (w) = weak or (s) = strong. Systems in which only a solution remained are marked as "S" (solution). Systems in which the gelator could not be dissolved even at the boiling point of the liquid are marked as "I" (insoluble). Solvents denoted with "*" are commercially available air home-fresheners form Bosque Verde with the respective register numbers: 81010750, 80851602 and 80961712 (see Fig. S1 for full composition of the different air fresheners).

Taking into account the former results, additional experiments were carried out for the gels derived from the natural flavor oil *(R)*-limonene.

3.3. Viscoelastic Properties of the Gels

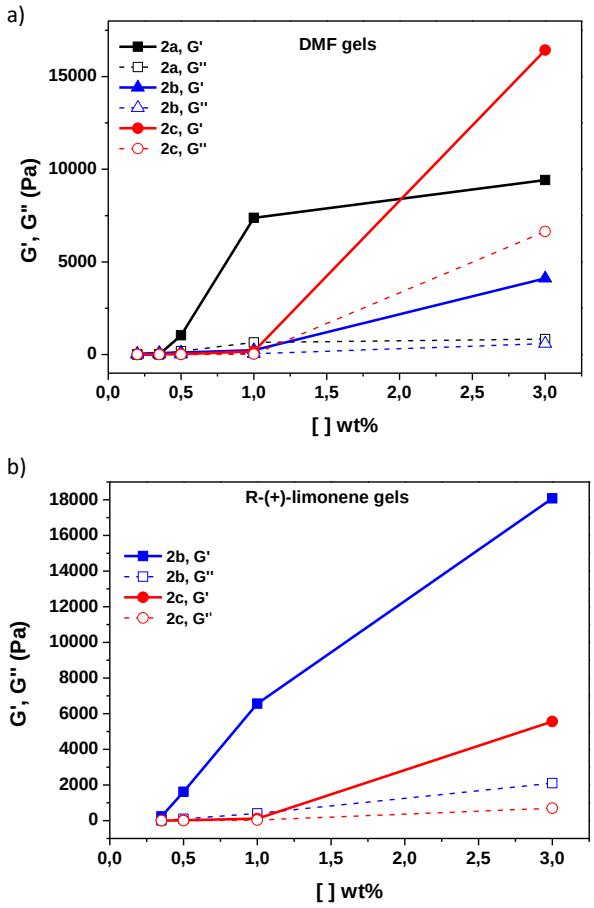

Figure 1 Storage (G') and loss modulus (G") obtained from frequency sweeps with 0.1% strain *vs* LMWG weight loading (wt%) obtained for 2a-c at 0.1 % oscillation strain: a) in DMF; b) in (*R*)-limonene.

Rheological measurements were made for **2a–c** in DMF or *(R)*-limonene to obtain more detailed quantitative data on the gels formed. First, amplitude sweeps were performed to establish the linear viscoelastic regions. As an example, LMWG **2b** at 1 wt % in *(R)*-limonene (Figure S2b) showed a linear behavior up to 1% strain. The frequency sweeps were measured in the linear viscoelastic range, with either 0.01% or 0.1% strain, in order to get data for lower strength organogels (see Figure S3a for **2b** in DMF). To obtain storage (G′) and loss moduli (G′′) of the gels prepared, values in Figure 1 were taken from the frequency sweeps with 0.1% strain, as at lower concentrations with 0.01% strain not enough reliable data were obtained (Figure S4), although the amplitude sweeps showed that, for some

samples at 0.1% strain, data were below the linear range (see Figure S2a for **2b** at 1 wt % in DMF). Figure 1 depicts a comparison of the G′ and G″ values obtained for the different gels formed in either DMF or *(R)*-limonene as a function of the amount of LMWG used at 20 °C. Compound **2a** showed an increase of the storage modulus at the lowest concentrations in comparison to **2b,c** in DMF, which could be associated with the lower molecular weight for **2a** and with its different topology. However, just by an increase in the concentration up to 3 wt %, strong gels with G′ > 3000 Pa were obtained for all samples, in particular for **2c** and **2a** (Figure 1a). Similar trends were observed using data from frequency sweeps with 0.01% strain (Figure S4a).

A different situation was observed when *(R)*-limonene was used as the solvent. First, the bis-urea **2a** showed a lack of solubility in this medium (Table 1). In addition, in opposition to what had been observed in DMF, the tripodal urea **2b** provided stronger gels in comparison to **2c** for all the concentrations evaluated (Figure 1b). Thus, **2b** was identified as the most suitable LMWG to obtain strong gels in *(R)*-limonene. Similar trends were observed using data from frequency sweeps with 0.01% strain (Figure S4b).

The thermal stability of the gels was then evaluated. Previous studies with **2a** had suggested that the gel structure can be preserved in some solvents even at temperatures close to 100 °C.[61] Rheological measurements indicated that the gel formed in DMF at 1 wt % of **2b** was stable up to 60 °C, above which the supramolecular interactions responsible for the formation of the gel weaken and the sample melts to a viscous liquid (Figure S5). However, at the same concentration, **2c** presents higher thermal stability, keeping its gel-like consistency with stable values of G′ and G″ until 110 °C. During these experiments, some solvent evaporation cannot be avoided when temperatures approach the boiling point. This is exemplified in Figure S5 for DMF (bp 153), where at temperatures close to 100 °C some increase in the values of G′ and G″ is observed before the disruption of the gel is detected at temperatures above 110 °C. This can be attributed to some solvent evaporation leading to an increase in the actual concentration of gelator.

The mechanical properties of the gels in *(R)*-limonene as a function of temperature are presented in Figure 2. The LMWG **2b** displayed a thermal stability similar to that observed in either DMF or DMSO, losing its solidlike character above 60 °C. It is worth noting that the LMWG **2c** showed a particular

thermal behavior. First, the gel in *(R)*-limonene melted at higher temperature than in DMF, being stable up to 140 °C. In addition, the mechanical properties indicated the existence of some structural transformations upon heating at relatively low temperatures. The results depicted in Figure 2b show that, in the 20−65 °C range, both G′ and G″ decrease significantly, leading to a material behaving as a viscous solution at ~40 °C. However, above 70 °C the gel recovered its original strength again and only lost the solidlike properties above 140 °C. A similar situation is depicted when the values of tan δ as a function of temperature are represented for **2c** (Figure S7).

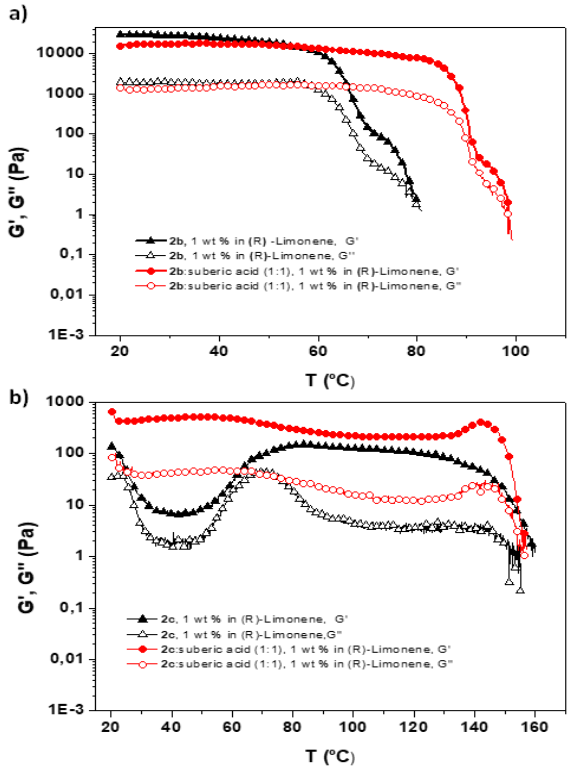

Figure 2 Dependence of storage modulus (G') and loss modulus (G") with the temperature for a gelator mass fraction of 1 wt% in (*R*)-limonene. a) triangles: molecule **2b**. dots: equimolecular mixture **2b** : suberic acid. b) Triangles: molecule **2c**. Dots: equimolecular mixture **2c** : suberic acid. Measurements were carried out at a heating rate of 2 ºC/min, a constant frequency of 1 Hz and 0.1 strain.

^{1}H NMR studies in DMSO-d_6 also provided information on the thermal behavior of the gels formed in this solvent (Figure 3 and Figure S6). The LMWGs considered in this work contain two main functionalities able to participate in hydrogen bonding: urea fragments with N−H hydrogen bond donor (HBD) ability and C=O hydrogen bond acceptor (HBA) ability and amide fragments with N−H HBD ability and C=O HBA. In addition, **2c** contains a tertiary amine group able

to act as a HBA. In ^{1}H NMR, downfield shifts for the N−H HBD groups are the main criteria for defining their involvement in hydrogen bonding and accordingly their participation in the self-assembly of noncovalent polymeric structures leading to the formation of gels. Thus, the higher observed shifts detected for the amide groups indicate that these groups are involved to a greater extent in the formation of hydrogen bonds in the self-assemblies formed. As expected, the urea groups present in the organogelators are involved in strong bifurcated hydrogen bonds, as indicated by the shift of the signals assignable to the NH of the urea (a and b in Figure 3). However, the largest shift (from 7.9 ppm at 23 °C to 7.4 ppm at 120 °C) can be attributed to the intermolecular hydrogen bond associated with the amide group (NH−C=O···HN−C=O, signal c in Figure 3a). This fact highlights the importance of the amide in order to define the properties of the corresponding LMWG.

The broadening of the proton signals (and eventually their disappearance) is a common feature of polymeric systems, either covalent or noncovalent. This is associated with changes in the relaxation times that are related with the molecular weight of the polymer; this is dependent on the probability of exchanging energy and particularly on the facility with which the different nuclei (of the same kind) involved can lose their homogeneity. When the temperature is increased, the equilibrium between the molecules in the gel fibrils and those in solution starts to be shifted toward the disruption of the gel and the increase of the molecules in solution, which is reflected in an increase of the relaxation times, leading to a narrowing of the signals and a higher visibility for them. This phenomenon is maximum when the gel is completely broken and has been used for the measurement of the thermal stability of gels.[61] In the spectra of **2b,c,** the signals of the LMWGs intensify when the temperature is raised (see traces in Figure 3 and Figure S6). Hence, this indicates that the polymeric network of intermolecular supramolecular interactions is weakened and finally destroyed. Upon cooling, the formation of the gel is re-established, as shown by the decreased intensity, broadening, and shift of the main proton signal characteristics of the LMWG (Figure 3). In good agreement with the rheological measurements, the gels obtained showed a transition in the NMR spectra at ca. 60 °C for compound **2b** and at ca. 120 °C for **2c**.

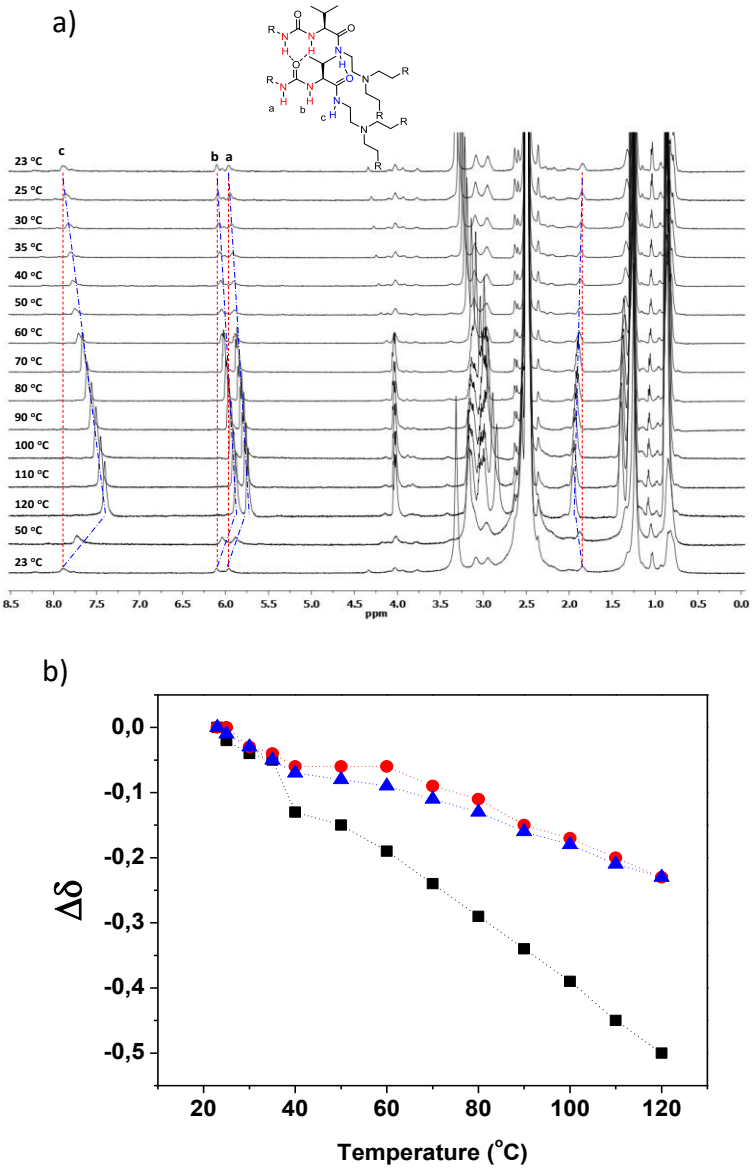

Figure 3 a: ^{1}H NMR (500 MHz) spectra of **2c** in DMSO-d_6 (4 mg/mL) at different temperatures, first heating from rt to 120 °C and then cooling back to rt (last two spectra at the bottom). b: Δδ *vs* temperature; squares: signal c, circles: signal b, triangles: signal a.

These supramolecular interactions explain the formation of a well-defined network based on intermolecular H-bonding interactions leading to strong gels with good thermal stability. This also explains the absence of gelation or the formation of weak gels in solvents able to participate in hydrogen bonding and interfere in the formation of such a network (Table 1). This explains the different behaviors observed between limonene and geraniol containing hydroxyl groups. This interference seems to be much less important for the tripodal derivative **2c** displaying a C_3 symmetry. This compound forms a strong gel in DMF and a

weak gel in geraniol and remains insoluble in MeOH, while **2b** only forms a weak gel in DMF, is soluble in geraniol, and forms a weak gel in MeOH.

MMFF calculations were in good agreement with the model proposed on the basis of ^{1}H NMR studies. This is illustrated in Figure 4, showing the structure obtained though minimization of a set of three interacting molecules for **2b,c**. For the sake of simplicity, the model was built from a molecule containing a short alkyl chain bonded to the urea group. Models reveal that the overall number of H bonds is larger in the assembly formed by **2c** than in the that by **2b** due to the presence of the additional amide group and the increase in symmetry in its structure. This higher symmetry could also favor a more favorable interaction of the long alkyl tails. The combination of both elements may account for the enhancement of the thermal stability of the gels formed by **2c**.

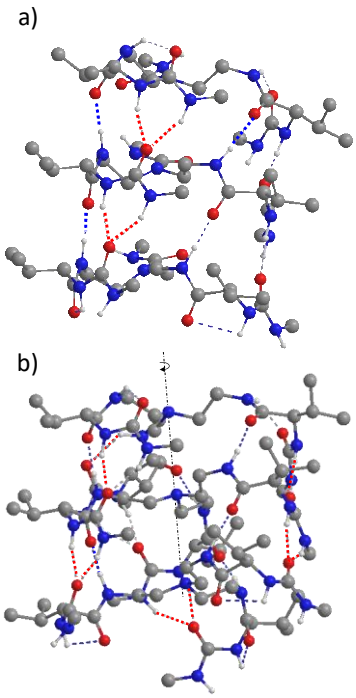

Figure 4 MMFF molecular proposed aggregation model: a) **2b**; b) **2c**.

3.4. Viscoelastic Properties of the Gels in the Presence of Suberic Acid

The presence and the adequate positioning of functional groups in the gelator molecules allow a consideration of their potential for acting as supramolecular hosts for different guests, in particular for carboxylic and poly(carboxylic

acids).[69,70] This host–guest interaction can be used as a chemical trigger to reinforce or weaken the gel structure.[71,72,73] Thus, after some computational modeling, an evaluation of the effect of suberic acid as a possible host molecule to tune the supramolecular structures defined by **2b,c** was carried out. The effect of suberic acid on the mechanical properties of the gels at 1 wt % of LMWGs **2b,c** is shown in Figure 2 and Figure S5. The gels were prepared using an equimolecular ratio of suberic acid to gelator in DMF or *(R)*-limonene. In the case of DMF, only small deviations were observed on comparison of the resulting thermal stability with one of the gels in the absence of the added acid, with the introduction of the acid slightly decreasing the strength of the gel (Figure S5). However, the presence of suberic acid in the gels obtained in *(R)*-limonene had a well-defined effect (Figure 2). In the case of **2b** the presence of suberic acid increased the thermal stability of the gel from ca. 60 to 90 °C (Figure 2a), while similar values of G′ and G″ were maintained. On the other hand, for **2c** the presence of suberic acid suppressed the variations of G′ and G″ observed at low to medium temperatures, yielding stable values of tan δ from 25 °C until ca. 150 °C (Figure 2b and Figure S7). In the case of **2c** and suberic acid some increase in the values of G′ and G″ is observed at temperatures (130 °C) close to the boiling point, which must be ascribed to some solvent evaporation leading to an increase in the actual concentration of the gelator before reaching the temperatures at which disruption of the gel is detected. This is not observed for **2c** alone as, in this case, the disruption of the gel starts to be observed at this temperature.

3.5. Slow Release of (R)-limonene

Finally, the gels were evaluated as potential supramolecular delivery systems for bioactive volatile compounds, being assayed for the controlled release of *(R)*-limonene. The delivery of *(R)*-limonene was initially studied by isothermal TGA at 35 °C under a N_2 flow (10 mL/min), following the observed weight loss

[69] *Anion recognition by oligo-(thio)urea-based receptors;* Jia, C.; Zuo, W.; Zhang, D.; Yang, X.J.; Wu, B.; *Chem. Commun.* **2016**, *52*, 9614-9627.
[70] *Anion binding with urea and thiourea derivatives;* Bregović, V. B.; Basarić, N.; Mlinarić-Majerski, K.; *Coord. Chem. Rev.* **2015**, *295*, 80-124.
[71] *Molecular recognition through divalent interactions with a self-assembled fibrillar network of a supramolecular organogel;* Escuder, B.; Miravet, J. F.; Sáez, J. A.; *Org. Biomol. Chem.*, **2008**, *6*, 4378-4383.
[72] *Anion-tuned supramolecular gels: a natural evolution from urea supramolecular chemistry;* Steed, J. W.; *Chem. Soc. Rev.* **2010**, *39*, 3686-3699.
[73] *Supramolecular gels: using an amide-functionalized imidazolium-based surfactant;* Cheng, N.; Kang, Q.; Xiao, J.; Du, N.; Yu, L.; *J. Colloid Interf. Sci.* **2018**, *511*, 215–221.

associated with the fragrance released. Figure 5 depicts the release profiles obtained, under those conditions, for liquid *(R)*-limonene and for different organogels. The release profile of the fragrance was significantly slower in the case of the organogels. These results suggest that the fragrance was physically entrapped inside the supramolecular structure defined by the assembly of the LMWG molecules, increasing the *(R)*-limonene release time.[74] From a view of these release profiles, the data could be well fitted by a simple first-order kinetics according to eq 1:

$$1\text{-}f = e^{-k_f t} \qquad (1)$$

where f is the fraction of *(R)*-limonene released at time t and k is the first-order rate constant.[75]

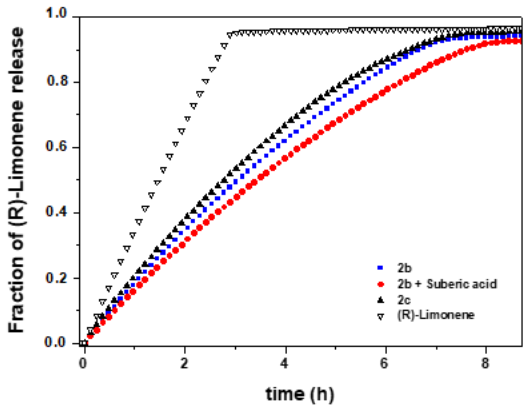

Figure 5 Fraction of (*R*)-limonene released vs time, as measured by TGA of the samples at 35 ºC under a N_2 flow of 10 mL/min. ▽: (*R*)-Limonene. ▲: organogel formed with 1 wt % of **2c** in (*R*)-limonene. ■: organogel formed with 1 wt % of **2b** in (*R*)-limonene. ●: organogel formed with 1 wt % of an equimolecular mixture of **2b** and suberic acid in (*R*)-limonene.

Table 2 summarizes the main parameters obtained for the different systems by adjusting the experimental data to this mathematical model. The results showed an increase of the time required to achieve the fragrance release for all of the gels. The best results were achieved with the organogels formed by **2b**, in particular for the equimolecular combination of **2b** and suberic acid. In this case, the times required to achieve a fragrance release at either 50% or 75%

[74] *Correlation between rheological properties and limonene release inpectin gels using an electronic nose;* Monge, M. E.; Negri, R. M.; Giacomazza, D.; Bulone, D.; *Food Hydrocolloids* **2008**, 22, 916-924.
[75] *Encapsulation and Controlled Release of Fragrances from Functionalized Porous Metal–Organic Frameworks*; Liu, Y.; Wang, Y.; Huang, J.; Zhou, Z.; Zhao, D.; Jiang, L.; Shen, Y.; *AIChE J.* **2019**, *65*, 491-499.

were 3.46 and 5.7 h, respectively (entry 4, Table 2). These times were ca. 2.5−2.3 times longer than the time observed in the blank experiment containing just liquid *(R)*-limonene. The presence of suberic acid was less significant in the case of **2c**, displaying very similar release profiles in the presence and absence of the acid (Figure S8).

Table 2. Kinetic parameters for the release of (*R*)-limonene under isothermal TGA conditions. [a]

Entry	gel	k_f (h^{-1})	$t_{50\%}$ (h)	$t_{75\%}$ (h)
1	-	0.3341± 0.0003	1.49	2.25
2	**2c**	0.127± 0.002	2.8	4.6
3	**2b**	0.114± 0.007	3.07	5.06
4	**2b** +suberic acid	0.101± 0.004	3.46	5.7

[a] The experiments were performed at 35 °C using a N_2 flow of 10 mL/min. The experimental data were adjusted by exponential regression to a first order model $1-f = e^{-kft}$ using the equation $y = A1\ \exp(-x/t_1) + y_0$, with k_f (release rate constant) = $(1/t_1)$. The $t_{50\%}$ and $t_{75\%}$ values represent the time required for the release of 50% and 75% of the fragrance, respectively.

Scanning electron microscopy (SEM) images were obtained for the xerogel prepared by drying the organogel prepared with 1 wt % of **2b** in *(R)*-limonene with supercritical CO_2 (Figure S9). Although the temperature required (80 °C at 80 bar) could affect the nature of the aggregates formed, it seems that the combination of pressure and temperature preserves the expected fibrillar self-assembled structure in the gel. On the other hand, supercritical CO_2 drying provided the milder conditions needed to obtain samples appropriate for SEM analysis. For instance, heating using a vacuum oven was also attempted, but this was unsuccessful. For DMF, the nanostructures observed were collapsed or ill-defined aggregates of fibers (figures attached), from which individual fibers could not be properly analyzed. Under similar conditions, a viscous residue was formed from *(R)*-limonene gels. The images in Figure S9 show that the LMWG **2b** self-assembles into fibers that further form hierarchical aggregates and develop a three-dimensional fibrous network able to entrap the solvent (flavor oil) molecules controlling their release. The release profiles correlated with the strength of the corresponding supramolecular network. The obtained rates (**2b** + suberic acid < **2b** < **2c**) follow the opposite trend observed for gel strength in rheological studies (**2b** + suberic acid > **2b** > **2c**). The stronger the supramolecular network, the more efficient the *(R)*-limonene entrapment and the slower the release.

In the view of results obtained by TGA, the release of 3 mL of *(R)*-limonene was evaluated at 30 °C by monitoring the weight loss at regular time intervals. The results obtained for the liquid fragrance and for the organogels formed with 1 wt % of **2b** or **2c** are summarized in Figure 6. The experimental data were again adjusted to the first-order model, and the main parameters obtained are presented in Table 3. The results obtained for the gel obtained using the equimolecular mixture **2b** + suberic acid were less reproducible, most likely because of its higher hygroscopicity. Under these conditions (30 °C), the organogel from **2c** released 50% of *(R)*-limonene in 4.6 days and 75% in 11.6 days and that from **2b** required 9.5 and 24 days, respectively. These times were significantly longer than those observed for liquid *(R)*-limonene (2.6 and 5.4 days). It is clear that these LMWGs, especially **2b**, present an excellent potential to develop supramolecular delivery systems for bioactive compounds in comparison with standard encapsulation techniques.[76]

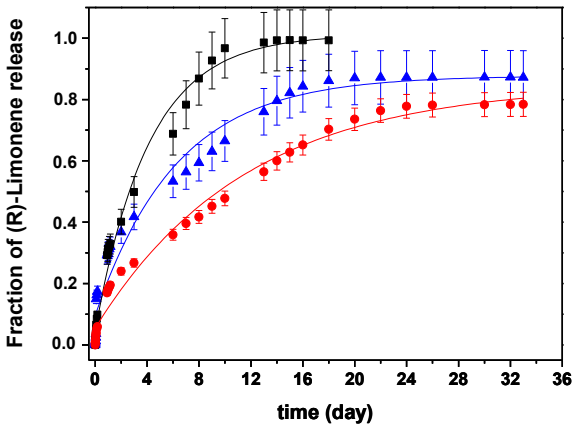

Figure 6 Fraction of (*R*)-limonene released at rt (20-23 °C) as a function of the time (days) starting from 3 mL of (*R*)-limonene. ■: pure (*R*)-limonene. ▲: organogel formed with 1 wt % of 2c in (*R*)-limonene. ●: organogel formed with 1 wt % of 2b in (*R*)-limonene.

[76] *Sustainable Chemistry Considerations for the Encapsulation of Volatile Compounds in Laundry-Type Applications*; Bruyninckx, K.; Dusselier, M.; *ACS Sustainable Chem. Eng.* **2019**, *7*, 8041-8054.

Table 3. Kinetic parameters for the release of (*R*)-limonene at 30 ºC. [a]

Entry	gel	k (h^{-1})	$t_{50\%}$ (day)	$t_{75\%}$ (day)
1	-	0.242± 0.003	2.6	5.4
2	**2c**	0.159± 0.002	4.6	11.6
3	**2b**	0.086± 0.001	9.5	24

[a] The experiments were performed at 30 ºC in a 12 mL glass vial. Gels were formed with 1% wt of the corresponding gelator in 3 mL of *(R)*-limonene. The experimental data were adjusted by exponential regression to a first order model $1-f = e^{-k_f t}$ using the equation $y = A1\ \exp(-x/t_1) + y_0$, with k_f (release rate constant) = $(1/t_1)$. The $t_{50\%}$ and $t_{75\%}$ values represent the time required for the release of 50% and 75% of the fragrance, respectively.

The results here presented show that N-functionalization of the nitrogen atom in the central spacer in C_2-symmetry pseudopeptidic compounds represents a very useful approach toward the preparation of biocompatible urea-based tripodal LMWGs not displaying C_3 symmetry, as illustrated by compound **2b**. This approach can allow a significant increase in the attainable molecular diversity and the achievement of a fine-tuning of the LMWG behavior. Despite the loss in symmetry and the lack of one amino acid fragment, in comparison with **2c**, compound **2b** shows a remarkable ability to gelate, at low concentrations (ca. 1 wt %), a variety of organic solvents. Tripodal compounds **2b** and **2c** both show an increased gelating ability in most studied solvents in comparison to the bis-urea derivative **2a**, which seems reasonable given their higher functional degree. NMR studies on the gels formed with these pseudopeptidic derivatives suggest that supramolecular hydrogen-bonding interactions involving the amide groups present can be more relevant than those in which urea fragments participate. This represents a unique feature for self-assembled systems involving pseudopeptidic compounds. According to its higher symmetry and functionalization, intermolecular supramolecular interactions are stronger for **2c**, in agreement with the results obtained for other tris-urea derivatives. This is clearly reflected in the high thermal stability of the gels formed with this compound, which can be stable up to temperatures close to 150 °C in some instances, as has been found in some other urea-pseudopeptidic LMWGs. In contrast, such strong interactions do not allow enough solubility in some solvents as to provide gels; this is the case for MeOH, where **2c** is fully insoluble while **2b** and **2a** afford the corresponding organogel. Interestingly, these LMWGs also achieved the gelation of a series of terpene flavors and fragrances, particularly tripodal compounds **2b,c.** It is remarkable

that the LMWG **2b** provided gels for limonene with significantly higher mechanical stability in comparison to **2c**.

The properties of the gels can also be tuned by the presence of additional species able to participate in the formation of supramolecular polymeric networks, as is the case of suberic acid. In this case the effect is dramatic in the case of the gel formed by **2b** + suberic acid in limonene, which maintains its stability and mechanical strength up to ca. 90 °C (from ca. 60 °C for the gel in the absence of suberic acid). For **2c**, no change in the thermal stability is observed, but it must be noted that the presence of suberic acid facilitates the appropriate ordering of the molecules in the fibrillar structure and the transitions observed at low to medium temperatures in its absence are no longer detected.

The capacity of the studied compounds to gelate terpenic natural oil flavors, even being able to form gels with complex mixtures, opens the way for their application in the controlled release of flavors and fragrances. Initial studies have shown that the stronger gels associated with compound **2b** provide slower release rates for limonene. The resulting release profiles compare very well with those obtained for the encapsulation of flavors in different materials, in particular considering the simplicity of the approach followed. Under conditions of passive release at room temperature, the time needed for the release of 75% of limonene is almost 4.5 times larger for the gel formed using 1 wt % of **2b** than for pure *(R)*-limonene (from 5.4 to 24 days).

4. Toc graphic

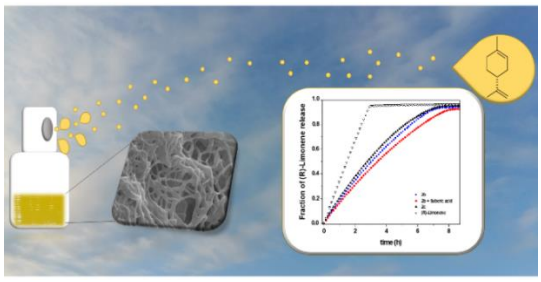

5. Supporting information

Gelation tests of **2c** and **2b** in three different commercial liquid fragrances, amplitude sweeps for **2b** in DMF and limonene, frequency sweeps for **2b** in DMF and limonene, dependence of the storage (G′) and loss moduli (G″) from the frequency sweeps with 0.01% strain with **2a–c** loading in DMF and limonene, dependence of the storage modulus (G′) on the temperature for the different

gelators in DMF, ^{1}H NMR (500 MHz) spectra of **2b** in DMSO-d_6 at different temperatures, evolution of the loss factor with the temperature for **2c** and **2c** + suberic acid in limonene, fraction of *(R)*-limonene released vs time was obtained by TGA for **2c** and **2c** + suberic acid, SEM images of the xerogel from **2b** and limonene, and synthesis and characterization of compounds **2b,c**.

5.1. Synthetic Protocols and Structural Characterization

Synthesis of 2b. (2S,2′S)-N,N′-(azanediylbis(ethane-2,1-diyl))-bis(2-amino-3-methylbutanamide) (1.03 g, 3.42 mmol) was dissolved in anhydrous CH_2Cl_2 (100 mL) in a 250 mL two-necked bottom flask under a N_2 atmosphere, and triethylamine (1.04 mL, 7.51 mmol) and dodecyl isocyanate (1.81 mL, 7.51 mmol) were added at 0 °C for 15 min. Then, the reaction mixture was stirred at rt for 24 h. The solvent was vacuum-evaporated, and the solid obtained was recrystallized in isopropyl alcohol. Yield: 2.42 g (87%, sticky white solid). Characterization: mp 153−165 °C; $[\alpha]^{25}_D$ = −23.6 (c = 0.01, CH_3OH). IR (ATR): 3332, 3273, 3102, 2956, 2920, 2850, 1626, 1566, 1467 cm^{-1}. ^{1}H NMR (400 MHz, $CDCl_3$): δ 0.81 (t, 9H), 0.85 (d, 6H, J = 6.8 Hz), 0.89 (d, 6H, J = 6.7 Hz), 1.18 (s, 60H), 1.40 (t, 6H), 2.02 (m, 3H), 2.96 (m, 2H), 3.13 (m, 4H), 3.27 (m, 2H), 3.36 (m, 2H), 4.10 (s, 1H), 5.39 (s, 1H), 5.65 (s, 2H), 7.78 (s, 2H). ^{13}C NMR (125 MHz, $CDCl_3$): δ 14.0, 18.0, 19.4, 22.6, 27.0, 27.1, 29.3, 29.4, 29.6, 30.2, 30.3, 31.0, 32.0, 39.3, 40.6, 42.1, 47.6, 59.4, 158.5, 159.0, 174.0. HRMS (ESI-TOF)$^+$: calcd for $C_{53}H_{106}N_8O_5$ $(M + H)^+$, 935.8381; found, 935.83.

Synthesis of 2c. N,N′,N″-Tris(*L*-valine)-tren (1.84 g, 4.17 mmol) was dissolved in anhydrous CH_2Cl_2 (100 mL) in a 250 mL two-necked bottom flask under a N_2 atmosphere, and triethylamine (1.27 mL, 9.16 mmol) and dodecyl isocyanate (2.21 mL, 9.16 mmol) were placed in the flask at 0 °C for 15 min. Then, the reaction mixture was stirred at rt for 24 h. The solvent was vacuum-evaporated, and the solid obtained was recrystallized in isopropyl alcohol. Yield: 4.33 g (96%, white solid). Characterization: mp 125 °C; $[\alpha]^{25}_D$ = −15.6 (c = 0.01, CH_3OH). IR (ATR): 3272, 3099, 2957, 2919, 2849, 1626, 1560 cm^{-1}. ^{1}H NMR (500 MHz, *d*-DMSO:*d*-TFA): δ 0.81 (m, 27H), 1.19 (m, 54H), 1.34 (t, 6H), 1.92 (m, 3H), 2.93 (m, 3H), 3.03 (m, 3H), 3.31 (m, 6H), 3.38 (m, 3H), 3.54 (m, 3H), 3.87 (d, 3H). ^{13}C NMR (125 MHz, *d*-TFA): δ 14.6, 18.8, 19.8, 24.2, 28.2, 30.6, 30.7, 30.9, 31.0, 31.1, 31.2, 32.8, 33.6, 37.1, 48.3, 55.1, 63.7, 162.0, 178.3. HRMS (ESI-TOF)$^+$: calcd for $C_{60}H_{120}N_{10}O_6$ $(M + H)^+$, 1077.9464; found, 1077.94.

Urea based low molecular weight pseudopeptidic organogelators for the encapsulation and slow release of *(R)*-limonene

Index

Figure S1. Gelation tests of **2c** and **2b** in three different commercial liquid fragrances: "Vainilla" (Vanilla, 81010750, composition: 2-metoxi-*p*-cresol), "Orquídea" (Orchid, 80851602, composition: linalol, 4-*terc*-butylcyclohexyl acetate, 3-*p*-cumenyl-2-methylpropionaldehyde, 2-(4-*terc*-butylbenzyl) propionaldehyde, 1,2,3,5,6,7-hexahydro-1,1,2,3,3-pentamethyl-4H-inden-4-one, 2,4-dimethylcyclohex-3-en-1-carbaldehyde, damascenone, geraniol, hexyl salicilate and silcolide) and "Lavanda" (Lavender, 80961712, composition: linalol, 4-*terc*-butylcyclohexyl acetate, 1-(1,2,3,4,5,6,7,8-octahydro-2,3,8,8-tetramethyl-2-naphthyl)etan-1-one, cineole, 3-(4-*terc*-butylphenyl)propionaldehyde, 3-methyl-4-(2,6,6-trimethyl-2-cyclohexen-1-yl)-3-buten-2-one, citronellol, coumarin and *D*-limonene).

a)

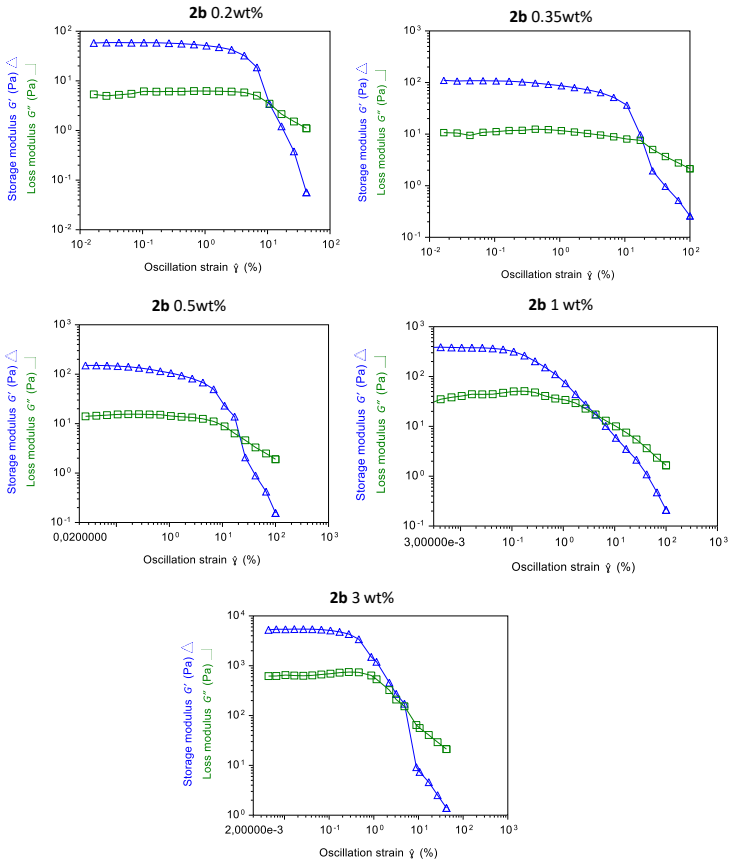

Figure S2a. Amplitude sweeps for organogels formed by **2b** in DMF at 20 ºC using different gelator contents.

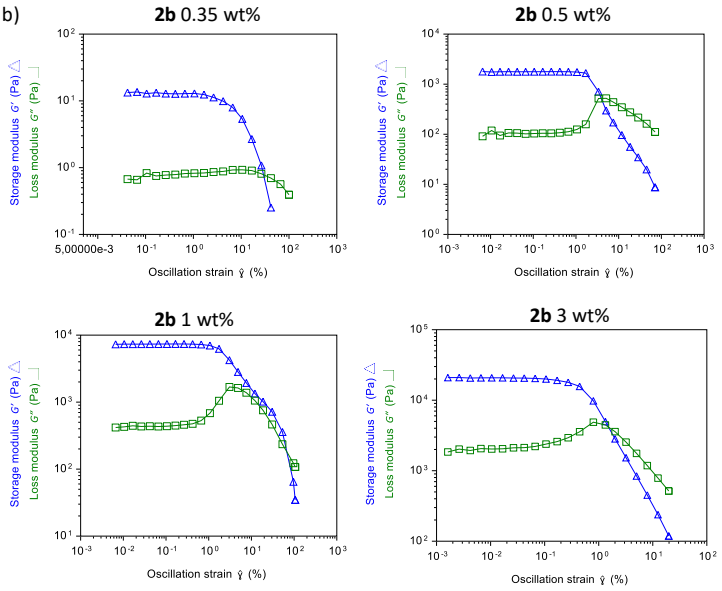

Figure S2b. Amplitude sweeps for organogels formed by **2b** in limonene at 20 ºC using different gelator contents.

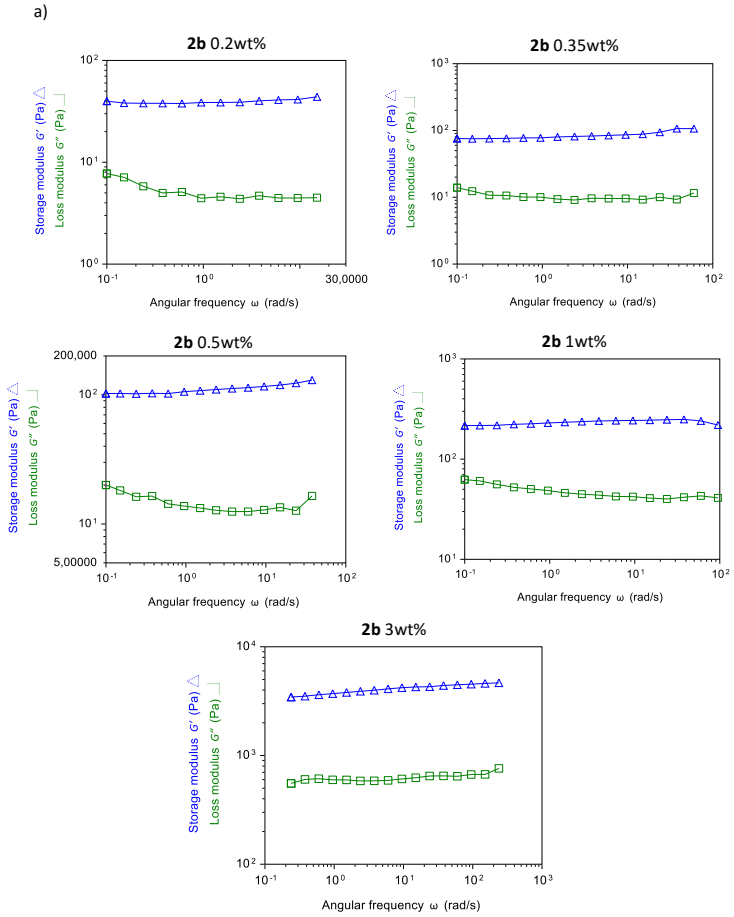

Figure S3a. Frequency sweeps with 0.1% strain at 20 ºC for organogels formed by **2b** in DMF using different gelator contents.

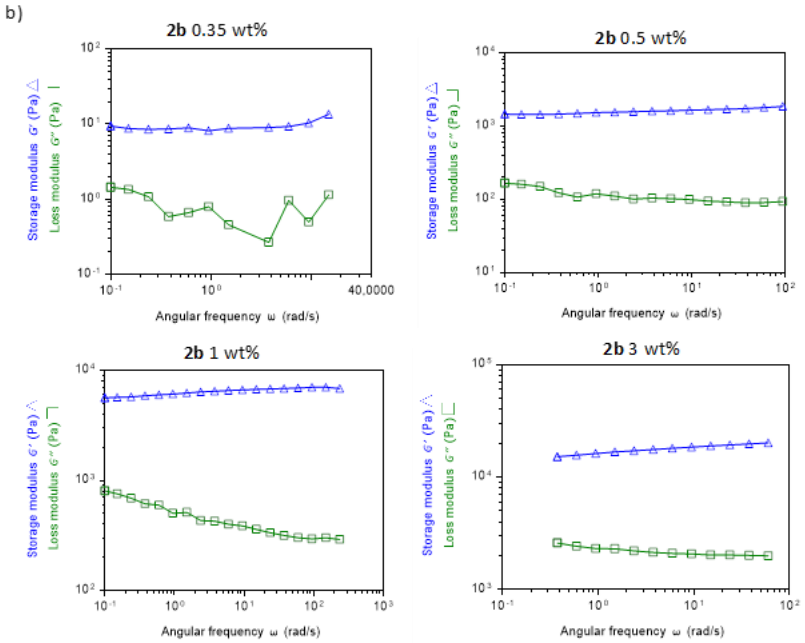

Figure S3b. Frequency sweeps with 0.1% strain at 20 ºC for organogels formed by **2b** in limonene using different gelator contents.

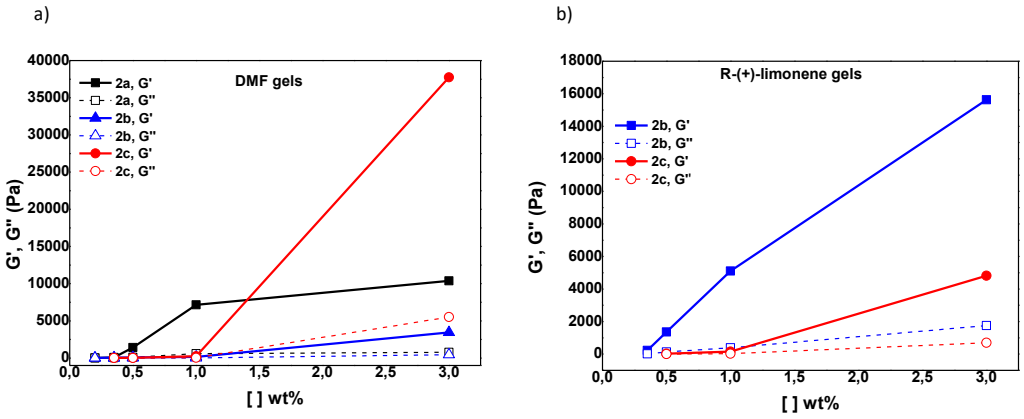

Figure S4. Storage (G') and loss modulus (G'') from the frequency sweeps with 0.01% strain vs LMWG weight loading (wt%) obtained for **2a**-**c** at 0.1 % oscillation strain: (a) in DMF; (b) in *(R)*-limonene.

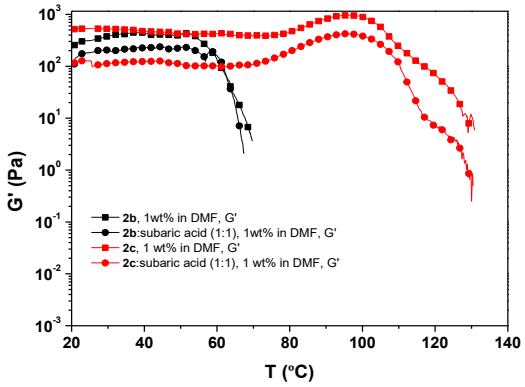

Figure S5. Dependence of the storage modulus (G') with the temperature for a gelator mass fraction of 1 wt % in DMF. All measurements were carried out at a heating rate of 2 ºC/min, a constant frequency of 1 Hz and 0.1% strain.

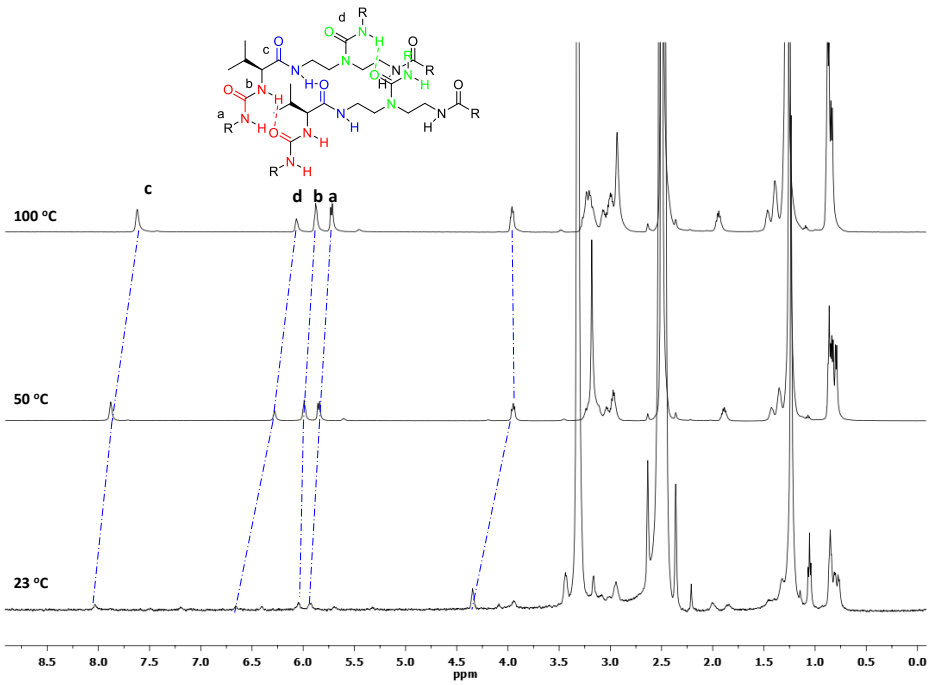

Figure S6. ^{1}H NMR (500 MHz) spectra of **2b** in DMSO-d_6 (4 mg/mL) at different temperatures.

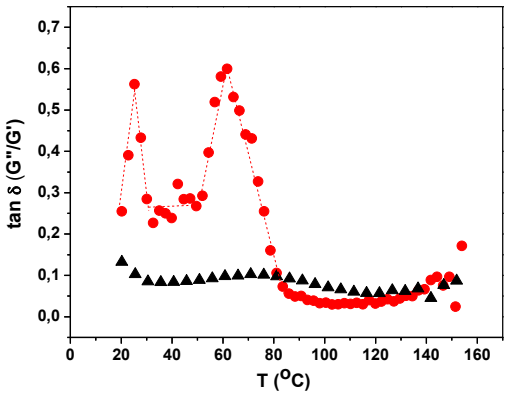

Figure S7. Evolution of the loss factor with the temperature. Dots: molecule **2c** (1 wt %) in *(R)*-limonene. Triangles: equimolecular mixture **2c** : suberic acid in *(R)*-limonene.

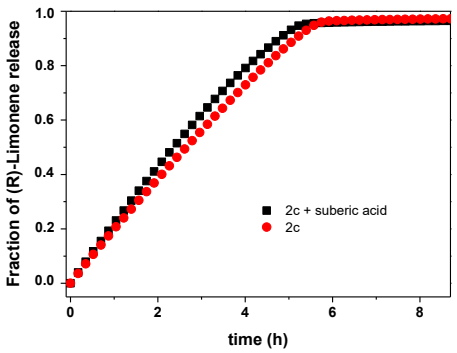

Figure S8. Fraction of (*R*)-limonene released vs time as obtained by TGA of the samples at 35 °C and under a N_2 flow of 10 mL/min. Dots: organogel formed with 1 wt% of **2c** in (*R*)-limonene. Squares: organogel formed with an equimolecular mixture of 1 wt% of **2c** and suberic acid in (*R*)-limonene.

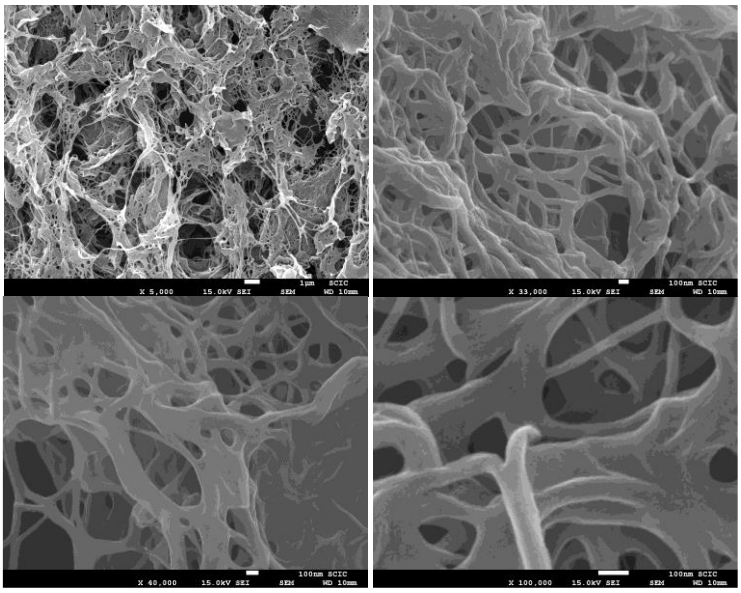

Figure S9. SEM images of the xerogel obtained by drying the organogel formed with 1 wt% of **2b** in (*R*)-limonene in supercritical CO_2 (T = 80 °C and 80 bar).

CHAPTER 4. Conclusions

CHAPTER 4. Conclusions

Conclusions for the work presented here have been shown and developed in each section. However, it is worth to highlight the most relevant and general ones in the following lines:

1) A better comprehension of the reaction mechanism for the synthesis of the tripodal imidazolium compounds has been achieved. The existence of well-defined supramolecular interactions between the imidazolium groups and the reacting imidazoles that facilitate the formation of tritopic systems once the first imidazolium group was formed, being the amide group from the amino acid moiety the key structural requirement for such supramolecular assistance to take place.

2) The potential of a series of tripodal imidazolium salts as chemotherapeutic agents has been demonstrated. At acidic pHe (6.2) the anticancer activity of some of the tripodal compounds has improved considerably, several of these compounds displayed selectivities against the control healthy cell line higher than 4. Moreover, the transmembrane anion transport studies has revealed moderate transport abilities suggesting that the observed biological activity is likely not the result of just their transport activity.

3) Imidazolium Gemini amphiphiles have been found to have excellent surfactants properties and it has been probed the importance of the position of the central aromatic spacer being the *para*-substituted compound the one that best-defined self-assembly processes in water at the μM region. Moreover optical microscopy and SEM allowed to observe the formation of spherical aggregates (vesicles) in water and the large apparent hydrodynamic radius obtained from LS measurements suggests that the amphiphiles form large aggregates (300- 600 nm).

4) The antibacterial activity against two model bacterial strains has been demonstrated for new imidazolium salts containing different alkyl chains. The antibacterial activity of compound **3b** toward *B. subtilis* was found to be lower than the IC_{50} cytotoxicity value for the control cell line HEK-293, being a promising antibacterial agent. Moroever, the compound **3b**, the

one with the best antibacterial activity, was not aggregated at the antimicrobial response concentration, being the monomeric species the responsible of the bioactivity

5) It has been demonstrated the potential of silica-supported polymeric ionic liquid (PIL)-based stationary phases derived from a vinylic *L*-valine ionic liquid monomer and divinylbenzene (DVB) as the crosslinking agent for the synthesis of high thermal and efficient new gas stationary phases. The results demonstrated that DVB is an excellent modulator of the properties of the resulting polymeric phases, and the degree of crosslinking represents a key parameter to define the overall chromatographic efficiency of the resulting silica-coated columns.

6) New LMWGs from a new family of open chain-pseudopeptidic compounds functionalized with a pendant carboxylic group have been demonstrated to be excellent hydrogelator showing a rapid and reversible, ultrasound, pH and thermal responsiveness. The control drug release studies using a Franz Diffusion Cell with a pig skin membrane revealed that the hydrogels allow for a significantly slower release of the drugs. The release process could be fitted to different release mechanism models, with the best fitting achieved for the Ritger-Peppas model.

7) Low-molecular-weight organogelators has been synthesized containing alkylurea fragments attached to the amino end of different miminalistic pseudopeptidic structures with exceptional gelation properties in relevant active substances. Furthermore, the properties of the gels have been tuned by the presence of additional species able to participate in the formation of supramolecular polymeric networks.

CAPÍTULO 4. Conclusiones

Las conclusiones del trabajo se han presentado y desarrollado en cada sección. Sin embargo, cabe destacar las más relevantes y generales en las siguientes líneas:

1) Se ha logrado una mejor comprensión del mecanismo de reacción para la síntesis de los compuestos tripodales de imidazolio. La existencia de interacciones supramoleculares bien definidas entre los grupos imidazolio y los imidazoles reactivos que facilitan la formación de sistemas tritópicos una vez que se formó el primer grupo imidazolio, siendo el grupo amida del aminoácido el requisito estructural clave para que dicha asistencia supramolecular tenga lugar.

2) Se ha demostrado el potencial de una serie de sales de imidazolio tripodales como agentes quimioterapéuticos. A pHe ácido (6.2), la actividad anticancerígena de algunos de los compuestos tripodales ha mejorado considerablemente, varios de estos compuestos mostraron selectividades contra la línea celular sana de control superior a 4. Además, los estudios de transporte de aniones transmembrana han revelado capacidades de transporte moderadas que sugieren que la actividad biológica observada no sea probablemente el resultado de su actividad de transporte.

3) Se ha encontrado que los imidazolios anfifílicos Gemini tienen excelentes propiedades tensioactivas y se ha probado la importancia de la posición del espaciador aromático central, siendo el compuesto *para*-sustituido el que mejor define los procesos de autoensamblaje en agua en la región μM. Además, la microscopía óptica y SEM permitieron observar la formación de agregados esféricos (vesículas) en agua y el gran radio hidrodinámico aparente obtenido de las mediciones de LS sugiere que los anfífilos forman agregados grandes (300-600 nm).

4) La actividad antibacteriana frente a dos cepas bacterianas modelo ha sido demostrada para nuevas sales de imidazolio que contienen diferentes cadenas alquílicas. La actividad antibacteriana de **3b** hacia la bacteria *B. subtilis* era menor que el valor de citotoxicidad IC_{50} para la

línea celular de control HEK-293, siendo un agente antibacteriano prometedor. Además, el compuesto **3b**, el de mejor actividad antibacteriana, no se agregó a la concentración de respuesta antimicrobiana, siendo la especie monomérica la responsable de la bioactividad.

5) Se ha demostrado el potencial de los líquidos iónicos poliméricos (PIL) soportados en sílice como fase estacionaria, derivados de un monómero de líquido iónico vinílico de *L*-valina y divinilbenceno (DVB) como agente entrecruzante para la síntesis de nuevas fases estacionarias de alta eficiencia térmica en cromatografía de gases. Los resultados demostraron que DVB es un excelente modulador de las propiedades de las fases poliméricas resultantes, y el grado de reticulación representa un parámetro clave para definir la eficiencia cromatográfica global de las columnas revestidas con sílice resultantes.

6) Se ha demostrado que los nuevos LMWG de una nueva familia de compuestos pseudopeptídicos de cadena abierta funcionalizados con un grupo carboxílico colgante son excelentes hidrogelificantes que muestran una respuesta rápida y reversible a los ultrasonidos, al pH y térmica. Los estudios de liberación controlada de fármacos realizados utilizando una celda de difusión de Franz con una membrana de piel de cerdo revelaron que los hidrogeles permiten una liberación significativamente más lenta de los fármacos. El proceso de liberación podría adaptarse a diferentes modelos de mecanismo de liberación, con el mejor ajuste logrado para el modelo Ritger-Peppas.

7) Se han sintetizado organogelificantes de bajo peso molecular que contienen fragmentos de alquilurea unidos al extremo amino de diferentes estructuras pseudopeptídicas miminalistas con propiedades de gelificación excepcionales en sustancias activas relevantes. Además, las propiedades de los geles se han tuneado por la presencia de especies adicionales capaces de participar en la formación de redes poliméricas supramoleculares.